UNIVERSIDAD POLITÉCNICA DE MADRID

ESCUELA TÉCNICA SUPERIOR DE ARQUITECTURA





ROMAN MORTARS USED IN THE ARCHAEOLOGICAL SITES IN SPAIN AND TURKEY

A COMPARATIVE STUDY AND THE DESIGN OF REPAIR MORTARS

TESIS DOCTORAL

DUYGU ERGENÇ

Ingeniera Geológica y Máster en Restauración

Junio 2017

CONSERVACIÓN Y RESTAURACIÓN DEL PATRIMONIO ARQUITECTÓNICO

ESCUELA T ÉCNICA SUPERIOR DE ARQUITECTURA DE MADRID

ROMAN MORTARS USED IN THE ARCHAEOLOGICAL SITES IN SPAIN AND TURKEY

A COMPARATIVE STUDY AND THE DESIGN OF REPAIR MORTARS

Autor:

DUYGU ERGENÇ

Ingeniera Geológica y Máster en Restauración

Directores:

Dr. Fco. David Sanz Arauz

Doctor en Arquitectura por ETSAM, UPM

Dr. Rafael Fort González

Doctor en Geología Económica por UCM,

Senior científico en Instituto de Geociencias (CSIC-UCM)

2017

TRIBUNAL

Tribunal nombrado por el Mgfco. Y Excmo. Sr. Rector de la Universidad Politécnica de Madrid, el día de de 2017

Presidente:

Vocales:

Secretario:

Suplentes:

Realizado el acto de lectura y defensa de la Tesis Doctoral el día de de 2017 en la Escuela Técnica Superior de Arquitectura de la Universidad Politécnica de Madrid

EL PRESIDENTE LOS VOCALES

EL SECRETARIO

I hereby declare that all information in this document has been obtained and presented in accordance with academic rules and ethical conduct. I also declare that, as required by these rules and conduct I have fully cited and referenced all material and results that are not original to this work.



To my family

Acknowledgements

This thesis would not have been possible without the support and expertise of many people. First of all, I would like to express my sincere gratitude to my advisors, Dr. Fco. David Sanz Arauz and Dr. Rafael Fort González for their guidance and generous support, and for their encouragement and cordiality.

I would like to give a special mention to Rafael Fort González whose efforts I can honestly never repay. I am grateful to him for believing in me from the beginning, for his endless enthusiasm and farsightedness, for never retaining his scientific and academic support, for being involved in every little step of the research and for his detailed revisions. Without his motivational talks, "trans-language" communication skills and ever-smiling face I would not have been able to make it to this point.

This research was funded by the project CLIMORTEC (BIA2014-53911-R) of the program Geomateriales 2 (S2013/MIT2914) of the Community of Madrid. In addition, Francisco González Yunta and Cátedra PROEISCON Ltd. are acknowledged for the lime putty supply and financial aid.

Guidance from E.T.S. Arquitectura and advice from Dr. Felix Lasheras Merino, Dr. Juan Monjo Carrio and Dr. Maria del Mar Barbero Barrera were a great help to and are greatly appreciated. Thank to Dr. Pablo Guerra and Dr. Cristina Mayo Corrochano for their support at conferences. Thanks for the valuable comments and revisions of Dr. Javier Mosteiro, Dr. Soledad García Morales, Dr. Monica Alvarez de Buergo Ballester in the pre-defense, which helped me to improve the thesis. The evaluations of Dr. Mauro F. La Russa, Dr. Fabio Fratini and Dr. Federica Fernandez as external reviewers are highly appreciated. I am particularly grateful for the assistance given by Dr. Monica Alvarez de Buergo, not only for detailed revisions of the thesis and publications, but also for continuous support and encouragement, both academically and personally. I have learned a lot from you.

This Ph.D. research gave me an opportunity to collaborate with many colleagues with different professions. I am grateful to the archaeologists of the where that I worked: Ana Lucia Sanchez Montes and Sebastián Rascón Marqués at the archaeological site of Complutum, Pedro Dámaso and Miguel Alba of the Consortium of the Monumental City of Mérida, Dr. Serdar Hakan Öztaner at the archaeological site of Nysa, and Dr. Olivier Henry at the archaeological site Labraunda, not only for giving permission for sampling, but also for their assistance and guidance.

Thanks to CEI-Moncloa the collaboration between different universities and research organisms was made possible. In this regard, the Petrophysics Laboratory, whose director is Monica Alvarez de Buergo of the Institute of Geosciences (CSIC-UCM), played a large role in the majority of the experiments that were conducted. I appreciate Dr. Mª Carmen Vázquez Calvo for conducting MIP measurements and for calmly explaining every procedure in the laboratory to me, Dr. David Martín Freire Lista for conducting Portable XRF analysis and Blanca Gallardo López for helping me with the saturation and capillarity experiments. I extend my thanks to Silvia Santos for helping me with the measurement of limes even when I was in Lisbon and to Cristian Zapatero Martín for conducting MIP measurements and helping with technical drawings.

I consider myself fortunate for being a member of an active and dynamic group, the Applied Petrology for Heritage Conservation Research Group in the Institute of Geosciences (CSIC-UCM), whose head is Rafael Fort. First and foremost, I want to express my sincere gratitude to Miguel Gómez Heras for introducing me to this group, and also thank you very much for every time being there for scientific or life consultancy and friendship. Indeed, I am more than happy to work with every single group member. Your patience, helpfulness, dedication, joy and friendship, Friday scientific diffusion breakfasts and clockwork-like teamwork motivated me every day. This was undoubtedly the best work environment ever!

Specifically, Dr. Luz Stella Gómez-Villalba is highly appreciated for her advice and assistance in the dedicated interpretation of the crystals in SEM and XRD analyses and feedback, and

likewise Dr. Mª José Varas Muriel is highly cherished for her support with the microscopic observations. I am very much obliged to Dr. Mª Inmaculada Martínez Garrido for sharing her expertise to collect-process the climatic data and creating the enjoyable working environment every time. Thank you to Dr. Natalia Perez Ema for guidance in Mérida and the program, and also for sharing all kinds of resources and information with me, to Dr. Elena Mercedes Pérez Monserrat for her scientific and life support and advice and for solving every little problem I had with great efficiency, and to Dr. David Martín Freire Lista for his constant support, sharing his passion and knowledge. I would also like to thank Dr. Beatriz Camara Gallego, my conference organization team partner, for support and motivation, my officemate, Dr. Áranzazu Sierra Fernandez, for full time positivity and academic support and ideas, and José Andrés Lira Aguado for IT and laughter support. Many thanks to my *besugo*, Dr. Arianna Murru, to Dr. Nevin Mohamed Aly, to Dr. Giulia Frostieri, to Manuela Martino and to Vincenzo Renda for their support and friendship. I also wish to express my gratitude to Dr. Mauro F. La Russa for giving me suggestions that were useful every single time and academic support. I owe a lot to each of you.

Thanks to a Santander Iberoamerica mobility grant, I had the opportunity to be a part of two important laboratories in Portugal as a visiting researcher. I deeply thank Dr. Maria do Rosário Veiga and Dr. António Santos Silva of the National Civil Engineering Laboratory (LNEC) and Dr. António Candeias of the Laboratory of Hercules-University of Évora. I would like to express my gratitude for their valuable constructive guidance, useful criticisms and helping me with the interpretation of the results, especially in the repair mortar study. During the months of working with them, I learned so much about the mortars from their expertise and the dynamic work environment. The assistance of Dora Santos with mechanical physical tests, Dora Soares with XRD, TGA and Paula Menezes with thin section preparation, Dr. Sara Valadas with SEM analysis and Ana Margarida Cardoso for FTIR analysis is greatly appreciated. Thanks to Sofia Malanho, Giovanni Borsoi and Cláudio Cruz, Dr. Ana Fragata and Dr. José Mirão for warm company and academic support.

My grateful thanks are also extended to Carmen Valdehita Mayoral, María Ascensión Barajas López, Pedro Vicente Lozano Velasco in the Department of Petrology and Geochemistry of Complutense University of Madrid for helping me in the preparation of the vast number of samples, to Iván Serrano Muñoz for realizing XRD patterns in the Institute of Geosciences (CSIC-UCM), to Xabier Arroyo Rey, Isabel Gómez Pinilla, Francisco Coruña Llopis, Sol López Andrés for conducting TGA-DSC analysis at the CAI de Técnicas Geológicas of UCM, to Ana Vicente Montaña and Pedro Robredo Urbina for conducting SEM-EDS analyses at the National Centre of Electron Microscopy (CNME) and Antonio Prieto for assistance in the manufacturing of the mortar specimens and doing the mechanical tests in ETSAM.

I also would like to acknowledge Tom Kelso for very fast and efficient language revision, and my dear *enişte*, Phil Glauberman, for helping with verbalizing the research idea, language, academic and moral support.

I would also like to thank to my friends Uğur and Filiz Diri Akyıldız for giving me a ride to the archaeological sites in Turkey and their assistance in the fieldworks. Nor can I go without mentioning my friends, Ebru Susur, Hakan Karaosman, Evin Deniz, Şenay Dincer Koç, Filiz Diri, Elif Ensari, Funda Tan, Saadet and Sinan Yenigül and Mehmet Ali Üzelgün, and acknowledging their endless support and "Ph.D therapy sessions".

Last but not least, I am grateful to my dear Omar Cabañas for supporting me every single moment of this journey, listening what happened to my *piedras* day and night, looking after me like a child in the full-time writing period, introducing the "tomorrow more and better" policy into my life and believing in me even when I do not.

Finally, I would like to thank to my nearest and dearest academic consultants: my father, my mother and my sister, who are my role models. They inoculated me with learning more and more and taught me to stick to my way of knitting. Thank you for winding me up to come here and contenting yourself with Skype conversations. In tougher times, thank you for calming and soothing me every time I wanted to be next to you, but could not be. Thank

you very much for giving me financial, academic and emotional support during my doctoral studies and the rest of my life. Without your support and belief I could not have accomplished any of these things.

Structure of the thesis

This doctoral thesis which is based on combination of two main analytical studies is organized in **ten chapters**;

Chapter 1 includes a brief introduction, the state of art and the definition of the problem, the hypothesis and objectives of the study.

Chapter 2 explains the methodology used in this study in three parts. In the first subchapter, the Roman case studies and the fieldworks are presented, in the second subchapter materials and methods used in the design of repair mortars are given, and finally in the third subchapter the analytical methods used in the study are explained. Furthermore, the chapter includes additional literature survey which was regarded necessary.

Results of the analytical studies and their relevant discussions are presented individually.

Chapter 3 presents the results of the analytical study conducted on the case study Roman mortars.

Chapter 4 presents the discussion of the characterization the comparison of Roman mortars.

Chapter 5 gives the results of experimental study conducted on the repair mortars.

Chapter 6 presents the discussion of experimental study conducted on the repair mortars.

Chapter 7 discusses the compatibility of the repair mortars based on the Roman mortars.

Chapter 8 gives the conclusion of the study.

Chapter 9 presents the contribution of the thesis to the field.

Chapter 10 presents the future lines of work.

Then, **Bibliography**, **List of figures and tables** are presented.

In the last part **Appendices**, extended information gathered from analytical study is presented with subchapters;

Appendix A presents the macroscopic descriptions of studied Roman mortars,

Appendix B presents thin section images of studied Roman mortars,

Appendix C presents MIP graphics of studied Roman mortars,

Appendix D presents Roman mortar samples and laboratories used in experiments and technical leaflet of accelerator

Table of Contents

ABSTRACT **IX**

RESUMEN **XIII**

CHAPTERS

1. INTRODUCTION **1**

1.1. State of Art and Definition of Problem 14

1.2. Hypothesis and Objectives 25

2. METHODOLOGY of the THESIS **31**

2.1. Case studies and fieldworks 33

2.1.1. Complutum Archaeological Site 34

2.1.1.1. Description of the Site *34*

2.1.1.2. Historical Background of Excavations and Investigations *34*

2.1.1.3. The Regional Geology of Complutum *35*

2.1.1.4. Sampling and Architectural Description of the Buildings *35*

2.1.2. Mérida Archaeological Complex 46

2.1.2.1. Description of the Site *46*

2.1.2.2. Historical Background of Excavations and Investigations *46*

2.1.2.3. The Regional Geology of Complutum *47*

2.1.2.4. Sampling and Architectural Description of the Buildings *48*

2.1.3. Nysa on the Meander Archaeological Site *56*

2.1.3.1. Description of the Site *56*

2.1.3.2. Historical Background of Excavations and Investigations *57*

2.1.3.3. The Regional Geology of Complutum *58*

2.1.3.4. Sampling and Architectural Description of the Buildings *59*

2.1.4. Sanctuary of Labraunda 71

2.1.4.1. Description of the Site *71*

2.1.4.2. Historical Background of Excavations and Investigations *73*

2.1.4.3. The Regional Geology of Complutum *73*

2.1.4.4. Sampling and Architectural Description of the Buildings *74*

2.2. Materials and methods of repair mortar design 82

2.2.1. The decision making process of the ratios, conditions and preparations for tests 82

2.2.2. Manufacturing process 86

2.2.3. Nomenclature of prepared samples 92

2.3. Analytical methodology 95

2.3.1. Optical Microscopy 96

2.3.2 X-Ray Diffraction (XRD) 100

2.3.3 Thermogravimetric Analysis (TGA) 104

2.3.4. X-Ray Fluorescence (XRF) 111

2.3.5. Raman Spectroscopy 114

2.3.6. Colour Spectrophotometry 115

2.3.7. Surface Hardness (Equotip) 117

2.3.8. Mercury Intrusion Porosimetry (MIP) 119

2.3.9. Acid in/soluble parts and Grain size distribution 121

2.3.10. Scanning Electron Microscopy (SEM-EDS) 123

2.3.11. Phenolphthalein spray 124

2.3.12. Flexural and Compressive Strength 125

2.3.13. Air permeability 126

2.3.14. Ultrasonic Pulse Velocity (UPV) 127

2.3.15. Water absorption under vacuum 129

2.3.16. Water absorption through capillarity 131

3. RESULTS of CHARACTERIZATION of ROMAN MORTARS **133**

3.1. Complutum Archaeological Site 135

3.1.1. Macroscopic description of the samples 135

3.1.2. Colour Spectrophotometry 137

3.1.3. Surface Hardness (Equotip) 140

3.1.4. Optical Microscopy 141

3.1.5. Binder aggregate ratio and grain size distribution 148

3.1.6. X-Ray Diffraction (XRD) 152

3.1.7. Thermogravimetric Analysis (TGA-DSC) 154

3.1.8. X-Ray Fluorescence (XRF) 159
3.1.9. Mercury Intrusion Porosimetry (MIP) 166
3.1.10. Correlations of results according to architectural features 169
3.2. Mérida Archaeological Complex 171
3.1.1. Macroscopic description of the samples 171
3.1.2. Colour Spectrophotometry 173
3.1.3. Surface Hardness (Equotip) 175
3.1.4. Optical Microscopy 176
3.1.5. Binder aggregate ratio and grain size distribution 183
3.1.6. X-Ray Diffraction (XRD) 186
3.1.7. Thermogravimetric Analysis (TGA-DSC) 189
3.1.8. X-Ray Fluorescence (XRF) 193
3.1.9. Mercury Intrusion Porosimetry (MIP) 198
3.1.10. Correlations of results according to architectural features 201
3.3. Nysa on the Meander 205
3.3.1. Macroscopic description of the samples 205
3.3.2. Colour Spectrophotometry 206
3.3.3. Surface Hardness (Equotip) 208
3.3.4. Optical Microscopy 209
3.3.5. Binder aggregate ratio and grain size distribution 215
3.3.6. X-Ray Diffraction (XRD) 219
3.3.7. Thermogravimetric Analysis (TGA-DSC) 221
3.3.8. X-Ray Fluorescence (XRF) 226
3.3.9. Mercury Intrusion Porosimetry (MIP) 231
3.3.10. Correlations of results according to architectural features 233
3.4. Labraunda 235
3.4.1. Macroscopic description of the samples 235
3.4.2. Colour Spectrophotometry 237
3.4.3. Surface Hardness (Equotip) 239
3.4.4. Optical Microscopy 240
3.4.5. Binder aggregate ratio and grain size distribution 246

3.4.6. X-Ray Diffraction (XRD) 250

3.4.7. Thermogravimetric Analysis (TGA-DSC) 251

3.4.8. X-Ray Fluorescence (XRF) 257

3.4.9. Mercury Intrusion Porosimetry (MIP) 262

3.4.10. Correlations of results according to architectural features 265

4. COMPARATIVE DISCUSSION of ROMAN MORTARS 267

5. RESULTS of the TESTS on REPAIR MORTARS 293

5.1. Results of Microstructural and mineralogical analyses 295

5.1.1. Optical Microscopy in 28 and 180 days of curing 295

5.1.2. X-Ray Diffraction (XRD) in 28, 90, 120 and 180 days of curing 297

5.1.3. Thermogravimetric Analysis Differential Scanning Calorimetry (TGA-DSC) in 28, 90, 120 and 180 days of curing 287

5.1.4. Scanning Electron Microscopy (SEM) in 28, 90, 120 and 180 days of curing 293

5.1.5. Raman Spectroscopy in 28, 90, 120 and 180 days of curing 307

5.1.6. Phenolphthalein spray in 28, 90, 120 and 180 days of curing 309

5.1.7. Mercury Intrusion Porosimetry (MIP) in 28, 90, 120 and 180 days of curing 313

5.2. Results of Physical analyses 319

5.2.1. Surface Hardness (Equotip) in 28, 90, 120 and 180 days of curing 319

5.2.2. Air permeability in 28, 90, 120 and 180 days of curing 321

5.2.3. Ultrasonic Pulse Velocity (UPV) in 28, 90, 120 and 180 days of curing 323

5.3. Results of Hydric analyses 329

5.3.1. Saturation in 28, 90, 120 and 180 days of curing 329

5.3.2. Capillary absorption in 28, 90, 120 and 180 days of curing 334

5.4. Results of Mechanical analyses 338

5.4.1. Flexural Strength in 90, 120 and 180 days of curing 338

5.4.2. Compressive Strength in 90, 120 and 180 days of curing 338

6. DISCUSSION of the EXPERIMENTAL PART 355

7. COMPATIBILITY ASSESSMENT of ROMAN MORTARS and REPAIR MORTARS 379

8. CONCLUSIONS 393

9. CONTRIBUTION to the FIELD 401

10. FUTURE LINES of WORK 407

REFERENCES **409**

List of Figures **445**

List of tables **453**

APPENDICES

Appendix A- Macroscopic descriptions **455**

Appendix B- Thin section images **477**

Appendix C- MIP graphical data **591**

Appendix D- Samples and laboratories used in experiments **609**

Abstract

The quality of Roman mortars stands out, for their high durability since they have survived two millennia, in very good conditions of conservation. The characterization of these mortars will allow us to understand their behaviour and establish guidelines for new mortar designs that approximate the properties of the Roman mortars. The field of cultural heritage sciences has discovered the significance of this durable building material and the number of case studies in archaeological sites is increasing day by day; however, there is a lack of comparative studies of Roman mortars. Despite the standardization in construction in the imperial ruled lands, this study assumed that even if the climate, cultural and historical developments, and constructions were similar in the two Mediterranean extremes of the Roman Empire, the geology of raw materials obtained from the surroundings or imported from other areas plays an important role in the appearance, durability and functionality of the mortars. Accordingly, repair mortars prepared using the original raw materials and proportions as the Roman mortars may or may not be compatible; largely due to the curing conditions, which play an important role slow carbonation is taken into account. Innovative techniques may enhance carbonation.

This doctoral thesis compared the mortars collected from two archaeological sites in Spain and two other archaeological sites in Turkey, the western and eastern Mediterranean ends of the Roman Empire. In addition, an innovative study of repair mortar design was carried out using the knowledge acquired through their characterization and controlling carbonation.

The comparative study characterized the Roman mortars of Complutum and Mérida from Spain and of Nysa and Labraunda from Turkey, which date to the first century BC and fourth century AD. The mortars were examined in two groups according to ceramic inclusion: *opus caementicium* and *opus signinum*. This also was intended to define the variations in the technology of processing mortars in these two regions.

The samples were analysed using polarized optical microscopy (POM), X-ray diffraction (XRD), thermogravimetric analysis (TGA-DSC), X-ray fluorescence (XRF), colour spectrophotometry, surface hardness (Equotip), mercury intrusion porosimetry (MIP), acid in/soluble parts and grain size distribution.

Differences in construction techniques and thus in mortar technology were observed in the two regions. While the mortar compositions in Complutum and Mérida vary, Nysa mortars 'compositions were very close to each other. The majority of the mortars have hydraulic properties, even sometimes unrelated to their function. In Turkey, among the raw materials, more argillaceous sands or volcanic origin metamorphic crushed rock fragments including high proportions of feldspar, mica, schist and slate, which causes medium to high pozzolanic effect.

The results of this doctoral research show that between the two extremes of the Mediterranean Roman Empire the raw material of the environment was used, and there is no connection in the techniques of elaboration, which means that the quality of the mortars obtained from each site differed. These studies made it possible to determine technological differences in the elaboration of the mortars in both parts of the Mediterranean, and also provided compositional information about the different mortars from each site. This in turn made it possible to establish different construction phases and assign different buildings to which construction phases of the Roman cities.

In the second part of the thesis, repair mortars were prepared based on the empirical knowledge gained from the first part. In order to stimulate the carbonation process, two innovative methods were applied, curing in a climatic chamber with a relatively higher CO_2 atmosphere and spray application of a carbonating agent. Those samples were compared with control samples cured in laboratory conditions and evaluated after 28, 90, 120 and 180 days of carbonation through a number of analytical techniques. The analytical techniques used with the repair mortars included: polarized optical microscopy (POM), X-Ray diffraction (XRD), thermogravimetric analysis (TGA), scanning electron microscopy (SEM), Raman

spectroscopy, phenolphthalein reaction, color spectrophotometry, mercury intrusion porosimetry (MIP), flexural and compressive strength, surface hardness (Equotip), air permeability, ultrasonic pulse velocity (UPV), saturation and capillary absorption.

The mortars cured in the climatic chamber show advanced carbonation and almost full carbonation. Early calcite formation was observed only in chamber cured samples. Carbonation depth was higher in the mortars without ceramic; however, those with ceramic inclusion had higher degrees of carbonation and higher performances. Nevertheless, internal micro-cracks occurred due to the rapid process, and irregularly shaped crystals formed, which suddenly diminished hydric properties. Accelerator did not yield a specific difference, but better carbonation was observed due to the steadiness of the process. The crystals in the mortars without ceramic inclusion had rounded shapes. The mortars with ceramic content did better on the performance tests; however, cracks occurred as well. In general, the mortars with ceramic inclusion had more compact microstructures and more stable carbonation. Pozzolanic reaction products were not detected due to the low relative humidity conditions and/or the low pozzolanic activity of the Roman bricks and tiles used.

Having similar petrographic aspects, the newly prepared mortars and the Roman mortars show physical and hydric compatibility; however, mechanical properties are risky. Thus it is necessary to reduce the amount of ceramic in the mortars.

Although with chamber curing optimum carbonation results were obtained, the appearance of cracks as well as the difficulty of using this method in the field makes us inclined to prefer to use the accelerator for repair mortars, with the recommendations of the reducing the proportion of ceramic used and curing in a humid environment.

Resumen

La calidad de los morteros romanos destaca, por lo general, por su alta durabilidad habiendo llegado, después de haber estado puesto más de dos milenios en obra, en muy buenas condiciones de conservación. La caracterización de estos morteros nos va a permitir entender su comportamiento y establecer las pautas para nuevos diseños de morteros que aproximen sus propiedades a las de los morteros romanos. El área de investigación en ciencias del patrimonio cultural ha descubierto hace tiempo estas buenas cualidades del mortero romano y el número de estudios de caso en yacimientos arqueológicos está aumentando día a día, sin embargo existe una carencia dentro de los estudios comparativos. Se supone que incluso si el clima, el desarrollo histórico-cultural y las construcciones son similares en los dos extremos del Mediterráneo dentro del Imperio Romano, la materia prima obtenida en el entorno geológico del yacimiento o importada de otras áreas tiene una importancia en la apariencia, durabilidad y funcionalidad de los morteros. En consecuencia, los morteros de reparación preparados utilizando las materias primas originales y las dosificaciones con los morteros romanos pueden ser o no ser compatibles en gran medida dependiendo de las condiciones de curado que juegan un papel importante cuando si se tiene en cuenta la carbonación lenta.

En esta tesis doctoral se realiza la comparación de los morteros de dos yacimientos romanos en España y otros dos yacimientos en Turquía, es decir, los extremos occidental y oriental del Imperio Romano Mediterráneo. Se realiza, además, un estudio innovador en el diseño de mortero de reparación utilizando los conocimientos adquiridos a través de su caracterización y controlando los procesos de carbonatación que experimentan estos morteros con el paso del tiempo.

En el estudio comparativo se caracterizaron morteros romanos de Complutum y Mérida de España y de Nysa y Labraunda de Turquía que se remontan a un periodo comprendido entre el siglo 1º a.C y el siglo 4º d. C. Los morteros se examinaron en dos grupos según la inclusión cerámica: *opus caementicium* y *opus signinum*. De esta forma se pretende definir las variaciones en la tecnología de elaboración entre estas dos regiones.

Las muestras se analizaron mediante Microscopía óptica polarizada (POM), Difracción de rayos X (XRD), Análisis termogravimétrico (TGA-DSC), Fluorescencia de rayos X (XRF), Espectrofotometría de color, Dureza de superficie (Equotip), Porosimetría por intrusión de mercurio (MIP), partes ácido solubles/insolubles y distribución del tamaño de los agregados.

Las composiciones de mortero en Complutum y Mérida son diferentes, al contrario de la homogeneidad encontrada en los morteros Nysa cuya composición es muy similar y muy diferentes a los del yacimiento de Labraunda . La mayoría de los morteros tienen propiedades hidráulicas incluso a veces no relacionadas con su función. En Turquía, entre las materias primas las arenas más arcillosas o los fragmentos de roca triturada del origen metamórficos y/o volcánicos, que incluyen también proporciones altas de feldespato y de mica, dan efecto puzolánico medio-alto.

Los resultados de esta investigación doctoral demuestran que en los dos extremos del Imperio Romano Mediterráneo se utilizaba la materia prima del entorno, no existiendo conexión en las técnicas de elaboración, además de que la calidad de los morteros recogidos en cada yacimiento es diferente. A partir de estos estudios se han podido determinar las diferencias tecnológicas en la elaboración de los morteros en ambas partes del Mediterráneo y también ha permitido proporcionar información de composición de los diferentes morteros en cada edificio del yacimiento lo que ha permitido establecer diferentes fases constructivas o asignar diferentes edificios en una fase de construcción determinada de las ciudades romanas.

En la segunda parte de la tesis, se prepararon diferentes morteros de reparación basados en el conocimiento empírico adquirido en la primera parte. Con el fin de estimular el proceso de carbonatación, se aplicaron dos métodos innovadores; curado en la cámara climática con una atmósfera de CO_2 relativamente más alta y aplicación de un agente acelerante de la carbonatación por medio de espray. Las muestras curadas se compararon con las muestras de control que se curaron en las condiciones de laboratorio y se evaluaron en 28, 90, 120 y 180 días de carbonatación. Para la valoración de sus cualidades se realizaron análisis de microscopía óptica de polarización, Microscopía Electrónica de Barrido, Espectroscopía Raman, Difracción de Rayos X (XRD), Análisis Termogravimétrico (TGA) reacción de Fenolftaleína, Espectrofotometría de Color, Porosimetría de Intrusión de Mercurio (MIP), Resistencia a la Flexión y Compresión, Dureza de Superficie (Equotip), permeabilidad al aire, velocidad del pulso ultrasónico (UPV), saturación y absorción de agua capilar.

Los morteros curados en la cámara climática mostraron carbonatación avanzada, encontrándose al final del estudio casi totalmente carbonatados. Se observó la formación incipiente de calcita solo en los morteros que se curaron en la cámara. La profundidad de carbonatación fue mayor en los morteros sin cerámica, sin embargo los morteros con cerámica tuvieron más alto nivel de carbonatación y mejor rendimiento. Pero debido a la rapidez de este proceso se produjeron grietas y se formaron cristales de hábito irregular que provocaron una disminución repentina en las propiedades. La aplicación de productos que favorecen la aceleración del proceso de carbonatación mostró la presencia de nuevas fases cristalinas en los morteros con cerámica. Sin embargo, en los morteros con contenido cerámico que respondieron mejor a las pruebas de valorización también se produjeron fisuras en su aglomerante. En todos los casos, los morteros que se utilizaron con cerámica mostraron una microestructura más compacta y una carbonatación más estable. Los productos de reacción puzolánica no pudieron detectarse debido a las bajas condiciones de

humedad relativa y/o a la baja actividad puzolánica de los ladrillos y tejas romanas utilizadas.

Al tener aspectos petrográficos similares, los nuevos morteros preparados y los morteros romanos mostraron una buena compatibilidad física y química; sin embargo las propiedades mecánicas no mejoraron, por tanto sería necesario mejorar esta propiedad disminuyendo la cantidad de cerámica en los morteros.

Si bien los morteros carbonatados en la cámara ha obtenido unos resultados de carbonatación óptima, la aparición de grietas así como la dificultad de utilizar este método en el campo hace que nos inclinemos por el uso del acelerante, recomendando la reducción en la proporción de cerámica utilizada y el curado en un ambiente más húmedo.

1 Introduction

This chapter includes a brief introduction to the research field, the state of art and the state of the importance, research questions, hypothesis and objectives of this doctoral research.

Reading history through architecture is important for deeply understanding the technological evolution and interactions among old societies that leads to building sustainable tomorrows. Accordingly, conservation of archaeological sites has a great importance. In 1931, The International Council of Monuments and Sites (ICOMOS) started to put the conservation actions in order with Athens Charter (Carta del Restauro) which is a pioneering attempt in the field that includes regulations for conservation and restoration actions for each country (Anonymous, 1931).

In 1956, archaeological excavations have been started to be done according to the principles of UNESCO Recommendations on International Principles Applicable to Archaeological Excavations (UNESCO, 1956).

Historic monuments were pointed out as historical evidence in the Venice charter in 1964, and underlined that authentic restoration and conservation should be done with the contribution of all possible sciences. Furthermore, in the restorations of the monuments and historic structures, every building material belonging to distinct construction periods should be taken seriously as they represent components of historical, archaeological or aesthetic value (ICOMOS, 1964).

In 1990, the ICOMOS charter for the protection and management of archaeological heritage underlined, multidisciplinary work, management of archaeological sites and investigations, minimum sampling and use of non-destructive techniques (ICOMOS, 1990).

In 2003, another charter about the conservation principles in architectural heritage was revealed by ICOMOS. In this charter the importance of multidisciplinary approaches and concern for every component of a building that reflects specific construction techniques of its period were similarly underlined (ICOMOS, 2003).

As it is indicated years ago in the Athens charter (Anonymous, 1931) and also valid in the present day, that every case should be treated individually, however an evaluation through a large scale approach would be eye-opening and beneficial in taking conservation

decisions. The impacts of Romanization on architecture that architectural features like roads, aqueducts, bridges etc. similar to the ones in Rome were used in other territories of the empire (Ward Perkins, 1994).

Reverse engineering and being so called historical detective work is possible with the investigation of the technology of building materials, especially in the human-made building materials of ceramics and mortars. The technology of mortars transmits the expertise in construction of its historical period (Crisci et al, 2004).

Throughout history, composite materials like mortars, plasters, renders with different binders and aggregates were used alongside other building stones and bricks for decorative or constructive purposes. The earliest findings of lime date back to the Pre-Pottery Neolithic period (10th – 9th millennium B.C.) as plaster for coating the walls at the site of Göbeklitepe, Turkey (Schmidt et al., 2011), in Aşıklı Höyük, Turkey (9th – 7th millennium B.C.) by chance having the pozzolanic properties (Hauptmann and Yalçın, 2000), Ain Ghazal, Jordan and Yiftahel, Israel (7th millennium B.C.) and Tell Abu Hureyra, Syria (8th – 7th millennium B.C.) (Carran et al. 2012). Wall paintings made by marl-lime plasters on the earthen structures (rammed earth) at Çatalhöyük (Anatolia, Turkey) date to 6000-7500 BC (Mellaart 1967; Çamurcuoğlu and Siddal, 2016). Boynton (1980) claimed that Egyptians also used some coatings of lime in different pyramids have been dated to ca. 5th millennium BC and 1400–1200 BC (Carran et al. 2012). On the other hand, Lucas and Harris (1962) and Ghorab et al. (1986) indicate that the Egyptians did not use lime in construction (they used gypsum) until Roman times. Gypsum has been used to prepare mortars and plasters since ancient times (Elsen, 2006). Other ancient civilizations, like those in India, China, and the Mayans and Aztecs in Mesoamerica used lime as a building material (Gárate Rojas, 1994; Carran et al. 2012). The first occasional use of lime in India was lining the pots and pans the houses of Kalibangan, Rajasthan (4th-3rd millennium BC), in China from the 2nd millennium BC, the use of lime was observed for the pillar foundations for roofing tile applications and evidences of lime uses (1st millennium BC) as plaster in the Mayan world at Cuello, Belize (Carran et al. 2012).

More examples of lime based mortars together with the deliberative use of reactive materials such as Santorini earth began with Greeks (Ritzouli et al. 2016) and become widespread throughout the Roman Empire. The Greek and Roman civilizations discovered that calcinations of marly limestones, i.e., with a concentration of aluminosilicates (clays) > 10% weight, yielded a binding material that hardened underwater (hydraulic setting) and had improved mechanical properties (Rodriguez-Navarro, 2004; Malinowski, 1981). Calcination of the air lime is produced by the heating of pure limestone (calcium carbonate) to about 900 degrees and is accompanied by a loss of 45% by weight, corresponding to the loss of carbon dioxide. The Romans used lime in constructions since the last two centuries of the Republic (200-100 BC). In addition to air lime, they regularly used lime mixed with either natural (pozzolana) or artificial (brick powder) pozzolanic materials, thus obtaining the *opus ceamentitious* and the *cocciopesto*. In other words, Roman mortar can be assumed to be equivalent to lime mortar, especially hydraulic lime mortar reflecting Roman architectural and engineering skills.

The Roman Empire begins in Rome then expanded to the east and west nearly at the same time. The Romans were present in the Iberian Peninsula for over 600 years, from 218 BC to AD 409 and brought about many changes, including the introduction of Roman languages, a legal system, and strong architectural and engineering skills (Figure 1-1). Rome created a united Spain which was to become the pride of the Roman Empire, but it took 200 years of fighting to get there - initially with the Cartaginians, then the Celts and Iberians[1] (Keay, 1988; Figueiredo et al, 2001; Muñoz Garrido, 2002).

Before the Romans, the Greeks dominate Asia Minor, today's Turkey (Akurgal, 1970). Greek architecture followed the pattern of the temple as its maximum expression, whereas the Roman architecture did it more through the constructions which serve to the state and the citizens. From this point, Greek architecture was essentially religious, while Roman

[1] During the flourishing state of the Roman Empire, Spain was known as the Roman Iberia. It was administratively parted into Hispania Ulterior and Hispania Citerior. It was even further divided into smaller regions: Hispania Taraconensis, Hispania Baetica and Lusitania(which nowadays is located in Portugal). These divisions remain a part of modern Spain, which has been divided into 15 regions (Keay, 1988; Figueiredo et al, 2001).

architecture was to a maximum civil and military level (Muños Garrido, 2002). The Romans used the irrigation systems in the lands they occupied. Within the boundaries there were connections and trade routes along which agricultural products and architectural raw materials were interchanged. After being empire, the control of technology in production and architecture was started to control by the centre (Adam, 1999).



Figure 1-1. Map of Roman Mediterranean (Laistner, 1929)

Roman architecture should have fed by antecedents. The Greeks did not use arches to any great extent, whereas arched structures are almost a hallmark of Roman civilization. The Romans learned much of their civil engineering from other people. It is known that the arch was inherited from the Etruscans, from the Greeks they learned about water supply by means of aqueducts, tunnelling techniques and the use of hydraulic cement (mortar), and in the Negev they took over and maintained the irrigation system of Nabataeans, with the assistance of Nabataean engineers (Keay,1988; Hill, 1996). The Romans have rightly been called the greatest civil engineers of ancient times, but the answer to their success lay in the ability to organize and administer large-scale projects and in their practical approach to

engineering problems. Their achievements, the sheer size and scope of their constructions were remarkable (Hill,1996). Widely shown engineering works are dams, roads, bridges, aqueducts, siphons and some other irrigation constructions.

The second century BC witnessed the start of unprecedented activity in the construction of masonry arched bridges (Figure 1- 2). The many arched bridge over the Guadalquivir at Cordoba was described by Al-Idrisi (Muslim geographer), and indeed it is noteworthy that Muslim writers often refer to Roman bridges with admiration (Hill,1996).

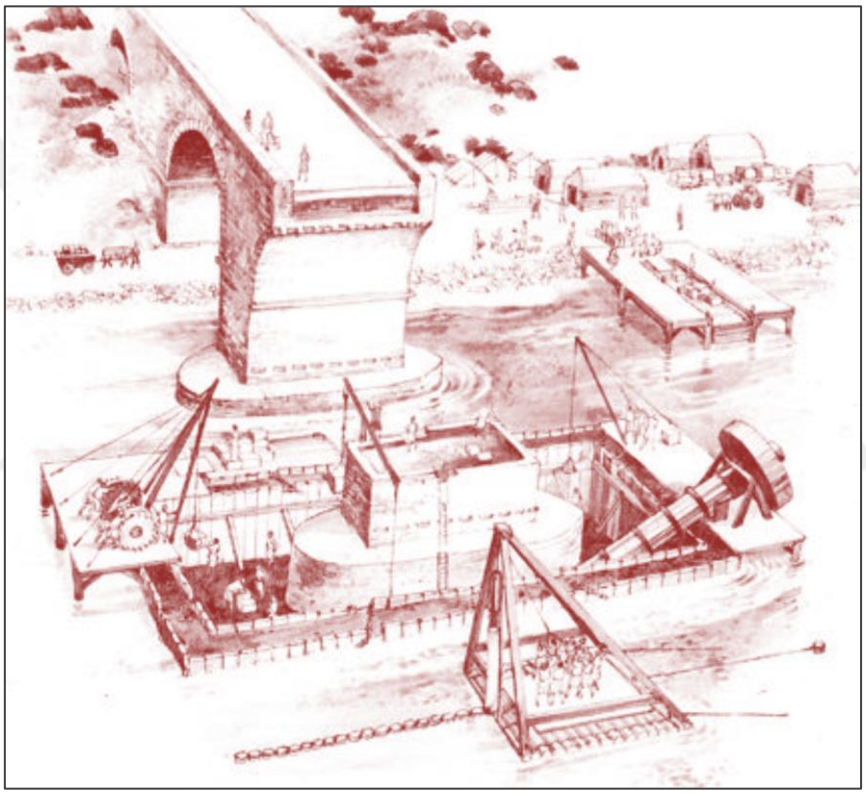


Figure 1- 2. Illustration showing the construction of bridge (Hamey and Hamey, 1990)

With the expansion of the empire, Roman engineers and architects set themselves to building roads, monumental scale buildings, bridges and for this they needed a durable mortar which could also set under water and thus they started to systematically use pozzolanic additives. Pozzolonic mortar was critical for water related construction with its ability of setting underwater. In order to reduce the impact of potential damage caused by

flooding, the number of piers was kept at a minimum and arches were constructed as large as possible. Cut-waters were placed ahead of the bridge piers to deflect tree trunks and debris that might be carried during a flood (Strickland, 2010). Pozzolanic materials include highly silica and/or alumina- siliceous compounds which can be found in volcanic origin rocks and clays. Its name comes from Pozzuoli in Italy as first mentioned by Vitruvius. In the presence of water or high humidity, finely powdered pozzolans are reactive with lime and procure calcium silicate hydrates (C-S-H) enhancing the mechanical strength (Blanco Varela et al. 2004). When there is lack of natural pozzolans, artificial pozzolans namely ceramics were used (Adam, 1999; Giavarini, 2010). Likewise, according to Jackson et al (2014) the durability and toughness of the mortars in Roman Empire came from pyroclastic volcanic rock, silt sized Pozzolane Rosse ash and as conglomerate sized tuff and brick *caementa*,. The term *caementa* refers to the larger size coarse aggregates in the Roman concrete masonries. The practice of the use ceramic as a pozzolan in lime mortar dates back to the 1st c. BC (MacDonald, 1965) and was introduced to Roman architecture from the Middle East (Akman et al. 1986).

In using concrete for construction, the initial step is preparing the foundation which was placed on the bedrock typically for the construction of large structures. Investigations of Roman structural remains have established a rather customary type of masonry foundation that consisted of large stone rubble, with mortar with a depth of about one meter (Strickland, 2010).

To create a voussoir arch, one half of this ring of stones was simply stood up on its ends. These ends rested on piers made of stone blocks mortared together with pozzolana mortar in the typical Roman arch bridge (Figure 1-3). The weight of the stone and concrete of the bridge itself compressed the stones together, making an extremely strong arch (Gedacht, 2004; Hamey and Hamey, 1990).

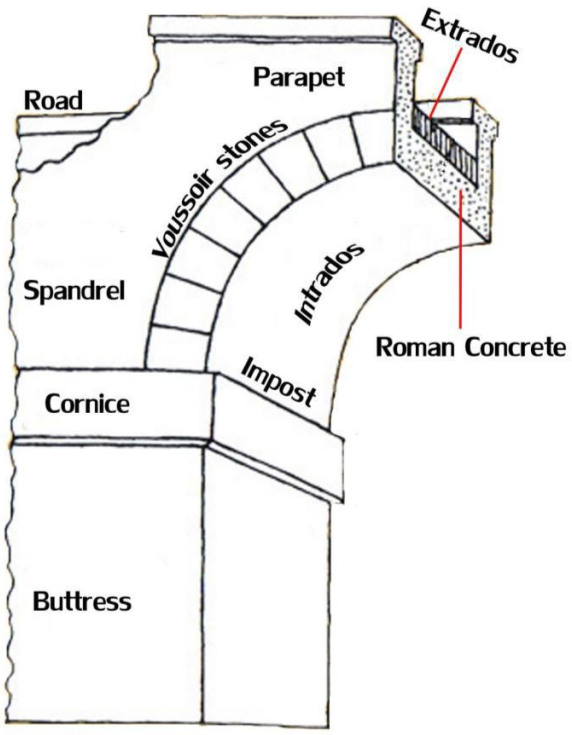


Figure 1- 3. Illustration showing the elements of a Roman bridge (redrawn after Hamey and Hamey, 1990)

The Romans built nearly 53000 miles of roads linking the capital to their far-flung empire (Hamey and Hamey, 1990). Major roads began in Rome and spread in every direction, spawning commerce, communication, and travel, while permitting rapid movement of Roman legions. The roads covered the empire like a latticework, joining the different territories (Figure 1-4). This included Italy, Germany, France, and Spain; the roads even extended as far north as Britain. To the east and south the roads connected the Balkans, Greece, Turkey, the Middle East, and North Africa, including Egypt and Tunisia (Figure 1-5). It is sure that a network of communications facilitated the movement of materials and especially of knowledge and specialized personnel for the execution of these works.



Figure 1- 4. Construction of a Roman road (Hamey and Hamey, 1990)

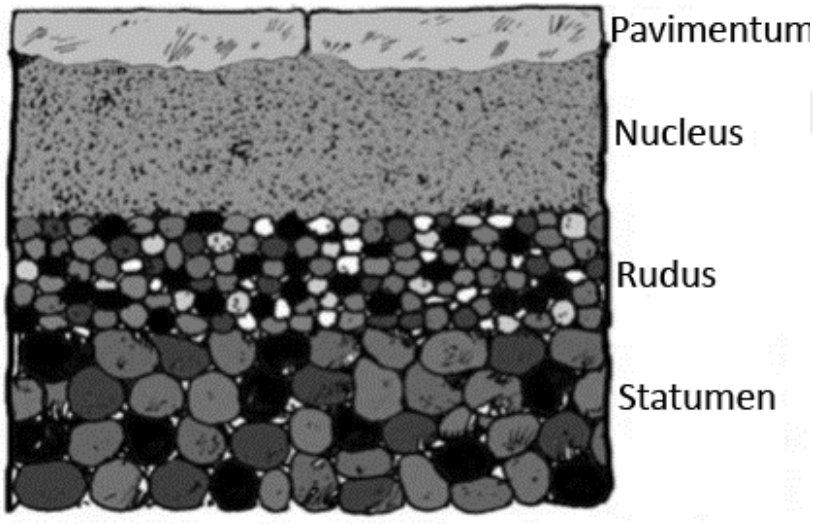


Figure 1- 5. Section of a Roman road, according to the Vitruvius' description (Hamey and Hamey, 1990)

It is very important to understand well the terminology in this field, in which there is an excess of words used by different branches of science. In order to understand the construction process clearly, the definition of terminology is necessary.

Limestone (calcium carbonate, $CaCO_3$) chips are burnt in a lime kiln and quicklime (CaO) is produced (eq. 1). The chemical reaction for this process is called calcination. The smaller fragments provide a better calcination (Cizer et al., 2012a).

$$CaCO_3\,(s) + \text{heat}\ (800\text{-}900°C) \rightarrow CaO\,(s) + CO_2\,(g) \quad \text{(eq. 1)}$$

After losing carbon dioxide (CO_2) during the calcination process, limestone turns in to calcium oxide (CaO) which is also called quicklime, burnt lime and calcined lime (Leslie and Hughes, 2002) (Figure 1- 6).

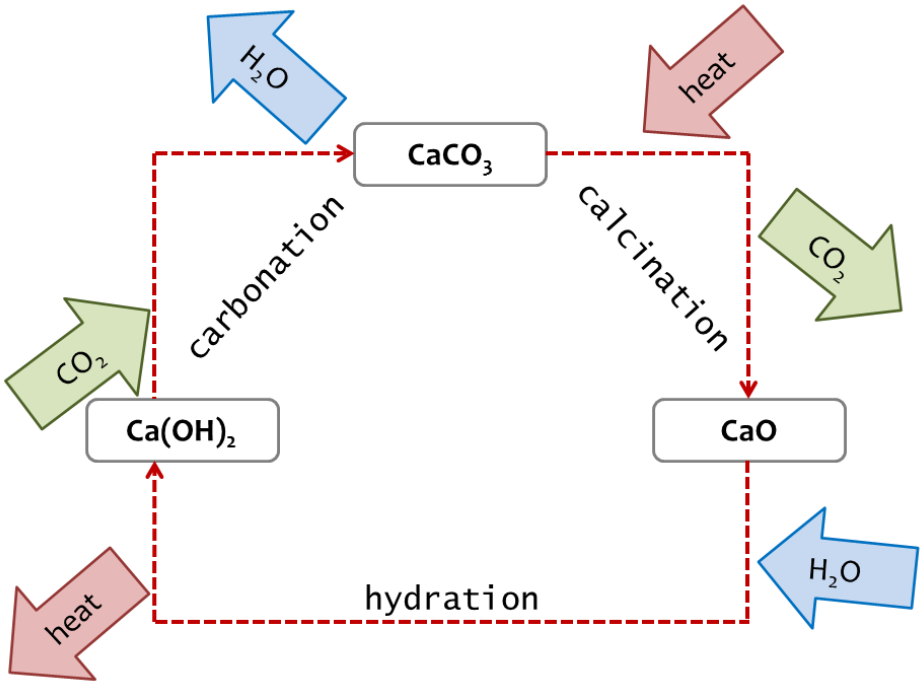


Figure 1- 6. Lime cycle

John Smeaton an English civil engineer recognized the hydraulic properties of lime derived from clay impurities in 1756 and later Louis Vicat divided limes into three classes in 1837: hydraulic lime which sets water or damp conditions, semi-hydraulic lime which partially sets under damp conditions and non-hydraulic limes which do not set under damp conditions and (Barbero-Barrera et al. 2014; Elsen et al. 2012; Carran et al. 2012).

Hydraulic limes, which achieve hydraulic setting in the presence of water, are obtained from burning limestones that contain clay impurities. The reactive aluminates and silicates in the clay combine with the lime to give the hydraulic properties. The speed of set relates directly to the amount of clay in the limestone. The limes varied from those giving a very slow set which could be slaked to form putty, to those giving a very rapid set and which would not slake at all. The hydraulic limes were described as "feebly", "moderately" and "eminently" hydraulic where the percentage of active impurities directly related to the speed of set (Rodriguez-Navarro,2004; Carran et al. 2012).

Upon calcination of impure limestones, clays dehydroxylate at 400 to 600°C. The resulting silica and alumina combine with CaO formed after the decomposition of $CaCO_3$ at 950 to 1250° C, to produce calcium aluminates and silicates. These limes are also called natural hydraulic limes (Callebout et al., 2001).

Non- hydraulic limes are known as 'pure', 'fat' or 'rich' lime. It is of high calcium content (≥90%), and is produced from a pure or almost pure limestone. It should not contain more than 5-6% impurities. High-calcium limes slake very rapidly, and harden slowly in mortar, being entirely dependent on external agents for the setting action (Rodriguez-Navarro,2004).

Furthermore, the dimension of stone chips has an influence on the resulting quicklime. Burning smaller size limestone chips requires less time and temperature and heat should be increased gradually (Elert et al. 2002).

If the temperature is low, then the lime would be under-burnt and unreacted calcium carbonate would be present. In the contrary case, if the temperature is high the lime would be over burned having low reactivity and workability (Rodríguez-Navarro, 2004).

Slaking (also called hydration) is the process of adding water to CaO to form calcium hydroxide ($Ca(OH)_2$, portlandite) (eq. 2). Slaked lime is also called as lime putty and hydrated

lime (Boynton 1980; Rodríguez-Navarro, 2004). The term hydration is used in the production of dry powdered hydrate while slaking refers to lime putty production (Elert et al. 2002).

$$CaO\ (s) + H_2O\ (l) \rightarrow Ca(OH)_2\ (aq) \quad \text{(eq. 2)}$$

The amount and purity of limestone and water have and direct relation with slaking as well as the temperature and stirring (Elert et al. 2002).

In Greek and Roman times, non-hydraulic limes were used (Hamey and Hamey, 1990). Its hydraulicity was provided by adding highly reactive silica and alumina aggregates, which cause pozzolanic reactions resulting in high bonding and strength (Rodríguez-Navarro, 2004; Mertens et al. 2009). In a wider context, Romans started to use volcanic origin aggregates, ceramic fragments and dust as artificial pozzolanic material (Stefanidou, 2016).

It is worth mentioning that in the west after the collapse of the Roman Empire, the practice of making natural and artificial pozzolanic mortars had somehow disappeared. On the other hand, in the eastern Roman Empire namely Byzantines continued the tradition and apparently passed the secrets on to Ottomans (Siddal, 2011; Weber, 2016). With the industrialization in the west mortars had been made with natural hydraulic limes, while in the east "khorasan mortar" was being made with pozzolanic additives in the regions under the rule of Ottoman Empire (Akman et al. 1986).

The last stage of the lime cycle is carbonation, when the atmospheric CO_2 dissolves in the alkaline pore solution where it reacts with slaked lime ($Ca(OH)_2$) leading to the precipitation of calcite ($CaCO_3$) and the release of water (eq. 3).

$$Ca(OH)_2\ (s) + CO_2\ (g) \rightarrow CaCO_3\ (s) + H_2O\ (l) \quad \text{(eq. 3)}$$

Carbonation is the crucial step where all of the constituents of the mortar are found together and the reactions between them along with external factors determine the mechanical resilience the final mortar. There are so many effective parameters that depending on the presence of them, carbonation process may last centuries.

1.1 State of Art and Definition of the Problem

The increasing knowledge of cultural heritage not only enriches society with answers to questions about our historic origins, but can also provide better-informed solutions to current environmental and construction-related problems which interact with broader socioeconomic factors. Europe's cultural heritage is a significant combination of many different cultures and currents of architectural style, and approaches to conservation (Cassar et al. 2004). Scientific research for cultural heritage needs to develop in a way that embraces this multitude of techniques and styles. In order to improve the application of scientific and technological methods within a humanistic/art /historical/architectural/sustainability framework, intercultural-multi-disciplinary and comparative research is needed (Cassar et al. 2001; van Balen, 2005; Elsen, 2006).

Aesthetics, function, construction materials, and environmental conditions are important factors in both architectural criticism and historic preservation. The fields of cultural heritage restoration and conservation science must consider these factors, and they should be regarded as inherently multidisciplinary. Heritage conservation science deals with the material conservation aspect of the field. Accordingly, the identification and documentation of building materials, their weathering processes, consolidation and the developing of new repair materials and methods are highly significant for furthering the field of cultural heritage management. One of the most challenging and promising subjects of interest in materials conservation science is the complex array of mortars; especially hydraulic lime mortar technology.

Recent studies on historic lime mortars focus on many aspects of this technology. These include determining the performance properties and raw materials, and to find compatible repair mortars for historic structures (Alvarez et al, 2000; Moropoulou et al, 2000; van Hees et al, 2004; Luxan and Dorrego, 2004; Elsen, 2006; Cizer et al. 2011). Binder:aggregate, water:binder ratios and aggregate properties (e.g. grain size distribution, grain shape, etc) are exceedingly related to the performance of mortar. Raw material characteristics and production technologies of lime mortars contribute to variability in structural conditions and

composition. Therefore, analysing hydraulic mortars is crucial for the evaluation of the structural performance of historic buildings. In the context of conservation, it is very important to determine the most appropriate reconstruction technique and materials for the restoration of historic buildings. In order to make a decision to use new materials, the original materials must be rigorously documented and analysed.

The need to understand better what is behind the resilience and good state of conservation of Roman lime mortar after two millennia make it an important research area after the wide use and the negative effects of Portland cement, especially in restoration of historic structures (Sabbioni et al. 2001, Mosquera et al. 2002; Elert et al. 2002; Varas et a., 2008; Smith et al. 2010).

As mentioned by Elsen (2006), studies on mortars vary according to research interests, goals, and methodologies involving experimentation and sampling. Mortar studies in conservation science include characterization of antique mortars only for documentation purposes (Lanas et al, 2004; Çizer, 2004; Blanco-Varela et al, 2004; Sanchez-Moral et al, 2005; Ortega et al, 2008; Özkaya and Böke, 2009; Mertens et al. 2009; Magalhães and Veiga, 2009; Sanjurjo-Sánchez et al. 2010; Miriello et al. 2010; Drdácky et al. 2013; La Russa et al. 2016). Specific information about a historic mortar is also collected and analysed to prepare compatible repair mortars. These studies often have focus on the hydraulicity of the binder, binder/ aggregate ratios and granulometry of aggregates (Pavia et al, 2006; Budak et al, 2010; Ventola et al. 2011; Arizzi et al. 2012). Aggregate characteristics and reactions between lime binder are of interest as well (Zendri et al. 2004; Arizzi and Cultrone, 2013). In the review of Rodriguez-Navarro (2004) highlights that Vitruvius (2005) claimed the optimal binder to aggregate ratio as 1:3. Roman and Greek lime mortars with considerable age difference had very similar textural and compositional characteristics and some researchers have found that the binder/aggregate ratio was 1:2 (Elsen 2006). Some researchers have studied the causes and effects of degradation of old mortars (Varas et al, 2008; Sabbioni et al, 2001), while recently some important studies have been conducted utilizing independent dating methods to discern different building phases through history (Hale et al, 2003; Geodicke,

2004; Rampazzi et al. 2006; Velosa et al. 2007; Sandrolini et al. 2010; Schueremans et al. 2011; Ventola et al. 2011; Marziali et al. 2013). Even though radiocarbon dating technology seems like a perfect solution, it is still not affordable by most of the archaeologists. It is also not guaranteed to get precise results every time, as very fine grain size volcanic aggregates are dispersed in the lime binder (Marra et al. 2011) which may cause age discrepancies within and among samples. Because of these drawbacks relative dating still maintains its importance in the field.

Characterization methods of historic mortars are determined several times by several researchers. First by Veiga et al (2001) then by RILEM technical committee "Characterization of historic mortars with respect to their repair" (Hughes and Callebaut, 2002; van Hees et al. 2002; Middendorf et al, 2005a, b) and then by Crisci et al (2004), Candeias et al (2005), Sandrolini and Franzoni (2010) and Santos Silva et al (2010). Characterization of materials include physical properties like density, porosity, water absorption capacity, mechanical properties like compressive, flexure and triaxial strength; and microstructure like mineralogical and petrographic properties. Velosa et al. (2010) emphasize the difficulty of working with archaeological mortar samples due to their insufficient amounts and irregular shapes, therefore mechanical and physical tests cannot be conducted in general.

Lime lumps which are frequently seen in historic mortars have been investigated by several researchers (Bakolas et al. 1995; Callebaut and Van Balen, 2000; Hughes and Cuthbert, 2000; Callebaut et al. 2001; Elert et al. 2002; La Russa et al. 2015; 2016). These lumps either can be present before or during the mixing process (Bakolas et al. 1995). Also lack of water during the slaking process, dry slaking, and insufficient seasoning may all lead to their formation (Callebaut et al. 2003). Lumps include traces from original limestone due to incomplete calcination and hydration process. Fully carbonated lumps which already exist before the mixing process have clear boundaries with the binder. On the other hand, if lump formation occurs during the mixing process it appears well integrated into the binder (Bakolas et al. 1995). The binders with lumps have less capillary pores, and therefore shrinkage cracks. Besides, the inclusion of the lumps leads to more elasticity and thus high durability (Cabellaut

et al. 2003). Hughes and Cuthbert (2000) claim that lumps are the indicators of hot lime mixing method in which quicklime, aggregate and water are mixed.

Most of the studies on Roman mortar characterization focused on monuments located in the centre of the Empire in Italy: mortars used in the constructions of Monte Sannace, Bari (Bruno et al. 2004), the Coliseum, Rome (Silva et al. 2005), Saint Callistus and the Domitilla catacombs at Rome (Sánchez-Moral et al. 2005), the Forum and Markets of Trajan, the Baths of Caracalla (Jackson et al. 2009; 2010). The mortars of Pompeii (Miriello et al. 2010) and the Theatre of Marcellus (Jackson et al. 2011) are characterized. Jackson et al. (2013) also investigated the Roman seawater submerged mortars in Bay of Puzoli.

Drádcky et al. (2013) claim that mortars taken from upper elevations (0-20 m) of Pillar of Ponte di Augusto (Narni) are made up of hydraulic limes while the ones from lower elevations (20-37.5 m) are pozzolanic mortars including volcanic aggregates. Different pozzolan types and mortars in Villa dei Quintili (Rome) have been petrographically and geochemically characterized (Belfiore et al.2015). Belfiore et al. (2016) made further a statistical analysis on the pozzolanic activity of those mortars by energy-dispersive X-ray spectroscopy (EDS) elemental maps and image analysis. Marra et al. (2011) studied several pozzolans from Albanian Hill that were used in the mortars, and Marra et al. (2015) petrographically and geochemically characterized the pozzolanic mortars and their volcanic aggregates in Temple of Capitoline Jupiter. La Russa et al. (2015) did the petrographic, chemical, characterization of the submerged mortars in underwater Roman city of Baia and reported that both hydraulic and non-hydraulic limestones and pumice as pozzolanic constituent were used to produce the lime mortar. Izzo et al. (2016) characterized mortar based materials from Villa San Marco in the ancient Stabiae (Napoli) and found out different characteristics at each level of plasters and mosaic mortars containing ceramic and volcanic aggregates. Leone et al. (2016) presented the characterization of the plasters in the walls of Herculaneum.

In Portugal, historic mortars have been studied by several researchers; Candeias et al. (2005) explain the characterization procedure and; Velosa et al. (2007) characterized the mortars of Coimbra channels, aqueducts and other water bearing constructions, in terms of micro-structure, binder/aggregate ratio, particle size distribution, and mineralogy. Roman mortars of Ammaia especially *opus signinum* mortars with different sized ceramic aggregates are characterized by Cardoso et al (2014). In the thermal analysis studies and characterization of the mortars from Troia and from Mertola researchers found that mortars with ceramic fragments when fired suffered a greater mass loss in the range of 200-650ºC, a common indicator of mortar hydraulicity (Silva et al. 2006a, b).

Topličić-Ćurčić et al. (2014) worked on the Mediana archaeological site in Serbia. In Belgium Notre Dame Cathedral in Tournai was characterized (Mertens et al 2009; Elsen et al.2011). Mortars from a Roman villa in Mošnje mortars together with the pigments in the wall paintings of Ljubljana were investigated in Slovenia (Kramar et al., 2011; Gutman et al., 2016). Coutelas (2011) makes a correlation between construction phases through the petrographic characterization of the mortars in Gallo Roman Bath in Le Vieil-Evreux in France. Mortars taken from the ancient city of Jerash in Jordan were investigated by Bany Yaseen et al. (2013). Gliozzo et al (2009) investigated production techniques by studying the mortars from the Thamusida Roman site in Morocco and found that the mortars which have quartz and carbonate sand aggregates have high amount silica but low hydraulic characters.

In Greece, Zamba et al (2007) did the characterization of Saithidai Heroon Podium in Ancient Messene (Peloponnesus), and Papayianni and Stefanidou (2007) characterized ancient mortars at the site of Olynthos and referred their durability to the use of silica reactive with lime and well grading of aggregates. After performing a physic-mechanical and chemical characterization of mortars in the Roman site Dion, Papayianni et al. (2013) prepared repair mortar mixture proposals. Pachta et al. (2014) analysed bedding and plastering mortars from cisterns and baths located in Greece, collected in old monuments from the Roman, Byzantine and Ottoman periods. That study revealed the presence of brick dust in Roman and Byzantine mortars apart from the aggregates.

In Turkey, lime mortar characteristics have been determined in the ancient cities of Sagalassos (Degryse et al. 2002) and Kyme (Miriello et al. 2011); the Serapis Temple in Pergamon (Özkaya and Böke 2009) and Roman baths in Ankara (Güleç and Tulun 1997). Besides, mortars from Roman sites in Western Anatolia (Uğurlu Sağın, 2012; Uğurlu Sağın and Böke, 2016) and mortars and plasters from Tarsus in south-eastern Turkey (Pekmezci and Ersen, 2010) have been characterized. In addition, Oğuz et al. (2014) studied mortars with other building materials used in Roman Bath in Myra, Kurugöl and Güleç (2015) characterized the mortars of the Roman basilica in Amasra, northern Turkey.

Among the researchers in Spain interest on mortars started to increase nearly two decades ago. Palomo et al. (2004) determined the characterization procedure for historic mortars after the European project in which they were involved in (EDAMM, 2002) concerningdeterioration of historic and modern hydraulc mortars. As the Roman period architecture can be found in a widespread geography, in Spain Roman mortars of Pollentia (Balearic Islands) was investigated by Genestar et al. (2006), as well as mortars of Mithraeum house of Mérida by Franquelo et al. (2008) and Robador et al. (2010). Roman mortars in La Rioja (Pavía and Caro, 2008), in Santa María La Real (Guipúzcoa) (Ortega et al., 2008) are characterized. Guerra Garcia (2015) worked on Roman mortars with ceramic aggregates in Val de la Viña (Guadalajara), Rotonda de Mejorada (Madrid), Las Arenas (Badajoz) and La Magdalena (Madrid) and claim the reaction rims around the ceramics with higher amount of calcium appear in cases where there is no ash inclusion. Recently, Ontiveros-Ortega et al. (2016) presented a detailed characteriztaion of mortars from Roman city Italica in Seville and reported that very little ceramic inclusion is found in mortars and the homogeneity in aggregtae sizes and ratios implies a premeditated mortar manufacturing.

The only comparative study available is the project ROMACONS in which maritime Roman concrete and its reproduction was investigated by high number of researchers between the years 2001 and 2009 (Brandon et al. 2014). In that project, numerous core samples which were drilled with high technologies from the harbours in central and eastern side of Mediterranean basin including southern Turkey were studied.

The are several parameters that effect the carbonation, hydration and the final quality and durability properties of the mortars which are principally binders, additives, and water and their ratios, organic/ inorganic additives, curing duration and conditions. Researchers have worked on the blended mortars with different combinations of the above mentioned factors, besides the interest on lime mortar that increased with the emerging harmful effects of the Portland cement, especially on the historic structures and sustainability issues.

For conservation and restoration, the maximum compatibility can be obtained either by using the same materials and the same composition of the old mortar and other building materials or the closest composition and the new materials which provide the similar properties (Velosa et al. 2010; Valek et al. 2000). Sánchez Moral et al. (2004) studied carbonation mechanism of mortars produced on the base of Roman mortar characteristics and found out that hardening temperature is crucial, higher temperatures lead to higher and faster calcination but lower carbonation.

In the International RILEM Workshop on Repair Mortars for Historic Masonry, which was held in Delft, The Netherlands in 2005 experimental procedures were discussed (RILEM, 2005). Characterization procedures for the repair mortar studies are defined by Van Balen et al (2005); RILEM Technical Committee (2009), Schueremans et al. (2011). Van Hees (2012) and Groot (2016) re-evaluated those decisions and resulting properties of lime mortars. Mineralogical and chemical characterization of the old mortars as well as the definition of the function is crucial in order to determine the characteristics of the repair mortars.

Arandigoyen et al. (2005) and Arizzi and Cultrone (2014) studied the water transport in the lime mortars, and Lanas et al. (2004; 2006) and Hughes and Taylor (2009) investigated the mechanical properties of lime mortars cured at different conditions. Important conclusion revealed in the study of Arandigoyen and Alvarez (2007) which state that lime mortars have a higher plasticity and even a small amount of lime in cement mortars can cause a sudden increase in plasticity while the opposite leads a slight decrease.

The effects of weathering on lime mortars have been studied by Arizzi et al. (2012) through accelerated ageing including salt attack and rain simulation after three months of curing. Higher CO_2 exposures are utilized by several reserachers in order to accelerate the carbonation (Cultrone et al. 2005; Morandeau et al. 2014). Cultrone et al. (2005) did researched on carbonation process in different types of mortars, in a carbon dioxide rich environment (1.25 dm^3) and showed that although only in 8 days almost all portlandite is transformed into calcite not fully carbonation could be gathered. Pozzolanic products were observed in low amounts and air entraining agent leads round shape in pores

There are several studies on repair mortars with different intrinsic and extrinsic factors. One step further, the mortar applications in the field and their monitoring are important to be reliable; however the control of the work is more difficult because the properties of the "laboratory specimen" change according to the properties of the adjacent material and therefore the compatibility and the overall working system in the masonry become important issues. Arizzi and Cultrone (2016) tested different binder: aggregate ratios and wet packing method to achieve the optimum water content in the mortar mixes and claim that wet mixing is preferable due to lower porosity however still leave points to search such as dissolution of lime in water.

Researchers at Leuven, Belgium, show a specific emphasis on carbonation as being a milestone of the lime cycle (Van Balen and Van Gemert, 1994;Knapen et al., 2009; Çizer et al., 2010; 2012a; 2012b). More fundamental materials research studies on mortars use combinations of advanced analytical techniques with the aim of enhancing knowledge of the burning, mixing, hydration and carbonation processes and of identifying different mineral phases (Çizer et al 2016; Elert et al 2002).

New mortars that are designed based on the compositions of the historic mortars and cured 15 months have been evaluated according to their acquired mechanical properties in the research of Moropoulou et al. (2005). Only hydraulic lime mortar and naturally pozzolanic-

lime putty mortar show a higher mechanical and chemical development. Artificially pozzolanic-lime powder mortars have the best mechanical response (Lanas et al., 2004).

Case studies of compatible repair mortars preparation and their monitoring on historic structures occupy a significant place in the literature (Lubelli et al., 2009; Bromblet et al. 2009; Bonazza, 2009; Veiga, 2010). Çizer at al. (2010) draw attention to the compatibility of the repair mortars in the restoration projects and studied by mineralogical, chemical and physical aspects. Arizzi and Cultrone (2012) mentioned the inappropriateness of dolomitc lime which leads more shrinkage and lower carbonation degree, mechanical properties. Arizzi et al. (2016) present a complete comparative study of laboratory and on-site of the mortars to use in the restoration of a 16th century palace. Two types (high and low aggregate content) of rendering mortar were applied to the walls as two layers with this order or as one mixed layer. Performances of the renders were characterized mineralogically, texturally and chromatically after 15 months, and also in the laboratory. The materials employed were dry hydrated lime, carbonate aggregate and perlite as a lightweight aggregate, metakaolin, as a water-retaining agent (cellulose derivative) and a plasticizer (polycarboxylate) as an additive; the research group utilises the proportions and characteristics of the mortars from their previous works (Arizzi & Cultrone, 2012, 2014; Arizzi et al. 2012). They recommend using the same binder: aggregate ratio at all layers of rendering mortars but smaller grain size in external layer.

Some results that can be extracted from the extensive investigation of Barbero-Barrera (2012) are that the mortars with diatoms -silica rich algae- having high water absorption and water vapour permeability are appropriate for the last but not exterior render layers, in addition the higher diatoms is the higher reflectance but the lower thermal conductivity and also grain size distribution has an direct influence on porosity.

The results of the analyses suggest the use of same binder: aggregate ratio plasters but finer aggregates in the superficial layer (Barbero-Barrera et al. 2013) and a mortar application in relatively damp and cool weather conditions. The most suitable mortar mix is that which

shows the lowest volume of micro-pores and a small volume of larger pores (up to 50 μm) to prevent the water absorption provided by the water vapour permeability.

Velosa et al. (2010) discuss the compatibility concerns about repair mortars and the historic mortars between Roman and modern times. Characterization of the mortars taken from various sites, buildings and periods was accomplished through optical microscopy, SEM-EDS, XRD, XRF, TGA/DTA techniques and compressive strength, water absorption by capillarity, grain size distribution after acid dissolution (Velosa et al. 2010). Furthermore, soluble salts, which are responsible for most of the materials decay, were studied in order to get similar results in new mortars. Moreover research states that the appropriate testing procedure should include cracking susceptibility, water intake and mechanical resistance and application in-situ in the field (Velosa et al. 2010).

Sepulcre Aguilar (2005) examined the effects of pozzolanic additives on restoration mortars in a wide extent with the use of aerial lime, natural hydraulic lime and cement as binder and metakaolin and sepiolite as additives in different proportions and curing conditions. As mentioned by other authors, he states that the addition of metakaolin causes early higher mechanical resilience and in addition, setting under cold water increase hardening. Stefanidou (2016) measured the properties of mortars with natural pozzolans, stating the positive effect of fine grains on pozzolanity, the adherence property. Metakaolin lime mortars have been tested by several researchers; with mechanical and physical properties of mortars prepared using lime putties, sands and metakaolin from different sources (Velosa et al. 2008; Bokan Bosiljkov and Valek, 2009;Faria and Martins, 2013; Santos Silva et al. 2014; Gameiro et al. 2014; Pavlík and Užáková, 2016). Nežerka et al. (2014) compared the properties of lime mortars produced with the metakaolin and ceramic dust and found that metakaolin mortars have more pozzolanic properties. On the other hand, Joao Silva et al. (2009) demonstrate that a 10% replacement of aggregates with fine ceramics show significant improvement on performance and the increase in shrinkage cracks is negligable.

Investigations on different additives have been intensely continuing; Barbeo Barrera (2011) added additives to lime mortars in order to increase the thermal behaviour and decrease the energy consumption in the building. Fusade and Viles (2016) examined the effects of different concentrations of wood ash as an additive on lime mortars' properties and attained a result of increase in drying rate, number of micropores and degree of carbonation. Researchers of the University of Navarra, Izaguirre et al. (2010) investigated fibre reinforcement, water repellent and retaining additives on lime mortars exposed to different environmental conditions, Duran et al. (2016) used polynaphthalene sulfonate, Pérez-Nicolás et al. (2016) used lignosulfonate as superplasticizer to examine the effects on air lime-metakaolin mortars and gathered higher workability and mechanical properties.

Velosa and Veiga (2001), Veiga et al. (2009) and Arizzi and Cultrone (2012) examined the effects of different pozzolanic additives on air lime mortars. With a sustainable approach, Matias et al. (2014) investigated the use of ceramic wastes and Farinha et al. (2015) investigated sanitary ware wastes in which the results show a high strength and low water absorption, Stefanidou et al. (2014) showed that the use of recycled sand derived from the demolition of historic mortars improves the chemical reactions between binder and aggregate and thus their properties. Pahlavan et al. (2016) found that the addition of spent cooking oils to air lime mortars considerably reduces the capillary sorption. Fibre is added to increase mechanical properties (Stefanidou et al., 2016). Pachta and Papaiyani (2016) indicate a better performance of lime-pozzolan grouts with linseed oil rather than with casein.

Even with the enormous increases in analytical data and applied results derived from previous researches, further, more detailed comparative research is lacking in the field and will widen the scope of applied conservation science. It is seen that repair mortar is a highly dynamic subject and the literature is full of researches with different aggregates, additives, proportions and experimental conditions. Nevertheless, the use of original historic raw materials and more reliable methods to accelerate the carbonation are lacking.

1.2 State of importance, Research questions, Hypothesis and Objectives

Based on the gaps in the literature state of importance of this thesis comes to the forefront as:

This comprehensive comparative and experimental research is necessary to have a holistic point of view. Comparative regional studies are relevant and highly necessary for understanding past technologies and interactions, with a view towards investigating regional variability. This allows the comparison of buildings and their construction style, mortar raw material selection and technology. As buildings and requisite mortars were produced and utilized within a comparable historical, political, cultural, and environmental setting, analysis of the historic mortars at the case study sites provides a suite of parameters for a productive comparative study. Similarly experimental research allows examining the influence of the different components and different curing conditions on the mortar carbonation and characteristics.

This comparative and experimental study will enrich knowledge about European cultural history, and also together with the experimental part of the research it has a practical aim of providing scholars and practitioners of cultural heritage with scientific knowledge and methods to develop new technologies of restoration and preservation specific to the Mediterranean region.

The comparative study is appropriate as in the case study regions, regional climatic conditions are similar, and Roman structures are numerous, visible, well documented, and accessible. The goal of the research is ultimately to allow for better understanding of variability in architectural activities in the western and eastern Mediterranean Roman Empire. In the selection of the structures, construction period range is limited to within the first centuryBC -including the Republic era- and fourth century AD, during which time, building performance was highest in Roman Empire (Figure 1.2-7).



Figure 1.2 - 7. Europe map bringing Spain and Turkey to focus

In the studied cases, construction style and technology, mortar raw material selection are evaluated and compared. As buildings and requisite mortars were produced and utilized within a comparable historical, political, cultural, and environmental setting, analysis of the historic mortars at the case study sites provides a suite of parameters for a productive comparative study; at the borders of Roman Empire, western Mediterranean Spain and eastern Mediterranean Turkey encompass archaeological, architectural interactions and disconnections.

1.2.1. Comparative Research questions

Data generated by this thesis will serve to test hypotheses and improve theories about regional raw material exploitation and use, mortar binder : aggregate mixture proportions and deterioration causes, and will help to identify new compatible repair mortars. Broader research questions to be addressed include the following:

1. What aspects of mortar production technology are similar or different in two distinct regions of Roman Empire?

2. How do locally available raw materials and environmental conditions impact technological decisions?

3. Do variable construction techniques affect the selection and use of certain raw materials?

4. What are the states of deterioration and conservation of mortars in buildings at case study sites?

Expected Results:

-If locally available raw materials are similar in both regions, then it is expected that the mortar technology and durability will also be similar. Alternatively, if raw materials vary between the regions, then mortar technology and durability should co-vary accordingly. Variability in raw materials used to produce mortars and building stone also have implications for construction techniques.

-If mortar raw materials and mortar production methods differ between sites in Spain and Turkey, it is expected that geochemical analytical methods will document different reaction products of different aggregates. If different pozzolanic additives are used in the mortars, then it is expected to find different C-S-H and C-A-H reaction products.

-If the regional geologies, environmental conditions, state of conservation of mortars and structures at both case study locations are similar, then it is expected to find same compatibility of mortar and adjacent building stone.

-If the post-construction and current environmental conditions are similar in both regions, then it is expected that the mortars will display comparable states of deterioration. Otherwise, if the environmental conditions differ, then decay level should be different.

-Combined analytical results on mortar composition, and assessment of local weathering factors will provide data which will establish the causes of differences and similarities in mortars between the case study regions.

1.2.2. Experimental Research questions:

The aim of the second and experimental part of this thesis is to do an investigation on manufacturing of the replica Roman mortars gathered by the characterization data, together with the innovative methods to accelerate the carbonation.

1. What are the factors that influence the carbonation?

2. How different are the carbonation processes at different curing conditions?

3. Is it possible to have faster carbonation without worsening the physical, mechanical and hydric properties?

4. Is it possible to have a common formula for the repair mortars in a specific region?

Expected Results:

-Theoretically, excess of CO_2 and accelerator product should increase the carbonation rate.

-If the ceramic aggregates are reactive enough and conditions are appropriate pozzolanic reactions should occur.

-Regarding to the mechanical and hydric properties, higher values are expected in the mortars with ceramic inclusions due to better bonding and water suction, respectively.

-At the end of the experimental campaign mortar blends may be still not fully carbonated even in the accelerated ones.

-If the performance of the mortars is good enough they can be used as the substitution of the much deteriorated original Roman mortars, and even can be used in new constructions.

After those mentioned specific research questions and expected results, a **hypothesis** to be evaluated within this thesis is that;

Romans brought the standardization and centralization to the constructions. However, even if the climate, cultural-historical context, and constructions are similar, it may be that the locally variable geology plays a role in the observed ingredients, appearance, durability and functionality of mortars. Accordingly, repair mortars prepared using the original raw materials and proportions with the Roman mortars may or may not be compatible depending much on the curing conditions which play important role when taken into account the slow carbonation. Innovative techniques may aid to get improved carbonation.

The main aim of this thesis is to compare the occidental and oriental Roman mortars (Spain and Turkey) and to make suitable repair mortars with the gained empirical knowledge. It would not be incorrect to evaluate the thesis in two parts. The first part focuses on extracting data from mortars of Roman archaeological sites and comparable structures situated in Turkey and Spain in order to achieve the specific research objectives within the framework of increasing knowledge on mortar production technology and use, an important aspect of Mediterranean historic technology. Moreover, to understand better the working mechanism of Roman mortars and construct a bridge to repair mortar studies empirical knowledge implication is important. Therefore the final goal is to design a repair mortar based on the data obtained in the composition of these mortars that may be used in the restoration of archaeological sites.

The main goal of the comparison of the Roman mortars address the aforementioned research questions, and elucidate the similarities and differences in mortar technology employed at opposite ends of the Roman Mediterranean. This will be achieved by distinguishing the components of raw materials, and assessing environmental conditions at archaeological sites which all affect durability, and functionality of mortars. In accordance with the aforementioned comparative research questions, sub-objectives are determined as follows;

Specific comparative research objectives:

1- To determine the characteristics of regional (in Spain and Turkey) Roman mortars

2- To find out the differences/similarities in the materials and production techniques and to examine if there is a transfer in the technology or not.

3- To examine the effects of the characteristics of the constituents and bonding between them on the performance of the whole mortar

4- To examine the environmental conditions that may affect building scale, construction methods, and differences in durability of mortars.

The main goal of the experimental repair mortar study address the aforementioned experimental research questions; to make repair mortars with similar properties that have Roman mortars and control the carbonation in different conditions. To answer the aforementioned experimental research questions sub-objectives are determined as follows;

Specific experimental research objectives:

1- To find and select the composition of the replica Roman mortars

2- To examine if the different curing conditions lead to a faster carbonation.

3- To use a set of experimental procedure to better follow the evolution in carbonation

4- To correlate properties of the Roman mortars and the newly carbonating mortars

With these mentioned sub-objectives of the experimental part it is possible to bridge the understanding of newly carbonating mortars and the Roman mortars, and accordingly to understand better the mortar system and discuss the applicability of the new repair mortars to archaeological sites and/or buildings.

2 The Methodology of the thesis

The methodology of this study is presented in three sections; first, the case studies and fieldwork used in the comparative study; second, the materials and methods of the experimental study, and finally, the analytical techniques used to characterize the Roman and new mortars. All three parts of the methodology are directly related to how each method will answer the research questions.

2.1 Case Studies and Fieldworks

The cases selected for the comparative study were Complutum and Mérida in Spain and Nysa and Labraunda in Turkey (Figure 2-1).



Figure 2-1. The archaeological sites indicated in Figure 1.2-7

In the fieldworks, the sites were documented systematically, and the sampling was done with the guidance of archaeologists. Note that, the samples were collected with hammer and chisel with the intention of minimum destruction, but also to obtain a sufficient number of samples to provide statistically precise results. Mortars were sampled regarding their function and the type of construction. The presence or absence of ceramic inclusion in the mortars was the main focus in the classification of the mortar samples since the very different properties it yields were the most remarkable aspect of the fieldwork. In this doctoral study, the mortars were categorized according to their ceramic content, and the terminology, *opus caementicium* and *opus signinum* was used.

Opus caementicium, also known as Roman concrete, is the revolutionary construction style made of lime, aggregate, pozzolan and water that was used to build immense core masonries. The faces are dressed with other building materials in various opus types. *Opus signinum* refers construction material that includes ceramic fragments. In this study, the mortars with ceramics are called *opus signinum*; and those without ceramics are called *opus caementicium*.

2.1.1 The Complutum Archaeological Site

2.1.1.1 *Description of the Site*

The archaeological site of Complutum is a complex of archaeological remains from the eponymous ancient Roman city located on in the plain the Henares River in Alcalá de Henares (thirty five kilometres northeast of Madrid, Spain. It has been a World Heritage Site since 1998 (Figure 2.1- 2).

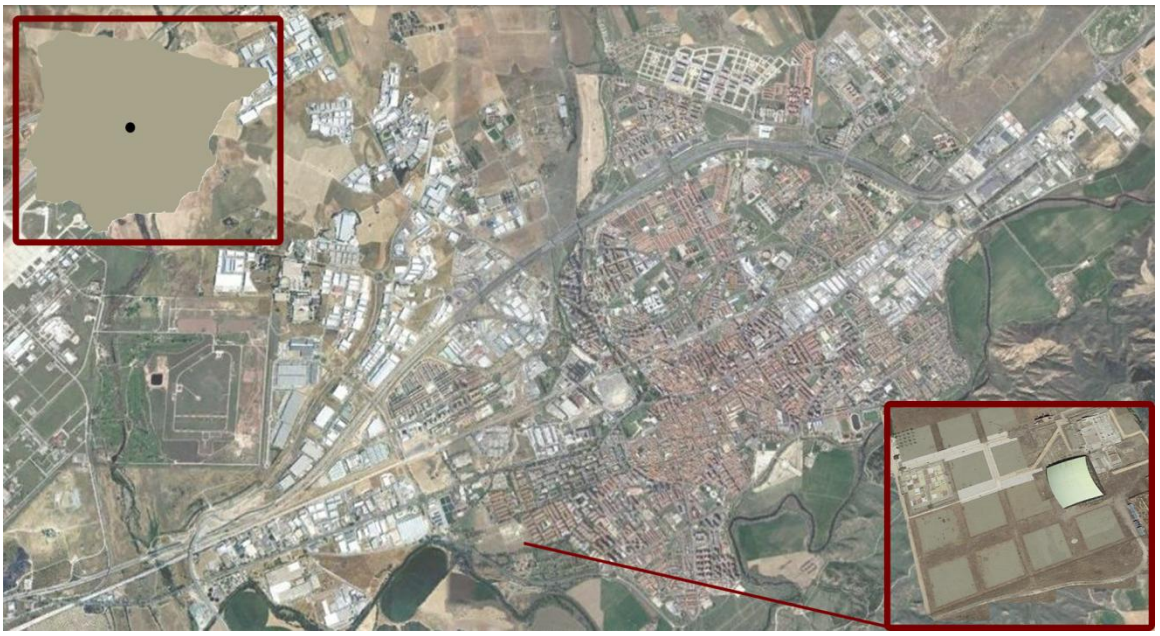


Figure 2.1- 2. Map showing the localization of Complutum (Aerial photograph from Google Earth)

2.1.1.2 *Historical Background of Excavations and Investigations*

The Roman city of Complutum (Alcalá de Henares) has antecedents in pre-Roman times, built in two phases: first in the time of Augustus. The second and last construction was realized in the period of Claudius, before the middle of the first century AD. The city had a remarkable development after the mid third century, the regeneration of urban infrastructures, deep remodelling of public buildings and the development of domestic architecture. From an advanced, but imprecise date in the fifth century AD, its buildings begin to dismantle progressively while developing a more dispersed urbanism, which defined the landscape until the Islamic invasion in the eighth century (Rascón Marqués et al. 2009).

Since 1985, archaeological excavations have been being conducted by the General Directorate of Historic Heritage of the Community of Madrid and Alcalá de Henares Town Hall. Complutum was declared to be of cultural interest in 1988, and since 2008 has been part of the open-air museums integrated in the network of open public sites in the Community of Madrid.

2.1.1.3 *The Regional Geology of Complutum*

The area of Alcalá de Henares is part of the whole of the upper basin of the Tagus. Complutum is in the terraces of the Henares River, which include Quaternary age sands and gravels, sandy clays, carbonate nodules and crustal limestones. In the south Miocene age clay loams, brown clays and micaceous sands are also present (Figure 2.1- 3).

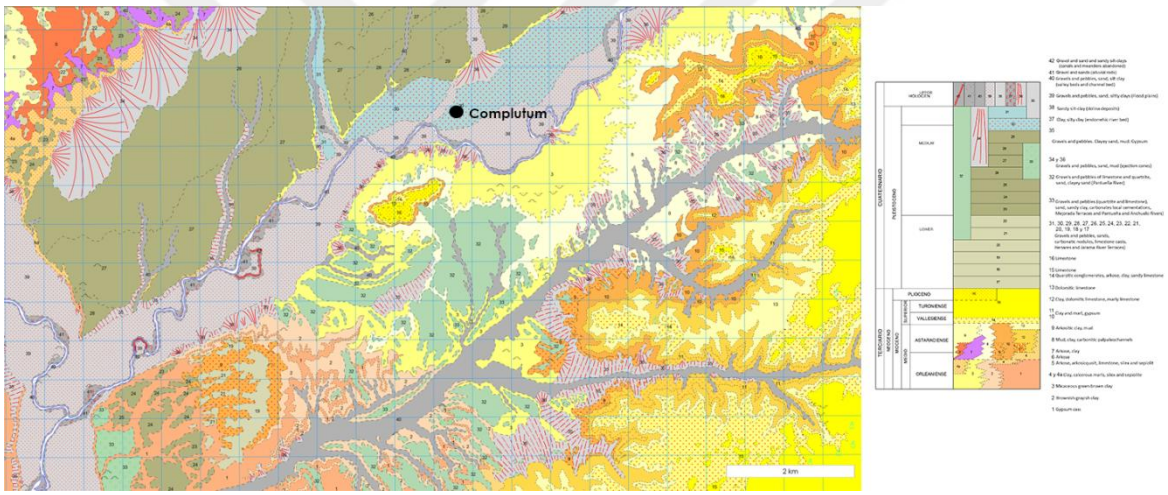


Figure 2.1- 3. Geological map of Alcalá de Henares (IGME, 1928)

The climate in Alcalá de Henares where Complutum is located is warm and temperate. There is more precipitation in winter than in summer. In Complutum, the temperature ranges between−4.5-38.7◦C, relative humidity between 10-61.08 %, and the maximum rainfall and CO_2 concentration recorded are 3.6 mm and 575 ppm, respectively (Martinéz Garrido et al. 2016).

2.1.1.4 *Sampling and Architectural Description of the Buildings*

The main site of Complutum has a surface area of more than 50 hectares, and an important belt of suburbs beyond that. It is a city of hypodermic urbanism, organized in blocks of 1

actus (ca 36x36 m), with a rational system of sanitation and porticos in almost all the streets. Several private houses are known, in the Mediterranean models of atrium, peristyle or courtyard (Rascón Marqués and Sánchez Montes, 2009).

A total of 42 samples of *opus caementicium* and *opus signinum* type mortars were collected from the Criptoporticus, the North and South Baths, the Cuadriporticus, the Basilica, the Monumental Façade, the House of Marte, the House of Atrium, the sewers and the cuadrifrontal arch (Figure 2.1- 4, Figure 2.1-5 and Table 2.1-1). The bridge is located relatively far from the actual archaeological site. It is marked with red point in Figure 2.1-2. It was sampled to determine if there is a correlation between it and the other collected samples.



Figure 2.1- 4. General plan of the Complutum archaeological site (the large red area in the center is the forum and House of Grifos, next to it in the west, the House of Atrium, the House of Marte, and in the six blocks west, the cuadrifrontal arch

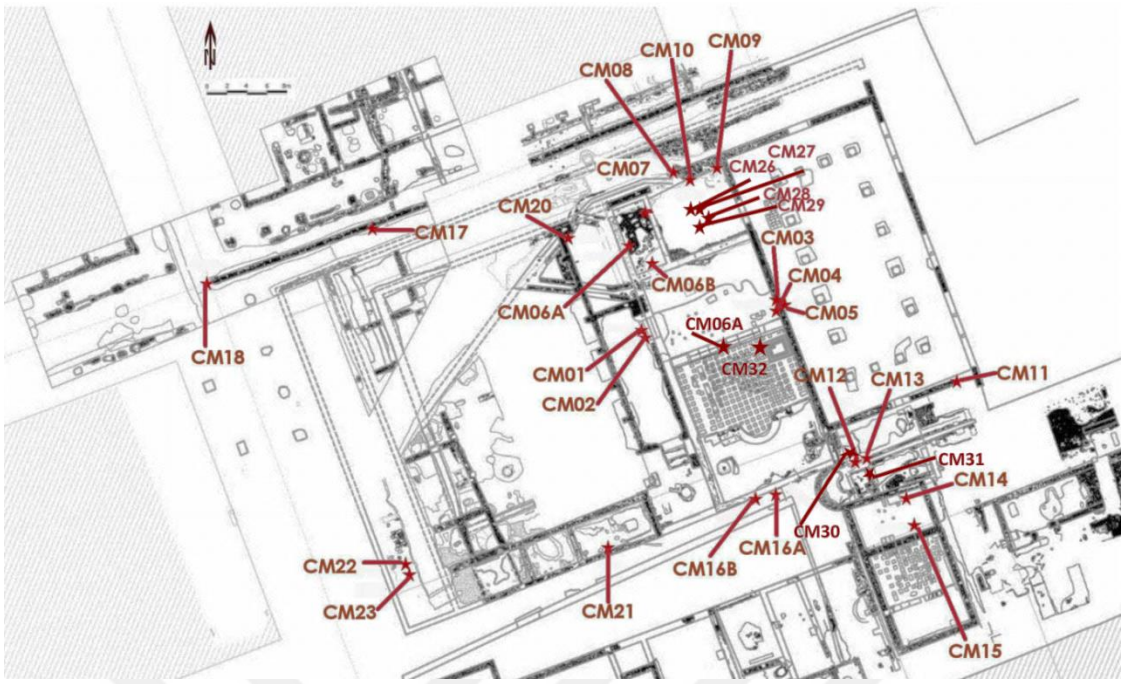


Figure 2.1- 5. Plan of the forum of Complutum with sampling points (the large red zone in Figure 2.1-4)

Table 2.1- 1. Description of the samples

Sample	Opus Type	Description	Construction Phase
CM1	*Opus Cementicium*	Criptoportico East Wall (half south), Wall of *specus* of reused canalization. Attached to entrance towards *tepidarium* from criptoportico.	1
CM2A	*Opus Cementicium*	Criptoportico East Wall (half south)	2
CM2B	*Opus Cementicium*	Criptoportico East Wall (half south)	2
CM3	*Opus Cementicium*	North Bath Conduit of hipocaustum. Pillar of separation wall of hipocaustum from tepidarium with caldarium. Eastern side.	1
CM4	*Opus Cementicium*	North Bath Conduit of *hipocaustum* of separation wall of *hipocaustum* from *tepidarium* with *caldarium*. Eastern side. Structure of closure of conduit.	2
CM5	*Opus Signinum*	North Bath Pillars of conduit of *hipocaustum* of separation	1

		wall of *tepidarium* with *caldarium*. Eastern side. Coating of the pillars.	
CM6A	*Opus Caementicium*	North Bath Floor of hipocaustum of caldarium. Northern side.	1
CM6B	*Opus Signinum*	North Bath Floor of Natatio of frigidarium. Western side.	1
CM7	*Opus Signinum*	North Bath Coating of walls of pool of *frigidarium*	1
CM8	*Opus Cementicium*	North Bath Wall of apse of the closure of opening of frigidarium of thermal baths. Elevation of opus caementicium.	2
CM9	*Opus Cementicium*	North Bath Façade Frigidarium	1
CM10	*Opus Signinum*	North Bath North wall of *frigidarium*. Marble coating mortar to the wall.	?
CM11	*Opus Cementicium*	Basilica South wall (east half).	1
CM12	*Opus Cementicium*	South Bath Canalization. Water entrance of natatio from frigidarium. Mortar of south wall of specus.	2-1
CM13	*Opus Signinum*	South Bath Canalization. Water entrance of natatio from frigidarium. Coating mortar of interior south wall of *specus*.	2-1
CM14	*Opus Cementicium*	South Bath Seperation wall between frigidarium and tepidarium.	2-1
CM15	*Opus Cementicium*	South Bath Seperation wall between tepidarium and caldarium. Elavation of *hipocaustum*. Mortar sample is in the brick arch.	2-1
CM16A	*Opus Cementicium*	Canalization under Decumano IV Canalization of drainage of north and south thermal baths.	1
CM16B	*Opus Cementicium*	Canalization under Decumano IV Canalization of drainage of north and south thermal baths. Direction E-W.	1
CM17	*Opus Cementicium*	Canalization under Decumano III *Specus* of canalization, north wall. Drainage of north and south buildings of of decumano III. Interior rendering mortar of the wall.	1
CM18	*Opus*	Canalization under Cado IV Vault of canalization.	1

	Cementicium	Drainage where the canalization poures under Decumano III and east and west buildings of Cardo IV. Sample is at the tie of two canalizations.	
CM20	*Opus Cementicium*	Monumental Façade Northern pillar, located at western facade, foundation. Over the covering of canalization.	2
CM21	*Opus Cementicium*	Cuadriportico Southern side South wall of south branch. Room 1(east). Foundation.	1
CM22	*Opus Cementicium*	Cuadriportico Western side Floor	1?
CM23	*Opus Signinum*	Cuadriportico Western side Floor	1?
CM24	*Opus Signinum*	House of Marte Specus of the canalization, east wall. Drainage from impluvium of Atrium towards the general sewerage of decumano III.	1
CM25	*Opus Signinum*	House of Atrium Decorative fountain of atrium. Exterior coating mortar.	1-2
CM26	*Opus Signinum*	North Bath Frigidarium floor highest level	?
CM27	*Opus Signinum*	North Bath Frigidarium floor 3	?
CM28	*Opus Cementicium*	North Bath Frigidarium floor level 2	?
CM29	*Opus Cementicium*	North Bath Frigidarium floor bottom level	?
CM30	*Opus Signinum*	South Bath wall	2
CM31	*Opus Cementicium*	South Bath caldarium floor	2
CM32	*Opus Cementicium*	North Bath hipocaustum floor	?
CM33	*Opus Cementicium*	North Bath hipocaustum floor	?
CM34	*Opus Cementicium*	Arch pillar	?
CM35	*Opus Signinum*	Arch pillar	?

CM36	*Opus Cementicium*	Arch pillar	?
CM37	*Opus Signinum*	Bridge pillar	?
CM38	*Opus Cementicium*	Bridge pillar	?

Samples of Roman colonial architecture that combine the plasticity of the opus with stone can be observed in the forum of the city. During the reign of Claudius, a basilica, a thermal bath and a *Cuadriporticus* were built. At some point in the third century AD a series of conversions were done to these buildings. A large administrative building, the Curia, near the Basilica, won prominence over the baths, which lost their hygienic and aesthetic function, to become representative buildings of the state for government and administration. This conversion was particularly important because it led to the construction of a new structure that served both as façade and access to this new concept of the building: a *Criptoportucus* on which supports a monumental building. It was constructed with opus *caementicium,* presumably lined with stone elements. In the middle of fourth century AD, new restorations were done to the buildings (Rascón Marqués and Sánchez Montes, 2015).

The *Cryptorporticus* is an underground gallery. Built with thick walls and paved with herringbone bricks; it was used as an entrance to the Curia. Its walls, vaults and the floor were constructed with *opus caementicium* and ceramic rhombs (third century AD) (Rascón Marqués and Sánchez Montes, 2009).

The Basilica, which was a trade and administrative building was built during the time of Claudius and was restorated in the last quarter of the third century AD. It was a covered building with a central nave surrounded by a corridor separated by a series of columns. The floor was *opus signinum,* which had a polished appearance when it was in use. The walls were coated with white plaster and decorated with marble (Rascón Marqués and Sánchez Montes, 2009) (Figure 2.1- 6).

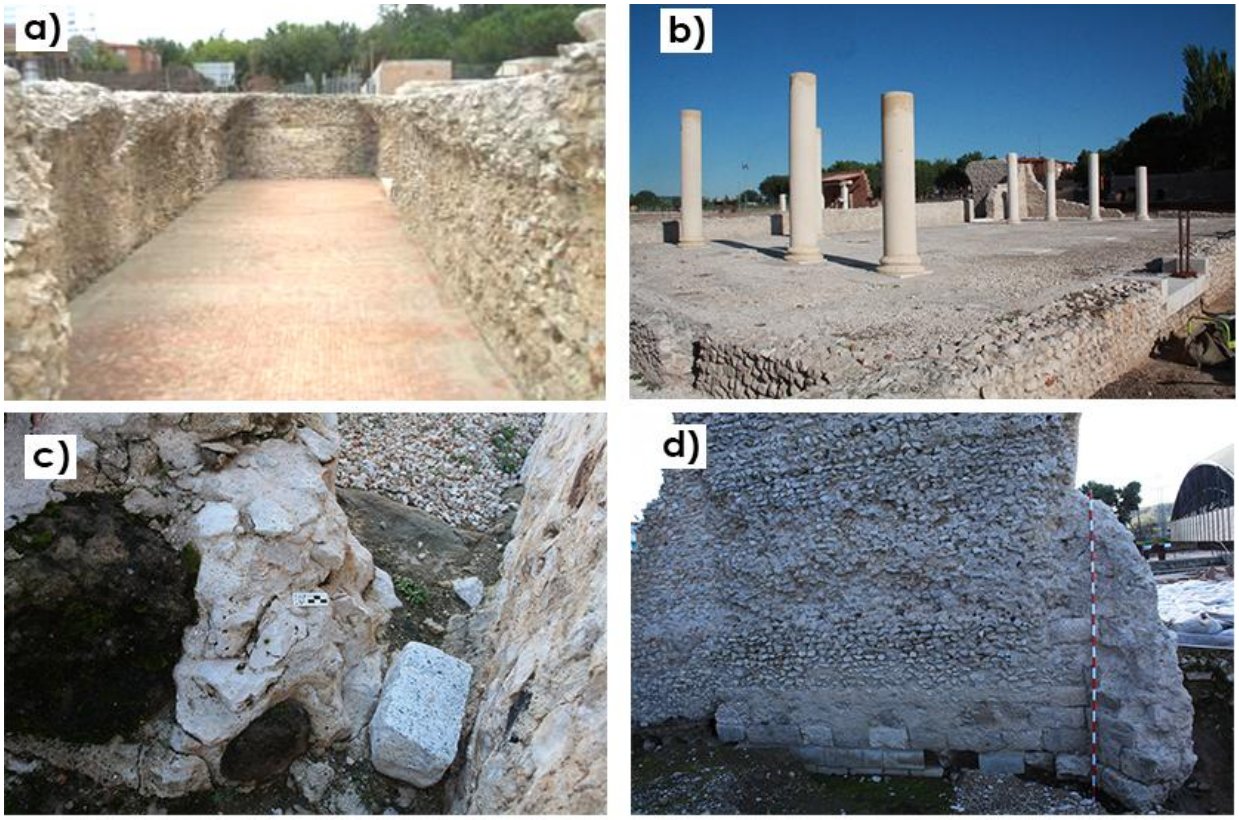


Figure 2.1- 6. a) Criptoporticus b) Basilica c) North Bath separation wall between the tepidarium and the caldarium d) monumental façade

In the third century AD, when the North Bath was converted into Curia, new wall was built, the neighbouring wall to the older wall, with the same typology and a smaller size. The North Bath next to the Basilica was constructed in two phases starting in 50/60 AD and later, at the end of the third century AD (second phase) it was transformed into a Curia. The *caldarium* is the principal element and the *tepidarium is the largest spaces. The frigidarium* with a *natatio* (pool) is situated next to *tepidarium*. The floor is large brick pavement with *opus signinum (*Rascón Marqués and Sánchez Montes, 2009*)*.

The South Bath was built during the remodelling of the North Bath-Curia space at the end of the third century AD. It is a smaller building than its predecessor, and the architecture of the new thermal bath is linear. Its north side has a small *apodyterium* (dressing room) and a *frigidarium* with a *natatio* (pool). Its south side has a *tepidarium* and a *caldarium* (Figure 2.1- 6c, Figure 2.1- 7, Figure 2.1- Figure 2.1- 9a).

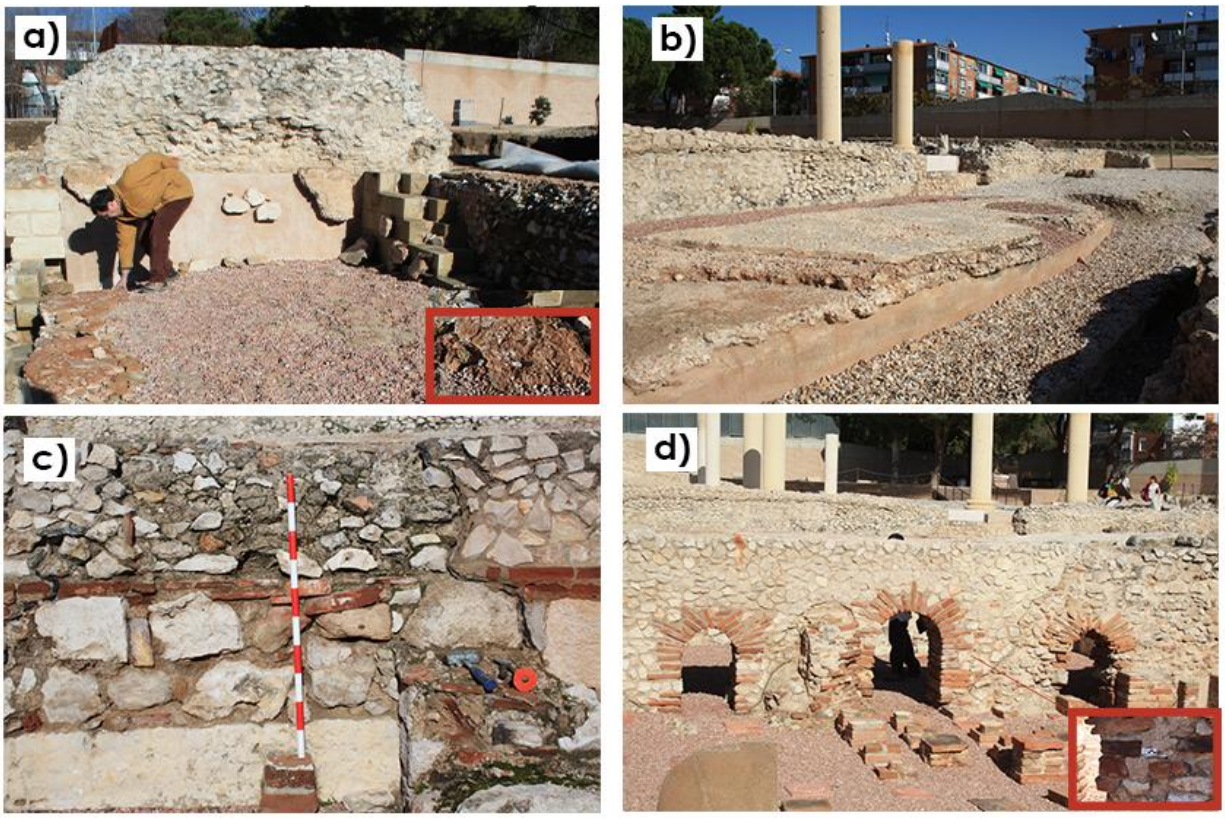


Figure 2.1-7. a) North Bath *frigidarium* northern wall b) North Bath *frigidarium* floor c) South Bath separation wall between the *fragidarium* and the *tepidarium* d) South Bath separation wall between the *tepidarium* and the *caldarium*, elevation of *hypocaustum*

The House of Marte and the House of Atrium have a central *atrium,* which is a courtyard without columns, and a central *impluvium* to collect rainwater. In the site, there is a network of sewers in an orthogonal lattice (Figure 2.1- 8a-d). On the House of Marte, a channel of ceramic tiles carried water from the *impluvium* (Figure 2.1- 8f).

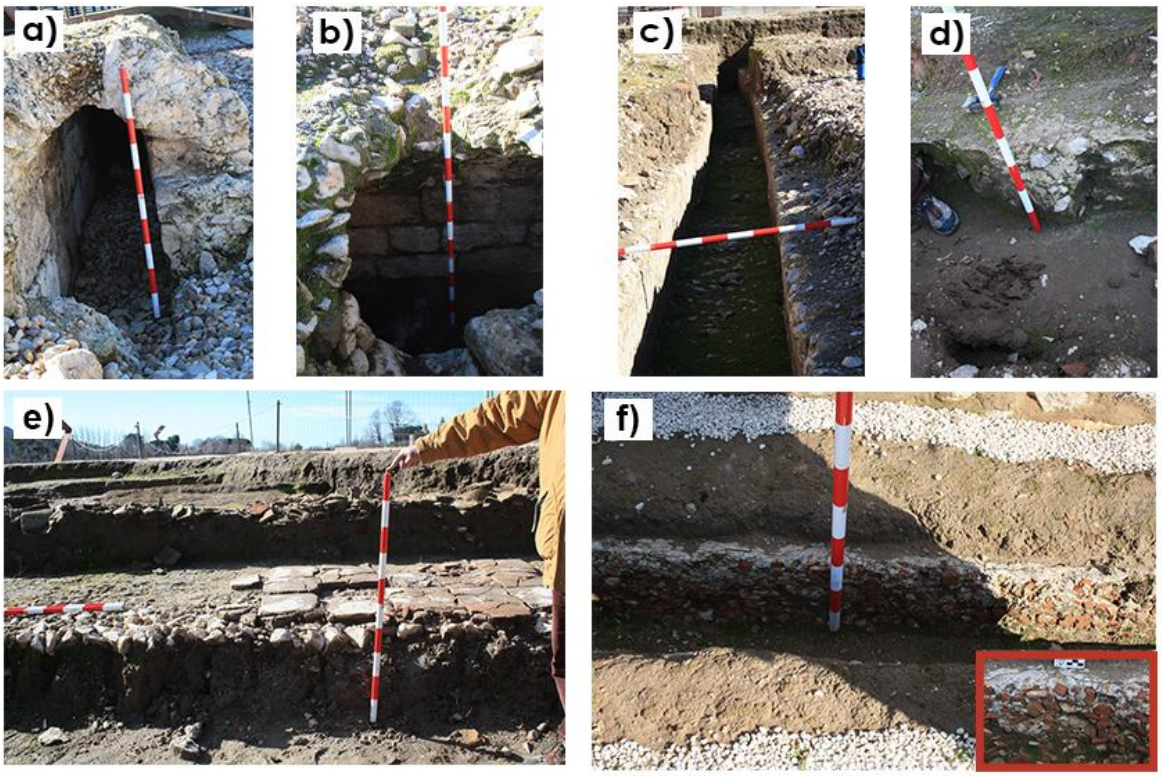


Figure 2.1-8. a-d) sewers e) Cuadriporticus western side floor f) House of Marte floor

There are other examples of Roman public architecture in and around the city, which are the Zulema Bridge over the Henares River and the quadrilateral arch over the western entrance to Complutum. Sampling was done in order to investigate whether they were constructed in the same period (Figure 2.1- 9c, d).

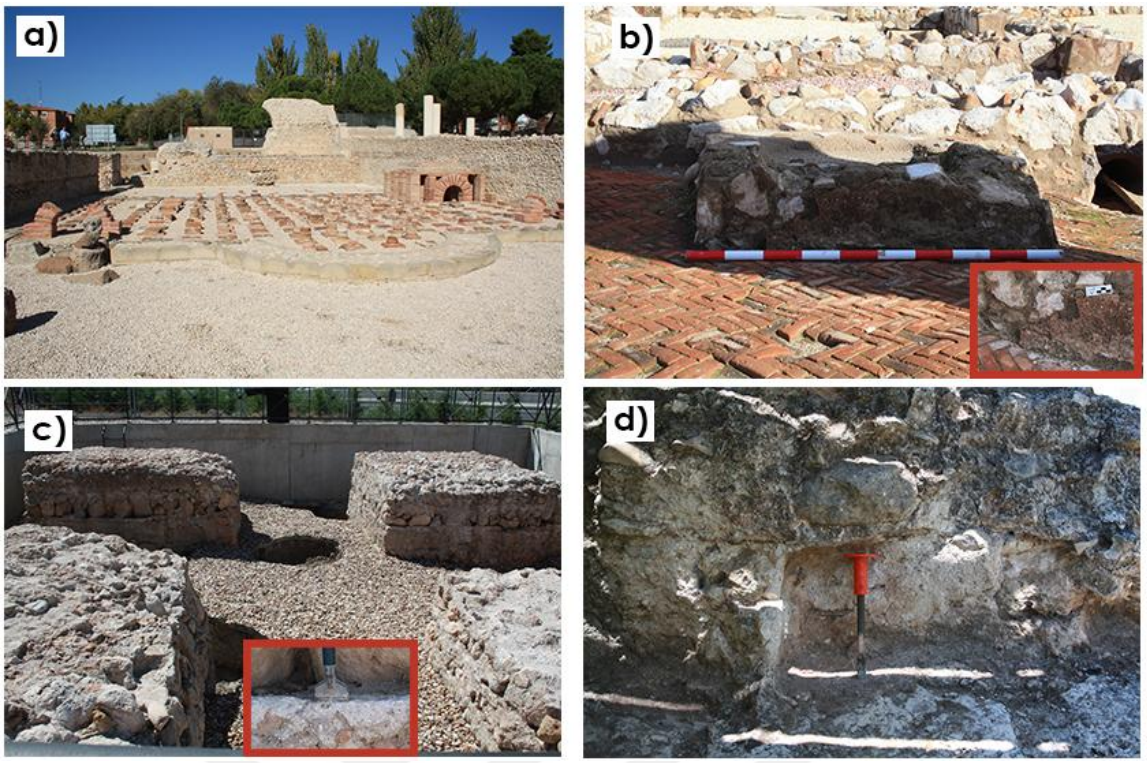


Figure 2.1- 9. a) North Bath caldarium b) House of Atrium fountain c) pillars of the cuadrifrontal Arch d) Zulema Bridge

The construction materials and types of opus of the public and domestic architecture are abundant and of different natures, like the construction techniques employed (Sánchez Montes, 2013).

The documented construction materials in the site are in the first place, stone, which includes quartzites (for foundations and baseboards), gypsum and limestone sandstones (in the form of ashlars or pillars for foundations and/or baseboards, amalgamated with mortars of lime and sand or clay, for thresholds, jambs and lintels, supporting elements or the corner posts of walls); plaster and marble (for floors and baseboards covering walls) and clay, which was used both crude (for walls and roofs) and cooked (for roofs, pipes and decorative elements). The finish of the rammed earth walls and other structures were covered with gypsum and lime based plasters and wall paintings in the House of Grifos (Ergenç et al. 2015; Martinéz Garrido et al. 2016). The wall paintings and their mortars were studied, and climatic data were collected from inside and outside the structure (Figure 2.1- 10).

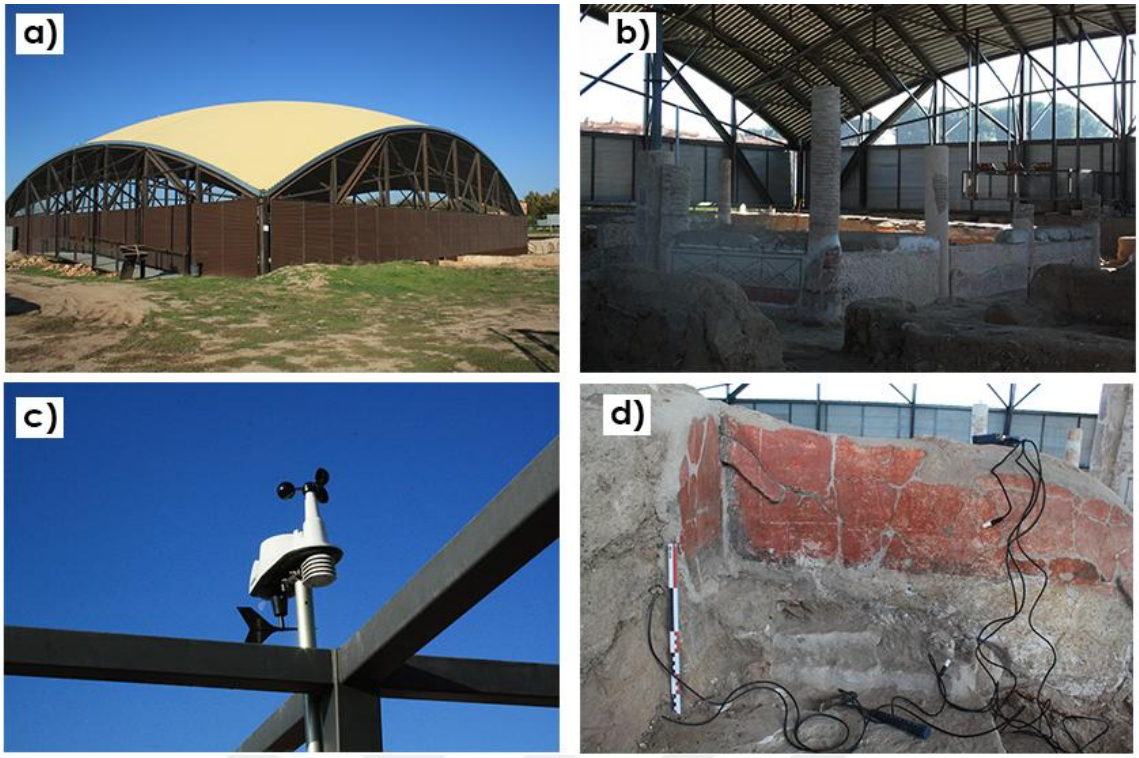


Figure 2.1- 10. House of Grifos a) exterior b) interior c) meteorological station d) sensor network in earthen wall with wall painting

The types of opus documented in Complutum are *opus quadratum*, the ordinary masonry for foundations and base of walls; and *opus caementicium* for elevations of walls, vaults and canalizations; *opus tesellatum* and *opus sectile* pavements and *opus testaceum* in the form of *spicatum* for soles, in the form of bricks for floors, walls and/or columns.

A total of 42 mortar samples were collected from Complutum. For detailed description of them, please see Appendix I.

2.1.2 Mérida Archaeological Complex

2.1.2.1 *Description of the site*

Mérida is located near the centre of the region of Extremadura at 217 meters above sea level. The Roman city of Augusta Emerita is in Merida, to the north of the province of Badajoz, crossed by the Guadiana River. Merida is the capital of the Autonomous Community of Extremadura (Figure 2.1- 11).



Figure 2.1-11. Location map of Mérida

2.1.2.2 *Historical Background of Excavations and Investigations*

Mérida was founded as a Roman colony in the year 25 BC by order of Emperor Octavio Augustus to serve as retirement home to the veteran soldiers (*emeritus*) of the legions, V Alaudae and X Gemina (Alba, 2005).

In the beginning of the fifth century AD, Mérida began to undergo barbarian invasions, becoming the capital of the entire Visigoth Kingdom of Hispania in the sixth century. At the

beginning of the eighth century AD the city fell into Muslim hands, in which it remained until its reconquest by the Christians in 1230.

Since 1983 it has been the capital of the Autonomous Community of Extremadura, and the city's architecture was declared a World Heritage Site by UNESCO in 1993.

In Mérida, the first archaeological intervention was conducted for a period of three years made in 1791 by Manuel de Villeña Mozillo who made several sheets with measurements, drawings and texts. The first excavation was done in 1911 by José Ramón Mélida, and the first restorations were performed in the early 1920s with the anastilosis project on the theatre.

With the help of the Directorate General of Fine Arts, through the Superior Board of Excavations and Antiquities, work began on the Theatre and the Amphitheatre and the bullfight tower was built.

The continued interest of the specialists motivated the visit of qualified archaeologists such as the German hispanist Adolf Schulten, and Professor Ian Richmond, professor and director of the British School in Rome, who helped to give international prestige to the discoveries.

2.1.2.3 *The Regional Geology of Mérida*

The Mérida massif can be considered Cadian reactivated volcanic arch (Bandrés et al., 1999; Mota López, 2015). Orthogneisses, amphibolitic series, Precambrian age volacanoclastic rocks, including greywacke, biotitic schist, the black rock series including black quartzites, greywacke, pelite, amphibolites with medium regional metamorphism are present along with Precambrian age diorites-granodiorites, quartz diorites slate, quartzite (Figure 2.1- 12). In addition to that there are several granite outcrops in the surroundings of Mérida, granitodis and monzogranites are found as well (Mota López, 2015).

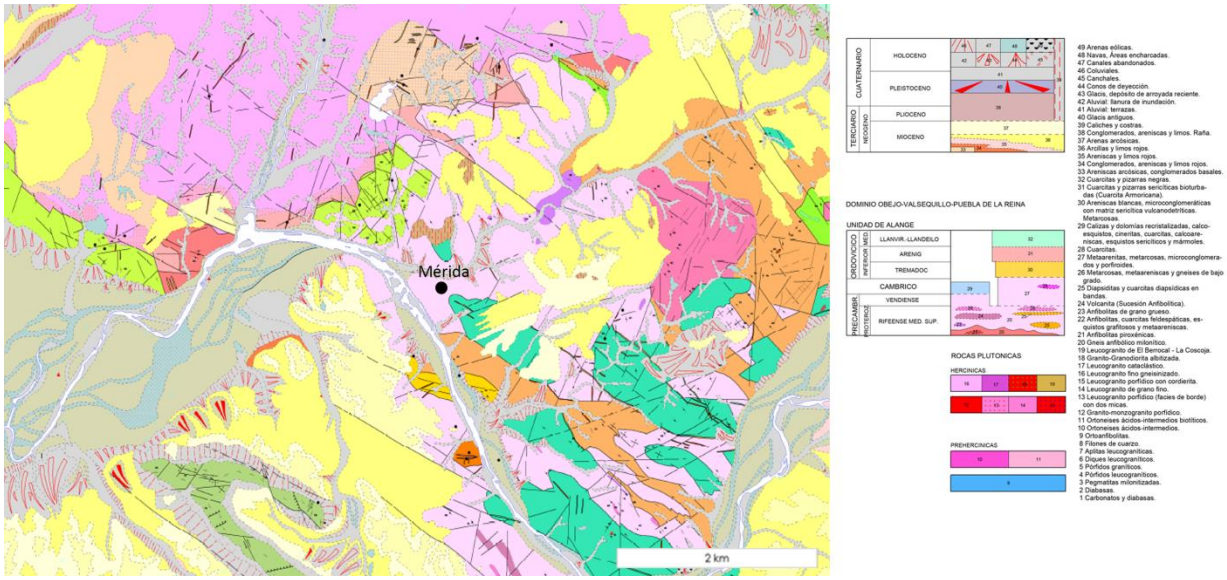


Figure 2.1- 12. Geological map of Mérida (IGME, 1991)

Mérida has a subtropical Mediterranean climate. The average annual temperature is 17°C. Temperature reach at 40 °C in July-August and fall to around 2-3 °C at December. Its maximum annual rainfall is 60 mm (IGME, 1991), and its average CO_2 concentration between May and July is 600 ppm.

2.1.2.4 *Sampling and Architectural Description of the Buildings*

Merida has an important architectural heritage, with numerous examples of constructions of great interest. For this thesis, samples were taken from the San Lazaro Aqueduct, the Amphitheatre, Circus, the Archaeological Remains of Viñero, Resti Thermal Bath, Alcazaba and Moreria (Figure 2.1- 13, Table 2.1- 2).

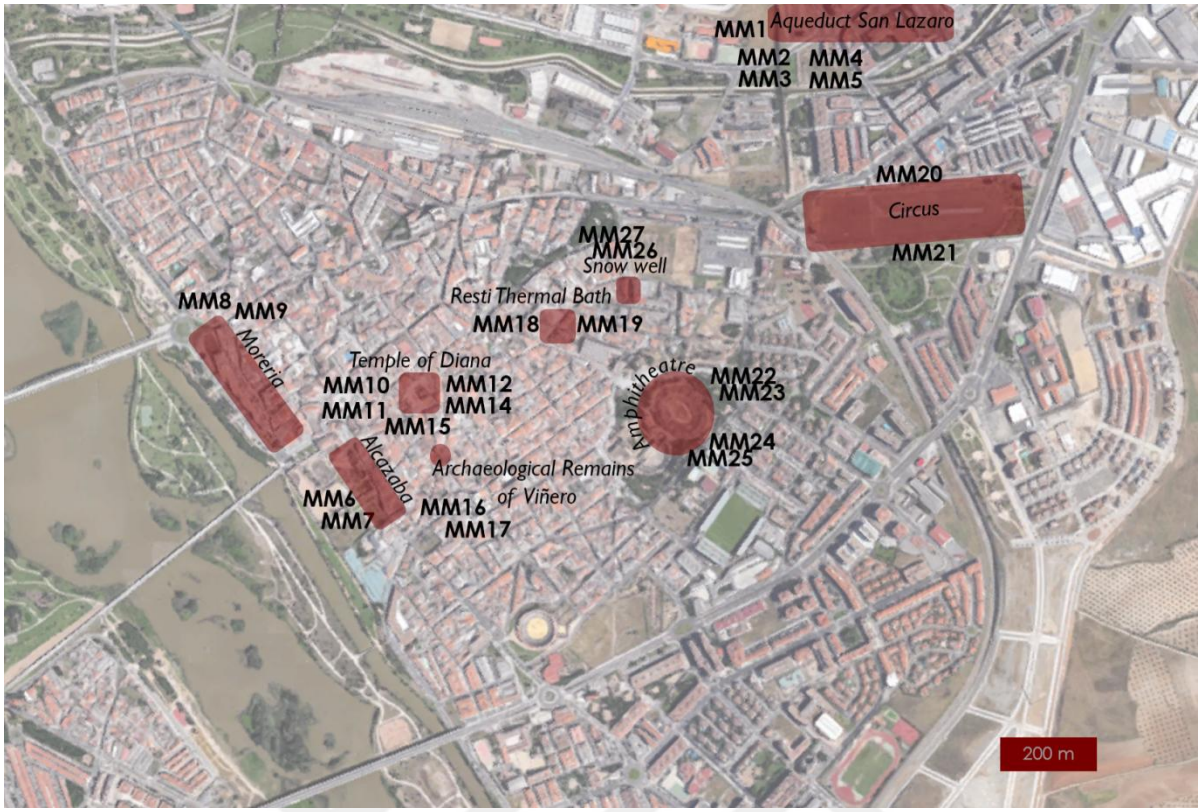


Figure 2.1-13. Locations of the sampling points

Table 2.1- 2. Collected samples from Mérida

Code	Opus Type	Location	Construction Phase
MM1	*Opus Caementicium*	San Lazaro Aqueduct lining	1c/3c AD
MM2	*Opus Caementicium*	San Lazaro Aqueduct channel	1c/3c AD
MM3	*Opus Caementicium* +*Opus Signinum*	San Lazaro Aqueduct channel	1c/3c AD
MM4	*Opus Caementicium*	San Lazaro Aqueduct tile	1c/3c AD
MM5	*Opus Caementicium*	San Lazaro Aqueduct channel floor	1c/3c AD
MM6	*Opus Caementicium*	Alcazaba wall	1-2 c AD
MM7	*Opus Caementicium*	Alcazaba wall	1-2 c AD
MM8	*Opus Caementicium*	Moreria wall	Roman
MM9	*Opus Caementicium*	Moreria wall	Roman
MM10	*Opus Caementicium*	Temple of Diana floor	1 c BC
MM11	*Opus Caementicium*	Temple of Diana channel vault	1 c BC
MM12	*Opus Caementicium*	Temple of Diana pillar	1 c BC
MM13	*Opus Caementicium*	Temple of Diana pillar	1 c BC

MM14	*Opus Caementicium*	Temple of Diana temenos	1 c BC
MM15	*Opus Caementicium*	Temple of Diana temenos	1 c BC
MM16	*Opus Caementicium*	Vrinero	Roman
MM17	*Opus Caementicium*	Vrinero	Roman
MM18	*Opus Signinum*	Resti Thermal Bath lining	Roman
MM19	*Opus Caementicium*	Resti Thermal Bath wall	Roman
MM20	*Opus Caementicium*	Circus wall	1 c AD
MM21	*Opus Signinum*	Circus wall	1 c AD
MM22	*Opus Signinum*	Amphiteatre	1 c BC
MM23	*Opus Signinum*	Amphiteatre	1 c BC
MM24	*Opus Caementicium*	Amphiteatre summa cavea	1 c BC
MM25	*Opus Signinum*	Amphiteatre summa cavea	1 c BC
MM26	*Opus Caementicium*	snow well	Roman
MM27	*Opus Signinum*	snow well	Roman

The Amphitheatre was constructed in 8 BC. It is located in the same geographic location with the theatre, which is in the northeast and east of the theatre. The dimensions of the amphitheatre are main axis, 126 m and minor axis, 102 m (Pizzo, 2007; Ramírez Sábada, 2003).

Topographically speaking, the building is adapted to the existing geological terrain and, specifically, to a double hill that crosses the area in a north-south and east-west direction (Pizzo, 2007). It was abandoned by the fourth century AD and until the beginning of the twentieth century it remained partially buried.

As in almost all Roman buildings of this type, its stands are divided into three sectors: *ima*, *media* and *summa cavea*, leaving only remains of the latter. Sampling was done in the periphery wall and *summa cavea* (Figure 2.1- 14).

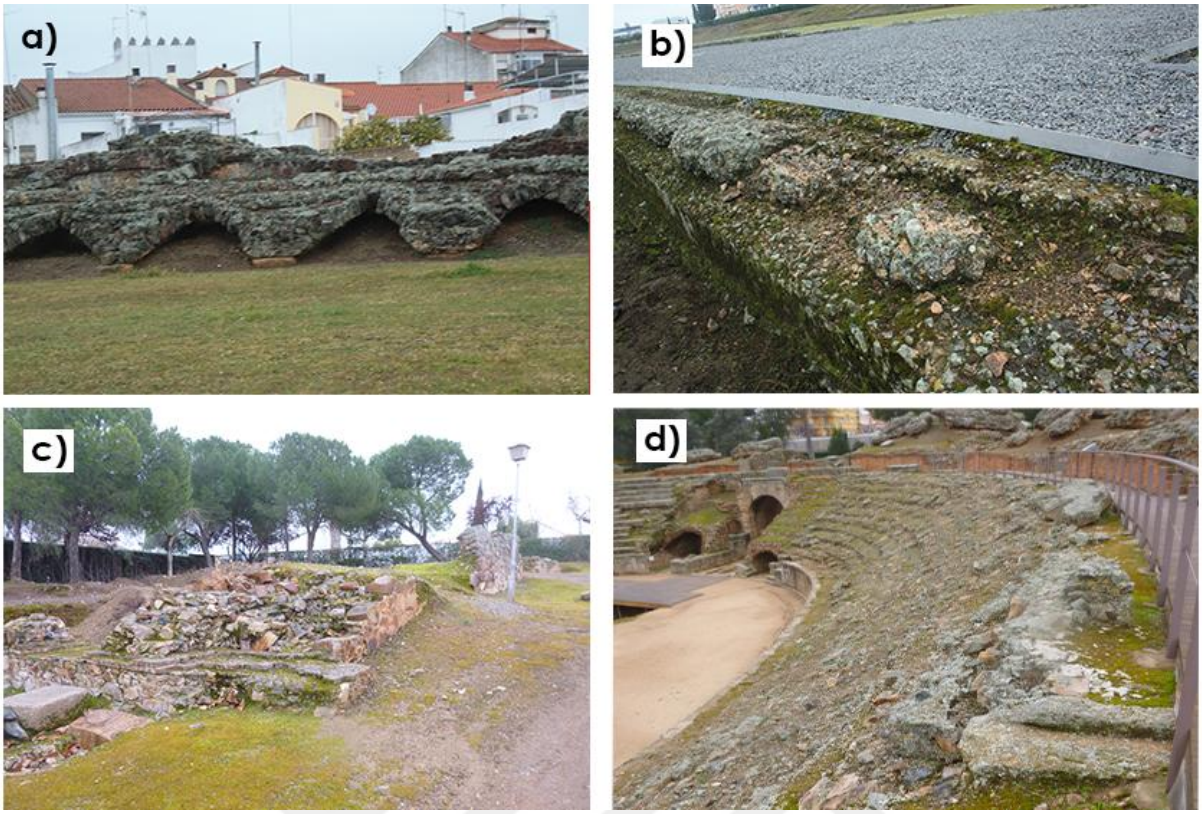


Figure 2.1- 14. a, b) Circus c,d) Amphitheatre

The Circus was an enclosure for chariot races built at the beginning of the first century AD. Erected outside the city and with an oval plant of about 440 m long by 115 m wide, it corresponds to the common model of this type of Roman works, with an elongated oval shape oriented from east to west with two major parallel sides and two minor ones, one that closes in a semicircle and another one that does so in a straight line curved at its ends. The façade was at its western end; the less curved, and at the time was covered with granite and enhanced with a decoration based on attached pilasters of the same material (Barroso and Morgado, 1996).

The stands were distributed in a classic way in three sectors: *ima*, *media* and *summa cavea*. The stands were raised on a high podium on its two major sides, taking advantage of the slope of the land in its south section and raised above vaults in the north section.

The Aqueduct of San Lázaro is one of the three pipes that provided water to Emerita Augusta. When this aqueduct had to cross the depression of the river Albarregas a large set of arches was built to support the pipes. Of all the set only we have three imposing pillars with two of their joining arches, located beneath the structure (Figure 2.1- 15, Figure 2.1- 16).

The original aqueduct was built in two phases at the third quarter of the first century AD and the end of third century AD. In the sixteenth century a new aqueduct was built using many of the Roman's ashlars, so it was almost destroyed.



Figure 2.1- 15. The San Lázaro Aqueduct

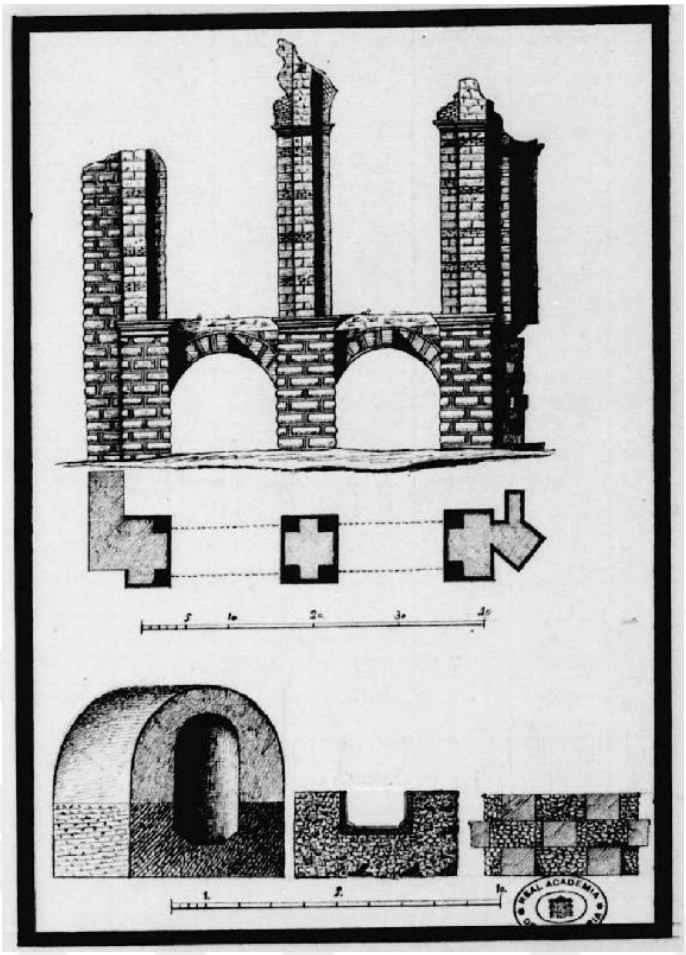


Figure 2.1- 16. Drawing of San Lázaro (Prado and Mariño, 1798-1801)

The Roman wall of Alcazaba is a structure located under the perimeter wall west of the Alcazaba. According to the seventeenth-century historian Bernabé Moreno de Vargas, this is a construction from the time of the Roman emperor Trajan (98-117 AD).

The Temple of Diana was erected at the same time as the foundation of the city at the end of first century BC. The length of the preserved podium on the west side is 31. 87 m, and on the east side, 32. 20 m. The length of north façade is 19. 33 m, and the length of south façade is 18. 75 m (Pizzo, 2007).

The temple is located in a central and slightly elevated area of the city. It has rectangular plant and with six columns in its front. Its main facade is crowned by a pediment in the shape of a semicircular arch. The colonnade, with attic bases, ribbed shafts and capitals of

Corinthian order, rests on a high podium of ashlars and is crowned by a moulded cornice (Figure 2.1- 17).

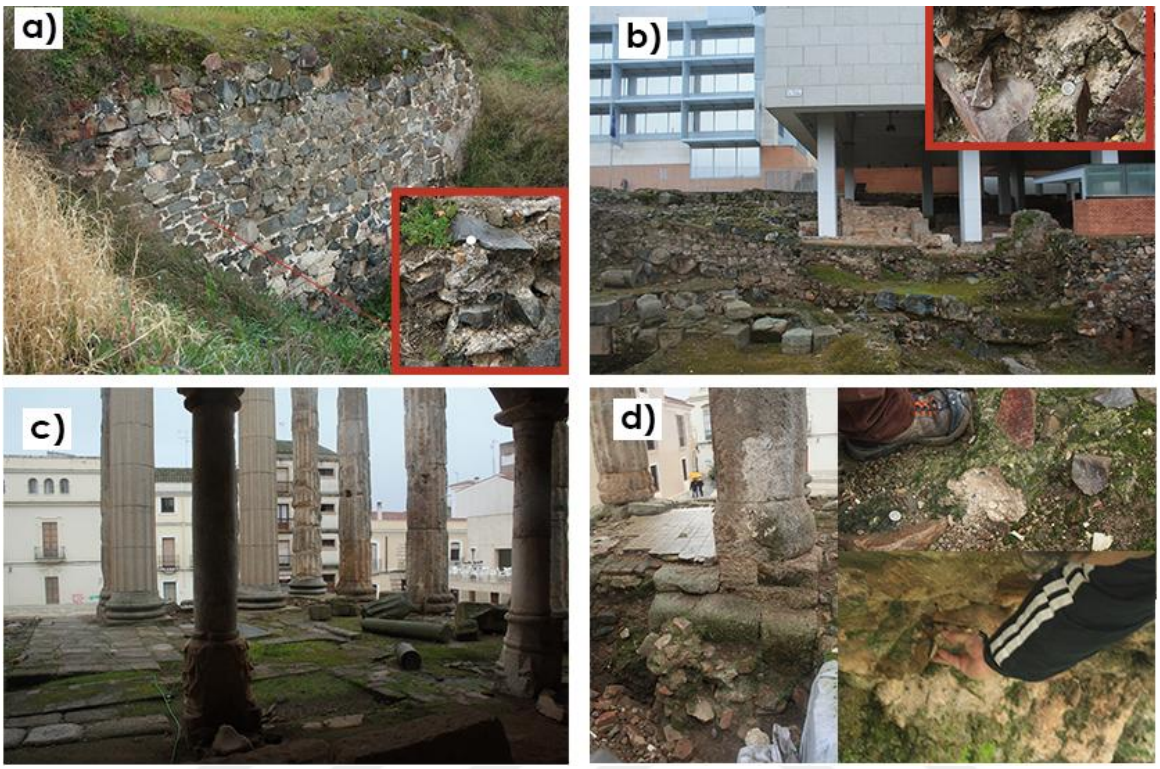


Figure 2.1-17. a) Alcazaba b) Moreria c, d) Temple of Diana

There is no sufficient information about the archaeological remains of Viñero and the thermal bath Resti, but they are known to have been constructed in Roman times from the personal communication with the archaeologists of Monumental Consortium of Mérida (Figure 2.1-18).

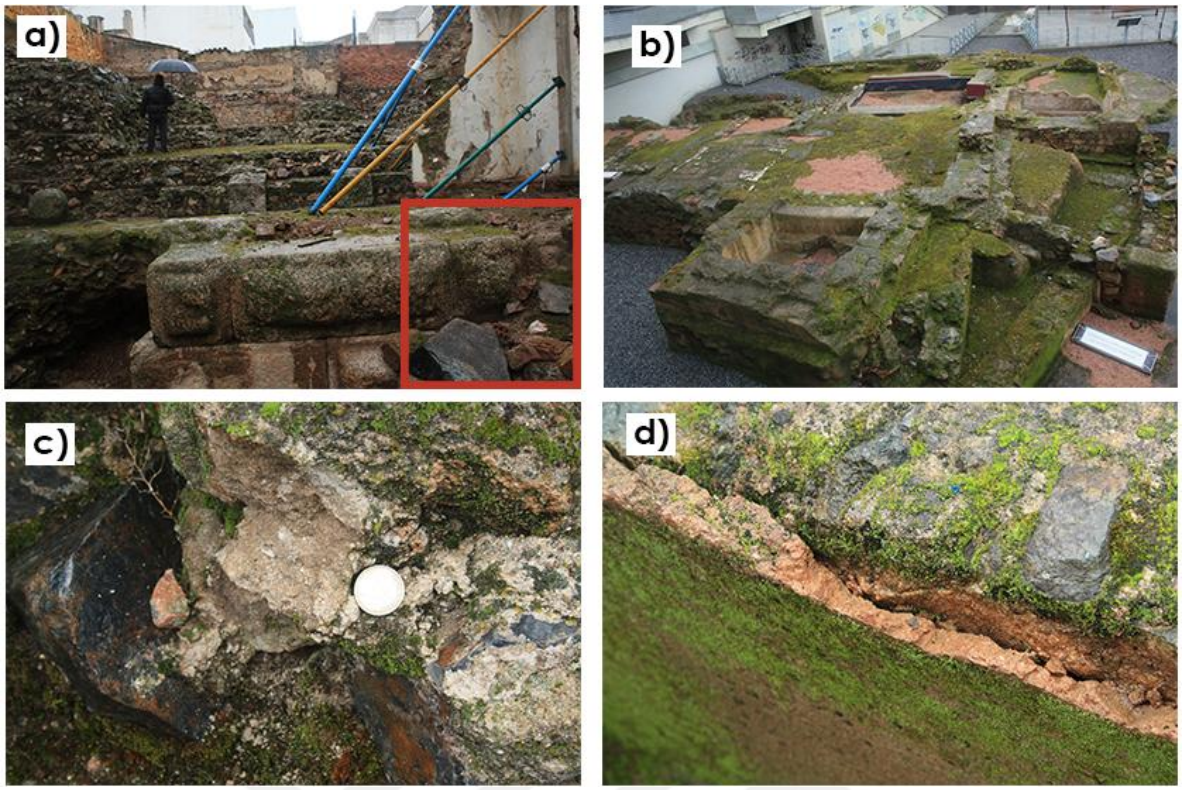


Figure 2.1-18. a, c) archaeological remains of Viñero b, d) Resti Thermal Bath

A total of 27 mortar samples were collected from Mérida. For detailed descriptions of the samples, please see Appendix II.

2.1.3 Nysa on the Meander

2.1.3.1 *Description of the site*

Nysa is located 30 km east of the city of Aydın, north of Meander (Büyük Menderes) River and on the southern cliff of Messogis (Aydın) mountain (Figure 2.1- 19). Nysa, which is situated near the border of Caria and Ionia, Asia Minor, is one of the important Carian centres, and its importance was derived from its productive Meander basin. Furthermore, the main transportation and trade route passing through the city and it was culture and education centre. The remains are allotted on the slopes on the sides of the Stream of Meander River where the streets and buildings of the ancient city constructed according to the topographic conditions. The city was under the rule of three empires where the post Hellenistic buildings Roman and Byzantium architecture are seen (Öztaner et al., 2014; Kadıoğlu and Kadıoğlu, 2008).



Figure 2.1-19. Aerial map of Turkish southwestern region showing the region where Nysa is located

The city was founded in the Hellenistic period by Antiochos I Soter (281-261 BC) for his wife Nysa with her name. The information was gathered from Byzantian Stephanos (sixth century AD). The earliest epigraphic data were gathered from the beginning of the Hellenistic period. From the inscriptions that date to the third century BC, it is known that a religion

centre was situated 3 km west of the city and improved the city's economy. One inscription records that in the first century BC the city was on the Roman side in the wars between Roma and Mithtadates (Öztaner et al., 2014). The geographer, Strabon, who had lived in Nysa in the early years of the first century AD, commented in his writings about Nysa that it as a centre of culture and education (Yurtsevenler, 2013; Freely, 2004).

According to the findings, the city had alterations in the Byzantium period (fourth to thirteenth centuries). After the thirteenth-fourteenth centuries, the Seljuks, Menteşe and Aydınoğulları seigniors began their reigns, and the settlement moved to the town of Sultanhisar (Yurtsevenler, 2013; İdil, 1993). At the end of the Hellenistic period, the newly developed architectural techniques of the Roman period can easily be seen in Nysa.

The gymnasium, the theatre, and the amphitheatres are situated on the west side of the city, and the agora and Geronticon are on the east side. Most of these buildings are regarded as architectural remains dating from the Late Roman Period, due to the differences in their structure and the additions that were made. The region is full of geothermal wells as a result of geological faults. Recorded earthquakes in the region affected the city many times in history (Yurtsevenler, 2013).

2.1.3.2 *Historical Background of Excavations and Investigations*

The German archaeologist, Walther von Diest, and his team conducted excavations between 1907 and 1909 (von Dies, 1913). In 1921, the Greek archaeologist, Konstantin Kourouniōtēs, made excavations in the Geronticon (Kourouniōtēs, 1924). The İzmir Archaeology Museum continued the excavations in the 1960s in the theatre and Geronticon, and in the 1980s the Aydın Archaeology Museum did short-term excavations-interventions in the *cavea* of the theatre. Between 1990 and 2010, excavation and restoration works were conducted by a team headed by Vedat İdil from Ankara University (İdil, 1999). Since 2012, excavations and restoration works have been continued by the head of Aydın Archaeology Museum and with the scientific consultancy of archaeologist from Ankara University, Serdar Hakan Öztaner.

Walther von Diest made a plan of the structure during his excavations in 1907 and 1909, but this was only a general plan and many aspects of the structure were not examined in detail (von Diest, 1913). Between 1921 and 1922, Konstantin Kourountiotis excavated some parts of the Geronticon's *cavea*, *orchestra*, *scaenae frons* and the *stoa* to the south. In these excavations, statue bases belonging to a rich man from Nysa, Sextus Julius Maior Antoninus Pythodoros, and to members of the Antonine imperial family, were found, along with many marble architectural blocks related to the façade of the structure (Kadıoğlu and Kadıoğlu, 2008).

2.1.3.3 *The Regional Geology of Nysa*

Nysa is located in the northern side of the Büyük Menderes graben, which is one of the main active tectonic structures in Turkey. The geological setting of Nysa and its surrounding base on Alluvium and Neogene deposits containing conglomerates, siltstone, mudstone and shale alternations. The north and south Permo-Carbon Göktepe Formation consists of phyllite, marble and metaquartzite and Paleozoic-Precambrian micaschist, and in the south Cambrian-Precambrian age gneisses are present (Figure 2.1- 20) (Bozkurt and Satır, 2000; Yalçıner et al. 2009)

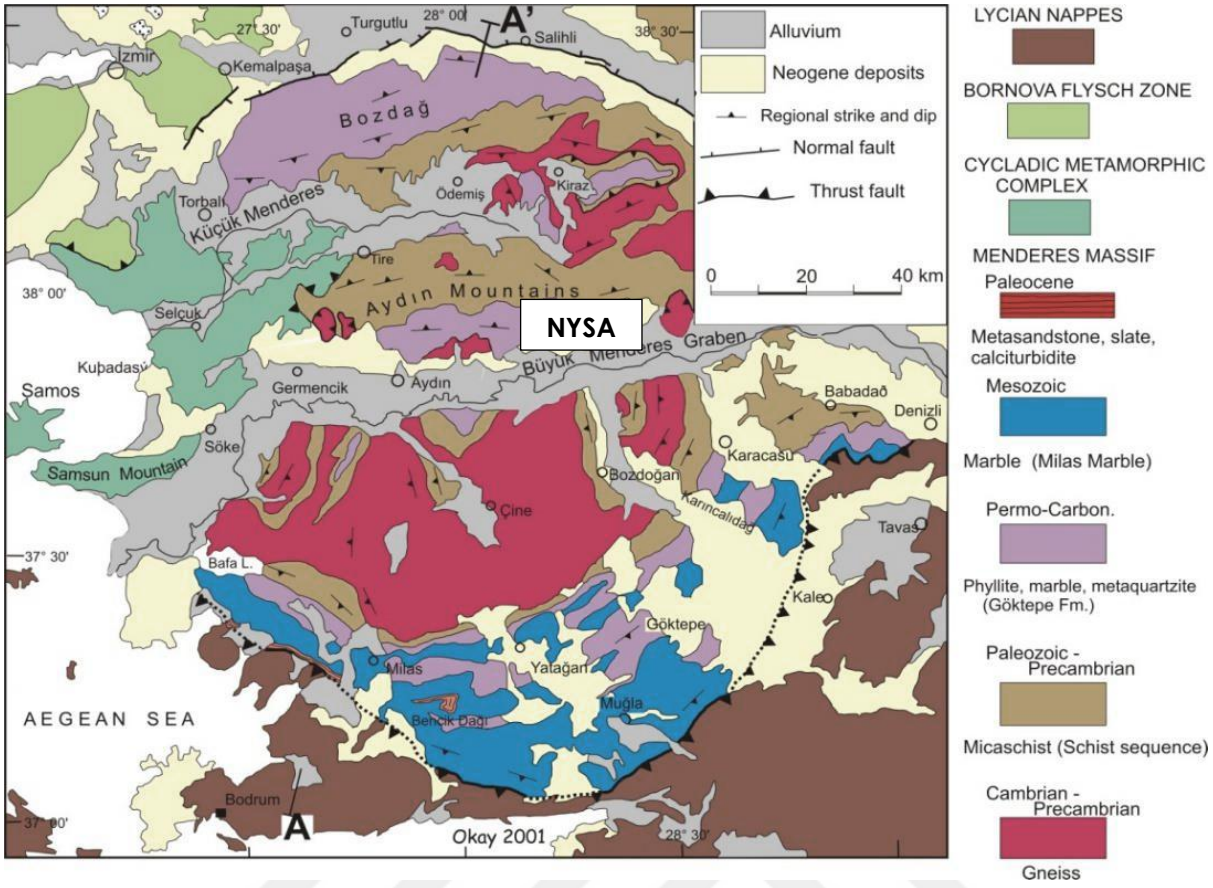


Figure 2.1-20. The Geological Setting of Nysa and its surroundings (Okay, 2011)

Marble, metaquartzite, garnet mica-schist and gneiss are abundant in the vicinity and are used as building stone in the site (Yalçıner et al. 2009).

The climate in Aydın where Nysa is located is generally warm and temperate. The winter months are much rainier than the summer months. The rainiest months are November, December, January and February. The average annual temperature is 17.8 °C (3-38° C). The average Relative Humidity is 60% and maximum annual rainfall is 80 mm (climate-data.org/location/178/).

2.1.3.4 *Sampling and Architectural Description of the Buildings*

Roman mortars from Roman two bridges and a tunnel connecting the both sides; along with samples from gymnasium, cistern, theatre, library, stadium in the west, the agora, basilica shop, Geronticon and the Roman baths on the east side (Figure 2.1- 21, Figure 2.1- 22). The

samples were classified in two groups according to their ceramic content as *opus caementicium* and *opus signinum* (Table 2.1- 3).

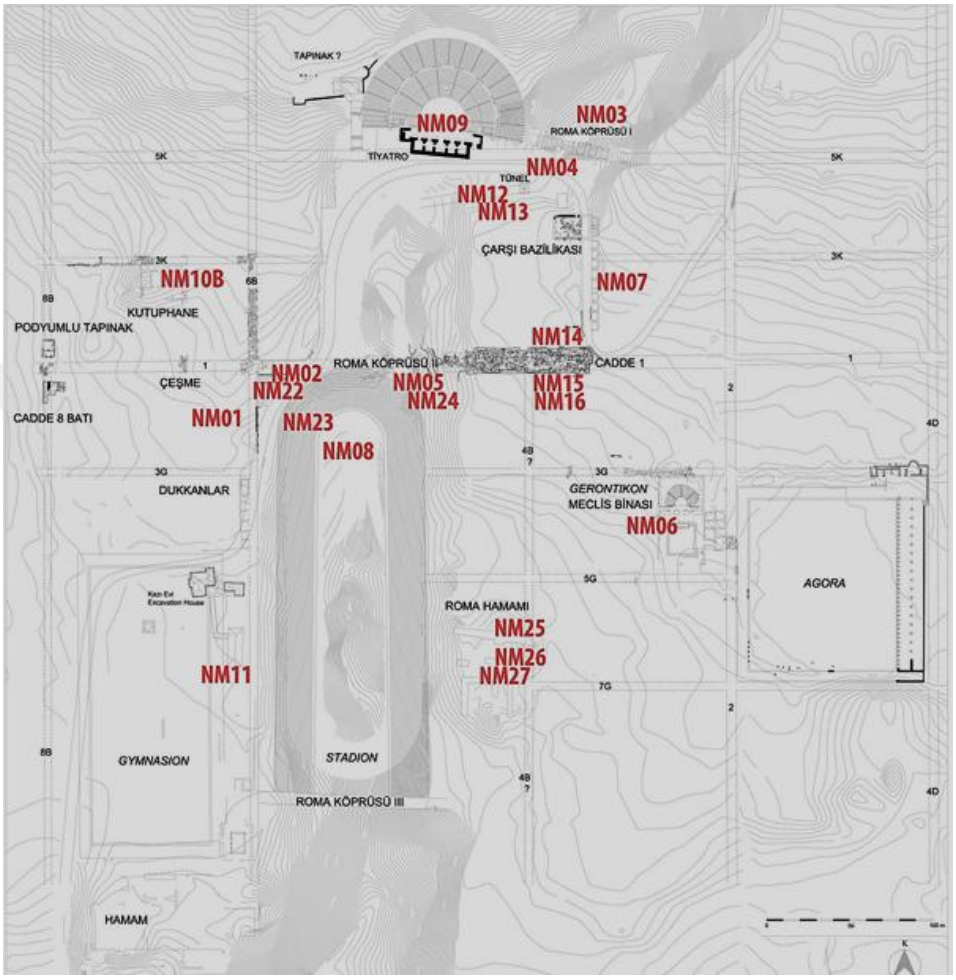


Figure 2.1- 21. Plan of Nysa and sampled points

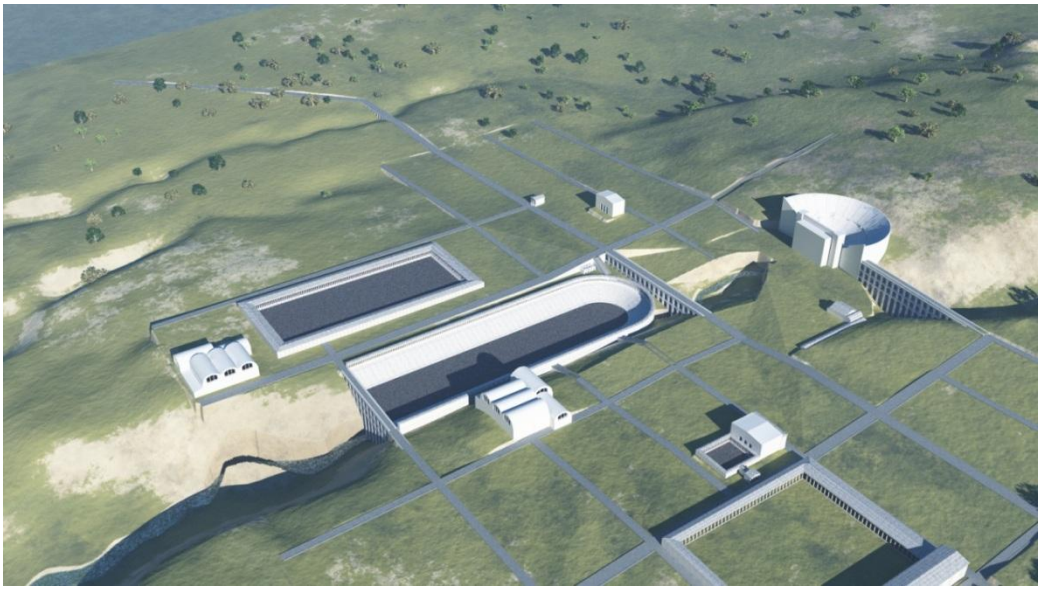


Figure 2.1- 22. 3D model of Nysa in a south eastern view showing the gymnasium, stadium, theatre, bridges, agora and street system by Saldaña (2014)

Table 2.1- 3. Sampled mortars in Nysa on Meander

Samples	Opus Type	Location	Construction Phase
NM01	*Opus caementicium*	Cistern	Roman
NM02	*Opus caementicium*	2nd Bridge West pillar	Roman
NM03	*Opus caementicium*	1st Bridge	Roman
NM04	*Opus caementicium*	Tunnel	Roman
NM05	*Opus caementicium*	2nd Bridge East pillar vault	Roman
NM06	*Opus caementicium*	Gerontikon	1st AD
NM07	*Opus signinum*	Basilica 3rd arch	Roman
NM08	*Opus signinum*	Stadium	Roman
NM09	*Opus*	Theatre	1st BC

	caementicium		
NM10	*Opus caementicium*	Library	1st AD
NM11	*Opus signinum*	Gymnasium	Early Roman
NM12	*Opus caementicium*	Tunnel Upper level	Roman
NM13	*Opus caementicium*	Tunnel Lower level	Roman
NM14	*Opus Caementicium*	Agora Road Pavement	Roman
NM15	*Opus signinum*	Agora Road Water level, around the water tube	Roman
NM16	*Opus signinum*	Agora Road Coating	Roman
NM22	*Opus caementicium*	2nd Bridge West pillar vault	Roman
NM23	*Opus signinum*	Stadium	Roman
NM24	*Opus caementicium*	2nd Bridge East pillar vault	Roman
NM25	*Opus signinum*	Thermal Bath Middle arch	Roman
NM26	*Opus signinum*	Thermal Bath Last arch	Roman
NM27	*Opus caementicium*	Thermal Bath Next to water tube	Roman

The cistern (*Nympheaum*) dates to Roman times and has three niched walls constructed by 4-5 cm cut stones and mortars. In the main walls, holes for the water pipes are present. The sampling was done in the main wall, at a height of 10 cm from ground level (Figure 2.1- 23a).

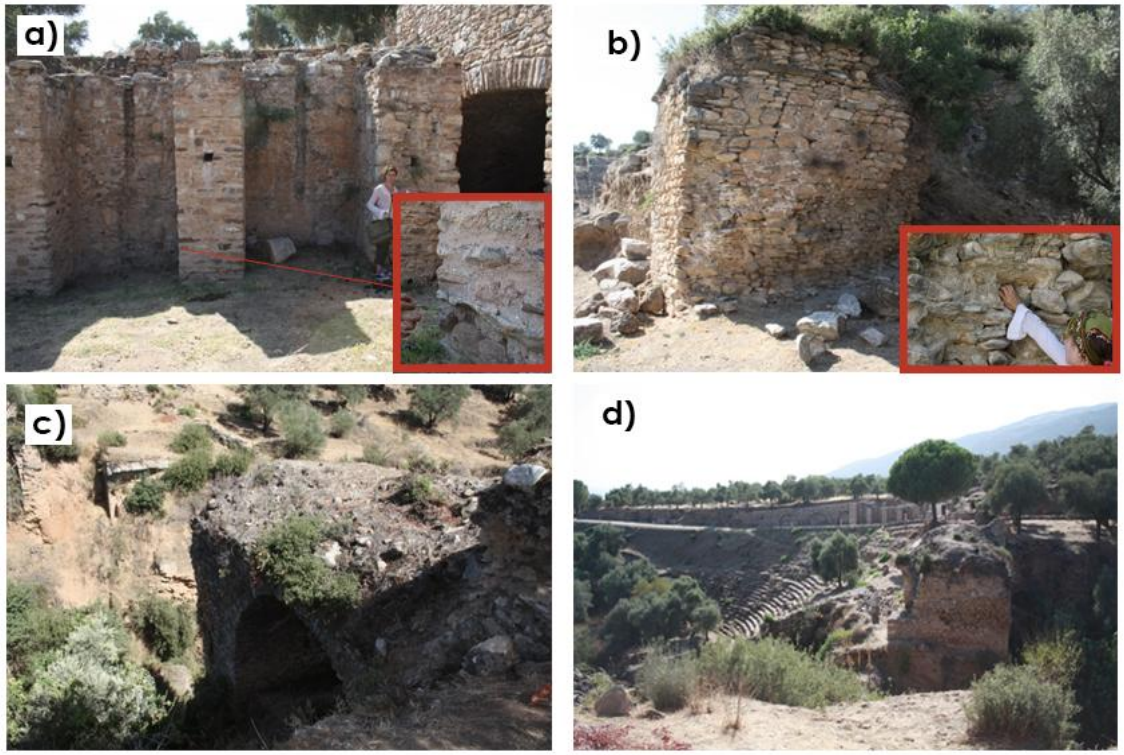


Figure 2.1-23. a) cistern b) pillars of first bridge c) second bridge d) Stadium from the two bridges.

The pillar of the first bridge is situated relatively far from the stream valley (Figure 2.1- 23b). The construction of the bridge is mortar with rubble stones. On the other hand, the pillars of the second bridge with vaulted structures are still present on both the east and west sides of the valley (Figure 2.1- 23c, d). Both of the bridges were demolished in the earthquake that occurred in Nazilli in 1899 (Idil, 1999).

Another important water-bearing structure to cope with the river crossing the city which was designed by Romans is the tunnel. To control and re-orient the stream flows they constructed a 100 m long vaulted tunnel. It starts from the level of the theatre and ends in the northeast of the theatre after passing the first bridge (Figure 2.1- 24). Mortar samples from it were collected from the lower and upper level of the tunnel (Figure 2.1- 25a, b).

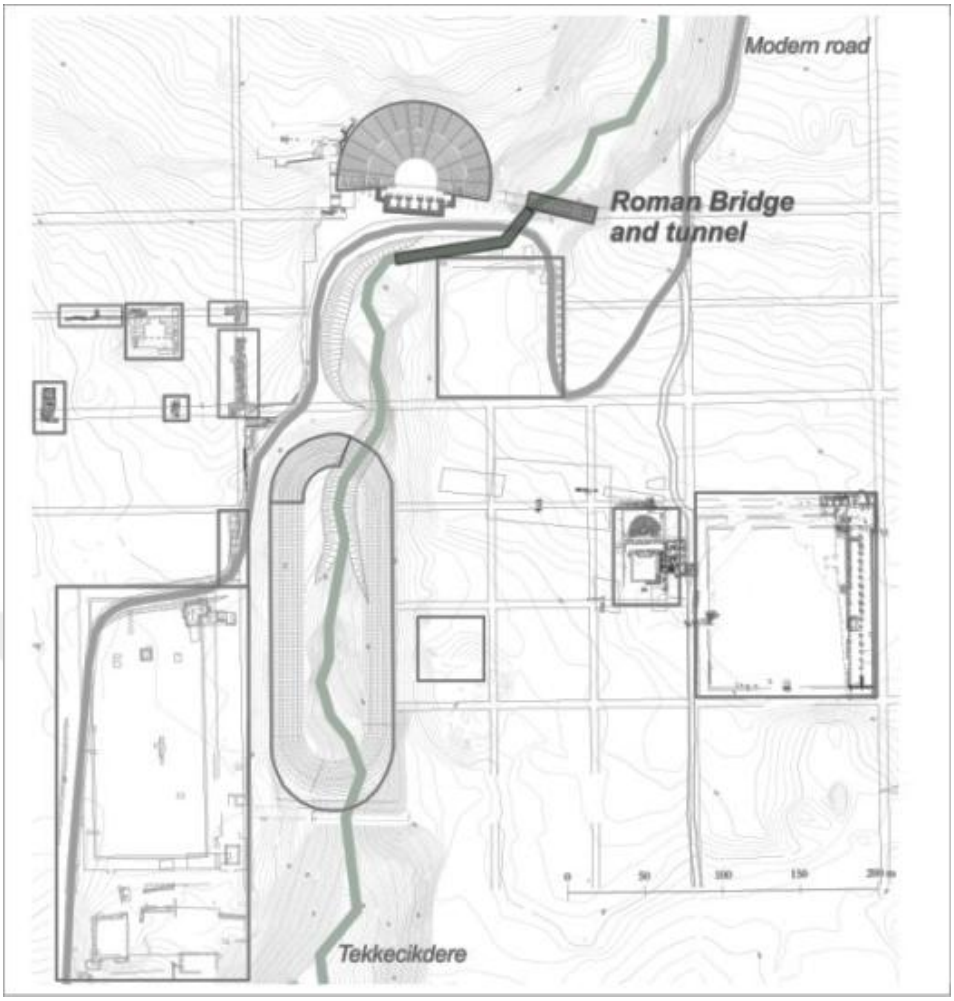


Figure 2.1-24. Map of Nysa by Yurtsevenler((2013) pointing out the water road with the location of the Roman Bridge and tunnel



Figure 2.1- 25. a, b) Tunnel c,d) Geronticon

The council building for elders of the city, the Geronticon, on the northwest side of the Agora was built in the first century AD. The building has a 28 m x 24 m rectangular plan in a semicircle shape that resembles a theatre (Figure 2.1- 25c). Its *cavea* consists of 12 rows of seats and 5 stairways (Kadıoğlu and Kadıoğlu, 2008). The mortar sample was collected from the back masonry part (Figure 2.1- 25d).



Figure 2.1- 26. Aerial photo of the site showing the Stadium, the Road, the Cistern, the Bridge and the Theatre (modified from photo in Nysa excavation archive, 2014)

The stadium, also called an amphitheatre by Strabo, was built on the slopes of the valley with the stream crossing through the middle of the city. It is a good example of construction solutions for topographic difficulties found by Roman architects and engineers (Figure 2.1-26). The use of an arch-vault system in the foundation is proof of this. Although the main form is conserved, some parts of the construction have been deformed by damage and deterioration caused by flooding (Figure 2.1- 27a).

The Gymnasium's remains are visible when entering the archaeological site from south. It is located on the southeast side of the archaeological site, and the modern road passes through the area where it is. It has not been fully excavated because of current limitations. It dates to Late Hellenistic Early Roman period. In addition, its construction techniques indicate that the building was reconstructed in several periods. The function of the arched structure is not clear, but the wall behind the arch, where the sampling was done, is thought to be the

external wall of a bath complex inside the Gymnasium((Kadıoğlu et al. 2013; Öztaner,2010) (Figure 2.1- 27b).

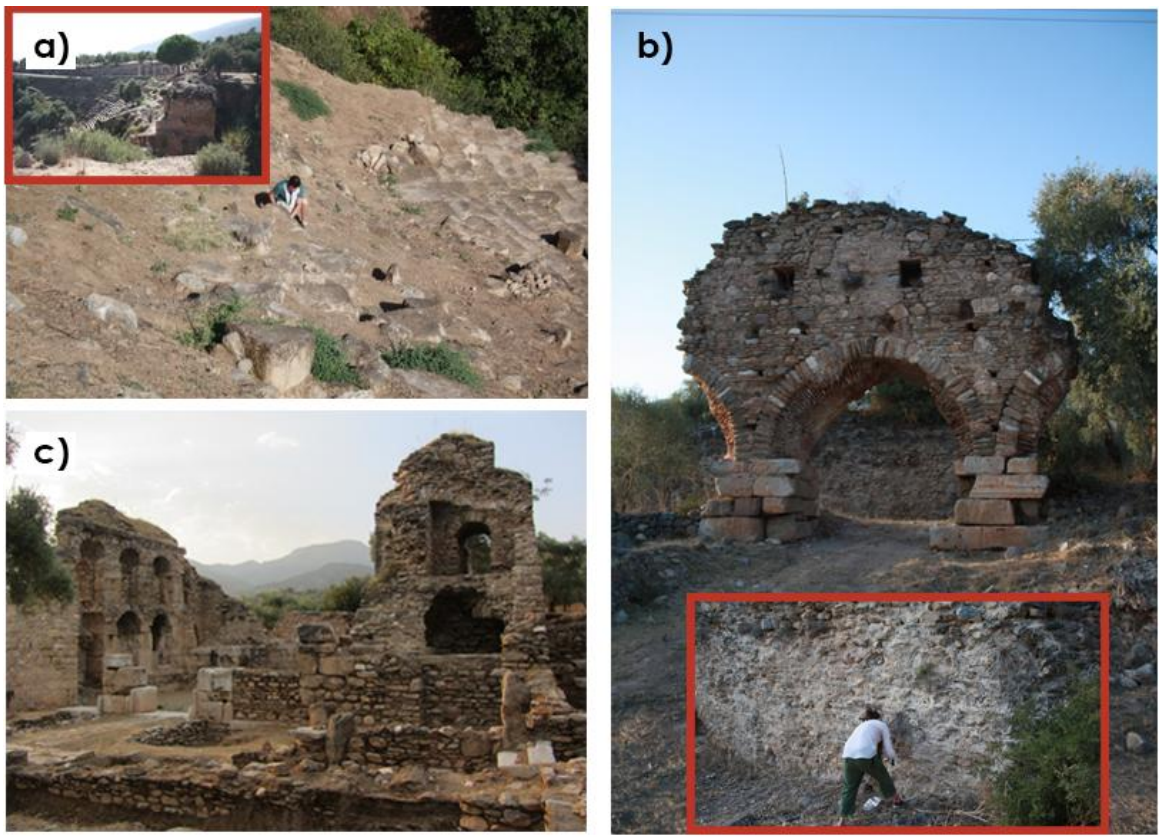


Figure 2.1- 27. a) Stadium *Suma Cavea* b) Arched structure in the southern part of Gymnasium c) Library

The Library of Nysa which is thought to have been used around 130 AD, is one of the best conserved libraries in Anatolia (Kadıoğlu and Kadıoğlu, 2008). The building which has the characteristics of Hellenistic and Roman libraries shows similarities with the libraries of Ephesus and Sagalassos, both built in the second century AD (Johnson, 1984; Mamoli, 2007). The two story building is 25 x 15 m, with square pilasters on both sides of the walls and deep niches to place books (Figure 2.1- 27c). The typology of the library matches other Roman Imperial libraries with extra rooms on the ground floor (Figure 2.1- 27). During the later periods, the building could have been used as a court and was restorated in the fourth-fifth century AD

(Uygun, 2013; Hiesel and Strocka 2006). The sampling was done from the wall, which was mainly constructed by aligning cut stones and/or filling the gaps between rubble stones and mortars (Uğurlu Sağın, 2012).

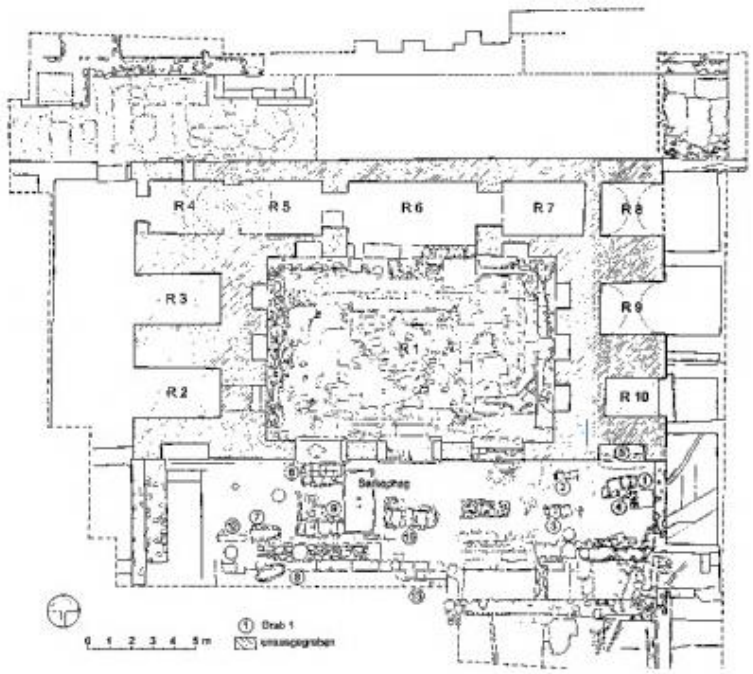


Figure 2.1- 28. Nysa Library ground floor plan (Uygun, 2012 ; Heisel and Strocka, 2006)

The theatre was built in the late Hellenistic period and had important renovations during the Roman period. It is 73 x 99 m and consists of the horseshoe-shaped *cavea*, the orchestra, the proscenium and the stage building with a three-story straight *scaenae frons* (Kadıoğlu and Kadıoğlu, 2008). Mortar was collected from the Anatolian-Roman style *Scanae frons* (Figure 2.1- 29b).

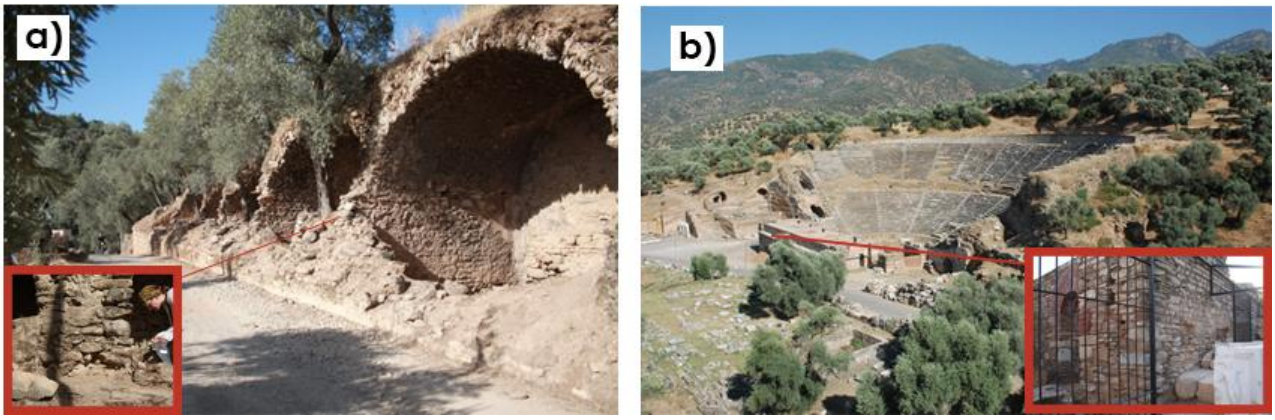


Figure 2.1- 29. a) Basilica shops b) Theatre

On the way from the theatre to the Agora, Basilica shops are situated on the left of the modern road. No detailed information is available due to the lack of excavations. Sampling was done from the basements of the vaults (Figure 2.1- 28a). North-south and east west streets were probably planned during the Hellenistic period (Kadıoğlu and Kadıoğlu, 2008) and renewed with the increase of constructions in the Roman period. In the columned Agora road, samples were taken from the coating mortar near the water tube and from the floor (Figure 2.1- 30).



Figure 2.1- 30. The Agora Road in the middle, coating mortar near water tube on the left and floor on the right

The Thermal Bath was recently excavated, and although there is a lack of information, its construction style helps to date it to the Roman period. With the existing remains it is difficult to determine the function. Samples were taken from the collateral arches and the mortar near the terracotta tube in the arch (Figure 2.1- 31).

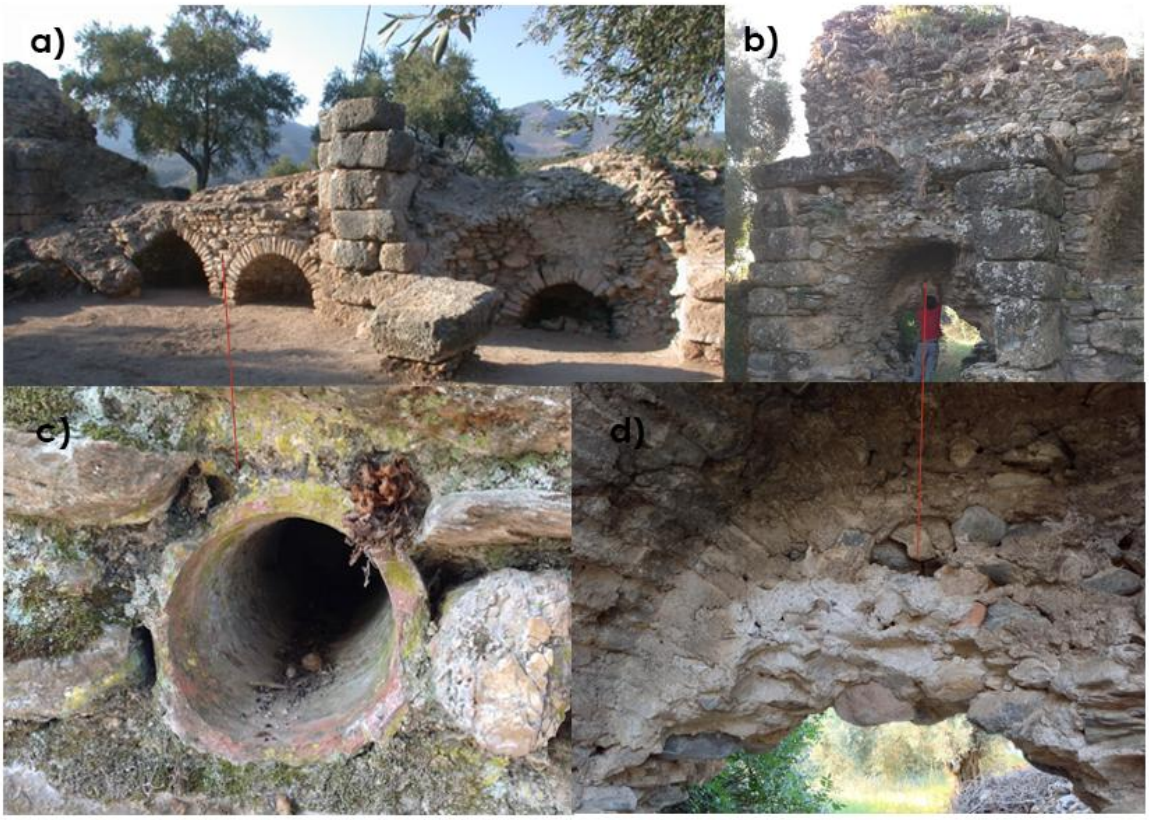


Figure 2.1- 31. The Thermal Bath

A total of 22 mortar samples were collected from Nysa. For detailed descriptions of the collected samples, please see Appendix III.

2.1.4 The Sanctuary of Labraunda

2.1.4.1 *Description of the Site*

Caria is the ancient name of the area in western Anatolia's Aegean Coast, from south of the Meanders River to Lycia. Labraunda, considered the most important sanctuary in western Caria, did not belong to any city. Instead it was used by people in the surrounding (labraunda.org).The sanctuary is located at 14 km north of the modern town of Milas, in south-western Turkey (ancient Caria) and was built in the seventh century BC (Figure 2.1- 32).

Labraunda was as a national sanctuary for the ancient Carians known as sanctuary of Zeus Labraundos. Hieron is situated on the Latmos Mountains (Baran, 2010; METU, 2013; Akurgal,1985).



Figure 2.1- 2. Location map of Labraunda

Most of the monuments were built under the rule of the Persian dynasty of the Hecatomnids in the fourth century BC. Andron A and Andron B were constructed in second century BC. Androns were banquet buildings for the ritual dinners after the sacrifices to the gods. Under the rule of Romans it was developed architecturally. The site also has three Byzantine period constructions (Figure 2.1- 33) (METU, 2013; Akurgal, 1985). The Early Roman Imperial age was a turning point for Labraunda, which lost its relative importance after the period of

Hekatomnids, the Sanctuary regained its popularity during the reign of –Claudius (Çakmaklı, 2016). The use of the sanctuary was intensified again, and new logistical needs came up in this period. The construction of the East Bath is the first known logistic addition from this period (Blid 2010).

According the ancient sources, Labraunda was a sacred area 11.6 km away from Milas. Strabon stated that the marble used in the sanctuary was thought to have been extracted and transported from the quarries on the other side of Milas by wooden sledges. Considering the fact that Labraunda is 650 m higher than the Milas plain, this would have been done with the help of animals to ascend the steep roads (labraunda.org). The analytical investigation showed that there were two types of marbles. One is pure calcite, and the other has dolomite crystals (Labraunda 2013 Report).



Figure 2.1- 33. Labraunda sanctuary from the northwest (2013)

2.1.4.2 *Historical Background of Excavations and Investigations*

It is known that Labraunda was discovered in the eighteenth century; however, there was little information. In the nineteenth century, the sanctuary was rediscovered by several European travellers; Austrian military Anton Prokesch, German writer Hermann Pückler-Muskau, Charles Fellows and French epigraphist Philippe Le Bas, W.H. Waddington, British Lieut. R. M. Smith, French epigraphist Georges Cousin (Hellstöm, 2007).

In the twentieth century, archaeological excavations were begun at Labraunda in 1948 by Swedish archaeological team which led by Axel W. Persson from Uppsala University. In 1951, Gösta Säflund continued the excavations. Alfred Westholm head of the excavation in 1960, re-dated the Andron C to the Roman Imperial period. Pontus Hellström and Karl Larsonn from Uppsala University led the excavations in 1987-2002 and 2004-2012, respectively, (Baran, 2010; Hellström, 2007). Currently, excavations are being conducted by a French-Turkish archaeological team led by Olivier Henry (Henry et al. 2015).

2.1.4.3 *The Regional Geology of Labraunda*

Labraunda is located on Cambrian-Precambrian age gneiss formations in the Menderes Massif. It is surrounded by Permo Cambrian age phyllite, metaquartzite and Mesozoic age Milas marble, Cambrian Precambrian age Gneisses Paleozoic Precambrian age micaschist, Paleocene metasandstone, slate and Neocene deposits (Figure 2.1- 34)(Yalçıner et al. 2009). Mainly, augen gneiss and marble from the southern part of the Menderes Massif were used as the building stones in Labraunda (METU, 2013). Like Nysa, the region of Labraunda is seismically active.

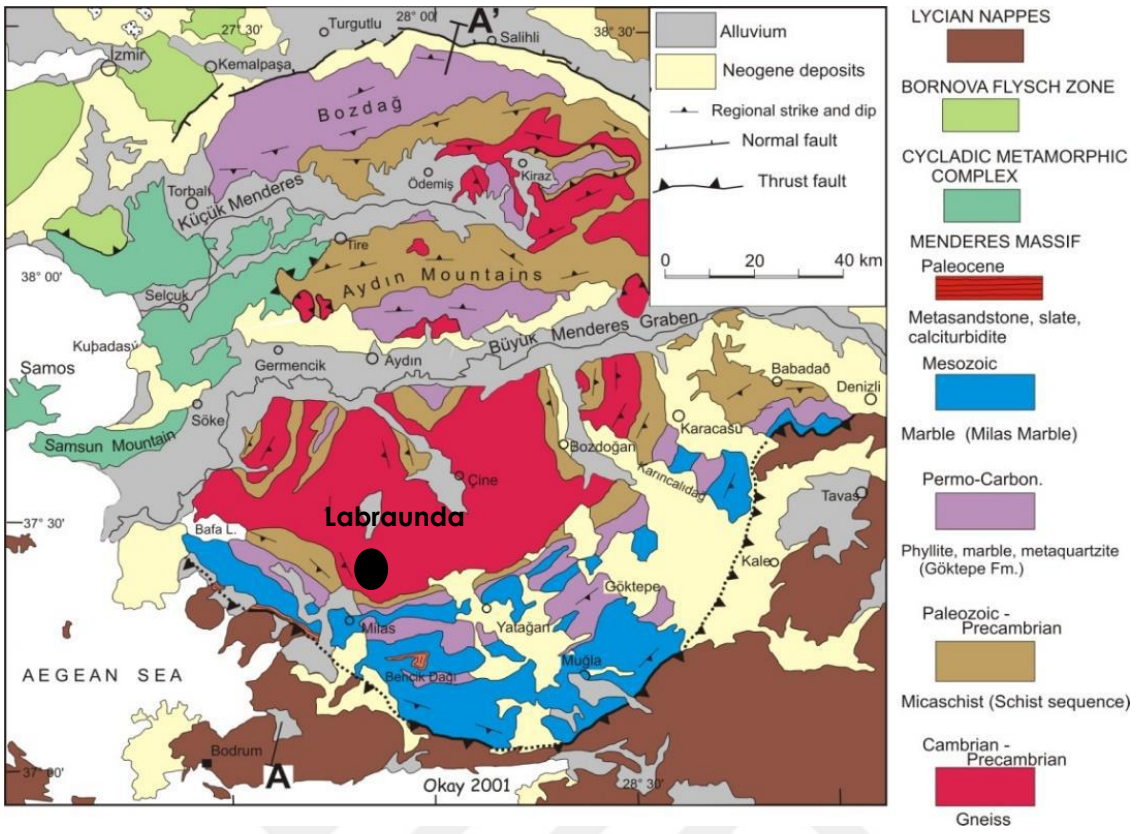


Figure 2.1- 34. Geological map of Muğla-Aydın region (after Okay, 2001)

The climate of Milas where Labraunda is located is generally warm and temperate. There is more rainfall in the winter than in the summer. The temperature here averages 18°C and the maximum annual rainfall is 130 mm (climate-data.org/location/10596/)

2.1.4.4 *Sampling and architectural description of the buildings*

The Roman period buildings at Hieron are the interest of this doctoral research. Andron C, Well House with a terrace, the West Stoa and the adjacent terraces, the East and South Baths, the hypostyle building, restorations of the Doric House, were constructed during the Roman reign (first-fourth centuries AD) (Figure 2.1- 35, Table 2.1-4)).

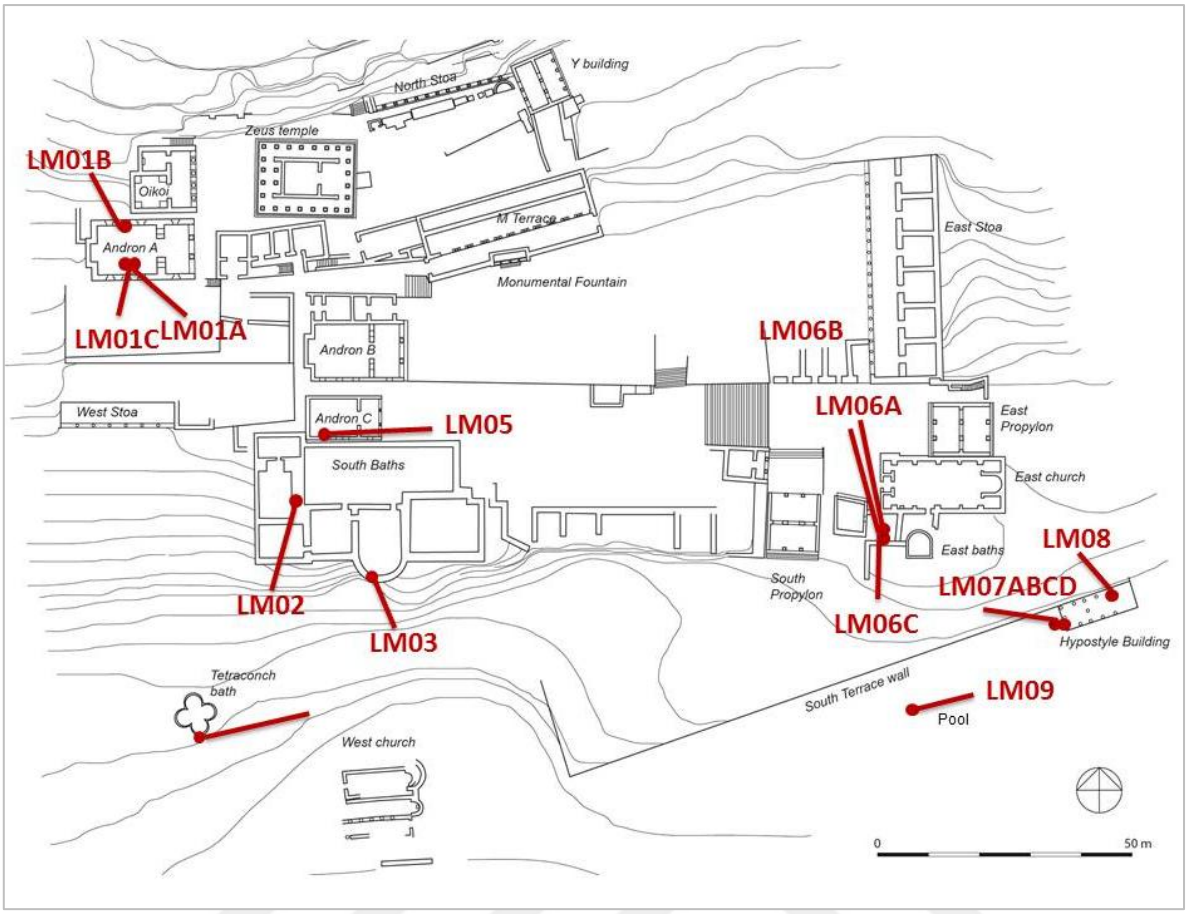


Figure 2.1- 35. Plan of the Sanctuary showing sampling points

Table 2.1- 4. Sampled mortars from Labraunda

Code	Opus Type	Location	Construction Phase
LM01A	*Opus signinum*	Andron A Floor	351-344 BC
LM01B	*Opus caementicium*	Andron A Repair mortar	?
LM01C	*Opus caementicium*	Andron A Fallen plaster piece	351-344 BC
LM02	*Opus caementicium*	South Bath Wall	3-4 c AD
LM03	*Opus caementicium*	South Bath Wall	3-4 c AD

LM04A	*Opus caementicium*	Tetraconch bath Wall	4 c AD
LM04B	*Opus signinum*	Tetraconch bath Floor	4 c AD
LM05	*Opus caementicium*	Andron C south wall	1 c AD
LM06A	*Opus signinum*	East bath Floor	1 c AD
LM06B	*Opus caementicium*	East bath	1 c AD
LM06C	*Opus signinum*	East bath wall	1 c AD
LM07A	*Opus signinum*	Hypostyle building Floor bottom level	Roman
LM07B	*Opus signinum*	Hypostyle building Floor second level	Roman
LM07C	*Opus signinum*	Hypostyle building Floor third level	Roman
LM07D	*Opus signinum*	Hypostyle building Floor fourth level	Roman
LM08	*Opus signinum*	Hypostyle building Ultimate layer 2nd phase of construction	Roman
LM09	*Opus signinum*	Pool In front of south terrace wall	1 2 c AD

Andron A is a sacred building that was constructed in the Hellenistic period. The reason to study this structure is because it has mortars in the floors, which are unlikely in Hellenistic architecture. This could be considered either a special building with unique construction according for its age or Roman period restoration (Henry et al. 2015). The building is located southeast of the excavation and has dimensions of 13 x 20 m (Figure 2.1- 36). It has double walls without mortar. A small piece of plaster found near window opening was collected as well.

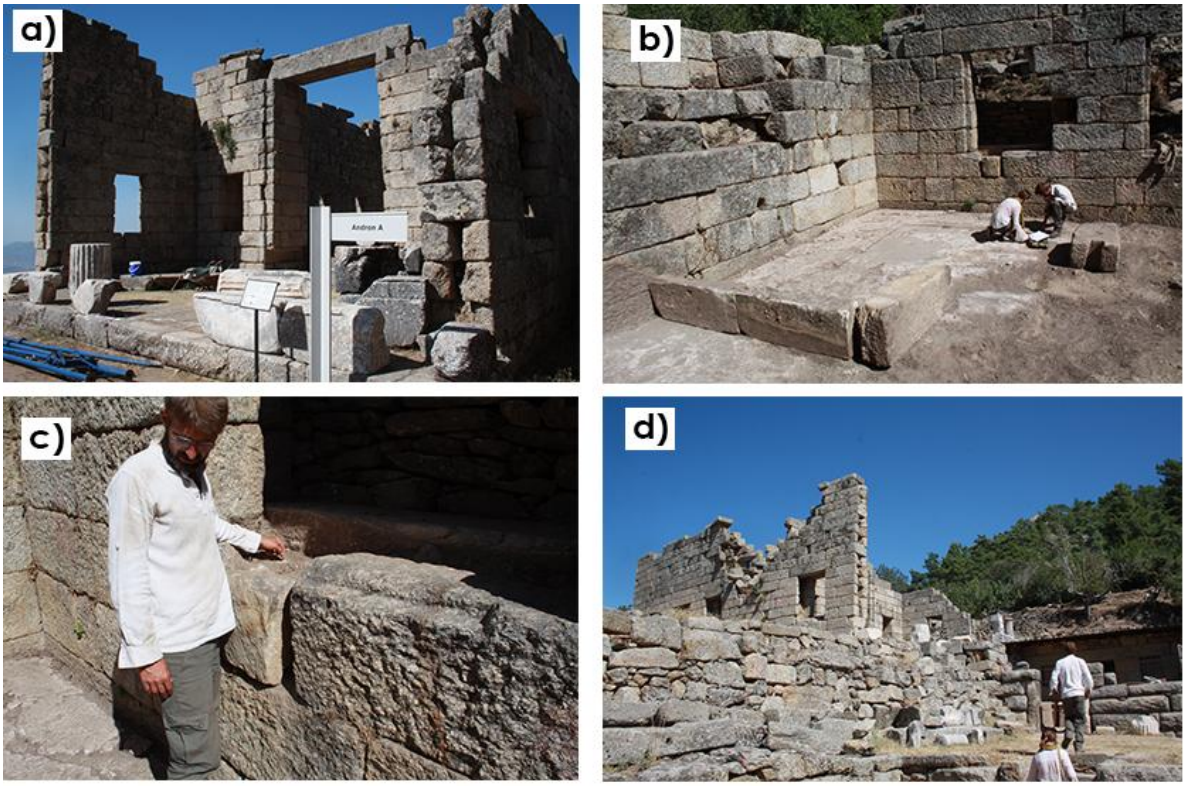


Figure 2.1- 3. Andron A

The largest building in the sanctuary, even in all of Lycia, is the South. It has an area of 1000m^2 and 7 rooms. The style of the construction of the walls with mortar is similar to that of the Tetraconch Bath and dates back to third-fourth century AD (Figure 2.1- 37a, b). Andron C was built in first century AD, function of the building is not clear yet but thought to be another sacred building. Two columns and walls were excavated (Figure 2.1- 36c,d) (Bild, 2012).

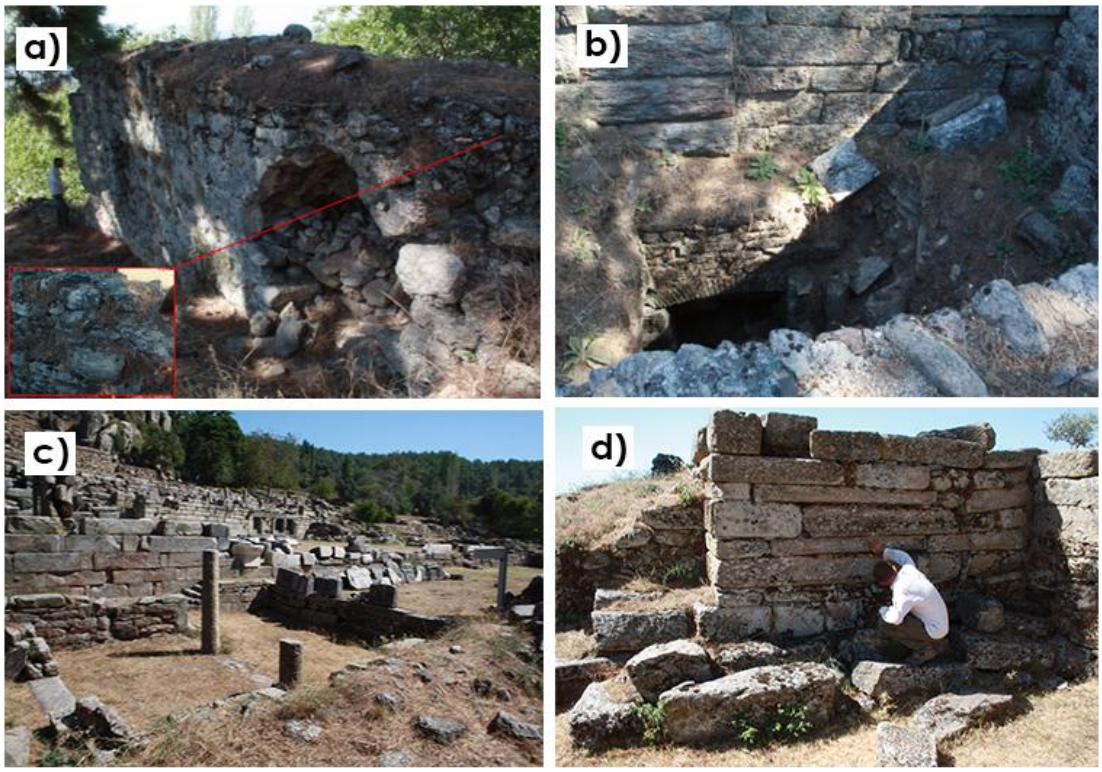


Figure 2.1- 37. a, b) South Bath c,d) Andron C

The Tetraconch building dates to the early fourth century and was built to function as the *sudatorium* of the bath complex of a private villa. The hypocaust is well conserved. In the fifth and sixth, the complex saw some restoration. It is thought to have last functions as a lime kiln (Figure 2.1- 38, Figure 2.1- 39).

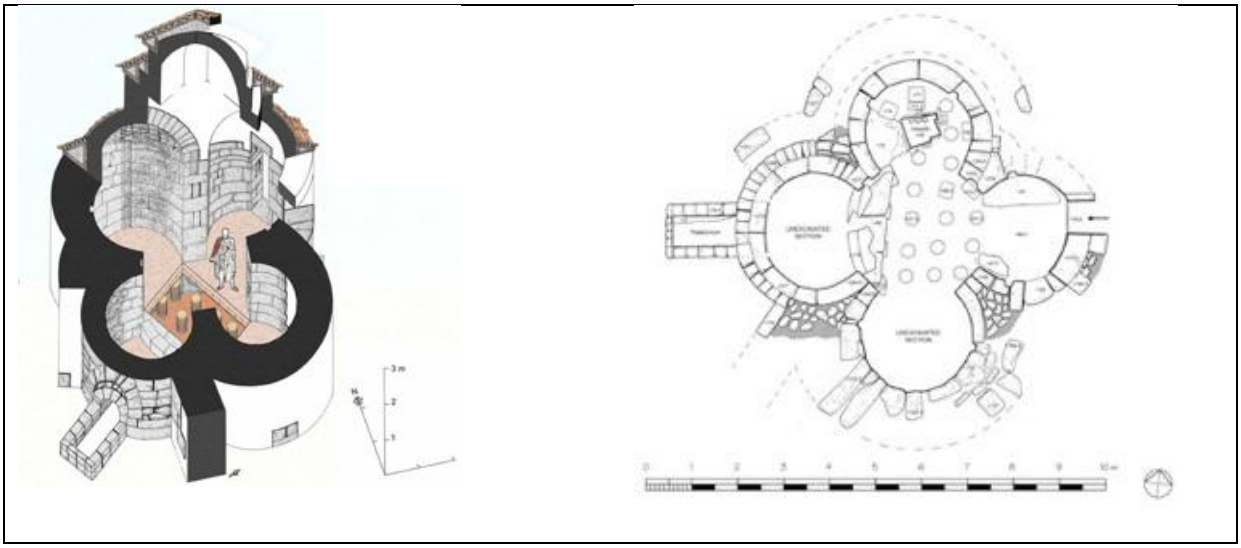


Figure 2.1-38. Tetraconch Building (Reconstruction by J. Bild on the left and the plan on the right, - www.labraunda.org, access date: 30.7.2015)



Figure 2.1-39. Tetraconch Bath

In the East Bath, the *sudatorium/ caldarium* is well conserved with its hypocaust (Bild, 2006). The Hypostyle is another water-related building. This columnar structure at the eastern end of the large retaining wall has not been fully excavated. Its function is thought to have been a place for visitors to wash (Figure 2.1- 40). Where the pool (*natatio*) is located in the south of the South Terrace was partly excavated, and mortar from the wall of the pool was sampled (Figure 2.1- 39).

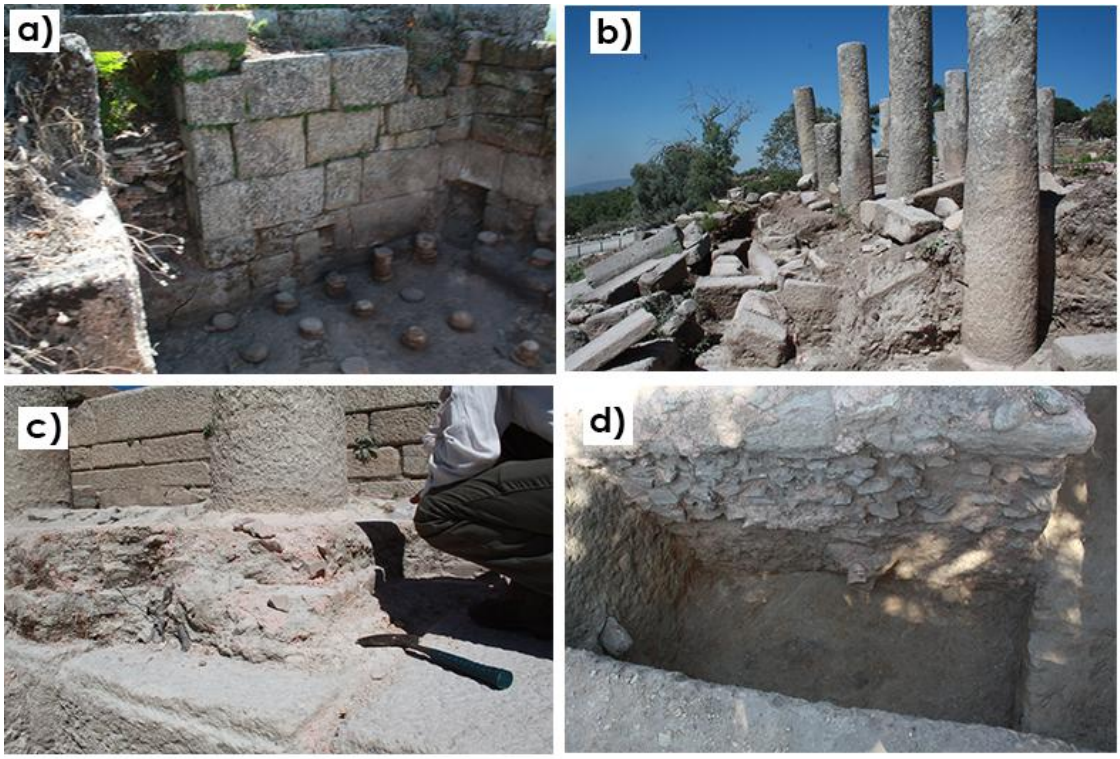


Figure 2.1-40. a) East Bath b, c) Hypostyle Building d) Pool (*natatio*)

In order to monitor the carbon dioxide (CO_2) amount, temperature (°C) and relative humidity (RH %) at the site, a data logger was placed in the warehouse under the shelter (Figure 2.1-40). Unfortunately, only one month of data were gathered, which are shown in Figure 2.1-41.



Figure 2.1- 41. Data logger measuring CO_2, T and RH in the warehouse

A total of 17 mortar samples were collected from Labraunda.

For detailed descriptions of the collected samples, please see Appendix IV.

2.2 Materials and Methods used in the repair mortar design

2.2.1 The decision making process of the ratios of the ingredients, curing conditions and preparations for tests

After the research done on the Roman mortars at the first part of the doctoral thesis, accordingly the repair mortars proportions were decided. Two kinds of mortar mixture were prepared. The first one M1 includes lime and sand aggregate whereas the second one M2 has lime as binder and sand and ceramic aggregates.

After comparing the literature (Table 2.2- 5)The proportion of the admixture M1 were decided from the common repair mortar proportion (Vitruvius, 2005; Velosa et al. 2009) and the apparent density and void ratio of the standard sand, in M2, the calculation was based upon the binder aggregate (sand and ceramic) ratio of *opus signinum* mortars in Complutum. The proportion in volume is 1:3 in M1 and 1:0.5:1:2 in M2. By weight the composition of the M1 turned to 1:3.3 and M2 1:0.7:1.4:2.2 (Table 2.2- 6).

Table 2.2- 1. Information gathered from the of previous studies

	Güney, 2012	**Vejmelkova et al. 2012**	**Lanas et al 2004**
Specimen dimension	5 cm^3 cubes	40x40x160 mm	40x40x160 mm
Duration (days)	28, 60, 90, 120	28	3,7,28,91,182,365
Flow%	70±10%		
Ambient	85%RH 20C		60±10%RH, 20±5C
# of cubes	24, 12	18(4x4x1.6) 6(5x5x2.5) 3(7x7x7) 5(5x5x2) 6(2r=5)	180
Water:Lime:poz:agg	1.3:1:0.5:2 1.2:1:1:1		1:1,1:2,1:3, 1:4,1:5
Analysis	1) Bulk density and effective porosity 2) Water vapour	1)Bulk density, matrix density, open porosity	1)three point flexural test 2)compressive

	permeability 3)Water impermeability 4) Hydric dilatation 5)Shrinkage of repair mortars during setting 6)Modulus of elasticity (Emod) 7)Uniaxial compressive strengths of mortars by point load measurements 8)Free $Ca(OH)_2$ content in the prepared pozzolanic lime mortar cubes 9)Thin section analysis 10) (SEM) (EDX) 11) XRD analyses	2)bending strength 3)compressive strength 4)fracture, 5)freeze&thaw resistance 6)Water vapour permeability 7)Wimp 8)thermal	strength 3)xrd 4)TG/DTG 5)FTIR 6) Pore structure 7)SEM

Table 2.2-6. Proportions of the prepared mortars (l: lime, s:sand, cd: ceramic dust, cd: ceramic fragment)

	M1 (l:s)	**M2 (l:cd:cf:s)**
Volume proportion	1:3	1:0.5:1:2
Weight proportion	1:3,3	1:0.7:1.4:2.2

For the ceramic aggregate in M2 15 kg Roman bricks and 5 kg Roman tiles of Complutum were crushed and sieved according to the granulometry of the *opus signinum* mortars in the site (Table 2.2- 7, Figure 2.2- 42, 43).

Table 2.2- 7. Granulometric distribution of the ceramic and sand aggregate (weight percentage %) (Sieve apertures are given in mm)

	>2	1<x<2	0,5<x<1	0,25<x<0,5	0,125<x<0,25	0,063<x<0,125	<0,063	Σ
ceramic	30	15,43	8	16	3,61	1,78	3	78
sand	0	3,86	8	7	2,41	0,45	0	22
%	30	19	16	23	6	2	3	100

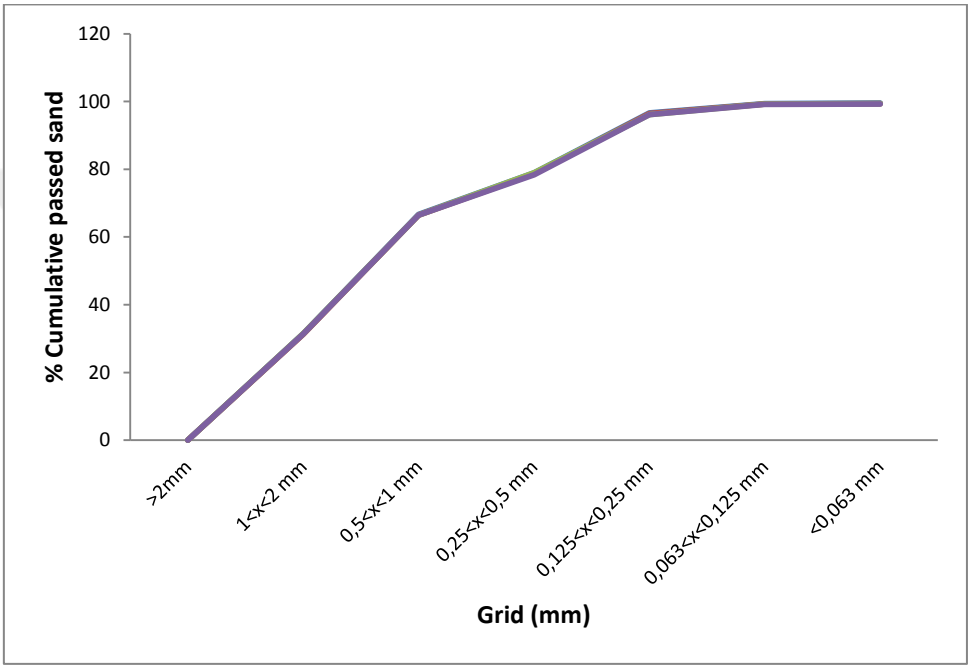


Figure 2.2-42. Particle size distribution of standard sand

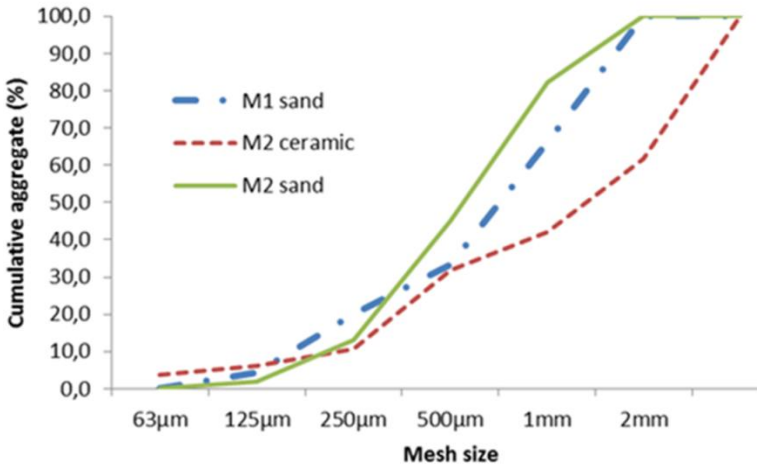


Figure 2.2- 43. Particle size distribution used in M2 mortars

The properties of the ingredients are given below (Table 2.2- 8).

Table 2.2- 8. Density of the constituents and water ratio of lime putty

	Density (g/cm³)	**Water ratio (%)**
Lime putty	1,36	84,95
Standard sand	1,48	
Ceramic	1,33	

2.2.2 Manufacturing process

Roman age ceramics which were gathered from Complutum archaeological site, were grinded and sieved according to the decided granulometry (Figure 2.2- 44- Figure 2.2- 47).

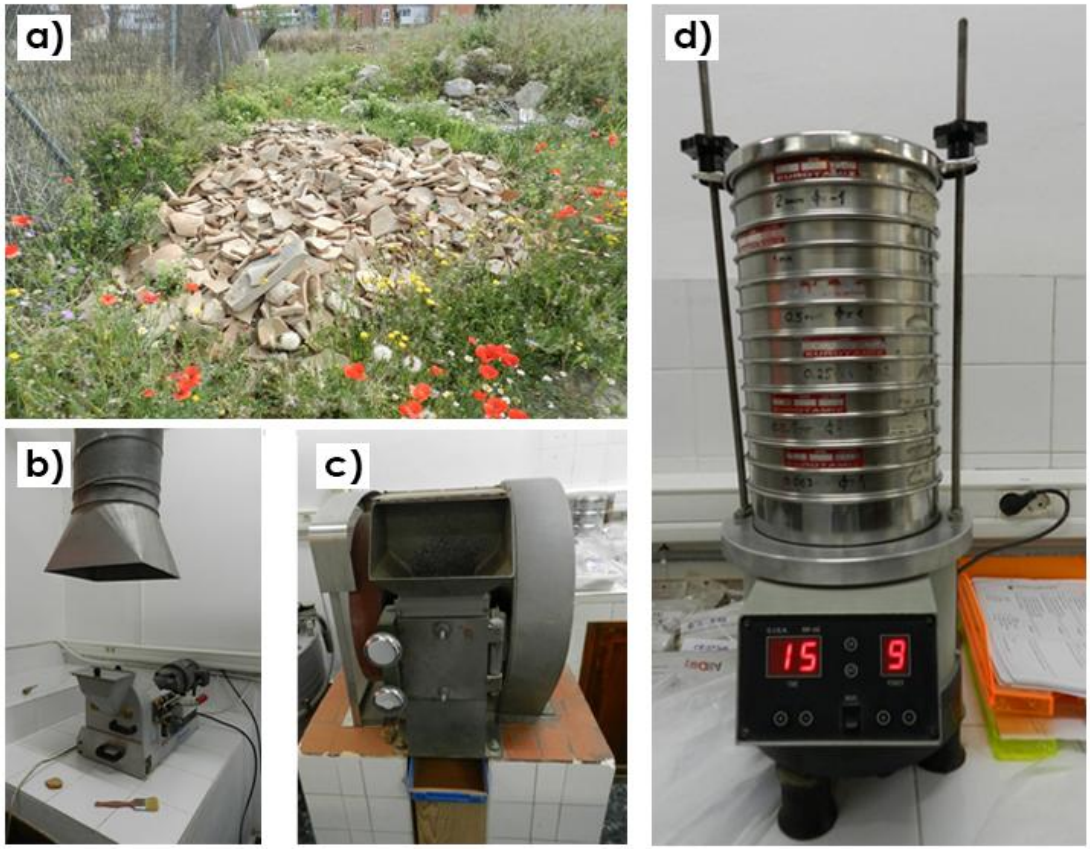


Figure 2.2- 44. a) Roman ceramics in Complutum archaeological site b,c) crushing and grinding machines d) sieving

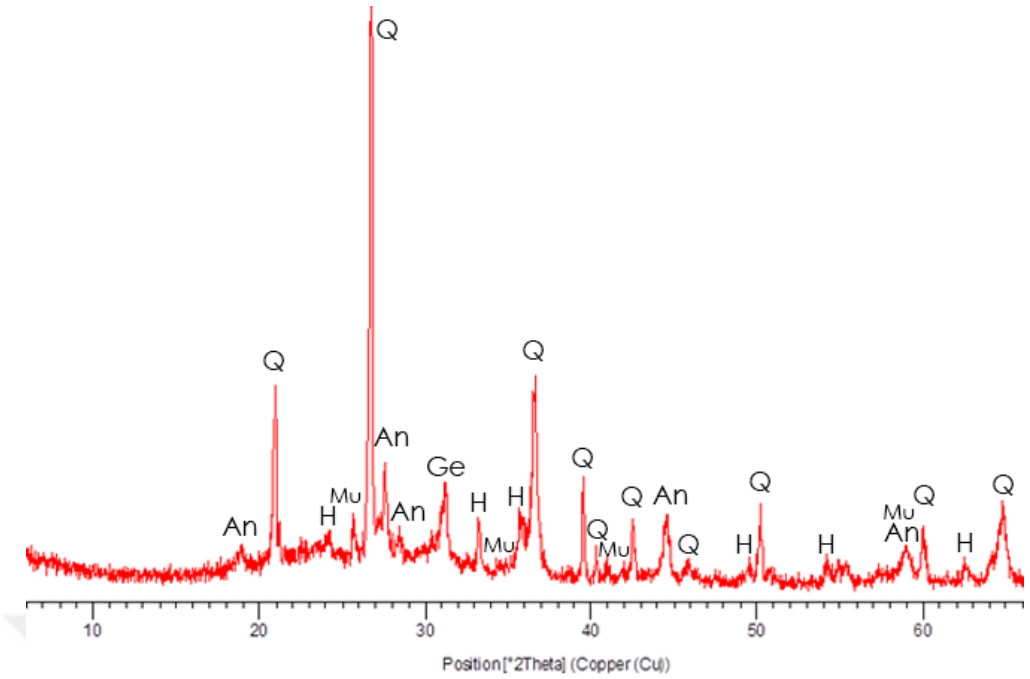


Figure 2.2-45. X-Ray Diffraction pattern of Roman tile from Complutum (Q. Quartz, An: Anorthite, H: Hematite, Ge: Gehlenite, Mu: Mullite)

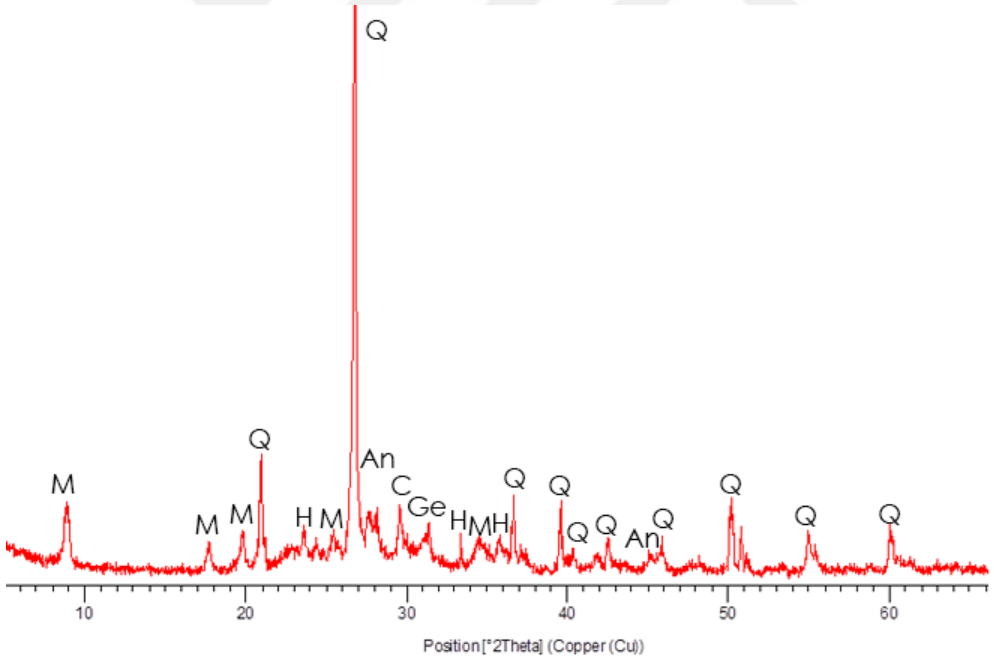


Figure 2.2-46. X-Ray Diffraction pattern of Roman brick from Complutum (Q. Quartz, An: Anorthite, H: Hematite, Ge: Gehlenite, M: Mica)



Figure 2.2- 47. Ceramic aggregates with different granulometries

Silicic (98%) sand aggregates were obtained from Eduardo Torroja Institute. CEN-NORMSAND sand is standardized according to EN 196-1 with controlled grain size distribution. The quartzitic sand grains are rounded, with and silica content comes 1350 g ± 5 g in every pack (Figure 2.2- 48).

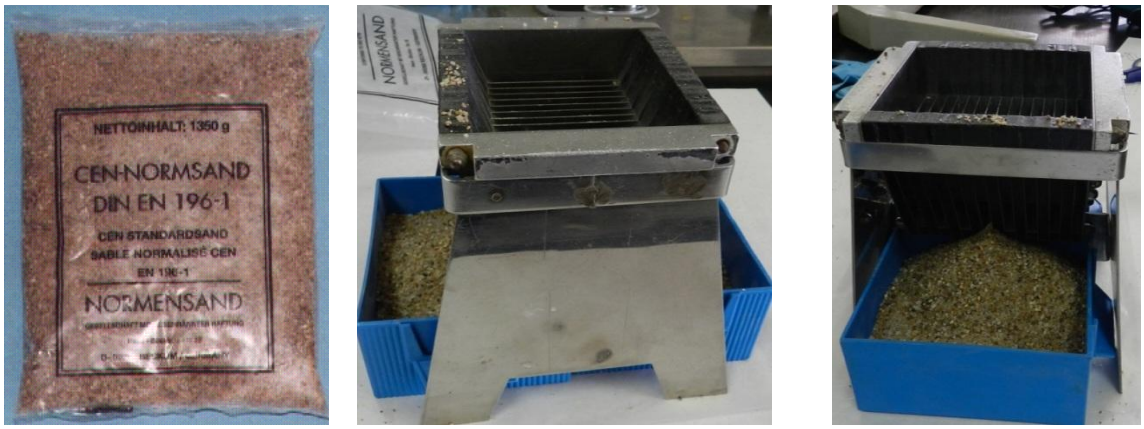


Figure 2.2- 48. Standard sand and the apparatus used for the separation

Before manufacturing of the mortars necessary for experimental part, some trials were realized. Mortars were prepared in the Construction Laboratory of ETSAM.

First, aggregates than the lime putty was added to the admixtures that water was added slowly in the mechanical mixer tank as much as it was needed until the adequate workability (Figure 2.2- 49a, b, c) was obtained. 96 metallic moulds of 160 mm x 40 mm x 40 mm were manually filled with the high attention of smoothness and compactness of the rectangular prism specimens (Figure 2.2- 49d) and left in the humid room with the conditions: 25 ˚C, 60 % RH.

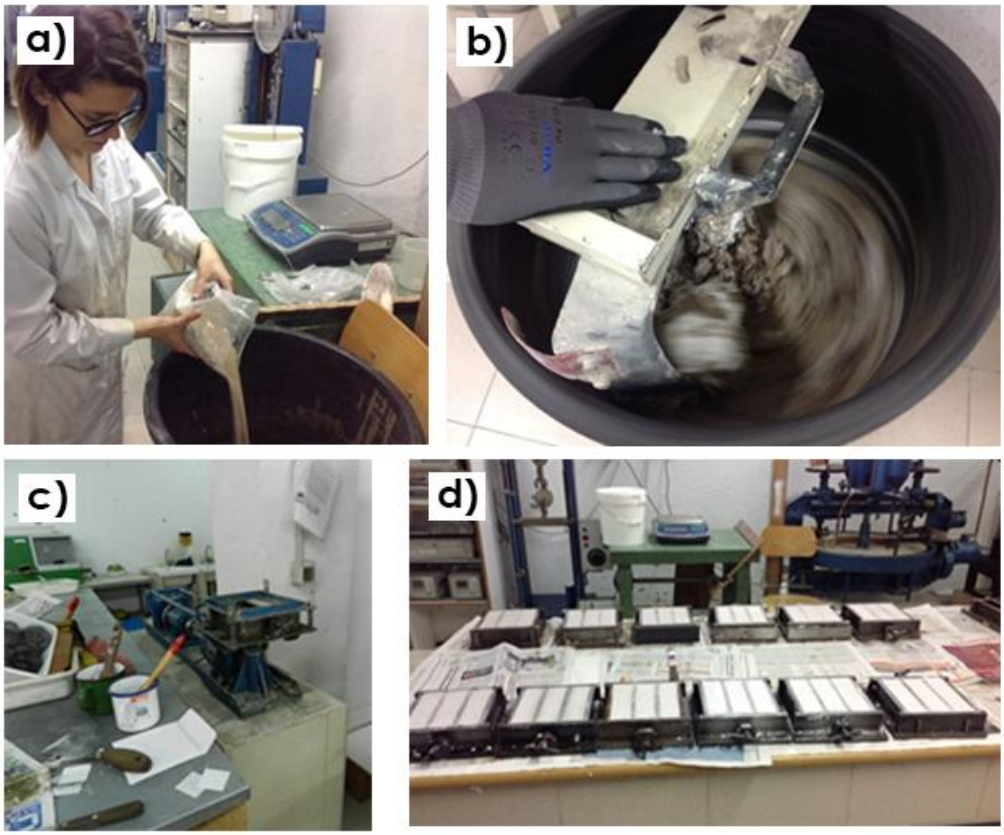


Figure 2.2- 49. Steps of manufacturing



Figure 2.2- 50. Manufactured mortar specimens

They were de-moulded after two weeks (Figure 2.2- 50) and 32 specimens were put into the climatic chamber (Dicometal) with conditions 20˚C, 60 % RH, 1600 ppm. The aim of the use of chamber is keep the conditions constant. 64 specimens were left in laboratory conditions 25 ±3 ˚C, 34 ± 8 % and 703 ± 116 ppm (Figure 2.2- 51, Figure 2.2- 52).

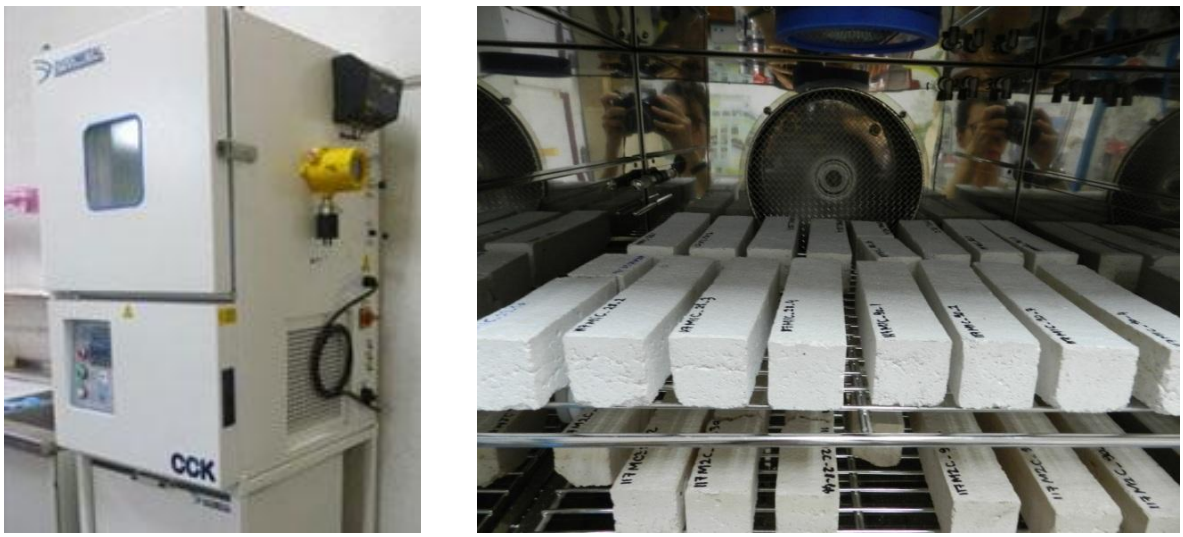


Figure 2.2-51. Climatic chamber (left), mortar samples in the climatic chamber (right)



Figure 2.2- 52. Samples cured at laboratory conditions

After demoulding, an accelerator product DiloCarb was sprayed to 36 samples in the laboratory (Figure 2.2- 51). DiLoCarB which is a variation of CaloSil®, composed of ethanol, diethyl carbonate and water. Decomposition of diethyl carbonate to ethanol and carbonate ions occurs when contact with calcium hydroxide ($Ca(OH)_2$). Because of promoting reactions it leads a faster and more complete carbonation. This reaction is much faster than carbonation reaction with CO_2 from atmosphere and allows the conversion of $Ca(OH)_2$ into $CaCO_3$.

Table 2.2-9. Environmental conditions in the laboratory between the test days (T: temperature, RH: relative humidity)

	0-28 day	**28-90 day**	**90-120 day**	**120-180 day**
T (°C)	24	28	24	22
RH (%)	40	30	33	38
CO_2 (ppm)	544	668	756	823

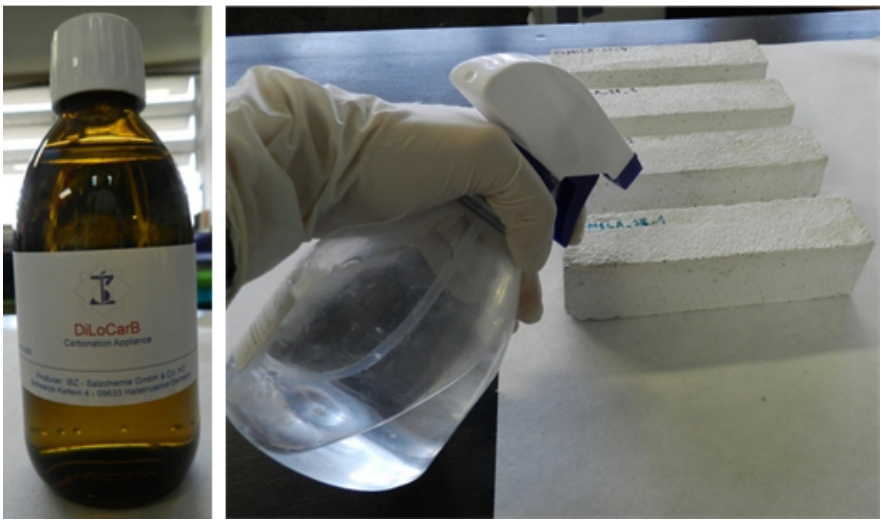
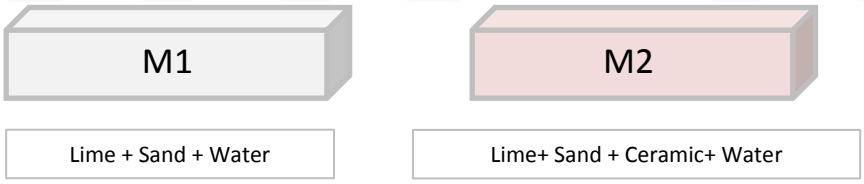


Figure 2.2-53. DiloCarb spraying on samples

2.2.3 Nomenclature of prepared samples

The nomenclature of prepared samples is the mixture type (M1,M2), curing conditions(L: laboratory, LA: laboratory with accelerator and carbonation date (28,90,120, 180) (Figure 2.2-54).



M:	C:	L:	A:
Mortar	Chamber	Laboratory	Accelerator

Figure 2.2- 54. Schematic illustration of nomenclature of samples

In every sample micro-structural analysis including optical microscopy, XRD, TGA-DTA, Mercury Intrusion Porosimetry (MIP) and SEM were conducted (Figure 2.2- 55). In three samples of every type of mortar first ultrasonic velocity, water absorption capillarity, water saturation and surface hardness then flexural strength were measured and ultimately the

three half of the samples that was broken in the flexural strength test were used to measure compressive strength. Phenolphthalein solution at 0,5% in alcohol was applied in fresh cutting surfaces -2cm thickness- of three samples of each type. Every experiment was repeated at age of 28, 90, 120 and 180 days.

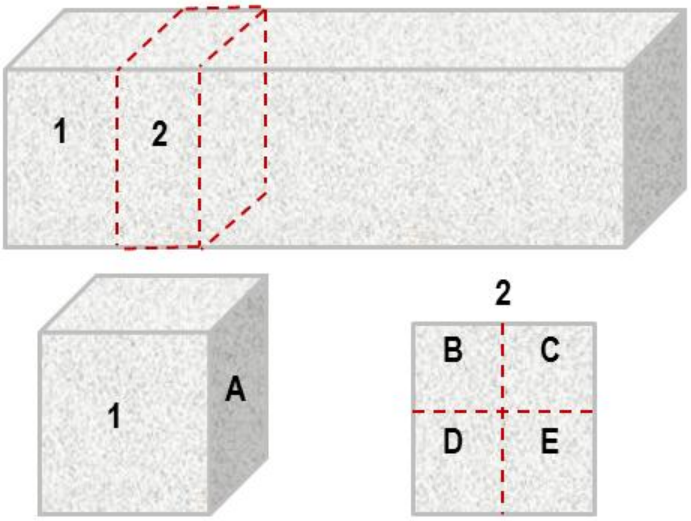


Figure 2.2-55. Illustration showing the sampling points in each simple (1: prism cut towards 4 cm inside, 2: 1 cm inside, Samples for A: phenolphthalein sprayed zone, B: XRD, C: TGA, D: SEM, E: MIP)

Physical tests were repeated every period on the same three mortar specimens in each group, for hydric tests same procedure was used for another three mortar specimens. Note that, after 28 days experiments apart from mechanical tests were realized because of the poor carbonation state (Table 2.2- 10). Ultrasonic pulse velocity values were determined all mortars casted for mechanical test (Me) in every stage, at 28 and 90 days therefore at 9 each, at 120 days 6 and at 180 days 3 each mortar specimens in each group were measured.

Table 2.2- 10. Schedule showing the mortar samples used for every experiment (M1: Lime and sand, M2: Lime, sand and ceramic, C: Chamber, L: Laboratory; LA: Accelerator,Mi: Microstructural tests, H: hydric tests, P: physical tests, Me: mechanical tets, every code of mortar specimen refers the number of specimen used in each test)

	C				L				LA			
28 days	M1C	Mi	M2C	Mi	M1L	Mi	M2L	Mi	M1LA	Mi	M2LA	Mi
90 days	M1C		M2C		M1L		M2L		M1LA		M2LA	
120 days	M1C		M2C		M1L		M2L		M1LA		M2LA	
180 days	M1C		M2C		M1L		M2L		M1LA		M2LA	
repeated	M1C	H	M2C	H	M1L	H	M2L	H	M1LA	H	M2LA	H
	M1C		M2C		M1L		M2L		M1LA		M2LA	
	M1C		M2C		M1L		M2L		M1LA		M2LA	
repeated	M1C	P	M2C	P	M1L	P	M2L	P	M1LA	P	M2LA	P
	M1C		M2C		M1L		M2L		M1LA		M2LA	
	M1C		M2C		M1L		M2L		M1LA		M2LA	
90 days	M1C	Me	M2C	Me	M1L	Me	M2L	Me	M1LA	Me	M2LA	Me
	M1C		M2C		M1L		M2L		M1LA		M2LA	
	M1C		M2C		M1L		M2L		M1LA		M2LA	
120 days	M1C		M2C		M1L		M2L		M1LA		M2LA	
	M1C		M2C		M1L		M2L		M1LA		M2LA	
	M1C		M2C		M1L		M2L		M1LA		M2LA	
180 days	M1C		M2C		M1L		M2L		M1LA		M2LA	
	M1C		M2C		M1L		M2L		M1LA		M2LA	
	M1C		M2C		M1L		M2L		M1LA		M2LA	

2.3 Analytical Methodology

The methodology of the characterization and the analytical techniques are illustrated (Figure 2.3- 56).

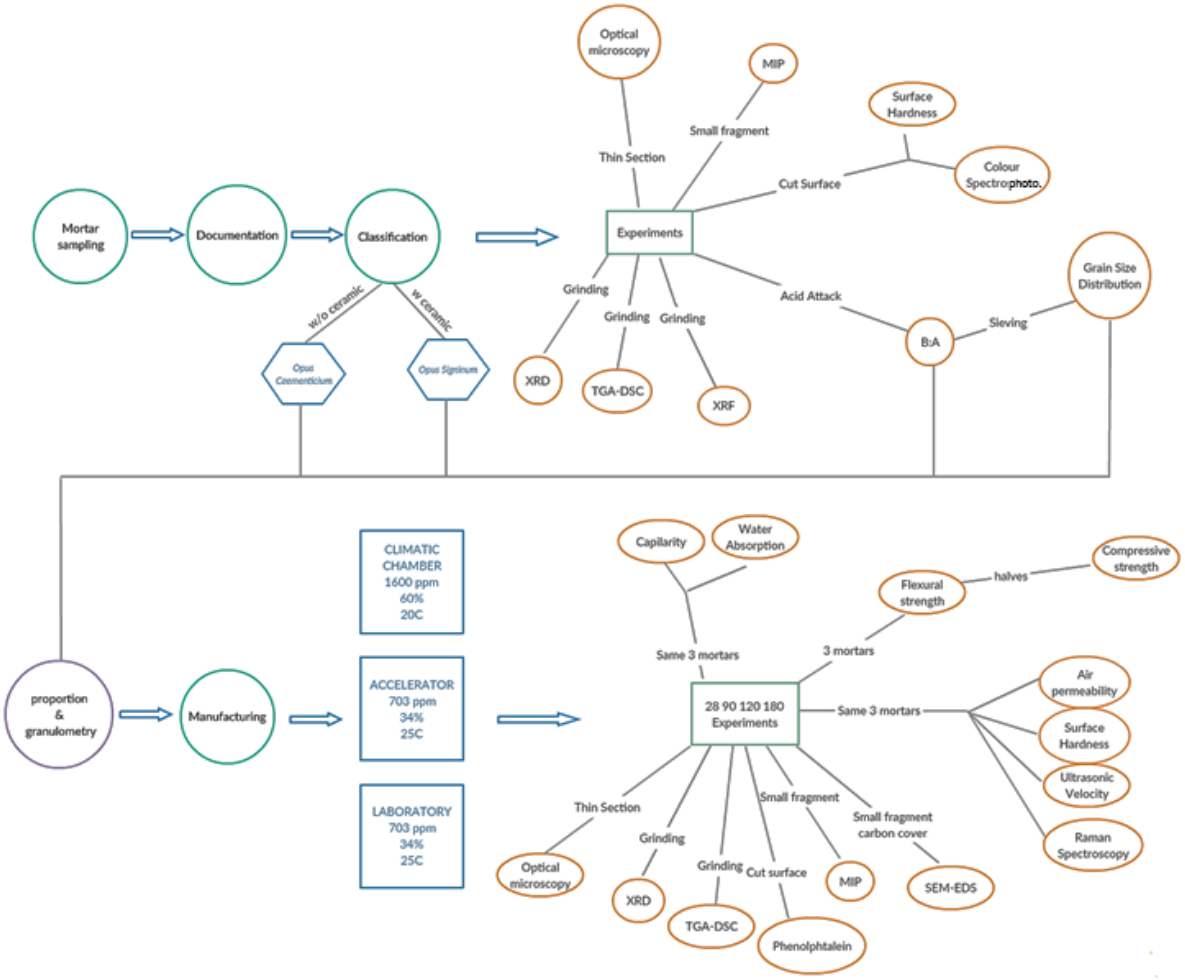


Figure 2.3- 56. Schematic illustration of conducted analytical researches

2.3.1 Optical Microscopy

Optical microscopy (OM), performed by the use of a polarized light microscope, is one of the oldest and most widespread tools for the mineralogical and petrographic investigation of minerals and rocks, although the fact that it is mostly applied to geologic samples is derived from purely historical reasons and it is generally applicable to all solid samples (Artioli, 2010).

OM with the binocular microscope equipped with incident and transmitted tungsten light, with the potential for observation of samples in cross-polar, allows determination of the mineralogy and distribution of components and their interrelationship. All compounds with valence electrons restrained in closed or local orbitals (ionic and covalent bonds, molecular compounds) absorb light in very narrow bands, so that the sample is largely transparent to light and the analysis can be performed in transmission mode. Most rock-forming minerals such as silicates, carbonates, etc. behave in this way (Figure 2.3- 57).

The majority of recent mortar characterization and/or identification studies propose optical microscopy and X-ray diffraction techniques as a first step in the qualitative identification of the different components of the mortar (Elsen, 2006).

Optical microscopy methods can be used to determine the aggregate size distribution of historic mortars and are very useful when the aggregate is acid soluble. Also, this method should be effective in mortars with complicated composition such as impure aggregate grains with mineral additions. It is useful in observation of reaction rims of mortar with adjacent material and/or air voids, lime lumps, new forming minerals due to degradation (Middendorf et al. 2005a).



Figure 2.3- 57. Photo taken during the microscopic observations

Different binder types, state of crystallinity of binder, grading, shape and mineralogy of the aggregates and can be determined with OM (Coutelas, 2003: Igea et al. 2012). Binder:aggregate ratios can also be estimated by microscopic observations. For more accurate analysis digital image analyses are used. OM is not only used to identify different mineralogical phases of mortar samples, aggregate, binder and the lithic fragments, but also for the identification of decay features of mortar (Ortega et al., 2008). In addition, in the repair mortar studies pozzolonic additives and carbonation process products are detected in the microscopic observations (Caner-Saltık et al. 2011, Ventolà et al. 2011).

Comprehensive phase and mineral identification can be seen in the ancient mortar characterization studies; Sabioni et al (2001) used microscope to identify the formation products that occurred in the sample surfaces as a result of the reaction of the mortars with atmospheric pollutants. OM is used by most of the researchers to define the petrographical characteristics of mortars; aggregates (Mertens et al. 2009), lithic fragments, (Santos Silva et al, 2010), binder aggregate bonding, secondary calcite precipitation in the pores, recarbonation of lime binder,(Sanchez-Moral et al. 2005; Igea et al. 2012) lime lump (Miriello et al. 2011), reaction rims around the ceramic aggregates (Özkaya and Böke, 2009; Vejmelková et al. 2012; Bany Yaseen et al. 2013, Robador et al. 2010; Duran et al. 2011).

Pavia (2006) examined hydraulicity of different mortars through petrography. More information gathered from the literature is presented in Table 2.3- 11.

Table 2.3- 11. Some microscopic observations in the literature

Miriello et al. 2011	calcite, anorthite, quartz, goethite, muscovite, vaterite, chlorite, albite; and the natural pozzolanic aggregates of these mortars consisted of quartz, plagioclase, muscovite, calcite, biotite, heulandite and opaque minerals.old mortar fragments
Stanislao et al. 2011	Tuff phenocrysts including sanidine, plagioclase, zeolite and clinopyroxene travertine, river pebbles including amphibolite and stony corals, fine grained pyroclastic binder, reaction rim between lime and scoria
Franquelo et al. 2008	brick aggregates were composed of quartz, anorthite, hematite, mica, calcite, muscovite; and lime mortars were consisted of quartz, calcite, mica and anorthite
Miriello et al. 2010	calcite, anorthite, analcime, leucite, sanidine, augite, phlogopite, albite, sillimanite, goethite, cowlesite, wollastonite, zircon, ludwigite and also CSH phases (hillebrandite, okenite, tobermorite, xonotlite); and lime mortars of brick aggregates contained calcite, quartz, albite, tobermorite, montmorillonite, andradite, augite, phlogopite, sanidine, nepheline, dypingite, plagioclase.

Petrographic observations were done on thin sections that were cut and impregnated in a stained resin then undertaken by polarized optical microscopy to examine the binder, the type and shape of the aggregate minerals and the structure of the entire mortar (Figure 2.3-58).



Figure 2.3- 58. Diamond disc cutting machine

The microscopic observations were carried out through polarized optical microscopy (POM) Olympus BX51 (equipped with a digital camera Olympus DP12 to capture images), on polished thin sections. Samples are impregnated in epoxy resin under vacuum to avoid air bubbles. Thin sections were prepared after cutting the mortar samples 3x4x1 cm then they were impregnated in resin and cut to 30μm width (Table 2.3-12).

Table 2.3- 12. Number of examined thin sections

Complutum	Mérida	Nysa	Labraunda	Repair mortars
25	19	19	13	24

2.3.2 X- Ray Diffraction (XRD)

X-Ray Diffraction (XRD) and optical microscopy are the primary mineralogical approaches to understand the nature of the mortars which researchers use. X-rays provide information on the exact nature of the crystalline substances identifying the mineralogical composition of the compound. The minimum amount needed for the analysis ranges from 10 to 100 mg and the minimum percentage of crystalline compound detectable is about 3-5% of the mass of the sample, this limit depending upon the crystallinity of the material. One of the advantages of XRD is that the analysis must be done directly on the powdered sample without putting it in solution and therefore the sample after the analysis can also be used again for additional investigations (ICCROM, 1999; Artioli, 2010).

In the examined material, each crystalline phase contains a set of characteristic reticular planes that allow its identification. A diffractogram is a listing of the spacings of these planes, represented by a series of peaks. Each diffraction angle is represented in a peak and the set of these peaks is denominated X-ray diffractogram. Identification of minerals was done by three peaks of greater intensity among several characteristic peaks as in case of the lower crystallinity high amount of peaks reveal (Pérez-Monserrat, 2012).

The first question of the research is the binder of mortars. If the evocation is necessary, most of the historic mortars are lime based and sand used as aggregate, thus about in all studies calcite is found as the main component and quartz as secondary (Alvarez et al, 2000; Biscontin et al. 2002).

The fundamental concern of the characterization is the rest, namely the other constituents of aggregates and pozzolanic materials. Microscopy is not sufficient in that manner so that should be collaborated with XRD. Differentiation of the binder types can be possible by XRD method (Igea et al. 2012)even though mostly the overlapping and masking by the peaks of other minerals are the concern encountered. However XRD can only detect the crystalline phases which are the product of carbonation, is insufficient in distinguishing the carbonate in the aggregate and in the lime binder. Besides, amorphous phases like calcium silica gel

cannot be detected (Middendorf et al, 2005a). But Miriello et al. (2010) remind the fact that the peaks for C-S-H phases were not measured in some samples does not mean that they are not present. Rather, may exist in the form of gels of very low crystallinity. The complex silicates diffraction peaks arise very closely together so individual identification of these components is difficult. Even after acid treatment the diffraction patterns for the samples are very similar and no differences can be established between those from different zones. However, Alvarez et al (2000) and Sanjurjo-Sánchez et al (2010) state that an estimation of siliceous nature can be done through initial qualitative and semi-quantitative composition of the aggregate fraction. Yet not all the investigations focus on the clay fragments, some researchers made a detailed analysis between 30 and 37- (2θ) (2.97A° –2.42A°) to find calcium and calcium–aluminium silicates which provide hydraulic properties to the binder. Varas et al. (2005), Glaize et al. (2009), Özkaya and Böke (2009), Miriello et al. (2010, 2011) made a detailed study of C-S-H forms and reported that the aggregates include kaolinite and kaolinite-smectite, as well as traces of anorthite and gehlenite, and a small amount of calcium silicate hydrate (hillebrandite, okenite, tobermorite) which indicates the presence of hydraulic compounds. Sanchez-Moral et al. (2005) utilize XRD in detecting the secondary mineral analcime.

Sabbioni et al. (2001) detected a large amount of microcrystalline gypsum, in many cases surrounding carbonaceous particles together with the pozzolanic material, the alite/belite phases and siliceous aggregate in the uppermost dark-coloured layers of mortars which is exposed to the atmosphere.

The study of ancient mortars presents helpful information for the relative dating of historic structures. This characterization requires the detailed identification of the ingredients of mortars and the determination of their proportions. Although the most of the dating studies based on other technologies XRD is used with other common mineralogical methods (Bruno et al. 2004). It is noteworthy that the XRD results in the study of Sandrolini and Franzoni (2010) show the presence of dolomite in the aggregate is definitely rare in the region where the work piece is located and helped in finding the sand's origin in the bed of the river nearby.

(Mota-López et al. 2016) found tremolite-actinolite in the mortars taken from theatre of Mérida thus prove the provenance of the sand aggregates which is outcrop in the *arena* of the amphitheatre. Other examples found in the literature are listed in Table 2.3- 13.

Table 2.3- 13. XRD findings in the literature

Sánchez-Moral et al. 2005	calcite, phyllosilicate, analcime and augite; and traces of feldspar and quartz
Jackson et al. 2011	calcite, analcime, leucite, diopside, vaterite and strätlingite; and natural pozzolanic aggregates were consisted of analcime, leucite, diopside, hematite and calcite
Jackson et al. 2009	Calcite, diopside, sanidine, leucite, analcime, and clay minerals
Jackson et al. 2010	Strätlingite which was defined as a calcium-aluminate cement hydrate was also specified by quartz, sanidine, analcime, biotite, ignimbrite, feldspar by
Degryse et al. 2002	sanidine, anorthite and also amorphous glass phases; and the pozzolans as plagioclase alkali-feldpar, augite, diopside, biotite and amphiboles
Kramar et al. 2011	calcite, dolomite, quartz and muscovite; whereas the brick aggregates were composed of dolomite, calcite, quartz and muscovite
Robador et al. 2010	brick aggregates as quartz, calcite, anorthite, hematite; and binders of lime mortars manufactured by these aggregates were composed of quartz, anorthite, mica, hematite

The identification of phases in combined mortars is, as expected, more complex, but distinctive peaks are always possible to observe. The use of clay (i.e. binders containing powdered bricks and terracotta) might also create extra difficulties, since mica phases, feldspars, pyroxenes, wollastonite, melilite are present. The complexity of the systems and lack of separation between patterns of several phases strongly restrict the potential of XRD as the main distinctive tool for the study of mortars.

It is suggested to separate the binder and whole mortar with aggregate before the analysis which helps in clarifying the nature of binder (Middendorf et al. 2005a, Santos Silva et al. 2006a). Nevertheless in the Roman mortars which have high consistency the mechanical separation is not possible at the most of the cases. XRD allows analysis of crystalline materials including binder phases and crystallized alteration products. Data from the testing of complex materials is difficult to interpret, and a highly skilled analyst is crucial. In terms of utility of XRD especially the C-S-H formations take place in the repair mortar studies since they present a critical value of adherence.

40°C dried samples were prepared by powdering < 50µm. Measurements where performed using a and Bruker D8 Advance X-ray diffractometer and spectra were taken in the following conditions: 40 kV and 30 mA at 2θ angles of 2–68° with a 0.020-step scan, a speed of 2° per minute, CuKa radiation and a graphite monochromator. Bruker EVA X-ray diffraction analysis software was utilized to interpret the diffractograms.

Table 2.3- 14. Number of mortar samples analysed by XRD

Complutum	Mérida	Nysa	Labraunda	Repair mortars
39	23	22	17	24

2.3.3 Thermogravimetric Analysis (TGA)

Thermogravimetric Analysis (TGA) is a technique in which the mass change is measured in a function of temperature of a in a controlled temperature and atmosphere. Using Differential Scanning Calorimetry (DCS), heat flow into a material causes many physical-chemical changes which generally have an important role in sample identification and characterization (Veiga et al. 2001; Artioli, 2010).

Thermal analysis can be carried out on very small samples and can positively identify the composition of certain components, including calcium carbonate, calcium hydroxide, calcium sulphate, calcium silicate hydrates, and depending upon the constituents remaining after ageing, complex calcium silicate and aluminate hydrates

Also thermogravimetric analysis and differential thermal analysis are performed to obtain a corresponding knowledge about the binder composition and purity.

TGA and DTA show a good concurrence with the other characterization techniques, and they are proved as a good method for the analysis of the ancient mortars(Alvarez et al. 2000, Bruno et al. 2004, Genestar et al.2006; Velosa et al. 2007, Özkaya and Böke, 2009, Uğurlu Sağın, 2012; Arizzi and Cultrone, 2012, Drdácky et al. 2013).

According to Schueremans et al. (2011), TGA and XRD provide confirmation to the presence of portlandite which cannot be determined by wet chemical analysis and also mineral phases related to the binder and sand fractions which allow better identification of the mortar constituents can be determined. The weight loss between 200 and 600 °C is attributed to the loss of the chemically bound water of hydraulic compounds (C–S–A–H and/or C–S–H) when techniques such as XRD, FTIR do not detect other compounds that decompose in the same temperature range, such as organic compounds, calcium or magnesium hydroxide, hydromagnesite, etc (Gelize et al. 2009).

Chemical reactions and physical transitions can be known through TGA-DSC. Thence, in mortar studies large number of scholars utilizes the technique to understand the hydraulicity,

even though it is not so simple to understand the hydraulicity of historic mortars every time (Elsen et al. 2012).

Percentages of weight losses at temperatures below 120˚C refer to hygroscopic water, weight loss at the temperatures between 200 ˚C and 600 ˚C was mainly due to loss of structurally bound water (H_2O) of hydraulic reaction products (C-S-H, C-A-H, etc.) (Bakolas et al.1995, Moropolou et al. 2000; Biscontin et al. 2002; Maravelaki-Lalaitzaki et al. 2003; Çizer, 2004).

Weight loss above 600 ˚C was mainly attributed to the release of carbon dioxide gas (CO_2) during the decomposition of calcium carbonates. Weight loss of structurally bound water occurs between 120 ˚C and 650 ˚C and carbon decomposition above 650 ˚C according to Cardoso et al. 2014. $Ca(OH)_2$ loses its chemically bound water between 350 and 550 ◦C (dehydroxylation) and $CaCO_3$ loses its chemically bound CO_2 between 600 and 900 ◦C (decarboxylation) (Lawrence et al. 2006). Bakolas, et al. (1995) demonstrates that weight loss attributed to early decomposition of the carbonates due to the presence salts occurs at 500-600˚C. In the study of (Cultrone, et al. 2005) initial weight loss until 110˚C is attributed to loss of the water in the lime putty. Another weight loss between 400 and 478˚C is caused by the loss of structural water present in portlandite. Ultimate weight between 600 and 715˚C is associated to the decomposition of calcium carbonates.

On the other hand Moropoulou et al. (2005) and Genestar et al. (2006) state that calcium carbonate decomposition occurs between 600 ˚C and 800 ˚C while Bonazza, et al. (2013) claim that it occurs between 590 ˚C and 790 ˚C. Silva, et al. (2006) state that weight loss at between 200 ˚C and 500 ˚C corresponds to chemically bound to hydrated aluminum silicates originated from pozzolanic reactions and between 500 ˚C and 900 ˚C calcium carbonates decompose. The more detailed peaks found by scholars are listed in Table 2.3- 15.

Ratio of CO_2/H_2O shows the inverse hydraulic character of the mortars. The inverse trend of hydraulicity (CO_2/H_2O) of the mortar samples is shown to augment exponentially with CO_2. Interpretations vary too from one scholar to another. Genestar et al. (2006) and Bonazza et

al. (2013) make the classification according to the graph. True lime mortars are grouped as CO_2 between 33-40% and structurally bound water lower than 3% CO_2/H_2O above 10 according to Moropolou et al (2000), in other study claims that the CO_2 correspond to over 32% and the ratio CO_2/H_2O between 7.5 and 10 (Moropoulou et al. 2005; Genestar et al. 2006) agree with Bonazza et al. (2013) except the range of CO_2 between 30-35% and the CO_2/H_2O ratio between 10 and 15. According to Maravelaki-Kalaitzaki et al. (2003) the typical lime mortars have less than 1.5% water chemically bound to hydraulic components and to CO_2 values between 30% and 38%. Whereas typical lime mortars (non-hydraulic) are characterised by less than 3% of structurally bound water to the hydraulic components (Genestar et al. 2006).

Ratio of the decomposition of calcium carbonates to structurally bound water is below 10 indicates the hydraulicity (Böke et al. 2008; Uğurlu Sağın, 2012). Non hydraulic mortars generally have CO_2/H_2O ratio about 5 (Elsen et al. 2011).

Hydraulic lime mortars are named after the classification CO_2 between 27% and 34% and H_2O between 4,1-6,1 % CO_2/H_2O=4,3-7,9% (Maravelaki-Kalaitzaki, et al. 2003). These mortars consist of approximately 1% of physically bound water, with low percentages of structurally bound water (3.5–6.5%) and CO_2 content that ranges between 24% and 34%, when calcareous aggregates prevail or even lower when aggregates of silicoaluminate nature are in excess. CO_2 to structurally bound water ratio ranges between 4.5 and 9.5, depending on the hydraulicity degree of the lime and on the aggregates composition (Moropoulou et al. 2005).

The so-called hydraulic mortars include all materials with an amount of structurally bound water to the hydraulic components lower than 3%, CO_2 between 27.5 and 35% and CO_2/H_2O ratio between 5 and 10 with calcareous aggregates or CO_2 surpassing 35% and CO_2/H_2O ratio over 10 for siliceous aggregates (Genestar et al. 2006)

Among hydraulic mortars more sub-classifications can be done. Artificial pozzolanic mortars are of ceramic powder as pozzolanic additive and brick fragments in the matrix of the

aggregates. Their physical bound water ranges between 1% and 4%, their structurally bound water between 3.5% and 8.5% and their CO_2 between 22% and 29% (Moropoulou et al. 2005). The crushed brick lime mortars show hydraulic water and CO_2 content in the range of 4–5% and 24–26%, respectively. This group presents higher hydraulic character than the hydraulic lime mortars (Maravelaki-Kalaitzaki et al. 2003).

Natural pozzolanic mortars present 4.5–5% of physical bound water, 5–14% of structurally bound water and CO_2 content that ranges between 12% and 20%. The CO_2 to structurally bound water ratio is lower than 3, which indicates mortars of high hydraulicity (Moropoulou et al. 2005). The pozzolanic mortars, showing more than 7% hydraulic water content and less than 20% CO_2, present the more advanced hydraulic character.

Thermal analysis (TG-DSC) was performed with a TA Instruments SDT-Q600, DSC Q-200 and General V4.1C DuPont 2000 thermogravimetric analyser, respectively, in a nitrogen atmosphere at a heating rate of 10 °C/min.

Table 2.3- 15. Number of mortar samples analysed by TGA

Complutum	**Mérida**	**Nysa**	**Labraunda**	**Repair mortars**
30	23	22	17	24

Table 2.3- 16. Weight losses and their corresponding compounds

	Hygroscopic water	**gypsum/ hydrated salts**	**structurally bound water (H_2O)**	**calcite decomposition (CO_2)**	**decarbonation $MgCO_3$**	**hydromagnesite**	**clay dehydroxilation**	**Quartz α→β**	**dehydroxilation of micaeous minerals**	**organic substances**
Ingo et al. 2014	30-120	120-200	200-600	600-1000						
Bakolas et al. 1995	30-120	120-200	200-600	>600 (500-600 if there is salt)						
Bakolas et al. 1998	<120	120-200	200-650	>650						
Alvarez et al., 2000	20-120		300-550	610-880	550-610	250,384,451,220,460		573		
Genestar et al, 2006	30-120	120-200	200-600	600-800						
Moropoulou et al. 1995	<120 (peak at 100)	120-200	200-600	>600	450-550, 860 (dolomite)		500-650°C,480, 520, 580, 660-773 (illite)	573		
Moropoulou et al. 2000	<120	120-200	200-600	>600				573		
Moropoulou et al 2005	<120		200-600	600-800						

Silva et al 2006			200-500	500-900			
Moropolou et al 2016	<120	120-200	200-600	>600			
Boke et al 2008			200-600	>600			
Arizzi et al. 2012			450-500	700-900			
Cardoso et al. 2014	<120	120-200	200-650	>650	450-550, 520-600 (dolomite)	300-400	573
Elsen et al.2000	<120	120-200	200-650	>650			573
Silva et al.2005	25-200		200-600	600-800			
Cizer et al 2004		100-200	450	500-800			
Bonazza et al 2013			200-600	590-690			
Cantisani et al 2002	<120	120-200	200-600	>600			
Uğurlu Sağın 2012			200-600	600-900			

Maravelaki -Kalaitzaki et al 2003	20-120	120-200	200-600	>600				573		
Alvarez et al., 2000	20-120		550-610	610-880	300-550					
Biscontin et al 2002	<120	120-200	200-600	>600						
Corti et al 2013	T_{amb}-120	120-200	200-600	>600				573	300-350, 630	
Bruno et al.2004			200-400	850, 900	700		100, 140, 500			400-500

2.3.4 X-Ray Fluorescence (XRF)

X-ray fluorescence (XRF) spectrometry is an elemental analysis technique with extensive use in science and industry. The basic principle of XRF is that when individual atoms are excited by an outer energy resource, they emit X-ray (fluorescent) photons of a characteristic energy or wavelength; therefore identification and quantification can be done by counting those emitted photons by sample. Major, minor and trace elements of solid and liquid phase samples can be identified by this technique. In the periodic table elements after carbon can be measured using XRF and for some elements XRF with detection limits are low as 1 ppm (part per million; 0.0001 %). The technique allows quantitative and semiquantitative analysis of geomaterials.

XRF is widely used in provenance studies when comes to trace elements which are signatures of the rocks. Lancester et al (2011) corrected the incorrect previous provenance information about the lightweight scoria and pumice used in the Roman concrete vaults with the help of XRF together with inductively coupled plasma mass spectrometry (ICP-MS) and optical microscopy.

Miriello et al (2012) did the characterization of mortars and plasters of the archaeological site Kyme in Turkey also utilizing XRF to determine the major elements. Crisci et al (2004)classified the mortar samples through graphical comparison of CaO/MgO and TiO2/Fe_2O_3 ratios gathered by XRF analysis. De Luca et al (2014) processed the geochemical data of major and rare earth elements obtained from XRF in line with Aitchison model (using logarithms of unnormalized oxide weight percent) to calculate additived-log-ratio (alr) transformations. Thereafter, alr coefficients of the mortar samples were grouped by Multivariate Cluster Analysis to determine the different construction phases. XRF was used to determine the major elements in the binder fraction and in the lumps in the study of Cantisani et al (2002), which served to estimate provenance of the lime used for the binder. Theodoridou et al (2013) investigated the pozzolanicity through chemical composition of the mortars belonging to late Bronze Age state that inverse relationship between silicon and calcium oxides and the linear relationship between silicon and aluminium oxides denote calcium aluminosilicate

formations after the reaction between lime and ceramics. More information is gathered from the literature (Table 2.3- 17).

Table 2.3- 17. Percentages (%) of major elements found in other mortar samples in previous studies

	Miriello et al. 2010	**Uğurlu Sagin 2012**	**Velosa et al. 2007**	**Jackson et al. 2009**	**Bany Yaseen et al. 2013**
SiO_2	32.3-45	39.3-79.3	28.4-51.2	42.-51.6	1.3-17.9
CaO	11.7-27.5	0.3-3.2	12.9-22.0	1.8-10.6	42.5-50.1
Al_2O_3	9.9-14.6	5.0-16.0	8.2-11.3	11.8-21.4	0.2-1.5
Fe_2O_3	5.1-8.4	2.2-7.5	2.2-3.5	9.4-11.1	0.1-0.8
MgO	2.8-8.4	0.4-2.9	1.4-4.4	1.4-5.1	0.5-1.3
Na_2O_3	1-3.4	0.4-2.2	0.7-1.1	0-1.3	0-0.9
K_2O	2.1-4.7	0.2-2.8	0.2-0.6	2.6-6.9	0.1-0.5
TiO_2	0.5-0.8	0.4-1.3	0.3-0.6	0.8-1.1	0-0.1
P_2O_5	0.1-0.5		66.5-83.4	0.2-0.7	0--0.3
MnO	0.1-0.1			0.1-0.2	-

For the X-Ray Florescence (XRF) analyses, the samples were grinded and pressed into a wafer. Analyses were realized in in the Centre of Scientific Instrumentation of University of Granada. The analyses were conducted on the powder with the laboratory equipment 4 kW wavelength-dispersive wavelength sequential spectrometer PHILIPS Magix Pro (PW-2440) with 4 kW X-Ray Generator and with the following configurations (Figure 2.3-59):

- Flow detector and one of unfolded scintillation and both inside the spectrometric camera and a sealed xenon detector to improve the sensitivity and limits of detection of some elements.

- Temperature stabilization systems in the spectrometric chamber, as well as a system for the stabilization of the PR gas flow for both pressure and temperature variations.

- X-ray tube of ultra-thin anode RH window to operate at 4KW

- Three primary collimators: 150 microns for quantitative work of high resolution, 550 microns for quantitative work and 700 microns for analysis of light elements.

- Six analyser crystals: LiF200, LiF220, Ge, PE, PX1 for analysis of Mg to O, and PX2

- Four filters: 200 and 750 micron aluminum, 300 micron bronze and lead

- Analytical software for qualitative and quantitative and semiquantitative IQ + analysis

- PHILIPS PW2540VRC Automatic Sampler with five 12-position trays

This instrumental equipment has the capacity to analyse elements from atomic number 11 onwards, in solid samples, either in high concentrations (major elements) or in traces. Typical detection limits are 0.01% for the major elements and 1-5 ppm for the traces.



Figure 2.3- 4. XRF equipment PHILIPS Magix Pro (PW-2440) (photo taken from the website: http://cic.ugr.es/servicios-y-unidades/ficha.php?codServicio=1&unidad=7, accessed date: 10.2.2016)

Table 2.3- 2. Number of Roman mortar samples analysed by XRF

Complutum	**Mérida**	**Nysa**	**Labraunda**
15	12	5	7

2.3.5 Raman Spectroscopy

Raman Spectroscopy is widely used in cultural heritage science as one of the main characterization tools (Casadio et al. 2016). The Raman signal is produced by exciting the material using a laser beam the excitation frequency and intensity is plotted. In mortar studies, increasingly with each passing day, Raman spectroscopy has been preferred by researchers because the technique allows identification of carbonates and silicates [Martinez-Ramirez et al. 2003; Lawrence, 2006; Vazquez Calvo et al. 2012; Ševčík et al. 2016). Moreover, particular attention is paid to handheld or portable Raman with being non-invasive method (Łydżba-Kopczyńska and Madariaga, 2016.).

The Raman measurement area is about 4µm although it is quite few, it should be considered that signals of un/carbonated binder, aggregate or the borders can overlap. Various components of the mortar can produce strong fluorescence [Newman et al. 2005; Lawrence, 2006; Casadio et al. 2016].

Characteristic peak of carbonate is shown at 1085cm^{-1}, calcite, aragonite and vaterite they all have distinctive peaks in the 700 – 800cm^{-1} range [Kontoyannis & Vagenas, 2000]. Peak at 3620 and 3640cm^{-1} are produced by $Ca(OH)_2$ (Dawson et al, 1973). 1086, 7122, 280, and 152 cm^{-1} calcite, 1008 cm^{-1} gypsum calcium oxalate monohydrate (whewellite; 1490, 1462, 895, and 502 cm^{-1}) can be used to assign the features in the sample (Edwards, 2002; www. rruff.com).

The portable- "Inspector Raman Delta Nu" Raman analyser was used was fitted with a 785nm diode laser whose maximum output power at the source was 120 mW and a thermoelectrically cooled, charge-coupled detector with a range of 200–2000 cm^{-1}.The integration time for recording the spectra was 5s at a resolution of 8 cm^{-1}. In every group same three mortars are tested each carbonation date, in total 72 samples are analysed.

2.3.6 Colour Spectrophotometry

Colour of the geomaterials is one of the key parameters in the characterization. In cultural heritage conservation science, chromatic scale defined by the *Commission International de l'Eclaraige* (CIE) is one of the most preferred methodologies (Figure 2.3-60). In L*, the 0 value in Z axis is associated to black colour and 100 value to white. Positive a*values indicates red and negative values to green in X axis, similarly positive b*values indicates yellow and negative values to bluein Y axis.

Used chromatic parameters are luminosity/brightness (L*), chromatic coordinates; green to red (a*) and blue to yellow (b*) and saturation/chroma (C*) which has the formula:

$C^* = ((a^*)^2+(b^*)^2)$

Color change (ΔE*) calculated according to the following formula:

$\Delta E^* = \sqrt{[(\Delta L^*)^2 + (\Delta a^*)^2 + (\Delta b^*)^2]}$.

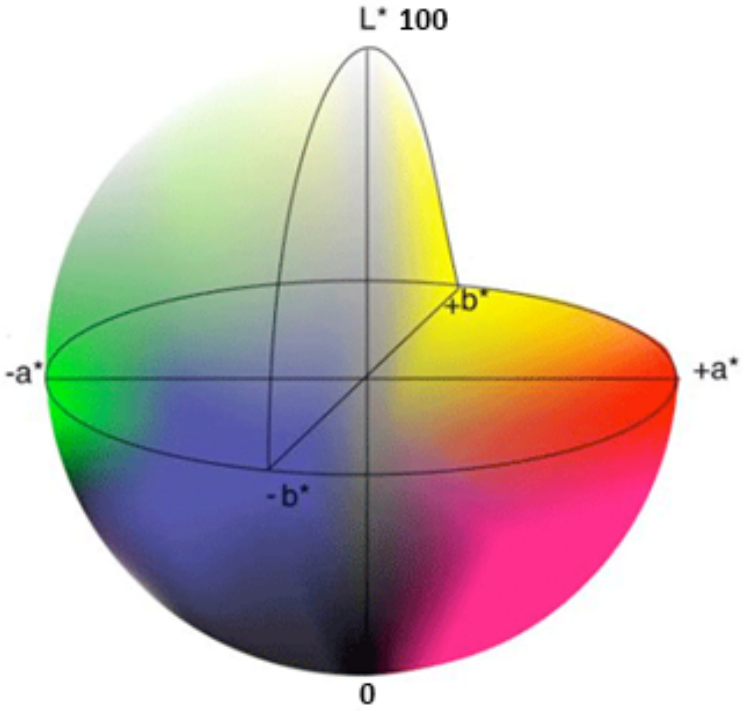


Figure 2.3- 60. CIE Lab parameters

There are other parameters that can be determined, such as White Index (WI) and Yellow Index (AI) defined by the American Society for Testing Materials (ASTM).

Colorimetric analyses were conducted through spectrophotometer CM 700d-Minolta 10 measurements were carried out in every Roman mortar sample fresh surfaces (Figure 2.3-61). In every measurement illuminant D65 at an observation angle of 10º was used. The measuring range was 4 mm diameter. For each sample colour has been measured and reported as CIE Lab coordinates mentioned above. (Fort, 1996; Alvarez de Buergo, 2012).

Secondly, spectrophotometer was used to measure the colour after the phenolphthalein sprayed to the carbonated samples in 90,120 and 180 days



Figure 2.3-61. Spectrophotometry Konica Minolta (photo taken from http://www.laboratoriopetrofisica.es/equipamiento.html, acces date: 18.3.2016)

Table 2.3- 19. Number of mortar samples analysed by Colour

Complutum	Mérida	Nysa	Labraunda	Repair mortars
27	19	21	11	24

2.3.7 Surface Hardness (Equotip)

Hardness is a physical-mechanical property of the surface of materials. It can be measured with different methods; among them we will highlight two: laboratory microdurometers, which measure either the Vickers hardness or the Knoop hardness of the materials. The first uses a diamond with a quadrangular pyramid that penetrates the material, measuring the crosshead of the footprint. The second calculates the depth of recorded signals or marks on the surface of a material by means of a diamond point with a determined force. Both are minimally destructive techniques.

A portable- and non-destructive technique (although an impact is generated on the surface of the material that could cause microcracking), is the measurement of the hardness by means of scalerometry, in which what is measured is the energy of rebound when generating an impact on the surface. Traditionally the Schmidt hammer is used, and lately there are lighter portable durometers (Equotip type).

This technique is used to determine the degree of deterioration of materials, to select replacement materials, to evaluate the efficacy of consolidating products, and in some cases, in conjunction with the ultrasound velocity technique, it has been possible to date the time of construction of some patrimonial structures (Pérez Ema et al. 2013; Viles et al. 2011).

The hardness experiment was applied with the instrument *Rebound microdurometer Leeb Equotip 3D; Proceq*. First, the experiment was carried on samples in the laboratory. The setup of the experiment was provided with the help of dough and cup because of the small size of the samples. Since a plain surface is necessary for the measurement, data was able to gather from on cut surfaces on Roman mortars and directly on prismatic repair mortar specimens (Figure 2.3- 62). On each Roman mortar sample ten measurements were recorded. Among repair mortars, every group of mortar with different curing condition has three samples and 5 measurements were conducted on each sample.

As Schmidt Hammer piston impacts with high energy on the surface so it is considered as destructive. To have an alternative Leeb rebound hardness test is designed and developed.

The equipment was designed for metals, however, in a decade it was broadly used on rocks rebound surface hardness and other materials rebound hardness with a attention on correlation between Leeb Hardness and Uniaxial Compressive Strength (Aoki and Matruska, 2008; Hujer, 2014).



Figure 2.3- 62. Equotip rebound tester

Table 2.3-20. Number of mortar samples analysed by Equotip

Complutum	Mérida	Nysa	Labraunda	Repair mortars
19	17	19	11	72

2.3.8 Mercury Intrusion Porosimetry (MIP)

Accessible porosity to mercury, pore size distribution and tortuosity can be obtained by the technique of mercury intrusion porosimetry, a destructive technique that requires a small amount of sample, which cannot subsequently be used because it is impregnated with mercury. It allows knowing the total porosity accessible to mercury, which covers a pore size range smaller than that determined with the porosity accessible to water. Likewise, it makes it possible to know the porosimetric distribution, macroporosity and microporosity.

The importance of determining macroporosity and microporosity is fundamentally based on the fact that, under equal conditions, microporosity tends to favor more the alteration of materials than macroporosity, mainly because of the smaller pore size, the higher the crystallization pressures.

The parameters obtained serve to characterize the material, to evaluate the degree of deterioration by natural or artificial alteration processes (durability), and, as in previous cases, to evaluate the effectiveness and durability of the materials (Farcie r al. 2005; Alvarez de Buergo, 2012).

Pore size distribution of the 3-4 g mortar samples were determined with the Micromeritics' AutoPore IV 9500 Series (Figure 2.3-63, Table 2.3-20). The equipment can measure pore diameters between 0.003 µm and approximately 1100 µm. Used mercury pressure is 0.2 psi[1] to 50 psi.

[1] pounds-force per square inch (1 psi = 0,00689476 MPa)



Figure 2.3-63. Porosímetry Autopore IV 9500; Micromeritic

Table 2.3-21. Number of mortar samples analysed by Mercury Intrusion Porosimetry

Complutum	Mérida	Nysa	Labraunda	Repair mortars
10	5	5	5	24

2.3.9 Acid in/soluble parts and Grain size distribution

Mix proportions and binder/aggregate ratios of historic mortars are traditionally determined by wet chemical methods. Several techniques have been proposed to segregate binder and aggregates, while acid dissolution is the most widespread method to extract binder in historic mortars (Groot et al. 2000; Casadio et al. 2005 and references therein). Yet, an important drawback of this method is that the concentrated acidic solutions dissolve the calcareous aggregate present (Ortega et al. 2008). Middendorf et al. (2005a) suggest the trial of multiple methods concerning the different solution reactions of every binder type. $CaCO_3$ can be highly effervescence when it is dissolving in even diluted acids with the release of CO_2. In order to dissolve magnesite the mortars should be attacked by hot HCl (Martin et al. 1999), in our study it was not considered necessary. In the literature some of the Roman mortar binder and aggregate ratios are as follows (Table 2.3-22):

Table 2.3- 22. Binder: aggregate ratios of the mortars from the previous studies

Miriello et al. 2010	30-50 % / 35-52 %
Miriello et al. 2011	67-83 % / 15-30 %
Kramar et al. 2011	35-65 % binder
Velosa et al. 2007	20-30 % binder

To determine the acid soluble/insoluble parts of the mortars, each 10 g of 40°C dried sample was dissolved in a beaker with 10 % HCl (1N) by folding and stirring. The remaining part (acid insoluble) were then filtered and washed four times dried again at 40 °C. The difference in the initial weight and acid insoluble weight allows calculating acid soluble and insoluble parts (Middendorf et al. 2005b).

The acid insoluble parts of mortar samples (aggregates) were sieved through a series of sieves with mesh sizes of 2000 µm, 1000 µm, 500 µm, 250 µm, 125 µm, 63 µm (Figure 2.3- 64). Weights that pass each sieve were recorded and cumulative percentages (Table 2.3- 22).

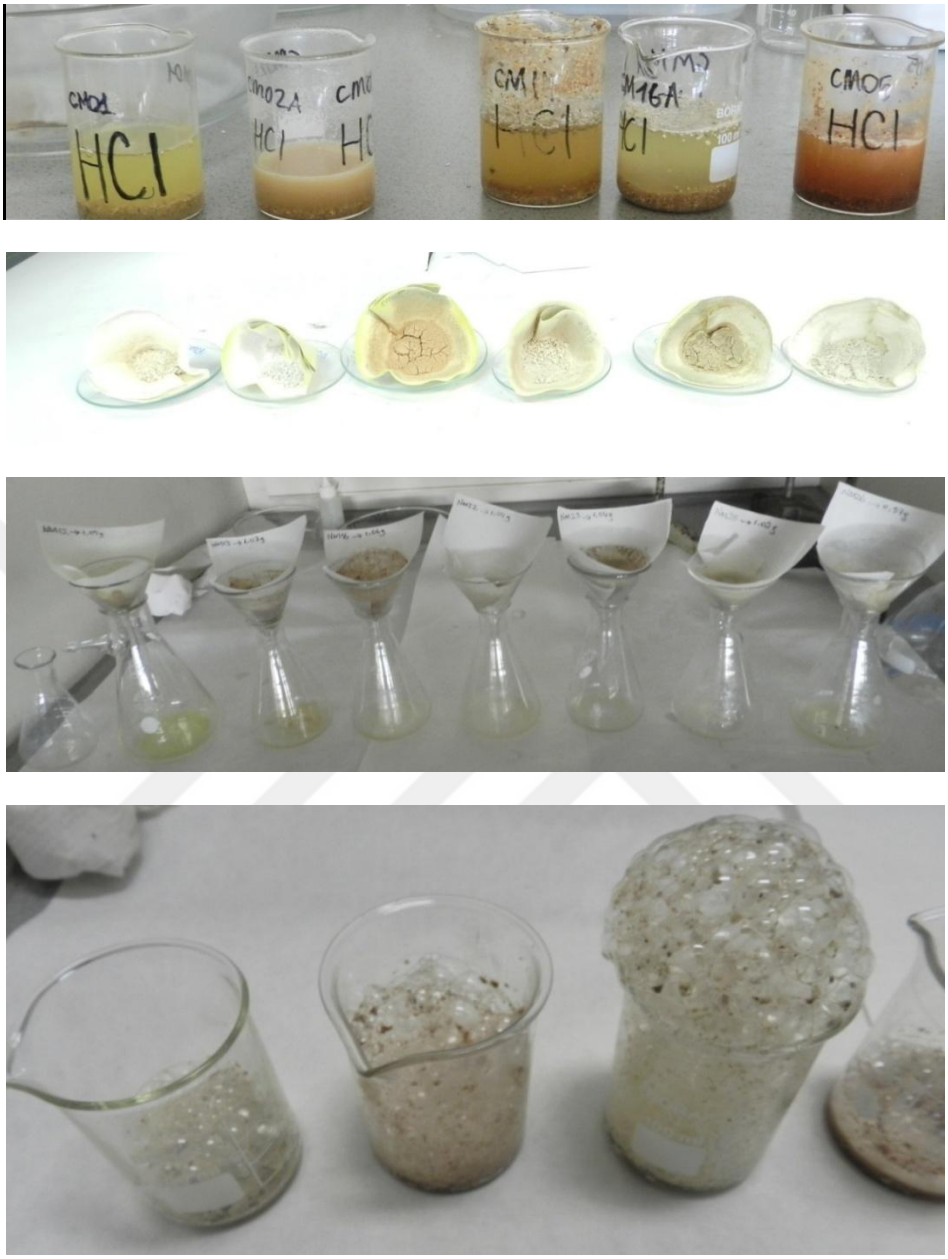


Figure 2.3- 64. HCl acid attack test

Table 2.3- 23. Number of mortar samples analysed by acid attack

Complutum	Mérida	Nysa	Labraunda
17	13	13	17

2.3.10 Scanning Electron Microscopy (SEM-EDS)

Scanning electron microscopy (SEM); electron microscopy with X-ray analysis (SEM/EDS); and SEM high resolution images of the surface of samples with magnification of up to 100000 x show the structure of the mortar. EDS allows elemental analysis of samples and SEM is used for characterization of morphologies and textural and compositional interrelationships of mortar components.

Nežerka et al (2014) could not detect interaction between the lime and crushed brick particles EDX mapping; however, the presence of only Ca in lime binder and the only presence of Al and Si on crushed bricks were seen. Jackson et al. (2014) found C-S-A-H acicular crystals including katoite, strätlingite, åkermanite. Duran et al (2014) reported that the thaumasite formed after weathering caused the decay of the C–S–H crystals.

The analyses were realized in The National Microscopy Centre (CNME) 24 repair mortar samples were analysed by SEM/EDS. Electron microscopy (SEM-EDS) studies were performed on a JEOL JSM 6400 scanning electron microscope fitted with an Oxford-Link Pentafet energy dispersive X-ray microanalyzer, approximately 1-2 cm^3 mortar samples are gold coated for the analysis (Figure 2.3- 65).

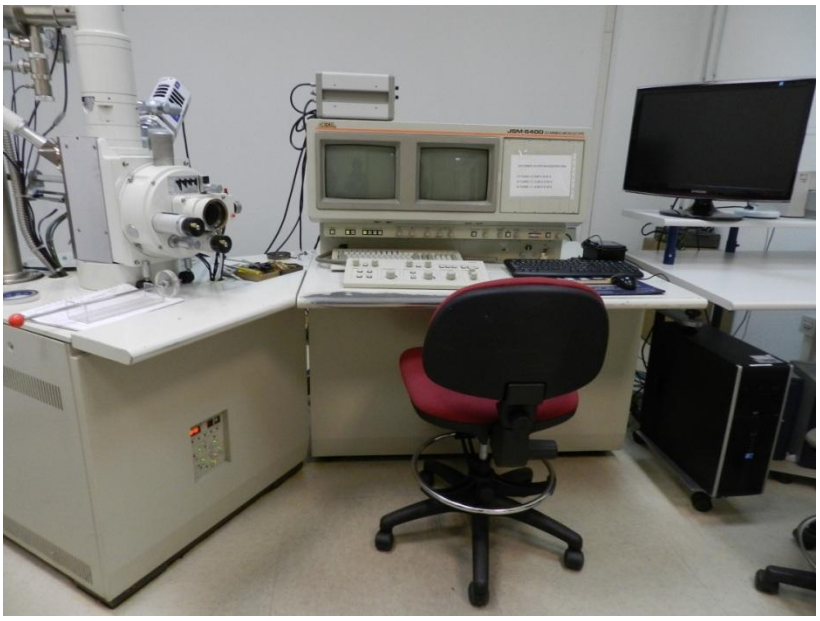


Figure 2.3- 65. SEM instrument in CNME

2.3.11 Phenolphthalein spray

As shown in Figure 2.3-65, Phenolphthalein is a chemical that is used to understand the acidity of the material. If the material surface is acidic or near neutral (pH < 8.2) it keeps colourless, on the other hand, it starts to turn out to pink at pH about 8.2 and colour changes completely at pH near 9.8 (Lawrence, 2006). This method is frequently used to measure the carbonation front of mortars by spraying phenolphthalein on a fresh broken surface of mortar (Verstrynge et al. 2011). Where the surface is stained deep pink it indicates the presence of the highly alkaline portlandite ($Ca(OH)_2$), whereas uncoloured areas indicate that the portlandite has carbonated into neutral calcite (Despotou et al. 2014).

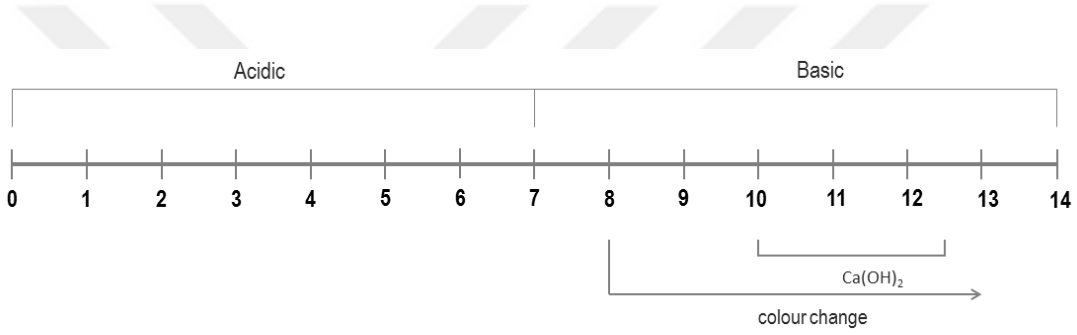


Figure 2.3- 66. pH scale classification. Calcium hydroxide average pH and Phenolphthalein changing colour start ranges (after Guimares, 2014; Lawrence 2006).

As calcium hydroxide has an average pH varying from 10 to 12.4, phenolphthalein staining is then an indicator of the presence of this high alkali. The limitations of the method cause by the rough changes in the alkali zone. 24 repair mortar samples were analysed by phenolphthalein spray, and colours were measured by spectrophotometer.

2.3.12 Flexural Strength and Compressive Strength

Mechanical properties of repair mortars are determined only. Although in the literature there are examples of measuring compressive and flexural strengths of historic mortars (Válek et al. 2005; Magalhães and Veiga, 2009) generally and in this study mechanical tests are not applied to Roman mortars due to the irregular forms.

Mortars have lower strength than adjacent building materials which serves balancing the masonry system. Among historic mortars which has compressive strengths between 0.5 and 3 N/mm^2 (Válek et al. 2005). Mechanical strength of repair mortars is affected by several factors like aggregate, porosity thus curing conditions and workability (Veiga et al. 2001; Lanas and Alvarez Galindo, 2003; Lanas et al. 2006; Matias et al 2014).

Mechanical tests are conducted by SCM3000 95 in the Construction laboratory of ETSAM Flexural and compressive strengths are performed according to the procedure UNE-EN 1015-11:1999. After 90 days mechanical tests were applied, 18 samples were analysed in each of mechanical tests. For the compression tests halves of the samples broken in flexural tests were used (Figure 2.3- 67).



Figure 2.3- 67. Compression and the instrument

2.3.13 Air permeability

Air permeability of the mortars was measured by handheld air permeameter Tiny-Perm-II by Vindum Engineeering New England Research Inc. Its air blowing vacuum generating probe has a rubber ring of 22 mm outer 9mm inner diameter (Figure 2.3- 68). In every group same three mortars are tested each carbonation date, in total 72 samples are analysed.

Air permeability (K) is calculated through air (T) value gathered in the measurement

$$T = -0.8206 \log_{10}(K) + 12.8737$$

The unit of the air permeability is millidarcys (mD).

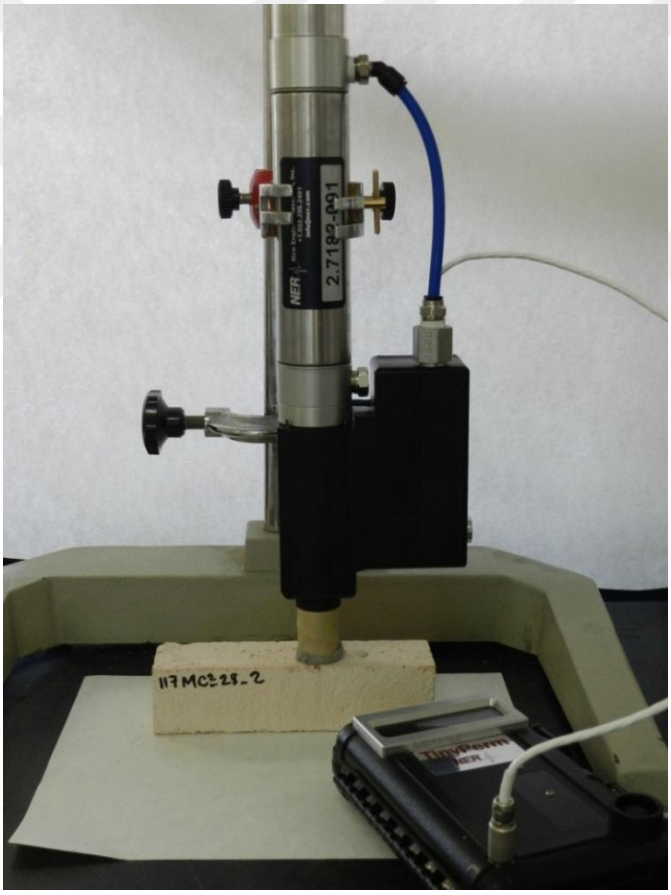


Figure 2.3- 68. Air permeameter

2.3.14 Ultrasonic Pulse Velocity (UPV)

Ultrasonic pulse velocity (UPV) as a non-destructive technique is highly preferred in cultural heritage science due to the information that provide. It is widely used in the diagnosis of the quality of the building materials such as metal, timber, ceramic, cement, mortar and stones. When the material is no homogeneous like the latter ones the response of the ultrasonic propagation waves are different. Several parameters that affect the ultrasonic waves should be taken into account in the interpretations (Fort, 2008). The equipment includes two transducers: emitter reveals ultrasound pulse with a certain frequency and the receiver receives the pulse signals throughout the material (Fort, 2008).

After the measurement the equipment gives the transfer time and the velocity is calculated by Eq. 2.3-1

UPV=d/t

d = distance between two transducers (mm)

t = time (μs)

Ultrasonic pulse velocity (UPV) was determined by the standard UNE 83-308-86 , five direct measurements on three axes of the samples were taken by PUNDIT CNS ELECTRONICS portable analyser, fitted with 1 MHz, 9mm diameter transducers and with utilizing coupling plastic (Figure 2.3- 69, Figure 2.3- 70).

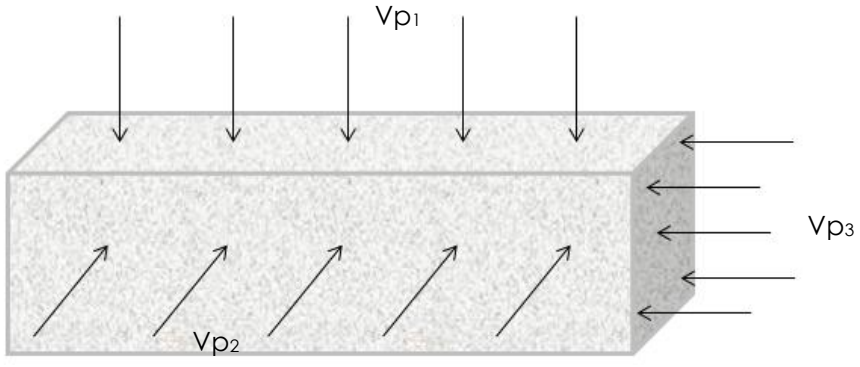


Figure 2.3- 69. Illustration of UPV measurements (Vp_1, Vp_2, Vp_3)

In the mechanical, physical and hydric experiments 3 mortar samples of each group were utilized. Exclusively in the UPV samples were measured before breaking in mechanical tests; in other words in each group in 28 and 90 days 9 samples were tested, 6 samples in 120 days and 3 samples in 180 days were measured. Presented values are the average values of the tested samples. In total, 162 samples were measured by UPV.

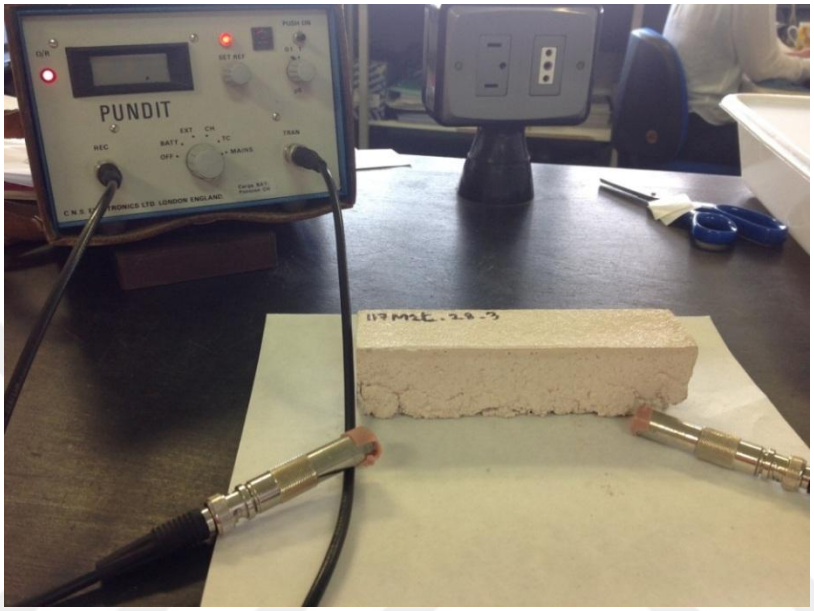


Figure 2.3- 70. Photograph showing UPV measurement

In addition, total Anisotropy índices (ΔM) were calculated (Eq 2.3-2).

$$(\Delta M)= 1- [2Vp_1/ (Vp_2+Vp_3)])*100 \qquad \text{Eq 2.3-2}$$

2.3.15 Water absorption under vacuum

Water absorption capacity (WAC) is the maximum water which a material can absorb under vacuum. Porosity is the empty voids in a solid mass. Open Porosity refers to accessible pores. Bulk (Apparent) Density is the ratio of the mass to the apparent volume of the sample. Real Density is the ratio of the mass to the real volume of the sample (RILEM, 1980).

Principal physical properties of mortars have been determined by researchers (Stefanidou and Papayianni, 2005; Velosa et al. 2007). 40°C dried samples were placed in the vacuum chamber two levels on top of each other with the help of meshes with minimum contact (Figure 2.3- 71). In order to provide the full access of water into pores air was vacuumed. After vacuuming, filled with distilled water and 24 hours left immersed. Calculations are carried out by using following equations (Eq 2.3.3- 2.3.6)

$$WAC\ (\%) = ((M_{saturated}-M_{dry})/M_{dry})x100 \qquad \text{eq. 2.3.3}$$

$$OP\ (\%) = ((M_{saturated}-M_{dry})/(M_{dry}-M_{immersed})x100 \qquad \text{eq. 2.3.4}$$

$$AD\ (g/cm^3) = (M_{dry} / (M_{saturated} - M_{immersed})) \times 100 \qquad \text{eq. 2.3.5}$$

$$RD\ (g/cm^3) = (M_{dry} / (M_{dry} - M_{immersed})) \times 100 \qquad \text{eq. 2.3.6}$$

M_{dry} = weight of dry sample,

$M_{immersed}$ = weight of sample in the water and

$M_{saturated}$= weight ofwet and wiped sample



Figure 2.3- 71. Vacuum chamber used in the saturation test

Saturation experiment was predicated by European Standard UNE-EN 1936:2007 water absorption capacity (WAC), open porosity (OP), apparent (AD) and real densities (RD) were determined by water vacuum saturation. Every testing period same group of samples were used. In total saturation test was conducted on 72 mortar specimens.

2.3.16 Water absorption through capillarity

Capillary rise is, by definition, the upward movement of ground water through a permeable wall structure causing the appearance of rising damp into the structure (Alfano et al. 2006).

Stefanidou and Papayianni (2005) examined the role of aggregates on the structure and behaviour of lime mortars by studying the influence of the aggregate content and the grain size on strength, porosity and volume stability of the mortars. They also measured capillary water penetration by suction according to the Normal 11/85 Karoğlou et al. (2013) besides studied the water vapour transfer rate of repair coated and uncoated plasters, used for masonries suffering by rising damp phenomena. Moreover they performed an ageing test with repeated cycles of capillary absorption of sodium sulphate solution, on brick–plaster-coating systems in accordance with Normal 11/85. Maravelaki-Kalaitzaki et al. (2003) conducted a research with hydraulic restoration mortars and presented the results of the physico-chemical characterization of original mortars and plasters and the evaluation of the repair ones prepared with natural hydraulic lime (NHL) as binding material and siliceous sand and crushed brick as aggregates. Water absorption measurements were carried out and the test was performed according to the methodology described in the normal UNI 10859.



Figure 2.3- 72. The experimental set up capillary test

For the water capillary rise experiment was done by adapting the European Standard for mortars UNE-EN 1015-18 (Figure 2.3- 72). The capillarity coefficient by contact between instants t_1 and t_2 ($Ccct_2$-t_1) is then calculated through the following expression:

$Ccct_2$-t_1 = (M2- M1)/(t_2-t_1).

Every testing period same group of samples were used. In total capillarity test was conducted on 72 mortar specimens. In the calculations 5, 10 and 90 minutes are taken into consideration.

3 Results of characterization of Roman mortars

This chapter presents the results of the analyses for the characterization of the Roman mortars of Complutum, Mérida, Nysa and Labraunda.

3.1 Complutum Archaeological Site

As it was illustrated in the previous chapter (Figure 2.3-56) two types (*opus caementicium* and *opus signinum*) mortars were collected from wall of *Criptoporticus*, Basilica shops, South Bath canalization and wall between *frigidarium, specus* of water supply lines and *tepidarium*, Monumental Facade, *Cuadriportico*, House of Marte and Atrio, floors of North and South Bath and pillars of Zulema bridge.

Collected samples were characterized multi-analytically. The results of the utilized techniques were described in macroscopic, physical, petrographic, mineralogical, and geochemical order.

3.1.1 Macroscopic description of the samples

Macroscopically *opus caementicium* mortars *in* Complutum site were porous mortars had white, crème, light brown colour binders with small size aggregates. They were consistent mortar with high cohesion. Poorly to well sorted grain size distribution was dominant. Lime lumps were visible by naked eye in the majority of samples. Binders had whitish light brown colour and light and dark to light sub-angular to angular sand grains (< 2 mm) and white colour quartz grains were observed. Pore and grain sizes were various, grain size distribution was poorly sorted (Figure 3.1-1). Detailed macroscopic description of every studied mortar sample was presented in appendix.

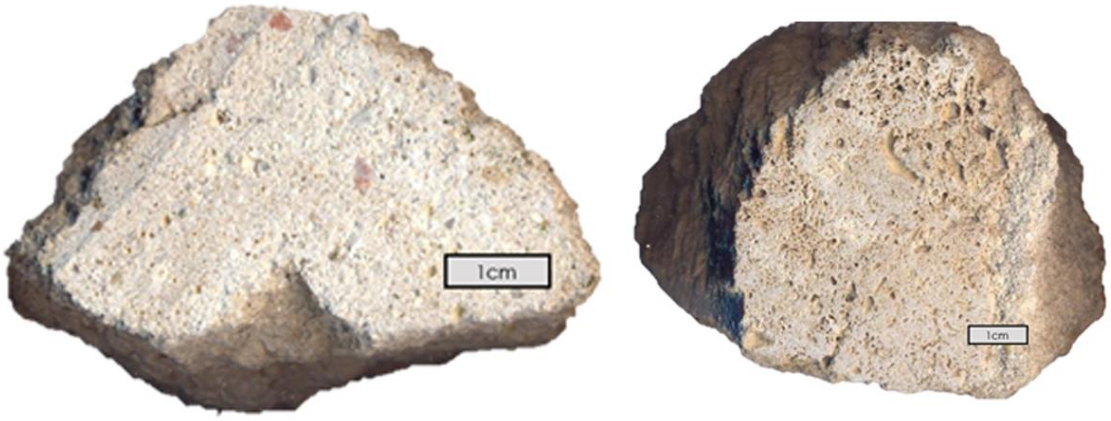


Figure 3.1-1. Examples of *Opus Caementicium* mortars (CM03 on the left, CM18 on the right, scale: 1 cm)

On the other hand *opus signinum* mortars which had reddish colour with the use of ceramics were encountered as coating mortar in separation wall between the *tepidarium* and the *caldarium* North Bath wall pool, *hipocaustum and frigidarium* floor and Cuadriportico, sewer and bridge pillar. The cohesion of the mortars was lower. Angular sub-angular ceramic aggregates were bigger in size and medium to well sorted in reddish colour matrix. Mortars of that type owned lower cohesion. Binder had reddish colour and angular ceramic aggregates (< 50 mm) were observed. Grain size distribution was medium to well sorted. Unlikely, sample CM07, coating mortar in the pool, had very big size angular ceramic aggregates and whitish binder (Figure 3.1-2).



Figure 3.1-2. Examples of *Opus signinum* mortars (CM10 on the left, CM07 on the right, scale: 1 cm)

3.1.2 Colour Spectrophotometry

The colours of both types of characteristic mortars of the site, determined by the spectrophotometry technique (see 2.1.6), showed different parameters. The *opus caementicium* mortars had high luminosity (70-85 units) and saturation between 5 and 15 units. In *opus signinum* the luminosity was less than 70 units (68-55) and the degree of saturation was higher than that of *opus caementicium* (Figure 3.1-3).

In the lightness vs saturation graph, the majority of samples were located in the zone (8-18,70-85) which indicated that were very pale whereas CM05,CM10,CM15,CM25 were located in (20,65) which indicated the tone between greyish and very pale, and CM13, CM24 were further away from them (25,58) which meaned they were dull (Figure 3.1-3).

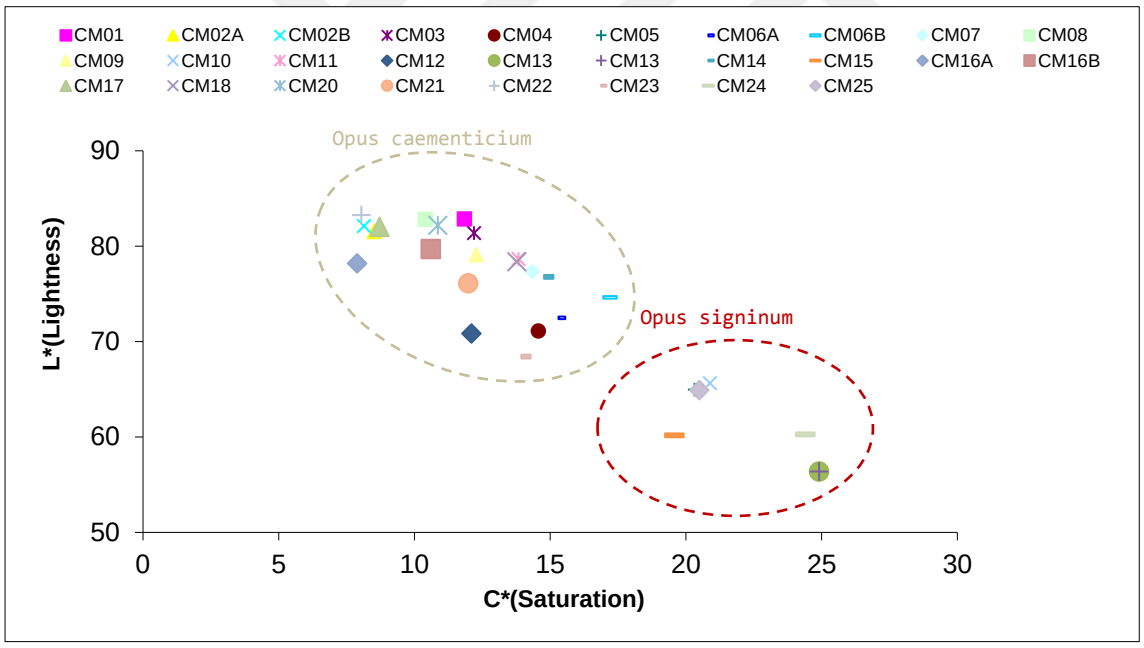


Figure 3.1-3. Lightness vs Saturation of Complutum mortars

M05, CM10, CM25 were *opus signinum* mortars with reddish colour whereas CM15 was *opus caementicium* in brick arch of separation wall between *tepidarium* and *caldarium*. CM13 and CM24 were the mortars in sewer and abundant with brick and tile fragments.

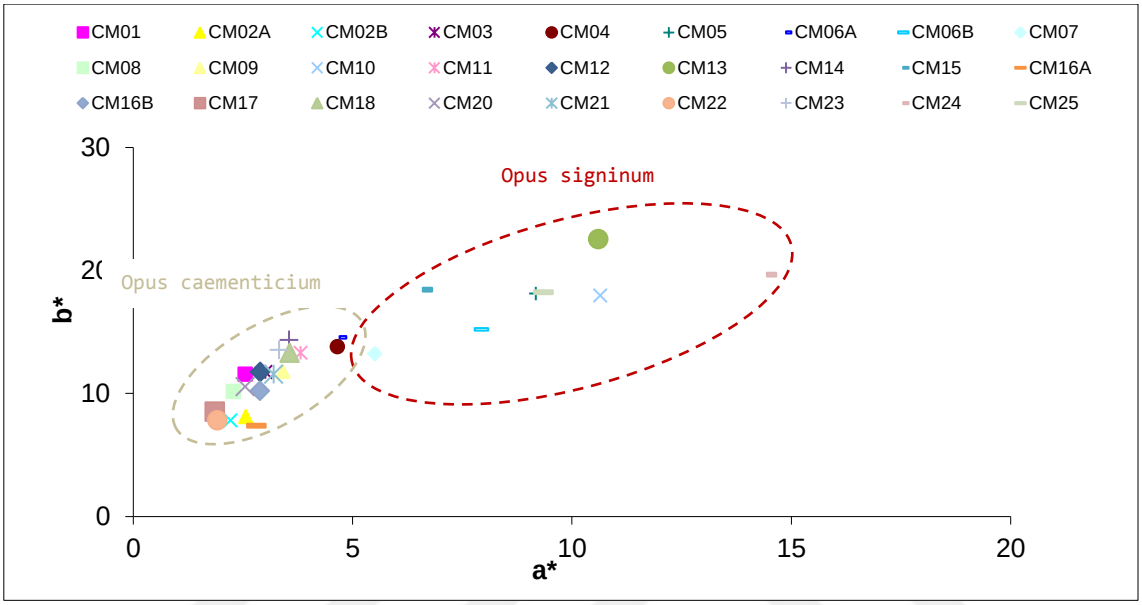


Figure 3.1-4. a* vs b* of Complutum mortars

The colour tone was also different between the two types of mortars. The *opus caementicium* presented lower values for the parameters a * and b *, while the *opus signinum* gave values indicating pinkish tone that was caused by the incorporation of brick dust. (Figure 3.1-4).

In the a* vs b* graph, the majority of samples were located in the zone (4.5,14), CM07 (5.5,13), CM15 (6.6,18.5), CM06B (8,15.2) whereas CM05, CM25 were located in (9,18) which indicated more reddish and yellowish range and CM10, CM13 were in the zone (10.6,23) and CM24 were further from them (14.5,20) (Figure 3.1-4). From spectrophotometry white and yellow indexes were obtained and as in concordance with other chromatic parameters

opus signinum mortars had negative values in white index and higher values in yellow index. *Opus caementicium* mortars showed higher white index and yellow index values around 10 (Figure 3.1-5).

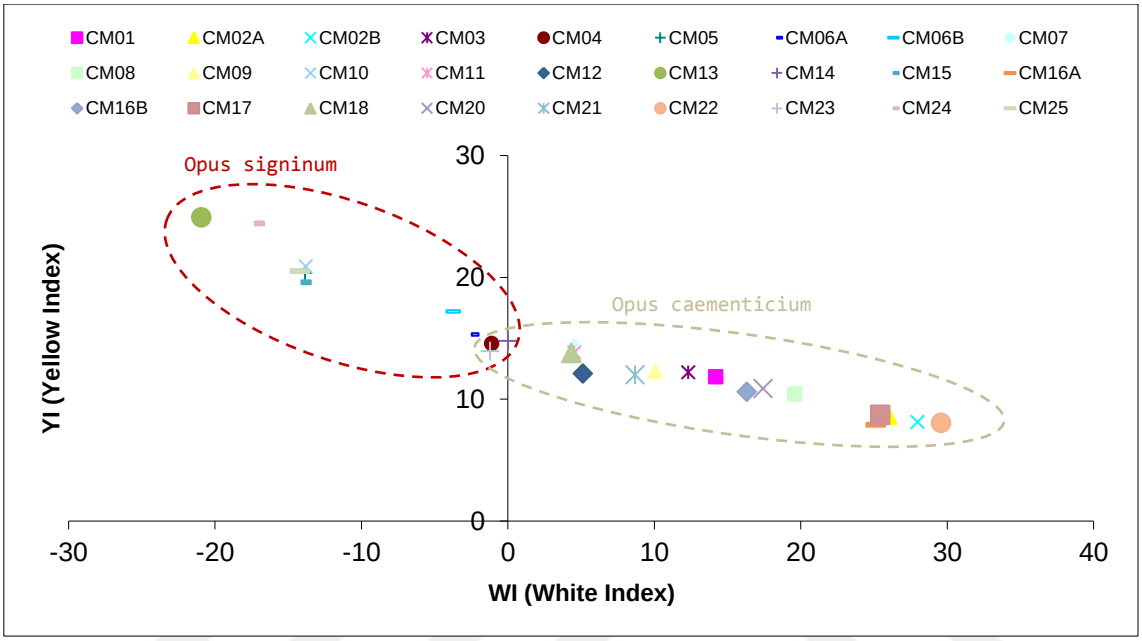


Figure 3.1-5. White index vs yellow index of Complutum mortars

3.1.3 Surface Hardness

As shown in the Figure 3.1-6 the mortar samples had highly variable surface hardness values changing between 84 leebs (CM05) and 442 leebs (CM02a). CM02a and CM02b showed the highest hardness values. They were second phase construction mortars of *Criptoporticus*. The mortar which belongs to first phase of construction had 143 leebs.

As it can be seen, the minimum hardness value is CM05 – coating mortar in the first phase of construction in North Bath, it can be assumed that it was due to type of mortar: *opus signinum* although other same type mortars showed higher strengths (e.g: CM07). It should be kept in mind that small sizes of the samples were used in the test.

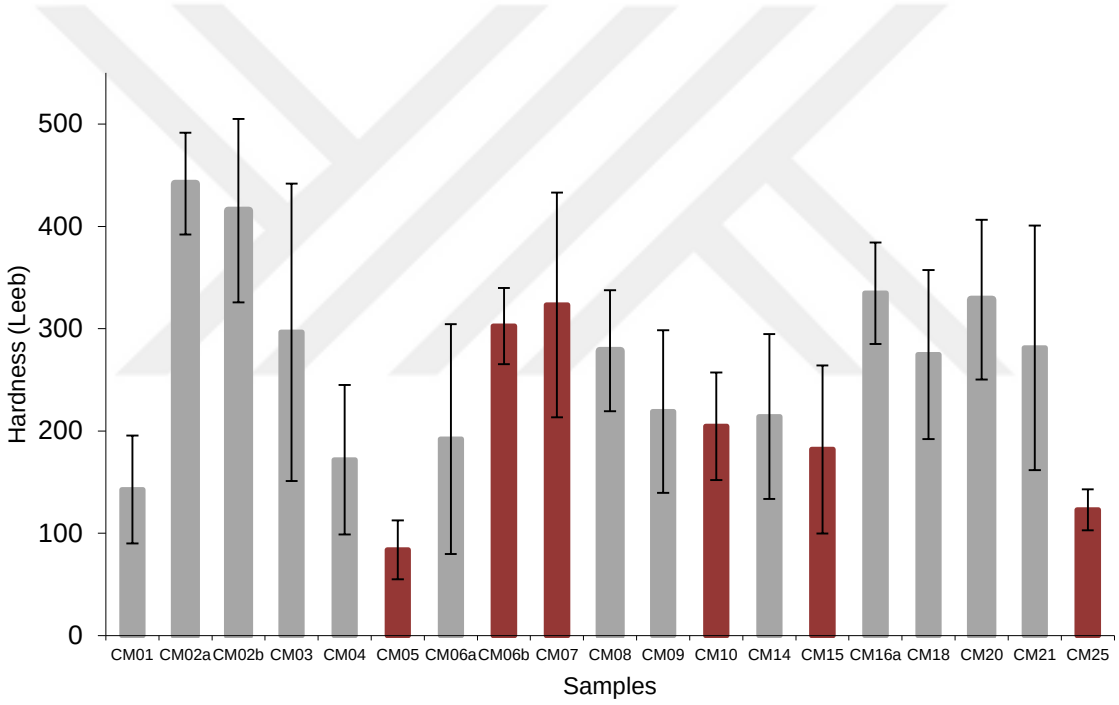


Figure 3.1-6.Surface hardness of Complutum mortars (grey: *opus caementicium*, red: *opus signinum*)

Sample which had the lowest superficial strength, CM05 and CM01 had more alkali reactive aggregate and less binder, according to XRF results, the low resistance could be related to this phenomenon. Nevertheless, samples CM02, CM08, CM16a had more aggregate than the binder as well, at the same time higher superficial strength.

3.1.4 Optical Microscopy

Regarding the classification of the mortars that we did as *opus caementicium* and *opus signinum* with their ceramic fragment, the petrographic observations varied.

Opus caementicium mortars had the binder (25% -50%) is of calcitic composition with angular and sub-angular grains of quartz (25%) of a size of 0.1-3.8 mm, together with feldspar and biotite, and sandstone, quartzite, slate and chamotte (Figure 3.1-7).

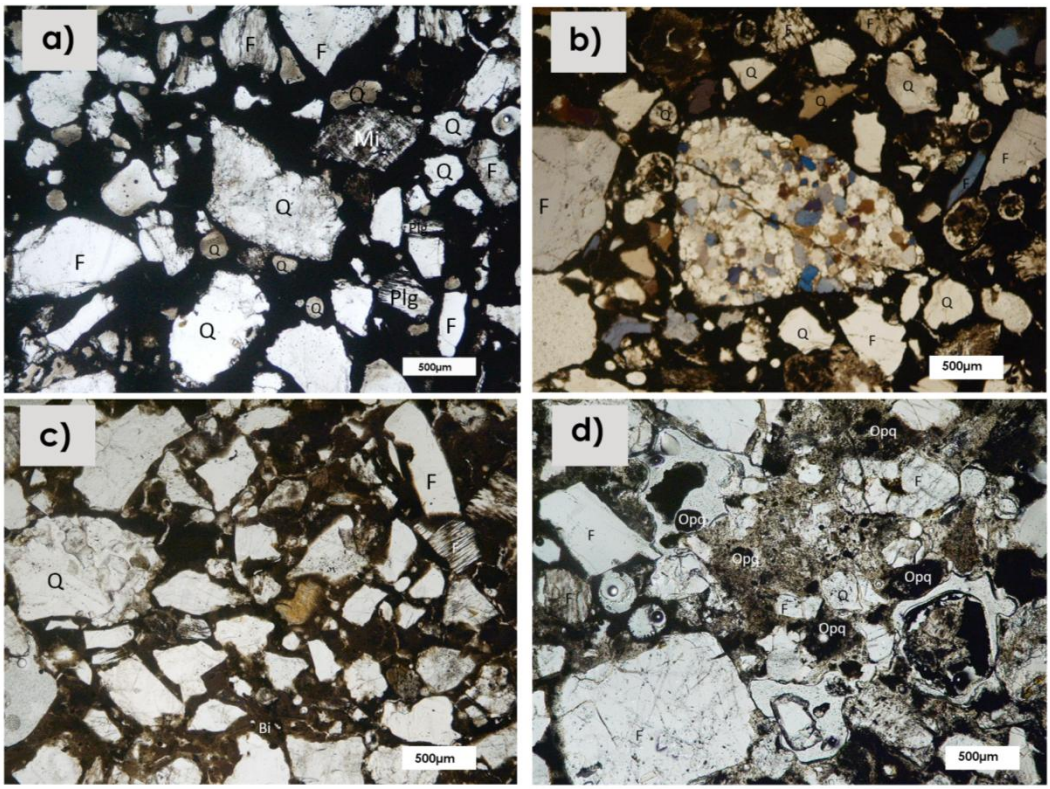


Figure 3.1-7. *Opus caementicium* mortars (a) CM01 plane polarized light b) sandstone in the middle of thin section image CM09 cross polarized light, c) CM11 plane polarized light, d) CM35 plane polarized light), Q: quartz, F: feldspar, Mi: microcline, Plg: plagioclase

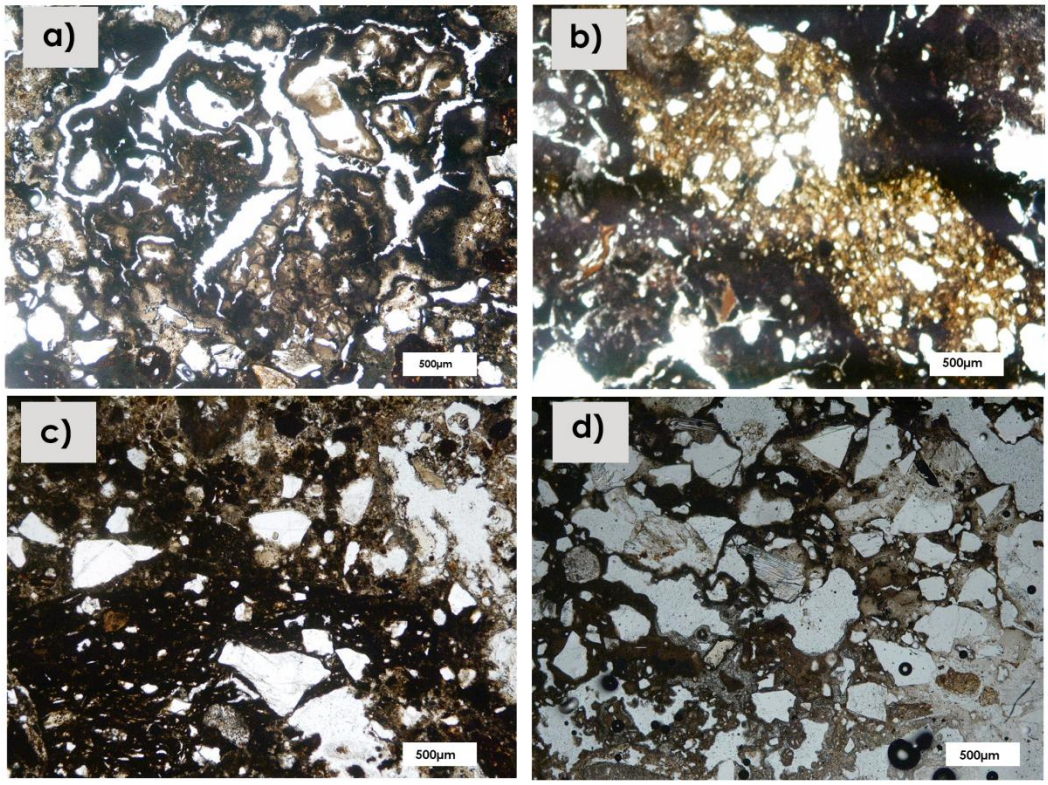


Figure 3.1-8. *Opus signinum* mortars (a) CM05 cross polarized light b) CM07 plane polarized light, c) CM10 plane polarized light, d) CM24 plane polarized light)

The mineralogical composition of *opus signinum* mortar was similar to that used in *opus caementicium*, differing in a greater amount of potassium feldspar, clayey appearance of binder and aggregate distribution. Under the microscope the binder was porous calcite, with medium-well sorted angular and sub-angular grains consisting mainly of quartz with a size of 100-600µm. The percentage of binder was 50% and of quartz grains of 30% (Figure 3.1-8).

In the majority of *opus caementicium* medium to well sort distributed aggregates were embedded in microcrystalline calcite binder. Lime lumps were seen and cracks in binder is often (Figure 3.1-9). Aggregates were mainly quartz and feldspar. Particle shapes were irregular and surface textures were changing between angular and sub-angular. It is seen that in Complutum generally silicic sand was used as aggregate, crushed rock fragments were rarely observed (Figure 3.1-10). *Opus signinum* mortars contained rounded to angular ceramic fragments where reactions in the border were discernible in some observations (Figure 3.1-11).

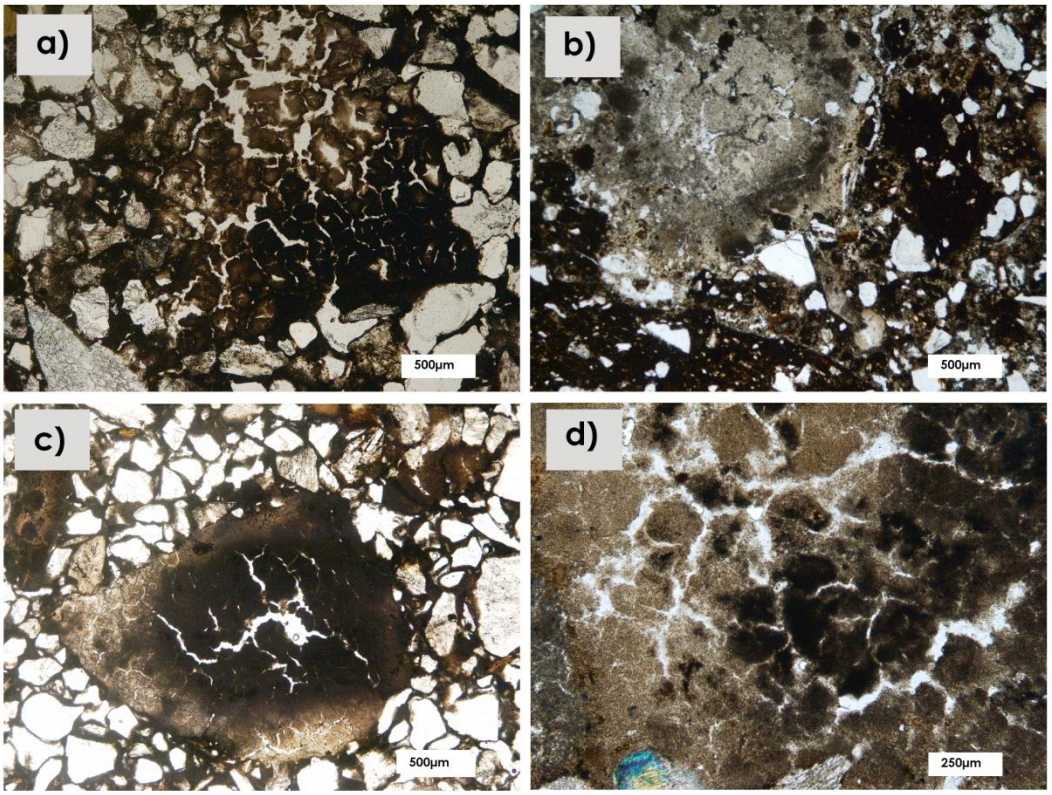


Figure 3.1-9. Lime lumps in a) CM14 b) CM10 c) CM21 d) CM04

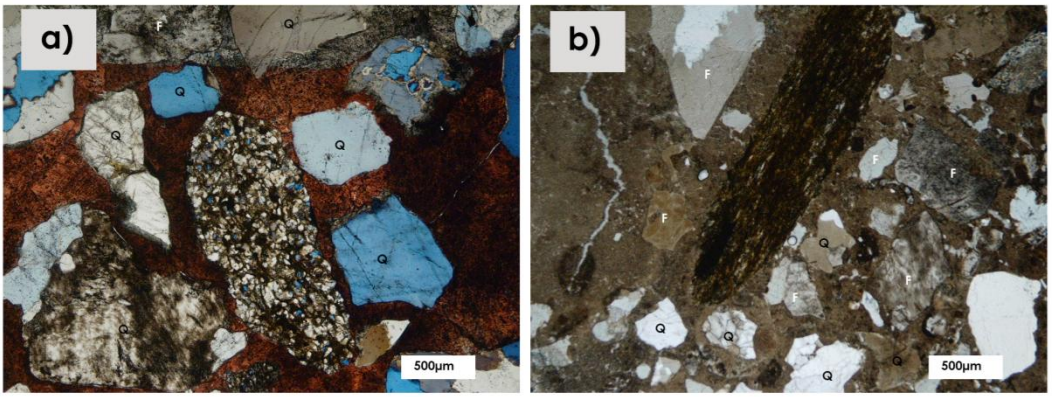


Figure 3.1-10. Photomicrographs a) sandstone in the centre CM02b (cross polarized light), b) slate in CM04 (plane polarized light Q: quartz, F: feldspar,

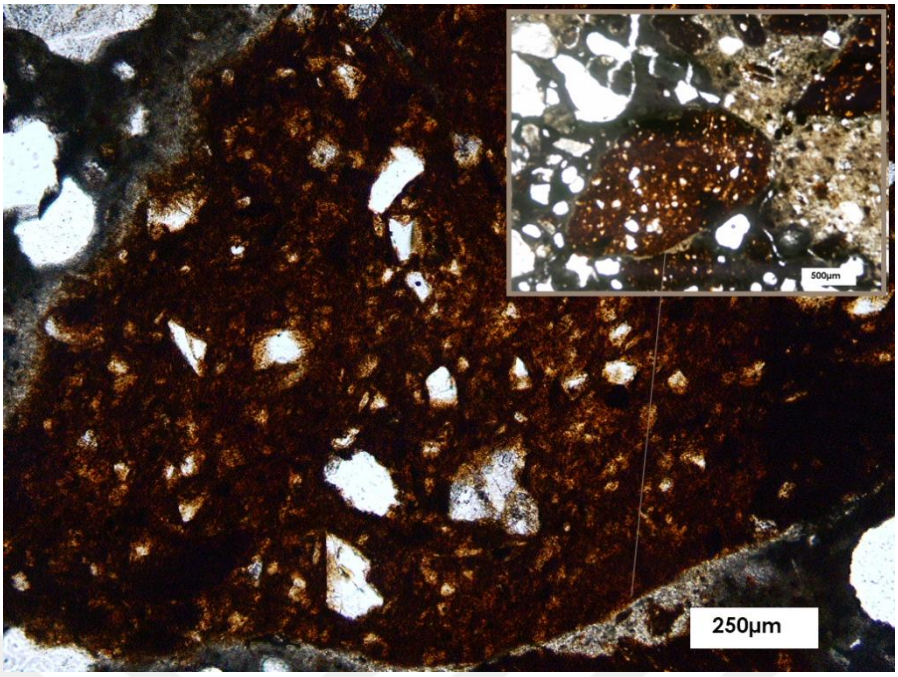


Figure 3.1-11. Rounded ceramic fragment in CM05 with reactions in the border

In sample CM02 and CM16 different binders are worthy of attention. Binder comprised white colour crystalline calcite (Figure 3.1-12), sample CM18 had white colour binder as well but the texture was cryptocrystalline.

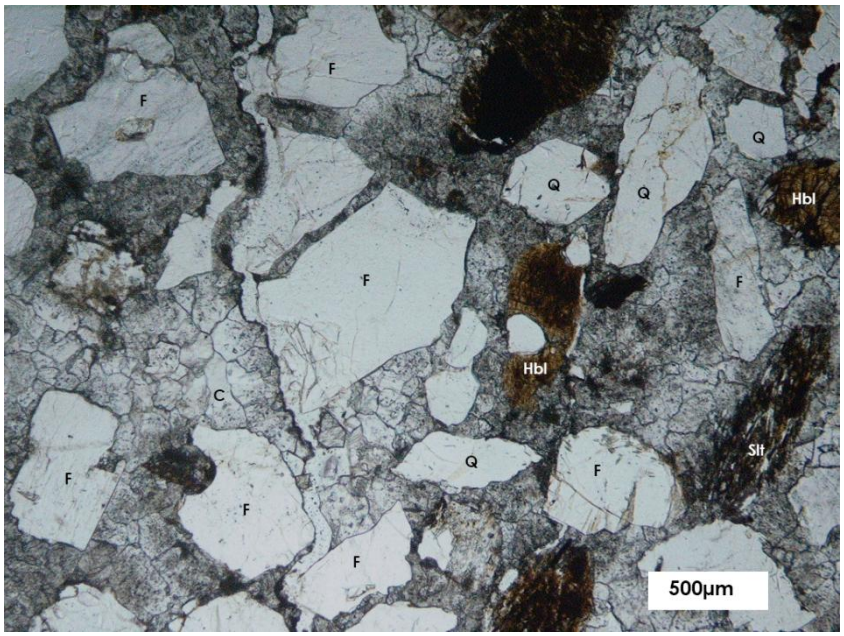


Figure 3.1-12. Photomicrograph of CM02a, Q: quartz, F: feldspar, Hbl: hornblende, Slt: slate, C: calcite

Table 3.1-1. Petrographical constituents of Complutum mortars (Qtz: quartz, Fsp: feldspar, Bt: biotite, Ms: Muscovite, Aug: augite, Px: pyropxene, Op: opaque mineral, Plg: Plagioclase, shr: shrinkage, pol: Qtz polycrystalline, crp: Qtz cryptocrstalline, inc.: inclusion).

	Samples	Binder	Minerals	Lithic and ceramic fragments, additives, others
Opus Caementicium	**CM01** Criptoporticus wall	Dark colour micritic calcite	Qtz, Fsp, Bt	
	CM02a Criptoporticus wall	White crystalline calcite	Qtz, Fsp	Slate clay
	CM02b Criptoporticus wall	White crystalline calcite	Qtz, Pl	sandstone
	CM03 North Bath wall	Dark colour micritic calcite	Qtz, Pl, Aug	
	CM04 North Bath wall	Brown colour micritic calcite, locally overburnt	Qtz, Fsp, Aug	Slate, chamotte, lime lump,
	CM06a North Bath floor	Brown colour micritic calcite, reaction zones recrytallization	Qtz, Fsp, Aug	Dark grey rock fragment
	CM08 North Bath wall	Dark colour micritic calcite	Qtz, Fsp, Aug	
	CM09 North Bath facade	Dark colour micritic calcite	Qtz, Fsp	sandstone
	CM11 Basilica wall	Dark colour micritic calcite	Qtz, Fsp, Op	
	CM14 South Bath wall	Brown colour micritic calcite, locally overburnt local recrystallization	Qtz, Fsp	lime lump, slate, ceramic

	CM15	South Bath brick arch	Dark colour micritic calcite	Qtz, Pl, Btferric incl.	Quartzite, lime lump
	CM16a	Sewer	White crystalline calcite recrystallization?	Qtz, Fsp, Op, Px	Ferric inclusions, quartzite, slate
	CM16b	Sewer	White crp calcite recrystallization	Qtz, Fsp, Bt	
	CM17	Sewer rendering	Dark colour micritic calcite clay?	Qtz, Fsp	
	CM18	Sewer	White cryp calcite recrystallization	Qtz, Fsp, Bt,	Slate/schist, polycrystalline Qtz, chamotte
	CM20	Monumental facade	White and dark cryp calcite recrystallization	Qtz, Fsp	underburnt lime lump
	CM21	Cuadriportico foundation	Dark colour micritic calcite	Qtz, Fsp, Bt	overburnt lime lump
Opus Signinum	**CM28**	North Bath frigidarium floor 2	Dark colour micritic calcite	Qtz, Fsp, Bt	
	CM05	North bath	Dark colour micritic calcite, reaction zones	Qtz, Fsp	Cracks and pores, slate
	CM06b	North Bath floor	Brown colour, reaction zones recrytallization	Qtz, Pl, clay, Op,	Old mortar, ceramic
	CM07	North Bath pool coating	Dark colour micritic calcite, reaction zones	Qtz, Pl, Bt,aug	Cracks, ceramic

	CM10	North Bath coating	Dark colour micritic calcite local recrystallization	Qtz, Pl, Ms, Op,	Ceramic lump,
	CM24	Sewer of House of Marte	Dark colour micritic calcite local recrystallization burnt parts	Qtz, Fsp, pyx	Reactive lithic fragment with rxtn rim, ceramic
	CM25	House of Atrium coating	Dark colour micritic calcite local recrystallization burnt parts	Qtz, Fsp	Charcoal, ceramic, reactive clast
	CM35	Arch pillar	White and dark colour micritic calcite Local recrystallization	Qtz, Fsp, Ms,	schist

3.1.5 Binder aggregate ratio and grain size distribution

After HCl attack soluble parts of the mortars were accepted as binder and insoluble parts as aggregates, as no calcitic grain was detected in microscopic observations. Percentages of binders and aggregates of the samples are listed below (Table 3.1-2).

Table 3.1-2. Acid soluble insoluble ratios (%) of Complutum mortars

		Samples	Binder%	Aggregate %	B:A
Opus Caementicium	**CM01**	Criptoporticus wall	48.51	51.49	1:1
	CM02a	Criptoporticus wall	33.02	66.98	1:2
	CM06a	North Bath hipocaustum floor	64.88	35.12	1:1
	CM08	North Bath frigidarium wall	31.83	68.17	1:2
	CM14	South Bath frigidarium wall	14.79	85.21	1:6
	CM15	South Bath brick arch	30.37	69.63	1:2
	CM16	Sewer	20.67	79.33	1:4
	CM18	Sewer vault	22.39	77.61	1:3
	CM22	Cuadriporticus floor	23.21	76.79	1:3
	CM29	North Bath frigidarium floor bottom level	55.80	44.20	1:1
	CM31	South Bath frigidarium floor	32.74	67.26	1:2
	CM33	South Bath caldarium floor	54.47	45.53	1:1
	CM38	Pillar of bridge	46.51	53.49	1:1
Opus Signinum	**CM05**	North Bath hipocaustum wall	33.90	66.10	1:2
	CM10	North Bath frigidarium coating	26.68	73.32	1:3
	CM26	North Bath frigidarium floor highest level	33.01	66.99	1:2
	CM34	Pillar of arch	26.91	73.09	1:3

As seen in Figure 3.1- 13 Complutum mortars proportions were distributed between 1:1 and 1:4 binder aggregate ratio (B:A).

CM01, CM06a, CM29, CM33 and CM38 had 1:1 B:A ratio. Indeed CM06a had less amount of aggregate; the reason for having this result might be the solution of carbonate aggregate in acid attack. B:A ratio of sewer mortar (CM16) is 1:4.

Grouping the mortars according to function was not possible because wall mortars from Criptoporticus (CM01 and CM02a) had 1:1 and 1:2, respectively, while mortars from walls of North Bath (CM05 and CM08) had both 1:2 and CM14 the sample from the wall of South Bath *frigidarium* showed 1:6. The variation could be related with the dimension of the aggregates.

Floor mortars in North Bath (CM26) and South Bath (CM31) had 1:2 ratio whereas floor mortar in *Cuadriporticus* (CM22) had 1:3. Mortars from arches CM15 and CM18 had 1:2 and 1:3 B:A ratios, respectively. Coating mortar (CM10) and pillar of Arch (CM34) belonging to *opus signinum* type had 1:3 ratio.

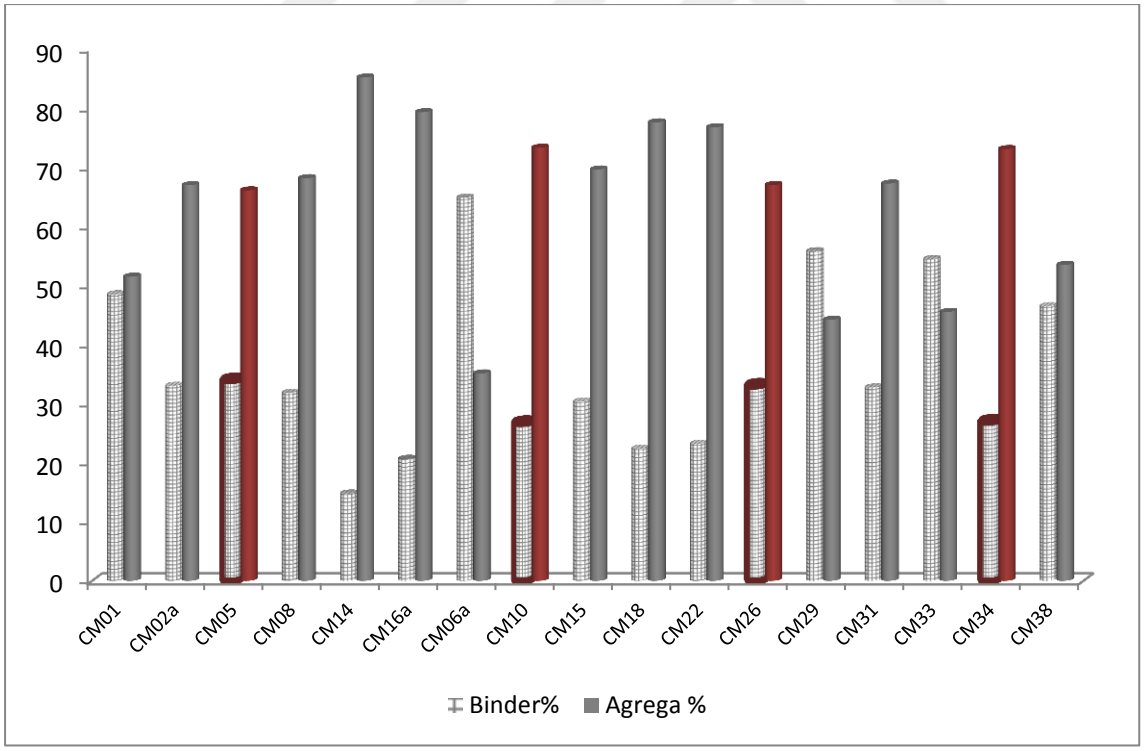


Figure 3.1- 13. Binder aggregate ratios of Complutum mortars (reds are *opus signinum* mortars)

Table 3.1-3. Weight passing each sieve in Complutum mortars

	Samples		>2mm	1<x<2 mm	0,5<x<1 mm	0,25<x<0,5 mm	0,063<x<0,25 mm	<0,063 mm
Opus Caementicium	**CM01**	Criptoporticus wall	0,91	8,51	45,47	33,15	10,51	1,45
	CM02a	Criptoporticus wall	0,63	15,85	50,31	22,89	9,43	0,88
	CM06a	North Bath *hipocaustum* floor	10,91	21,82	27,27	35,15	4,24	0,61
	CM08	North Bath *frigidarium* wall	0,28	6,75	44,16	32,63	14,77	1,41
	CM14	South Bath *frigidarium* wall	3,36	9,63	34,49	44,79	6,94	0,78
	CM15	South Bath brick arch	1,98	14,98	39,65	32,82	8,59	1,98
	CM16a	Sewer	3,84	4,32	45,86	36,25	8,88	0,84
	CM18	Sewer vault	0	9,57	38,03	41,4	10,35	0,65
	CM29	North Bath f floor bottom	21,07	18,67	27,36	20,89	6,47	5,55
	CM31	South Bath *frigidarium* floor	5,6	12,39	25,96	31,27	20,35	4,42
	CM33	South Bath *caldarium* floor	26,09	36,41	11,41	9,51	15,22	1,36
	CM38	Pillar of bridge	2,99	15,61	41,86	27,91	9,63	1,99
Opus Signinum	**CM05**	North Bath *hipocaustum* wall	12,89	16,05	26,79	31,09	12,46	0,72
	CM10	North Bath *frigidarium* coating	40	13,06	14,17	16,11	14,44	2,22
	CM26	North Bath *frigidarium* floor 4	53,35	12,54	8,45	15,45	8,75	1,46
	CM34	Pillar of arch	0	12,49	30,46	44,24	12,38	0,43

As seen in Figure 3.1- 14 grain size distribution of *opus signinum* mortars of coating (CM10) and floor (CM26) were identical, having the highest mass due to big ceramic aggregates (> 2mm). Other floor mortars (CM29 and CM33) of *opus caementicium* type had high values above 2mm, large sand aggregates, as well.

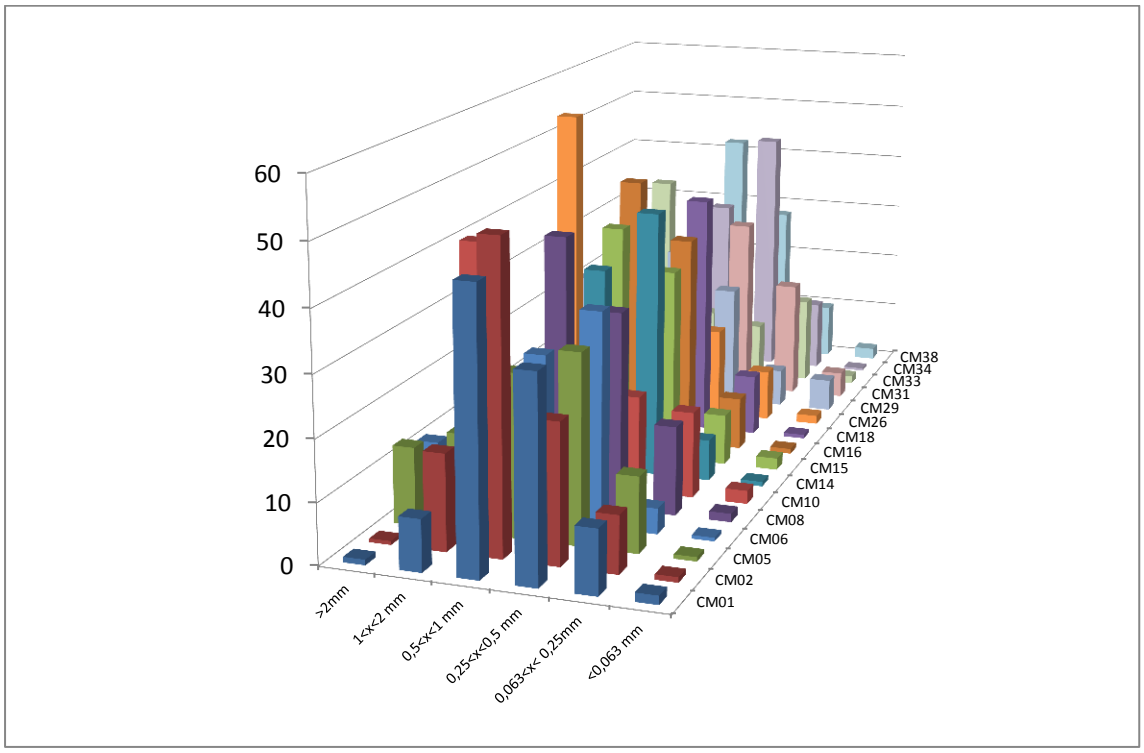


Figure 3.1- 14. Grain size distribution graph of Complutum mortars

Fine particles below 63µm generally included ceramic dust and/or additives. Coating mortar (CM10) supported the idea; however, in this case floor mortars (CM29 and CM31) had the highest values which may indicate pozzolanic additives. On the other hand, oddly enough other *opus signinum* mortar CM05 had low amount of fine particle.

3.1.6 X-Ray Diffraction

As it is illustrated in Figure 3.1- 15 and Table 3.1- 4, main constituents of Complutum mortars were quartz and calcite. Feldspar (albite and anorthite) was the secondary mineral that was found predominantly. *Opus signinum* mortars (CM05, CM10, CM13, CM23, CM26, CM27, CM33) had mica (biotite and muscovite) peaks coming from ceramic addition. Samples CM01 and CM02A showed gypsum peaks, as it is not seen in other samples it is thought to be present due to the air pollution, also different binder appearance could be related with gypsum.

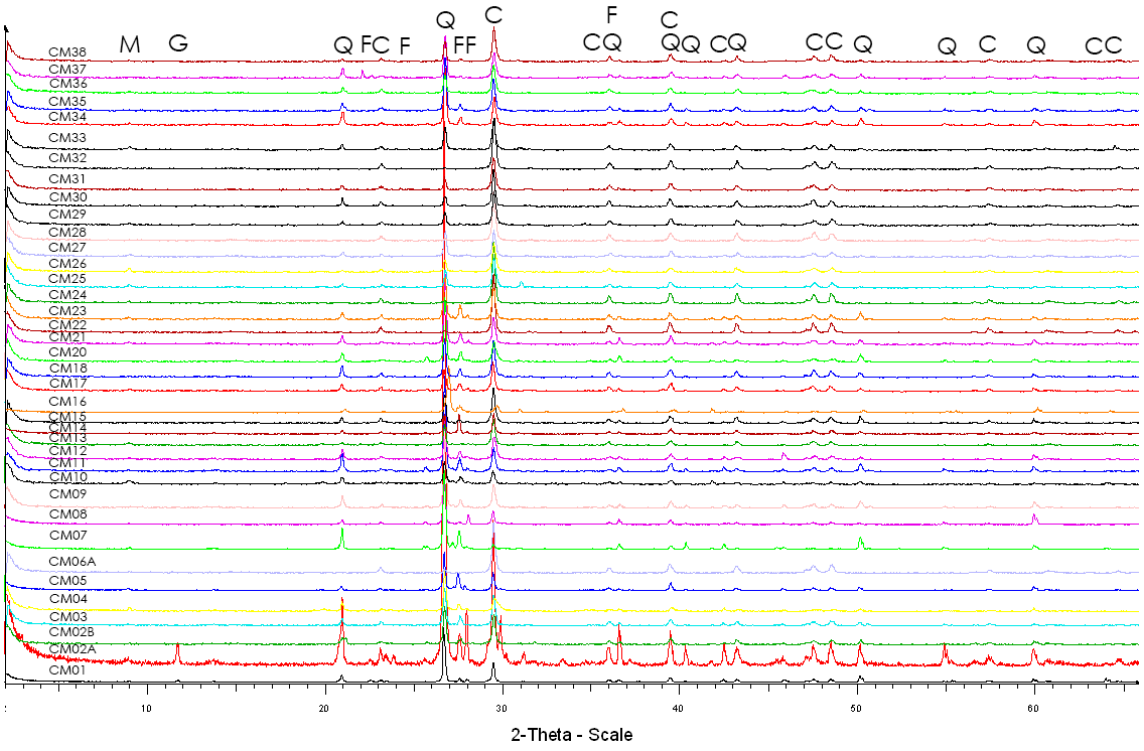


Figure 3.1- 15. XRD patterns of Complutum mortars (Q: quartz, C: calcite, F: feldspar, M: mica, G: gypsum)

Table 3.1- 4. Semiquantitative XRD analysis of Complutum mortars (++++: primary mineral, ++: secondary mineral, +: present, tr: trace)

	Samples		Quartz	Calcite	Feldspar	Mica	Gypsum
Opus caementicium	**CM01**	Criptoportico wall	++++	++	+	tr	+
	CM02a	Criptoportico wall	++++	++	+		+
	CM02b	Criptoportico wall	++++	++	+		

	CM03	North Bath wall	++++	++	+	
	CM04	North Bath wall	++++	++	+	+
	CM06a	North Bath floor	++	++++		
	CM08	North Bath wall	++++	++	+	+
	CM09	North Bath facade	++++	++	+	
	CM11	Basilica wall	++++	++	+	
	CM12	South Bath wall	++++	++	+	
	CM14	South Bath wall	++	++++	++	+
	CM15	South Bath brick arch	++	++++	+	
	CM16a	Sewer	++++	++	+	
	CM17	Sewer rendering	++	++++	+	+
	CM18	Sewer	++++	++	+	
	CM20	Monumental facade	++++	++	+	
	CM21	Cuadriportico foundation	++++	++	+	tr
	CM22	Cuadriportico floor	tr	++++		
	CM28	North Bath frigidarium floor 2	tr	++++		
	CM29	North Bath frigidarium floor bottom	tr	++++		
	CM30	South Bath wall	+	++++		
	CM31	South Bath Caldarium floor	++	++++	tr	
	CM32	North Bath floor	tr	++++		
	CM33	North Bath floor	++	++++		+
	CM36	Arch pillar	++	++++		
	CM38	Bridge pillar	++	++++	tr	
Opus signinum	**CM05**	North Bath coating	++++	++	++	+
	CM07	North Bath coating	++++	++	+	+
	CM10	North Bath coating	++++	++	++	+
	CM13	South Bath coating	++	++++	+	+
	CM23	Cuadriportico floor	++++	++	++	+
	CM24	House of Marte sewer	tr	++++		tr
	CM25	House of Atrium coating	++	++++		+
	CM26	North Bath frigidarium floor highest l.	++	++++	tr	+
	CM27	North Bath frigidarium floor 3	+++	++++	tr	+
	CM34	Arch pillar	++++	++	+	tr
	CM35	Arch pillar	++++	++	+	
	CM37	Bridge pillar	++++	++		

3.1.7 Thermogravimetric Analysis (TGA-DSC)

From the results of TGA/DSC analyses of the samples (Table 3.1- 5), percentages of weight losses up to 120°C, between 120-200°C, 200-600°C and 600-800°C were calculated which attribute to the loss due to hygroscopic water, gypsum dehydration, structurally bound water of hydraulic compounds and decomposition of calcium carbonate ($CaCO_3$), respectively (Moropoulou et al. 2000; Bonazza et al., 2013).

Table 3.1- 5.Weight losses (%) of the mortar samples

	Samples		<120°C	120-200°C	200-600°C	600-800°C	CO_2/H_2O
Opus Caementicium	CM01	Criptoporticus wall	1.44	0.42	2.71	9.48	3.50
	CM02	Criptoporticus wall	1.54	0.75	3.66	6.19	1.69
	CM06A	North Bath floor	0.81	0.31	3.38	37.64	11.14
	CM08	North Bath wall	3.28	1.27	6.75	15.64	2.32
	CM14	South Bath wall	0.77	0.18	2.44	11.77	4.82
	CM15	South Bath brick arch	0.94	0.21	3.88	22.25	5.73
	CM16	Sewer	1.53	0.35	1.51	4.93	3.26
	CM18	Sewer	0.55	0.24	2.02	19.81	9.81
	CM22	Cuadriportico floor	0.27	0.11	1.03	40.64	39.46
	CM28	North Bath floor 2	0.89	0.35	3.61	35.98	9.97
	CM29	North Bath floor bottom	2.01	0.56	3.99	25.91	6.49
	CM31	South Bath floor	2.22	0.69	3.99	21.21	5.32
	CM33	North Bath floor	2.05	0.54	3.21	18.64	5.81
Opus Signinum	CM05	North Bath coating	0.99	0.27	2.31	9.91	4.29
	CM07	North Bath coating	0.29	0.10	1.56	2.81	1.80
	CM10	North Bath coating	3.08	0.81	3.24	7.41	2.29
	CM26	North Bath floor 4	1.54	0.51	3.88	20.15	5.19
	CM27	North Bath floor 3	2.47	0.92	3.61	14.70	4.07
	CM35	Arco pillar	2.50	0.55	2.77	16.85	6.08
	CM37	Bridge pillar	1.56	0.68	4.58	13.93	3.04

The mortars in the floors of North Bath and Cuadriporticus had a higher percentage between 600-800°C. On the contrary, mortars in the South Bath wall and coatings had the lowest values. Figure 3.1- 16 presents the relation of CO_2/H_2O vs CO_2 % which serves to classify the mortars according to their hydraulic character (Bakolas et al. 1998, Moropoulou et al. 2000, Genestar et al. 2006, Cardoso et al. 2014). CO_2/H_2O is inversely related to hydraulicity (Bakolas et al. 1995, Moropoulou et al. 2000). Based on the data and graph, Böke et al. (2008), Uğurlu Sağın (2012) accepted as non-hydraulic mortar when CO_2/H_2O ratio higher than 10 like CM28, CM06 and CM22 by far Unlikely, according to (Moropoulou et al. 2000; Genestar et al. 2006) mortars that had H_2O higher than 3 were so called hydraulic mortars as a result, CM01, CM05, CM07, CM16, CM22 and CM35 do not possess hydraulic properties.

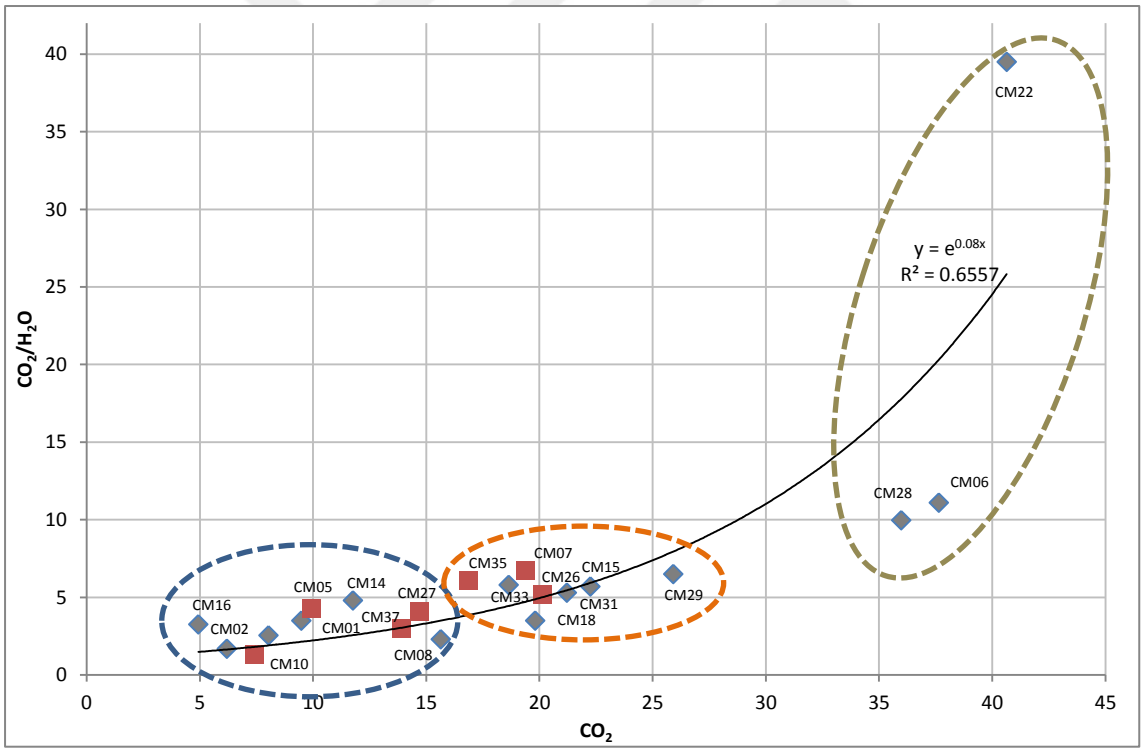


Figure 3.1- 16. CO_2/H_2O vs CO_2% graph of samples

From the graph (Figure 3.1- 16) several groups can be discerned. First group had CO_2/H_2O ratio below 5 and CO2 is below 20 (CM01, CM02, CM05, CM08, CM10, CM14, CM16, CM27, CM37) and can be defined as highly hydraulic lime mortars. The second group had

percentage of CO_2 between 15 and 30 and CO_2/H_2O ratio between 5 and 10 (CM07, CM15, CM18, CM29, CM31, CM33 and CM35) hydraulic lime mortars. Third group can be marked as CO_2 between 35 and 40 and CO_2/H_2O ratio between 10 and 15 (CM28 and CM06A) were true lime mortars according to classification of Moropoulou 2005. CM22 (sample from floor) is true lime mortar with high level of CO_2 or is limestone itself. The data of the TGA analysis of CM08 showed that it is naturally pozzolanic mortar (Moropoulou et al., 2005) CM26, CM27 and CM 31 can be classified as artificial pozzolanic mortars.

Phase transition peak of quartz at 573°C revealed at the thermograms of the samples CM01, CM02, CM05, CM07, CM08, CM14 and CM18 (Figure 3.1-17). From CM01, CM02a, CM08, CM15 had peaks around 120°C which indicate hydrated salts (Figure 3.1-17-Figure 3.1-19, Figure 3.1-20). In the samples having salts weight losses due to decomposition calcium carbonates begin at earlier temperatures. CM02a lost higher weight between 100°C and 150°C generating from gypsum (Figure 3.1- 17).

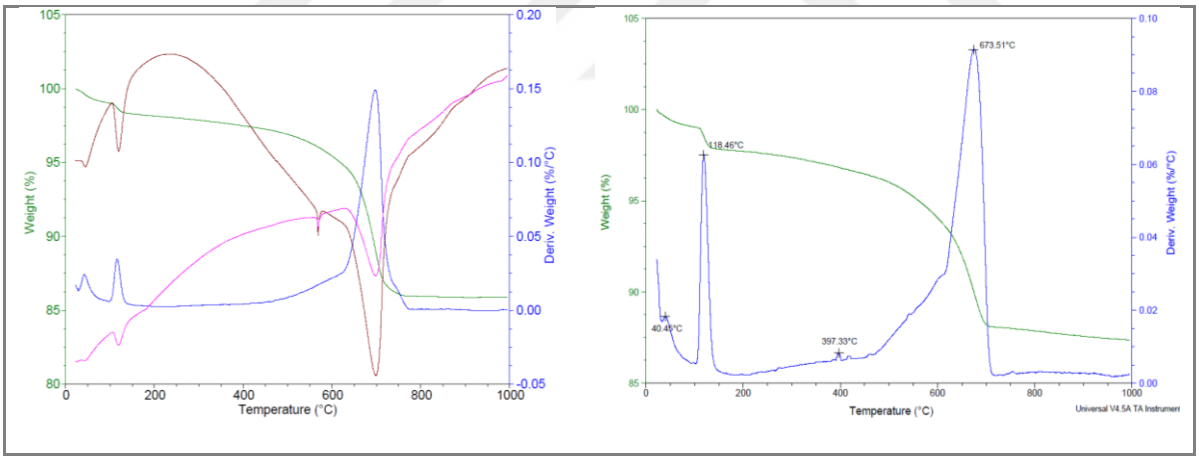


Figure 3.1- 17 Thermogram of CM01 (left) CM02a (right)

In addition, it is seen in Figure 3.1-17 and 18 CM02, CM05 and CM07 had peaks at 400°C in which clays were responsible. Indeed, DTA of sample CM07 had much more amount of peaks than a typical lime mortar. Weight loss around 450°C which is due to the magnesite or portlandite, weight losses at 560°C 720°C 750°C 780-790°C and 830°C, 860°C were generated probably due to clays and recrystallizations (Figure 3.1- 18).

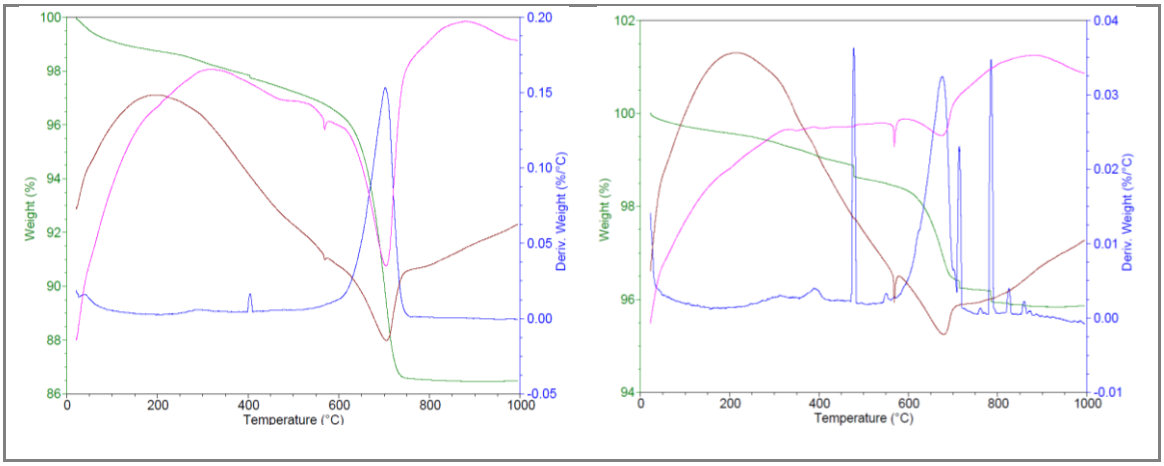


Figure 3.1- 18. Thermogram of CM05 (left) and CM07 (right)

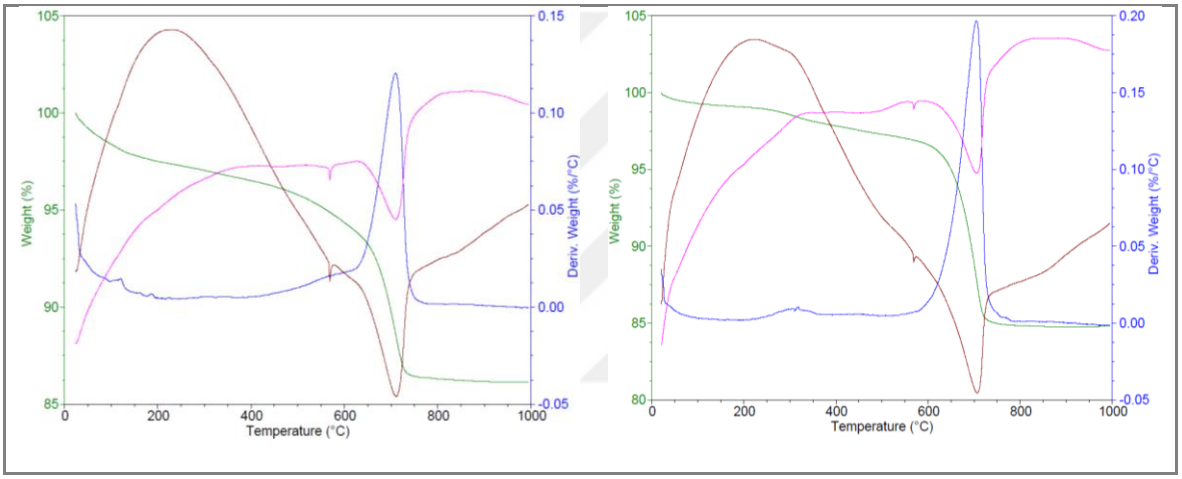


Figure 3.1- 19. Thermogram of CM08 (left) and CM14 (right)

CM14 had a well-marked weight loss between 200 and 400°C which may had caused by clay dehydroxylation (Figure 3.1- 19). CM15 and CM16 had peaks around 800 °C which showed the recrystallization (Figure 3.1- 20).

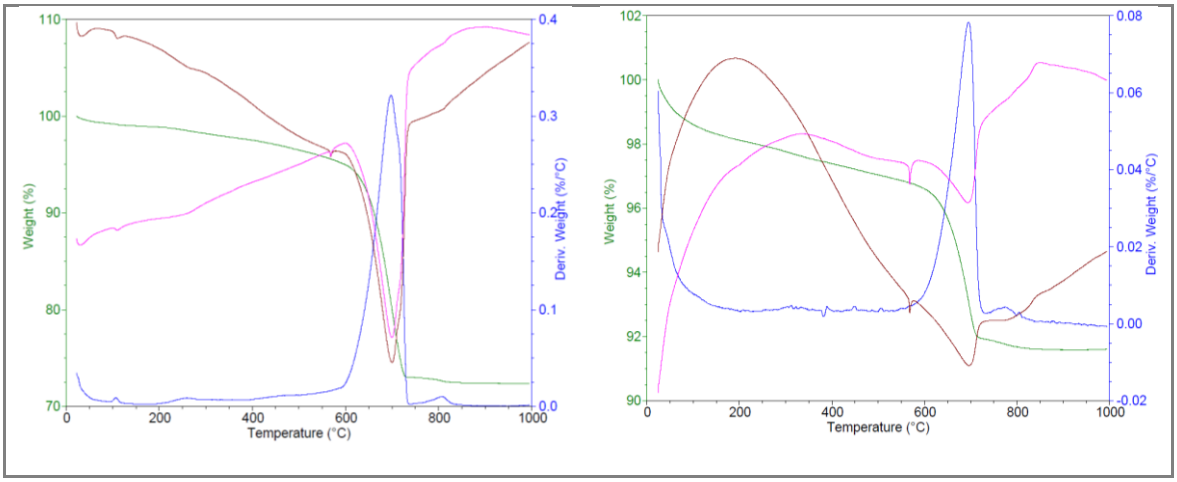


Figure 3.1- 20. Thermogram of CM15 (left) and CM16 (right)

Figure 3.1-21 was plotted to understand the correlation between the acid soluble insoluble parts of the mortars. Putting ahead the sample CM06 which had much higher binder than aggregate, samples were encountered in the zone of binder aggregate ratios between 0.2 and 1.3 on the other hand calcium carbonate percentage was in between 11 and 60%.

As seen below (Figure 3.1- 21) same grouping can be done as the plot of the inverse hydraulicity (CO_2/H_2O) vs CO_2 (Figure 3.1- 16). The aggregate and water ratios were in concordance. Only samples CM01, CM33 and CM29 were situated a bit far from the other samples due to the less aggregate amount.

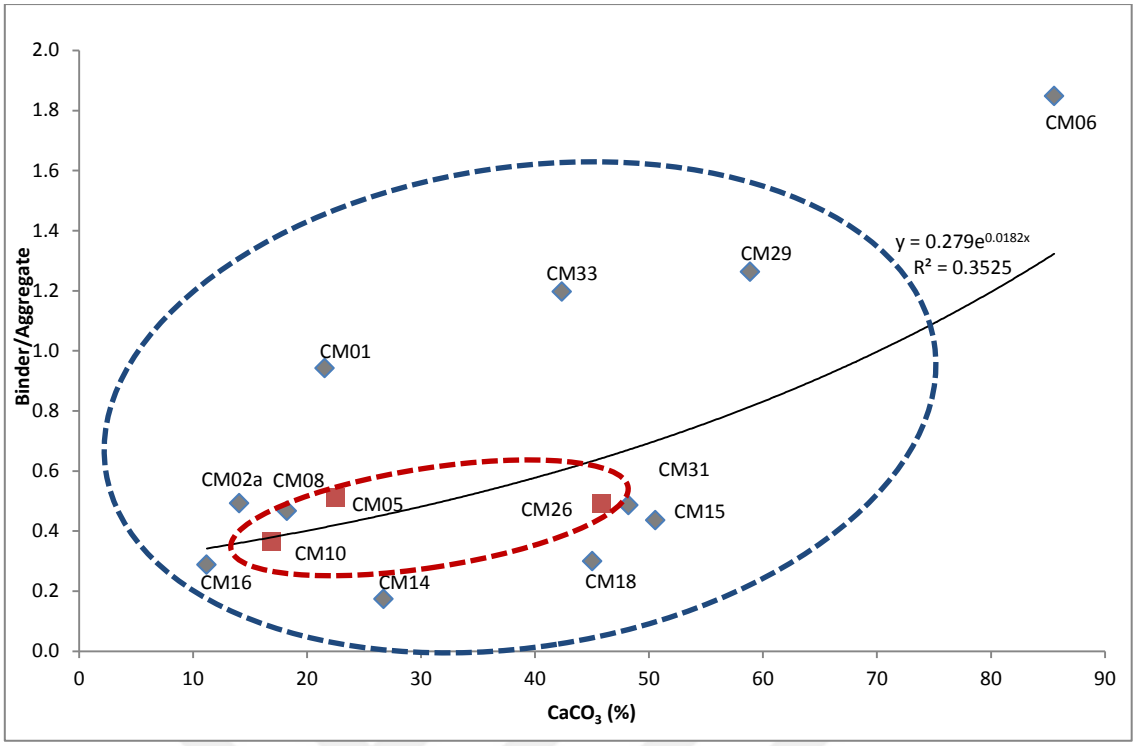


Figure 3.1- 21. acid in/soluble fraction vs $CaCO_3$ (%) from TGA of Complutum mortars (blue circle: *opus caementicium*, red circle: *opus signinum* mortars)

3.1.8 X-Ray Fluorescence (XRF)

In Table 3.1-6 elemental composition of the mortar samples is presented. CM27, CM35 had the highest MgO ratio and CM10, CM05, CM07, CM31 and CM29 follow them. In thermogravimetric analysis magnesite was also revealed in the thermograms of samples CM05 and CM07.

When y axis was basically considered as binder and x axis as aggregates Complutum mortars were aligned in two groups (Figure 3.1-22). CM35, CM05, CM10, CM01, CM02, CM08, CM14 and CM16 were having more SiO_2+ Al_2O_3+ Fe_2O_3 (60%-80%) less CaO+MgO (10%-20%). Second group having less SiO_2+ Al_2O_3+ Fe_2O_3 (30%-50%) more CaO+MgO (25%-36%) included CM27, CM15, CM07, CM37, CM29, CM31, CM33.

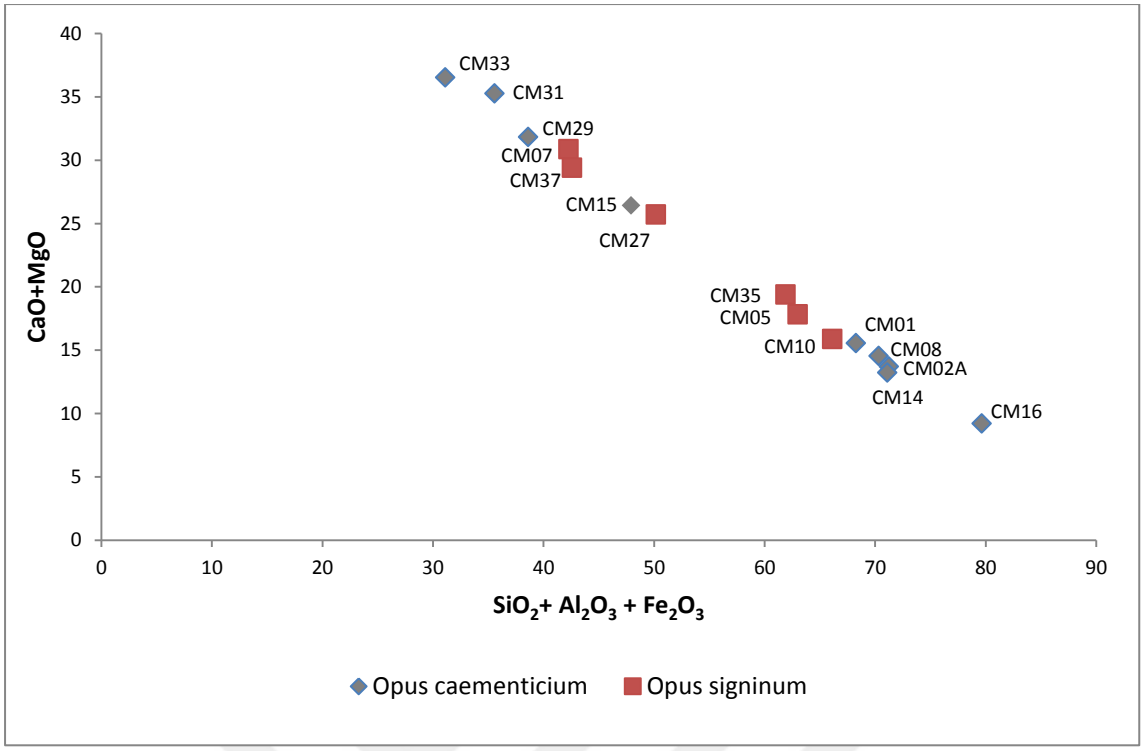


Figure 3.1- 22. CaO+MgO vs SiO_2+Al_2O_3+Fe_2O_3 graph of Complutum mortars

Table 3.1- 6. Major elements in Complutum mortars (%) (LOI: Loss of ignition)

	Samples		SiO_2	Al_2O_3	Fe_2O_3	MnO	MgO	CaO	Na_2O	K_2O	TiO_2	P_2O_5	LOI	Total
Opus Caementicium	**CM01**	Criptoportico wall	63.01	4.84	0.43	0.01	0.26	15.29	0.37	2.79	0.08	0.08	12.47	99.63
	CM02	Criptoportico wall	65.44	5.26	0.55	0.01	0.46	13.24	0.46	2.99	0.07	0.09	10.7	99.28
	CM08	North Bath wall	63.53	6.13	0.66	0.02	0.76	13.79	0.2	3	0.1	0.11	11.68	99.98
	CM14	South Bath wall	64.74	5.75	0.63	0.01	0.32	12.9	0.24	3.16	0.13	0.12	11.54	99.54
	CM15	Sewer	42.88	4.48	0.55	0.02	0.86	25.58	0.73	3.34	0.16	0.11	20.85	99.56
	CM16	Sewer	73.27	5.87	0.51	0.01	1.92	7.28	0.15	2.99	0.07	0.07	7.69	99.83
	CM29	North Bath floor bottom	33.33	4.37	0.91	0.02	2.11	29.73	0.41	2.11	0.22	0.2	25.88	99.29
	CM31	South Bath floor	28.54	5.53	1.51	0.04	2.59	32.69	0.28	1.52	0.31	0.23	26.08	99.32
	CM33	North Bath floor	24.66	4.92	1.53	0.03	1.61	34.93	0.29	1.57	0.23	0.23	29.39	99.39
Opus Signinum	**CM05**	North Bath coating	52.04	8.81	2.15	0.04	2.12	15.71	0.37	3.77	0.24	0.1	13.91	99.26
	CM07	North Bath coating	30.72	8.68	2.86	0.04	2.64	28.23	0.12	2.48	0.35	0.29	23.45	99.85
	CM10	North Bath facade	51.72	10.95	3.47	0.05	2.88	13	0.42	3.19	0.52	0.2	13.01	99.4

	CM27	North Bath floor	36.13	10.53	3.52	0.05	3.68	22.03	0.41	2.62	0.58	0.31	19.65	99.51
	CM35	Arco pillar	55.17	5.99	0.75	0.02	3.65	15.73	0.3	2.43	0.17	0.1	15.25	99.56
	CM37	Bridge pillar	36.24	5.24	1.1	0.02	1.25	28.15	0.24	1.86	0.36	0.11	25.15	99.71

Two groups that were gathered from previous graph (Figure 3.1- 22) revealed in TiO_2/Fe_2O_3 vs SiO_2/CaO graph as well (Figure 3.1- 23). First groupwa situated between 3-5 SiO_2/CaO and 0.1-0.25 TiO_2/Fe_2O_3 while second group was located below 1.6 SiO_2/CaO and 0.10-0.35 TiO_2/Fe_2O_3. CM16 was found separated from others due to high SiO_2/CaO ratio which had more quartz supported by XRD and microscopic analysis.

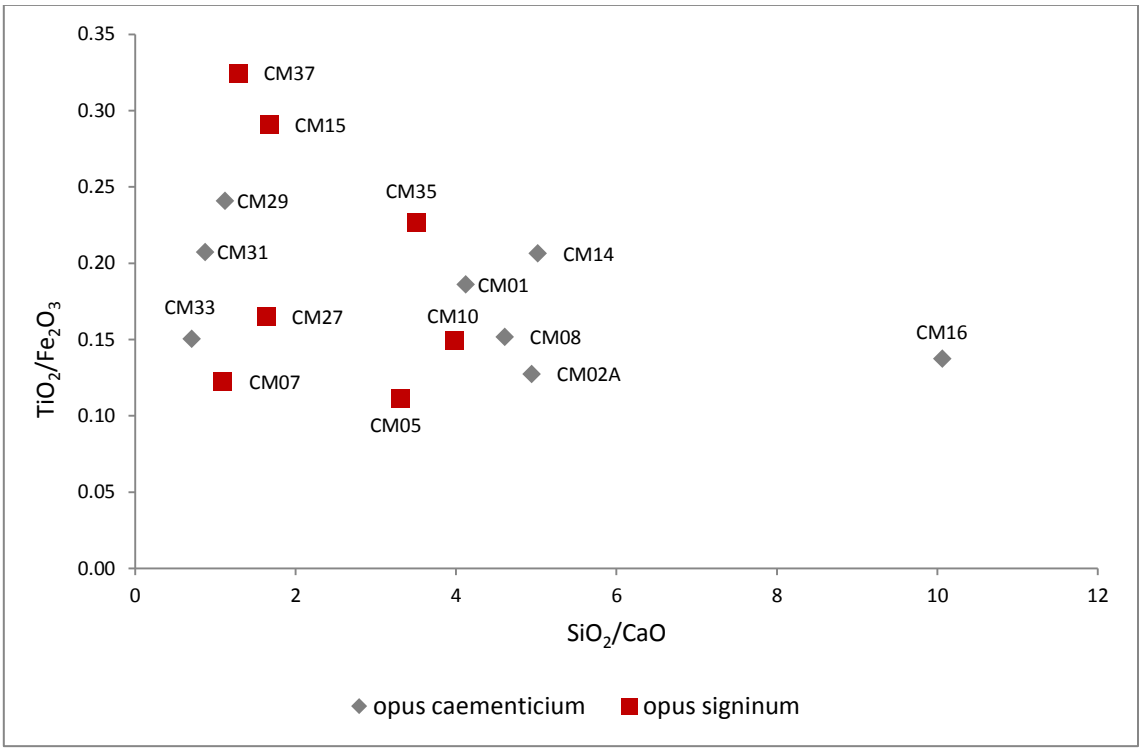


Figure 3.1- 23. TiO_2/Fe_2O_3 vs SiO_2/CaO graph of Complutum mortars

As Crisci et al. (2004) in their research used TiO_2/Fe_2O_3 vs CaO/MgO diagram (Figure 3.1-24) may help to classify mortars. Majority of mortars lay around 0.15 TiO_2/Fe_2O_3 and below 30 CaO/MgO indicating same origin and homogenity. Majority of *opus signinum* mortars were situated in the bottom of that zone however, sample CM37 from bridge stayed apart due to higher magnesium oxide and lower iron oxide content.

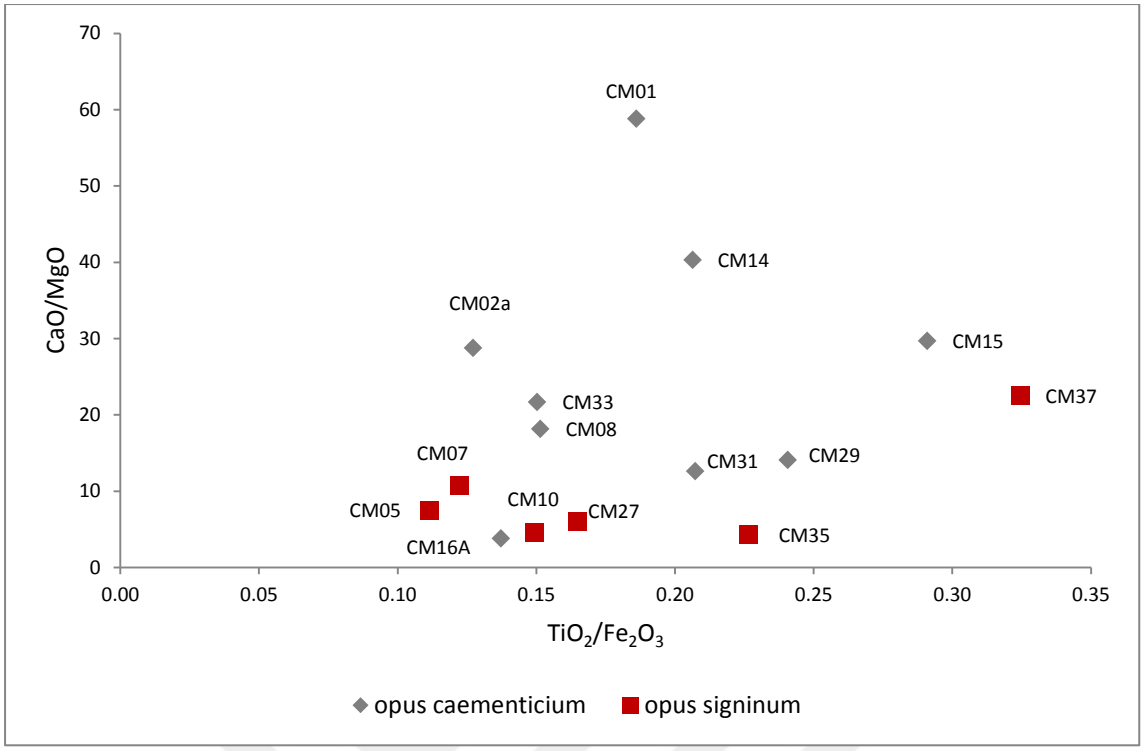


Figure 3.1- 24. CaO/MgO vs TiO_2/Fe_2O_3 graph of Complutum mortars

Correlation of trace element proportions can give idea about the employed raw materials. *Opus signinum* mortars were clustered into two groups, North Bath mortars CM05 and CM07 were belong to one, CM27, CM35 and CM37 were belong to another group with high Zr and Sr content (Figure 3.1-25). CM35 and CM37 were collected from pillars of arch and Zulema bridge which were not close to the forum of Complutum. The difference could be related to different time of construction. Although CM10 was coating mortar in the same building it was located further just like CM27. The reason behind this could be due to different use of raw materials in construction period or random selection.

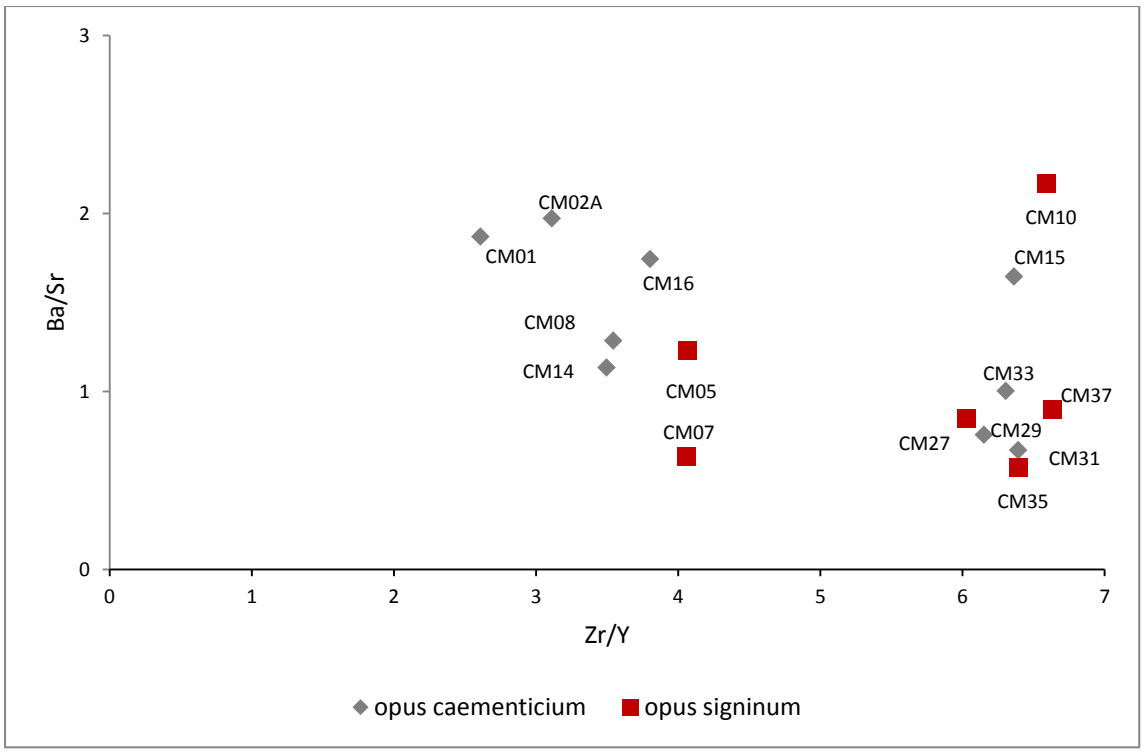


Figure 3.1- 25. Ba/Sr vs Zr/Y graph of Complutum mortars

3.1.9 Mercury Intrusion Porosimetry

Among the selected mortars CM02A had the lowest porosity and specific surface values but the highest bulk and real density values. The rest of the samples had the porosity values changing between 26 and 41.5%. It is not possible to interfere difference between different types of mortars through open porosity values, however it is seen that average pore diameter of *opus signinum* mortars were lower (Table 3.1- 7).

Table 3.1- 7. Parameters gathered by mercury intrusión (P: Porosity, APD: Average Pore Diameter (4V/A), BD: Bulk density, RD: Real density)

	Samples		P (%)	APD (µm)	BD (g/ml)	RD (g/ml)
Opus Caementicium	CM02	Criptoportico wall	5.86	0.09	2.47	2.63
	CM06	North Bath hipocaustum floor	26.31	0.12	1.85	2.51
	CM09	North Bath frigidarium wall	32.22	0.22	1.59	2.34
	CM15	South Bath brick arch	32.27	0.56	1.64	2.43
	CM16	Sewer	37.47	0.04	1.51	2.42
	CM31	South Bath frigidarium floor	31.83	0.13	1.68	2.47
	CM38	Pillar of bridge	28.48	0.06	1.71	2.39
Opus Signinum	CM07	North Bath pool coating	27.50	0.04	1.83	2.52
	CM10	North Bath frigidarium coating	33.74	0.07	1.51	2.27
	CM27	North Bath frigidarium floor 3	41.55	0.07	1.38	2.36

It can be said that *opus signinum* mortars (CM07, CM10 and CM27) had similar (quasi) unimodal distribution (Figure 3.1- 26) having the accumulation of pores in smaller pores between 10-0.01µm. CM07 showed nearly a unimodal pore size distribution. Little hump revealed between 10 µm and 5 µm and the other denser peak between 5 µm and 0.005 µm. Micropores were abundant.

On the other hand *opus caementicium* mortars pore sizes were more variable. Mortar from the sewer (CM16 and the one from the pillar of the bridge (CM38) had mainly micropores (1-0.005 µm) (Table 3.1- 8), mortar from the floor of South Bath (CM31) showed bimodal distribution, macropores between 100 µm and 8 µm and the midi and micropores between 5 µm and 0.01 µm were seen (Table 3.1- 8) (For detail see appendices).

Average porosity and bulk density of *opus caementicium* mortars were 28 % and 1.8 g/cm^3. *Opus signinum* mortars had slightly different values; average porosity and bulk density were 34 % and 1.6 g/cm^3 and the ratio of micropores were high in these mortars due to the higher deterioration.

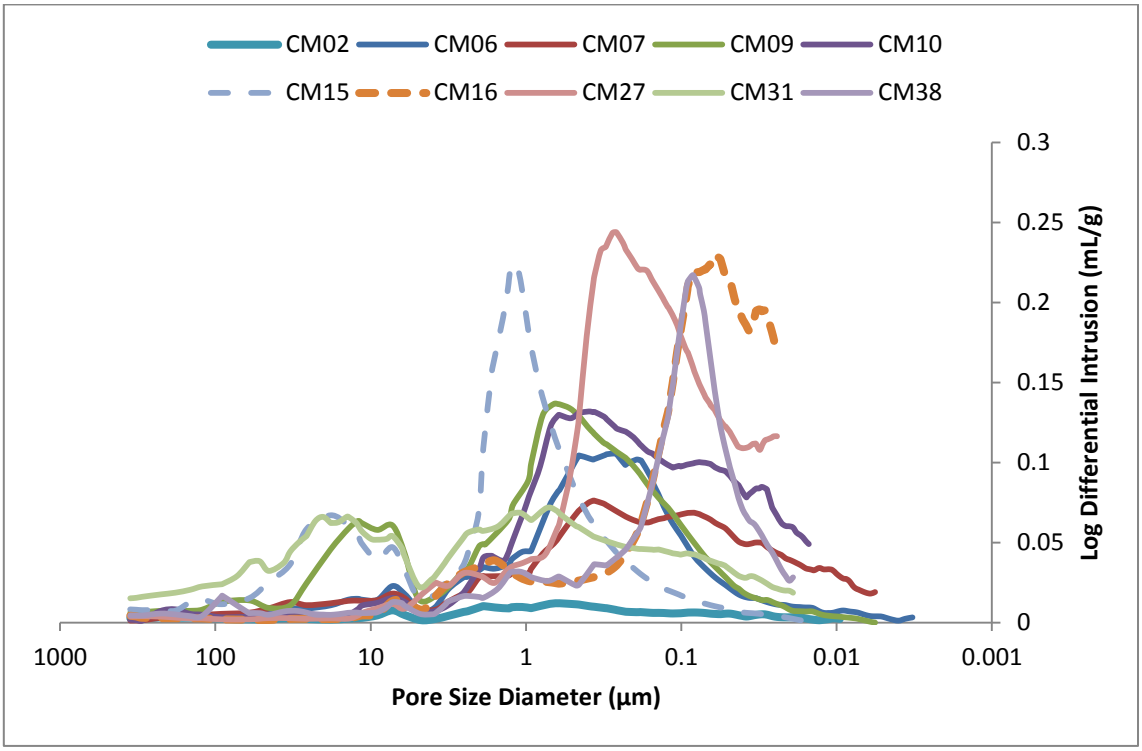


Figure 3.1- 26. Log differential intrusion versus pore size of the Complutum samples

Mortar taken from the wall of Criptoporticus (CM02) which had the lowest porosity showed a bimodal pore size distribution. Pores were dispersed less densely between 20 µm and 5 µm and more densely between 5 µm and 0.005 µm. Sample from floor of North Bath (CM06) showed nearly a unimodal pore size distribution. Little hump was seen between 10 µm and 5 µm and the other denser peak between 5 µm and 0.005 µm. Sample from the wall from the same building (CM09) showed a bimodal pore size distribution with less dense peak was seen on macropores between 50 µm and 7 µm and the other denser peak between 7 µm and 0.005 µm (Figure 3.1- 26. Table 3.1 -8).

Table 3.1- 8. Pore size distribution and percentages of micro and macropores

	Samples		Micro < 5 µm	Macro > 5 µm	< 0.01 µm	0.01 - 0.1 µm	0,1 - 1 µm	1-10 µm	10 - 100 µm	>100 µm
Opus Caementicium	**CM02**	Criptoportico wall	77,0%	23,0%	2,55%	17,98%	36,64%	26,36%	9,48%	6,99%
	CM06	North Bath floor	88,8%	11,2%	1,49%	13,17%	60,85%	16,83%	6,09%	1,57%
	CM09	North Bath frigidarium wall	76,7%	23,3%	0,28%	10,23%	53,12%	20,38%	14,04%	1,96%
	CM15	South Bath brick arch	71,5%	28,5%	-0,01%	3,07%	34,58%	39,40%	20,26%	2,70%
	CM16	Sewer	96,8%	3,2%	-19,28%	80,81%	25,80%	10,81%	1,10%	0,75%
	CM31	South Bath floor	61,4%	38,6%	-1,94%	14,34%	29,75%	26,71%	25,43%	5,71%
	CM38	Pillar of bridge	91,8%	8,2%	-4,93%	53,68%	35,40%	9,41%	4,81%	1,63%
Opus Signinum	**CM07**	North Bath pool coating	88,8%	11,2%	4,03%	33,11%	42,37%	12,39%	6,92%	1,19%
	CM10	North Bath coating	94,7%	5,3%	-3,76%	35,21%	54,00%	10,98%	2,28%	1,29%
	CM27	North Bath floor 3	97,3%	2,7%	-12,21%	41,88%	60,32%	8,30%	1,04%	0,66%

CM15 showed a bimodal pore size distribution. Less dense peak was seen again on macropores between 80 µm and 5 µm and the other denser peak between 5 µm and 0.005 µm (Figure 3.1- 26). CM16 showed a bimodal pore size distribution. No macropore was observed. Less dense hump was seen between 10 µm and 0.5 µm and the other denser peak between 5 µm and 0.01 µm (Figure 3.1- 26, Table 3.1- 8).

When we look at the binder aggregate ratios of the samples we may claim that increase in aggregate ratio, decrease in modal and accumulation of pores below 1µm which is accepted as small capillary pores forming in the binder (Thomson et al., 2004). Unlikely, the sample CM06a which had less aggregate than binder indeed had the pores in similar sizes. However, aggregates were needed to not had shrinkage cracks in the mortar. The reason for the same curve could be the cracks and fissures.

Considering the same function of mortar, coating mortars (CM07 and CM10) were parallel while mortars from floors of North Bath (CM06a) and South Bath (CM31) showed pretty different distributions. Besides, Thomson et al (2004) and Lourenço et al (2014) state that pores larger than 100 µm were responsible for the water permeability, accordingly mortar from *Criptoporticus* wall (CM02) and South Bath floor (CM31) had higher permeability properties which is an indicator of deterioration despite the good condition of the mortars.

3.1.10 Correlations of results according to architectural features

Similarities/differences in the raw materials and properties of mortars can be used to had estimation about the construction periods of the buildings, bearing in mind that for the precise results cross-referencing of the archaeological data would be necessary (Barluengo et al. 2014).

In Complutum there were two phases of construction. First construction phase corresponds to first century BC and second phase corresponds to third century AD. In walls of Criptoporticus two collected mortars account for different phases, and the difference was clear in composition after the proof of the analytical techniques. The binder of latter construction mortar had different carbonation degree that was revealed after microscopic observations, surface hardness test, XRF and mercury intrusion porosimetry. On the other hand, both of the samples had gypsum; however, it could be related with the weathering.

Sewer mortars had the different aspect in the binder and they were belonging to first phase construction. As a result, if there was not any archaeological misinterpretation of the mortars, the carbonation degree of the binder was not related to the time, more to the conditions.

When look at the proportions of the mortars in North Bath and South Bath it was seen that binder: aggregate ratios of the mortars in the walls and the floors were 1:1 at first phase and 1:2 at second phase. It can be interpreted that in the second phase of construction to increase the aggregate amount was a conscious decision, probably to prevent shrinkage cracks. Grain size distributions of floor mortars were similar.

Another observation on the different level of mortars in floor in North Bath showed that two bottom levels were *opus caemneticium* mortars with 1:1 B:A ratio and overlapping two layers were *opus signinum* mortars with 1:2 ratio.

The same increase in aggregate amount through ages was seen in coating mortars. Complutum mortars did had low amount of fine grains which may be both ceramic dust and pozzolanic additions like fly ashes or clays.

In floors, true lime mortars without hydraulic properties were used as well, which was revealed in Cuadriporticus and North Bath. XRF, together with TGA showed that floor mortars and coating mortars in two Baths were highly carbonated. Elemental composition of *opus caementicum* floor mortars and mortars in the pillars of Zulema bridge and Arch were similar which indicated that same raw materials were used. It may also refer to the same time construction.

3.2 Mérida Archaeological Complex

Collected samples were characterized multi-analytically. The results of the utilized analytical techniques were described in macroscopic, physical, petrographic, mineralogical, geochemical order then mercury intrusion porosimetry were presented.

3.2.1 Macroscopic description of the samples

In Mérida *opus caementicium* mortars were collected from walls of Moreria, Alcazaba, archaeological remains of Viñero, amphitheatre and circus. In general, porous mortars had crème, light brown colour binders with small size aggregates. They were consistent mortar with high cohesion. In some samples lime lumps were visible by naked eye. Dark to light sub-angular to angular sand grains (< 4 mm) and rock fragments were observed. Samples collected from aqueduct were classified as *opus caementicium* except the sample with reddish binder (MM3sig) due to the white colour binder and aggregates however the difference of them should be noted that they consist of angular rock fragments (>2 cm) which is called *caementea.* Pore and grain sizes were various, grain size distribution is poorly sorted (Figure 3.2- 27). In the sample MM5 from aqueduct organic additive (straw) and fly ashes were detected (Figure 3.2- 28).



Figure 3.2- 27. Examples of *opus caementicium* mortars in Mérida (on the left MM3 having both types of mortars and MM15 on the right)



Figure 3.2- 28. Straw in the sample MM5

There were a few *opus signinum* mortars which had reddish colour sample collected from the aqueduct San Lazaro basement, floor in the Temple of Diana, coating mortars in Resti Bath and seats in amphitheatre. The cohesion of the mortars was high. Angular sub-angular ceramic aggregates were bigger in size and medium to well sorted in reddish colour matrix. Mortars of that type own lower cohesion. Binder had reddish colour and angular ceramic aggregates (< 1 cm) were observed. Grain size distribution is poorly sorted (Figure 3.2- 29).



Figure 3.2- 29. Examples of opus signinum mortars in Mérida (on the left coating mortar in Bath MM18 and mortar from amphitheatre MM22 on the right)

3.2.2 Colour Spectrophotometry

Figure 3.2- 30 showed that the majority of the mortars lay down to the werea corresponding between 8.5-15 C* and 68-80 L*. MM3 ceamenticium and MM5 had higher lightness and lower saturation and MM3 signinum and MM18 showed the opposite. It is expected with ceramic content.

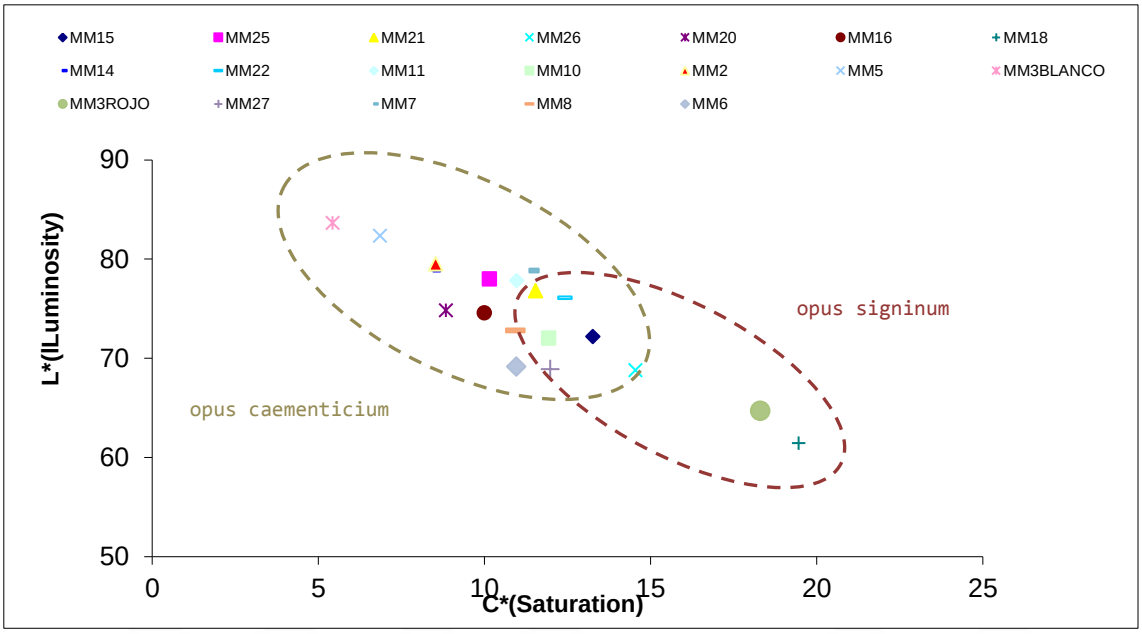


Figure 3.2- 30. Luminosity vs Chrome of Mérida mortars

In Figure 3.2- 31 the trend of those two groups were reversed, as higher the a* values higher the redness and higher the b* refers to yellowness, mortars lay down to below 4 a*, 4 and 16 b* and MM3sig and MM18 were located seperated with higher than 10 values. In addition, mortars from San Lazaro aqaeduct had lower b* values than others while they had the highest lightness (L*).

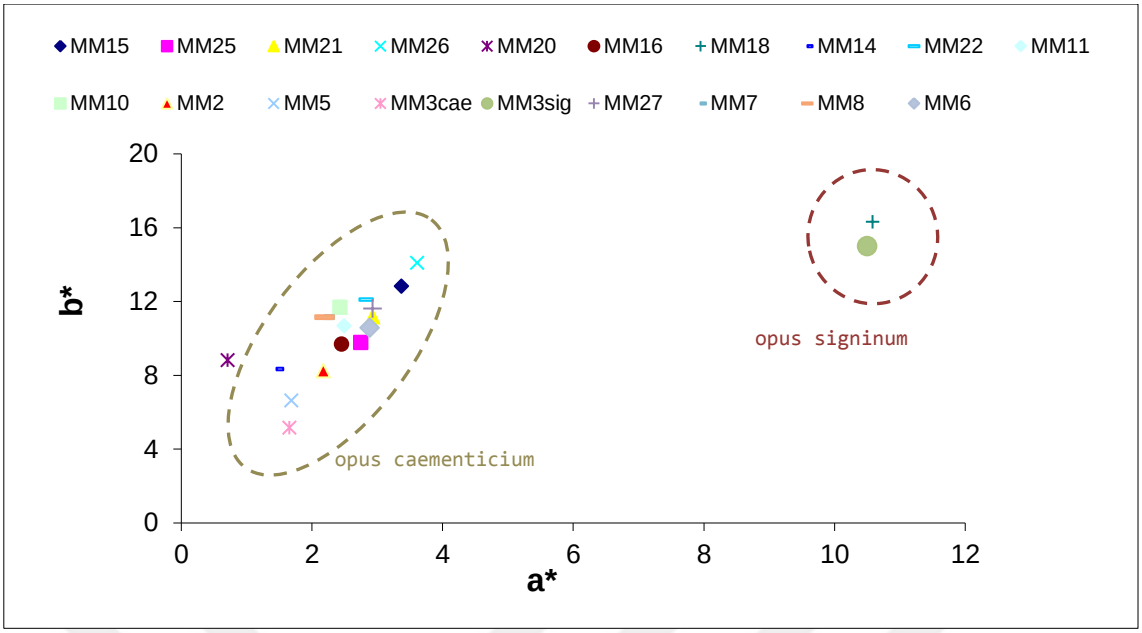


Figure 3.2- 31. Chromatic parameters b* vs a* of Mérida mortars

Figure 3.2- 32 showed that whiteness and yellowness of the samples were in concordance with other chromatic longitude values (Figure 3.2- 30, Figure 3.2- 31). The majority of the samples were grouped in the middle of the diagram. Reddish mortars MM3sig and MM18 had higher yellow index at the same time minus zero white indexes and samples MM3cae and MM5 had higher whitish index (34, 41) as expected.

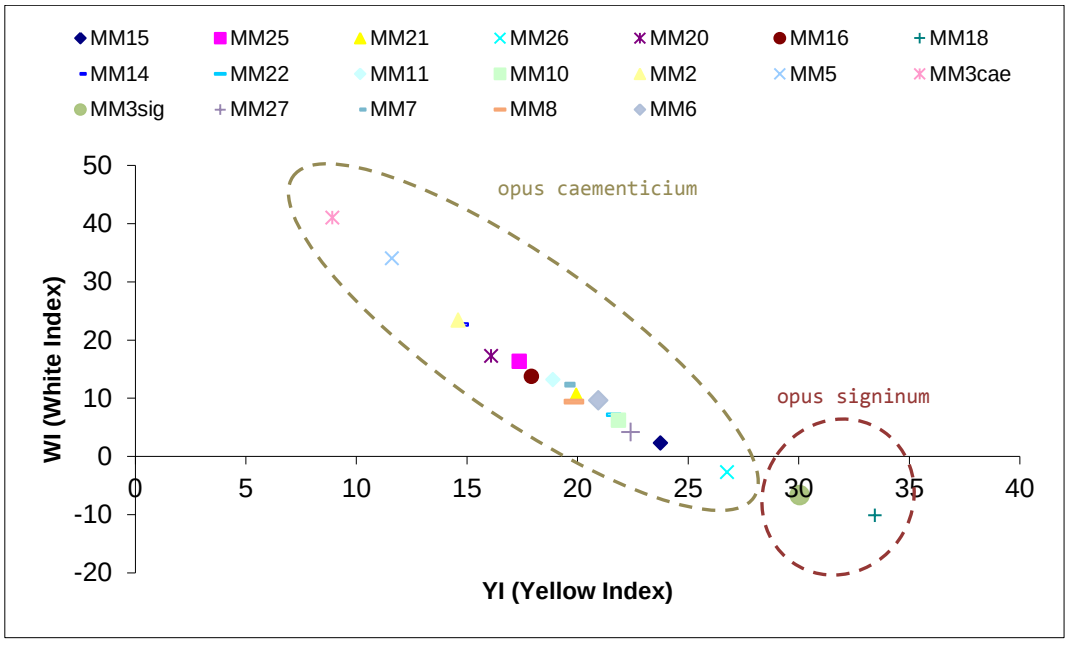


Figure 3.2- 32. White index vs yellow index of Mérida mortars

3.2.3 Surface Hardness

As shown in the Figure 3.2- 33 the surface hardness values of the samples vary between 100 and 420 leebs. The lowest hardness values belong to *opus signinum* mortar MM21 and highest value belongs to MM3 *caementicium* mortar. Apart from these two extreme values the rest of the samples had values changing between 200 Leeb (HL) and 300 Leebs (HL).

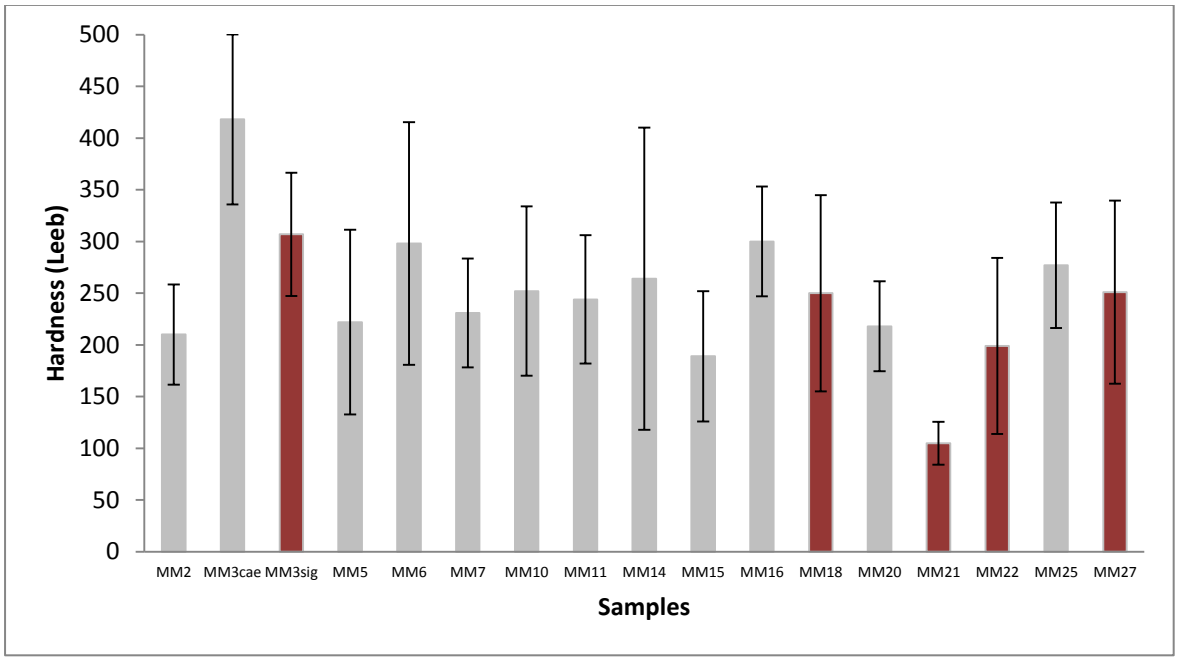


Figure 3.2- 33. Surface hardness values of Mérida samples

3.2.4 Optical Microscopy

Opus caementicium mortars had is of micrite size calcitic binder (25% -40%) with angular to rounded grains (25-30%) (Figure 3.2- 34). Medium to poorly sorted grains were embedded in dark colour carbonated lime binder. Up to 250 μm angular grains were well distributed and large grain feldspar phenocrysts or rock fragments (>3 cm) make the distribution poorly sorted. Aggregates were composed of rounded to angular quartz, feldspar and somehow mica, crushed rock fragments from surrounding, monzogranite, diorite, slate, quartzite and schist (geo map). Reaction rims were observed on aggregates.

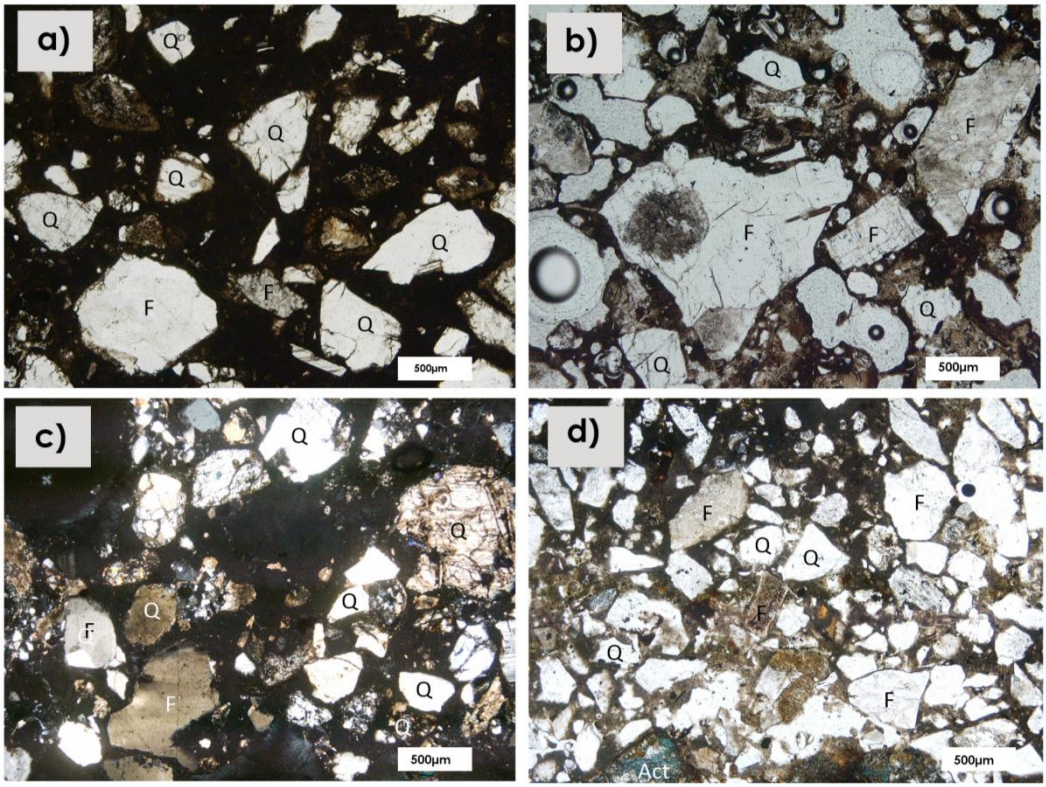


Figure 3.2- 34. *Opus caementicium* mortars (a) MM2 plane polarized light b) MM14 plane polarized light, c) MM16 cross polarized light, d) MM26 plane polarized light), Q: quartz, F: feldspar, Act: actinolite

As shown in Figure 3.2- 35 binder of *opus signinum* mortars had micrite size calcitic binder and lighter than *opus caementicium* mortars is of (40%-50%) with angular to rounded quartz grains and ceramic fragments (25-30%).Bond between the ceramic fragments and the binder is high frequently reaction rim is observed. Grain size distribution is poorly sorted. Aggregates were composed of rounded to angular quartz, feldspar and somehow mica, crushed rock fragments from surrounding, monzogranite, diorite, slate, quartzite and schist (Figure 2.1- 11).

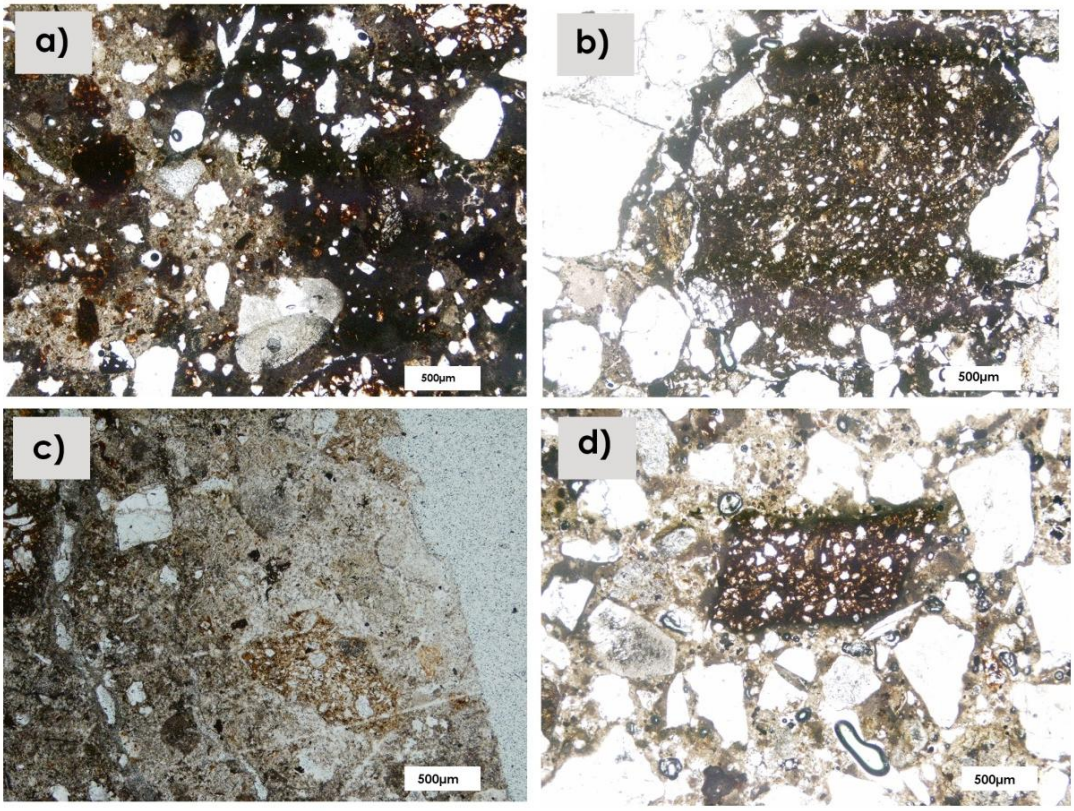


Figure 3.2- 35. Opus signinum mortars (a) MM18 plane polarized light b) MM22 plane polarized light, c) MM21 plane polarized light, d) MM27 plane polarized light)

Metamorphic rocks like diorite, metagranite, quartzite, slate and monzogranite were found in the mortars (Figure 3.2- 36). The reaction rims and irregular boundaries of the lithic and ceramic fragments indicate the reaction between the lime (Figure 3.2- 37).

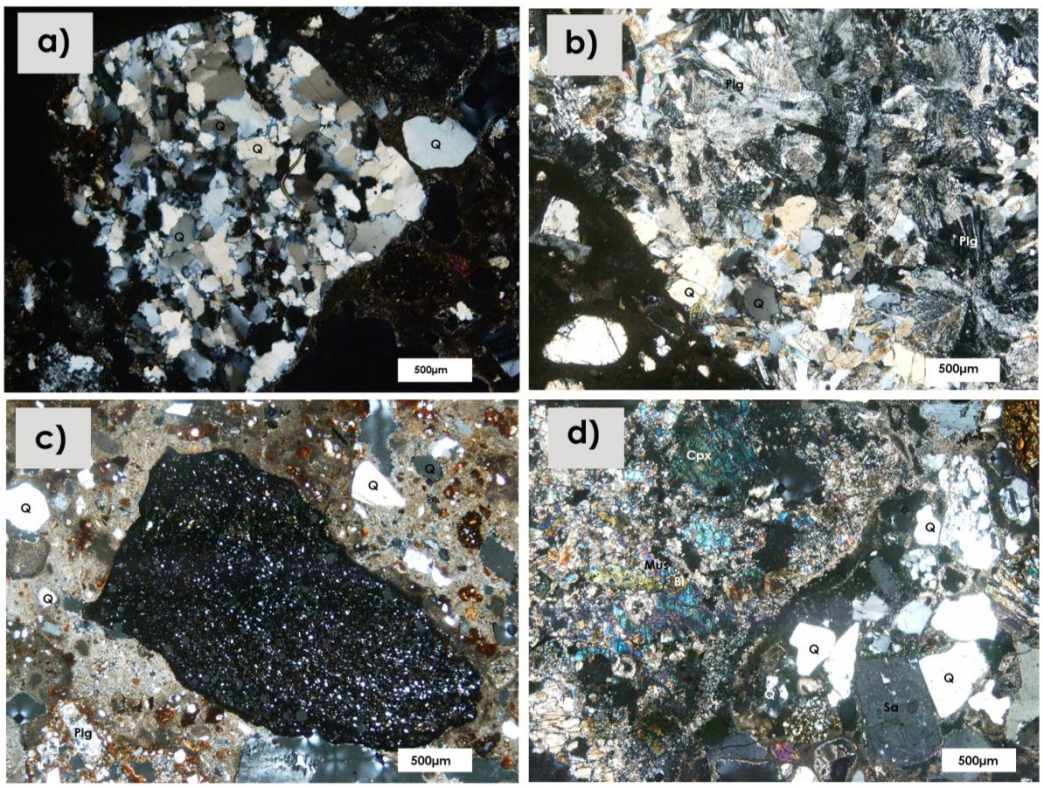


Figure 3.2- 36. Rock fragments encountered in Mérida mortars a) quartzite in MM10 b) monzogranite in MM2 C) slate like metamorphic rock in MM18 d) granodiorite in MM16 (cross polarized light)

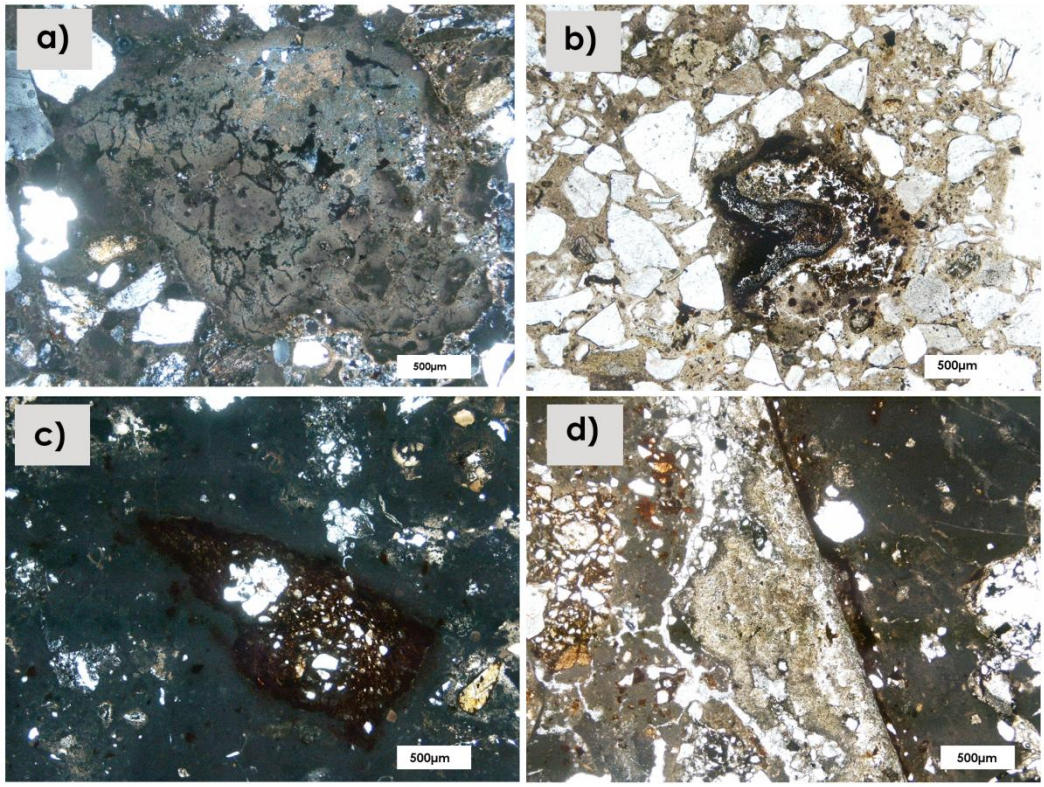


Figure 3.2- 37. a) lime lump in MM7 b) reactive rock fragment and rim around it in MM26 c) angular ceramic fragment with reaction rim in MM5 d) in MM3 (plane polarized light) scale: 500 µm

Table 3.2- 9. Petrographical constituents of Mérida mortars (Qtz: quartz, Fsp: feldspar, Cal: calcite, Bt: biotite, Ms: Muscovite, Am: amphibole Hbl: Hornblende, Act: Actinolite,, Op: opaque mineral, shr: shrinkage, pol: Qtz polycrystalline, crp: Qtz cryptocrstalline, inc.: inclusion).

	Samples		Binder	Minerals	Lithic and ceramic fragments, additives, others
opus caementicicum	MM2	San Lazaro Aqueduct	Dark colour micritic calcite	Qtz, Fsp, Am, Op, Cal	diorite, quartzite, monzogranite, graywacke
	MM3 cae	San Lazaro Aqueduct	Dark colour micritic calcite	Qtz, Fsp, Op, Hbl, Bt	Ceramic, lime lump, diorite, large feldspar, amphibolite
	MM5	San Lazaro Aqueduct	Dark colour micritic calcite	Qtz, Fsp, Bt, Ms, Op	Charcoal, ceramic, amphibolite
	MM6	Alcazaba wall	Dark colour micritic calcite	Qtz, Fsp,	Quartzite, ceramic, slate, schist
	MM7	Alcazaba wall	Dark colour micritic calcite, locally clayey appearance	Qtz, Fsp,	Overburnt lime lumps, quartzite, graywacke ceramic, schist,
	MM9	Moreria wall	Dark colour micritic calcite	Qtz, Fsp, Hbl	Diorite, lime lump
	MM10	Temple floor	Dark colour micritic calcite	Qtz, Fsp,	Quartzite, , graywacke, lime lump, lime inclusion
	MM11	Temple floor	Dark colour micritic calcite	Qtz, Fsp,	slate
	MM12	Temple channel	Dark colour micritic calcite	Qtz, Fsp, Hbl, Bt	Quartzite, lime lump, large feldspar

	MM14	Temple Temenos wall	Dark colour micritic calcite	Qtz, Fsp, Bt	Diorite, large microcline
	MM15	Temple Temenos wall	Dark colour micritic calcite	Qtz, Fsp	Slate, schist, lime lump
	MM16	Viñero wall	Light color binder	Qtz, Fsp, Hbl	Amphibolite, schist, graywacke, lime lump
	MM20	Circus wall	Dark colour micritic calcite	Qtz, Fsp,Hbl, Op	quartz diorite, quartzite, lump
	MM25	Amphitheatre	Dark colour micritic calcite	Qtz, Fsp, Bt	lime lump, large feldspar, small amphibolite
	MM26	Snow well	Dark colour micritic calcite	Qtz, Fsp, Act	Lime lump, monzogranite
opus signinum	MM3sig	San Lazaro Aqueduct	Dark colour micritic calcite	Qtz, Fsp	ceramic
	MM18	Bath coating	Dark/light colour micritic calcite	Qtz, Fsp	Ceramic, slate
	MM21	Circus wall	Light color binder	Qtz, Fsp	ceramic
	MM22	Amphitheatre	Dark colour micritic calcite	Qtz, Fsp	Ceramic, greywacke, lime lump, quartzite
	MM27	Snow well	Dark colour micritic calcite	Qtz, Fsp	ceramic, slate, schist, lime lump

3.2.5 Binder aggregate ratio and grain size distribution

After HCl attack soluble parts of the mortars were accepted as binder and insoluble parts as aggregates. Percentages of binders and aggregates of the samples are listed below (Table 3.2- 10).

Table 3.2- 10. Binder and aggregate ratios (%) of Mérida mortars

	Samples		Binder%	Aggregate %	B:A
Opus caementicium	**MM1**	Aqueduct coating	27.77	72.23	1:3
	MM2	channel	32.86	67.14	1:2
	MM3	channel	35.73	64.27	1:2
	MM6	Alcazaba wall	46.55	53.45	1:1
	MM8	Moreira wall	24.16	75.84	1:3
	MM10	Temple floor	20.6	79.4	1:4
	MM14	Temenos wall	26.75	73.25	1:3
	MM16	Viñerowall	19.45	80.55	1:4
	MM20	Circo wall	12.4	87.6	1:5
Opus signinum	**MM24**	Amphiteatre	27.16	72.84	1:3
	MM18	Resti Bath coating	40.04	59.96	1:1
	MM22	Amphitheatre	16.05	83.95	1:7
	MM27	Snow well	29.23	70.77	1:2

Mérida mortars showed variety in binder aggregate ratio (B:A)(Figure 3.2- 38) The higher amount of mortars had 1:3 ratios which were MM1, MM24, MM8 and MM14. Among the rest, MM6 and MM18 had 1:1, MM2 and MM27 had 1:2, MM10 and MM16 had 1:4. MM22 and MM20 had much more aggregates that had the B:A ratios 1:5 and 1:7 respectively.

The higher aggregate proportion of the samples from thermal bath is the use of large dimension ceramic fragments.

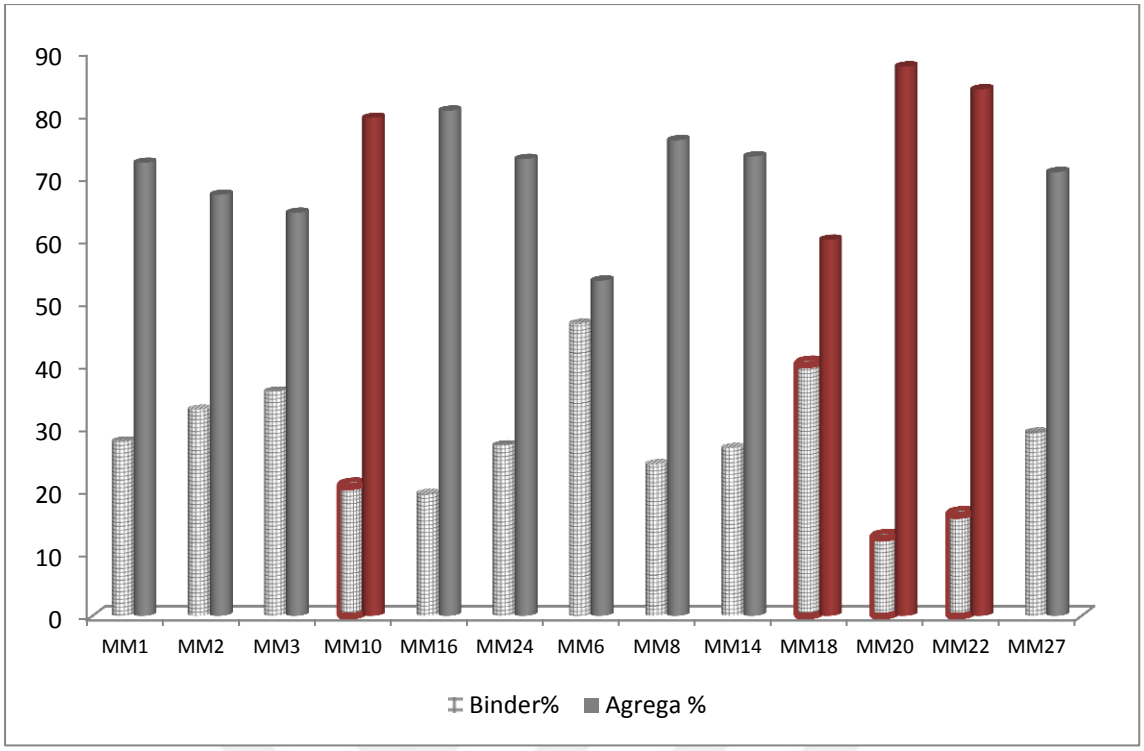


Figure 3.2- 38. Binder aggregate ratios of Mérida mortars (reds are *opus signinum*)

As seen in Table3.2- 11 and Figure 3.2- 39, , MM3 MM1 and MM8 had higher percentage above 2 mm. MM2 MM24, MM14 and MM27 follow them. Ignoring the large fragments generally Mérida mortars showed symmetric distribution with the highest intensity in the medium size grains between 0.25 mm and 1mm. Another noteworthy result was the relatively higher amount of fine grains (<63 µm) which may be ceramic dust or pozzolanic additives.

Table 3.2- 11. Weight passing each sieve in Mérida mortars

	Samples		>2mm	1<x<2 mm	0,5<x<1 mm	0,25<x<0,5 mm	0,125<x<0,25 mm	0,063<x<0,125 mm	<0,063 mm
opus caementicium	**MM1**	Aqueduct	68,31	6,49	6,49	5,71	4,42	4,94	3,64
	MM2	Aqueduct	36,84	14,21	22,11	14,21	5,79	1,58	5,26
	MM3	Aqueduct	72,20	3,86	5,79	4,63	3,86	5,02	4,63
	MM6	Alcazaba wall	14,84	16,13	25,48	20,65	8,71	8,06	6,13
	MM8	Moreira wall	57,14	8,90	8,67	9,13	8,20	4,68	3,28
	MM14	Temple Temenos wall	25,98	20,34	19,12	13,97	9,31	6,37	4,90
	MM16	Viñero wall	6,56	8,40	39,37	35,43	6,30	1,57	2,36
	MM24	Amphiteatre	26,59	17,34	19,94	20,81	7,51	4,05	3,76
opus signinum	**MM10**	Temple floor	6,22	12,43	30,00	35,95	8,11	3,24	4,05
	MM18	Resti Bath coating	15,00	17,94	20,29	22,35	11,47	8,24	4,71
	MM20	Circus wall	1,27	3,81	38,84	40,29	8,53	3,45	3,81
	MM22	Amphitheatre	1,17	5,36	26,34	34,73	17,48	9,09	5,83
	MM27	Snow well	16,62	10,65	36,36	24,42	5,45	2,60	3,90

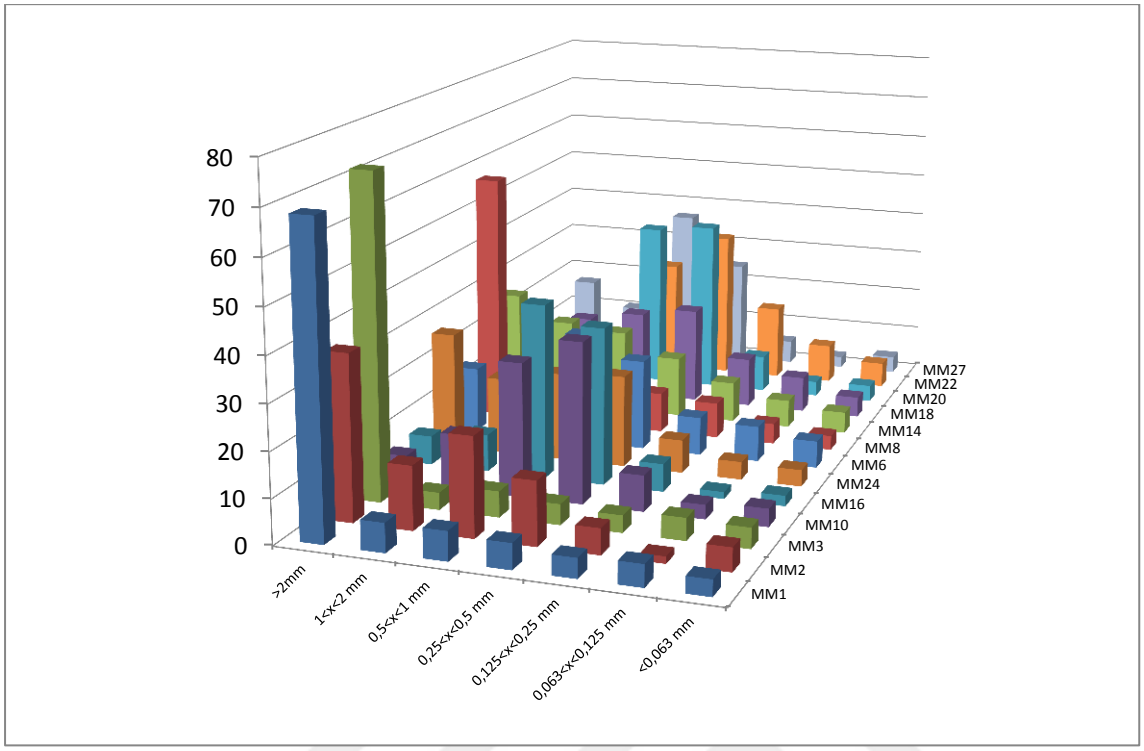


Figure 3.2- 39. Grain size distribution graph of Mérida mortars

3.2.6 X-Ray Diffraction

As it illustrated in Figure 3.2- 40 main constituents of Mérida mortars were quartz and calcite. Feldspar was the secondary mineral that was found predominantly. MM3sig (aqueduct), MM10 (Temple floor), MM20 (circus wall) and MM22 (amphitheatre) had mica peaks. Actinolite peaks reveal at MM10 (Temple floor), MM18 (Bath coating) and MM20 (circus wall). Some of the *opus caementicium* mortars showed the same peaks as well, like MM6, MM7, MM14, MM25, MM26 and MM27. Chlorite was seen in the XRD patterns of MM12 MM17 and MM25 which can be a consequence of deterioration.

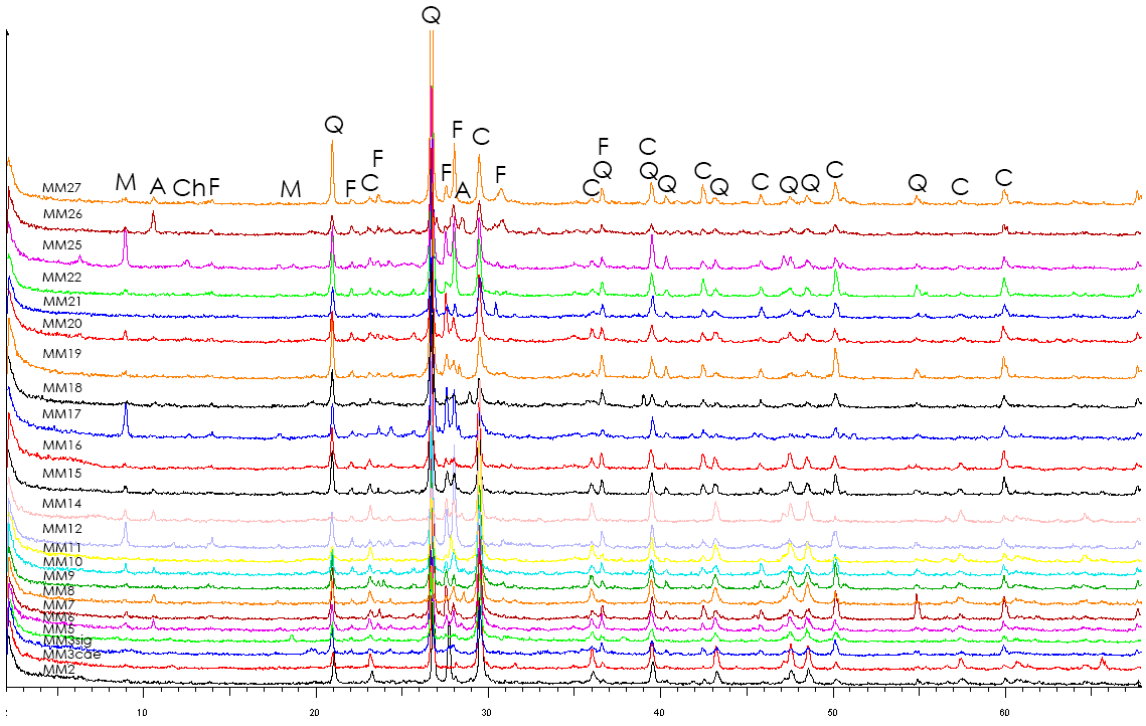


Figure 3.2- 40. XRD patterns of Mérida mortars (Q: quartz, C: calcite, F: feldspar, M: mica, Ch: Chlorite, A: Actinolite)

Semi quantitative analysis of the minerals from XRD analysis is listed below (Table 3.2- 12).

Table 3.2- 12. Semiquantitative XRD analysis of Mérida mortars (++++: primary mineral, ++: secondary mineral, +: present, tr: trace)

	Samples		Quartz	Calcite	Feldspar	Mica	Actinolite	Chlorite
opus caementicicum	MM2	San Lazaro Aqueduct	++	+++			tr	
	MM3cae	San Lazaro Aqueduct	++	+++	+	+	tr	
	MM5	San Lazaro Aqueduct	+++	+++	+	+	tr	
	MM6	Alcazaba wall	+++	++	+	+	+	
	MM7	Alcazaba wall	+++	++	+	+		
	MM8	Moreria wall	+++	+++	+		+	
	MM9	Moreria wall	+++	+++	+	tr		
	MM10	Temple floor	+++	++	+	+	+	
	MM11	Temple floor	++	+++	+			
	MM12	Temple channel	+++	++	+	+		+
	MM14	Temple Temenos wall	+	+++	+	+	+	
	MM15	Temple Temenos wall	+++	++	+	+	+	
	MM16	Viñero wall	+++	++		tr		
	MM17	Viñero wall	+++	+	+	+		+
	MM19	Bath coating	+++	++	+	tr		
	MM20	Circo wall	+++	++	+	+	+	+
	MM25	Amphitheatre	+++	++	++	+		+
	MM26	Snow well	+++	++	+		+	
opus signinum	MM3sig	San Lazaro	+++	++	+	+		
	MM18	Bath coating	+++	+	+		+	
	MM21	Circo wall	+++	++	+			
	MM22	Amphitheatre	+++	++	++	+	+	
	MM27	Snow well	+++	+	+	+	+	

3.2.7 Thermogravimetric Analysis (TGA-DSC)

From the results of TGA/DSC analyses of the samples (Table 3.2- 13) percentages of weight losses up to 120°C, between 120-200°C, 200-600°C and 600-800°C were calculated which attribute to the loss due to hygroscopic water, gypsum dehydration, structurally bound water of hydraulic compounds and decomposition of calcium carbonate ($CaCO_3$), respectively (Moropoulou et al. 2000; Bonazza et al., 2013).

Table 3.2- 13. Weight losses (%) of the mortar samples

Samples			<120	120-200	200-600	600-800	CO_2/H_2O
opus caementicium	MM2	San Lazaro	3.26	1.03	4.52	14.40	3.19
	MM3cae	San Lazaro	2.59	0.89	4.41	19.51	4.42
	MM5	San Lazaro	3.16	1.50	7.02	11.27	1.61
	MM6	Alcazaba wall	2.05	0.64	3.65	13.34	3.65
	MM7	Alcazaba wall	1.32	0.31	3.40	11.63	3.42
	MM8	Moreira wall	1.85	0.43	4.27	22.08	5.17
	MM9	Moreira wall	0.95	0.25	4.27	17.21	4.03
	MM10	Temple floor	1.98	0.43	3.95	10.80	2.73
	MM11	Temple floor	2.44	0.50	3.51	19.87	5.66
	MM12	Temple channel vault	2.05	0.65	2.80	6.81	2.43
	MM14	Temenos wall	1.37	0.22	3.17	21.17	6.68
	MM15	Temenos	0.92	0.29	2.70	10.13	3.75
	MM16	Vrinero wall	2.81	0.77	2.92	10.35	3.54
	MM17	Vrinero	2.68	0.35	2.38	5.07	2.13
	MM19	Bath wall	1.72	0.44	3.53	8.43	2.39
	MM20	Circo wall	1.99	0.40	3.32	8.46	2.55
	MM25	Amphiteatre	1.25	0.38	3.13	9.42	3.01
	MM26	Snow well	1.32	0.52	4.70	10.85	2.31
opus signinum	MM3sig	channel	3.32	1.03	4.08	8.80	2.16
	MM18	Bath lining	2.21	0.78	3.58	5.39	1.51
	MM21	Circo wall	1.59	0.39	3.33	10.74	3.23
	MM22	Amphithea tre	1.08	0.45	4.20	7.35	1.75
	MM27	Snow well	0.85	0.33	3.64	10.97	3.01

Figure 3.2- 41 presents the plot of CO_2/H_2O vs CO_2 % which serves to classify the mortars according to their hydraulic character (Bakolas et al. 1998, Moropoulou et al. 2000, Genestar et al, 2006, Cardoso et al., 2014). CO_2/H_2O is inversely related to hydraulicity (Bakolas et al. 1995, Moropoulou et al. 2000). Based on the data and graph, Böke et al. (2008), Uğurlu Sağın (2012) accepted as non-hydraulic mortar when CO_2/H_2O ratio higher than 10. According to this approach, there was no non-hydraulic mortar among Mérida mortars. Another approach is that mortars that had H_2O higher than 3 were so called hydraulic mortars (Moropolou et al. 2000; Genestar et al. 2006). So, MM12, MM15, MM16 and MM17 were supposed to be true lime mortars.

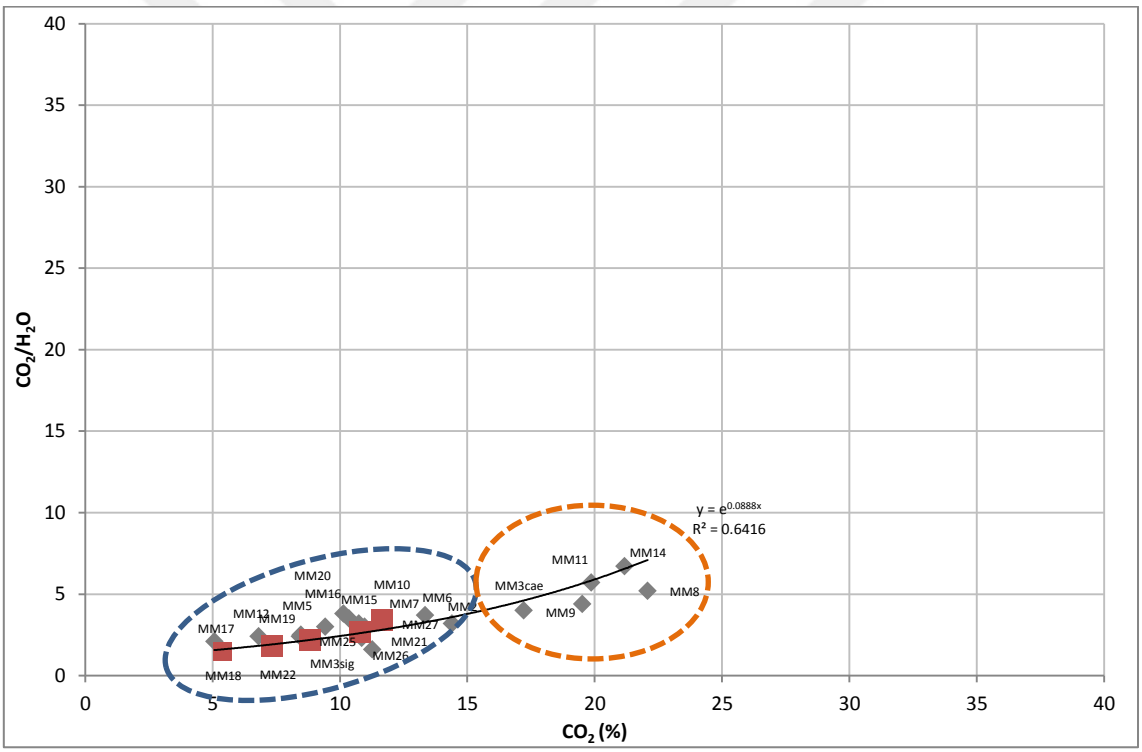


Figure 3.2- 41. CO_2/H_2O vs CO_2% graph of samples

From the graph several groups can be discerned. First group had CO_2/H_2O ratio below 4 and CO_2 was between 5-15 (MM2, MM3sig, MM5, MM6, MM7, MM10, MM12, MM15, MM16, MM17, MM18, MM19, MM20, MM21, MM22, MM25, MM26, MM27) and can be defined as highly hydraulic lime mortars. The second group had percentage of CO_2 between 15 and 25 and

CO_2/H_2O ratio between 4 and 8 (MM3cae, MM8, MM9, MM11, MM14) hydraulic lime mortars. It was also observed that all of the *opus signinum* mortars lay down between 5-12 CO_2 % in the first group. The dissolution of lime was more frequently seen in those mortars.

All mortars showed phase transition peak of quartz at 573°C. MM3cae, MM3 sig, MM16, MM18 showed peaks at 180°C those can be attributed to salts (Figure 3.2 – 42 - Figure 3.2-44).

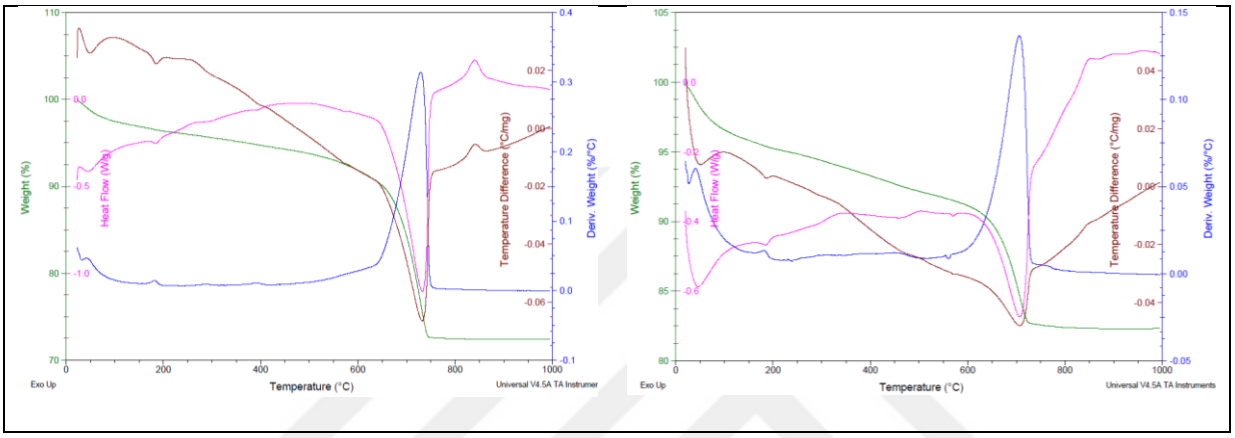


Figure 3.2- 42. Thermogram of MM3 *caementicium* (left) and *signinum* (right)

Although the sample MM5 was almost identical to sample MM3 cae they own highly different thermograms. MM5 had weight loss between 170 and 200°C and between 300 °C and 400 °C (magnesite) and calcium carbonate decomposition occur between 500 and 750 °C. This phenomenon indicated that the first weight loss was due to salts that cause earlier decomposition degrees (Silva, 2003). Weight loss below 100°C was the indication of free water probably related to the ceramics.

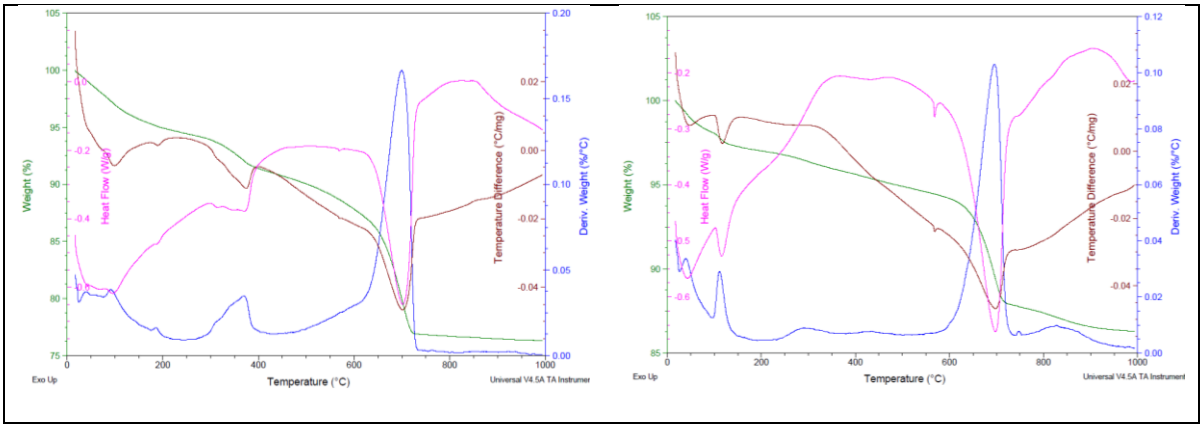


Figure 3.2- 43. Thermogram of MM5 on the left MM12 on the right

MM12, MM5, MM7, MM10 had a well-marked weight loss between 200 and 400°C due to magnesite content. In addition, MM12 had peaks at 750°C and over 800°C which implies recrystallization and calcite as aggregate and weight loss between 100 and 150°C due to the hydrated salts.

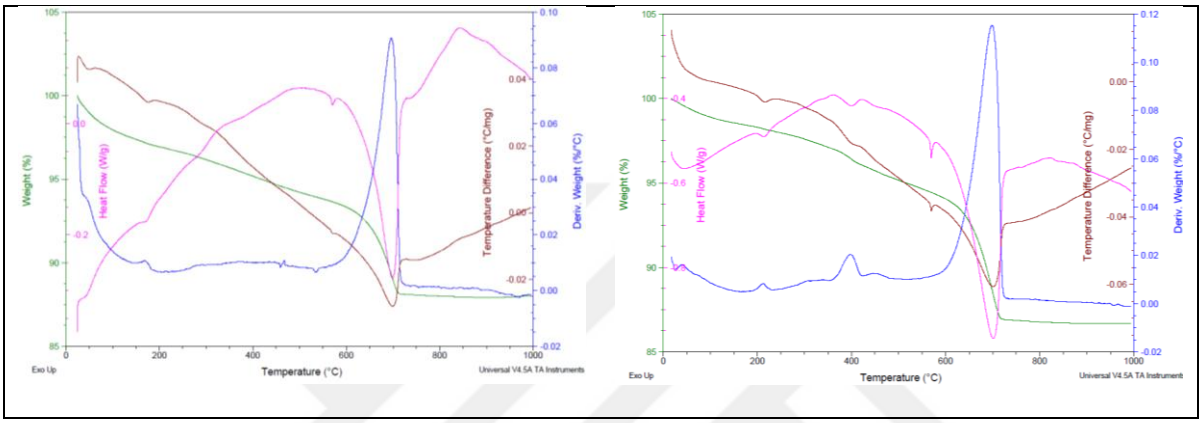


Figure 3.2- 44. Thermogram of opus signinum mortars (MM18 on the left and MM22 on the right)

MM22 had peak at 200°C and weight loss around 400°C which indicates magnesite (Figure 3.2 - 44). Binder aggregate ratios vary between 0.1 and 0.9 on the other hand calcium carbonate percentage was in between 10 and 50% (Figure 3.2- 45). The results coincide with the previous grouping, *opus signinum* mortars were placed in the left zone in the first group. Sample MM18 (Bath) and MM6 (Alcazaba) binder aggregate ratio was higher than the CO_2/H_2O ratio which make us think that they own highly reactive aggregates.

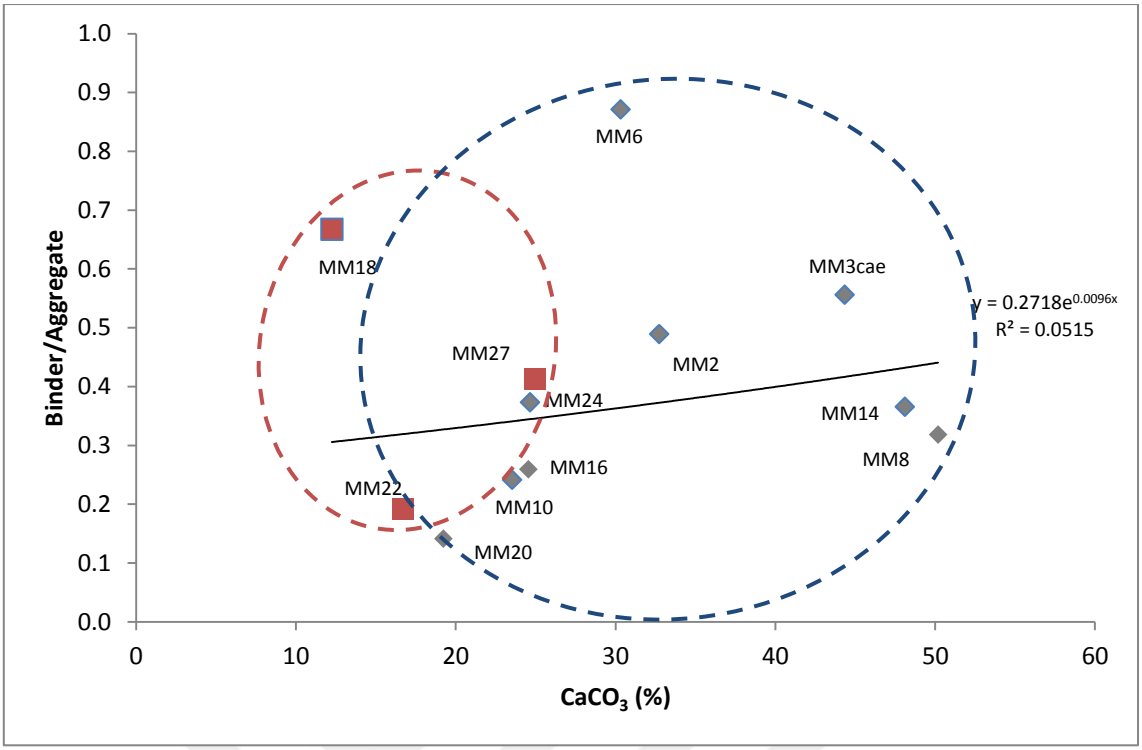


Figure 3.2 – 45. acid in/soluble fraction of Mérida mortars (red circle: *opus signinum*, blue circle: *opus caementicium* mortars)

3.2.8 X Ray Fluorescence (XRF)

Table 3.2 – 14 shows the geochemical composition of the mortar samples. It was revealed that Mérida mortars had high amount of MgO. Although in thermogravimetric analysis no specific peak associated to magnesite which was revealed in sample MM3cae, it had the highest amount of magnesium in elemental analysis.

.

Table 3.2- 14. Major elements of the Mérida mortars (%) (LOI: Loss of ignition)

	Samples		SiO_2	Al_2O_3	Fe_2O_3	MnO	MgO	CaO	Na_2O	K_2O	TiO_2	P_2O_5	LOI	Total
opus caementicium	**MM2**	channel	47.64	5.39	0.98	0.03	5.13	20.84	0.65	1.38	0.09	0.14	18.35	100.61
	MM3c	channel	41.74	10.79	5.01	0.08	7.11	15.95	0.68	0.98	0.5	0.21	17.31	100.36
	MM6	Alcazaba wall	37.58	3.44	1.15	0.02	4.04	27.88	0.45	0.84	0.09	0.15	23.62	99.26
	MM8	Moreira wall	30.55	4.65	1.42	0.03	3.23	30.87	0.97	0.79	0.17	0.28	26.32	99.28
	MM10	Temple floor	56.44	7.13	1.62	0.05	3.29	14.29	1.93	1.43	0.18	0.84	12.35	99.55
	MM14	Temenos wall	48.17	9.13	1.46	0.04	1.74	17.86	2.42	3.23	0.14	0.25	14.88	99.32
	MM16	Vrinero wall	65.44	6.5	1.28	0.04	3.65	9.8	1	1.63	0.14	0.12	9.72	99.32
	MM24	Amphiteatre	49.12	8.4	1.86	0.06	4.46	15.61	1.71	2.53	0.17	0.22	15.26	99.4
opus signinum	**MM18**	Bath lining	46.82	11.78	5.14	0.11	5.65	12.6	1.11	1.44	0.6	0.29	13.78	99.32
	MM20	Circo wall	62.64	8.62	2.17	0.06	5.17	8.14	1.63	2.04	0.2	0.24	8.75	99.66
	MM22	Amphiteatre	66.99	6.59	1.75	0.03	1.71	9.57	1.37	1.77	0.26	0.12	9.45	99.61
	MM27	Snow well	47.45	6.64	4.17	0.09	5.49	15.75	1.5	1.17	0.49	0.54	16.69	99.97

When y axis as binder and x axis is considered as aggregates in Figure 3.2- 46, it is possible to classify the samples. MM16, MM20 and MM22 were drawn apart with low CaO+MgO content and very high SiO_2+ Al_2O_3+ Fe_2O_3 content. Among the rest of the samples two groups can be discarded: first group having 50-70% alkali reactive aggregates and 15-25% binder and second group with <50% alkali reactive aggregates >30% calcitic binder includes MM6 and MM8 which were *opus caementicium* mortars. In the first group in centre both *opus caementicium* and *opus signinum* mortars were involved.

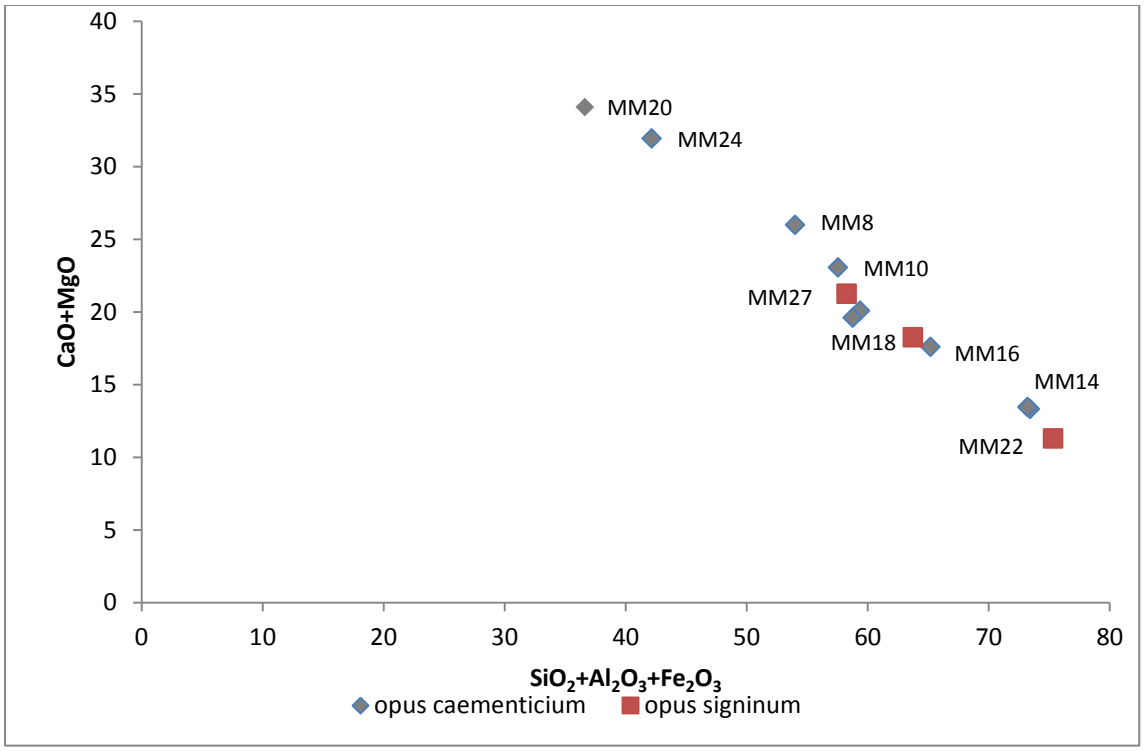


Figure 3.2- 46. CaO+MgO vs SiO_2+Al_2O_3+Fe_2O_3 graph of Mérida mortars

The majority of samples were situated close to each other 2-4 SiO_2/CaO and 0.09 TiO_2/Fe_2O_3 (Figure 3.2- 47). *Opus caementicium* mortars MM6 and MM8 having higher amount of binder were at left and MM16 and among *opus signinum* mortars MM22 was seen at right side apart.

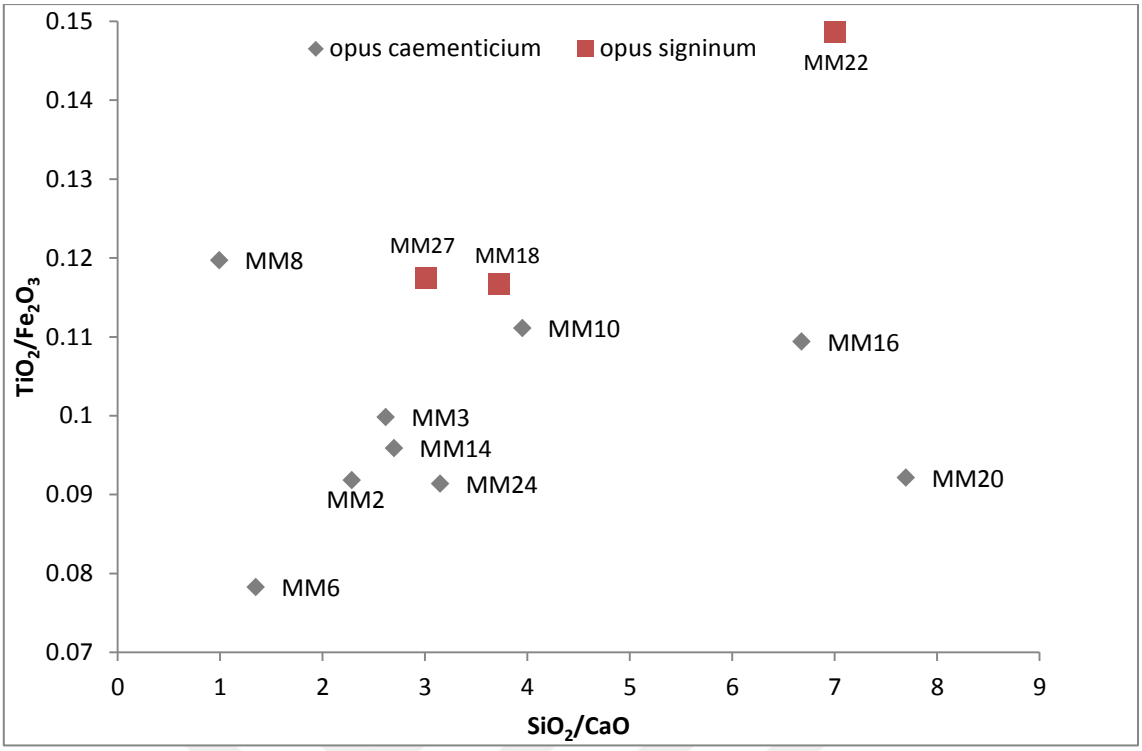


Figure 3.2- 47. TiO_2/Fe_2O_3 vs SiO_2/CaO graph of Mérida mortars

TiO_2/Fe_2O_3 vs CaO/MgO diagram (Figure 3.2- 48) allows similar distinction among mortars. Only, MM14 stays apart rather than MM16 here.

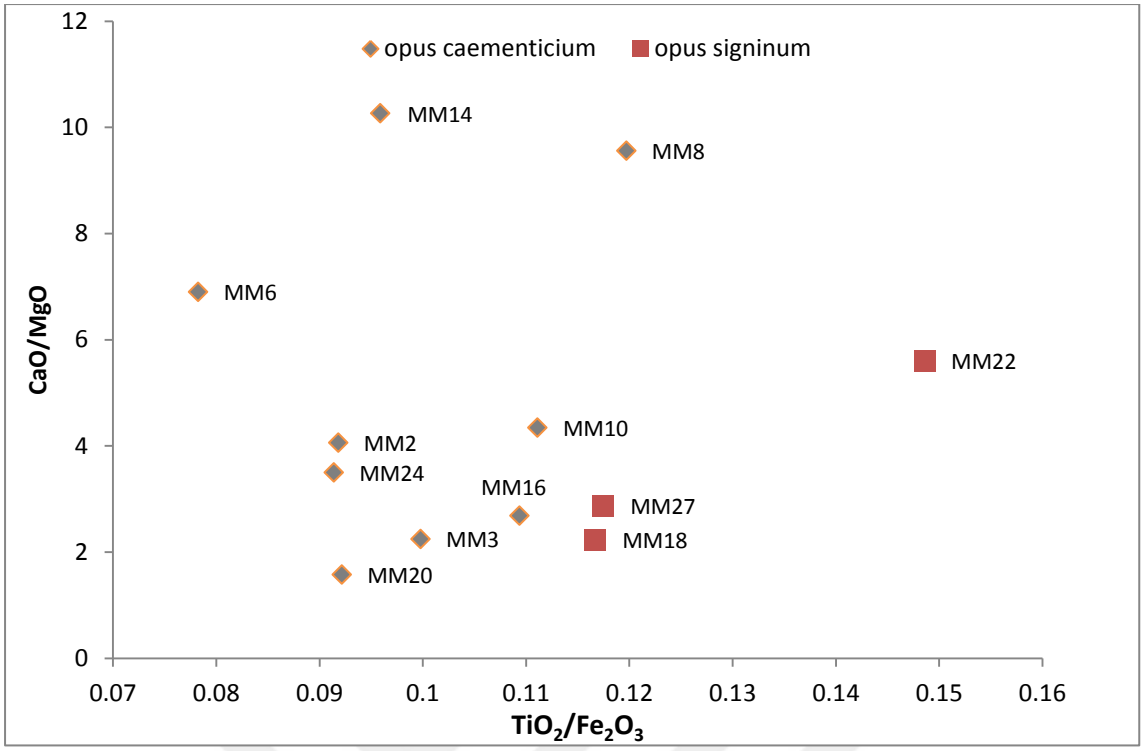


Figure 3.2- 48. CaO/MgO vs TiO_2/Fe_2O_3 graph of Mérida mortars

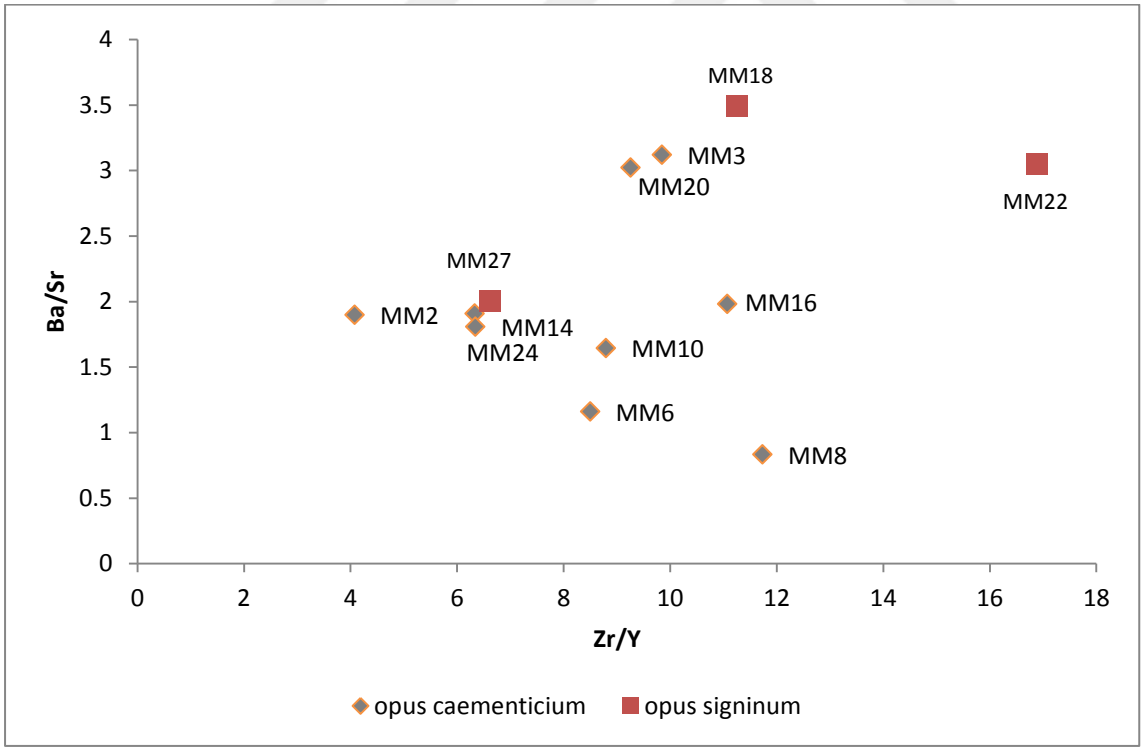


Figure 3.2- 1.Figure 3.2- 49. Ba/Sr vs Zr/Y graph of Mérida mortars

3.2.9 Mercury Intrusion Porosimetry

Sample MM8 had the highest porosity and highest average pore diameter, on the other hand MM26 had the highest bulk and real density value. *Opus signinum* class mortar MM22 had medium porosity among the samples. Average porosity and density of *opus caementicium* type mortars were 30% and 1.69 g/cm^3, respectively. In *opus signinum* there was not such a great difference; these values were 28% and 1.66 g/cm^3 (Table 3.2- 15). The reason of this distinct result can be the ceramics and rocks used in the mortars were less porous or there was less cracks/deterioration. In addition, keep in mind that in Mérida the sampled mortars were mostly *opus caementicium* type thus the variability was higher.

Table 3.2- 15. Parameters gathered by mercury intrusion (P: Porosity, APD: Average Pore Diameter (4V/A), BD: Bulk density, RD: Real density)

Samples		P (%)	APD (4V/A) (µm)	BD (g/ml)	RD (g/ml)
MM8 (OC)	Moreira wall	40.12	0.22	1.4	2.33
MM10 (OC)	Temple floor	30.54	0.04	1.73	2.49
MM14 (OC)	Temenos wall	26.53	0.13	1.76	2.39
MM26 (OC)	Snow well	24.62	0.14	1.89	2.5
MM22 (OS)	Amphitheatre	28.88	0.18	1.66	2.33

MM8 showed a quasi trimodal distribution. It had macropores greater than 100 µm and from 100 µm to 0.005 µm a wide pore size distribution was interrupted with a peak between 50 µm and 10 µm (Figure 3.2- 50).

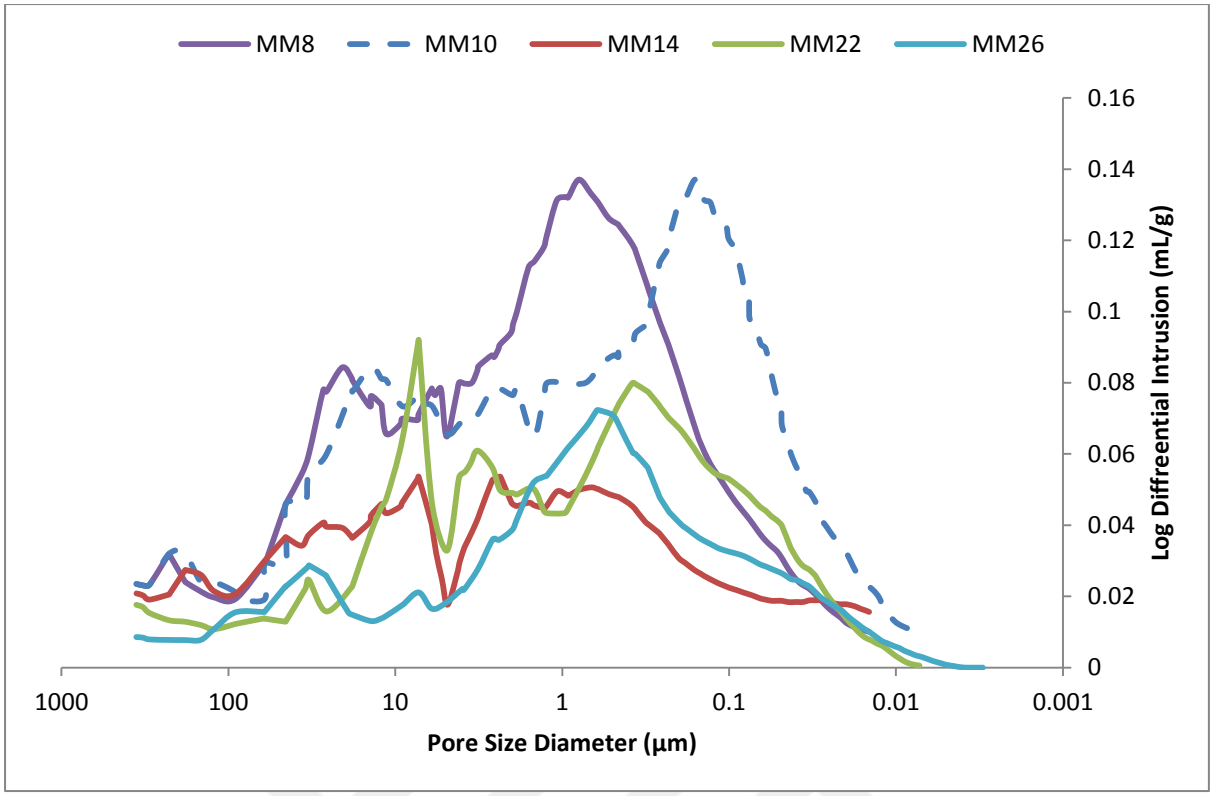


Figure 3.2- 50. Log differential intrusion versus pore size of the Mérida samples

Pore size distribution of MM10 however, a little peak between 80 µm and 20 µm, 10 µm and 8 µm, 5 µm and 3 µm before the highest accumulation of pores which was between 1 µm and 0.1 µm, Micropores were distributed mainly between 0.5 µm and 0.008 and 0.008 and 0.003 µm. MM14 showed quasi bimodal pore size distribution. It had macropores and till 8 µm first peak and the second between 8 µm and 0,005 µm with two humps on midi and micro pores zones.

In MM22 pores were distributed variously. Macropores were present and little peak in between 50 µm and 20 µm, the highest narrow peak was between 20 µm and 8 µm and with less macropores, the highest peak narrow range was between 11 µm and 8 µm, wide peak between 1 µm and 0,005 µm. MM26 showed a bimodal distribution first 80 µm and 10 µm, the second accumulation was between 8 µm and 0,005 µm (Table 3.2- 16).

Table 3.2- 16. Pore size distribution and percentages of micro and macropores

Samples		Micro < 5 µm	Macro > 5 µm	< 0.01 µm	0.01- 0.1 µm	0,1 - 1 µm	1-10 µm	10 - 100 µm	>100 µm
MM8 (OC)	Moreira wall	67.5%	32.5%	-0.47%	8.21%	35.63%	32.07%	19.62%	4.94%
MM10 (OC)	Temple floor	70.5%	29.5%	2.71%	30.03%	24.04%	24.24%	11.45%	7.54%
MM14 (OC)	Temenos wall	58.1%	41.9%	-1.52%	12.30%	26.69%	29.87%	24.05%	8.60%
MM26 (OC)	Snow well	77.9%	22.1%	0.74%	15.70%	41.02%	24.49%	14.29%	3.76%
MM22 (OS)	Amphitheatre	72.7%	27.3%	0.10%	15.48%	36.81%	30.97%	12.48%	4.17%

3.2.10 Correlations of results according to architectural features

The mortars obtained from San Lazaro aqueduct and from the rest of the city had different appearances. In the channel of aqueduct there were several levels. In the core of the walls of channel white-crème colour mortar with small aggregates were used and on top of it a mortar with greater aggregates of both ceramic and dark coloured rock fragments (*caementa*) were placed. In very white colour binder fly ashes were present. These mortars had more magnesium content than others. On top of it, *opus signinum* type reddish mortar with angular ceramic aggregates was used to cover the channel. A thin, grey colour plaster, between these two layers can be observed by naked eye. The ultimate layer was applied with rounded off edges in the channel not only to let the water flow better but also prevent from deteriorations which may cause by the pressure of water (Jimenez Martin, 1977; Robador et al. 2010). Robador et al (2010) stated that in the aqueduct channel in Mitraeum House the high quality lime binder, siliceous sand and ceramic aggregates were used. It perfectly matches the Sanz Lazaro aqueduct mortars and the mentioned house was constructed late first early second century AD, meaning that they use the same construction style in the same period.

Other encountered *opus signinum* mortar was coating mortar in Thermal Bath which had medium to poorly sorted ceramic aggregates embedded in very red binder. The rest of that type mortars in snow well or in amphitheatre had appearance closer to *opus caementicium* mortars, accordingly, the use of ceramic was not thought to be in purpose. Instead, by casualty they could had added ceramic. In the rest of the city these mortars had crème/ light brown colour binder and poorly sorted aggregates which were smaller in size. Spectrophotometry results exhibited that the coating mortars, which were typical *opus signinum* type mortars, from aqueduct and Bath had saturation values between 15 and 20 and luminosity values around 60. On the other hand, the mentioned discernible white colour binders from aqueduct made the mortars situated between high luminosity the rest of the samples showed homogeneity in colour between 8.5-15 C* and 65-80 L*.

Binder: aggregate values of the coating mortars which were in *opus signinum* group were 1:1. Besides, floor mortars had 1:4 B:A ratio. Proportions of wall mortars varied in the city. Alcazaba and Bath mortars had 1:1 ratio, Moreria 1:3, Viñero wall 1:4 and Circus 1:5. If the rule deduced from Complutum that "adding more aggregate to mortar latter centuries" was applied to Mérida as well, Alcazaba and Thermal Bath were supposed to be the earlier constructions while, the others were latter.

In all of the mortars fine grains (<63µm) were in high amounts this was an indicator that the mortars had higher pozzolanicity. This "fine grain" may include fly ashes which were visible by naked eye as well. Ignoring the large fragments bigger than 2 mm, the rest of the distribution was symmetric.

In the microscopic observations the use large rock fragments were frequently encountered. Raw materials from surrounding were used as revealed in previous studies as well (Robador et al. 2010; Mota-López et al. 2016). Monzogranite, slate, schist, quartzite and were the metamorphic examples. In addition, sedimentary and igneous rocks were present as well such as graywacke and diorite. Actinolite was a silicate mineral that was found in that rocks in the outcrop in the *arena* of the amphitheatre (Mota-López, 2015) and revealed in the mortars in both microscopic and XRD analysis. The addition of that rocks and minerals together with fly ashes caused the alkali silicate reaction and a better bonding between lime and aggregate. The reaction rims around the aggregates could be the demonstration of the phenomenon.

It was possible to approximate the same construction period mortars according to the rock fragments. Diorite was encountered in the mortars of San Lazaro aqueduct and Circus and Moreria wall. Knowing that circus was constructed in the first century AD, mortars of aqueduct could be from the first construction phase and the Moreria construction can be conjectured as first century AD. Accordingly, mortars from archaeological remains of Viñero and Snow well had monzogranite, greywacke and amphibolite just like the mortars from the channel of aqueduct San Lazaro; therefore both of the archaeological remains of Viñero

and snow well were probably constructed at the same period. Alternatively, mortars of amphitheatre and Temple of Diana, which were constructed in first century BC, contained quartzite, schist, greywacke and amphibolite. Hence, archaeological remains of Viñero and Resti Bath had the possibility to had been constructed in first century BC. Furthermore keep in mind that archaeological remains of Viñero were thought to be part of a temple in the forum next to the Temple of Diana. Under microscopic observations particle distribution of snow well mortars were noted differently than others, they had medium sorted grain size distributions also this may be an indicator of a different phase of construction.

On the other hand, in XRF results we saw that the mortar that was sampled from the wall in front of the entrance of amphitheatre was slightly different from others in composition. It had less calcium and iron than other samples. Similarly, mortars from Circus, Viñero and Temple of Diana had high SiO_2 and low CaO values and on the contrary, mortars of Moreria and Alcazaba walls had higher CaO and the highest loss of ignition values thus the most carbonated binders.

According to the classification done after TGA data, among *opus caementicium* type mortars of San Lazaro, Moreria and Temple of Diana wall and floor were classified as hydraulic mortars and the rest were highly hydraulic lime mortars laying down the 5-15 % CO_2. Besides, mortar sample from aqueduct which had the highest structurally bound water content was the sample with straw. Organic additives and fly ashes were supposed to support the hydraulicity. The presence of saline phases was detected in the mortars of San Lazaro, Temple of Diana, amphitheatre and Circus from TGA which coincided with the chlorites revealed in XRD analysis.

Mortars with high pozzolanity were encountered in Bath coating and Alcazaba wall. There may not be any specific reason for Alcazaba wall if there was not undiscovered water related function; already the used reactive rock fragments gave the hydraulic property to the mortars.

In Temple of Diana all of the sampled mortars were *opus caementicium*, including the floor and basement mortars as well. Basement mortars which can be described as lower level floor mortar had beige colour and had similar large rock fragments with other samples from channel vault and *temenos* walls. The mortar from floor upwards on the other hand had crème colour and only slate was present as rock fragment with poorly sorted quartz and feldspar. The sample from the channel in front of the temple, lower level foundation mortar, the inner wall of *temenos* had higher hydraulic properties than others (Ergenç and Fort, 2017).

3.3 Nysa on the Meander Archaeological Site

Collected samples were characterized multi-analytically. The results of the utilized techniques were described in macroscopic, physical, petrographic, mineralogical, and geochemical order.

3.3.1 Macroscopic description of the samples

In Nysa of Meander *opus caementicium* mortars were collected from wall of tunnel, theatre, library, pillars of bridge and next to pipeline in the arch of Bath. Porous mortars had white, crème, light brown colour binders with small-big size aggregates (<1.2 cm). They were consistent mortar with high cohesion. Poorly to medium sorted grain size distribution was observed. Lime lumps were visible by naked eye in the majority of samples. Although mortars collected from tunnel had quite darker colour they can be classified both as *opus caementicium* mortars due to the absence of ceramic aggregate and *opus signinum* mortars due to the fact that binder colour implies ceramic dust (Figure 3.3- 51).

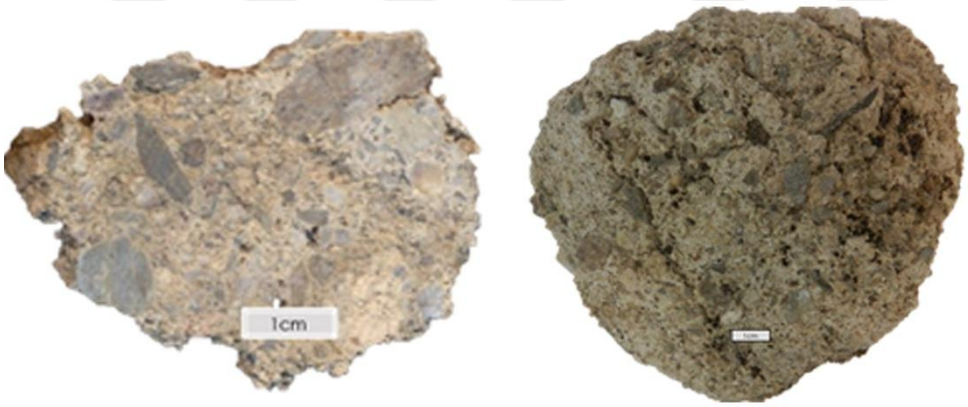


Figure 3.3- 51. Examples of *Opus Caementicium* mortars (NM05 on the left, NM24 on the right)

Opus signinum mortars which had reddish colour with the use of ceramics were encountered in the arches of basilica shop and bath, in the road floor and as coating mortar, Stadium and Gymnasium. The cohesion of the mortars was lower than *opus caementicium* mortars. Angular and sub-angular ceramic aggregates were bigger in size and medium to well sorted in reddish colour matrix. Mortars of that type own lower cohesion. Binder had reddish colour

and angular ceramic aggregates (< 5 mm) were observed. Grain size distribution was medium to well sorted.

Binder had reddish brown colour and light and dark to light sub-angular to angular sand grains (< 4 mm) and white colour quartz grains were observed. Pore and grain sizes were various, grain size distribution was poorly sorted (Figure 3.3- 52).



Figure 3.3- 52. Examples of *Opus Signinum* mortars (NM13 on the left, NM16 on the right)

3.3.2 Colour Spectrophotometry

The colours of both type of opus mortars of the site, determined by the spectrophotometry technique (see chapter part 2.1.6), were different. *Opus caementicium* mortars had high luminosity (65-75 units) and saturation between 10 and 15 units. In *opus signinum* the luminosity was less than 70 units (60-70) and the degree of saturation was higher than that of *opus caementicium* (Figure 3.3- 53).

It was seen from Figure 3.3- 53 that the majority of the mortars were clustered together between 10 and 15 saturation (Chrome) and 60-75 luminosity, 4 samples NM16, NM23, NM09 and NM15 were shifted to right. Those were the samples with ceramic aggregates and reddish binders.

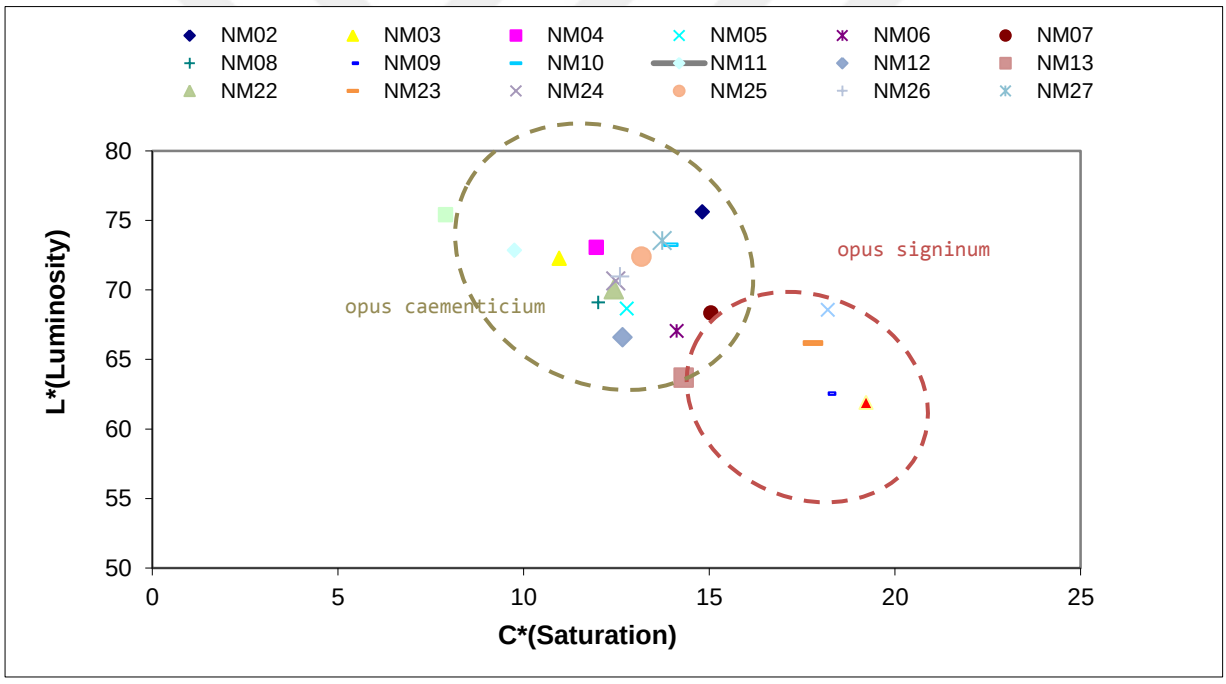


Figure 3.3- 53. Luminosity vs Chrome of Nysa mortars

The colour tone was also different between the two types of mortars. The *opus caementicium* presents lower values for the parameters a * and b *, while the *opus signinum* gives values indicating pinkish-red tone (a* values between 4 and 10 and b* values between 10 and 15) due to the incorporation of brick dust (Figure 3.3- 54). The trend of those two groups were reversed, as higher the a* values higher the redness and higher the b* refers to

yellowness, NM23, NM6 and NM15 were again located seperated from the rest of the samples due to higher red (a*) values, sample NM09 which had high saturation like others , appears to had more yellow. NM07 had more a* values while the majority of the samples lay down between 2 and 5 in a* and 10 and 15 in b*.

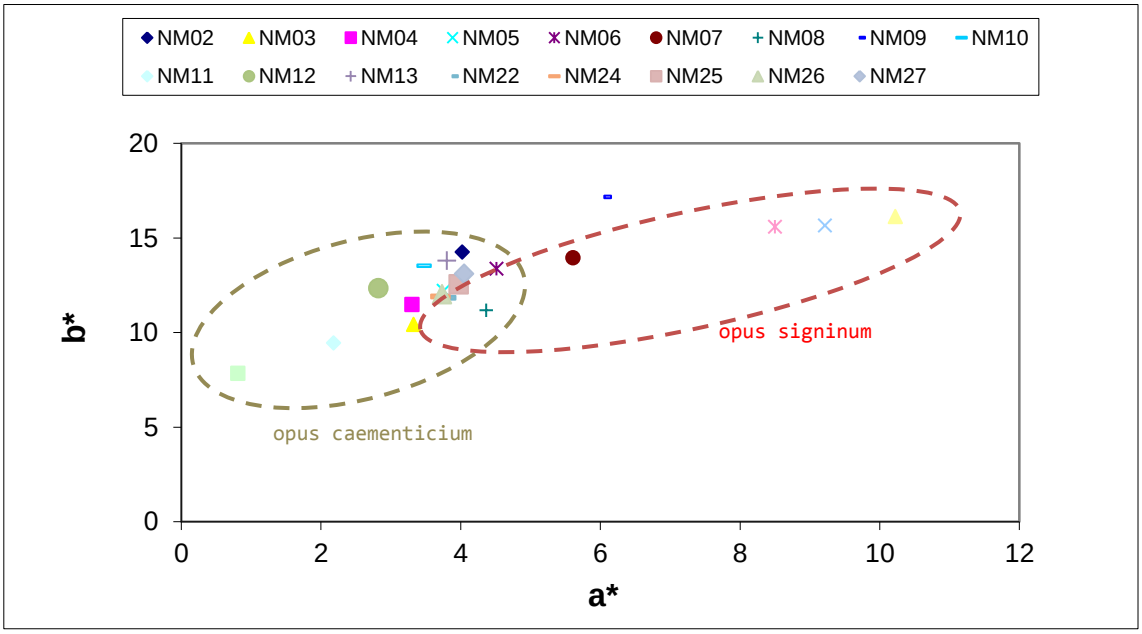


Figure 3.3- 54. Chromatic parameters b* vs a* of Nysa mortars

3.3.3 Surface Hardness

As shown in the Figure 3.3- 55 the *opus caementicium* samples had hardness between 170 and 240 leebs with the exception of Agora road mortar (NM14).The lowest hardness values belong to bridge 1 (NM03), theatre (NM09) and library (NM10). Stadium mortars NM08 and NM23 had identical values (179 leebs).

Bridge 2 (NM05 and NM24), cistern (NM01), lower level tunnel mortars (NM04 and NM13), Geronticon (NM06) had close values following them. NM02, NM07, NM22 and NM27 had average values around 240 leebs.

Among the *opus signinum* group mortars from arches of Bath construction (NM25 and NM26) had the highest surface hardness values. Basilica (NM07) and gymnasium (NM11) had intermediate values and stadium mortars showed the least hardness.

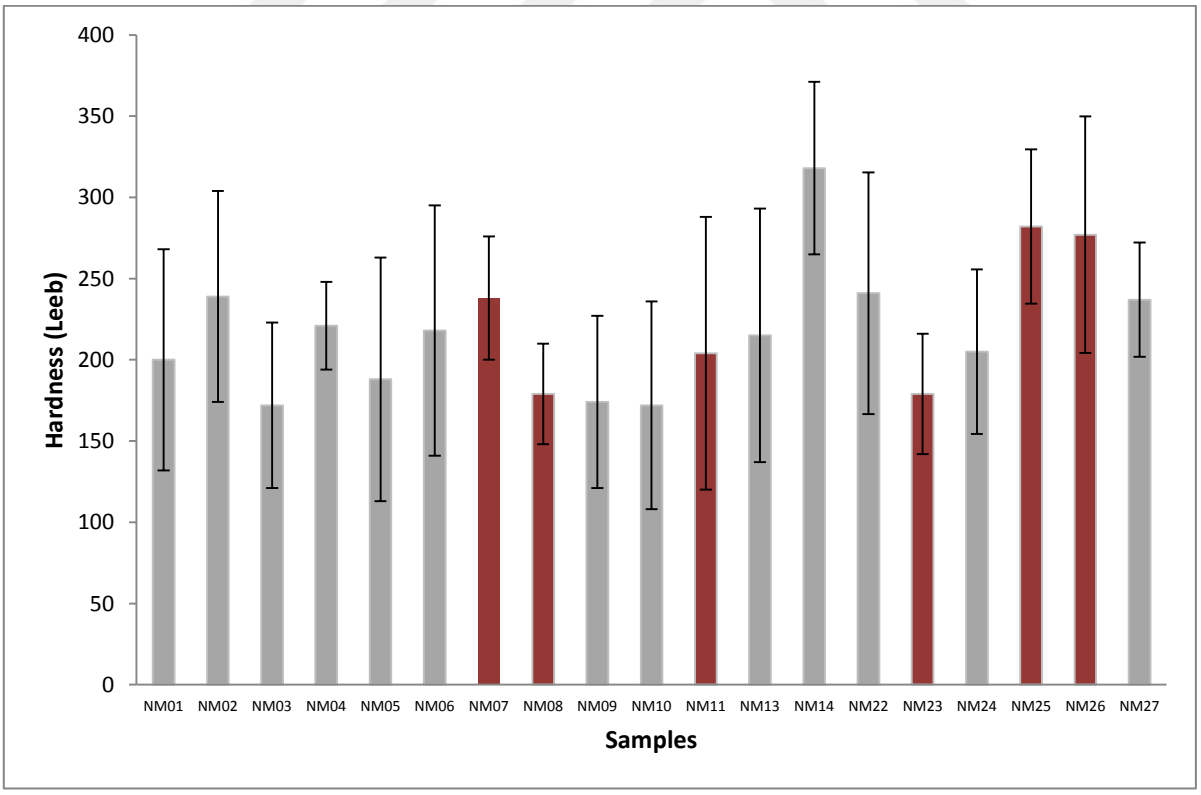


Figure 3.3- 55. Surface hardness values of Nysa samples

3.3.4 Optical Microscopy

Opus caementicium mortars had medium to poor grain size distribution the proportion can be estimated as 30-40% binder and 60-70% aggregates mainly consisting of quartz grains. High amounts of rounded, sub-rounded pores were interconnecting sometimes (Figure 3.3- 56a). Apart from quartz, feldspar and biotite (Figure 3.3- 56b), calcite was observed in the sample from bridge (Figure 3.3- 56c). Particle shapes were irregular and surface textures were changing between angular and sub-angular. In the matrix dense clay was observed. Various dimensions of gneiss, marble, schist rock fragments, ceramic fragments were observed. Old mortars were used in Gerontikon (NM06) as filler and theatre (NM09) which indicate different construction phases and/or restorations. Shrinkage cracks due to rapid drying were observed around the aggregates in the mortars (Figure 3.3- 56d).

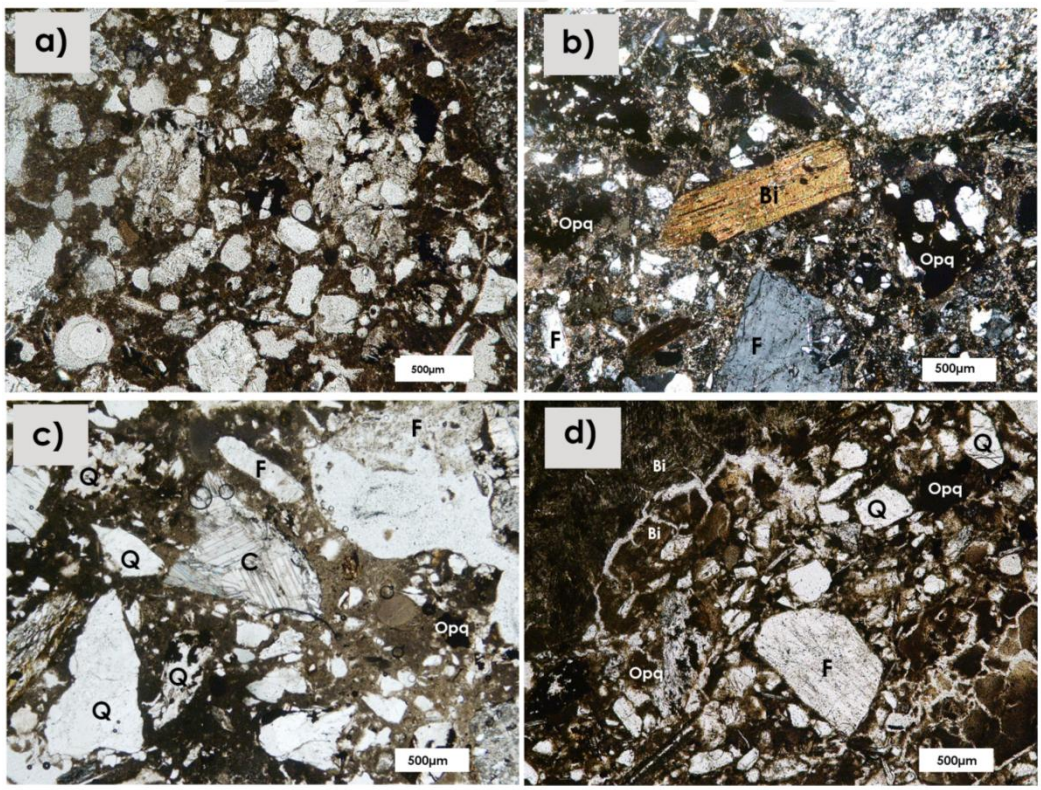


Figure 3.3- 56. *Opus caementicium* mortars a) NM02 b) NM04 c) NM24 d) NM10 (Q: quartz, C: calcite, F: feldspar, Bi: biotite, Opq: Opaque mineral)

On the other hand *opus signinum* mortars had large ceramic aggregates very well integrated to lime binder. Opaque minerals, quartz, feldspar and in some sample other lithic fragments were present as well. Recrystallization in the pores and cracks were occasionally observed (Figure 3.3- 57). Grain size distribution was poorly sorted.

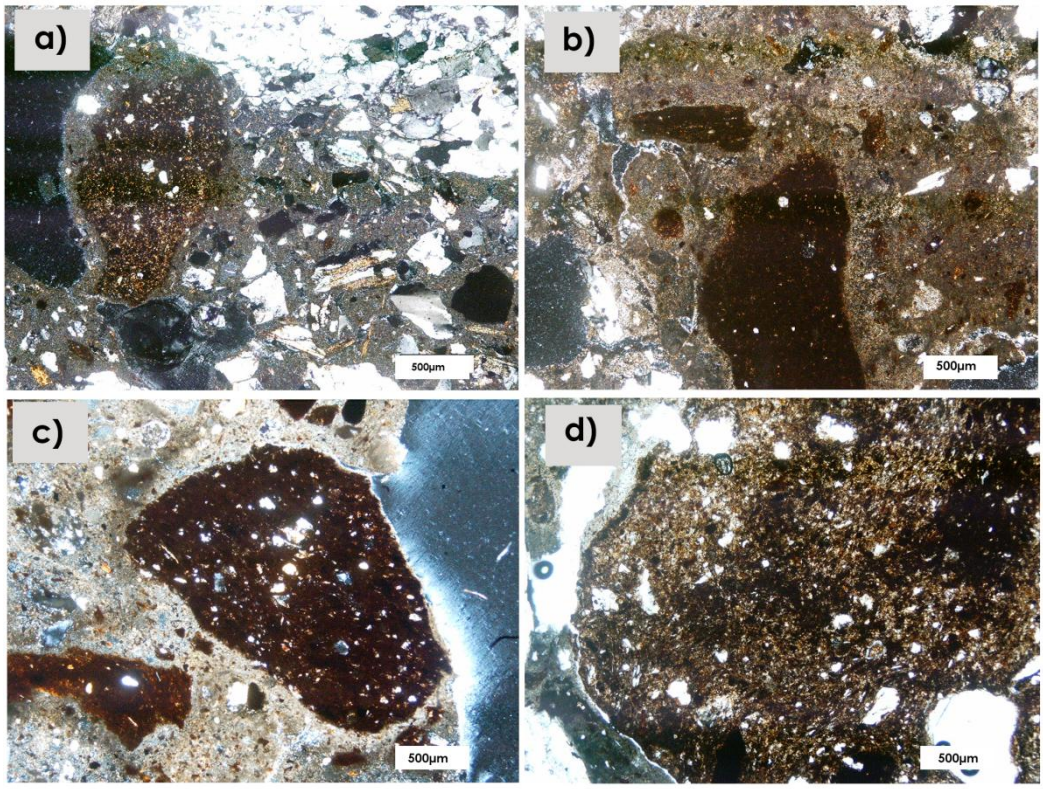


Figure 3.3- 57. *Opus signinum* mortars a) NM08 b) NM11 c) NM15 d) NM16

Under plane polarized light in *opus caementicium* mortars binder appears with dark colour generally, only in theatre (NM09), library (NM10) and locally second bridge east pillar mortars (NM24) had lighter colours. The difference comes from recrystallization of carbonated binder which was seen lighter colour. This phenomenon existed in all *opus signinum* mortars. It could be the re-precipitation as a result of carbonate dissolution of the lime binder matrix.

Various dimensions of crushed rock fragment aggregates like gneiss, marble, metaquartzite, garnet mica-schist which were abundant in the vicinity (Figure 2.1- 20) were encountered in the mortar samples (Figure 3.3- 58).

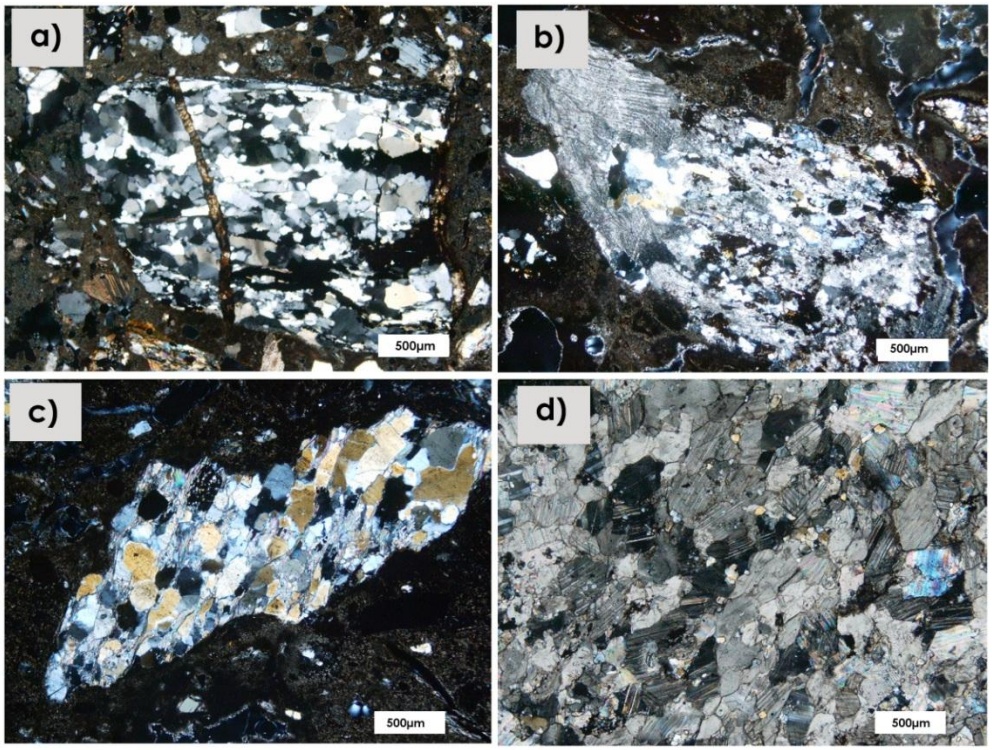


Figure 3.3- 58. Rock fragments found a) quartzite in NM02 b) schistositic metamorphic rock in NM04 c) metaquartzite in NM24 d) marble in NM26

Besides, reaction rims around the ceramic and lithic fragments were observed in Nysa mortars (Figure 3.3- 59). All samples had highly porous un/carbonated lime binder that place to place showed shrinkage cracks due to rapid drying. Clayey appearance was common in all of the mortars. Lime lumps were not frequent in the mortars.

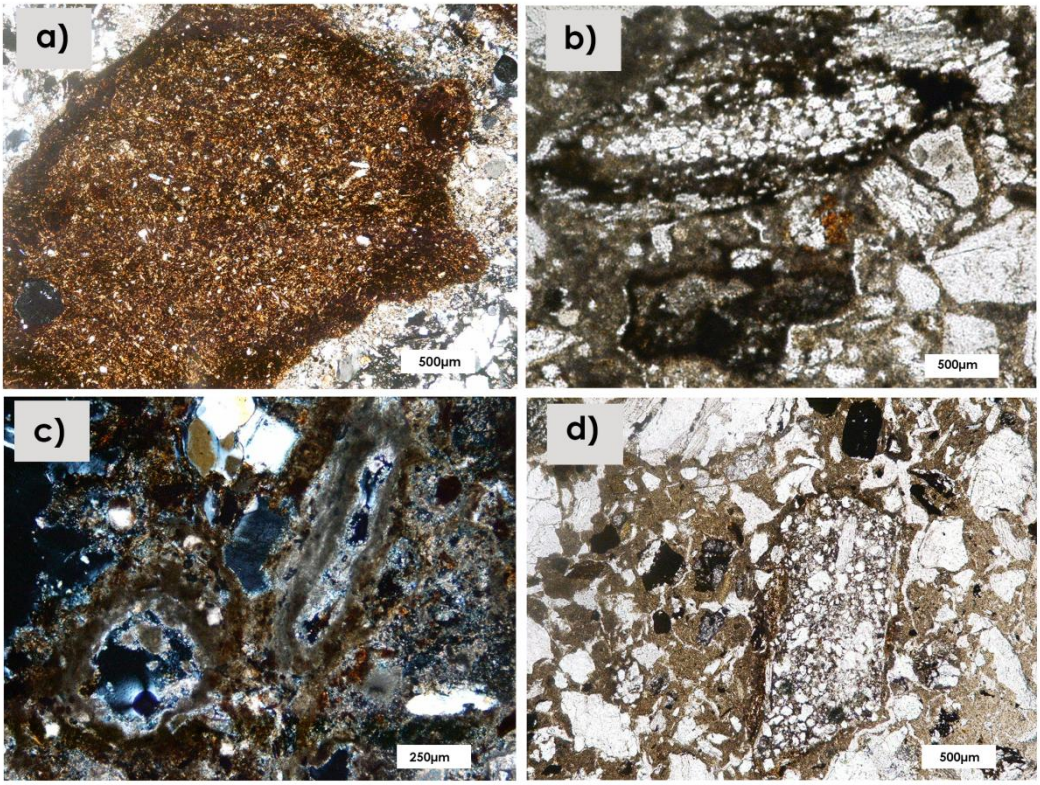


Figure 3.3- 59. Reaction rim around a) ceramic fragment in NM07 b) polycrystalline sliicic rock in NM05 c) recarbonation and recrystallization around pores in NM15 d) old mortar relict in NM06

The petrographic observations were categorized below (Table 3.3- 17). In cistern and first ridge only gneiss, in the west pillar of second bridge in addition to gneiss, quartzite and slate in the east pillar of the same bridge, Agora floor, stadium and theatre. Library and bath mortars comprise marble fragment as well.

Table 3.3- 17. Mineralogical composition of the mortars (Qtz: quartz, Fsp: feldspar, Cal: calcite, Mca: Mica, Op: opaque mineral, shr: shrinkage, inc.: inclusion)

	Samples		Binder	Minerals	Lithic and ceramic fragments, additives, others
Opus Caementicicum	NM01	cistern	Dark colour micritic calcite	Qtz, Fsp	gneiss
	NM02	bridge 2W	Dark colour micritic calcite	Qtz, Fsp	gneiss, quartzite, chamotte,
	NM03	bridge 1	Dark colour micritic calcite	Qtz, Fsp	gneiss
	NM04	tunnel low	Dark colour micritic calcite	Qtz, Fsp, Mca	gneiss, schist
	NM05	bridge 2E	sparitic calcite	Qtz, Fsp	gneiss, ferric inclusion
	NM06	Geronticon	Dark colour micritic calcite	Qtz, FspMca	gneiss, elongated polycrystalline rock
	NM09	Theatre	light colour micrite	Qtz, Fsp	gneiss, slate
	NM10	Library	brown colour micrite	Qtz, Fsp	gneiss, marble
	NM22	Bridge 2 W	Dark colour micritic calcite	Qtz, Fsp	gneiss, slate, quartzite
	NM24	bridge 2E	dark/ light colour binder	Qtz, Fsp, Cal	gneiss, slate, schist
Opus Signinum	NM07	Basilica arch	light colour micrite	Qtz, Fsp, Op	gneiss, quartzite, ceramic
	NM08	Stadium	brown colour micrite	Qtz, Fsp	gneiss, ceramic,
	NM11	Gymnasium	brown colour micrite	Qtz, Fsp, Mca	gneiss, ceramic
	NM15	Agora floor	light colour micrite	Qtz, Fsp	gneiss, ceramic, slate
	NM16	Agora coating	light colour micrite	Qtz, Fsp	gneiss, ceramic, polycrystalline quartz
	NM23	Stadium	light colour micrite	Qtz, Fsp	gneiss, ceramic, slate
	NM26	Bath arch	brown colour micrite	Qtz, Fsp	marble, ceramic, slate, quartzite

3.3.5 Binder aggregate ratio and grain size distribution

After HCl attack soluble parts of the mortars were accepted as binder and insoluble parts as aggregates. Percentages of binders and aggregates of the samples were listed below (Table 3.3- 18).

Table 3.3- 18. Binder and aggregate ratios (%)

	Samples		Binder (%)	Aggregate (%)	B:A
opus caementicium	**NM02**	Bridge 2 W	20.49	79.51	1:4
	NM04	Tunnel low	20.29	79.71	1:4
	NM05	Bridge 2 E	25.1	74.9	1:3
	NM10	Library	28.22	71.78	1:3
	NM12	Tunnel up	23.64	76.36	1:3
	NM13	Tunnel low	25.26	74.74	1:3
	NM22	Bridge 2 W	16.67	83.33	1:5
opus signinum	**NM08**	Stadium	24.56	75.44	1:3
	NM11	Gymnasium	25.19	74.81	1:3
	NM16	Agora coating	28.37	71.63	1:3
	NM25	Bath arch	22.18	77.82	1:4
	NM26	Bath arch	14.43	85.57	1:6

As illustrated below (Figure 3.3- 60) the majority of Nysa mortars had 1:3 binder aggregate ratio (B:A). Among them, mortars from stadium (NM08), gymnasium (NM11) and coating mortar in Agora road (NM16) were *opus signinum* mortars with ceramic dust. *Opus caementicium* mortars collected from the east pillar of second bridge (NM05), library (NM10), lower and upper layer of tunnel (NM12 and NM13) had 1:3 proportion as well. NM02, NM04 and NM25 had 1:4 while other mortar from west pillar of second bridge NM22 showed 1:5 ratio and other bath arch mortar NM26 had 1:6 binder: aggregate ratio.

The higher aggregate proportion of the samples from thermal bath was the use of large dimension ceramic fragments. In different mortars taken from water related civil works (bridge and tunnel) grain size distribution varied; mortars from the lower part of the tunnel (NM4 and 12) and west pillar of second bridge the aggregate granulometry were superiors

to the mortars of east pillar of second bridge and another sample of west pillar of second bridge (NM22) and upper level of the tunnel (NM13) (Table 3.3- 19).

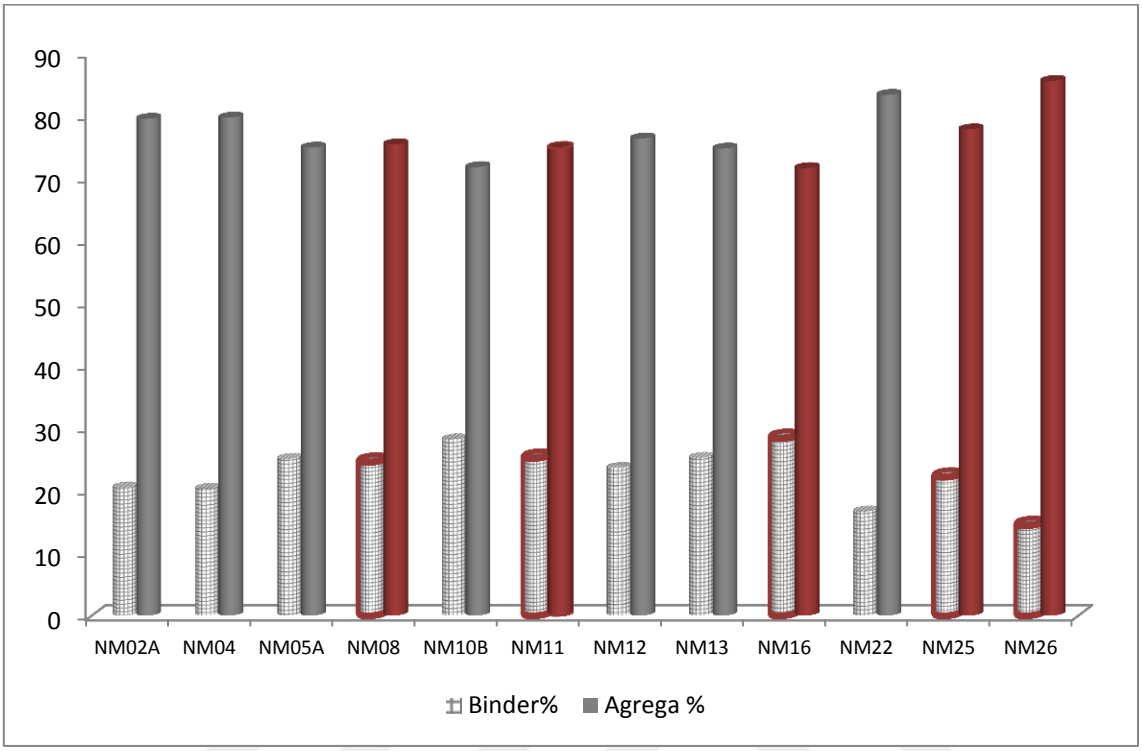


Figure 3.3- 60. Binder aggregate ratios of Nysa mortars

Table 3.3- 19. Weight passing each sieve (%)

Samples			>2mm	1<x<2 mm	0,5<x<1 mm	0,25<x<0,5 mm	0,125<x<0,25 mm	0,063<x<0,125 mm	<0,063 mm
opus caementicium	**NM02**	Bridge 2 W	18.20	20.33	21.99	15.84	12.53	8.27	2.84
	NM04	Tunnel low	51.82	10.91	11.82	11.21	8.48	3.64	2.12
	NM05	Bridge 2 E	28.80	19.37	21.20	15.18	9.42	3.93	2.09
	NM10	Library	23.44	17.45	20.05	14.32	13.28	7.81	3.65
	NM12	Tunnel up	42.42	12.34	14.94	12.55	9.09	5.63	3.03
	NM13	Tunnel low	25.80	20.55	17.58	13.70	13.01	6.85	2.51
	NM16	Agora coating	52.90	11.11	8.45	8.45	9.42	6.04	3.62
	NM22	Bridge 2 W	52.56	15.35	13.49	9.30	6.05	1.86	1.40
opus signinum	**NM08**	Stadium	19.23	16.92	22.56	19.23	13.08	5.90	3.08
	NM11	Gymnasium	28.72	22.98	19.84	11.23	9.40	5.48	2.35
	NM25	Bath arch	51.49	16.78	9.66	6.21	6.67	5.98	3.22
	NM26	Bath arch	28.42	26.42	26.32	12.63	3.16	1.05	2.00

As seen in Table 3.3- 19 and Figure 3.3- 61, grain size distribution of *opus signinum* mortars of coating (NM16) and arch of bath (NM25) were identical, having the highest mass due to big ceramic aggregates (> 2mm). Tunnel mortars (NM04 and NM12) apart from the similarly high values above 2mm, had symmetric distribution. Mortars of east and west pillars of bridge (NM05 and NM22) as well as gymnasium (NM11) and tunnel mortars (NM13) showed descending distribution. The difference in the grain size distribution despite the homogeneity in binder aggregate ratios implies that in time of elaboration the sizes of the grains did not had great importance.

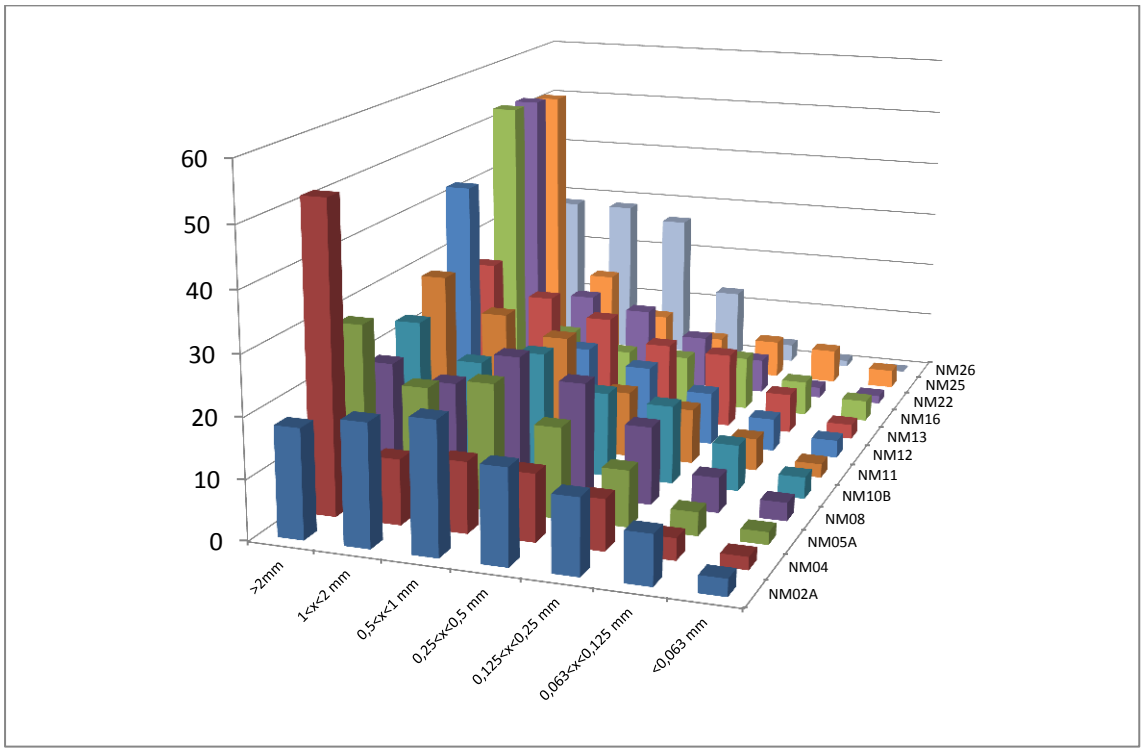


Figure 3.3- 61. Grain size distribution graph of Nysa mortars

Fine particles below 63μm may include ceramic dust and/or pozzolanic additives. NM16, NM08 and NM25 had the ceramic dust and relatively high amount of fine particles could be ascribed to pozzolanic additives in the mortars of bridge (NM02), library (NM10) and tunnel (NM12).

3.3.6 X-Ray Diffraction

The results of semi-quantitative analysis XRD showed that quartz, calcite, albite/anorthite and biotite were the omnipresent mineralogical constituents. In the samples NM01, NM15, NM16 and NM23 calcite is more abundant, whereas in NM02A, NM12, NM25, NM26 and in NM27 both present in equal amounts and quartz was predominant in the rest of the samples (Figure 3.3- 62). The majority of the diffractograms of the samples include kaolinite/phillipsite peak (~7.17 Å). Considering the present mica in the mortars was coming from ceramics, it can be interfered that firing temperature of the ceramics in the mortar is below 900˚C. Above this degree, high temperature mineral phases mullite and crystoballite were observed rather than mica and amorphous structure (Cardiano et al 2004; Franquelo et al. 2008). In addition, various mica types existed in the metamorphic rocks which were used in the mortars, therefore there are plenty of resources for mica and phyllipsite or kaolinite.

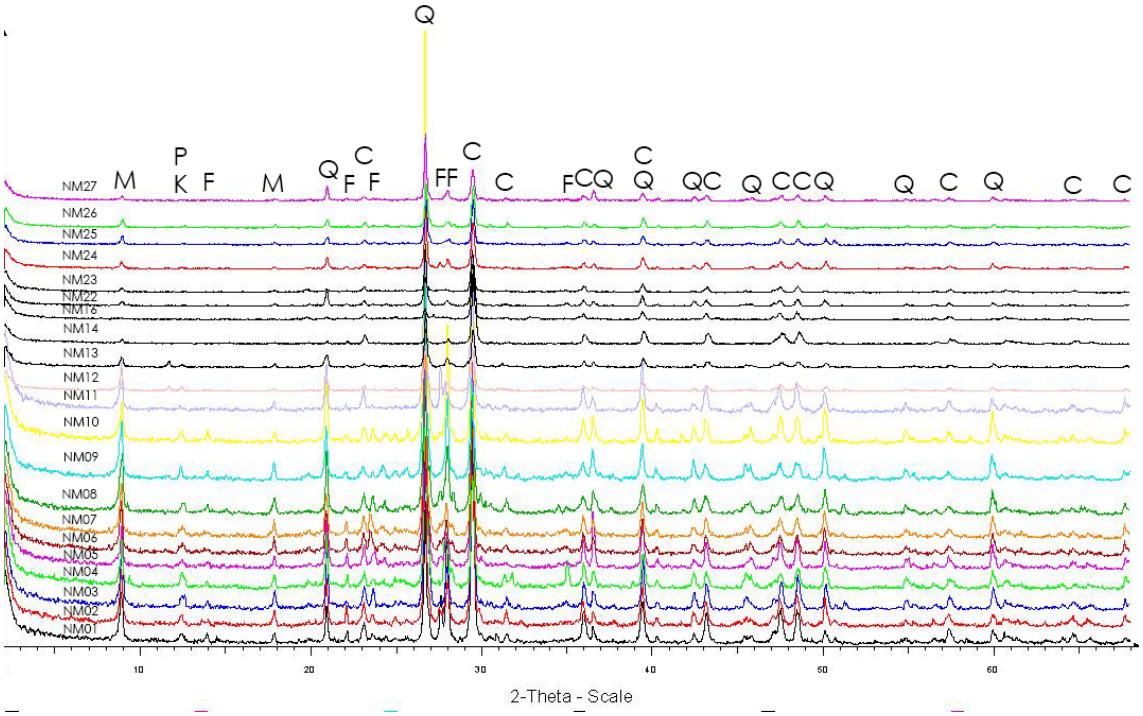


Figure 3.3- 62. XRD patterns of Nysa mortars

In Table 3.3- 20 crystal amounts were listed semiquantitatively.

Table 3.3- 20. Semiquantitative XRD analysis of Nysa mortars (++++: primary mineral, ++: secondary mineral, +: present, tr: trace)

	Samples		Quartz	Calcite	Albite	Mica	Kaolinite/Phyllipsite	Gypsum
opus caementicium	**NM01**	cistern	++	+++	+	+	+	
	NM02	Bridge2W	+++	+++	+	+	+	
	NM03	Bridge1	+++	++	+	+	+	
	NM04	Tunnel lower	+++	++	+	+	+	
	NM05	Bridge2E	+++	++	+	+	+	
	NM06	Geronticon	+++	++	+	+	+	
	NM09	Theatre	+++	++	+	+	+	
	NM10	Library wall	+++	++	+	+	+	
	NM12	Tunnel upper	+++	+++	+	+	+	+
	NM13	Tunnel lower	+++	++	+	+	+	+
	NM14	Road floor	+	+++	+	+		
	NM22	Bridge 2W	+++	++	+	+		
	NM24	Bridge 2E	+++	++	+	+		
	NM27	Bath pipeline	+++	++	+	+		
opus signinum	**NM07**	Basilica arch	+++	++	+	+	+	
	NM08	Stadion	+++	++	+	+	+	
	NM11	Gymnasium	+++	++	+	+		
	NM15	Road pipeline	+	+++	+	+		
	NM16	Road coating	+	+++	+	Tr		
	NM23	Stadion	+	+++	+	+		
	NM25	Bath arch	+++	+++	+	+		
	NM26	Bath arch	+++	+++	+	+	+	

3.3.7 Thermogravimetric Analysis (TGA-DSC)

From the results of TGA/DSC analyses of the samples (Table 3.3- 21), percentages of weight losses up to 120°C, between 120-200°C, 200-600°C and 600-800°C were calculated which attribute to the loss due to hygroscopic water, gypsum dehydration, structurally bound water of hydraulic compounds and decomposition of calcium carbonate ($CaCO_3$), respectively (Moropoulou et al. 2000; Bonazza et al., 2013).

Table 3.3- 21. Weight losses (%) of the mortar samples

	Samples		<120	120-200	200-600	600-800	$C0_2/H_2O$
opus caementicium	**NM01**	cistern	0.49	0.18	3.94	16.64	4.2
	NM02	Bridge2W	0.54	0.42	3.8	15.01	4.0
	NM03	Bridge1	0.49	0.39	2.5	14.25	5.7
	NM04	Tunnel lower	0.61	0.2	4.61	9.03	2.0
	NM05	Bridge2E	0.83	0.53	3.25	14.02	4.3
	NM06	Geronticon	0.53	0.54	3.16	15.59	4.9
	NM09	Theatre	0.33	0.21	3.24	8.72	2.7
	NM10	Library wall	0.51	0.39	2.99	12.25	4.1
	NM12	Tunnel upper	0.9	0.82	2.84	13.13	4.6
	NM13	Tunnel lower	1.98	1.35	4.38	9.82	2.2
	NM14	Road floor	0.71	0.25	2.29	31.27	13.7
	NM22	Bridge 2W	1.72	0.78	4.55	12.29	2.7
	NM24	Bridge 2E	0.84	0.45	3.4	11.51	3.4
	NM27	Bath pipeline	1.6	0.73	3.85	11.05	2.9
opus signinum	**NM07**	Basilica arch	1.08	0.68	4.19	11.18	2.7
	NM08	Stadion	0.33	0.27	4.08	8.75	2.1
	NM11	Gymnasium	1.09	0.61	4.42	13.05	3.0
	NM15	Road pipeline	2.98	1.12	4.5	15.34	3.4
	NM16	Road coating	3.34	1.34	4.89	15.31	3.1
	NM23	Stadion	3.83	1.38	3.49	12.45	3.6
	NM25	Bath arch	4.86	0.74	9.25	7.45	0.8
	NM26	Bath arch	2.03	0.88	3.4	13.42	3.9

The civil works (bridge, road and tunnels and the cistern) were those that present a higher value corresponding to range 600-800°C, except lower level tunnel mortars. In the mortars of

Gerontikon, gymnasium and library which had a higher value. The peer samples from stadium and the bath had different values. The theatre had a lowest CO_2 value.

Figure 3.3- 63 presents the plot of CO_2/H_2O vs CO_2 % which serves to classify the mortars according to their hydraulic character (Bakolas et al. 1998, Moropoulou et al. 2000, Genestar et al, 2006, Cardoso et al., 2014). CO_2/H_2O was inversely related to hydraulicity (Bakolas et al. 1995, Moropoulou et al. 2000). Based on the data and graph, Böke et al. (2008), Uğurlu Sağın (2012) accepted as non-hydraulic mortar when CO_2/H_2O ratio higher than 10 like NM14. According to the classification of Moropoulou et al. (2005) NM25 was natural pozzolanic mortar and NM11, NM15 and NM16 were artificial pozzolanic mortars. Mortars that had H_2O higher than 3 were so called hydraulic mortars (Moropolou et al. 2000; Genestar et al. 2006).

Based on the positions in the graph (Figure 3.3- 63) three groups can be obtained. First NM14 can be separated as non-hydraulic lime mortar with its high ratios of CO_2 and low ratio of structurally bound water to hydraulic compounds, second group located between 5 and 10 % of CO_2 and CO_2/H_2O ratio <5, which includes NM04, NM08, NM09, NM13 and NM25 and the other group which contains the rest of the samples which lay down 10-20% CO_2 and CO_2/H_2O ratio below 10. Mortars of the first group had high hydraulic characters and the second group had hydraulic character only.

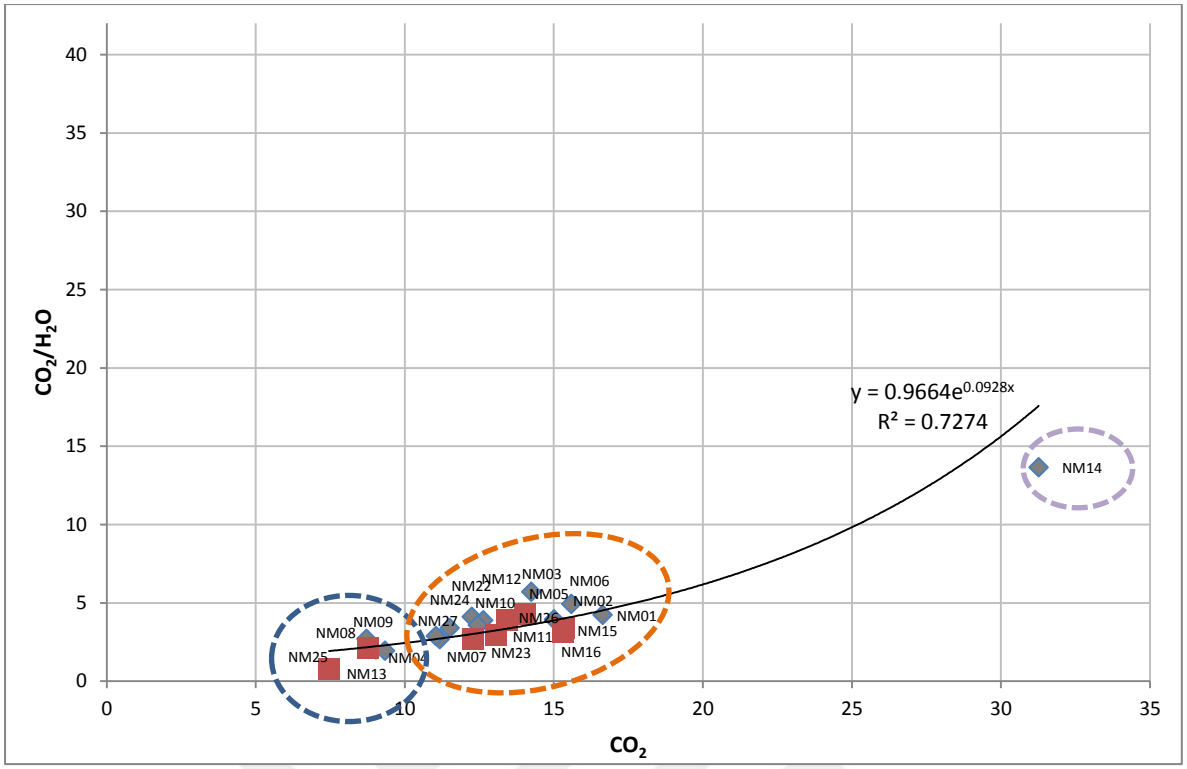


Figure 3.3- 63. CO_2/H_2O vs CO_2% graph of samples

Indeed, the values gathered from TGA-DSC analysis were lower than the values of other mortars that other scholars analysed. Bonazza et al. (2013) had the same phenomenon in their work and claimed that the reason could be partial dissolution of calcite in the binder.

Considering the thermograms different peaks at different ranges more information can be gathered about the characterization of mortars. All of the mortars had peaks around 573°C which indicates phase transition of quartz.

As illustrated at Figure 3.3- 64 NM04 had a well-marked weight loss between 400 and 600°C magnesite decomposition in addition; peak at 250°C indicates hydromagnesite (Cardoso et al. 2014).

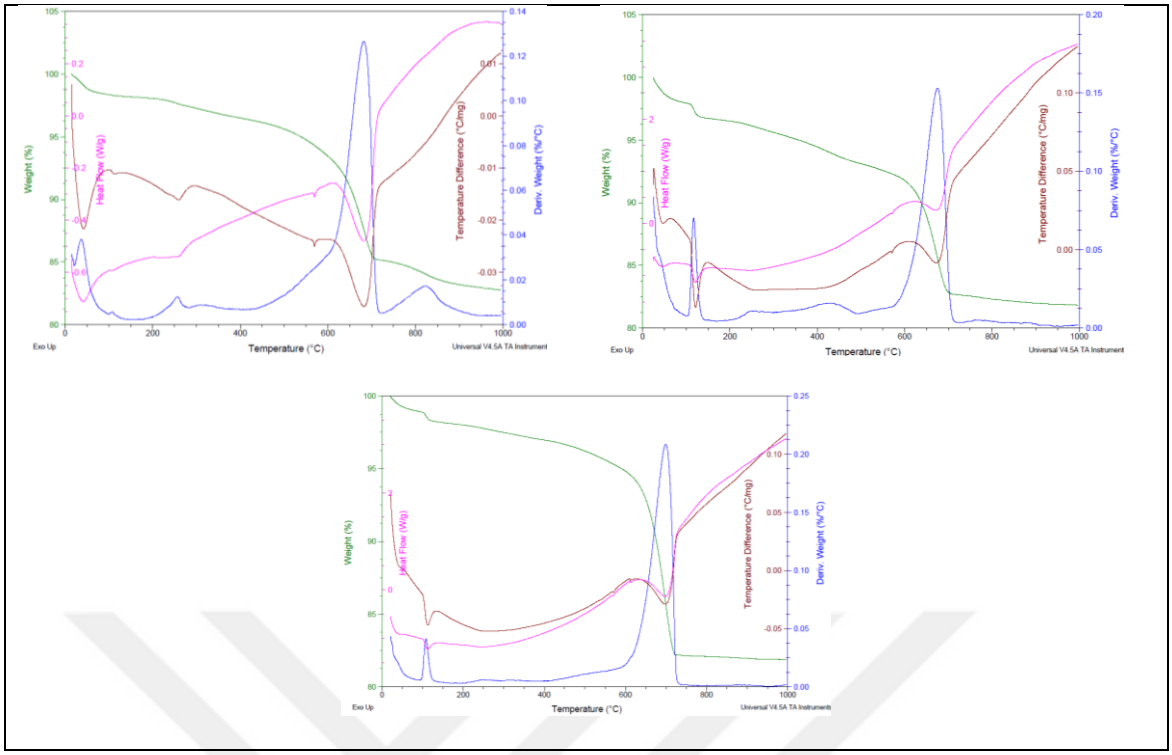


Figure 3.3- 64. Thermogram of mortars from tunnel a) NM04 b) NM12 c)NM13

Just like NM04 and NM08, NM09 had peak at 100 °C 250 °C, 450 °C and 530°C indicating magnesite content and weight loss after 800 °C indicating recarbonation (Figure 3.3- 64 – Figure 3.3- 66). NM09, NM11, NM12, NM13, NM25 had peaks at 120 which indicates gypsum. In the thermograms of NM12 and NM13 peak at 120°C was associated with hydrated salts.

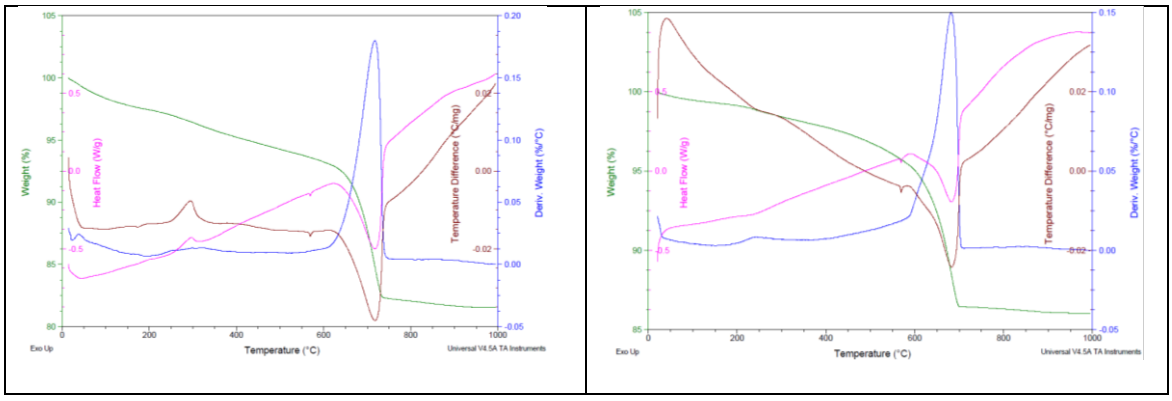


Figure 3.3- 65. Thermogram of mortar from arch of Basilica shops (NM07) (left) stadium (NM08)

NM07 had at 300°C due to organic material and or charcoal (Figure 3.3- 65). In the thermogram of NM25 at peak around 800°C may be associated to recarbonation or calcite as aggregate. Early weight loss of carbonates could be related with the magnesites as had peak at 450°C, peak at 120°C for hydrated salts as well (Figure 3.3- 66).

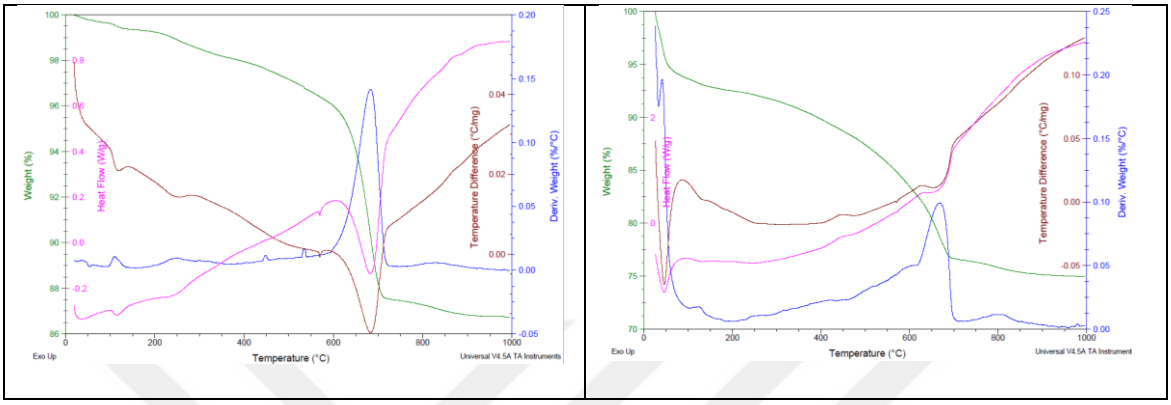


Figure 3.3- 66. Thermograms of mortar sample from theatre (NM09) (left), arch from Thermal Bath (NM25) (right)

Figure 3.2- 67 was plotted to understand the correlation between the acid soluble insoluble parts of the mortars and calcium carbonate content calculated from data obtained from thermogravimetric analysis. Another relevant point was that same samples were grouped together with CO_2/H_2O vs CO_2 graph. Apparently, samples having lower weight loss due to decomposition of carbonates and higher water content were located in the centre 25-35 B:A and 15-20% $CaCO_3$%. Similarly, samples having more binder and less structurally bound water content lay down to the zone located between 26-35% CaCO3% and 0.15-0.40 B:A.

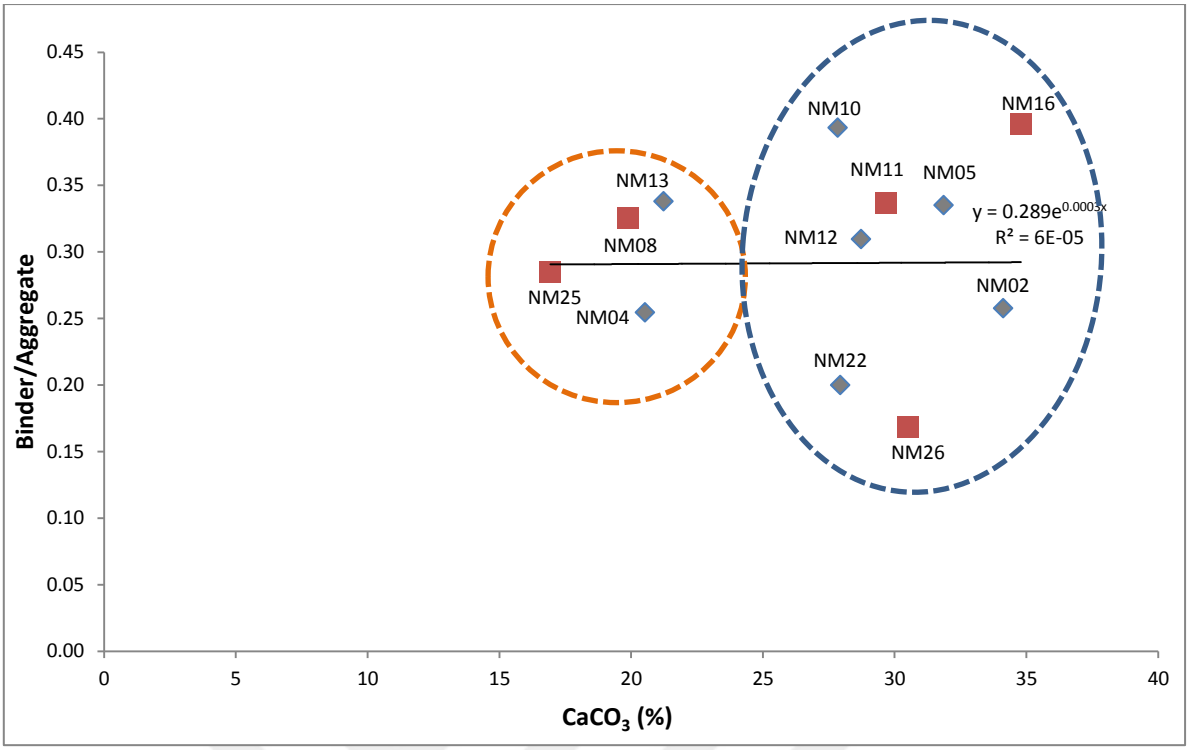


Figure 3.3- 67. Acid in/soluble fraction vs $CaCO_3$ (%) from TGA of Nysa mortars

3.3.8 X-Ray Fluorescence (XRF)

Table 3.3- 22 presents the chemical composition of the mortar samples. Magnesite that was revealed in thermogravimetric analysis of the lower level mortar in tunnel NM04 it was supported by XRF data as well. It had more magnesium oxide (MgO) content which indicates higher workability plasticity, water retention property and thus durability of the mortar.

Table 3.3- 22. Major elements of the Nysa mortars (LOI: Loss of ignition)

	Samples		SiO_2	Al_2O_3	Fe_2O_3	MnO	MgO	CaO	Na_2O	K_2O	TiO_2	P_2O_5	LOI	Total
OC	**NM02**	Bridge2W	53.03	7.19	3.03	0.06	0.82	13.27	0.21	1.68	0.35	0.2	19.69	99.53
	NM04	Tunnel lower	54.6	8.94	3.91	0.07	2.79	9.72	2.51	3.15	0.62	0.21	12.65	99.16
	NM05	Bridge2E	56.63	7.98	3.45	0.07	0.94	13.26	1.18	2.05	0.49	0.21	13.4	99.66
OS	**NM07**	Basilica arch	54.47	9.18	3.85	0.07	1.25	12.57	1.4	2.07	0.74	0.29	13.37	99.25
	NM11	Gymnasium	54.96	8.13	2.59	0.05	1.18	15.27	1.68	2.05	0.46	0.2	12.98	99.54

When y axis as binder and x axis was considered aggregates in reliable classification of mortars was as follows: all of the mortars were in the same line regarding to SiO_2+ Al_2O_3+ Fe_2O_3 and CaO+MgO content. Nysa mortars were clustered together having 10-20% binder and 60-70% alkali reactive aggregates (Figure 3.3- 68). There was not any significant difference between different types of mortars.

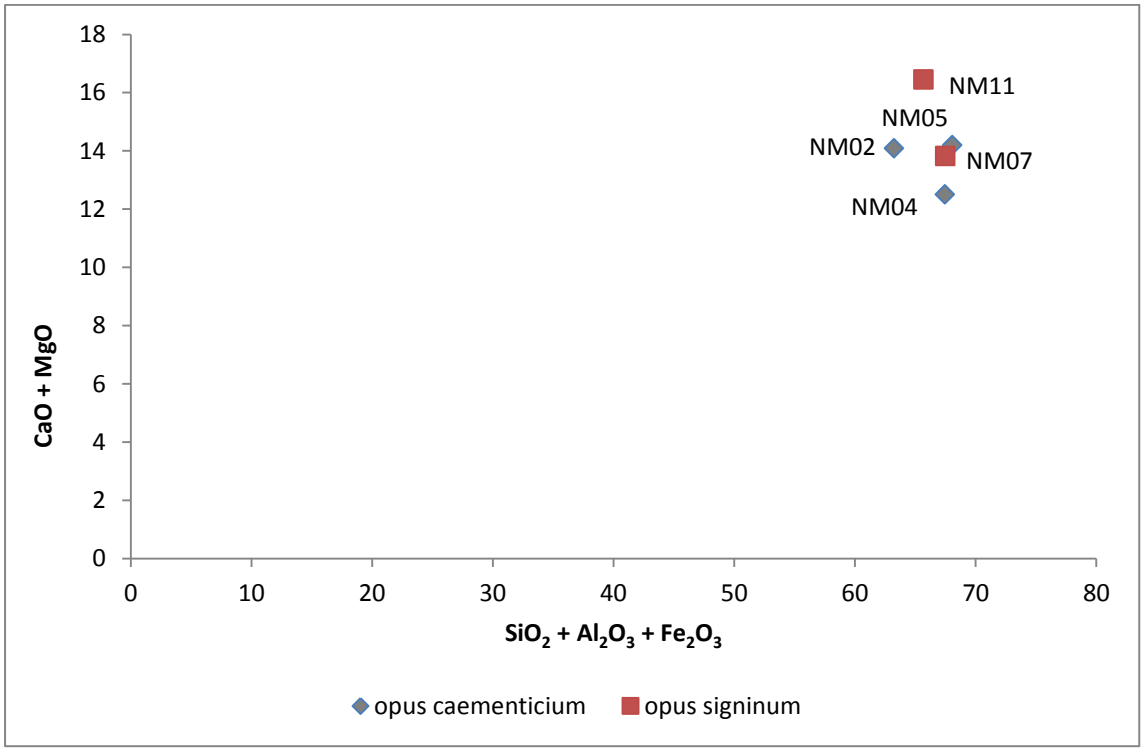


Figure 3.3- 68. CaO+MgO vs SiO_2+Al_2O_3+Fe_2O_3 graph of Nysa mortars

It was seen that *opus signinum* mortars were slightly separated from other and NM04 separated from others at TiO_2/Fe_2O_3 vs SiO_2/CaO graph (Figure 3.3- 69) due to very low amount of CaO, it was seen that NM02 had the most homogeneous composition with more iron content as well.

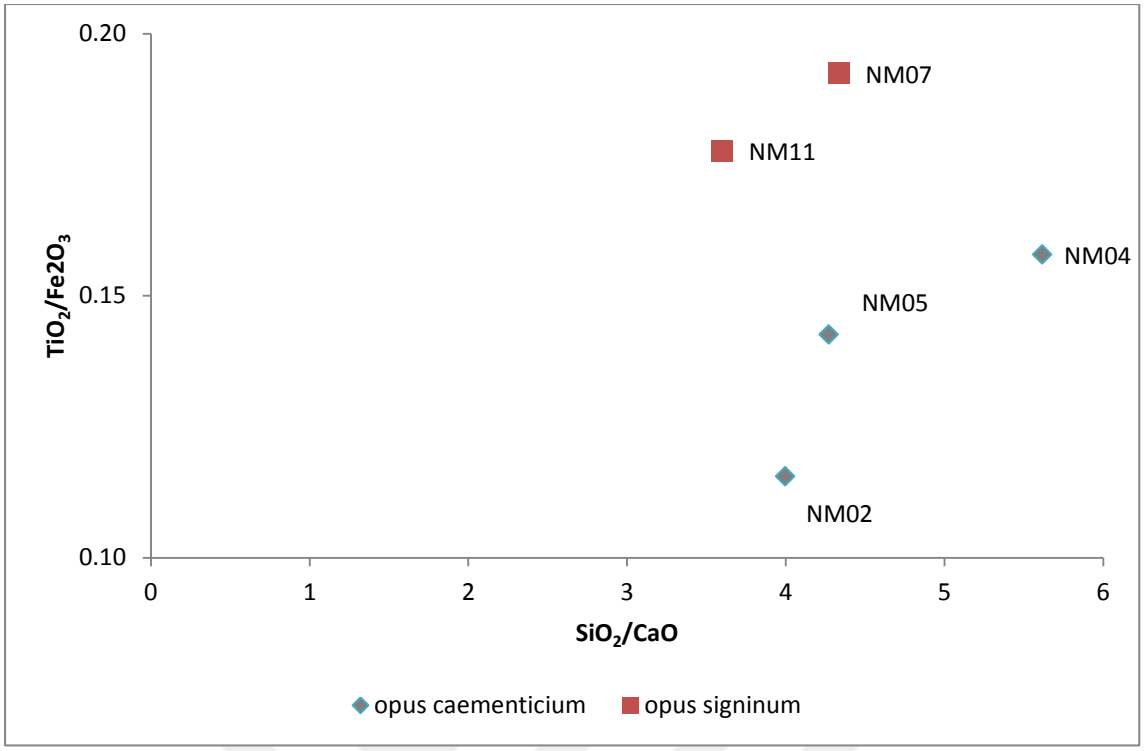


Figure 3.3- 69. TiO_2/Fe_2O_3 vs SiO_2/CaO graph of Nysa mortars

Correlation between the ratios TiO_2/Fe_2O_3 and CaO/MgO (Figure 3.3- 70) serves to classify mortars according to their aggregates and binders (Crisci et al., 2004). Analysed mortars had TiO_2/Fe_2O_3 between 0.1 and 0.2 that close values imply homogeneity in the mortar compositions, CaO/MgO ratios make a difference that NM04 stays below with higher magnesium it had.

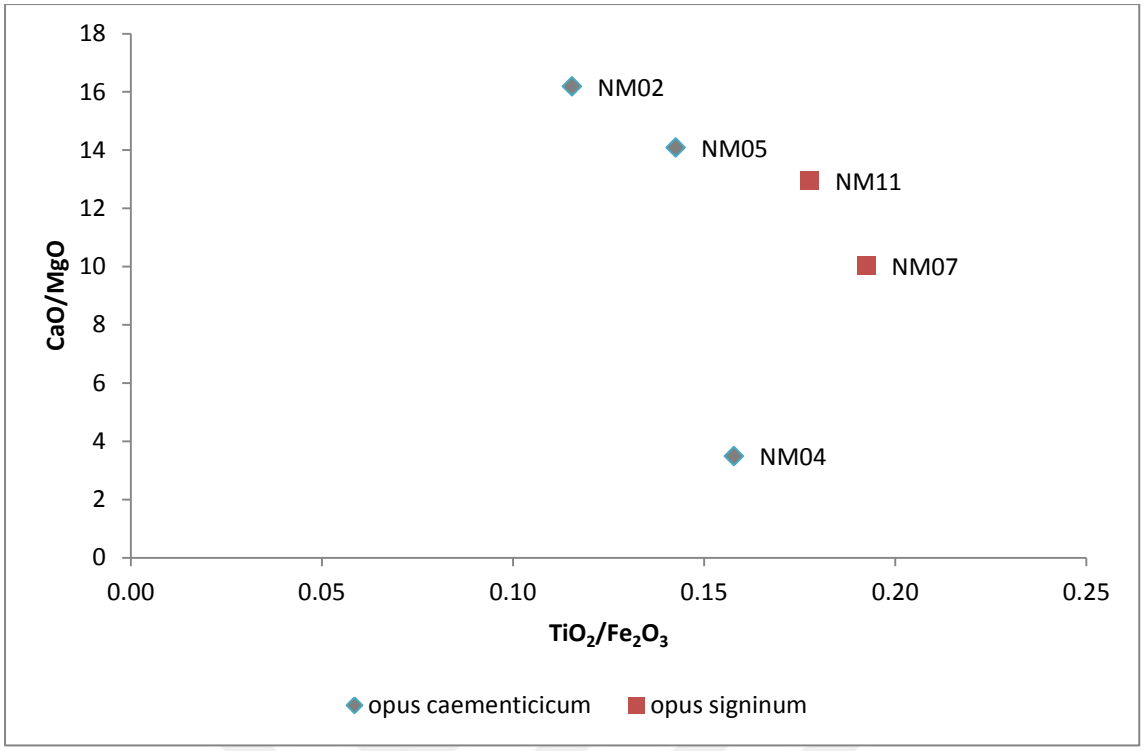


Figure 3.3- 70. CaO/MgO vs TiO_2/Fe_2O_3 graph of Nysa mortars

Both type of the mortars had the same lithic constituents, accordingly they were situated close to each other in the graph (Figure 3.3- 71).

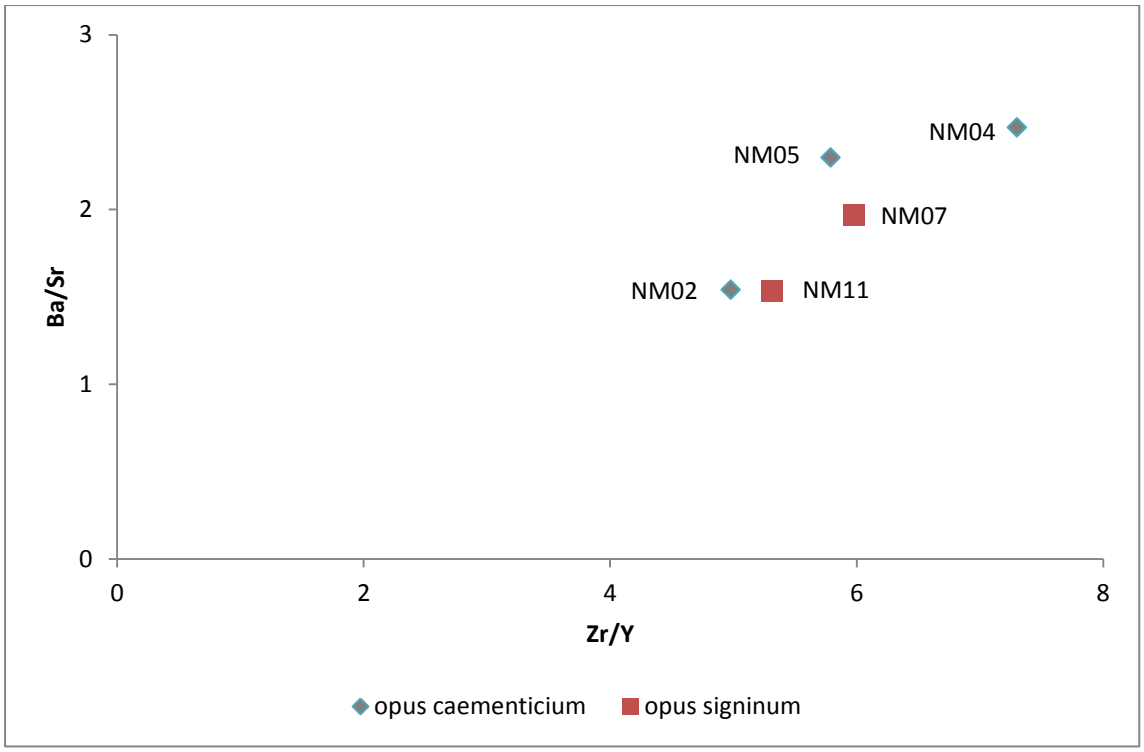


Figure 3.3- 71. Ba/Sr vs Zr/Y graph of Nysa mortars

3.3.9 Mercury Intrusion Porosimetry

Opus caementicium mortars NM12 and NM24 had highest bulk density values. Their average pore diameters were higher than the others. Moreover, NM12 had the lowest porosity and specific surface values (Table 3.3- 23). *Opus caementicium* mortars had porosity and density values like 23% and 2.9 g/cm^3 , respectively while *opus signinum* had these properties as 38% and 1.45 g/cm^3, respectively. As expected, micropore percentage was higher in *opus signinum* mortars.

Table 3.3- 23. Parameters gathered by mercury intrusion (P: Porosity, APD: Average Pore Diameter (4V/A), BD: Bulk density, RD: Real density)

	Samples		P (%)	APD (4V/A) (µm)	BD (g/ml)	RD (g/ml)
OC	**NM12**	Tunnel upper	17.13	0.15	2.05	2.48
	NM24	Bridge 2E	29.73	0.12	2.06	2.94
OS	**NM16**	Road coating	46.82	0.04	1.21	2.27
	NM23	Stadion	41.95	0.06	1.34	2.31
	NM25	Bath arch	24.75	0.07	1.8	2.39

As illustrated in Figure 3.3- 72 and listed in Table 3.3- 24, *opus caementicium* mortars NM12 had dispersed macropores from greater than 100 µm to 3 µm and the main highest distribution was between pore size distribution was between 1 µm and 0,1 µm. Micropores exist with less intensity. NM24 showed a bimodal distribution that first group of pores was between 10 µm and 5 µm and the second was between 5 µm and 0,005 µm.

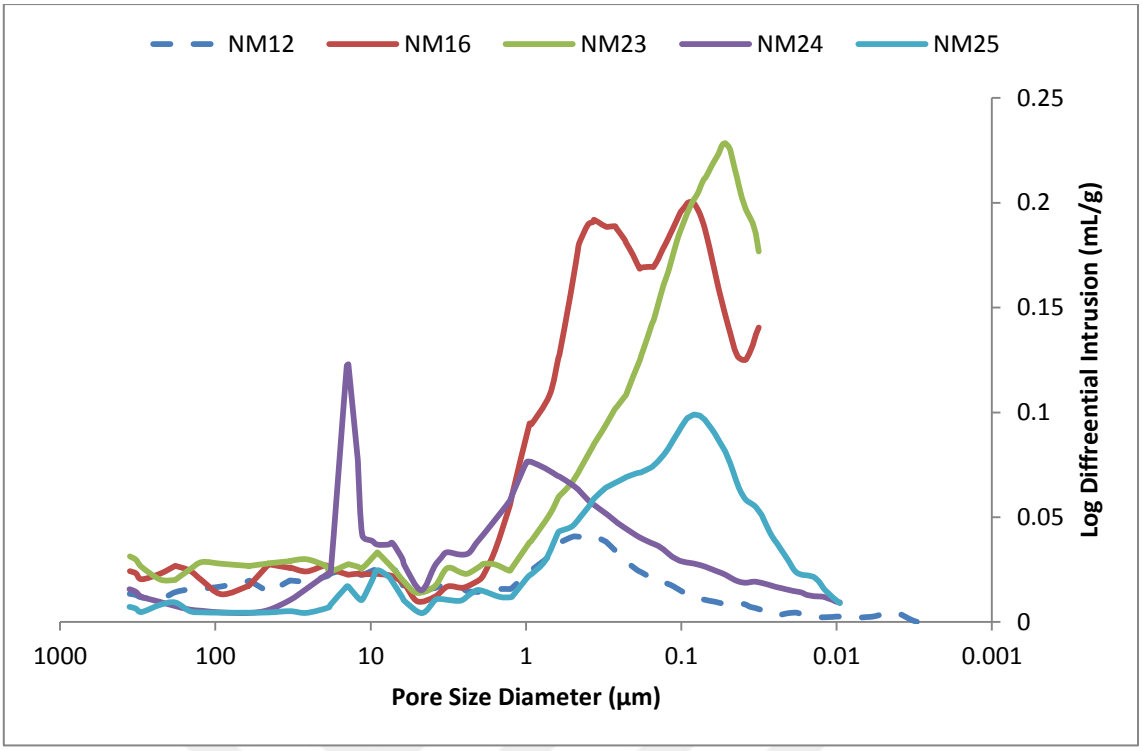


Figure 3.3- 72. Log differential intrusion versus pore size of the Nysa samples

Table 3.3- 24. Pore size distribution and percentages of micro and macropores

	Samples		Micro < 5 µm	Macro > 5 µm	< 0.01 µm	0.01 - 0.1 µm	0,1 - 1 µm	1-10 µm	10 - 100 µm	>100 µm
OC	**NM12**	Tunnel upper	59.6%	40.4%	1.65%	7.96%	36.39%	21.38%	23.48%	9.14%
	NM24	Bridge 2E	71.1%	28.9%	0.00%	13.44%	37.67%	26.57%	19.00%	3.33%
OS	**NM16**	Road coating	86.8%	13.2%	-20.24%	46.83%	53.61%	8.61%	7.12%	4.07%
	NM23	Stadion	81.9%	18.1%	-15.36%	54.46%	36.60%	9.03%	10.19%	5.08%
	NM25	Bath arch	88.8%	11.2%	0.18%	39.87%	42.77%	9.64%	5.04%	2.50%

Among *opus signinum* mortars, pore size distribution of NM16 basically accumulated on midi and micropores between 1 µm and 0,01 µm and smaller than 0,01 µm. Pore size distribution of NM23 basically accumulated on midi and micropores between 1 µm and 0,005 µm. NM25 showed a quasi trimodal distribution while the main and highest peak was between1 µm and 0,005 µm. The other little humps were greater than 100 µm and two peaks between 20 µm 8 µm.

3.3.10 Correlations of results according to architectural features

In the common public buildings of the city mostly *opus caementicium* mortars were preferred, with the exceptions of basilica, stadium and gymnasium. *Opus caementicium* types were porous mortars composing of crème/ light brown colour binder and poorly sorted small-medium size aggregates and lime lumps. Tunnel mortars were distinct with more brownish colour.

Gymnasium is not fully excavated indeed there is only an arched entrance and a masonry which the sampling was done. The use of *opus signinum* type mortar in that wall makes us think that it could belong to the aforementioned bath complex in the Gymnasium.

Similarly, in Stadium the use of *opus signinum* mortar was because of the construction in the slope of the stream valley that was closer to the stream than bridges pillars which were *opus caementicium* mortars. Tunnel mortars were classified as *opus caementicium* mortars due to the lack of ceramics however the darker colour and clay content showed that earth was used in the mortars which provide hydraulic properties. Among the rest of the water related constructions, *opus signinum* mortars were utilized in masonry of thermal bath and in Agora road as rendering mortars.

Opus signinum mortars had two sub-types one had red binder and medium sorted angular ceramic fragments the other was with light brown binder and including ceramic fragments. Except the more reddish mortars found in Road and Stadium, chromatic parameters of the mortars were not so different from each other.

Mortars from different functions had different properties, such as the floor mortar from the Agora Road was revealed as true lime mortar which showed the highest surface hardness.

With other properties as well Nysa mortars had close values in geochemical analysis as well. This fact indicates the homogeneity in the mortar execution. The majority of the samples had 1:3 binder:aggregate ratios. In the mortars from different pillars of second bridge, aggregate

amounts were changing. This may be a coincidence or different time of construction/restoration. In the mortars from Bath arches the aggregate amount seemed to be higher than the majority of mortars. All of the mortars had certain amount of fine particles below 63μm might include ceramic dust and/or pozzolanic additives or which could be clay particles. In Nysa,it was seen from the XRD analysis that, kaolinite/phyllipsite was present. In addition, the clayey appearance under the microscope indicated it as well. In the road and gymnasium mortars presence of clay was not observed.

Microscopic observations also demonstrated the interconnected rounded pores in *opus caementicium* mortars. Reaction rims around the ceramic fragments, recrystallization of carbonated binder and calcite re-precipitation in the pores were detected in *opus signinum* type mortars. Large metamorphic rock fragments were frequently used as aggregate in the mortars. The detected rocks were marble, gneiss and quartzite. Fly ash was present in some samples.

Mortar from theatre seemed slightly different from other mortars. It contained the fragment of same rock with the Gerontikon mortar but larger in size. The porosity and the grain size distribution were changing occasionally in the mortar. In addition, the thermogram of the sample was quite different from others as well. It could had been constructed in different period.

All mortars had hydraulic properties, except the floor mortar in Agora Road. The high clay amount in tunnel mortars was also proved by TGA analysis. In addition, those mortars had certain amounts of gypsum which could be related with deterioration. Hydraulicity degree was higher in the mortars of west pillar of the bridge than the ones of east pillar. Same was veridic in two different levels of tunnel. Different construction period and/or deterioration could be the reason for the pillars and conscious preference due to the water contact of the lower level mortar in tunnel.

3.4 Sanctaury of Labraunda

As it is illustrated in the previous chapter (Figure 2.3-56) two types (*opus caementicium* and *opus signinum*) mortars were collected from wall of Andron A and Andron C building and various water bearing constructions (East Bath, Tetraconch Bath, Hypostyle building, pool).

Collected samples were characterized multi-analytically just like other archaeological sites and presented in the same order.

3.4.1 Macroscopic description of Labraunda samples

Macroscopic description of every studied mortar sample is presented in appendix. *Opus caementicium* mortars *in* Labraunda were porous mortars had white, crème, light brown colour binders with small size aggregates. They were consistent mortar with high cohesion. Poorly to medium sorted grain size distribution was dominant. Lime lumps were not abundant. Binder had whitish crème colour and light and dark to light sub-angular to angular sand grains (< 4 mm) and white colour quartz grains were observed. Pore and grain sizes were various, grain size distribution was poorly sorted (Figure 3.4- 73). Ceramic aggregates were seen in the mortar sample LM03 from South Bath but the amount was low therefore it was not relevant to determine the type of mortar.

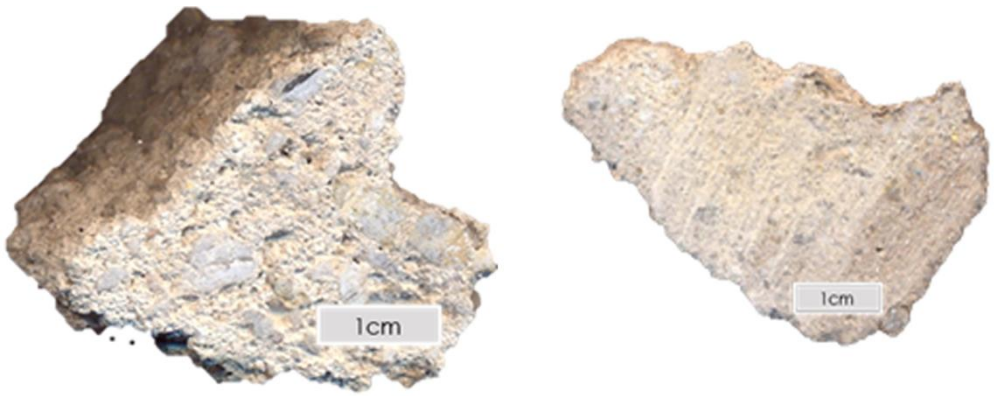


Figure 3.4- 73. Examples of *Opus Caementicium* mortars (LM04A on the left, LM06B on the right, scale: 1 cm)

In Labraunda the majority of collected samples were *Opus signinum* mortars which had reddish colour with the highly use of ceramics. They were encountered in floor of Tetraconch, East Bath and Hypostyle building, in the walls of pool, East Bath and Andron A. The cohesion of the mortars was lower. Angular sub-angular ceramic fragments (< 7 mm) were bigger in size and medium to well sorted in reddish colour matrix. Grain size distribution was poorly to well sorted (Figure 3.4- 74).

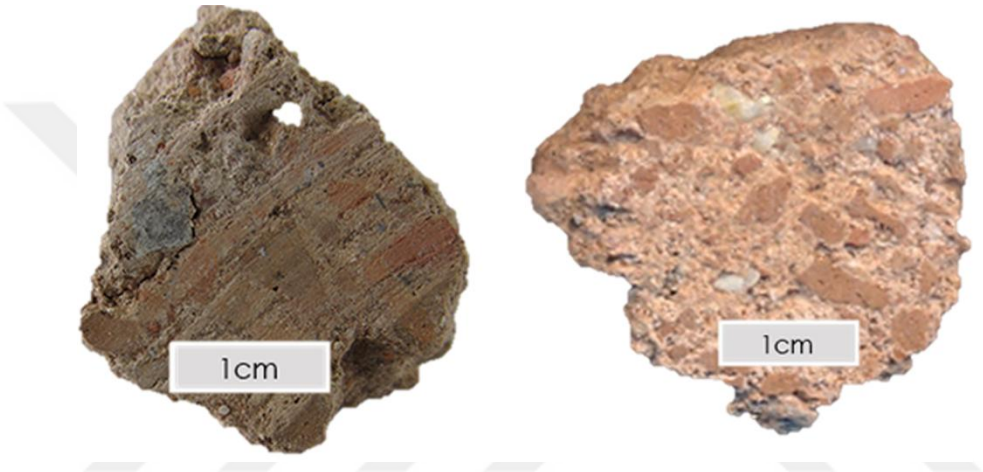


Figure 3.4- 74. Examples of *Opus Signinum* mortars (LM06A on the left, LM08 on the right, scale: 1 cm)

3.4.2 Colour Spectrophotometry

Figure 3.4- 75 depicts that sample LM02 had highest luminosity and the lowest saturation and sample LM09 and LM08 showed the opposite. Mortars taken from East Bath showed decreasing trend towards floor sample (LM06A), in other words that sample had more saturated color than wall mortars. In hypostile building samples nearly same trend was observed with higher L and C values. Contrarily, the sample from the lowest level of the floor had more luminosity and less stauration than the medium level mortar.

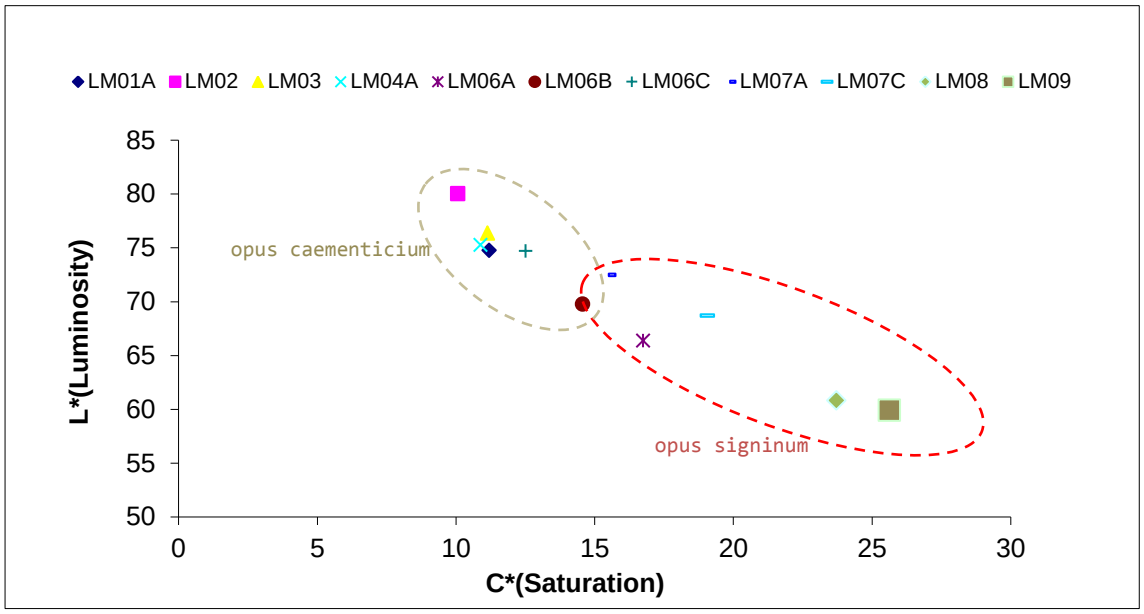


Figure 3.4- 75. Luminosity vs Chrome of Labraunda mortars

In Figure 3.4- 76 the trend of those two groups were reversed, as higher the a* values higher the redness and higher the b* refers to yellowness, LM06A sample embodies more red and yellow. In hypostile building mortars sample LM07C had yet higher values. In Figure 3.4- 77 LM02, LM03 and LM04A group together locating in the zone corresponding to 10 at b* and 3 at a* axis while LM01A had higher a* value in the same y line. Samples LM01A, LM03 and LM04A had almost same values of lighter color zone in two of the plots (Figure 3.4- 77). LM08 and LM09 again stand apart from other with higher values (12-15, 20-21).

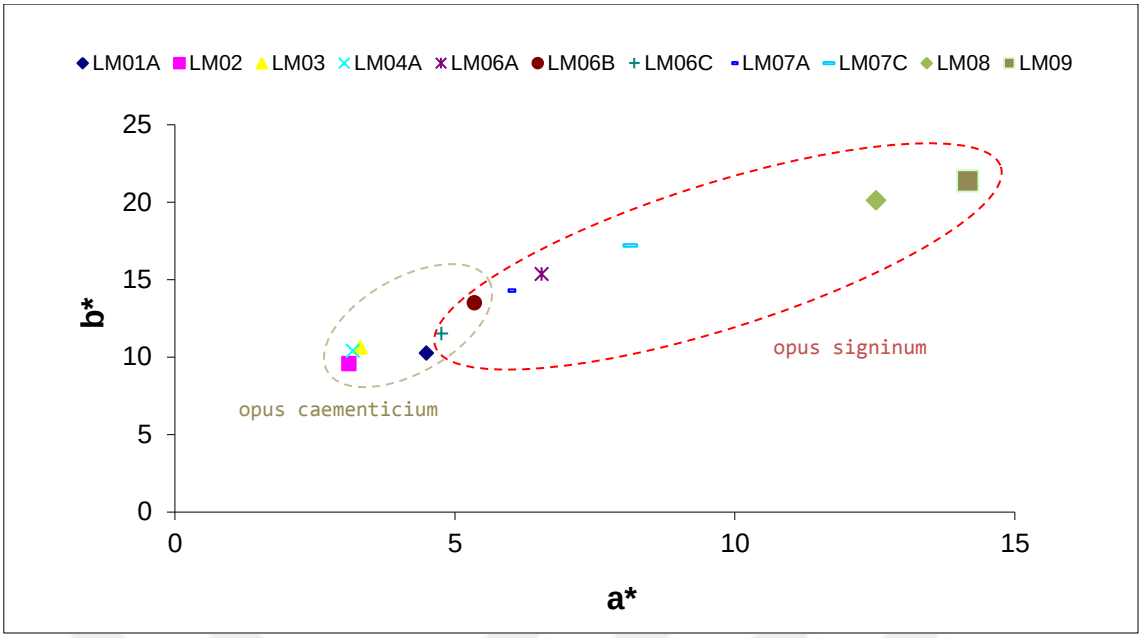


Figure 3.4- 76. b* vs a* of Labraunda mortars

Figure 3.4-77 exhibits a significant clustering of the samples with white and yellow index values similar to Figure 3.3- 53 but in a wider range. LM02 showed highest and positive WI on the other hand LM09 had the lowest and minus values in the same parameter hypostyle building samples had YI values between 25 and 35 and YI values 0 and -10.

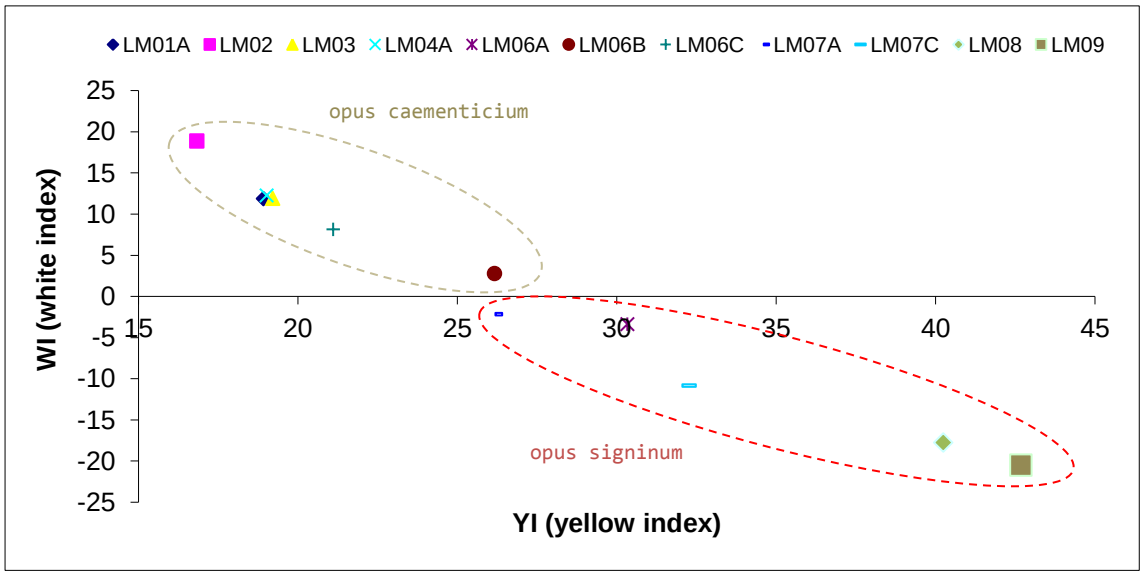


Figure 3.4- 77. White index vs yellow index of Labraunda mortars

3.4.3 Surface Hardness

As shown in the Figure 3.4- 78 *opus caementicium* mortars had surface hardness values between 150 and 175 leebs except the wall mortar on East Bath (LM06B) which had 200 leebs. Indeed, the *opus signinum* samples from East Bath had the lowest hardness values, sample from the floor (LM06A) showed 78 leebs, sample from the wall (LM06C) had 84 leebs surface hardness.

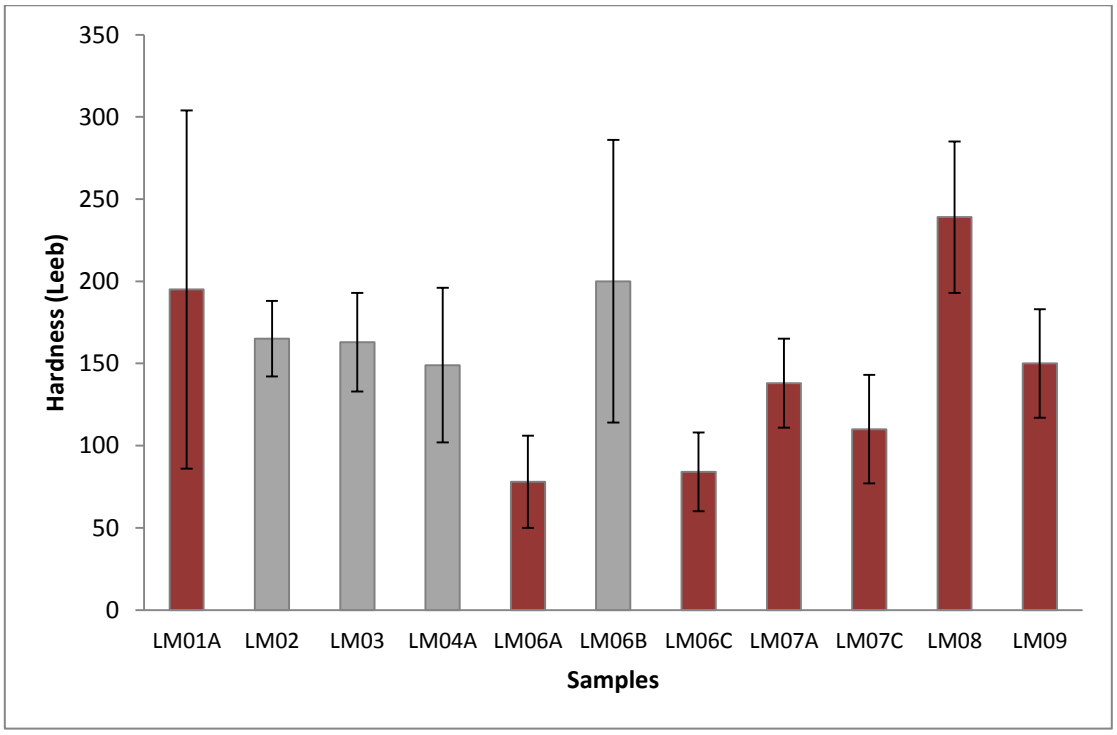


Figure 3.4- 78. Surface hardness values of Labraunda samples (gray: *Opus caementicium*, red: *Opus signinum*)

Samples from the floor levels in Hypostyle building come after those mortars; in the third level mortar sample (LM07C) 110 leebs reveals and the lowermost level (LM07A) 138 leebs was read. Pool rendering mortar sample (LM09) and sample taken from the wall of Tetraconch bath (LM04A) had the same values (150 leebs). Samples taken from the wall of the South Bath (LM02 and LM03) had almost the same surface hardnesses. Samples from the floor of Andron A (LM01A) and wall of East Bath (LM06B) had similar values, 195 and 200 leebs, respectively. Being not so high from the one value before (220 leebs) the highest surface hardness value belongs to the second phase of construction of hypostyle building (LM08).

3.4.4 Optical Microscopy

Raw materials of Labraunda mortars, reflects the regional geology (Figure 2.1- 32) and the other building materials used in the site In the thin section analyses, it is observed that nearly all samples had metamorphic rock fragments (mica schist, gneiss, quartzite) embedded in porous and micritic calcitic binder that porosity and different concentration of carbonation in the binder was observed.

As seen in Figure 3.4 - 79 in *opus caementicium mortars*, poorly sorted aggregates were embedded in brown dark brown colour microcrystalline calcitic binder. Apart from quartz feldspar and mica (biotite, muscovite) frequently rounded opaque minerals were observed besides the rock fragments. Larger size rock fragments were abundant which causes the poorly sorted distribution. The size of grains vary from 40 µm to 3 mm. Binder: aggregate ratio was visually estimated as 1:3.

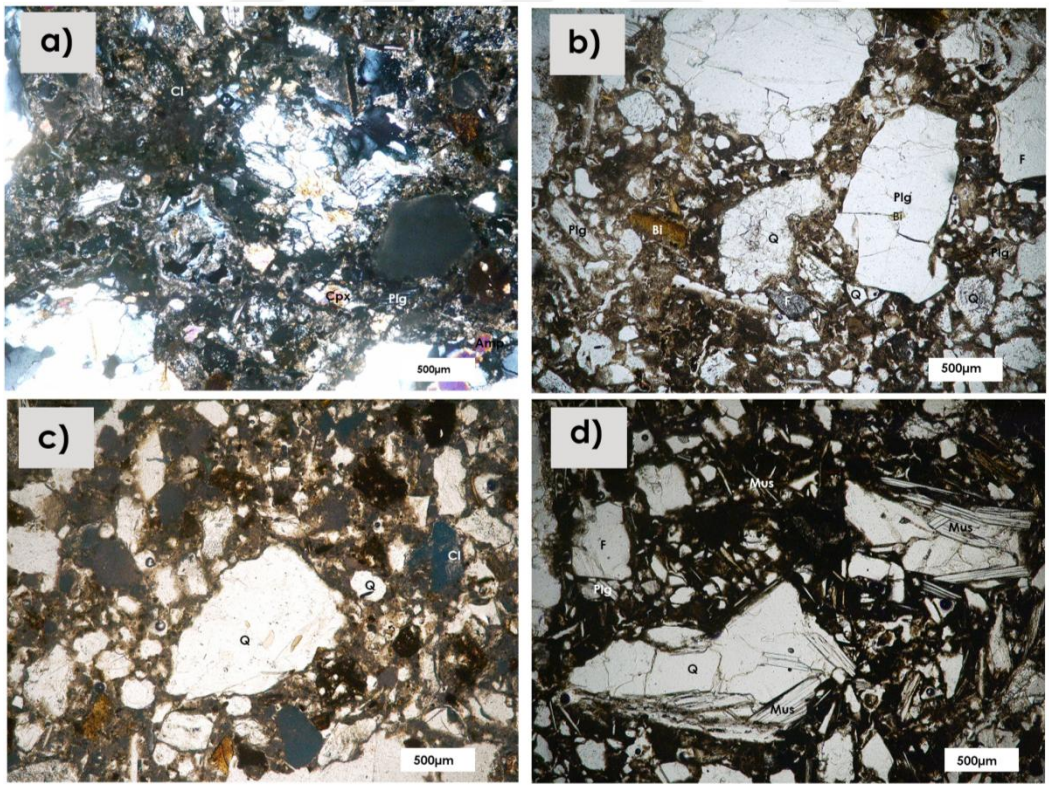


Figure 3.4- 79. Photomicrographs of *opus caementicium* mortars a) LM02 (cross polarized light) b) LM04A (plane polarized light) c) LM05 (plane polarized light) d) LM06B (plane polarized light) (Q: quartz, F. feldspar, Plg: plagioclase, Mus: muscovite, Cl: chloride, Cpx: clinopyroxene)

Metamorphic rock fragments such as metaquartzite and mica schist, gneiss were found in sub-rounded and angular shapes as well as angular feldspar, biotite and quartz grains and rounded opaque minerals. Over burned lime lumps and secondary calcite precipitations in the pores were present which was observed under cross polarized light (Figure 3.4- 80). In the binder place to place clayey appearance was observed.

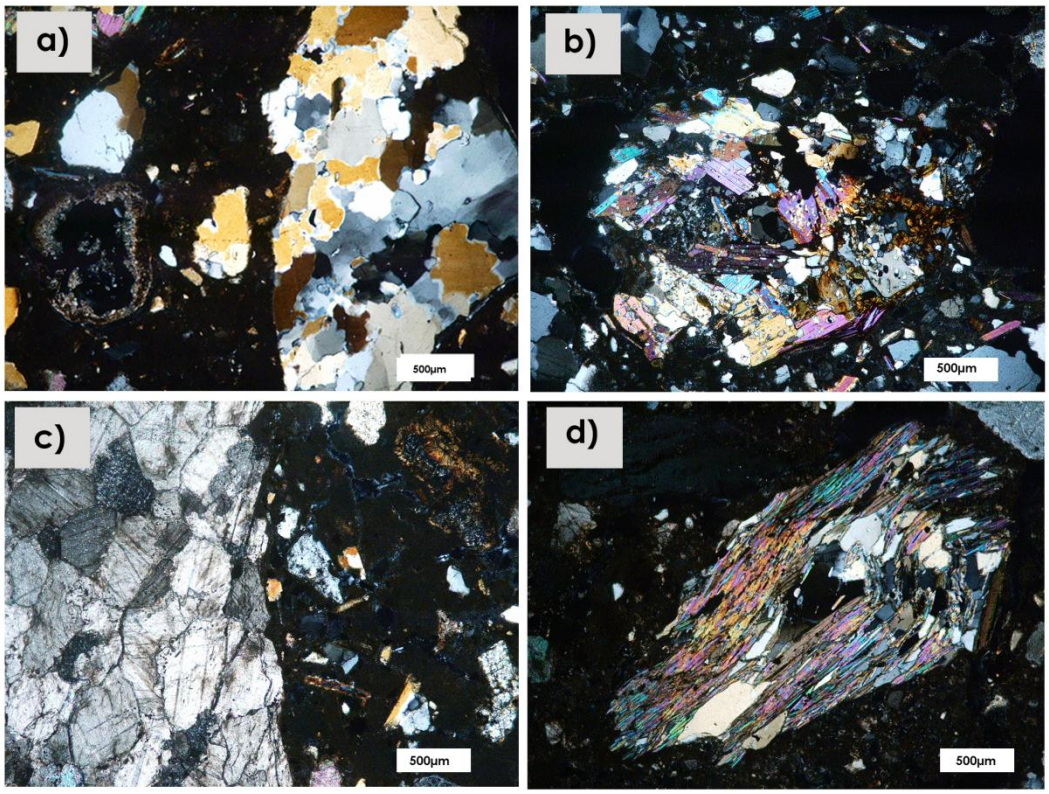


Figure 3.4- 80. a) Photomicrograph of LM01A from Andron A (cross polarized light) showing recrystallization in the pore on the left and quartzite on the right b)LM04A Photomicrograph of the mortar sample LM04A from the wall of Tetraconch Bath showing gneiss fragment (cross polarized light) c) Photomicrograph of the sample LM05 from Andron C wall (plane polarized light) marble fragment on the left LM05 d) LM07A showing augen eye gneiss mica group

Opus signinum mortars own 1.5mm up to greater than 3mm ceramic fragments were observed apart from the angular lithic fragments like other samples- quartzite, gneiss- (Figure 3.4- 81). Porous microcrystalline calcite binder had lighter colour under plane polarized light, locally darker colour. Sizes of aggregates were changing between 20 µm and 3mm. Visually

estimated binder: aggregate ratio is 1:3. Besides, locally recrystallization of carbonated microcrystalline calcitic binder was observed.

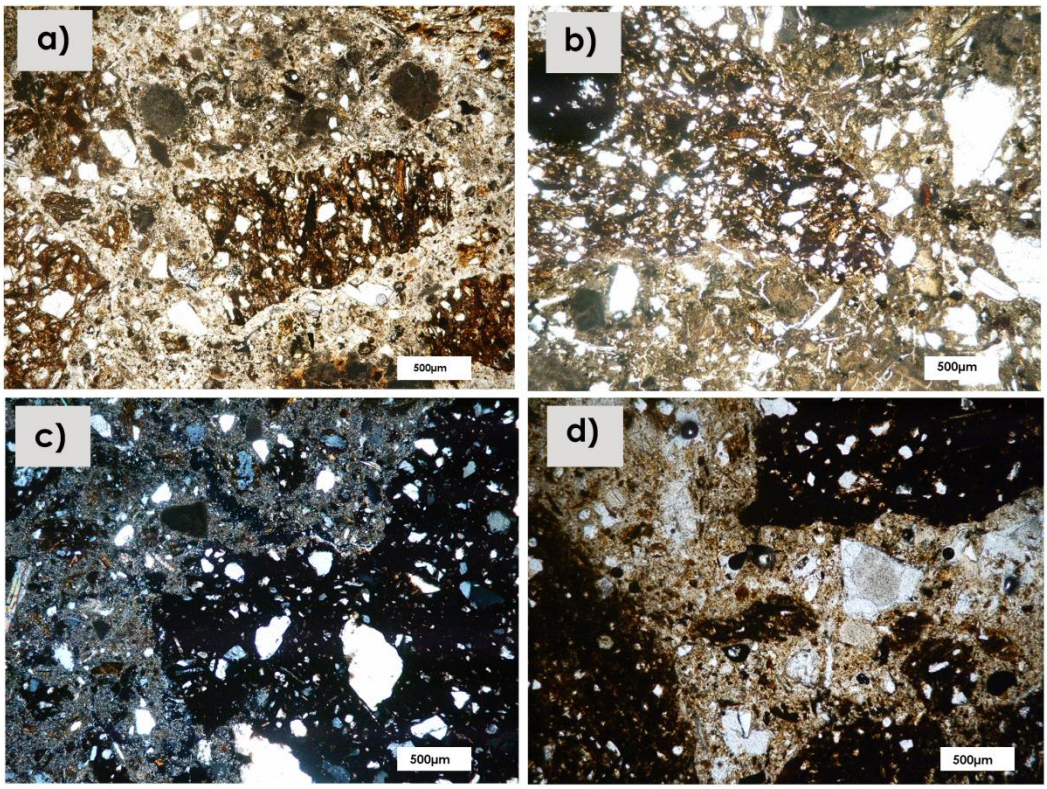


Figure 3.4- 81. Photomicrographs of *opus signinum* a) sample LM06A from the floor of East Bath (plane polarized light) showing ceramic fragment with its reaction rim in the centre b) LM04B (plane polarized light) Photomicrograph (x4p) of mortar sample from floor of Tetraconch Bath LM04B, showing the ceramic in the centre and metamorhphic rock fragment embedded in a porous lime binder with shrinkage cracks c) LM06C (cross polarized light) d) LM08 (plane polarized light)

Reaction rims around aggregates and chamotte were observed (Figure 3.4- 82a). Lime lumps with shrinkage cracks under burnt lime relicts with various dimension and forms were detected (Figure 3.4- 82b). Plaster sample from Andron A a different appearance with a well sorted grain size distribution of sharp edged feldspar and quartz in dark colour lime binder Calcite, feldspar and quartz grains were sub- angular to angular in shape. No lithic fragment was detected in the microscopic observations. Rounded opaque minerals (smaller than 1mm) and recrystallization in the pores were abundant. The sizes of grains vary from 100 µm

to1 mm. Binder: aggregate ratio was visually estimated as 1:2 (Figure 3.4- 82c). Moreover, clay and lime intrusions were observed (Figure 3.4- 82d).

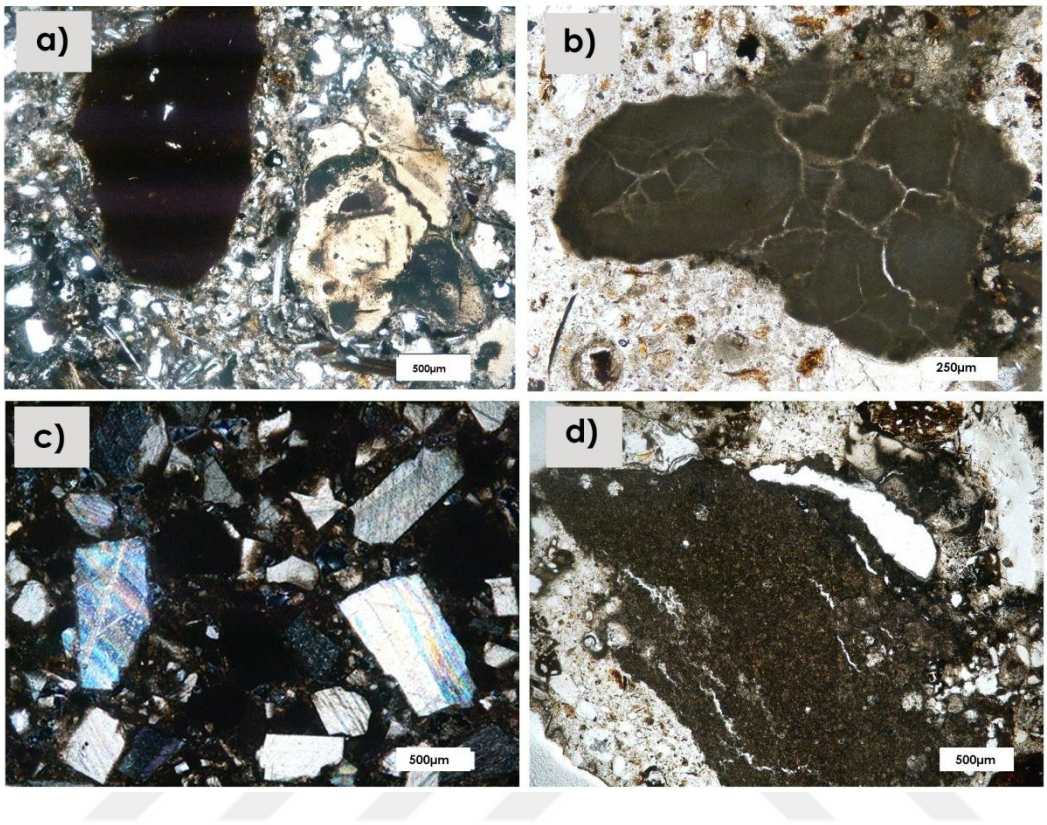


Figure 3.4- 82. Photomicrograph of a) LM02 b) LM06A c) LM01C d) LM06C

Minerals, lithic fragments and additives revealed in the microscopic observations can give valuable clues. Type and texture, size can indicate different construction phases or lack of control in elaboration of mortars.

Calcite grains were encountered in plaster sample LM01C, wall mortars from South Bath (LM02), Tetraconch Bath (LM04B) and East Bath (LM06C), they come from marble whose fragments were detected in wall mortars of Andron C (LM05) and East Bath (LM06C). It was thought to be Permo-Carbon age marble from because the same samples contain meta-quartzites from Göktepe formation as well (Figure 2.1- 32). In the samples LM02 and LM05 chamottes were encountered which contains high alumina and silica. Since they assess drying and hardening of mortar and prevent shrinkage, it would not be incorrect considering

its addition in purpose. It was curious that those two samples which had both chamotte were situated close to each other in the Sanctuary however belong to different construction periods. Hence, reuse of mortars or raw materials of the crushed mortars become an issue.

Lime lumps and inclusions were present in the Labraunda mortars except the hypostyle building floor mortars which indicate the hot lime technology in time of manufacturing of mortars. The absence of lumps in hypostyle building floor mortars may be an indicator of different construction period or care in the elaboration.

Microscopic observations are presented in Table 3.4- 25

Table 3.4- 25. Petrographic constituents of Labraunda mortars (Qtz: Pl: plagioclase, Cal: calcite, tour: tourmaline, Op: opaque mineral, Mca: Mica)

Samples			Binder	Constituents	Lithic and ceramic fragments, additives, others
Opus caementicium	LM01C	AndronA plaster	Dark colour micritic calcite	Qtz, Pl, Cal	-
	LM02	South Bath wall	Brown colour, recrystallization	Qtz, Fsp, Mca, Op	gneiss, chamotte, lump
	LM04A	Tetraconch Bath wall	Dark brown colour micritic calcite	Qtz, Pl, Mca	Metaquartzite gneiss, lump
	LM05	AndronC wall	Brown colour	Qtz, Fsp, Mca, Op	Marble, polycrystalline quartz, chamotte, lump
	LM06B	East Bath wall	Brown colour	Qtz, Fsp Mca	gneiss, mica group, feldspar phenocryst, lump
opus signinum	LM01A	AndronA wall	Dark colour micritic calcite	Qtz, Pl, Mca	Metaquartzite, gneiss, ceramic, feldspar phenocryst, lump
	LM04B	Tetraconch Bath floor	brown colour micritic calcite	Qtz, Fsp Mca,Cal	gneiss, ceramic, feldspar phenocryst, lump
	LM06A	East Bath floor	recrystallization	Qtz, FspMca,	ceramic, gneiss, lump
	LM06C	East Bath wall	porous light colour binder lime inclusions	Qtz, Fsp Mca, Tur, Cal	Metaquartzite, marble, ceramic, lump
	LM07A	Hypostile Floor bottom	light colour porous binder locally recrystallization	Qtz, FspMca	gneiss, mica group, feldspar phenocryst, ceramic, lump
	LM07B	Hypostile Floor 2	light colour porous binder locally recrystallization	Qtz, Pl Op	Ceramic, polycrystalline quartz
	LM07C	Hypostile Floor 3	light colour binder, recrystallization	Qtz, Pl Mca	gneiss, ceramic, feldspar phenocryst
	LM08	Hypostile Floor 4	light colour binder, recrystallization	Qtz, plg, Mca	Ceramic, gneiss

3.4.5 Binder aggregate ratio and Grain Size Distribution

After HCl attack soluble parts of the mortars were accepted as binder and insoluble parts as aggregates. Percentages of binders and aggregates of the samples are listed below (Table 3.4- 26).

Table 3.4- 26. Binder and aggregate ratios (%)

	Samples		Binder (%)	Agregate (%)	B:A
opus caementicium	**LM03**	South Bath wall	24.9	75.1	1:3
	LM04A	Tetraconch Bath wall	34.5	65.5	1:2
	LM06B	East Bath wall	31.76	68.24	1:2
opus signinum	**LM04B**	Tetraconch Bath floor	30.34	69.66	1:2
	LM06A	East Bath floor	22.85	77.15	1:3
	LM06C	East Bath wall	46.96	53.04	1:1
	LM07A	Hypostyle Floor bottom	18.23	81.77	1:4
	LM07B	Hypostyle Floor 2	15.96	84.04	1:5
	LM07C	Hypostyle Floor 3	5.93	94.07	1:15
	LM07D	Hypostyle Floor 4	2.09	97.91	1:49
	LM08	Hypostyle Floor 5	7.48	92.52	1:13
	LM09	Pool wall	12.33	87.67	1:7

As illustrated below (Figure 3.4- 83) binder aggregate ratios (B:A) of LM03 and of LM06A were 1:3, Tetraconch Bath mortars LM04Aa and LM04B had both 1:2 binder aggregate ratios like sample LM06B, LM06C was 1:1.

In the Hypostyle Building floor the basement mortar (LM07A) had the ratio of 1:4, mortar above it (LM07B) had 1:5 B:A. Uprising levels showed unexpected values, binder aggregate ratio of LM07C was 1:15 then sample LM07D had nearly no lime that had B:A, 1:49, upper level mortar sample LM08, second phase of construction, had the ratio was 1:13 and B:A of sample LM09 from pool had 1:7 ratio.

B/A ratio was very homogeneous in OC, but in *signinum* the binder content was very different depending on the constructive areas in which they were applied.

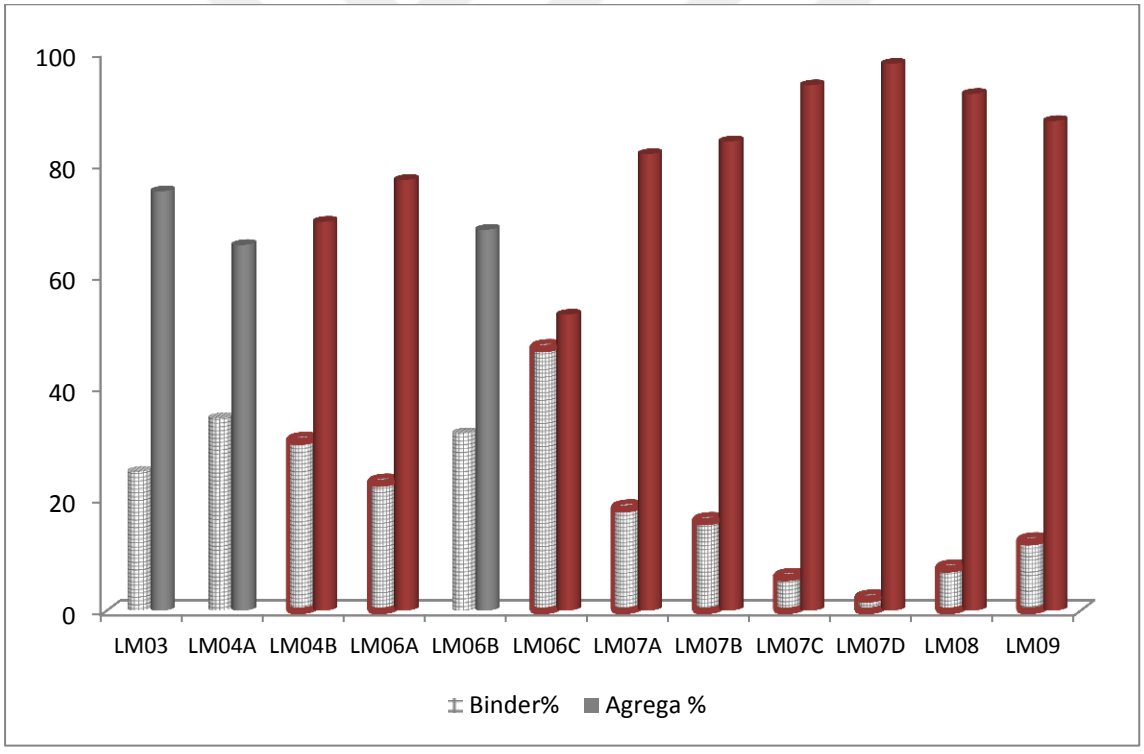


Figure 3.4- 83. Binder aggregate ratios of Labraunda mortars (reds are *opus signinum* mortars)

All Labraunda mortars showed descending grain size distribution (GSD) except mortar from the wall of East Bath (LM06B) (Figure 3.4- 84). Grain size distributions of floor mortars LM06A and LM07C were identical, big ceramic aggregates (> 2mm) of LM07D prevent to be in that group (Table 3.4- 27). Tetraconch Bath mortars LM04A, LM04B and second level of floor of

Hypostyle building LM07B had same GSD, also South Bath wall mortar sample LM03 and mortar from the uppermost level of floor of Hypostyle building LM08 had similar distributions and LM09 had the same distribution with ceramic aggregates. In the sample LM06C aggregate ratio passing through every sieve was lower.

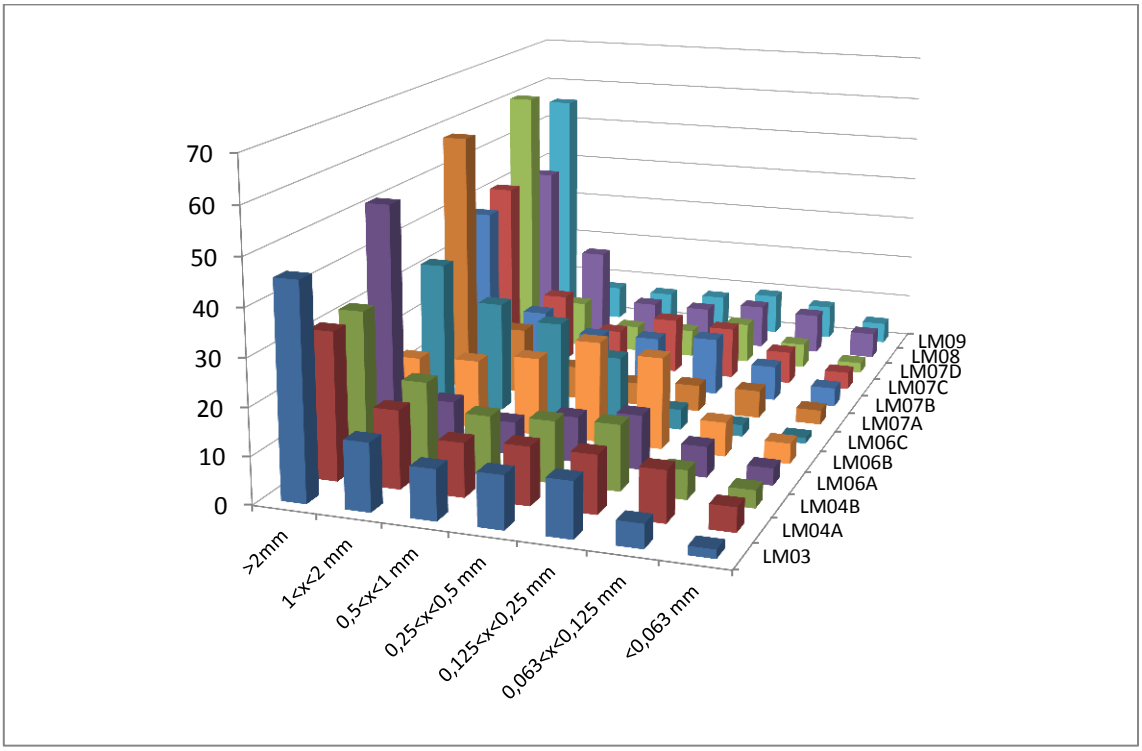


Figure 3.4- 84. Grain size distribution graph of Labraunda mortars

Table 3.4- 27. Weight passing each sieve (%)

	Samples		>2mm	1<x<2 mm	0.5<x<1 mm	0.25<x<0.5 mm	0.125<x<0.25 mm	0.,063<x<0.125 mm	<0.063 mm
opus caementicium	**LM03**	South Bath wall	45,36	14,32	10,61	11,14	11,67	5,04	1,86
	LM04A	Tetraconch Bath wall	31,43	16,57	11,43	12,29	12,29	10,86	5,14
	LM06B	East Bath wall	14,29	15,02	17,00	21,92	19,95	7,39	4,43
opus signinum	**LM04B**	Tetraconch Bath floor	31,99	18,28	12,63	13,17	13,98	6,18	3,76
	LM06A	East Bath floor	51,46	9,95	7,04	9,71	11,65	6,55	3,64
	LM06C	East Bath wall	31,85	24,20	21,02	14,65	4,46	2,55	1,27
	LM07A	Hypostyle Floor bottom	58,11	14,64	7,21	4,95	5,86	6,08	3,15
	LM07B	Hypostyle Floor 2	37,69	15,13	10,98	11,57	12,76	7,72	4,15
	LM07C	Hypostyle Floor 3	40,85	15,65	8,33	12,40	11,59	7,32	3,86
	LM07D	Hypostyle Floor 4	60,57	10,48	5,86	6,22	9,06	5,51	2,31
	LM08	Hypostyle Floor 5	39,26	19,86	8,08	8,08	9,93	9,01	5,77
	LM09	Pool wall	55,45	7,72	7,33	7,72	9,31	7,72	4,75

When considered that the fine particles (<63μm) may include ceramic dust and pozzolanic additives, LM08 and LM09 had the highest amounts and LM07C, LM04A and LM06B were following them. In the first three use of ceramic dust was obvious with high reddish colour of the mortars and in LM04A and LM06B those can be attributed to the clays or pozzolanic additives.

3.4.6 X-Ray Diffraction

All of the XRD graphs showed calcite, quartz, feldspar and mica peaks were seen. In diffractograms plaster sample LM01C from Andron A building, south bath mortar samples LM02 and LM03 calcite was the primary crystals wherever, calcite and quartz were seen equal in Andron C sample LM05 and East Bath sample LM06B. In the rest of samples calcite amount decrease and traces were encountered in LM01B -Andron A repair mortar, upper levels of floor of Hypostyle building LM07D, LM08 and Pool wall sample LM09 (Figure 3.4- 85).

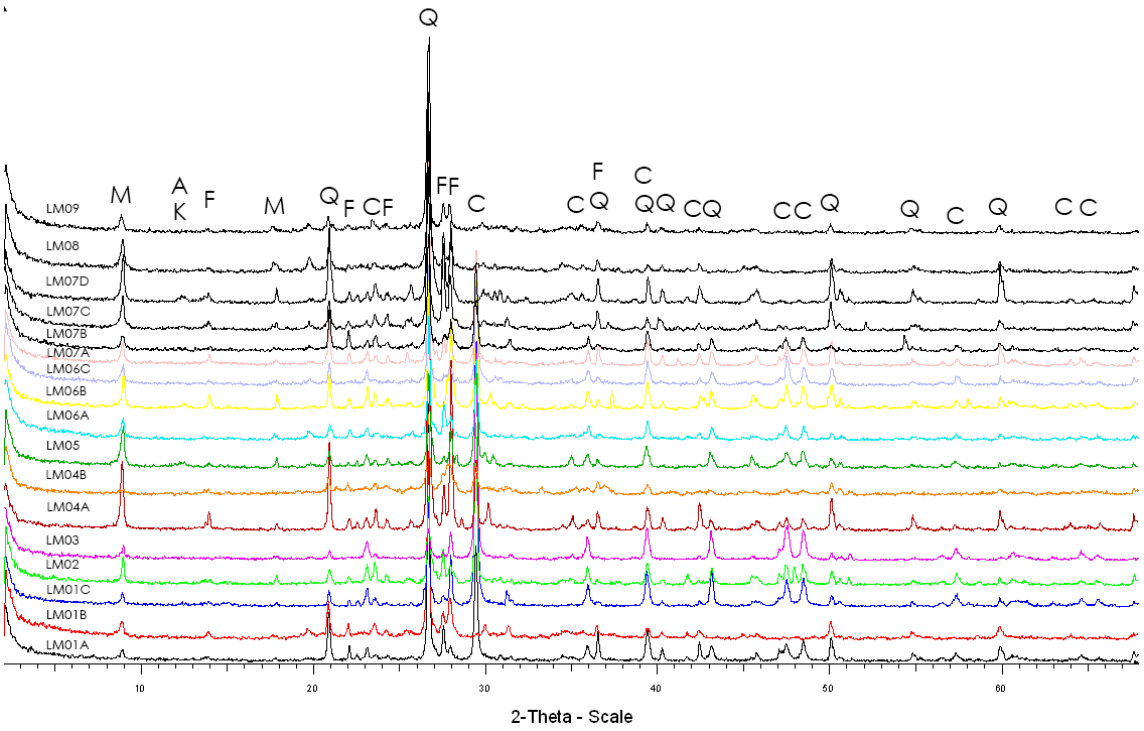


Figure 3.4- 85. XRD patterns of Labraunda mortars (Q: quartz, C: calcite, F: feldspar, M: mica, K: kaolinite, A: amphibole)

LM01C, LM02 and LM03 samples had fewer amounts of quartz peaks; it was confirmed by the optical microscopy that quartz grains were fewer. LM05, LM06B and LM07D showed kaolinite peak whose clayey appearance at matrix observed under microscope (Table 3.4- 28).

Table 3.4- 28. Semiquantitative mineralogical distribution of Labraunda mortars (Q: quartz, C: calcite, F: feldspar (albite, anorthite), K: kaolinite, Am: amphibole, M: Mica (muscovite, biotite), +++: abundant, ++: major, +: present, tr: traces found)

	Sample		Q	C	F	M	K/Am
opus caementicium	**LM01B**	AndronA Rep.mortar	+++	tr	+	+	
	LM01C	AndronA plaster	++	+++	+	+	
	LM02	South Bath wall	++	+++	+	+	
	LM03	South Bath wall	+	+++	+	+	
	LM04A	Tetraconch Bath wall	+++	+	++	+	
	LM05	AndronC wall	+++	+++	+	+	+
	LM06B	East Bath wall	+++	+++	++	+	+
opus signinum	**LM01A**	AndronA wall	+++	++	+	+	
	LM04B	Tetraconch Bath floor	+++	+	++	+	
	LM06A	East Bath floor	+++	++	+	+	
	LM06C	East Bath wall	+++	++	+	+	
	LM07A	Hypostyle Floor bottom	+++	++	++	+	
	LM07B	Hypostyle Floor 2	+++	++	+	+	
	LM07C	Hypostyle Floor 3	+++	+	+++	+	
	LM07D	Hypostyle Floor 4	+++	tr	++	+	+
	LM08	Hypostyle Floor 5	+++	tr	++	+	
	LM09	Pool wall	+++	tr	+	+	

3.4.7 Thermogravimetric Analysis (TGA-DSC)

From the results of TGA-DSC analyses of the samples, percentages of weight losses up to 120°C, between 120-200°C, 200-600°C and 600-800°C were calculated which attribute to the loss due to hygroscopic water, gypsum or hydrated salt dehydration, structurally bound water of hydraulic compounds and decomposition of calcium carbonate ($CaCO_3$), respectively (Moropoulou et al. 2000; Bonazza et al., 2013). Weight loss data was listed in Table 3.4- 29.

Sample LM03 having higher structurally bound water amount can be classified as hydraulic lime mortar according to the classifications of Moropoulou et al. 2000; ; Bonazza et al. (2013). With the classification of Cantisani et al. (2002) LM05 and LM06C can be counted as hydraulic mortars, as well. Their relatively higher weight loss due to the calcium carbonate decomposition (600-800°C) could be related with the marble fragment they possess. In addition they were grouped as artificial pozzolanic mortar according to Moropolou et al., (2005), Genestar et al. (2006).

Table 3.4- 29. Weight losses (%) of the mortar samples

	Samples		<120°C	120-200°C	200-600°C	600-800°C	CO_2/H_2O
Opus caementicium	**LM01C**	AndronA plaster	0,55	0,23	1,89	26	13,8
	LM02	South Bath wall	1,92	1,47	3,06	12,91	4,2
	LM03	South Bath wall	1,42	0,58	7,56	24,4	3,2
	LM04A	Tetraconch Bath wall	0,44	0,19	1,9	6,28	3,3
	LM05	AndronC wall	0,9	0,31	3,34	15,05	4,5
	LM06B	East Bath wall	0,82	0,25	2,67	12,56	4,7
Opus Signinum	**LM01A**	AndronA wall	1,34	0,43	2,7	12,63	4,7
	LM04B	Tetraconch Bath floor	0,33	0,22	2,11	3,08	1,5
	LM06A	East Bath floor	2,88	0,94	3,31	8,54	2,6
	LM06C	East Bath wall	2,27	0,68	3,49	14,23	4,1
	LM07A	Hypostyle Floor bottom	1,26	0,48	2,4	11,05	4,6
	LM07B	Hypostyle Floor 2	2,37	1,03	3,16	8,29	2,6
	LM07C	Hypostyle Floor 3	2,24	1,13	2,67	1,74	0,7
	LM07D	Hypostyle Floor 4	1,02	0,37	1,42	0,28	0,2
	LM08	Hypostyle Floor 5	3,52	1,49	3,3	0,81	0,2
	LM09	Pool wall	3,03	2,43	4,1	0,46	0,1

Figure 3.4- 86 presents the plot of CO_2/H_2O vs CO_2 % which serves to classify the mortars according to their hydraulic character (Bakolas et al. 1998, Moropoulou et al. 2000, Genestar et al, 2006, Cardoso et al., 2014). CO_2/H_2O was inversely related to hydraulicity (Bakolas et al. 1995, Moropoulou et al. 2000). Based on the data and graph, Böke et al. (2008), Uğurlu Sağın (2012) accepted as non-hydraulic mortar when CO_2/H_2O ratio higher than 10 like LM01C.

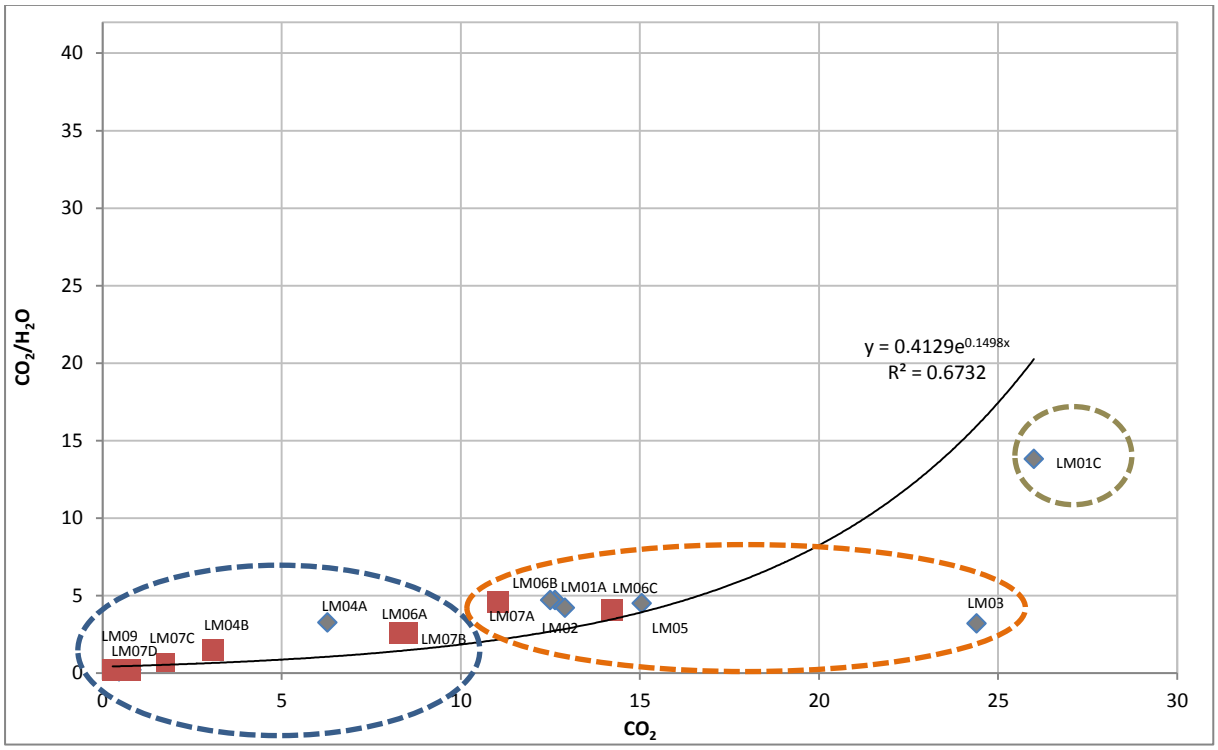


Figure 3.4- 86. CO_2/H_2O vs CO_2% graph of samples (blue circle: highly hydraulic, orange circle: hydraulic, green: non-hydraulic)

First group located below 5 on y axis and below 10 at x axis which was shown in blue circle in Figure 3.4- 86, LM09, LM07D, LM07C LM04 A and B, LM06A, LM07B can be classified as highly hydraulic lime mortars. LM07A, LM06B, LM06C, LM02, LM05 and LM03 which were grouped as hydraulic lime mortars while LM01C was true lime mortar without hydraulic properties according to TGA results. This was logical because it was plaster.

Mortar from pool (LM09) and upper levels of floor in hypostyle building (LM07C and LM07D) having close values near to intersection of the axes. Meanly they had so little amount of calcite and water. Weber (2016) claimed that historic mortars may had highly siliceous binder and low water as a consequence of the reaction between lime and pozzolanic additives. The reason for this phenomenon could be either consume of lime due to high pozzolanic reaction or the dissolution of binder in time. Both might had been occurred as well.

Considering the thermograms different peaks at different ranges more information can be gathered about the characterization of mortars. From graphs all of them had peaks around 573°C which indicates phase transition of quartz (Figure 3.4- 87 – Figure 3.4- 89). LM01C, LM04A and LM05 had peaks at 120 which may be attributed to salts.

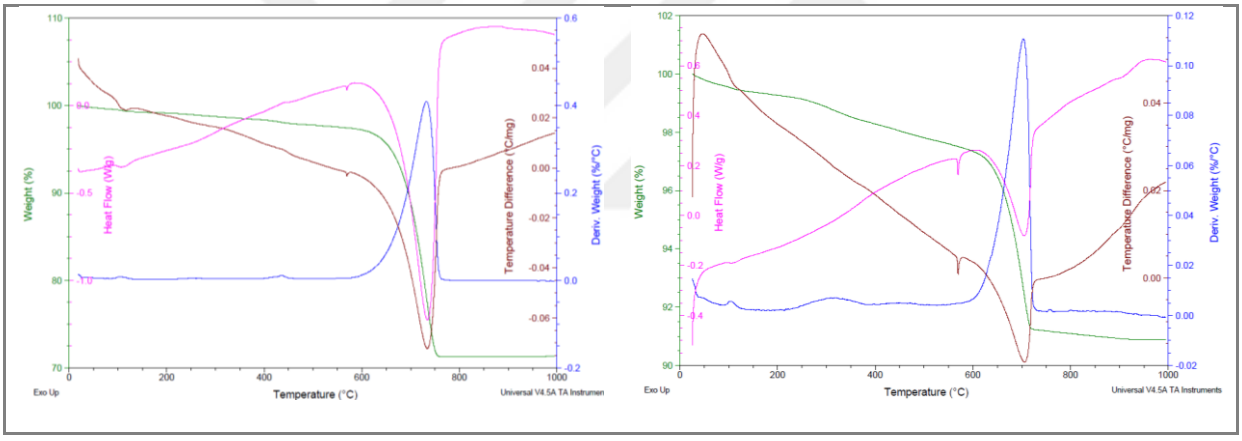


Figure 3.4- 87. Thermogram of LM01C (left) and LM04A (right)

LM03, LM04A, LM04B had weight loss between 200 and 400°C of 4.93%, 1%, 1.19% respectively (Figure 3.4- 88). It was probably related to dehydroxylation of clays. Clay minerals could be associated to the alteration product of the lithic aggregates or deliberative contribution to the carbonate binder (Crisci et al. 2004).

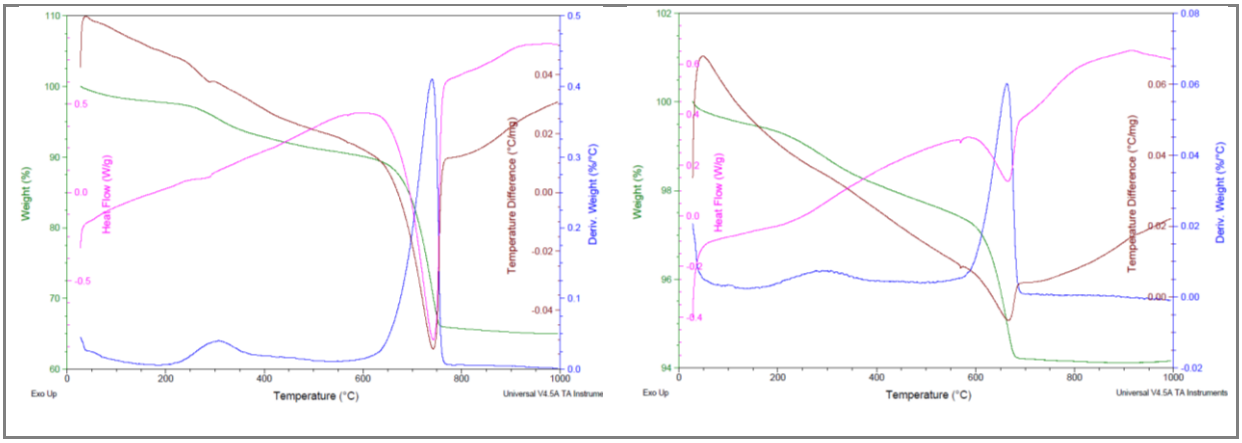


Figure 3.4- 88. Thermogram of LM03 (left) and LM04B(right)

LM06A had peak at 850 which indicates recarbonation or presence of calcite as aggregate (Silva, 2003). As illustrated in Figure 3.4- 89, LM07D had peaks at 200 and 650°C, which can be attributed to CSH also having weight loss between 400 and 500 indicate the presence of magnesite (Cardoso et al 2014). The thermograms imply ceramic or earthen material. High amount of weight loss below 120°C which indicates hygroscopic water responsible for movements of salts were appeared with peaks at LM07D, LM08 and LM09. LM08 had peak at 730 (calcium carbonate was not pure, recarbonated lime which includes some cementicious material, clay, CSH, CAH (Moropoulou et al. 1995) and LM09 had his major weight loss below 200°C.

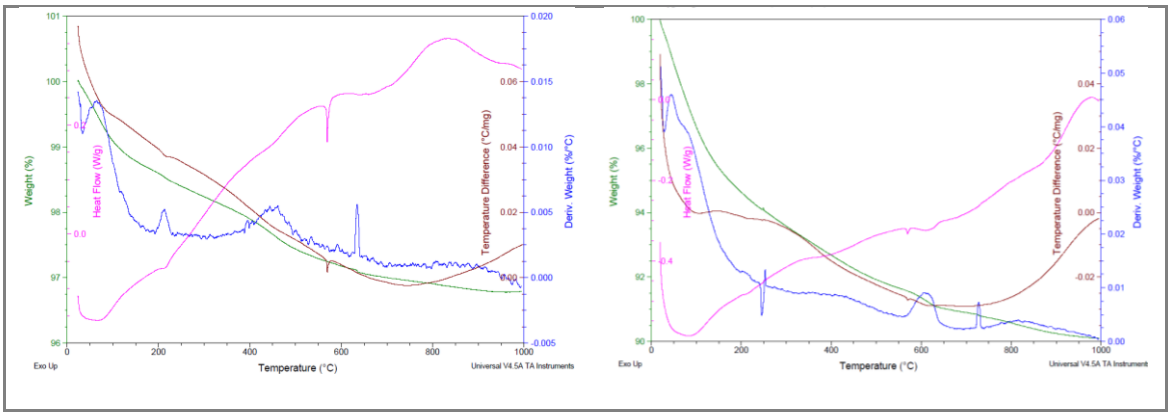


Figure 3.4- 89. Thermogram of LM07D (left) and LM08 (right)

Figure 3.4- 90 was plotted to understand the correlation between the acid soluble insoluble parts of the mortars and calcium carbonate ratio obtained from TGA analysis. Same

grouping can be done with "CO_2/H_2O vs CO_2" plot. Tetraconch bath wall and floor mortars (LM04A, B) had low binder and higher B/A ratios, floor of hypostyle building already low binder amount was decreasing from bottom level to top simultaneously B/A ratio. In East Bath sample taken from floor had less amount of binder and more aggregates than the mortar samples from walls. *Opus caementicium* mortar sample LM03 from South Bath wall had high $CaCO_3$ content which was also seen from TGA analysis, had low B/A ratio. The opposite would be expected due to the low amount of quartz peaks revealed in XRD analysis. It was seen that *opus caementicium* mortars were aligned in same binder aggregate ratio range and increasing carbonates percentages however there was no correlation found between the construction periods. *Opus signinum* mortar from the wall of East Bath (LM06C) lay in the zone of higher B/A and higher $CaCO_3$, the reason for this should be the marble fragment that affects the results of analyses. Therefore the sample theoretically should be situated around 25 x axis and 0.4 y axis. Similarly, marble fragment in LM03 mortar sample from the wall of South Bath resulted in high content of carbonates and higher B/A ratio.

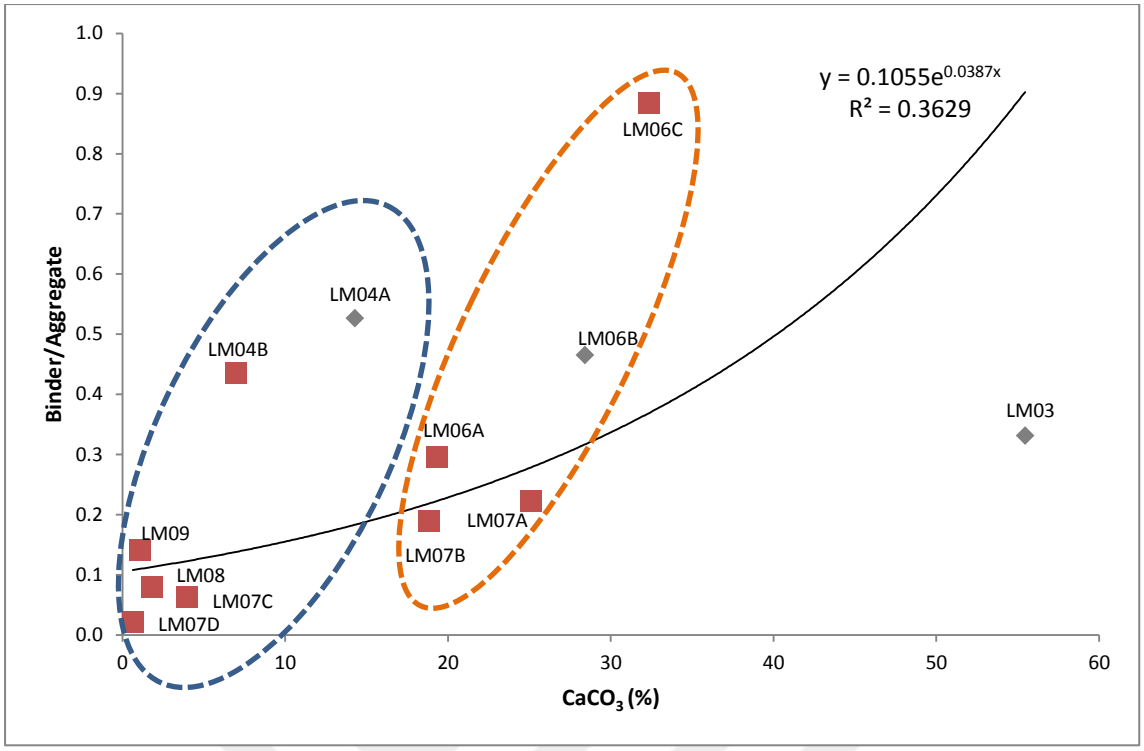


Figure 3.4- 90. acid in/soluble fraction vs $CaCO_3$ (%) from TGA of Labraunda mortars , same grouping with Fifure 3.4- 86, blue circle: highly hydraulic, orange circle: hydraulic)

3.4.8 X-Ray Fluorescence (XRF)

When y axis as binder and x axis was considered aggregates in Figure 3.1- 22 it was possible to classify the samples. LM08D and LM09 were drawn apart with low CaO+MgO content and very high SiO_2+ Al_2O_3+ Fe_2O_3 content. Among the rest of the samples two groups can be discarded: first group having > 50% alkali reactive aggregates and 15-25% calcitic binder and second group with <50% alkali reactive aggregates >25% calcitic binder. In Figure 3.4- 91 chemical compositions of the mortar samples was presented.

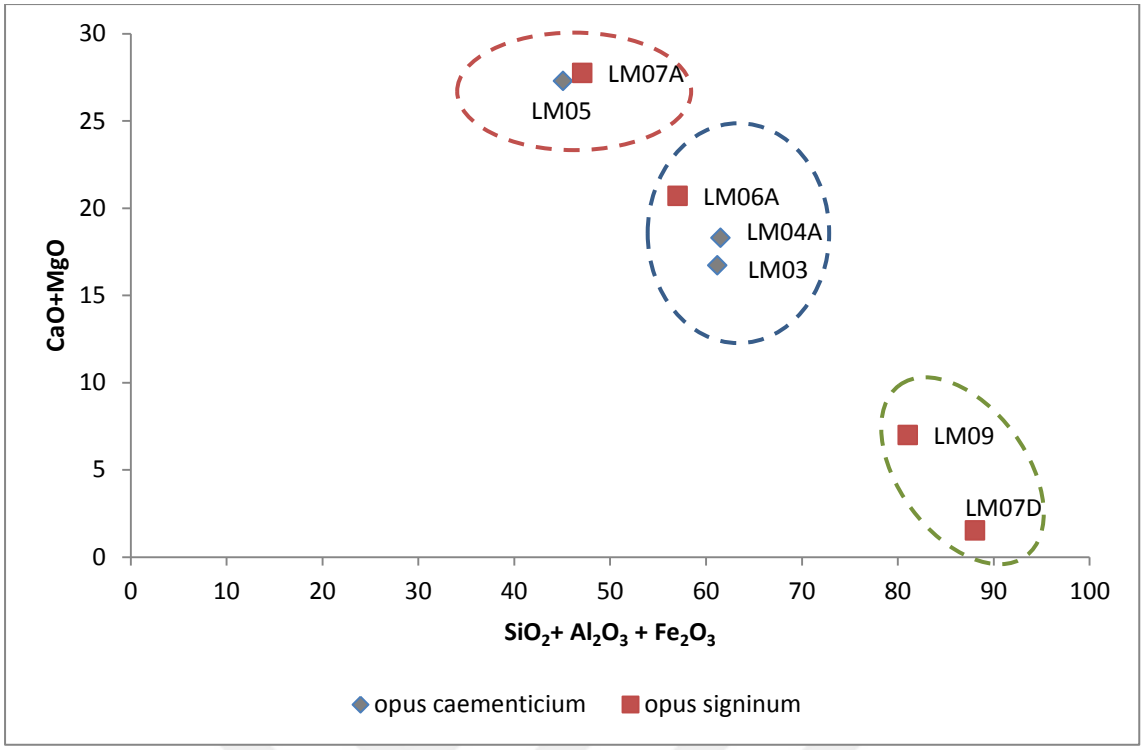


Figure 3.4 -91. CaO+MgO vs SiO_2+Al_2O_3+Fe_2O_3 graph of Labraunda mortars

It was seen that LM07D seperates from others at TiO_2/Fe_2O_3 vs SiO_2/CaO graph (Figure 3.4-92) due to very low amount of CaO but same TiO_2/Fe_2O_3 ratio with LM07A. This was enough to prove the use of same raw material in two samples from Hypostyle building floor. Among other samples which were located next to the y axis, LM03 which had richer content in Fe_2O_3. This was correlated with its low intensity of quartz peaks at XRD analysis and with high amount of weight loss between 200-400°C from thermogravimetric analysis can be associated to clays and hydraulic properties.

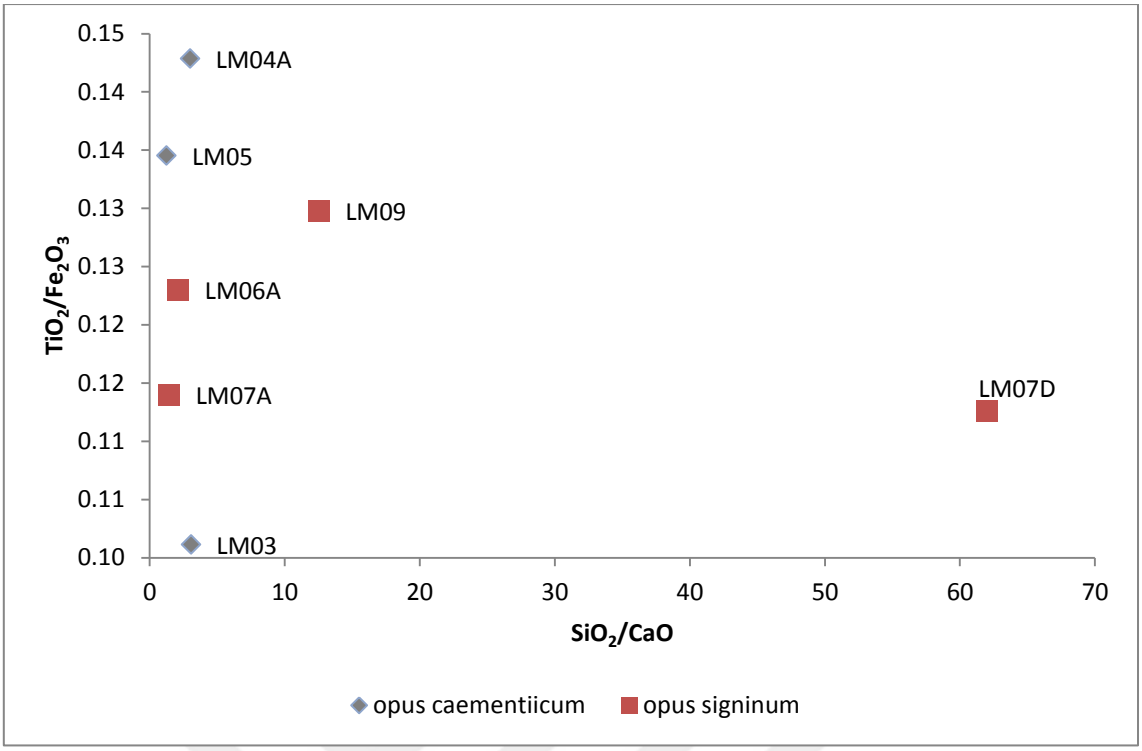


Figure 3.4- 92. TiO_2/Fe_2O_3 vs SiO_2/CaO graph of Labraunda mortars

Opus signinum mortars were situated in the core in the diagram (Figure 3.4- 93) while *opus caementicium* mortars were more dispersed. Among the mortars clearly fall into bottom portion of the diagram LM09 had higher magnesium and higher lower iron (Figure 3.4- 93). Again Hypostyle building floor samples were in the same range between 0.11 and 0.12 TiO_2/Fe_2O_3 ratio indicating same origin. In the rest, close values imply homogeneity in the mortar compositions (Table 3.4- 30).

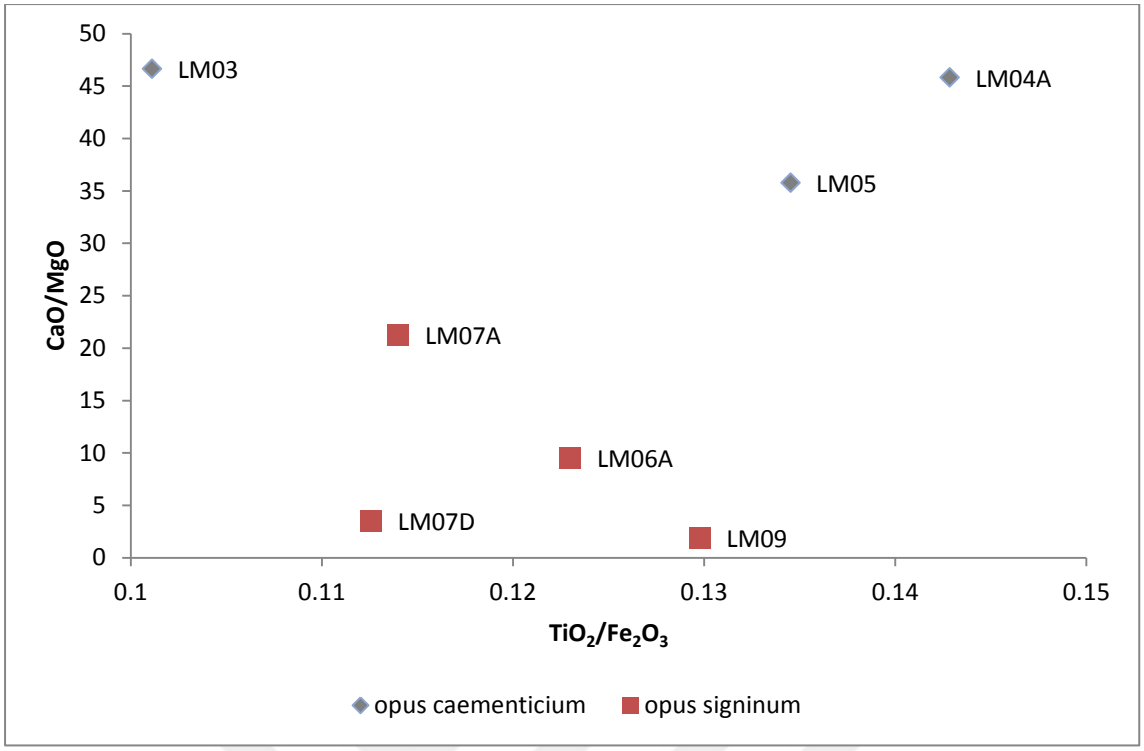


Figure 3.4- 93. CaO/MgO vs TiO_2/Fe_2O_3 graph of Labraunda mortars

Although in thermogravimetric analysis magnesite was revealed in sample LM07D it was not supported by XRF data.

Table 3.4- 30. Elemental composition of the Labraunda mortars (%) (LOI: Loss of ignition)

		Samples	SiO_2	Al_2O_3	Fe_2O_3	MnO	MgO	CaO	Na_2O	K_2O	TiO_2	P_2O_5	LOI	Total
opus caementicium	LM03	South Bath wall	50.11	10.2	0.89	0.02	0.35	16.36	1.92	4.57	0.09	0.18	15.39	100.07
	LM04A	Tetraconch Bath wall	53.72	7.04	0.77	0.01	0.39	17.91	1.44	2.79	0.11	0.21	15.55	99.94
	LM05	AndronC wall	33.18	9.67	2.23	0.03	0.74	26.54	1.57	2.19	0.3	0.86	23.2	100.52
opus signinum	LM06A	East Bath floor	39.22	14.08	3.74	0.07	1.94	18.76	1.01	2.53	0.46	0.72	17.99	100.51
	LM07A	Hypostyle Floor bottom	37.69	7.48	1.93	0.04	1.24	26.5	1.03	2.29	0.22	1.24	20.79	100.45
	LM07D	Hypostyle Floor 4	73.8	12.76	1.51	0.02	0.33	1.19	2.17	4.39	0.17	0.74	2.56	99.64
	LM09	Pool wall	58.14	17.68	5.24	0.09	2.34	4.65	0.95	2.77	0.68	0.51	7.17	100.23

Figure 3.4- 94 exhibits the use of raw materials and the difference in various levels of floor in Hypostyle building was worthy to note. It may be caused by the ceramic amount or may imply the different time of construction.

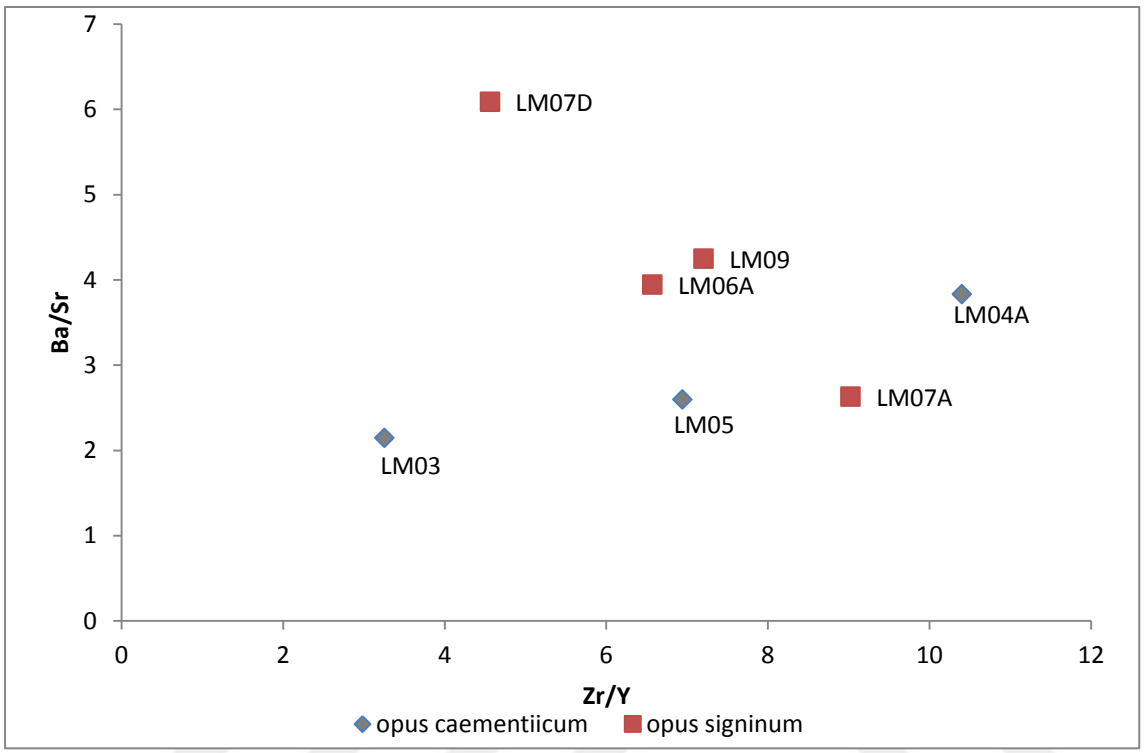


Figure 3.4- 94. Ba/Sr vs Zr/Y graph of Labraunda mortars

3.4.9 Mercury Intrusion Porosimetry

According to the values listed in Table 3.4- 31 LM03 stands among others with the lowest total porosity, together with the highest bulk density and average pore diameter values. On the other hand, LM06A had the highest total porosity and the lowest average pore diameter values. East Bath floor mortars had the highest porosity value. *Opus caementicium* mortars had 1.80 g/cm3 density and 26 % porosity values and *opus signinum* mortars had 1.2 g/cm3 density and 47 % porosity values. Micropore percentages were high in those mortars as well.

Table 3.4- 31. Parameters gathered by mercury intrusion (P: Porosity, APD: Average Pore Diameter (4V/A), BD: Bulk density, RD: Real density)

Samples		P (%)	APD (μm)	BD (g/cm^3)	RD (g/cm^3)
LM03	South Bath wall	25.4	0.16	1.82	2.44
LM06A	East Bath floor	50.61	0.05	1.21	2.44
LM07A	Hypostyle Floor bottom	26.97	0.06	1.78	2.44
LM07C	Hypostyle Floor 3	43.13	0.06	1.4	2.46
LM09	Pool wall	45.41	0.08	0.93	1.7

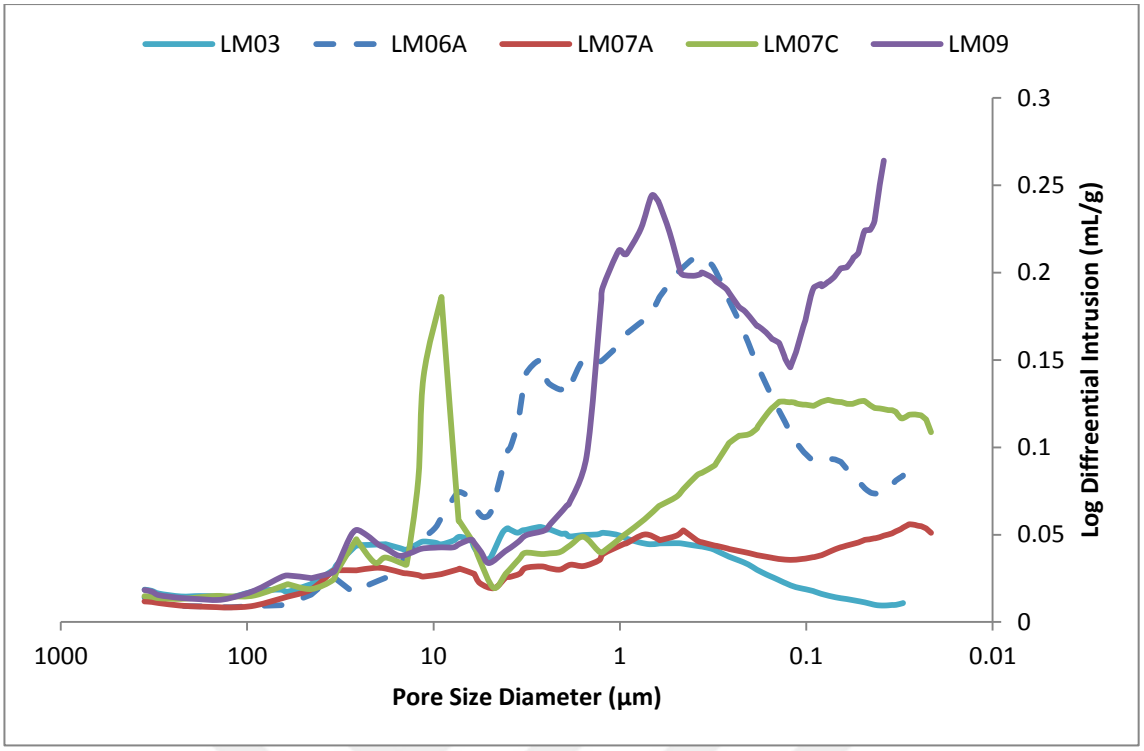


Figure 3.4- 95. Log differential intrusion versus pore size of the Labraunda samples

Sample LM03, from the wall of South Bath which belongs to *opus caementicium* type, had the lowest porosity and low amounts of macropores greater than 100 µm. The majority of pores were accumulated between 80 µm and 0.5 µm diameters with quasi bimodal distribution (Table 3.4- 32, Figure 3.4- 95).

Floor mortar from East Bath, (LM06A) showed nearly a unimodal pore size distribution however, a little peak between 80 µm and 20 µm, 10 µm and 8 µm, 5 µm and 3 µm before the highest accumulation of pores which was between 1 µm and 0,1 µm. Micropores were distributed mainly between 0.5 µm and 0.008 and 0,008 and 0,003 µm (Table 3.4- 32).

Table 3.4- 32. Pore size distribution and percentages of micro and macropores

Samples		Micro < 5 µm (%)	Macro > 5 µm (%)	< 0.01 µm	0.01 - 0.1 µm	0,1 - 1 µm	1-10 µm	10 - 100 µm	>100 µm
LM03	South Bath wall	59.7%	40.3%	-3.29%	8.25%	27.87%	36.47%	24.46%	6.24%
LM06A	East Bath floor	86.5%	13.5%	-13.66%	26.16%	47.69%	31.94%	6.35%	1.52%
LM07A	Hypostyle Floor bottom	72.7%	27.3%	-9.66%	33.21%	32.45%	22.87%	17.26%	3.86%
LM07C	Hypostyle Floor 3	73.1%	26.9%	-9.03%	39.00%	33.30%	19.81%	14.11%	2.82%
LM09	Pool wall	86.1%	13.9%	-24.55%	46.05%	49.27%	18.58%	8.67%	2.00%

In Hypostyle building bottom level (LM07A) and penultimate level from surface (LM07C) showed trimodal pore size distribution. First pore cluster was seen between 100 µm and 8 µm, the highest peaks were between and the other peaks were accumulated between 5 µm and 0.005 µm. Micropores between 0.1 and 0.008 µm were abundant and pores between 0,008 and 0,003 µm were higher than LM06A.

Surface hardness values of the samples were not directly depending on the hydraulicity and/or presence of pozzolanic aggregate. Sample which had the lowest superficial strength, LM06A, had highest total porosity and showed recrystallization of carbonated binder observed as lighter colour under microscope and as weight loss at 850°C at TGA-DSC analysis. Therefore the low strength value could be justified. The surface hardness values of the rest of the samples seemed not had direct relations with other analysis results.

3.4.10 Correlations of results according to architectural features

In the sanctuary Roman age buildings, except the Andron buildings, all of them were water related constructions. The majority of the collected samples were *opus signinum* type mortars having reddish/brownish binders and poorly sorted ceramic aggregates. Principally, because of the water related function *opus signinum* mortars could had been preferred. Nevertheless, mortars of Andron buildings contain ceramic as well similarly *opus caementicium* mortars were collected from the walls of South Bath and Tetraconch Bath which were same period construction mortars were similar in colour and surface hardness.

All floor mortars were *opus signinum* type and had strong reddish colour except the mortar sample from Andron A which had lighter colour. Remind that, the mentioned building was constructed in Hellenistic times and the presence of mortar was extraordinary. The microscopic observations showed that the same raw materials were selected; however, the lighter colour, less ceramic content prevented the assertion of the Roman period intervention. The plaster sample taken from that building was classified as true lime mortar with no hydraulic character and showed well sorted calcite, quartz and feldspar aggregates.

In Roman times at first century AD, Andron C building, East Bath and pool were constructed. The mortars collected from the wall of Andron C, the wall joint mortar and rendering mortar the floor mortar of *hypocaust* of the bath were *opus signinum* mortars. The certain construction period of hypostyle building was not known however with the same rock fragments and similar high content ceramic content imply that it was built in first century AD as well.

In the second construction period, third–fourth centuries AD, two other baths were constructed in the Sanctuary. This time, the only use of *opus signinum* mortars was seen in the floor of Tetraconch Bath, it could be related that the sampling was done from exterior walls.

Binder:aggregate ratios of the mortars in the wall were 1:1 in East Bath which was constructed in first century AD. In the walls of fourth century AD constructions, South and

Tetraconch Bath, this ratio decreased to 1:2 and 1:3 respectively. In floor mortars, the ratio was 1:3 in both of the construction phases. In Labraunda, the hypothesis of adding more aggregates in new constructions was valid only for wall mortars.

The pool mortar from wall and upper two levels of Hypostyle building were exceptional because they own so low amount of binder due to dissolution of lime. They were both were situated in the eastern part of the sanctuary it was thought that there should be a decay factor causing dissolution and preventing re-precipitation of calcite, which could be the immense rainfall.

Independent from the binder/aggregate ratio, all of the mortars showed descending grain size distribution, namely the high weight percent of the aggregates were in the higher aggregate size. It should be a conscious decision. Amount of fine grains below 63 μm were high in the water related buildings. In that, probably *opus signinum* mortars had ceramic dust *opus caementicium* mortars included pozzolanic dust grains. Furthermore, the angular shape of aggregates indicated that the raw materials gathered after crushing and grinding the rocks. When the geographical conditions of the site were concerned it was already expected.

Hypostyle building and pool mortars had the least carbonation degrees, and first century AD construction, Andron C, had the most carbonated mortar binder.

4 Comparative Discussion of Roman Mortars

This chapter compares and discusses the results of the characterization of Roman mortars from Complutum, Mérida, Nysa and Labruanda.

Mortars extracted from the same period constructions of four sites from the two extremes of Mediterranean Roman Empire were characterized. The aim of the characterization of these mortars was to find the differences and similarities in order to see architectural interactions and/or disconnections.

In the sites, independent from construction style, the collected mortars are classified as *opus caementicium* and *opus signinum* according to ceramic inclusion. In all of the archaeological sites, the majority of *opus caementicium* type mortars are porous mortars with medium size aggregates. In Nysa, the colour of the mortars is light brown in general. On the other hand, among Labraunda mortars, both light brown and whitish binders are found. This is related to the clay and pozzolanic additive content. The majority of this type of mortars in Spain have whitish crème colour. Mortars with very high luminosity are found in *Criptopoticus* of Complutum and in the aqueduct of Mérida. According to spectrophotometric measurements, this type of mortars in Spain are accumulated in a wider range between 70-85 L* and 6-15 C* where Complutum mortars have higher luminosity values. Mortars from Turkey lie between 65-80 L* and 10-15 C*, and Nysa mortars are uniform in colour except for two (theatre and pavement) mortars. Furthermore, microscopic and thermogravimetric analyses show that these mortars differ from the rest (Figure 4.1).

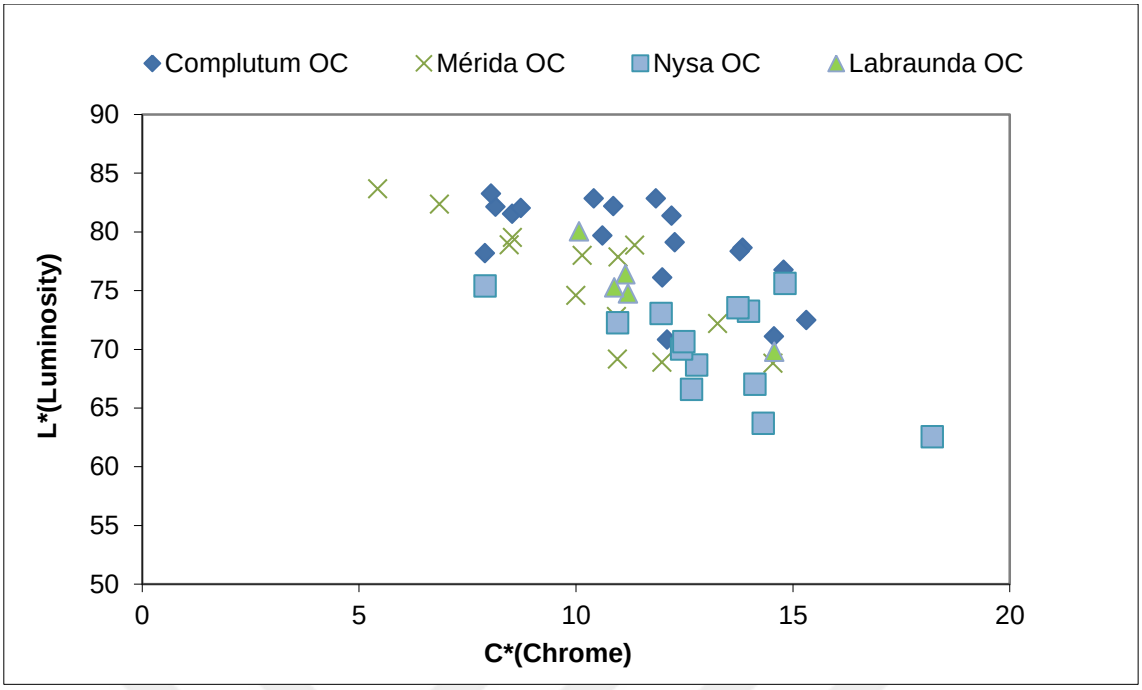


Figure 4. 1. Luminosity vs Chrome of *opus caementicium* samples (OC)

Of the *opus signinum* mortars examined, two distinct types were identified. The first and more common type has reddish binder and medium sorted small angular ceramic aggregates. The other type has larger angular ceramic fragments embedded in whitish binder. The first type is found in all the sites as coating mortar, floor mortar or masonry mortar in water-related structures. The second type is seen in Complutum as a marble coating mortar in North Bath, and in Mérida in San Lazaro aqueduct in the second layer of the channel; however, it has also dark coloured rock fragments. Figure 4.2 shows that Nysa and Mérida *opus signinum* mortars lie in the same (C*, L*) range (8-20, 62-77). Samples having the highest C* and the lowest L* values (10-25, 55-76) belong to Labraunda and Complutum.

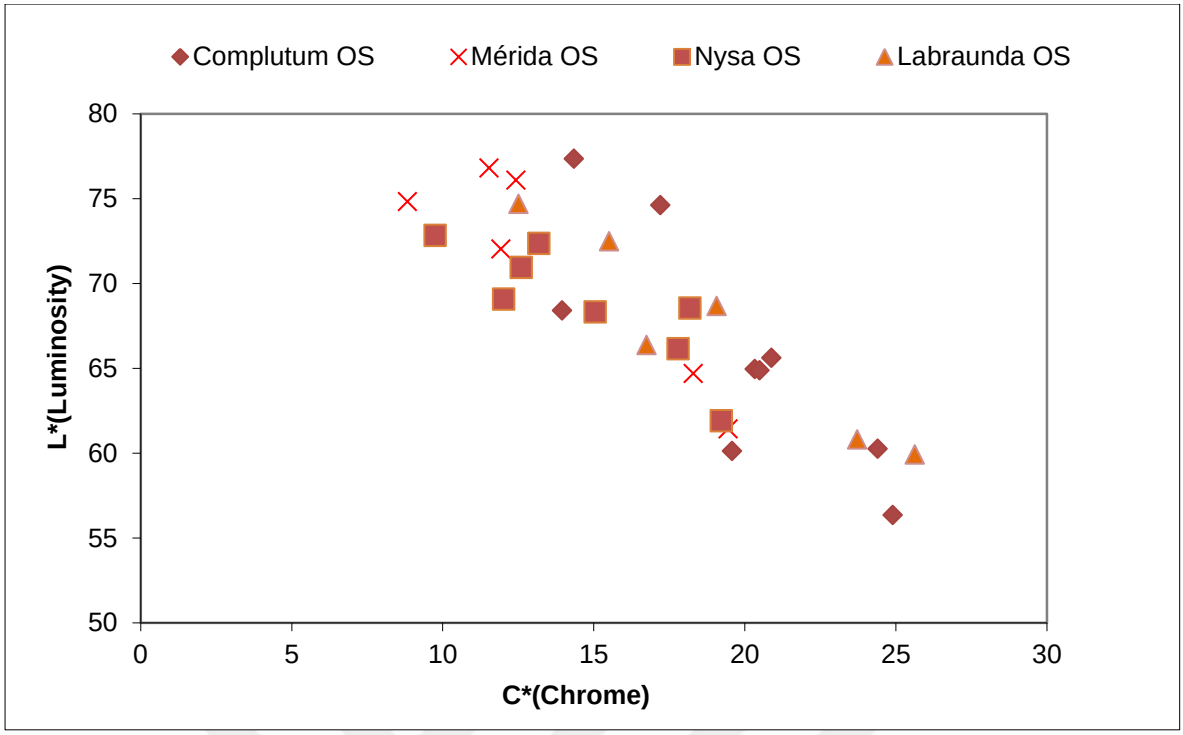


Figure 4. 2. Luminosity vs Chrome of *opus signinum* samples (OS)

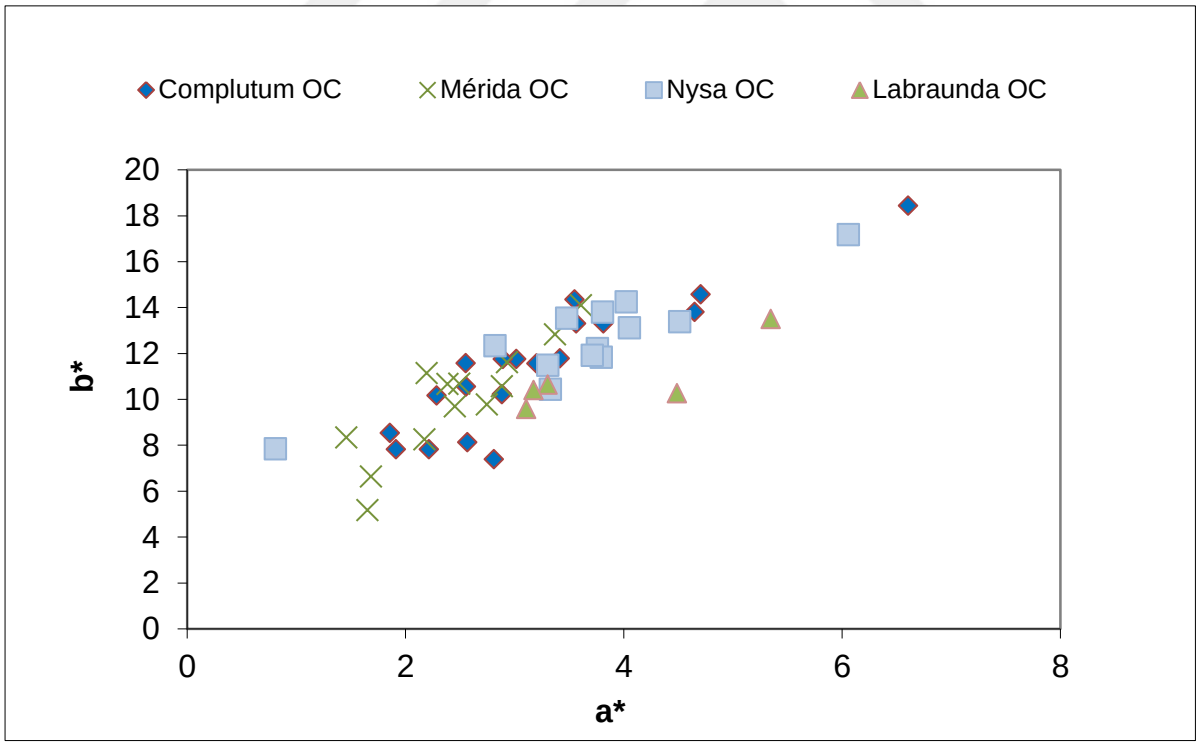


Figure 4.3. b* vs a* chromatic parameters of *opus caementicium* mortars

Among *opus signinum* mortars, Mérida has the least reddish tones, and reddish colours are most frequently seen in Complutum and Labraunda (Figure 4.4).

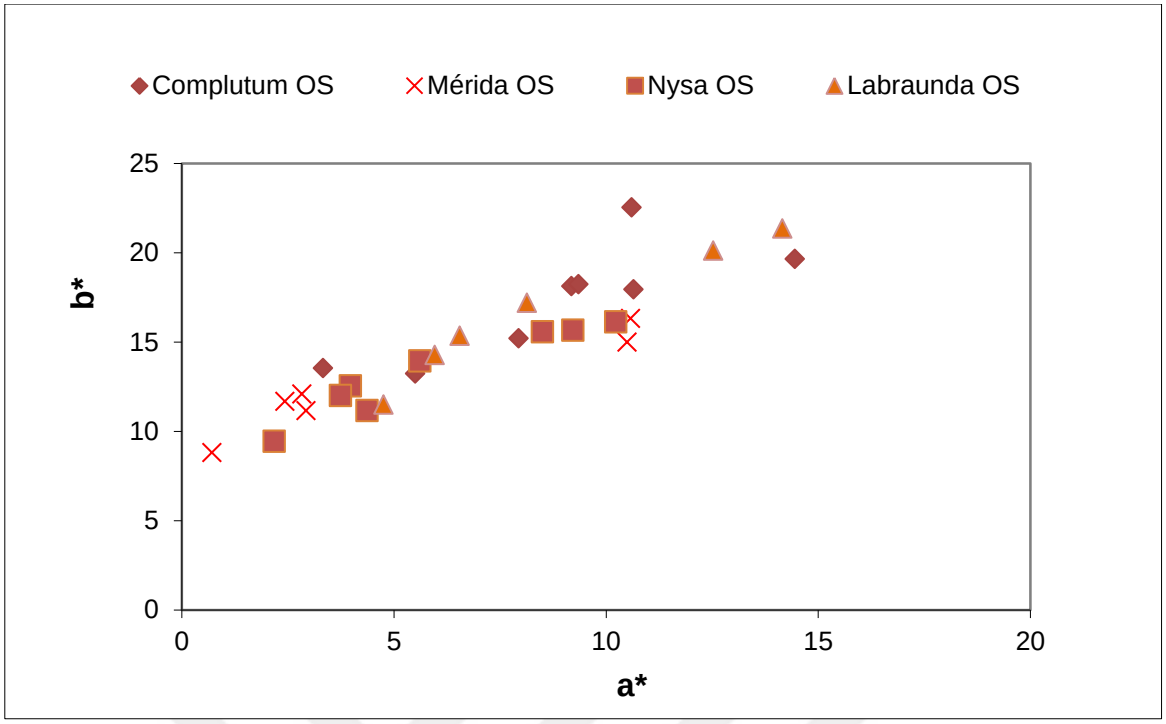


Figure 4.4. b* vs a* chromatic parameters of *opus signinum* mortars

Observation under the microscope provided petrographic information about mortar components. Figure 4.5 shows the schematic explication of the interpretations in optical microscopic analysis.

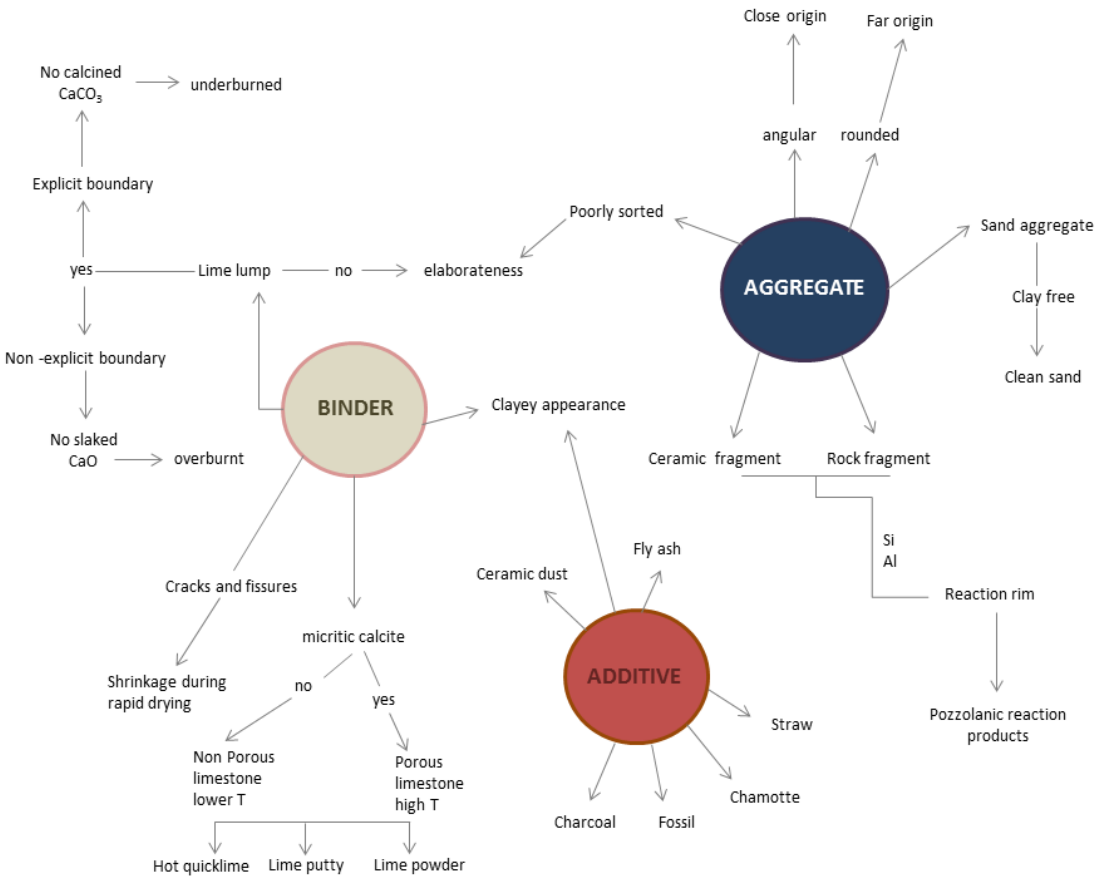


Figure 4.5. Flow chart showing the microscopic view of binder, aggregate and additives and possible information that can be gathered

In Complutum mortars, aggregates are composed of angular to sub rounded sand grains and rarely, medium size rock fragments of sandstone, quartzite and slate. The geology of the region includes sands, gravels, silts and clays from the terraces of Henares River. Nevertheless, no clay is found in the mortars. The builders seem to have preferred clean sand in the manufacturing of mortars.

In other sites, angular to sub rounded sand aggregates and large rock fragments constitute the aggregates. The aggregates of Mérida mortars include a large range of lithic fragments including diorite, metagranite, quartzite, slate and monzogranite. Since Nysa and Labraunda are situated in the same geological zone the rock fragments found there are similar as well. Gneiss, metaquartzite, and micaschist are observed in the Labraunda mortars, and garnet mica schist and marble are seen in the mortars of Nysa. The use of these rock fragments

provided alkali reactive minerals such as actinolite in Mérida and kaolinite-phillipsyte in Nysa and Labraunda. Relatedly, clayey appearance binder and reaction rims around the aggregates are observed here and there.

The raw materials used in the mortars reflect the regional geology in all of the archaeological sites. Apparently, in none of the sites was procurement of special aggregates from the manufacturers considered necessary, and aggregate selection was directly related to the geographical conditions. More sophisticated materials were bought, some of the marbles used in Mérida (pavonozetto) was gathered from Docimium, today's İncehisar on the western coast of Turkey (Barrientos Vera and Palma García, 2012).

In Complutum, Mérida and Nysa sub-rounded aggregate shapes are abundant, which indicates that builders used sands from riverbank. On the other hand Labraunda mortars aggregates are crushed rock fragments with angular forms. The dust and fragments of ceramics used for the *opus signinum* mortars were obtained from the remains after cutting the square bricks. Those bricks are supposed to have been manufactured close to the archaeological sites where they were used. Clays for the bricks either were transported from the river beds and from the closest alluvium deposits or purchased by central clay merchandiser. Due to the immense construction in the imperial period, there was industrial-like brick production, and special care was given to the aging of clays (Giavarini, 2010).

Figure 4.6 shows the binder aggregate ratios and calcium carbonate content, which are closest in the Nysa mortars. The common group consists all of the Nysa mortars and the majority of the Complutum, Mérida and Labraunda mortars, which lie in the bottom left sub-division of the diagram, 10-40 $CaCO_3$ (%) and is 1:2- 1:4 B:A. The second group is between 45-50 $CaCO_3$ (%).

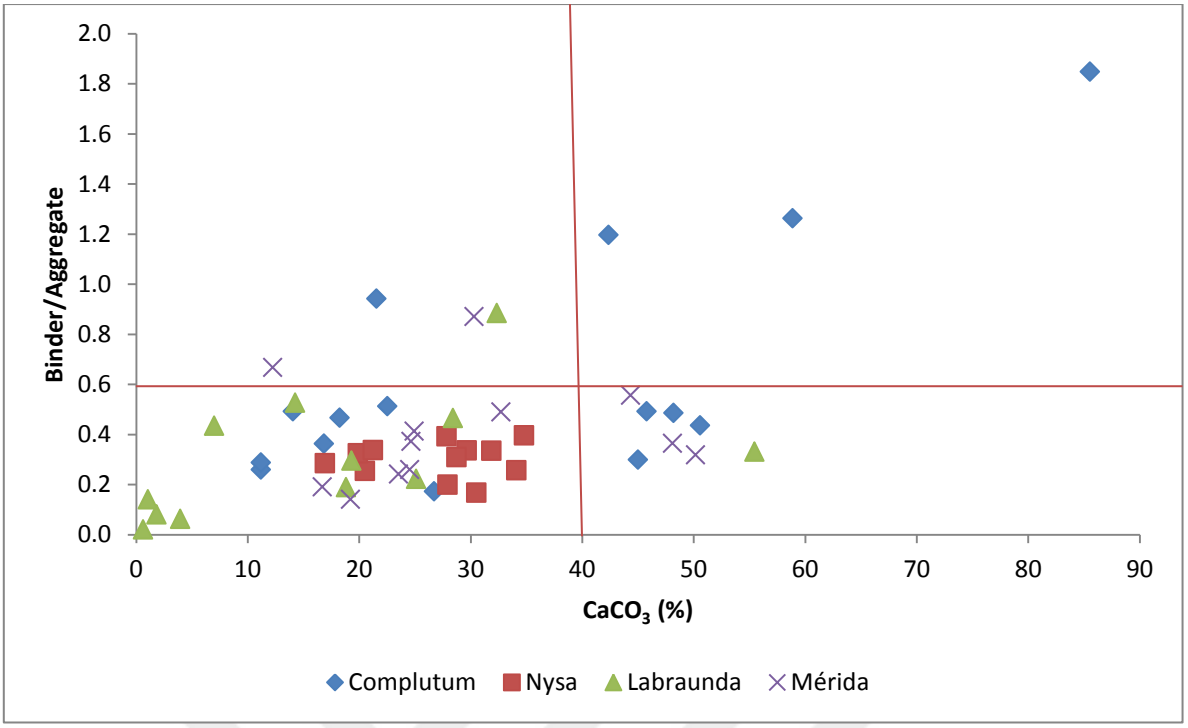


Figure 4. 6. B/A vs $CaCO_3$ (%) of mortars

The B:A ratio of the coating mortar in Mérida is different from those in Complutum and Labraunda. Floor mortars have 1:4 B:A ratio. The proportions of wall mortars vary in the city. Alcazaba and Bath mortars have a 1:1 ratio; Moreria, 1:3, Viñero wall, 1:4 and Circus 1:5. If the rule deduced from Complutum that "adding more aggregate to mortar occurred in later centuries" can be applied to Mérida as well, Alcazaba and Thermal Bath should be earlier constructions than the others. The mortars of Nysa date to Roman times but more precise information is lacking. Since the binder aggregate ratio of the majority of the mortars is 1:3 and the rest are with more aggregates it can be interfered that the buildings are constructed after the third century. AD.

There is a variety in the granulometry of the mortars in Spain, but in the mortars of Turkey, the particle size distribution of the aggregates exhibits more uniformity. The aggregates in Nysa mortars are symmetrically distributed, and those in Labraunda have a descending distribution with higher ratio of larger grains. This may be considered an indication of a special care in their manufacture.

As Figure 4.7 shows, the majority of the mortars and all the Mérida mortars studied have hydraulic character due to highly silicic rock fragments (Mota et al. 2016). The first group of samples are in the highly hydraulic zone which is between 5 and 15 CO_2 (%). Almost all the Nysa mortars are in that zone. Five Labraunda samples and one Complutum sample are closer to the intersection of the two axes with both low CO_2 and H_2O ratios because of their very low binder content. Another group includes more Complutum and Mérida mortars between 15 and 30 CO_2 (%). The rest of the mortars are dispersed after 10 CO_2/H_2O, which is inversely related to hydraulicity, are true lime mortars without hydraulic properties. They are floor mortars from the Road and the Bath and plasters from Complutum, Nysa and Labraunda, respectively.

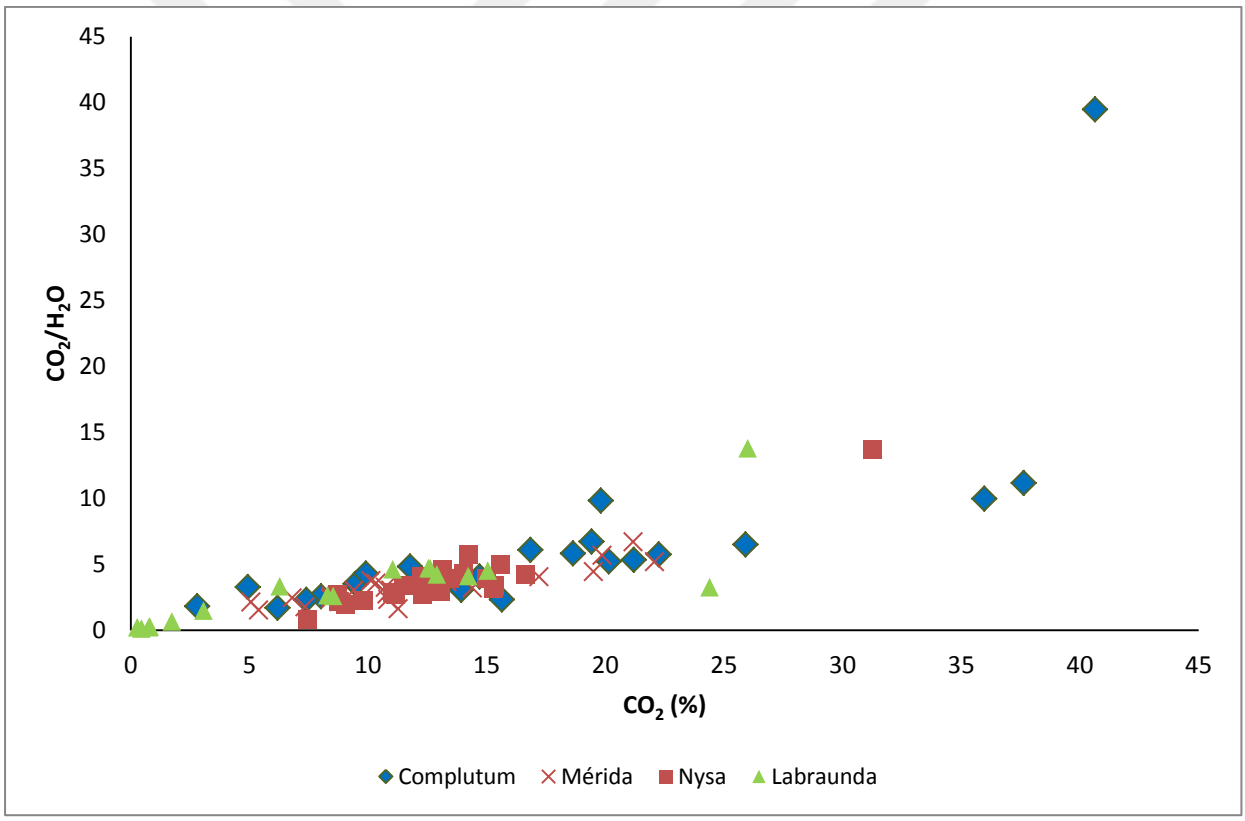


Figure 4. 7. CO_2/H_2O vs CO_2 plot of mortars

Figure 4.8 shows the relation between CaO+MgO and SiO_2+Al_2O_3+Fe_2O_3 can be roughly regarded as binder vs aggregate since in general the mortars do not contain calcareous aggregates. It demonstrates that, in Complutum and Mérida, there are two main groups of

samples. The first group of Complutum lies between 25-36 % lime and 30-50 % aggregate, and the second group has 10-20 % lime and 60*80 % aggregate.

In Mérida, the two groups are quite shifted. Two samples are in the first group with 32-34% lime and 35-40% aggregate, but the majority of the samples are in the second group with 55-75 % aggregate and 11-25 % lime. The *Opus signinum* type mortars in the second group are located closer to 90 on X axis and 0 on the Y axis.

In the mortars from Turkey, Nysa mortars are situated together united in the middle of the second group with 60- 70 % aggregate and 13-18 % lime. The Labraunda mortars are in three groups, of which the third group is *opus signinum* mortars with very low concentrations of lime.

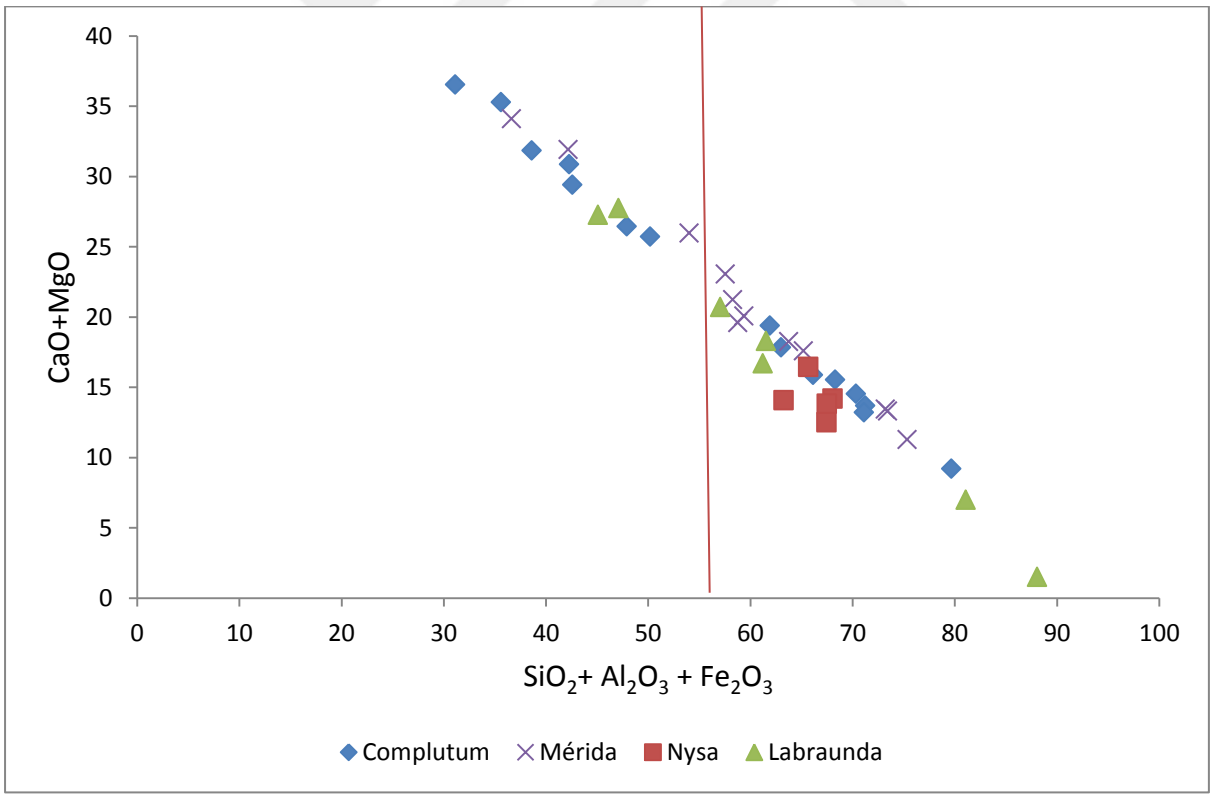


Figure 4. 8. CaO+ MgO vs SiO_2+Al_2O_3+ Fe_2O_3 plot of mortars

When the two types of opus mortars were examined separated in the same correlation (Figure 4.7), it was found that mortars of Nysa were the most uniform mortars, and that both

types of the mortars were similar in composition (Figure 4.9). The Mérida *opus signinum* mortars are close to each other while the *opus caementicium* is more dispersed. The Complutum mortars are in two groups, both for *opus caementicium* and *signinum* type mortars. The Labraunda mortars do not show any uniformity (Figure 4.10).

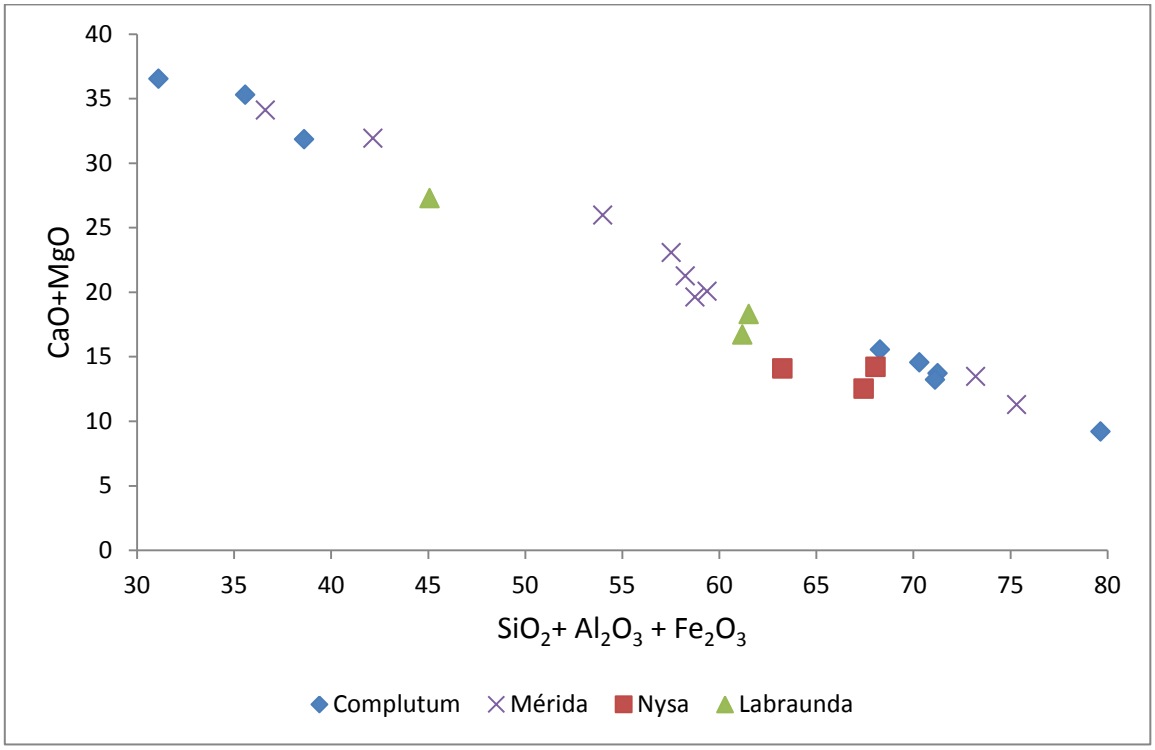


Figure 4. 9. CaO+ MgO vs SiO_2+Al_2O_3+ Fe_2O_3 plot of *opus caementicium* mortars

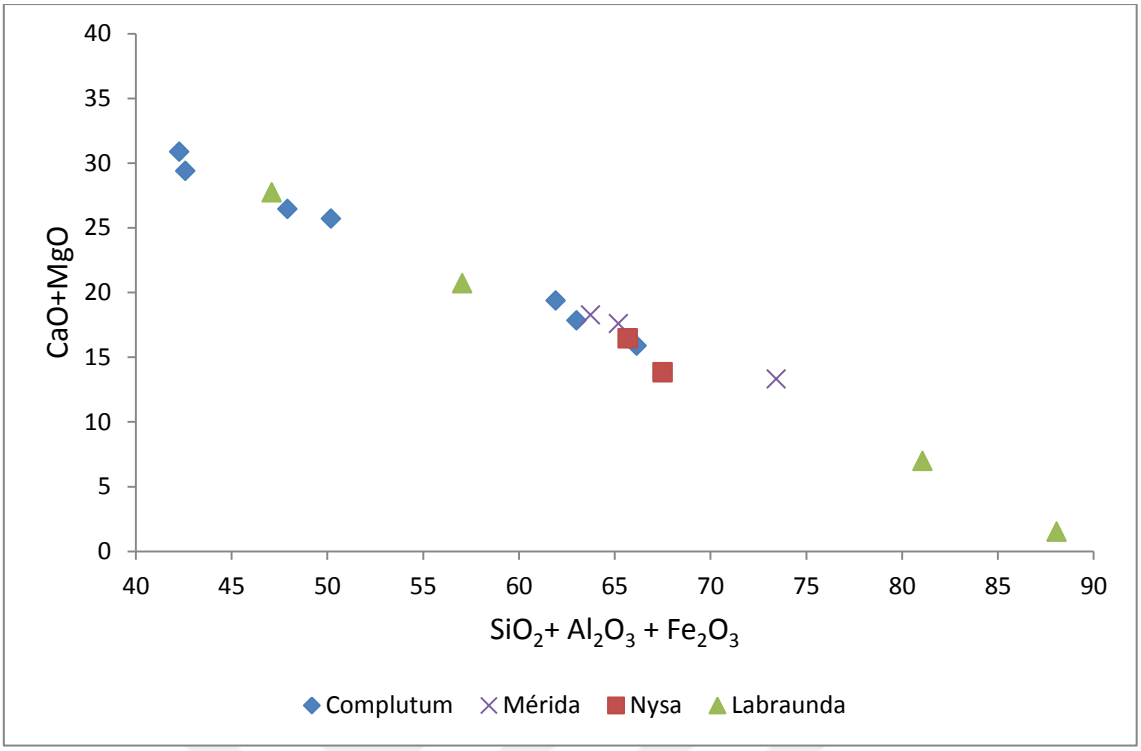


Figure 4.10. CaO+ MgO vs SiO_2+Al_2O_3+ Fe_2O_3 plot of *opus signinum* mortars

(Figure 4. 11) shows that the Mérida mortars are accumulated below 10 CaO/MgO and 0.07-0.15 TiO_2/Fe_2O_3, and the Labraunda mortars below 50 CaO/MgO and 0.10-0.15 TiO_2/Fe_2O_3. *Opus caementicium* mortars are in the upper portions. The aggregates do not vary as much as the binder content. The Complutum mortars show greater variety and are seen dispersed in the zone below 60 CaO/MgO and 0.10-0.35 TiO_2/Fe_2O_3. The *opus signinum* type mortars are dispersed below 23 on the y axis, which means that the ceramics used have distinct features and more difference in composition due to the different iron content.

The Mérida and Nysa mortars show more homogenous values in the centre of the diagram; however, the Labraunda and Complutum mortars are more dispersed. The Labraunda values vary due to the binder content, and the Complutum mortars are affected by both lime content and composition of aggregates. The aggregates used in the Complutum mortars have varied iron content, which may be attributed to clays, even in small amounts.

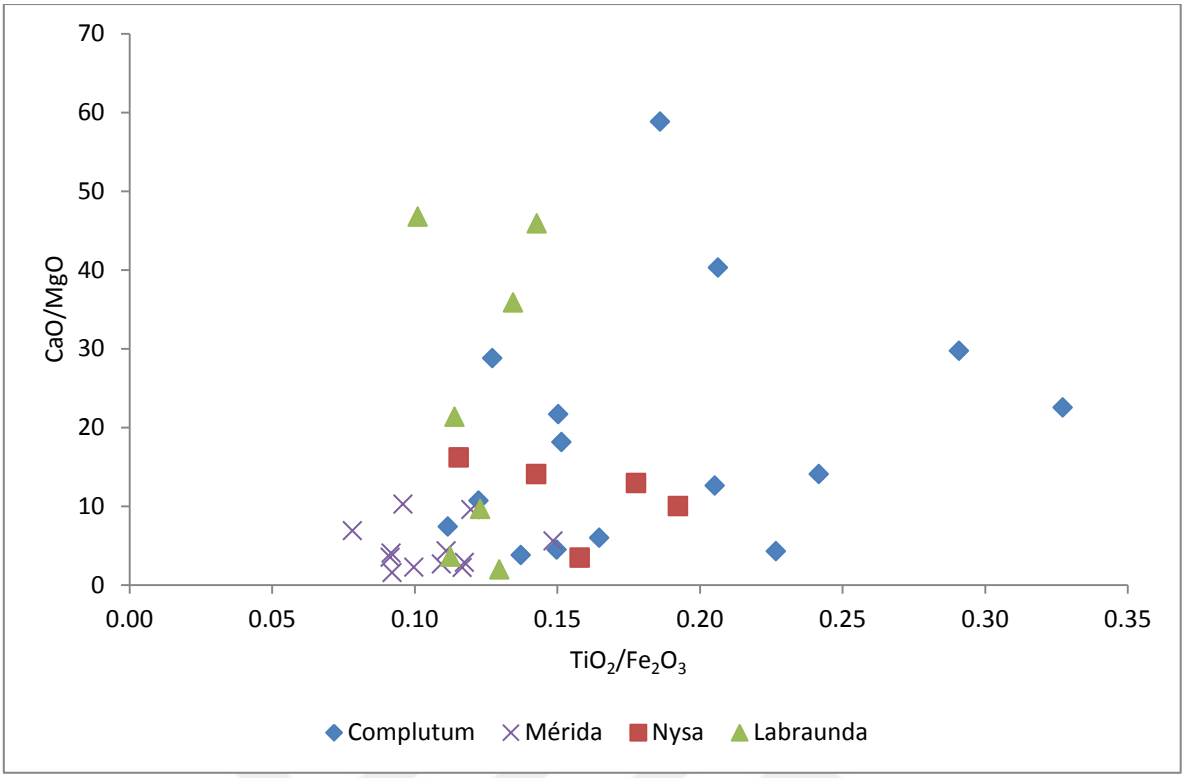


Figure 4.11. CaO/MgO vs TiO_2/Fe_2O_3 plot of mortars

The relation between immobile elements (Ti, Zr, Y, Nb) and more mobile elements (Ba, Rb, Sr, Si, Al, Na, K) is used to classify altered volcanic rocks (Marra et al, 2011; Sayit and Göncüoğlu, 2009). If the binder amount is high the trace elements are difficult to detect. Thus, the Ba/Sr ratio would be low, and high ratios of Zr/Y indicate rock fragments rather than ceramic fragments (Miriello et al. 2011). Subdividing the diagram (Figure 4.1- 12) into three zones, Nysa and the majority of Complutum mortars are situated in the left bottom indicating more homogeneity. Since the majority of the mortars collected from Mérida do not have ceramic fragments they are dispersed in the higher Zr/Y zone, and the Labraunda mortars are located in the upper zones (high Ba/Sr) in the diagram due to their low lime content.

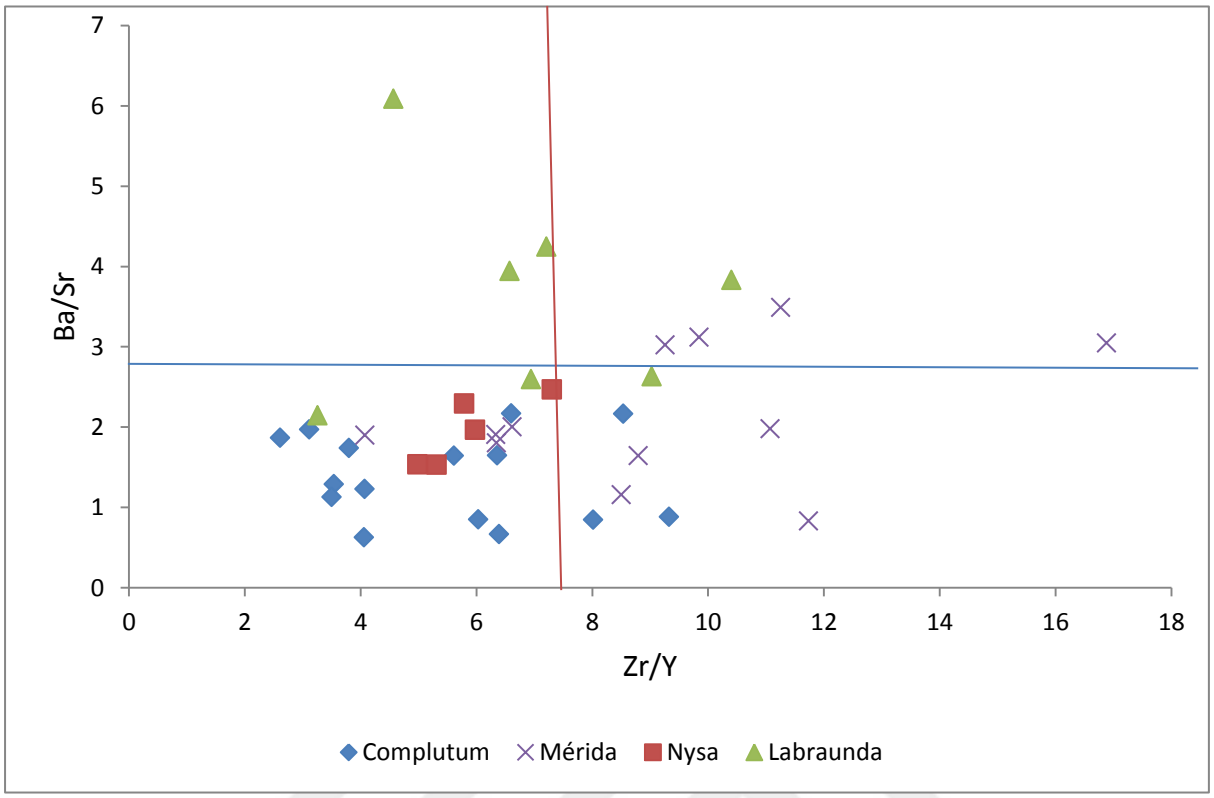


Figure 4. 12. Ba/Sr vs. Zr/Y plot of mortars

When we look at porosity and average pore diameter of the mortars from the archaeological sites in Turkey, two groups stand out. The *opus caementicium* mortars have medium porosity (below 30 %) while the *opus signinum* mortars have high porosity (40-50%) with smaller average pore diameters. On the contrary, both types of mortars in the archaeological sites in Spain lie in the middle of the diagram (30-40%) showing more uniform porosity. The Complutum mortars have slightly higher porosity and more variation among the samples. The *opus signinum* type mortars from Turkey have small pores and higher porosity (Figure 4. 13). There may be several explanations for this difference. The ceramics used in Turkey are more porous, so the measurements result in higher porosity or higher ceramic aggregates and less binder amount cause more rapid deterioration and thus, higher porosity. Furthermore, lime lumps which are thought to lessen the capillary pores and shrinkage cracks, are less frequent in these mortars (Cabellaut et al.2003).

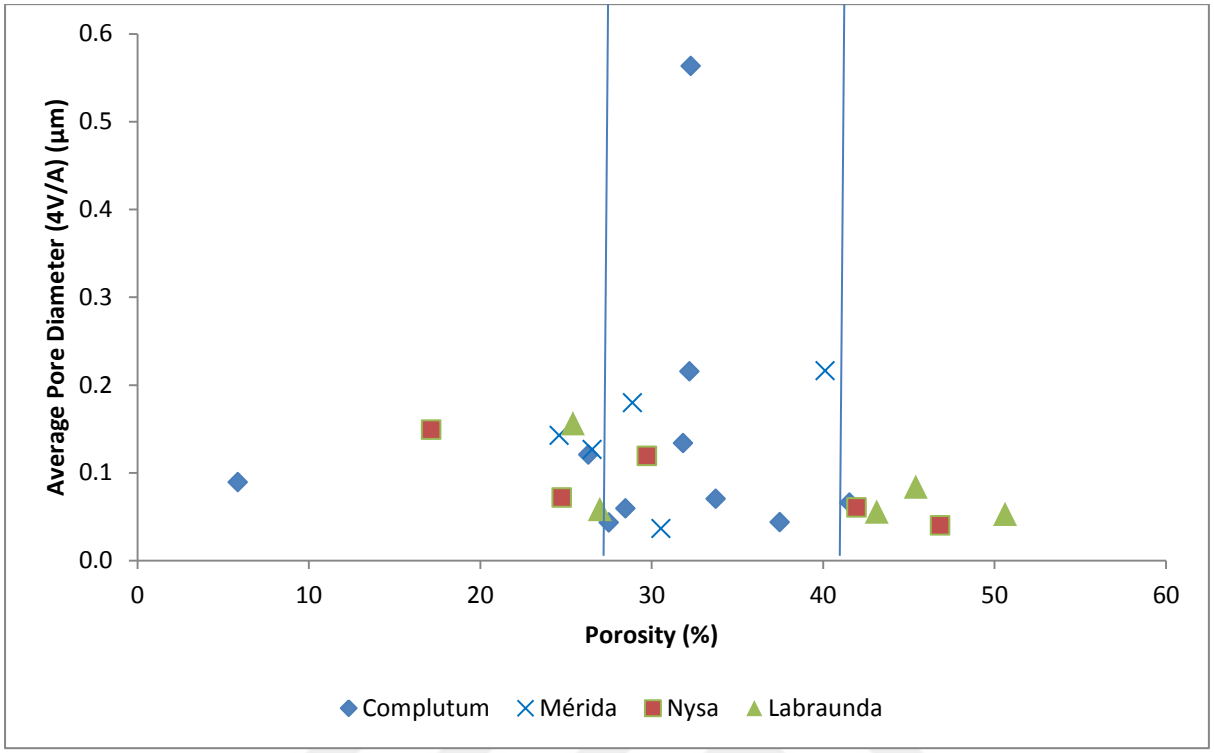


Figure 4. 13. Average Pore Diameter vs. Porosity of mortars

The Complutum mortars have more percentage of micropores, which can be considered as more susceptible for deterioration than macropores (Table 4.1).

Table 4.1. Physical properties of the mortars

		Mortar Samples		Average Pore Diameter (4V/A) (µm)	Bulk Density (g/cm³)	Apparent Density (g/cm³)	Porosity (%)	Micropores (%)	Macropores (%)
Spain	OC	CM02 A	Criptoportico wall	0,09	2,47	2,63	5,86	77	23
		CM06 A	North Bath floor	0,12	1,85	2,51	26,31	88.7	11.3
		CM09	North Bath facade	0,22	1,59	2,34	32,22	76.7	23.3
		CM15	South Bath brick arch	0,56	1,64	2,43	32,27	71.5	28.5
		CM16	Seawage	0,04	1,51	2,42	37,47	96.8	3.2
		CM31	South Bath floor	0,13	1,68	2,47	31,83	61.4	38.6
	OS	CM07	North Bath coating	0,04	1,83	2,52	27,50	88.8	11.2
		CM10	North Bath coating	0,07	1,51	2,27	33,74	94.7	5.3
		CM27	North Bath floor 3	0,07	1,38	2,36	41,55	97.3	2.7

		CM38	Bridge pillar	0,06	1,71	2,39	28,48	91.8	8.2
	OC	MM8	Moreira wall	0,22	1,40	2,33	40,12	67.5	32.5
		MM10	Temple floor	0,04	1,73	2,49	30,54	70.5	29.5
		MM14	Temenos wall	0,13	1,76	2,39	26,53	58.1	41.9
	OS	MM22	Amphitheatre	0,18	1,66	2,33	28,88	72.7	27.3
		MM26	Snow well	0,14	1,89	2,50	24,62	77.9	22.1
Turkey	OC	NM12	Tunnel up	0,15	2,05	2,48	17,13	59.6	40.4
		NM24	Bridge	0,12	2,06	2,94	29,73	71.1	28.9
	OS	NM16	Road coating	0,04	1,21	2,27	46,82	86.8	13.2
		NM23	Stadium	0,06	1,34	2,31	41,95	81.9	18.1
		NM25	Bath arch	0,07	1,80	2,39	24,75	88.8	11.2
	OC	LM03	South Bath floor	0,16	1,82	2,44	25,40	59.7	40.3
	OS	LM06A	East Bath floor	0,05	1,21	2,44	50,61	86.5	13.5
		LM07A	Hypostyple floor bottom	0,06	1,78	2,44	26,97	72.7	27.3
		LM07C	Hypostyple floor 3	0,06	1,40	2,46	43,13	73.1	26.9
		LM09	Pool coating	0,08	0,93	1,70	45,41	86.1	13.9

The surface hardness values of the mortar samples from the sites in Spain are higher than those of the mortars in Turkey of which the Labraunda mortars are more varied than the Nysa mortars, and the *opus signinum* type mortars show less hardness. This property does not directly depend on the hydraulicity and/or the presence of pozzolanic aggregate. Superficial hardness should be affected by carbonation degree or the conservation state of the mortar, rather than binder aggregate ratio or chemical composition.

When the research questions in the beginning of the study are asked again;

What aspects of mortar production technology are similar or different in two distinct regions of Roman Empire?

In Roman times, both lime putty and quicklime were used (Adam, 1999). For convenience, when quicklime was bought from the manufacturer, the mortar was either prepared *in situ* with hot lime technology (Moropoulou et al., 1995) or slaked in lime pits in a very humid environment. Alternatively, slaked lime (lime putty) could be directly acquired from the manufacturer and carried in closed baskets or amphora (Adam, 1999; Goldsworthy and Min, 2009).

It is difficult to tell whether quicklime or lime putty was used, from the lime lumps in the mortars because both are possible. Due to the unequal heat distribution in the lime kilns over-burnt CaO or under-burnt $CaCO_3$ together with insufficient water in slaking, lime lumps occurred in the mortar mixes (Pecchioni et al. 2014; Giavarini, 2010). Alternatively, they may have been caused by manufacturing of the mortars using hot lime method with quicklime and wet aggregate (Moropolou et al. 1995; Hughes and Cuthbert, 2000).

The geological zone of Labraunda and Nysa in Turkey does not have limestone, but marble outcrops. Small marble fragments were found in the Tetraconch bath in Labraunda, which is thought to have been used as lime kiln in the later centuries (Labraunda 2013 report). Considering that Roman builders preferred lime from pure limestone and marble is very close to the purest calcium carbonate, the calcination of marble makes sense. On the other hand, this hypothesis may be discarded primarily because a high quality building stone like marble would not have been wasted, secondly this operation would have been difficult. The lime was probably provided by manufacturers from further away. Lightweight quicklime blocks made of calcined limestone from a central kiln were easier to transport to the site (Goldsworthy and Min, 2009; Gotti et al 2008). According to the experiments in the previous studies, the micrite size calcite crystals indicate the use of aged lime putty (Rodriguez

Navarro et al. 1998) and the limestone was porous and fired at around 900 °C (Moropolou et al.1995).

As in cases in Spain, similar micritic calcitic binders imply aged lime putty gathered from porous limestone. Both of the two sites have limestone formations nearby, therefore the manufacturers could have been nearby, too, and since there are no traces of lime pits in the sites, it can be assumed that the lime putties were transported in amphoras. On the other hand, fly ashes were observed in the mortars of Mérida and Nysa, raising the possibility of burning limestone in lime kilns, which makes sense, especially to reduce expenses in large scale constructions. Note that in Nysa mortars, nearly no lumps are present, meaning that hot-lime technology is not a possibility (Hughes and Cuthbert, 2000), and special care must have been given lime production.

The Complutum mortars differ from the others in grain size distribution and aggregate use. Angular to sub-angular sand grains are medium to poorly sorted. Rarely, they include rock fragments of sandstone, and slate. In other archaeological sites, frequently crushed rock fragments were used which gives them a poorly sorted appearance.

The mortars from Nysa show homogeneity in manufacturing. They have similar colours and properties. The clayey appearance of the mortars comes from the argillaceous aggregates containing schist, slate, and gneiss. Different construction periods and/or deterioration may be the reasons for their variety in hydraulicity levels. Uğurlu Sağın (2012) found from tan analysis of their lime lumps that non-hydraulic limes from high calcium limestones were used as binder.

Less elaborateness was found in Labraunda mortars. When the prepared mortar blends had less workability, the builders would have added more lime which resulted in poor mixing and lime inclusions as observed in the microscopic observations of mortars from the East Bath. This might have been related to a lack of experience using an aggregate as absorbent as ceramic. It is known that bricks began to be used in Anatolia in the 2nd c. AD (Ward- Perkins, 1981; Uğurlu Sağın, 2012); however, in Labraunda *opus signinum* mortars dated to the 1st c.

AD refute this argument. Furthermore, there is another contradictory argument about the use of ceramic as an artificial pozzolanic aggregate as Roman building technique that came from Middle East in 1st c. BC (MacDonald, 1965; Akman et al. 1986) since this technology transfer would be less likely if it had not first been used in Turkey. Labraunda should be the best example of this influence. Indeed, in the sanctuary, the higher use of ceramic in the mortars is noteworthy and distinguishes it from other archaeological sites. In other words, in the same type of constructions such as the bottom levels of floors, walls, and renders *opus signinum* mortars were used rather than the *opus caementicium* mortars seen in other sites. This was either done intentionally to make water impermeable layers or by chance, given an abundance of ceramics for some reason.

How do locally available raw materials and environmental conditions impact technological decisions?

Socio-economic aspects in general affect the choices, but the raw materials tend to be gathered from the surroundings (Coutelas, 2011). Our study confirmed this statement since the raw materials were chosen from nearby geological formations. For instance, no extrinsic materials were used to increase pozzolanicity. Our research shows that so-called pozzolans or volcanic rocks are not indispensable, if the necessary mineral balance is obtained; other aggregates can provide pozzolanic properties as well. Argillaceous sands or volcanic origin metamorphic crushed rock fragments including high proportions of feldspar, mica, schist, or slate can provide medium-high pozzolanic effect.

Reaction rims around aggregates and ceramic fragments were detected in the Nysa, Labraunda and Mérida mortars. These rims are calcium silicate hydrate (C-S-H) and calcium aluminium silicate hydrate (C-A-S-H) formations. They are also encountered in *opus caementicium mortars* because of the silicate rich metamorphic rock fragments and fly ash in the binder. Fly ashes were either intentionally introduced or came from the lime kiln. They also create reaction products. However, in the Complutum mortars, reaction rims are rarely

observed; due to selection of mainly washed sand aggregate and the lack of fly ash. Brick was introduced to the first Greeks then the Romans from the Middle East (Akman et al. 1986). This may be why we find more *opus signinum* mortars in the archaeological sites in Turkey.

All of the archaeological sites have close average annual temperature values, but the rainfall is higher in Turkey, and frequent loop of heavy rainfall may prevent the mortars from acquiring auto-healing properties (dissolution-recrystallization). Since high relative humidity inhibits CO_2 penetration, re-precipitation of calcium carbonate after dissolution does not occur. Even if ceramic was used intentionally in the mortars with no water related function due to the high humidity conditions, future deterioration was not considered. Consequently, there is no evidence that Romans thought of long-term environmental conditions; however, long-term environmental conditions should be considered an important factor in the decisions we make about the repair of mortars today.

Do variable construction techniques affect the selection and use of certain raw materials?

Although both *opus caementicium* and *opus signinum* mortars have common aspects in all the archaeological sites, among the mortars in Spain, some mortars contain 1-2 cm brick fragments and *caementa*s, while in Turkey the fragment sizes do not reach 1 cm in mortars. In Spain reputed Roman large mass *opus caementicium* constructions can be found, while in Turkey, this construction practice is missing. Instead, lime mortars were used to bond irregularly shaped rubble stones.

Petrographic studies show that, in all of the mortars, aggregates were collected from the surroundings. Therefore, the use of ceramic was determinant for certain construction techniques. Common knowledge would expect to find ceramic in water bearing constructions, so the different types of mortar according their functions are shown in Table 4.2. It corroborates that ceramic dust was used in coating mortars and fragments in mortars with structural purposes as previous researchers have reported (Matias et al. 2014;

Moropoulou et al. 2005). Although some *opus signinum* mortars are present in the walls of Complutum, Nysa and Labraunda, the majority mortars from the walls are *opus caementicium*. In Complutum and Nysa, unexpectedly some water-related structures have *opus caementicium* mortars, and vice versa, some *opus signinum* mortars were found in the structures without any relation with water. The first phenomenon can be explained with the hydraulic property provided by the use of high silica aggregate, and the latter can be associated with the humid environment and/or coincidence. Under any circumstances, archaeologists should rethink the function of the buildings. All the coating mortars are water tight *opus signinum* mortars.

The pillars of bridge and arches have both opus types in Complutum whereas in Nysa all of the mortars collected from the pillars of bridges are *opus caementicium* mortars. In the arches, *opus signinum* mortars are used in the Bath in Nysa, whereas in Complutum, *opus caementicium* mortars are found. The construction techniques for water transporting channels are different for aqueducts, sewers and tunnels. The first one which we can observe, in Mérida, was constructed elaborately with two levels of mortars, consistent *opus caementicium* mortars in the core and *opus signinum* mortars above it. In the sewers of Complutum, only *opus caementicum* mortars are found. This is consistent with the different use of mortars for waste water transport and clean water supply in Le Vieil-Evreux (Coutelas, 2008). This difference shows that the supply of clean water was considered more important than waste water infrastructure. The tunnel in Nysa was constructed with irregular rubble stones and *opus caementicium* mortars with earth additives. All of the mortars have hydraulic characters with these raw materials. As the clean/waste water assessment mentioned above would suggest, the aqueduct was built more elaborately, than the tunnel, which in turn, was built more elaborately than the sewers. Floors are seen in both types: the temple in Mérida, the road in Nysa and the baths in Complutum have *opus caementicium* mortars, while in Complutum in *Natatio* and *Cuadriporticus* and in all the baths of Labraunda *opus signinum* mortars were used. Furthermore, floors composed of four levels are found in Complutum and Labraunda, in Complutum, the uppermost two levels are *opus signinum*

mortars, while in Labraunda, all the layers are *signinum*. Nevertheless, they are same in construction type since the binder amounts are higher in the bottom levels.

Table 4. 2. Mortar types according to function in the constructions, (OC: *opus caementicium*, OS: *opus signinum*)

	Wall	**Floor**	**Coating**	**Aqueduct-channel**	**Pillar**	**Arch**
Complutum	OCx 4 OS	OCx4 OSx2	OSx4	OCx2	OCx2, OSx2,	OC
Mérida	OCx 4	OC	OS	OCx3 OSx2		
Nysa	OCx 5 OSx1	OC	OS	OCx3*	OCx4	OSx2
Labraunda	OCx5, OSx2	OSx9	-	-	-	

Regarding the building type, both in Nysa and Mérida *opus signinum* mortars are preferred in the core of the wall of amphitheatres, *opus caementicium* mortars in *summa cavea*.

In Nysa, different types of mortars are seen next to the terracotta pipes. In the Agora Road, *opus signinum* mortar was used. On the other hand, in the arch of the Bath, *opus caementicium* mortar was observed. In another Roman site in Turkey, Sagalassos, the same practice was observed, and Degryse et al. (2002) explained that the *opus caementicium* mortar has a load bearing function or was used for placing water pipe. In Ottoman baths, inside the terracotta pipes, lime plaster with linseed oil, cotton and linen additives was used to obtain water impermeability (Tekin and Kurugöl, 2012). If this tradition was inherited by the Romans, the mortar next to terracotta pipe already does not have any water-related function. The reason for using ceramic in the mortar next to terracotta water pipe in the road would be its proximity to the groundwater and rising damp.

Opus caementicium mortars were used in the public buildings, although in the exceptions such as basilica, stadium and gymnasium, *opus signinum* mortars that have hydraulic property were used. Among the water-related constructions, *opus signinum* mortars were utilized in the arch of the Bath as coating mortar in the Agora Road. The mortars of cisterns,

tunnels and bridges are *opus caementicium* mortars. Except for one sample from the pavement of the Agora, the rest of the mortars have hydraulic properties. The use of mortar in tunnel vault construction differs according to level because the lower level mortars must have a hydraulic nature due to their contact with water. The mortars of the west pillar of the second bridge have more hydraulicity than those of the east pillar. Different times of construction and/or deterioration may be the reasons for this difference. Mica and argillaceous aggregates already provide the pozzolanicity of the Roman mortars of Nysa. The use of ceramics may have been intended to improve the mechanical quality and physical functions of the mortars (Ergenç et al. 2016).

Beyond the type of mortar, another distinct aspect seen within the mortars with different functions is the size of aggregates in all of the sites. Mortars used in walls have smaller aggregates and medium sorted distribution. On the other hand, larger size aggregates (*caementas*) are found in the marble coating mortar in Complutum and in the aqueduct San Lazaro in Mérida. Under load, coarse aggregates absorb energy and prevent the formation of shrinkage cracks in the binder (Stefanidou et al. 2015). This mentioned load is generated by water in case of Mérida and by marble in the case of Complutum. Whereas coating mortar with the same function in Nysa does not possess that much large aggregate, this may be explained by a lack of technical knowledge.

What are the states of deterioration and conservation of mortars in buildings at case study sites?

Climate induced environmental factors as well as air pollution affect building materials, and since mortars are more porous than other building materials they are more subject to deterioration. These external decay factors cause microstructural changes (Velosa et al. 2010). Rain water gives rise to lime dissolution with efflorescence and crypto-florescence generating stress after evaporation. Lime mortars have auto-healing properties such as recrystallization in cracks and pores due to the reaction with atmospheric carbon dioxide

(Lubelli, 2011). Generally, the dissolution and re-precipitation of carbonated binder was found in *opus signinum* mortars, which have a higher tendency to exhibit this phenomenon because reactions between the lime and ceramic dust lead more pozzolanic activity products which are dispersed throughout the mortar (Silva et al. 2005). The calcite dissolution phenomenon, which is frequently observed in Labraunda mortars from the Hypostyle and pool building, could be related to rainwater since the sanctuary is exposed to the highest average annual precipitation and lacks conservation.

In the fieldwork and during preparation for the analyses, it was observed that some mortars did not exhibit higher strength, and disintegration happened as well during extraction and cutting. This occurred rarely in the Complutum mortars and most frequently in Nysa and Labraunda mortars. This may be due to their kaolinite and illite content, which improves pozzolanic activity but at the same time, leads to deterioration as well. It should also be noted that Complutum sees the least rainfall.

Considering the porosity and surface hardness values, it can be deduced that state of conservation of the mortars in Turkey are poorer than those of the mortars in Spain. Some of the Labraunda mortars contain significantly low amounts of binder, which can be caused by the lack of recrystallization after dissolution of the lime. Although the Nysa mortars have uniform properties, their porosity and hardness values can be attributed to this.

The Spanish archaeological sites are more exposed to air pollution from traffic, etc. more than the Turkish cases. Mérida, is already the city, itself, the remains are integrated in the actual town. In Complutum, although the remains are fenced off, they are situated next to the city and the main highway. On the contrary, the Turkish sites can be considered more safeguarded. In Nysa, the road passes over the remains through the city, but the density of the traffic is low. Labraunda is situated on top of a mountain, and the remains are allocated far from the road. Surprisingly, gypsum, which can be formed as a consequence of the air pollution, was only found in two mortar samples from Complutum.

At the beginning, some expected results were attributed to the research questions, but after the evaluation of the results, some of them have slightly changed.

If locally available raw materials are similar in both regions, then it is expected that the mortar technology and durability will also be similar. Alternatively, if raw materials vary between the regions, then mortar technology and durability should co-vary accordingly. Variability in raw materials used to produce mortars and building stone also have implications for construction techniques.

This study found that the mortar technology was somehow different in Spain and Turkey in the same periods. Nevertheless, the large scale engineering solutions are still the same. On the other hand, in Labraunda and Nysa, the raw materials are similar; however, micropore rich porosity is higher in Labraunda, which makes the mortars less durable

If mortar raw materials and mortar production methods differ between sites in Spain and Turkey, it is expected that geochemical and petrograpgical analytical methods will document different reaction products of different aggregates. If different pozzolanic additives are used in the mortars, then it is expected to find different C-S-H and C-A-H reaction products.

Geochemical differences are caused by the petrographic and mineralogical properties of the aggregates. Alternatively, homogeneity in geochemical data is an indicator of the petrographic and mineralogical homogeneity. In the Nysa mortars homogeneity stands out. Reaction rims around the aggregates are encountered in the microscopic observations of the mortars from all of the sites, but less so in those from Complutum. Higher amounts of aluminium oxide in the samples with these rims can be an indicator of C-A-S-H (Rogers, 2011) however the hypothesis needs to be confirmed by SEM-EDS analysis.

5 Results of the tests applied on repair mortars

This chapter presents the results of the mineralogical, microstructural, physical, hydric and mechanical analyses in chronological order, 28, 90, 120 and 180 days.

5.1 Results of Microstructural and mineralogical analyses

Results are presented in the following order: microscopic observations, XRD, SEM-EDS.

5.1.1 Optical Microscopy in 28 and 180 days of curing

At 28 days, in M1 mortars poorly sorted rounded to angular shape silicic aggregates were embedded in the dark coloured lime binder. Quartzite and slate is observed lithic fragments apart from quartz sand grains. Binder had dark brown black colour. It is seen that interconnected pores were present between smaller aggregates. M1L had less cracks generating from the connection of pores.

In M2 mortars, ceramic aggregates were embedded in very dark coloured binder. Larger size shrinkage cracks connected to pores around the fragments were higher than the M1. M2C seemed to have fewer cracks compared to other ceramic added mortars at 28 days carbonation. The occasional grey colour of the binder comes from the portlandite (Pecchioni et al. 2014) (Figure 5.1-1).

At 180 days, secondary calcite precipitation around the aggregates and inside the cracks is clearly observed in the samples of both types of LA. In M1L no significant change was recorded whereas especially at M2LA and M2C mortars the filling of the pores and cracks were noted. Papayianni and Stefanidou (2006) state that crack occurring at the binder can be considered as normal when the mortars were cured at low RH environment.

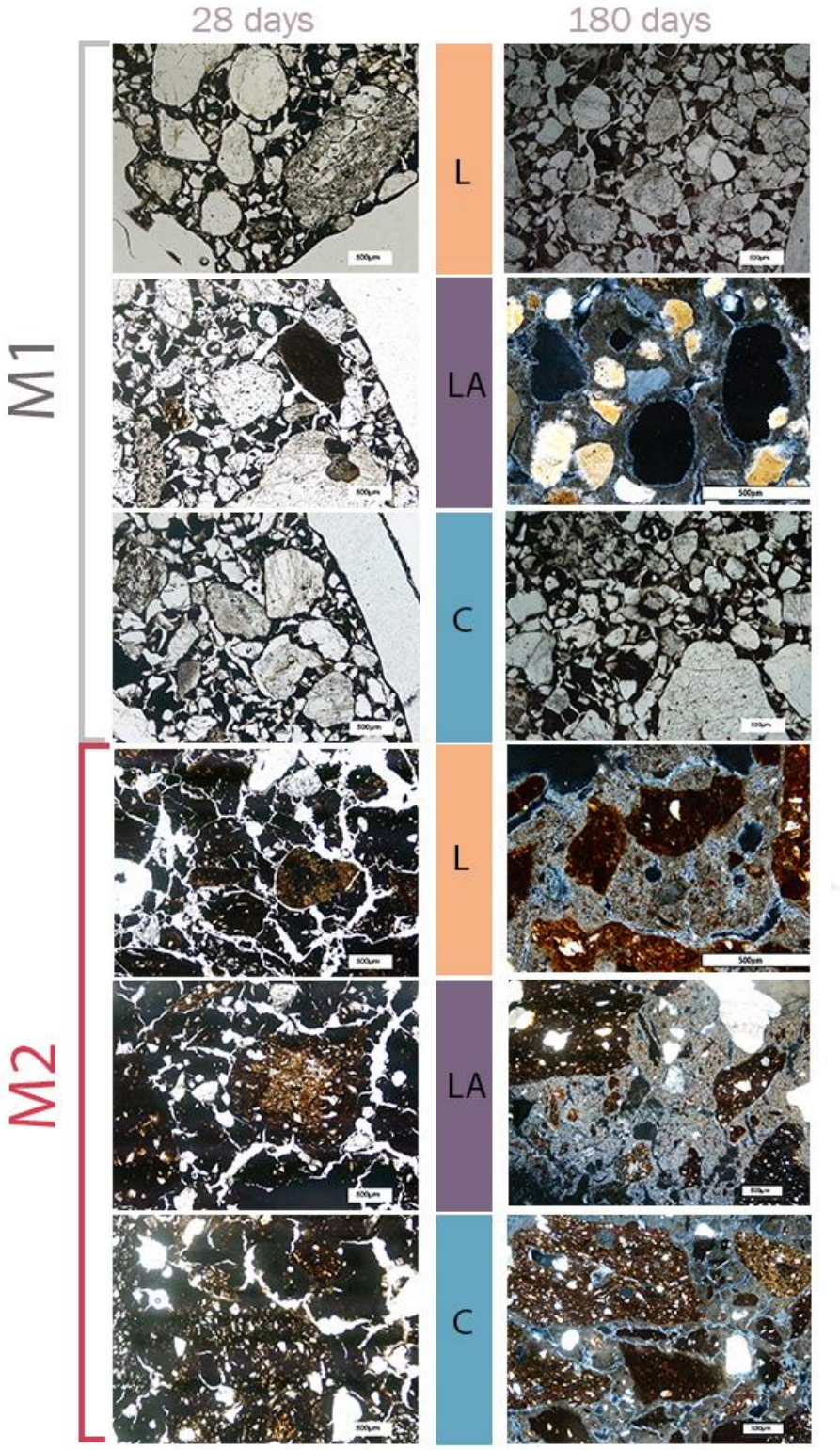


Figure 5.1- 1.Photomicrographs 28 days on the left 180 days on the right in the order, M1L, M1LA, M1C, M2L,M2LA, M2C, (M1LA180, M2L180, M2LA180, M2C180 are under cross polarized light), M1: lime, sand, M2: lime, sand, ceramic, L: Laboratory, LA: Accelerator, C: Chamber

5.1.2 X-Ray Diffraction (XRD) in 28, 90, 120 and 180 days of curing

The main mineralogical constituents in the M1 and M2 mortars were quartz and feldspar coming from the siliceous sand that was used as aggregate, together with portlandite and calcite from the binder[1]. Moreover, mica (biotite, muscovite), hematite, gehlenite and poorly crystalline amorphous phases were detected in the specimens with ceramics (M2)[2]. The main intention of XRD in this process was to observe the amount of decrease in portlandite and increase in calcite peaks' intensities however; the change in calcite was not such remarkable and portlandite was present at 180 days in all of the cured samples.

In fact, the decrease-increase in portlandite-calcite of the specimens was not so detectable in all of the diffractograms. Portlandite peaks indicate that the carbonation reactions did not consume all of the $Ca(OH)_2$. Knowing that the testing period was not enough for fully carbonation this result was expected. Moreover, the drawback of this analysis was that the different intensities in the XRD patterns which may have been caused by the different quantity or the unhomogenity of the sample prevent the quantification of the change in portlandite and calcite peaks. The detection of aragonite becomes more of an issue as it was the metastable polymorph of calcium carbonate.

The highest amount of calcite augment was reached at 180 days in M1 mortars cured at chamber while in M2 version of chamber the decrease of portlandite was more prominent. Also, decrease in portlandite peaks at 120 days was observed better in chamber cured and accelerator sprayed samples. Moreover aragonite was detected[3] in M1LA, M2LA, M1C and M2C at 28 days and laboratory cured samples at 180 days more clearly. Very well marked peak of aragonite at 28 days

[1] D-spacing of quartz, calcite and portlandite are (3.34, 4.26, 1.82 Å), (3.03, 3.85 Å) and (2.63, 4.9, 1.9 Å), respectively.
[2] between 20-35 2θ
[3] D-spacing of aragonite: 3.39, 2.70 Å

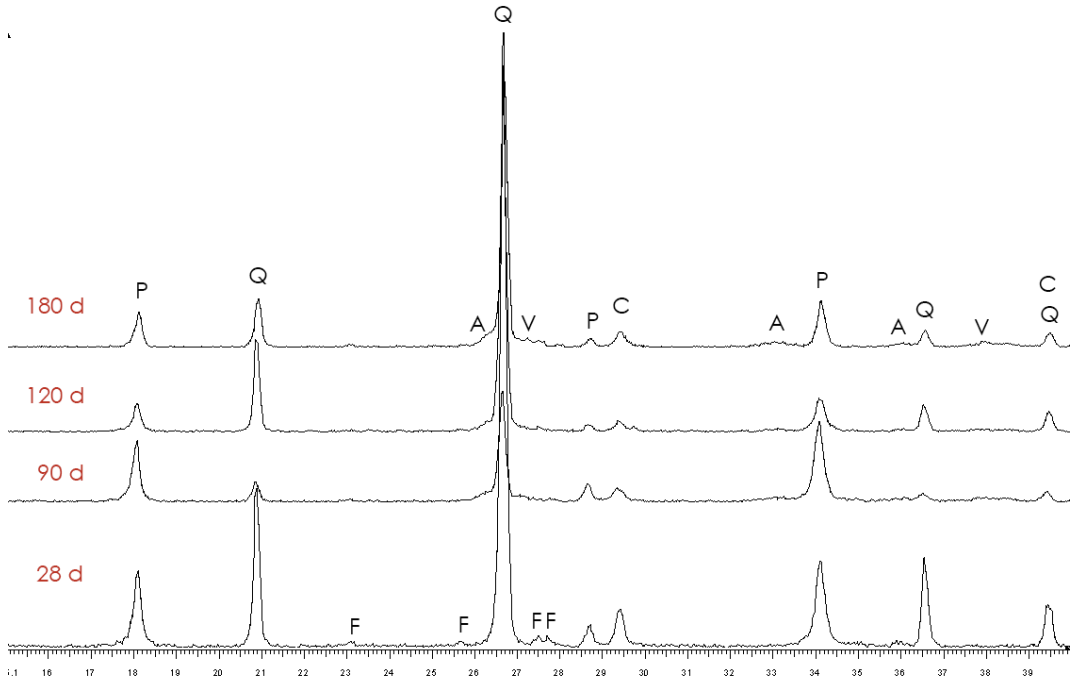


Figure 5.1- 2. XRD patterns of sample M1L during carbonation (P: Portlandite, C: calcite, Q: quartz, F: feldspar, A: aragonite, V. vaterite)

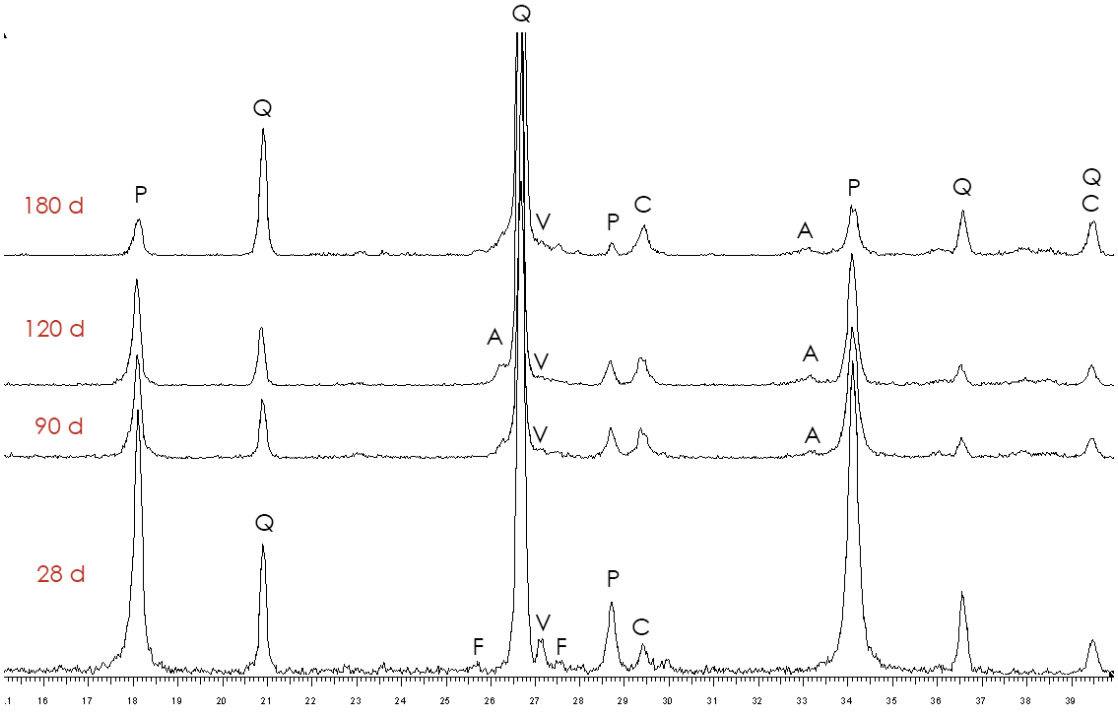


Figure 5.1- 3. XRD patterns of sample M1LA during carbonation (P: Portlandite, C: calcite, Q: quartz, F: feldspar, A: aragonite, V. vaterite)

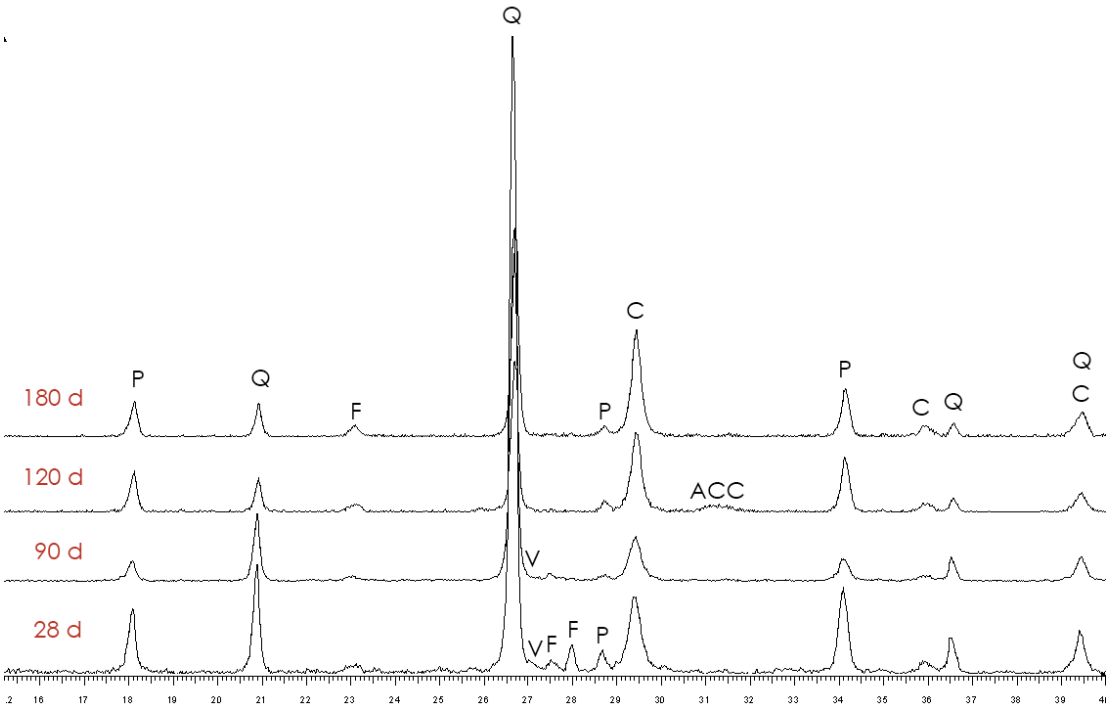


Figure 5.1- 4. XRD patterns of sample M1C during carbonation(P: Portlandite, C: calcite, Q: quartz, F: feldspar, A: aragonite, V. vaterite, ACC: Amorphous calcium carbonate)

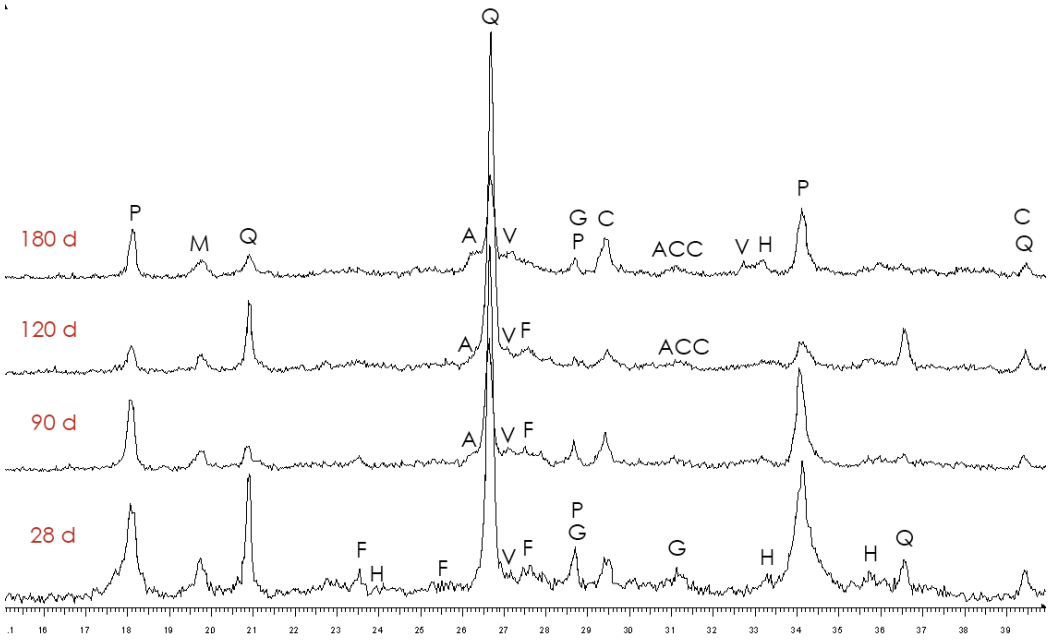


Figure 5.1- 5. XRD patterns of sample M2L during carbonation (P: Portlandite, C: calcite, Q: quartz, F: feldspar, A: aragonite, V. vaterite, ACC: Amorphous calcium carbonate, M: mica, G: gehlenite, H: hematite)

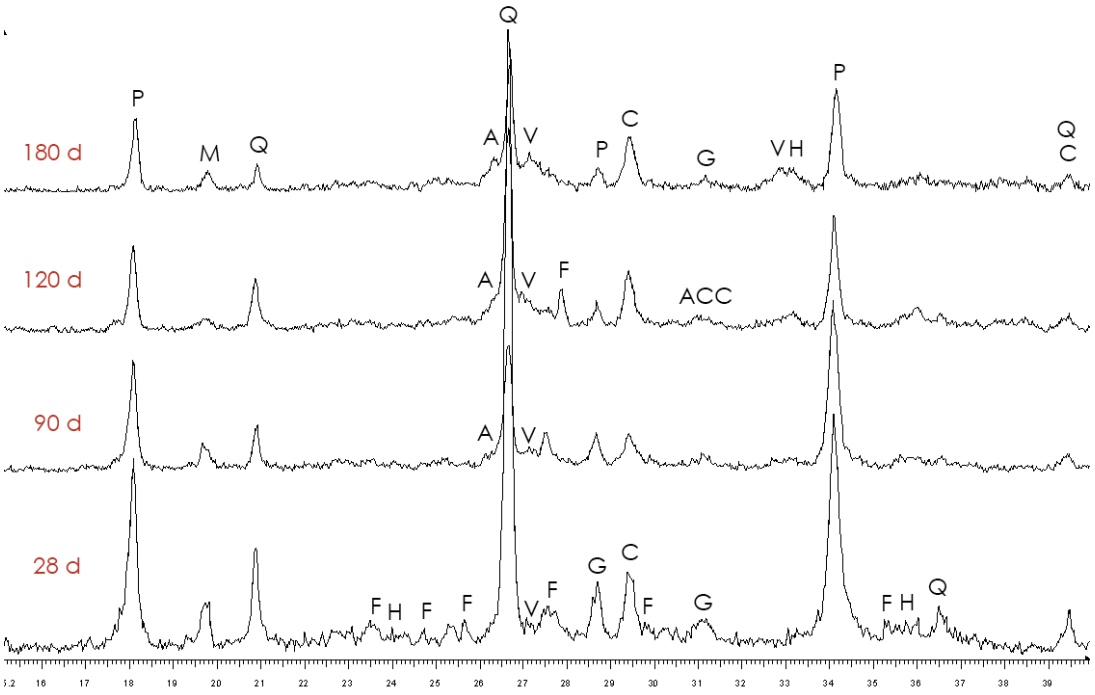


Figure 5.1- 6. XRD patterns of sample M2LA during carbonation (P: Portlandite, C: calcite, Q: quartz, F: feldspar, A: aragonite, V. vaterite, ACC: Amorphous calcium carbonate, M: mica, G: gehlenite, H: hematite)

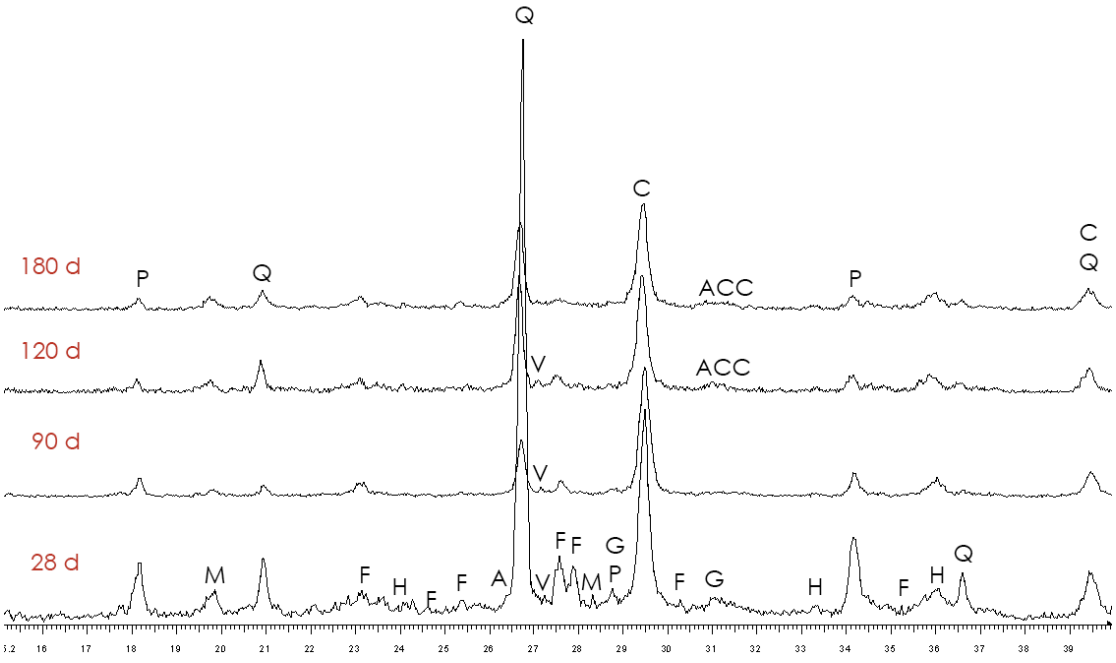


Figure 5.1- 7. XRD patterns of sample M2C during carbonation (P: Portlandite, C: calcite, Q: quartz, F: feldspar, A: aragonite, V. vaterite, ACC: Amorphous calcium carbonate, M: mica, G: gehlenite, H: hematite)

5.1.3 Thermogravimetric Analysis Differential Scanning Calorimetry (TGA-DSC) in 28, 90, 120 and 180 days of curing

Weight losses below 200 ˚C, between 350˚C-500˚C and 500˚C-750˚C from the data gathered from TGA-DSC analysis are listed in Table 5.1- 1. The second weight loss range was associated to $Ca(OH)_2$ dehydration and the weight loss between last temperature range occurs due to the decomposition of $CaCO_3$ so, those aforementioned compounds can be calculated with the formulas: (WL: weight loss, MM: molar mass)

$Ca(OH)_2$ (%) = ($WL_{Ca(OH)2}$ x $MM_{Ca(OH)2}$)/ MM_{H2O} (1)

$CaCO_3$ (%) = (WL_{CO2} x MM_{CaCO3})/ MM_{CO2} (2)

.

Table 5.1- 1. Results of TG-DSC analysis (WL: weight loss)

		<200˚C	WL 350˚C-500˚C	$Ca(OH)_2$ (%)	WL 500˚C-750˚C	$CaCO_3$ (%)
M1L	28	1.38	3.16	12.99	3.37	7.66
	90	2.07	2.39	9.83	6.26	14.23
	120	1.07	1.93	7.93	6.74	15.32
	180	0.55	1.26	5.18	7.23	16.43
M1LA	28	3.14	3.61	14.84	4.10	9.32
	90	1.84	3.14	12.91	5.39	12.25
	120	1.32	2.59	10.65	6.86	15.59
	180	1.58	1.2	4.93	6.98	15.86
M1C	28	1.22	3.1	12.74	7.22	16.41
	90	2.35	2.21	9.09	8.95	20.34
	120	2.11	2.04	8.39	11.31	25.70
	180	0.54	1.96	8.06	12.76	29.00
M2L	28	2.60	3.05	12.54	3.54	8.05
	90	2.19	2.66	10.94	5.66	12.86

	120	2.16	1.32	5.43	6.81	15.48
	180	1.32	1.12	4.60	9.11	20.70
M2LA	28	2.67	3.15	12.95	3.62	8.23
	90	2.19	2.54	10.44	5.97	13.57
	120	1.86	1.75	7.19	8.29	18.84
	180	1.38	1.46	6.00	9.39	21.34
M2C	28	1.76	1.41	5.80	9.28	21.09
	90	1.86	1.12	4.60	9.62	21.86
	120	1.66	0.61	2.51	10.71	24.34
	180	1.00	0.3	1.23	10.89	24.75

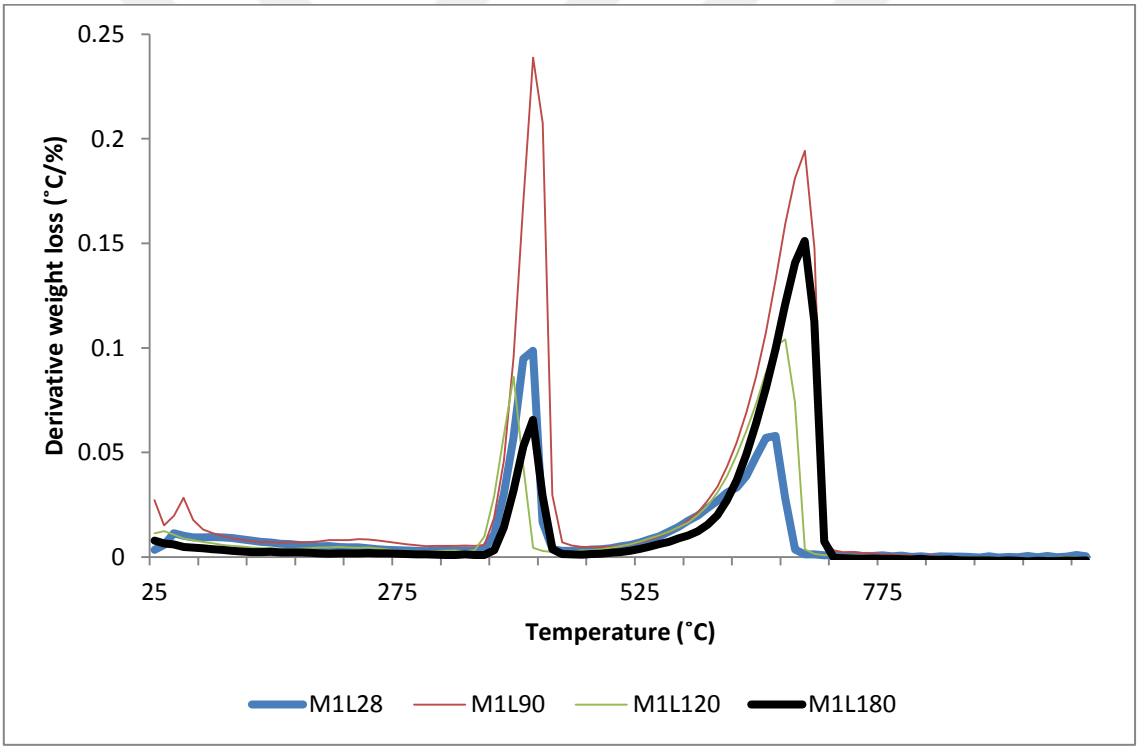


Figure 5.1- 8. Derivative weight loss of the sample M1L in different curing periods

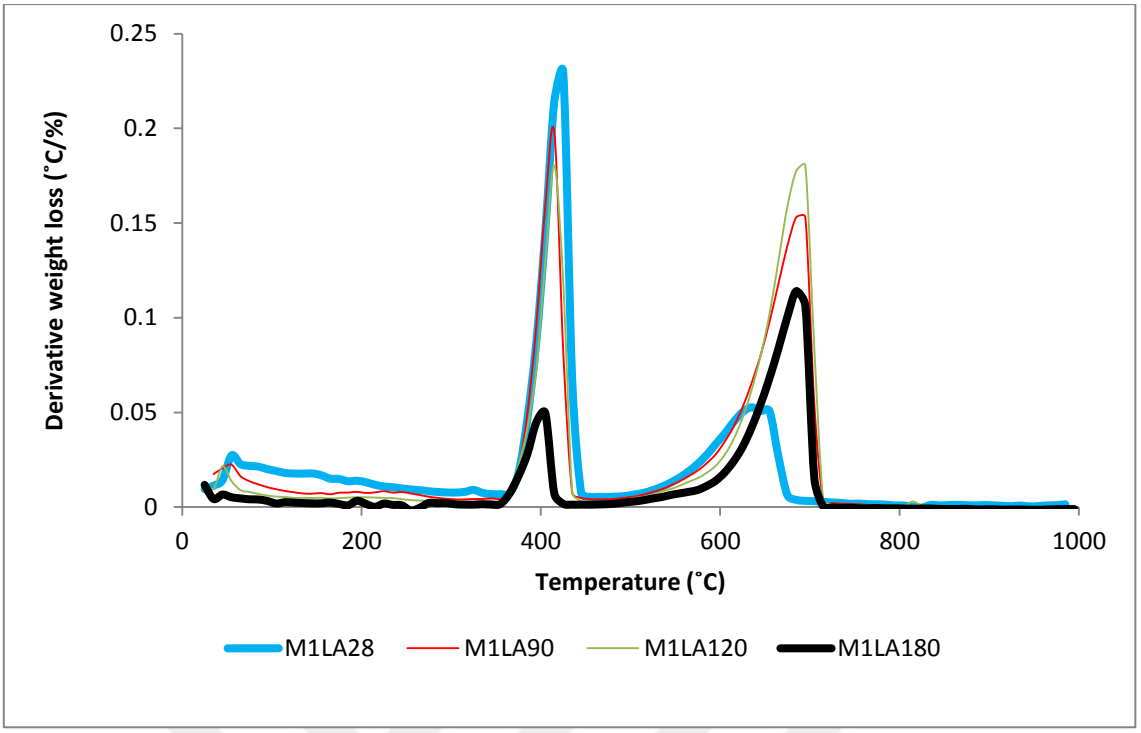


Figure 5.1- 9. Derivative weight loss of the sample M1LA in different curing periods

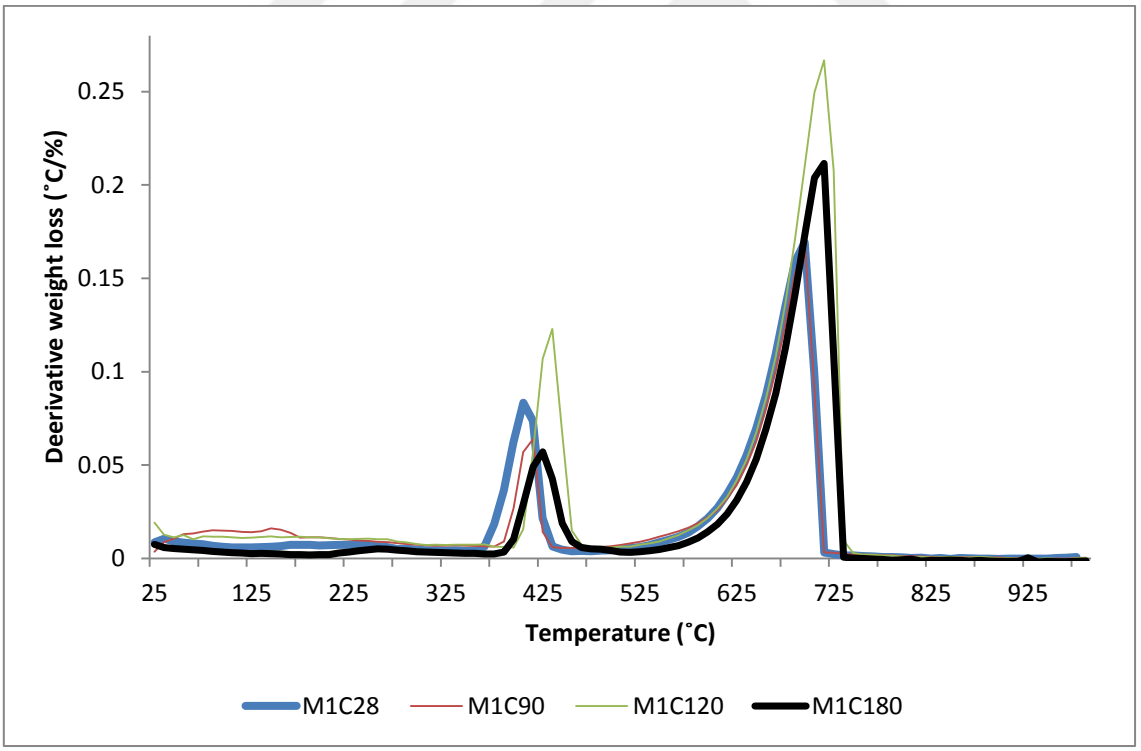


Figure 5.1- 10. Derivative weight loss of the sample M1C in different curing periods

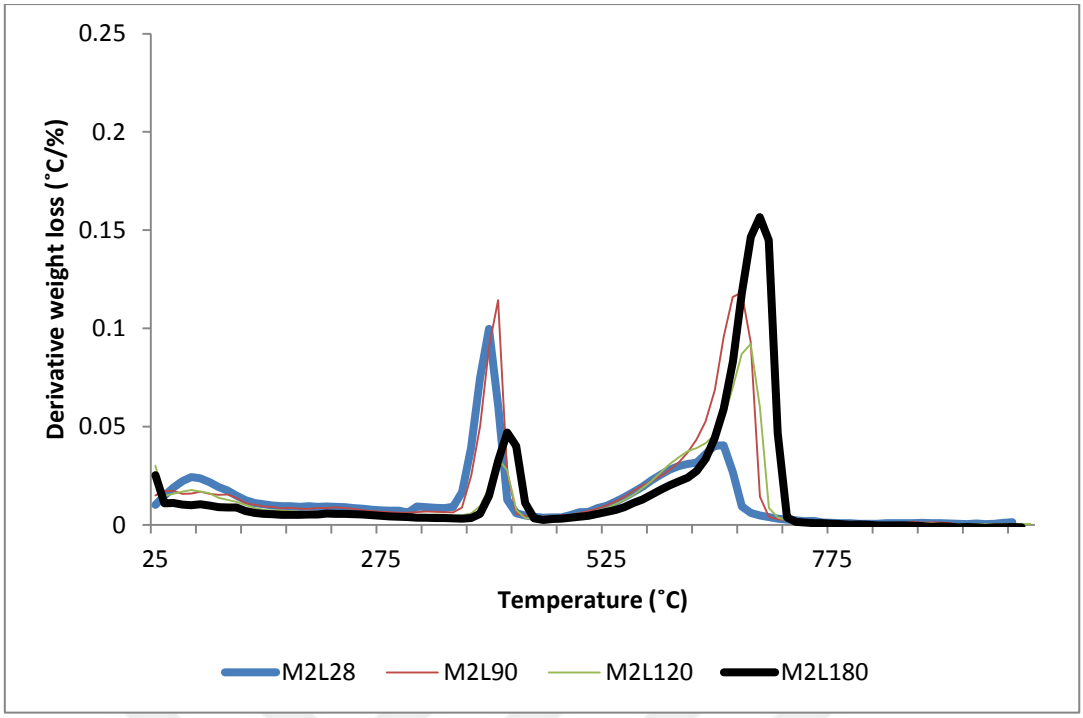


Figure 5.1- 11. Derivative weight loss of the sample M2L in different curing periods

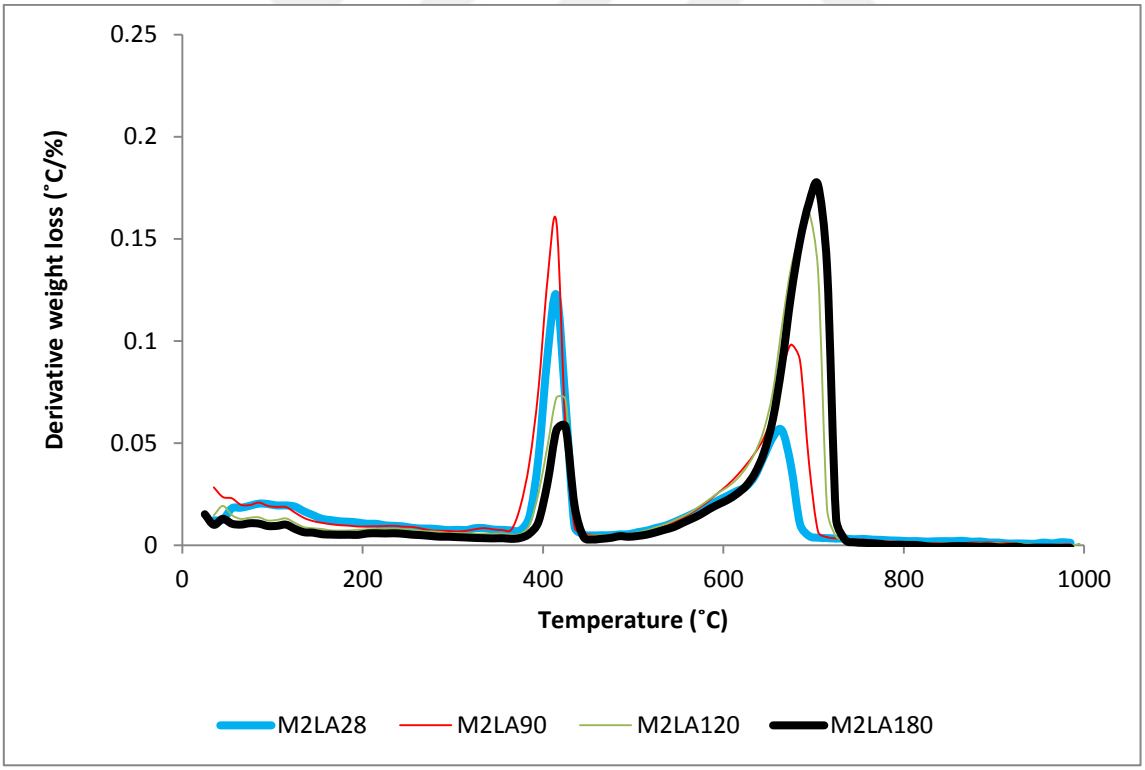


Figure 5.1- 12. Derivative weight loss of the sample M2LA in different curing periods

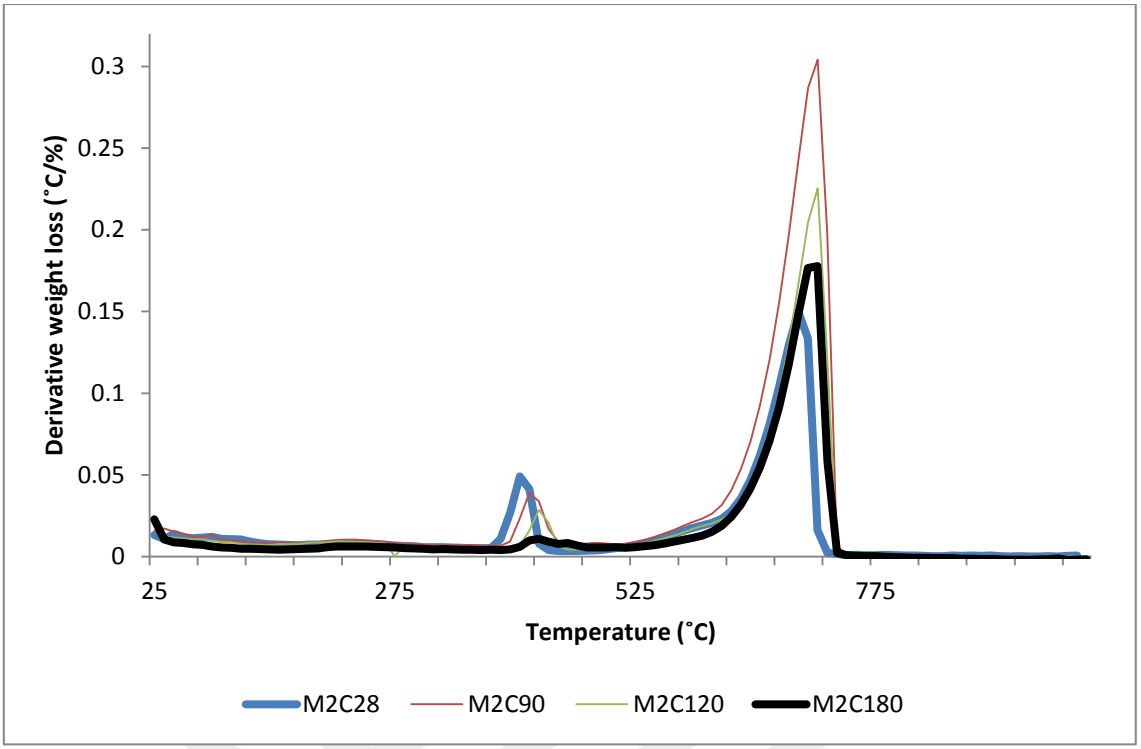


Figure 5.1- 13. Derivative weight loss of the sample M2C in different curing periods

The first and last derivative weight losses of the samples were evaluated because samples show anomalies between 90 and 120 days (Figure 5.1- 8- Figure 5.1- 13). After 180 days decrease in calcium hydroxide and increase in calcium carbonate was well observed. Moreover, in the thermograms the weight losses below 200 ˚C which was associated with the hygroscopic water coming from the ceramics which was higher in M2 mortar than in M1 at 28 days, but was decremented in other ages (Figure 5.1- 11).

TGA analysis was conducted also in the lime putty in order to have the initial parameters. It was revealed that 17.09 % weight loss and 7.44 % weight losses were attributed to portlandite and calcium carbonate, respectively. This means that lime putty consists of 70.86% calcium hydroxide and 16.46% calcium carbonate.

As a one further step, amount of portlandite that was consumed in the carbonation reaction and amount of calcite that was formed after the carbonation can be calculated by the equations 3 4: It is important to note that calcium carbonate content in the ceramics were taken into account as well (0.28% of $CaCO_3$ of 1 unit tile 3 unit brick).

Lime consumed (%) = Free lime (%)-$Ca(OH)_2$ (%) (3)

Calcite formed (%) = $CaCO_3$ (%)-($CaCO_3$ in the mortar + $CaCO_3$ in ceramics) (4)

Table 5.1- 1. Portlandite and calcite amounts during carbonation

	Consumed Portlandite (%)				Formed Calcite (%)			
	28	90	120	180	28	90	120	180
M1L	3.48	6.65	8.54	11.29	3.85	10.42	11.51	12.63
M1LA	1.63	3.56	5.83	11.54	5.51	8.44	11.79	12.06
M1C	3.73	7.39	8.09	8.42	12.60	16.54	21.90	25.19
M2L	0.83	2.43	7.94	8.76	4.68	9.50	12.11	17.34
M2LA	0.41	2.92	6.17	7.36	4.86	10.20	15.48	17.98
M2C	7.57	8.76	10.86	12.13	17.73	18.50	20.98	21.39

As listed in Table 5.1- 2, lime consumption in M1 mortar that was cured at chamber was slightly higher than laboratory cured sample at 28 and 90 days however the calcite formation was remarkably higher than others resulting the highest calcite formation after 6 months of curing.

Portlandite was not consumed so much in M2L and L mortars at early ages while calcite formation was relatively higher. In M2C mortars it was obvious that both the consumption of portlandite and calcite formation was high.

In Figure 5.1- 14 carbonation reaction ratios were presented. As in direct proportion with the results presented in Table 5.1- 2, M2C had the highest carbonation ratio ending at 96% and M1C follows in the earlier periods but end up with 80% like others. Among other samples carbonation begins around 30% and end up at approximately 80% carbonation. M1LA shows steadier carbonation path through 28, 90, 120 and 180 days, the ratio until 90 days of M1L was higher than the rest, and in M2L and M2LA mortars until 120 days the carbonation rate seem higher.

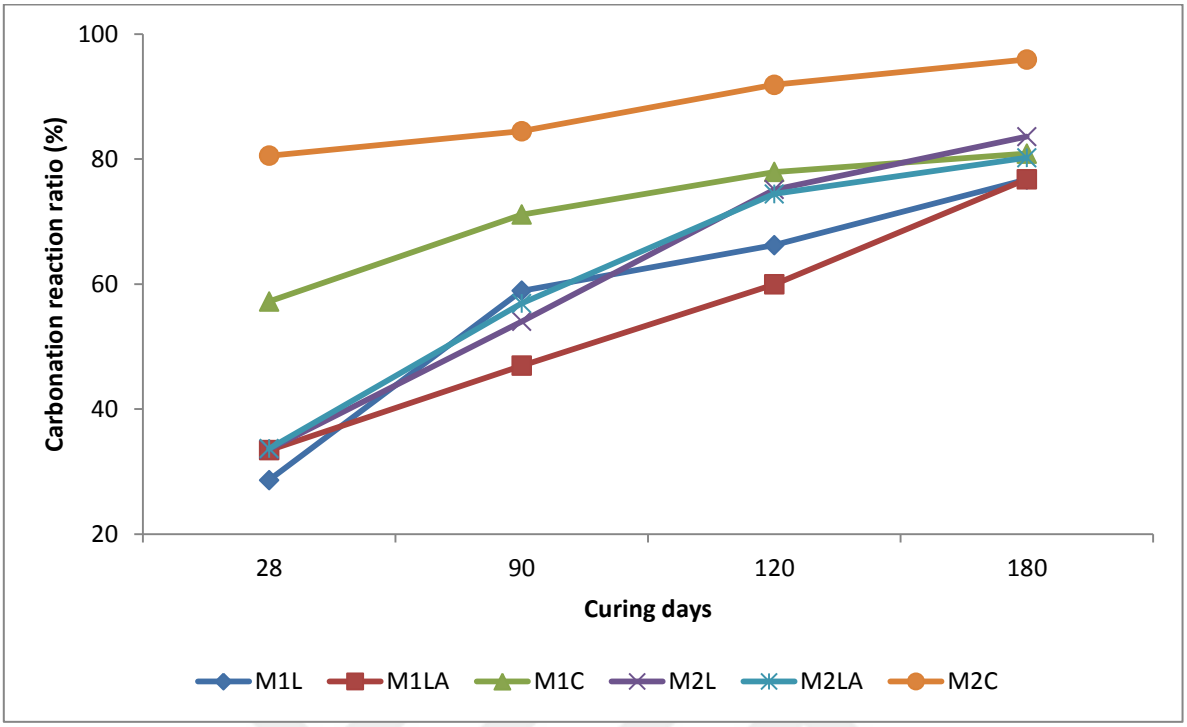


Figure 5.1- 14. Carbonation reaction ratio throughout the ages

5.1.4 Scanning Electron Microscopy (SEM) in 28, 90, 120 and 180 days of curing

It is known that calcium carbonate ($CaCO_3$) had three anhydrous polymorphs (calcite, aragonite, and vaterite) and other hydrous phases (monohydrocalcite and ikaite) and amorphous calcium carbonate (ACC) (Gomez Villaba et al 2012).

SEM analyses of all samples reveal the evolution in microstructure from 28 to 180 days. Bubble to platelet and hexagonal portlandite crystals turn into scalenohedral and then rosette shape calcite crystals in 120 days (Figure 5.1- 17, Figure 5.1- 24, Figure 5.1- 26). Aged lime putties provide smaller plate like shape portlandite crystals and larger surface area thus more water absorption (Rodriguez Navarro et al. 1998; Cazalla et al. 2000).

In the SEM images of the acicular aragonite crystals were present. Although in the beginning they were thought of C-S-H crystals EDS spectra of the stick shape crystal in Figure 5.1- 18 reveals only calcium and oxygen. Temperature, pH, ion concentration and presence of

additives have effect on polymorph type, morphology and size of precipitated calcium carbonate (Jung et al.,2000; Garcia-Carmona et al. 2003; Domingo et al. 2006; Cizer et al. 2008; Gomez-Villaba et al. 2012).

It was seen in the previous studies that different polymorphs of calcium carbonate can be formed; calcite is stable whereas aragonite is the least stable polymorph. Among the metastable $CaCO_3$ polymorphs, low temperature environment favours formation of vaterite, while aragonite is generated in high temperature environment (Martinez Ramirez et al. 2003). In the samples of our study only calcite and aragonite crystals were observed. Remember that in our study the curing temperatures were around 20˚C, therefore the absence of vaterite instead of aragonite was a contradictory to the previous assumptions.

At 28 days M1C mortar had highly amount of 2.5 μm length scalenohedral calcite crystals and place to place nano-size ACC polymorphs. Irregular shape pores exist and bonding between aggregate and binder is poor (Figure 5.1- 15)

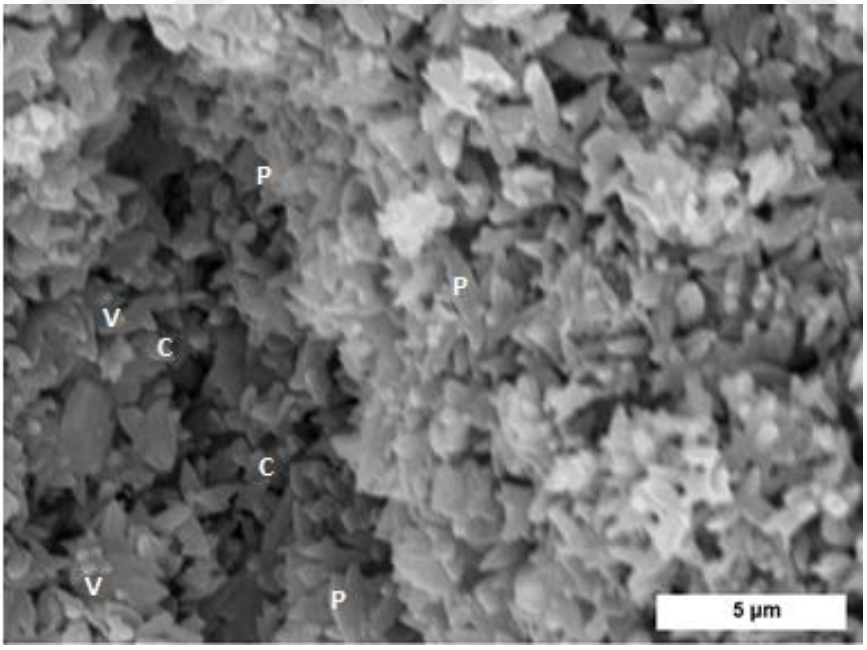


Figure 5.1- 15. SEM image of sample M1C at 28 days (P:portlandite, V: vaterite, C: calcite)

The distance between binder and aggregate was measured as 19.23 μm in M1L mortar which had irregular form or pseudo-hexagonal, scalenohedral and 3.8 μm platelet

portlandite crystals were heaped on top of each other. 3.84 µm and 8.7 µm length acicular aragonite crystals and very small ACC were observed as well.

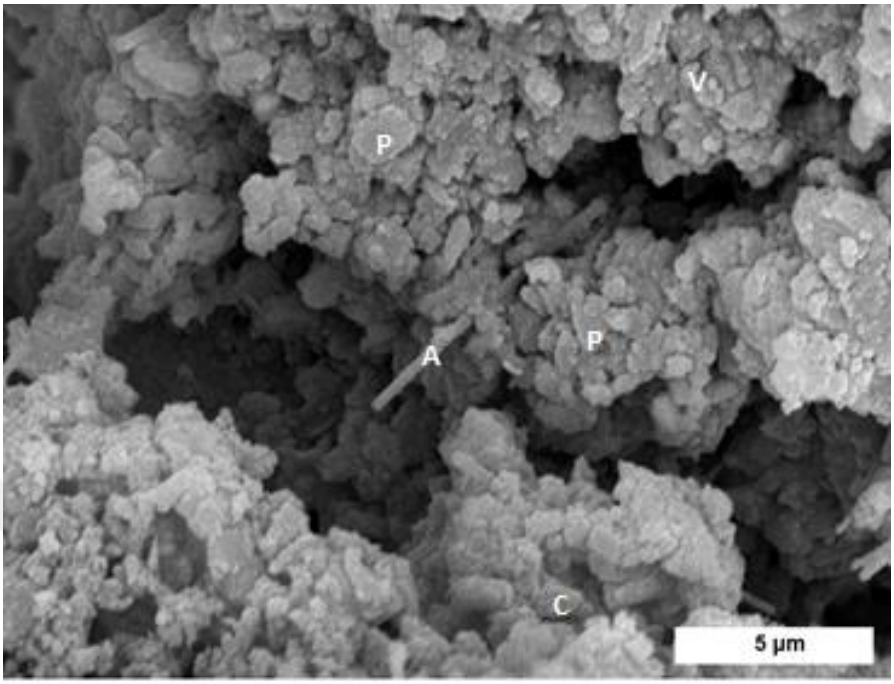


Figure 5.1- 16. SEM image of sample M1L at 28 days (P:portlandite, V: vaterite, A: aragonite)

At 28 days M1LA had 4-5 µm plate like portlandite crystals and bubble shape nano size vaterite, in general binder and 20 µm stick shape aragonite crystals pores were irregular in form.

At 28 days M2L mortar apart from the smaller size ones shows 1.2 nm length aragonite crystals located on top of the quartz grain. Binder was composed of irregular formed plate like portlandite crystals (Figure 5.1- 17).

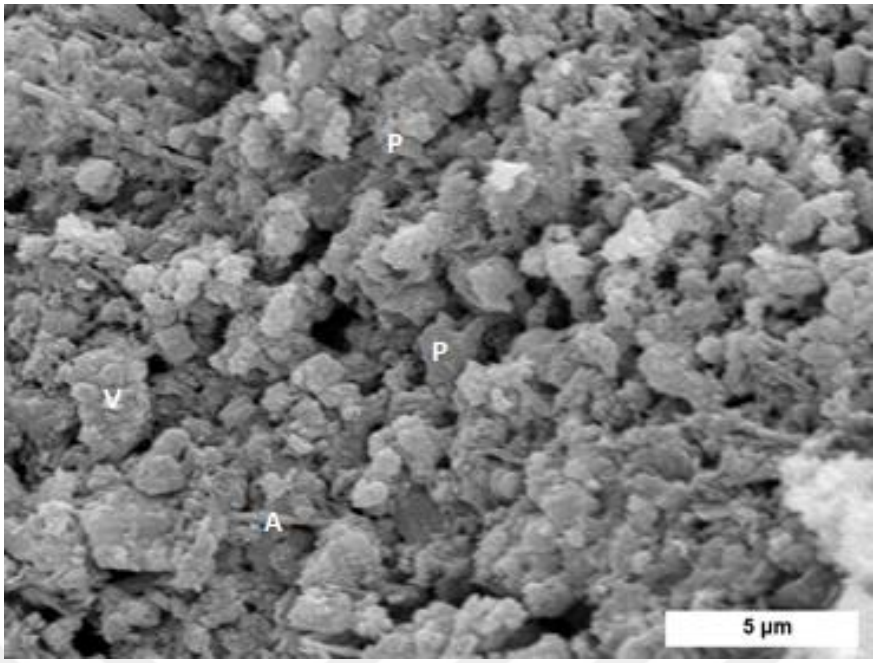


Figure 5.1- 17. SEM image of M2L at 28 days (P:portlandite, V: vaterite, A: aragonite)

In M2LA 7 µm size pores and 16 µm wide cracks were observed. Shapes of the portlandite crystals were plate like until 10 µm aragonite crystals were observed (Figure 5.1- 18).

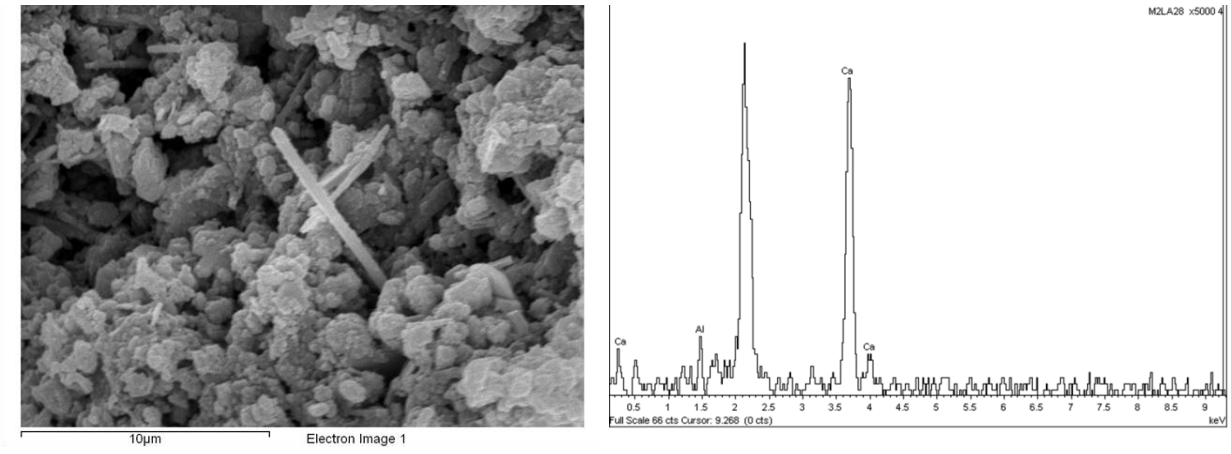


Figure 5.1- 18. SEM image and EDS stick shape crystal in the sample M2LA at 28 days

At 28 days of carbonation in the SEM image of M2C high amount of irregular shape pores observed. Besides, smaller ACC on the platelet portlandite crystals were seen (Figure 5.1- 19).

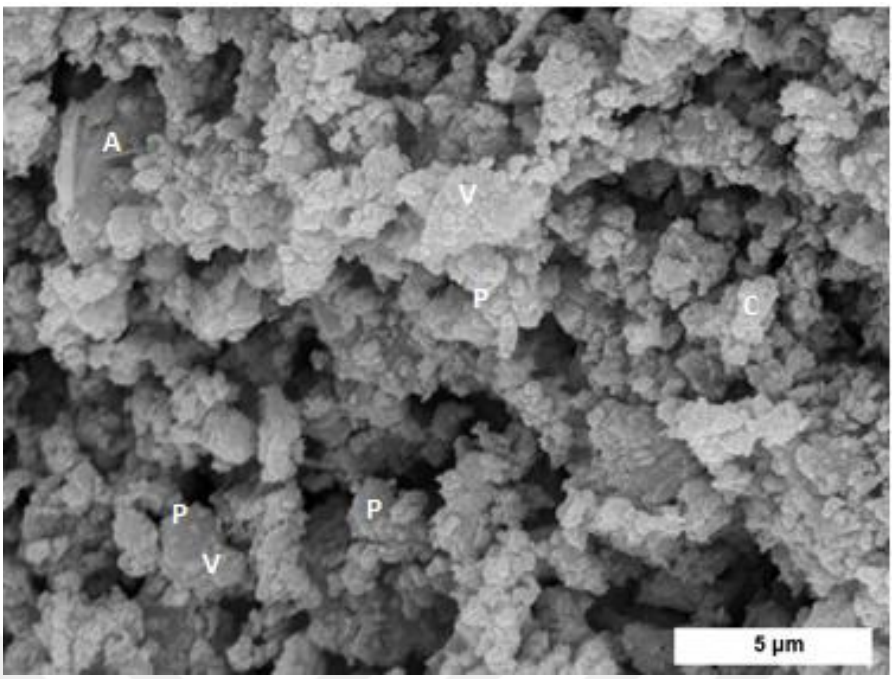


Figure 5.1- 8. SEM image of sample M2C at 28 days (P:portlandite, V: vaterite, A: aragonite, C: calcite)

At 90 days scalenohedral calcite crystals keep abundance at sample M1C with slightly higher sizes and 5 µm aragonite acicular crystals (Figure 5.1- 20).

As seen in Figure 5.1- 21 10 µm acicular aragonite crystals were situated above the ACC polymorphs and platelet portlandite crystals. Those rounded polymorphs were precursors of crystal form of scalenohedral shape calcite crystals. pores were seen in 6 µm length.

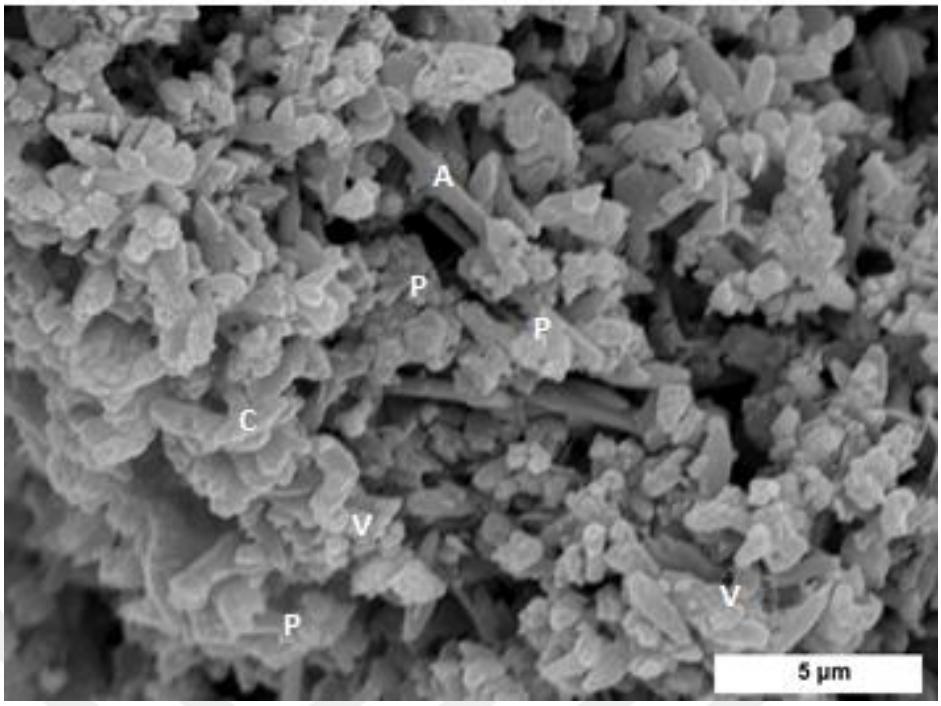


Figure 5.1- 20. SEM image of sample M1C at 90 days (P:portlandite, V: vaterite, A: aragonite, C: calcite)

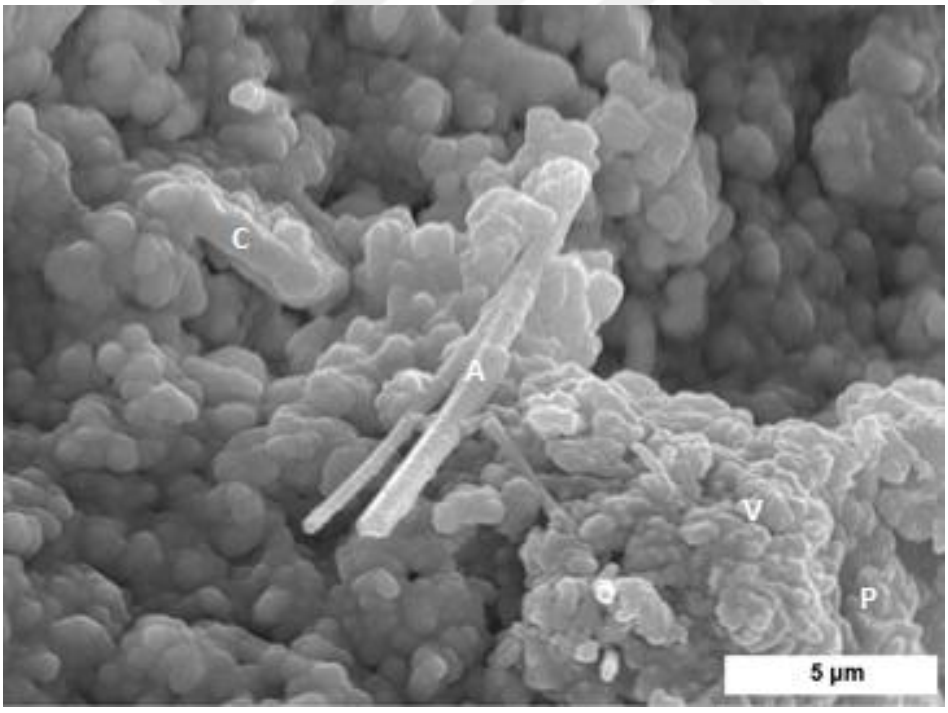


Figure 5.1- 21. SEM image of M1LA at 90 days (P:portlandite, V: vaterite, A: aragonite, C: calcite)

In sample M2C crystals lose their shape a little bit that scalenohedral like irregular form calcite crystals were abundant smaller size stick shape aragonite crystals were present as well (Figure 5.1- 22).

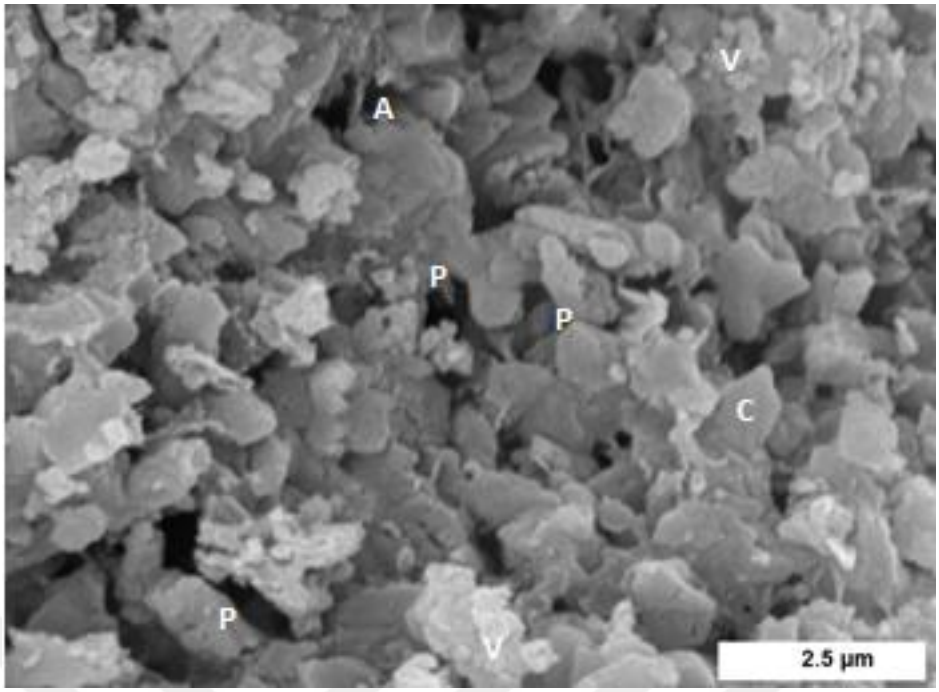


Figure 5.1- 22. SEM image of sample M2C at 90 days (P: portlandite, V: vaterite, A: aragonite, C: calcite)

M2L had various size aragonite crystals together with corroded scalenohedral calcite crystals. Pseudo rhombohedral shape calcite crystal was observed too next to the plate like portlandite crystals (Figure 5.1- 23).

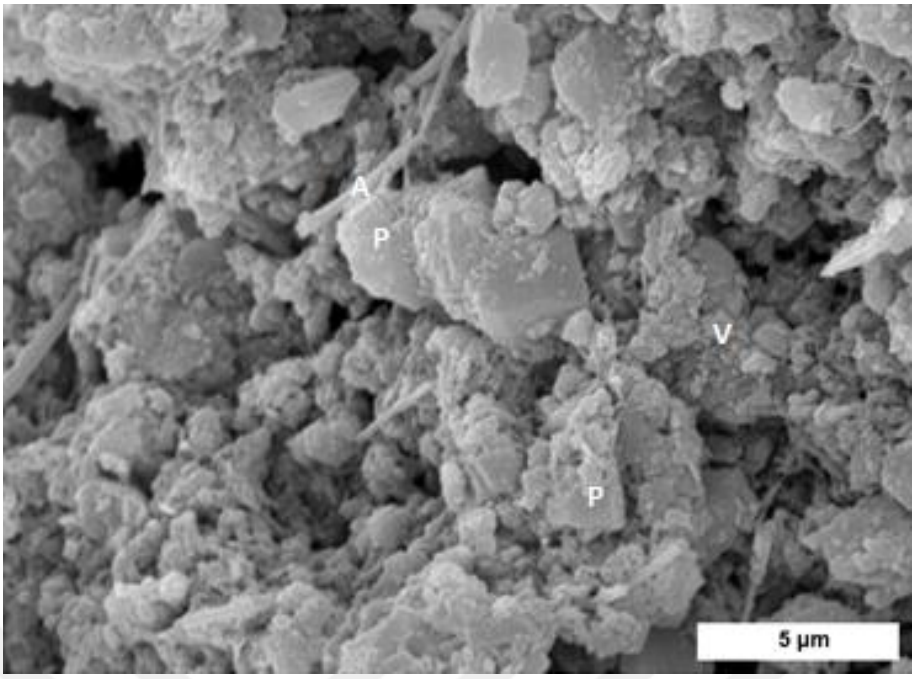


Figure 5.1- 23. SEM image of sample M2L at 90 days (P:portlandite, V: vaterite, A: aragonite)

At 120 days it was seen that scalenohedral calcite crystals in M1C lose their well-defined shapes, aragonites and portlandites still exist and on the other hand porosity seems decreasing (Figure 5.1- 24).

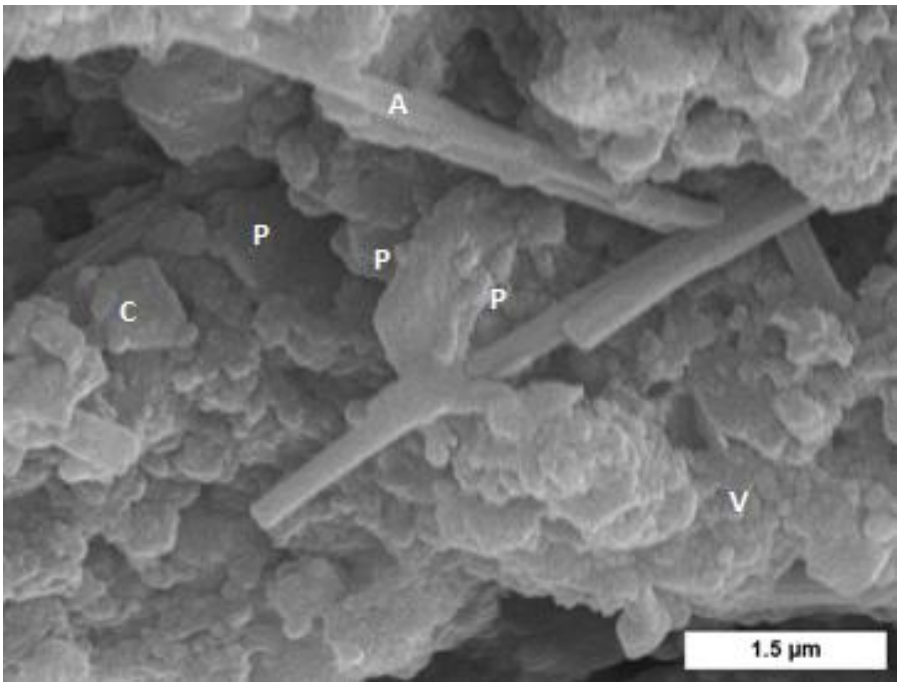


Figure 5.1- 24. SEM image of M1C at 120 days (P:portlandite, V: vaterite, A: aragonite, C: calcite)

At 120 days corroded scalenohedral calcite crystals appear with abundance in M1L and M1LA.

Sample M2C at 120 days show large amount of short thick stick shape aragonite crystals which were placed next to each other were observed 1.3 mm far from surface of the sample (Figure 5.1- 25). Scalenohedral and pseudo hexagonal calcite crystals and platelet portlandites with small size ACC were present as well.

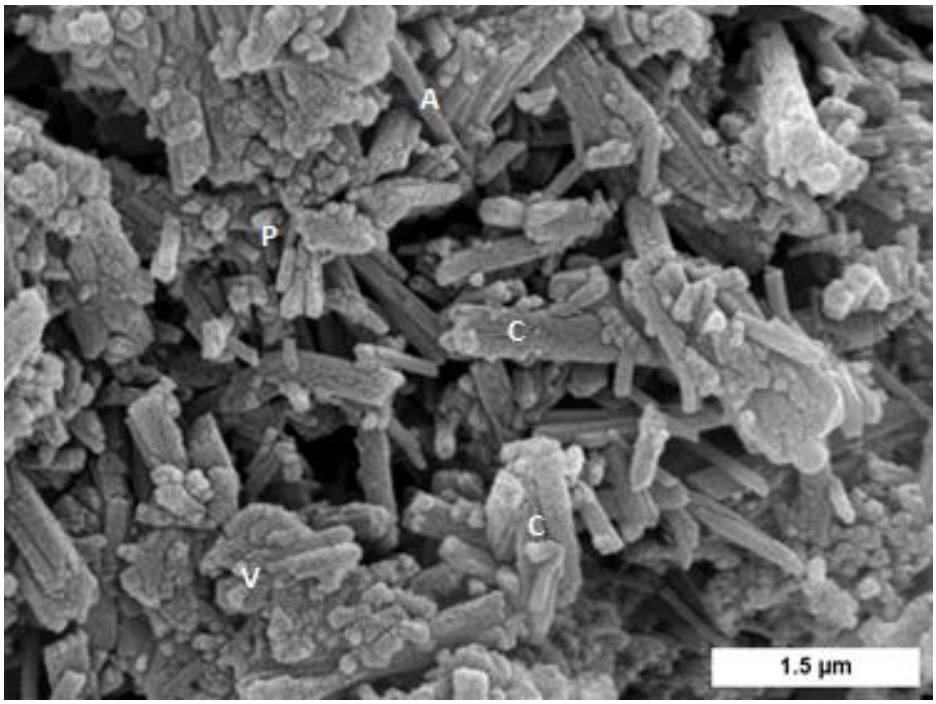


Figure 5.1- 25. SEM image of sample M2C at 120 days (P:portlandite, V: vaterite, A: aragonite, C: calcite)

Crystal morphology of M2L changes at 120 days, 2.72 mm inside of the sample seems to be composed of scalenohedral and hexagonal calcite crystals which were accumulating and forming rosette shape crystals and large number of acicular aragonite crystals (Figure 5.1- 26Figure 5.1- 26).

Similarly M2LA had mostly scalenohedral calcite crystals with more rounded morphology compared to specimen M2L. It should be ACC transformation into calcite and seems like rosette shape calcite crystals were close to be formed.

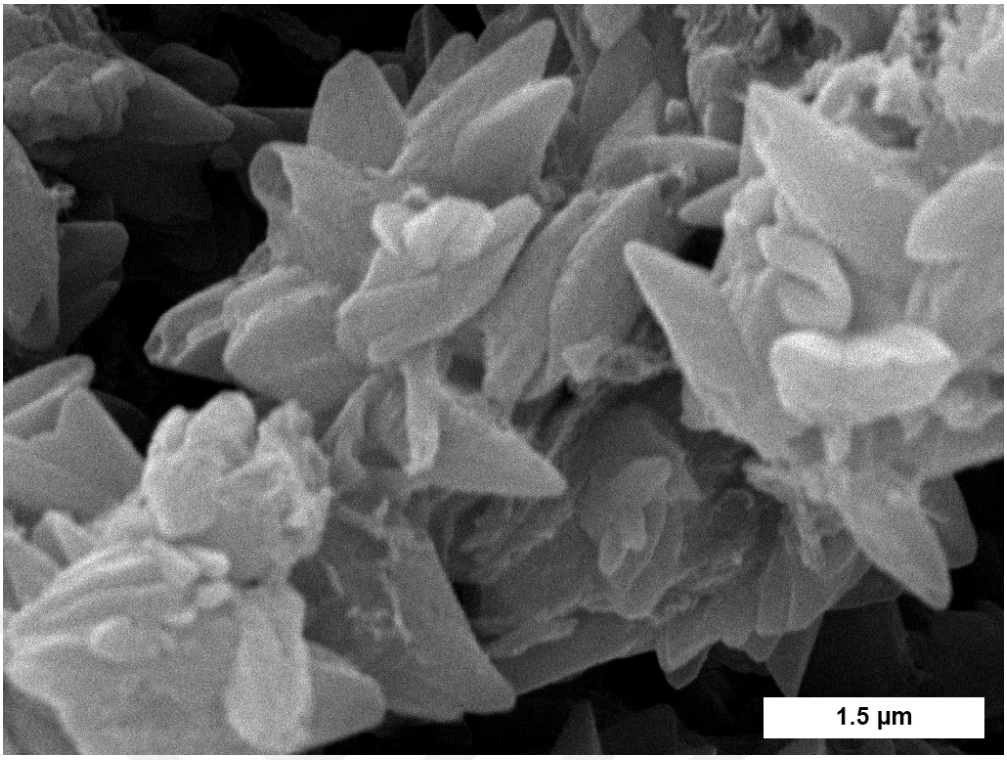


Figure 5.1- 26. SEM image of M2L at 120 days

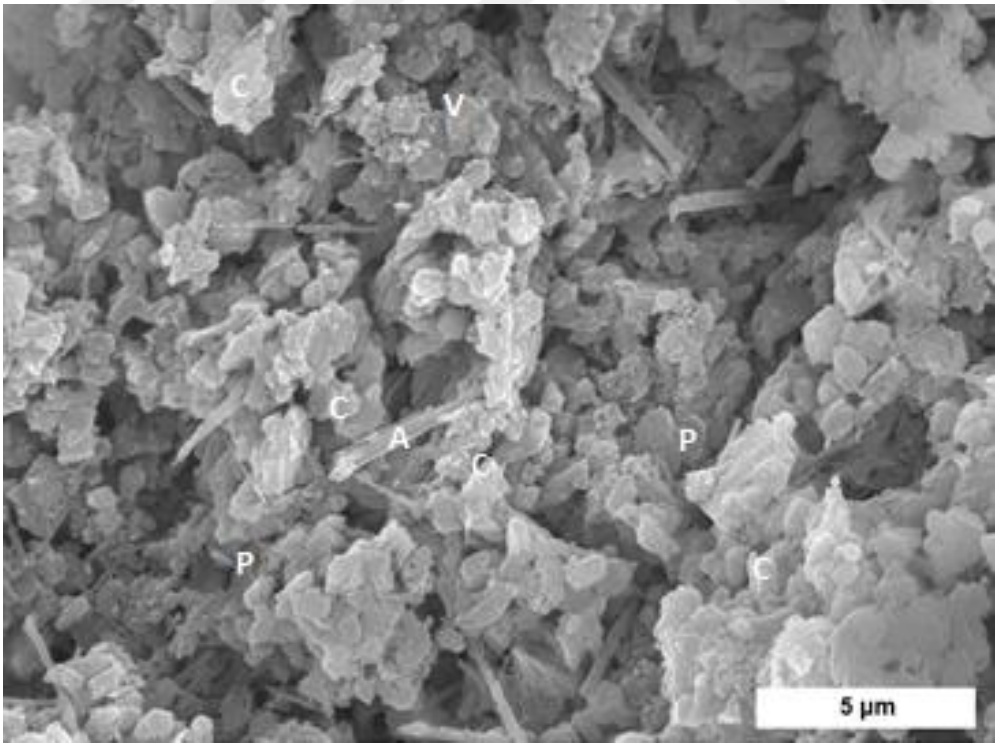


Figure 5.1- 27. SEM image of M1L at 180 days (P:portlandite, V: vaterite, A: aragonite, C: calcite)

At 180 days at deeper zones (3.08mm) of the mortar M1L hexagonal and scalenohedral calcite crystals together with acicular aragonite crsytals were observed (Figure 5.1- 27).

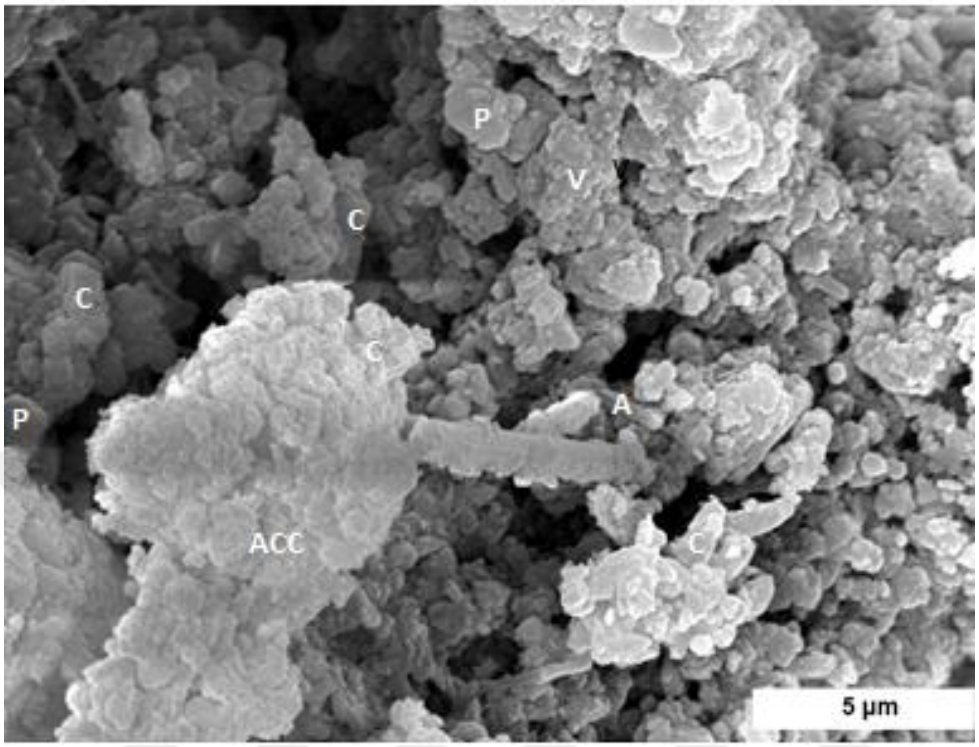


Figure 5.1- 28. SEM image of M1LA at 180 days (P:portlandite, V: vaterite, A: aragonite, C: calcite)

It is seen that at 180 days bubble shape ACC of previous ages turn into more irregular shape scalenohedral-like calcite crystals. Crystal heaping on each other was seen. Pores still exist approximately 4 µm in size.

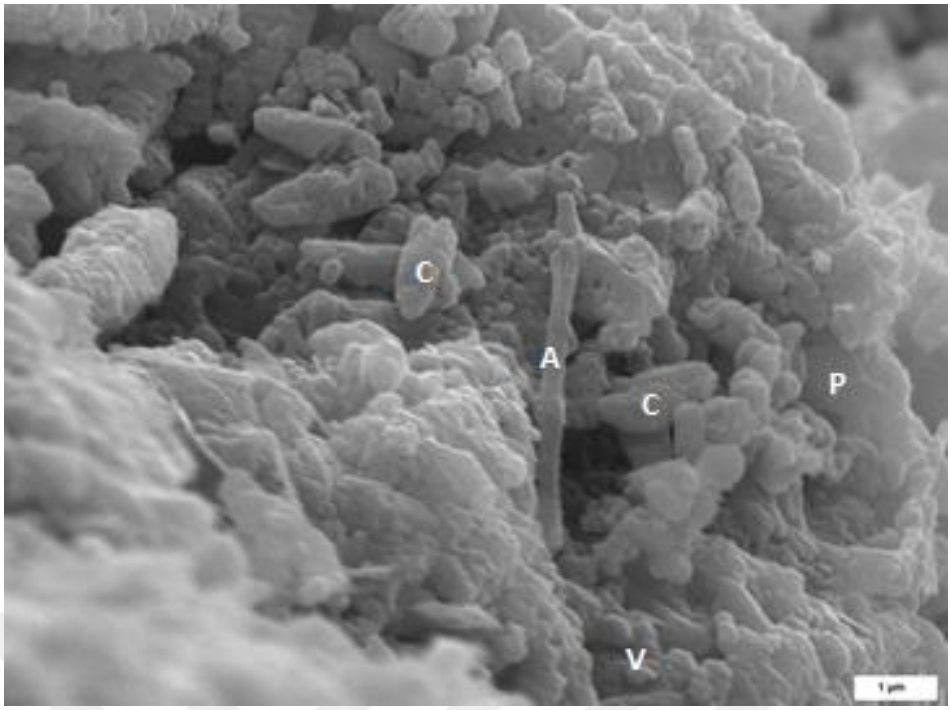


Figure 5.1- 29. SEM image of sample M1C at 180 days (P:portlandite, V: vaterite, A: aragonite, C: calcite)

At 180 days M2C had at 4 mm deep abundances of approximately 5 μm length aragonite crystals and rosette shape calcite crystals (Figure 5.1- 30).

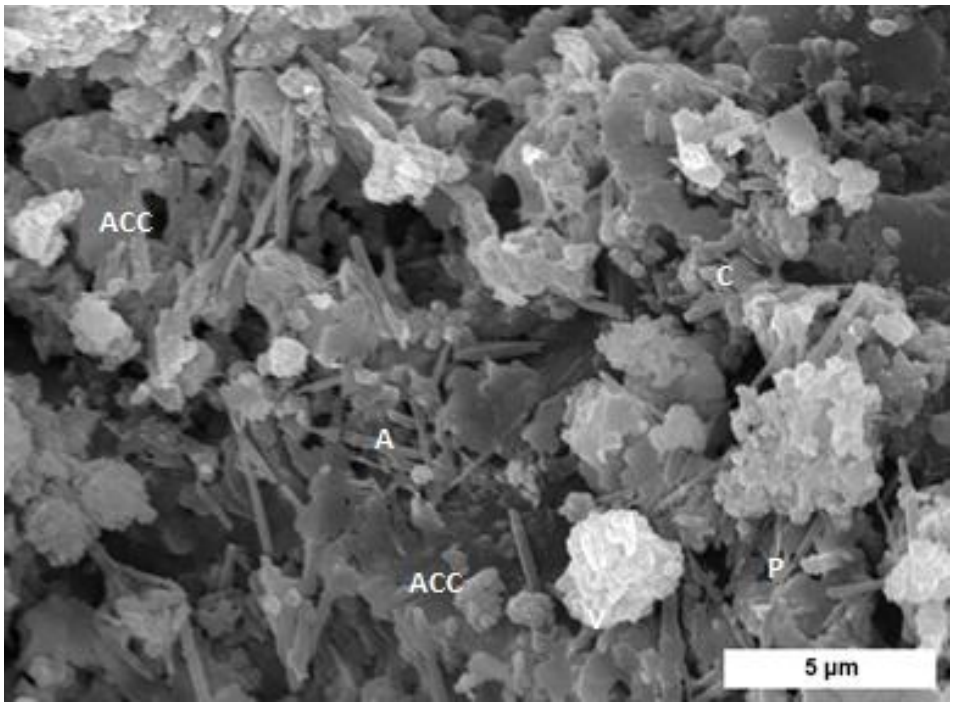


Figure 5.1- 30. SEM image of the sample M2C at 180 days (P:portlandite, V: vaterite, A: aragonite, C: calcite, ACC: amorphous calcium carbonate)

Likewise 4 mm from surface M2L had aragonite and irregular morphology calcite crystals. Decrease in amount of pores was discernible whose sizes were 1.5 μm approximately (Figure 5.1- 31).

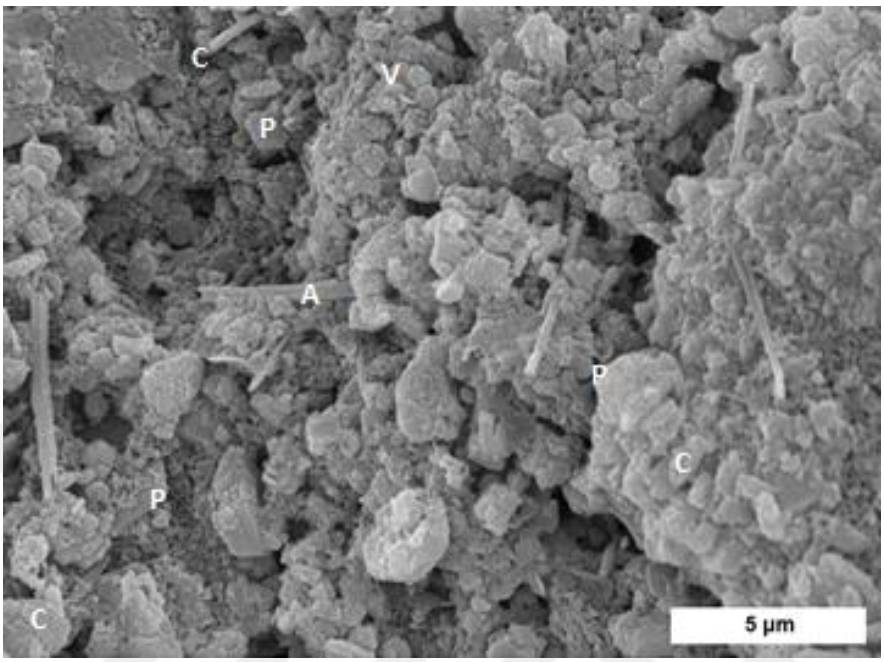


Figure 5.1- 31. SEM image of M2L at 180 days (P:portlandite, V: vaterite, A: aragonite, C: calcite)

The lower humidity during curing of samples causes not very well defined crystal morphologies (Nezerka et al., 2014). Research of Çizer et al. (2008) state that scalenohedral crystals transform into rhombohedral shape calcite crystals when exposed to high CO_2. However, the mentioned CO_2 exposure and relative humidity was higher. Acceleator leads formation of more rounded crystal shapes which changes at 180 days.

5.1.5 Raman Spectroscopy in 90, 120 and 180 days of curing

The slowest carbonation seems to be in M1L sample. Peaks of portlandite (285,9, 361.6 400.5) were seen more densely at M1L sample 90 days. Furthermore, except M1L specimen in the other mortars show Ca-O bonding peak (200-400) and peak due to Ca-Si bonding at sample M2L was detected (Domingo et al. 2006). Quartz peaks were seen in all of the samples except M2LA (Table 5.1- 3). Other strength signals from other constituents should have

hindered. Hematite from ceramics were expected in M2 mortars to support the XRD analysis however its peaks (227, 294, 411, 502, 614) (Iordanidis and Garcia-Guinea, 2013) could not be detected. .

Table 5.1- 3. Raman peaks at different periods

	90 days	120 days	180 days
M1L	467.7 – 1085.6 – 1380.1 – 285.9 – 361.6 – 400.5 – 465.9 – 639.8 – 1085.7 – 1380.2	1085.6 – 1085.7 - 463.9 – 465.9 – 1208.4 – 1302.5- 1380.2	360.6 – 1085.6 1085.7– 463.9 -465.9 – 601.6
M1LA	1085 - 465	353.4 – 465.9 1085.7 – 1284.1 – 1380.2	465.9 – 283.9 – 901.6 – 1085.7 – 1380.1
M1C	461.6 –463.9 - 1083.6 – 1087.7	1083,6 – 1118.4 – 705.2 – 463.9 – 279.3 – 1380.2 – 1085.7	1085.6 –1085.7 - 465.9 – 279.8 -1380.2 – 463.9
M2L	988.8 – 1085.6 – 1316.2 – 1380.1 – 434.5 – 280.3 – 508.9 – 634.6 – 1085.6 -852.9 – 1118.5 – 1293.6 – 1363.6	1085.7 – 1118.5 – 1291.5 – 1085.6 – 461.9	1085.6 1087.6–1380.1 – 1281.2
M2LA	1085 – 1083.5 – 1394.5 – 1540 – 284.4 – 712.8 – 1085.6 – 1380.1	1087.6 – 1087.6 – 1536.6 – 686 – 259.3	1087.6 – 1085.6 – 1380 – 1118.5 – 1291.5
M2C	1083 – 1380 – 278 – 709 – 461.6	1085.7	1083.5 – 1085.6 – 513 - 714

5.1.6 Phenolphthalein spray test in 28, 90, 120 and 180 days of curing

Phenolphthalein sprayed samples show no significant change except chamber-cured samples. At 28 days, M1C had dark pink circle 14mm from outside and whitish pinkish colour the rest and M2C had this darker zone larger, rounded edge square shape and 9mm from outside (Figure 5.1- 32). In the following ages, the different colour cores cannot be observed however the lightening of colour were observed in both M1 M2 chamber cured samples (Figure 5.1- 33- Figure 5.1- 35). In the other curing conditions the colour change is clearer after 120 days.

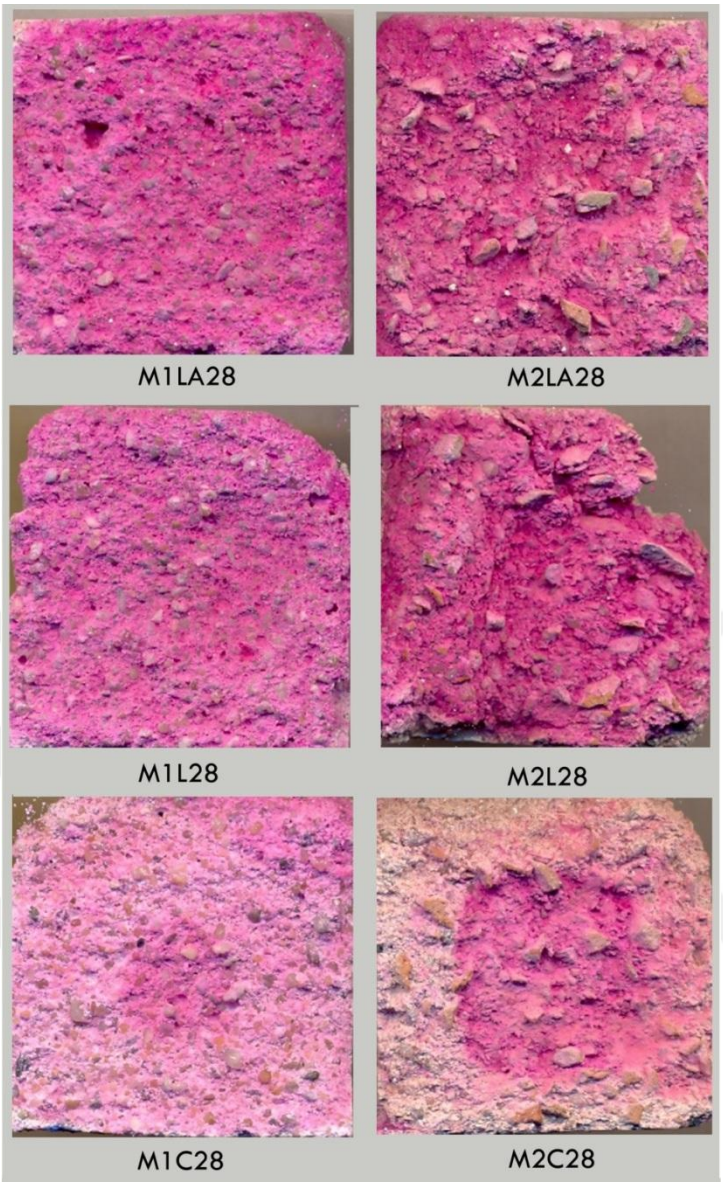


Figure 5.1- 32. Phenolphthalein sprayed samples after 28 days of curing

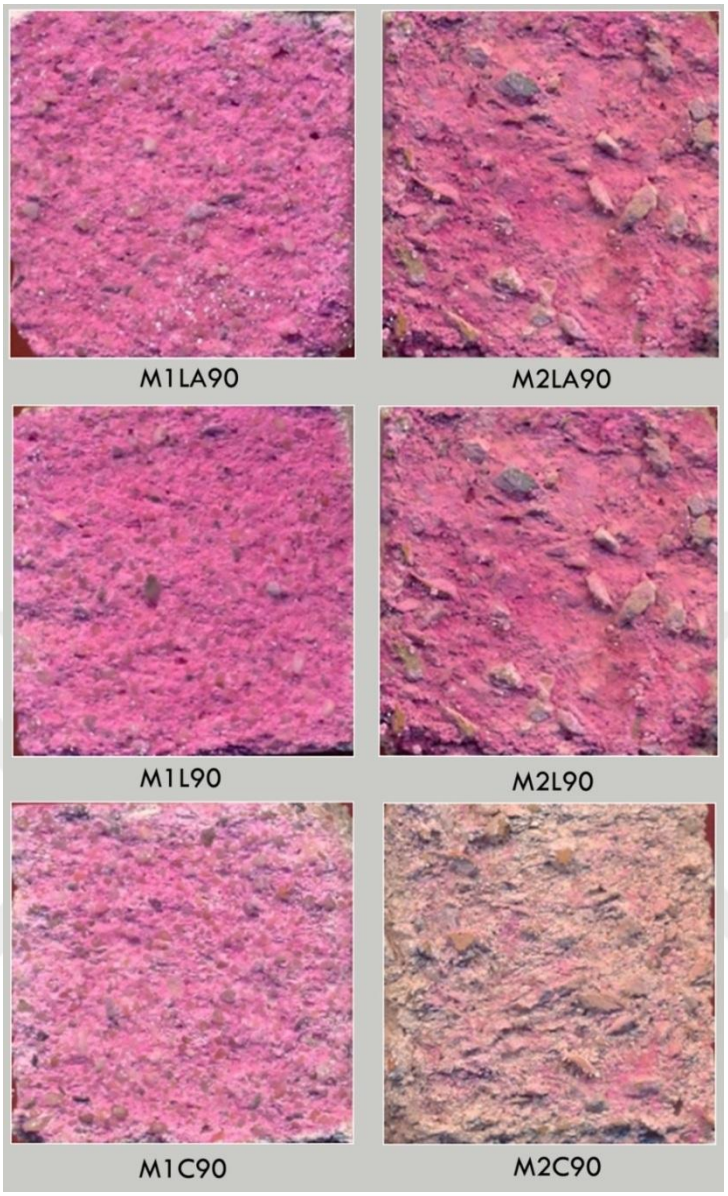


Figure 5.1- 33. Phenolphthalein sprayed samples after 90 days of curing

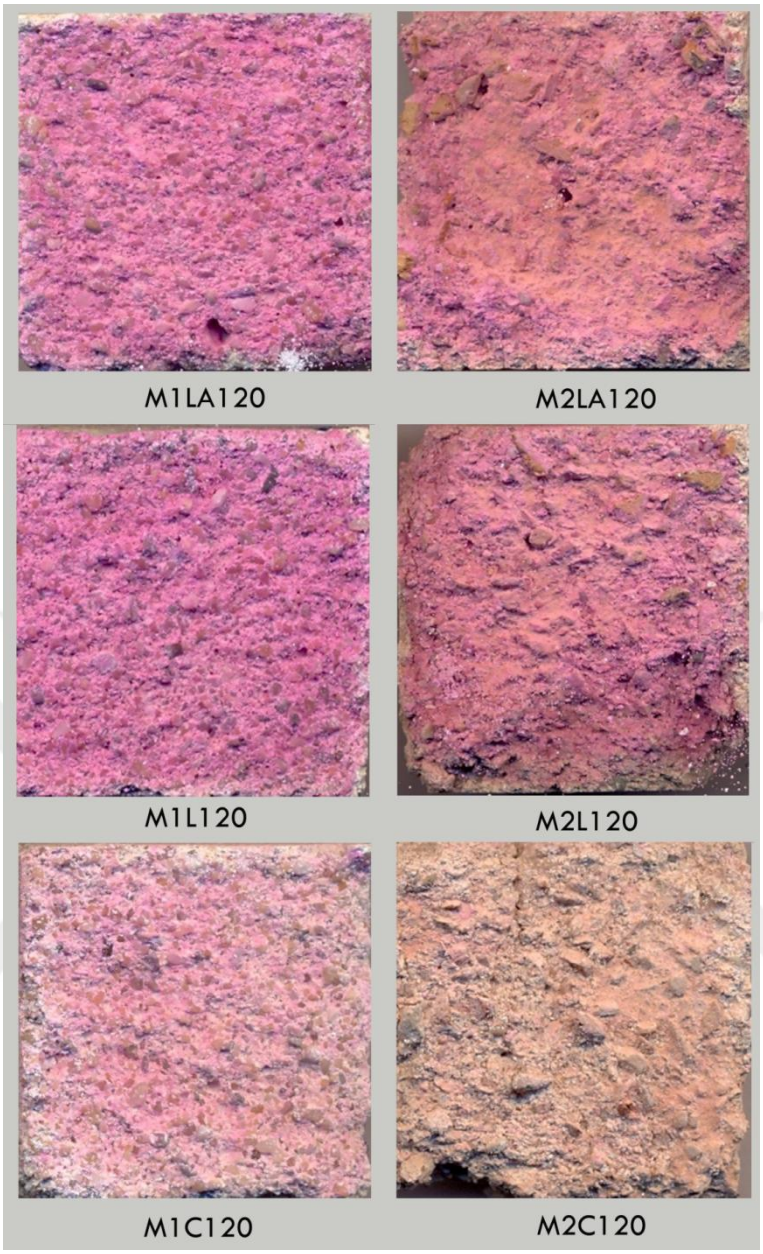


Figure 5.1- 34. Phenolphthalein sprayed samples after 120 days of curing

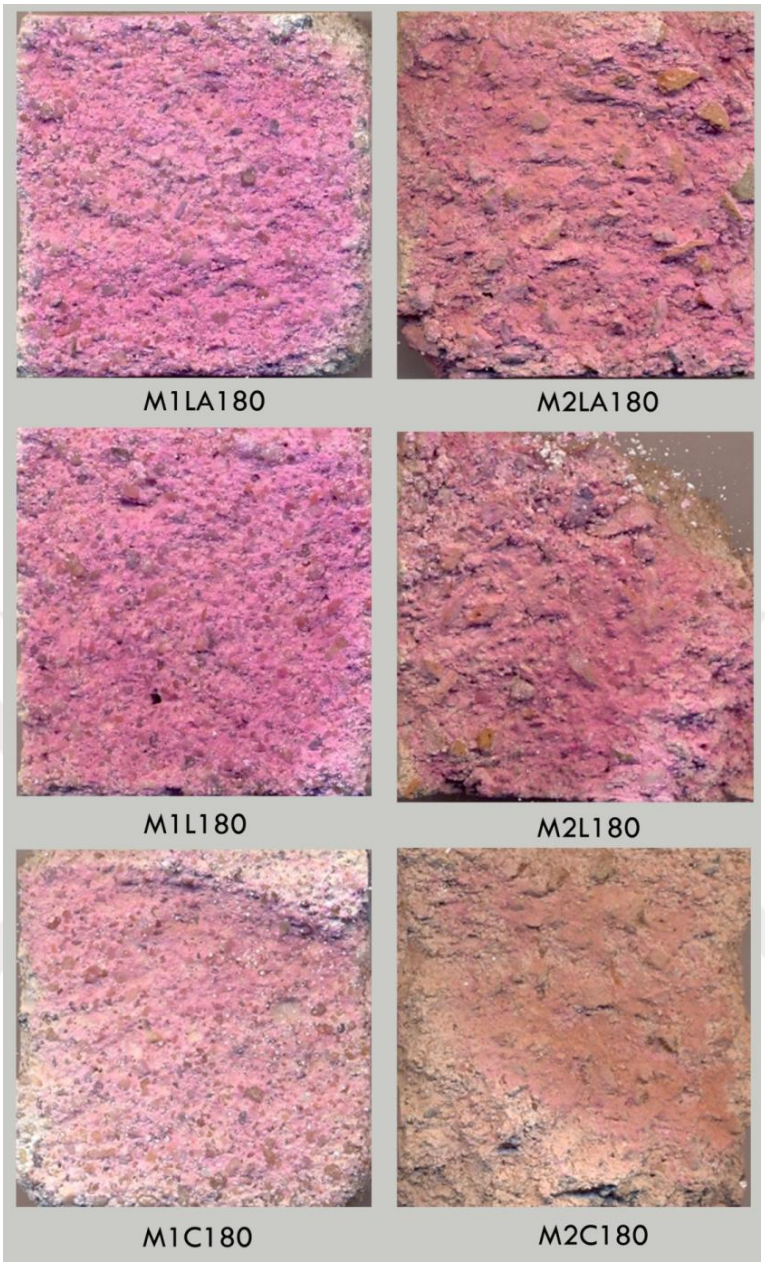


Figure 5.1- 35. Phenophtalein sprayed samples after 180 days of curing

5.1.7 Mercury Intrusion Porosimetry (MIP) in 28, 90, 120 and 180 days of curing

In M1 mortars total porosity generally ranges around 25 % with the exception of sample M1L at 180 days which shows 38% total porosity, it was possibly because of the cracks generated by the mercury intrusion pressure during the measurement as the mortar samples still had poor bonding between aggregates and lime binder. Chamber cured M1 samples own larger pore sizes and smaller specific surface areas compared to other samples of same mixture (Table 5.1- 4).

M2 mortars had higher total porosity and specific surface area as expected due to the ceramic dust and fragment inclusion. Because the ceramic aggregate was more porous than sand aggregate thus the amount of entrained air was higher. Among M2 mortars, samples that were cured in the climatic chamber show lower values except 120 day in which the porosity and average pore diameter rise and specific surface decreases (Table 5.1- 4). As mentioned before, the reason may be the occurred cracks due to the pressure during measurement. In both samples M2L and M2LA porosity rise at 90 days due to the shrinkage cracks upon hardening and then decrease with the filling of the pores and cracks by recrystallization as confirmed by the microscopic observations (Figure 5.1- 1).

M1L shows a porosity increase at 180 days due to increased cracks and M2L shows a significant decrease at 180 days of the porosity occurs because of the formation of new mineral phases (calcite, aragonite) inside the pore system.

Table 5.1- 4. Physical properties gathered from MIP

Samples		Porosity (%)	Average Pore Diameter (4V/A) (µm)	Specific Surface Area (m^2/g)
M1L	**28**	26	0.27	2.19
	90	24	0.24	2.17
	120	25	0.29	2.01
	180	38	0.24	2.13
M1LA	**28**	26	0.24	2.45
	90	23	0.29	2.04
	120	24	0.26	2.06
	180	25	0.30	1.85

M1C	**28**	25	0.34	1.62
	90	26	0.37	1.57
	120	24	0.28	1.91
	180	26	0.34	1.74
M2L	**28**	43	0.11	11.51
	90	47	0.12	10.98
	120	41	0.15	8.34
	180	28	0.12	10.18
M2LA	**28**	37	0.12	9.11
	90	42	0.10	13.58
	120	41	0.14	8.98
	180	39	0.21	5.39
M2C	**28**	37	0.13	8.58
	90	37	0.14	7.32
	120	46	0.26	5.23
	180	39	0.16	7.27

Pore size distributions that were measured by MIP show bimodal distribution in all the mortars. In M2 mortars, amount of the pores between1 and 0.01 μm were higher whereas in M1 mortars the intensity of the two models was same. All of M1 mortars of the curing conditions had a peak around 8-9 μm at 28 days at 120 days M1C mortar shows the peak at 11 μm like M1L mortars does in all of the ages. In the chamber cured at 180 days micropores between 0.1 and 0.01 μm occur as an indication of connecting micropores.

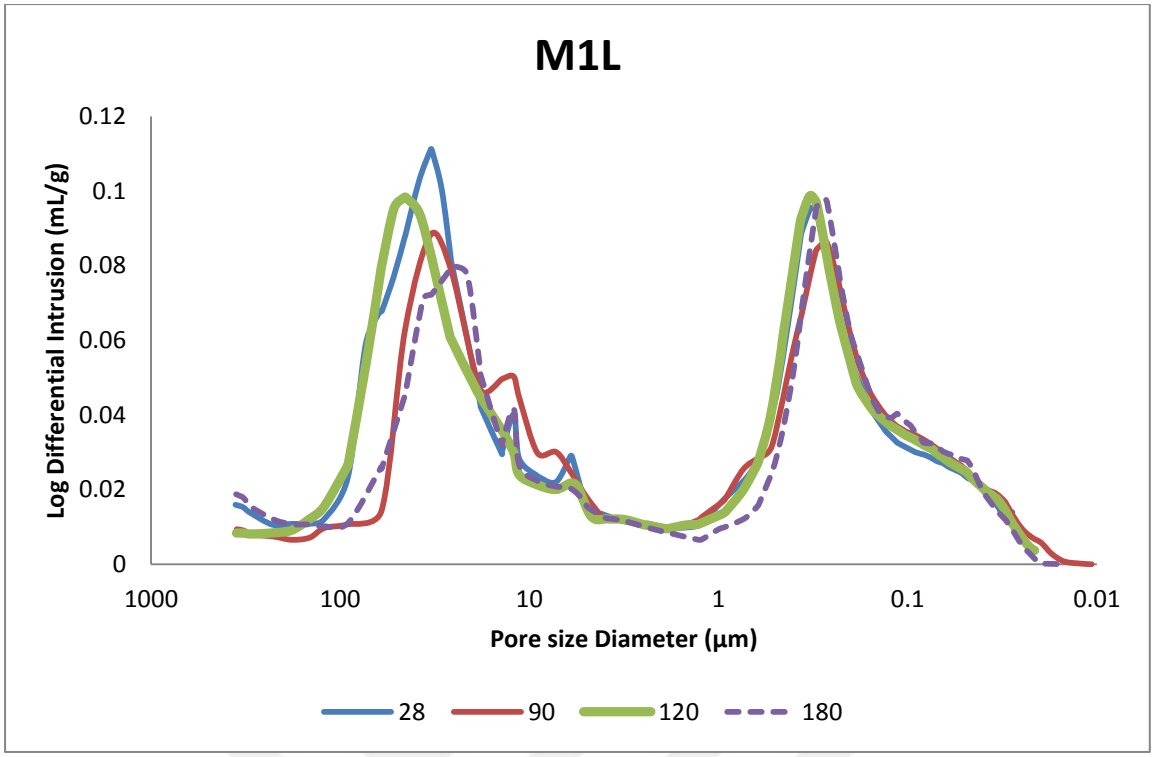


Figure 5.1- 36. Pore size distribution of sample M1L in tested periods

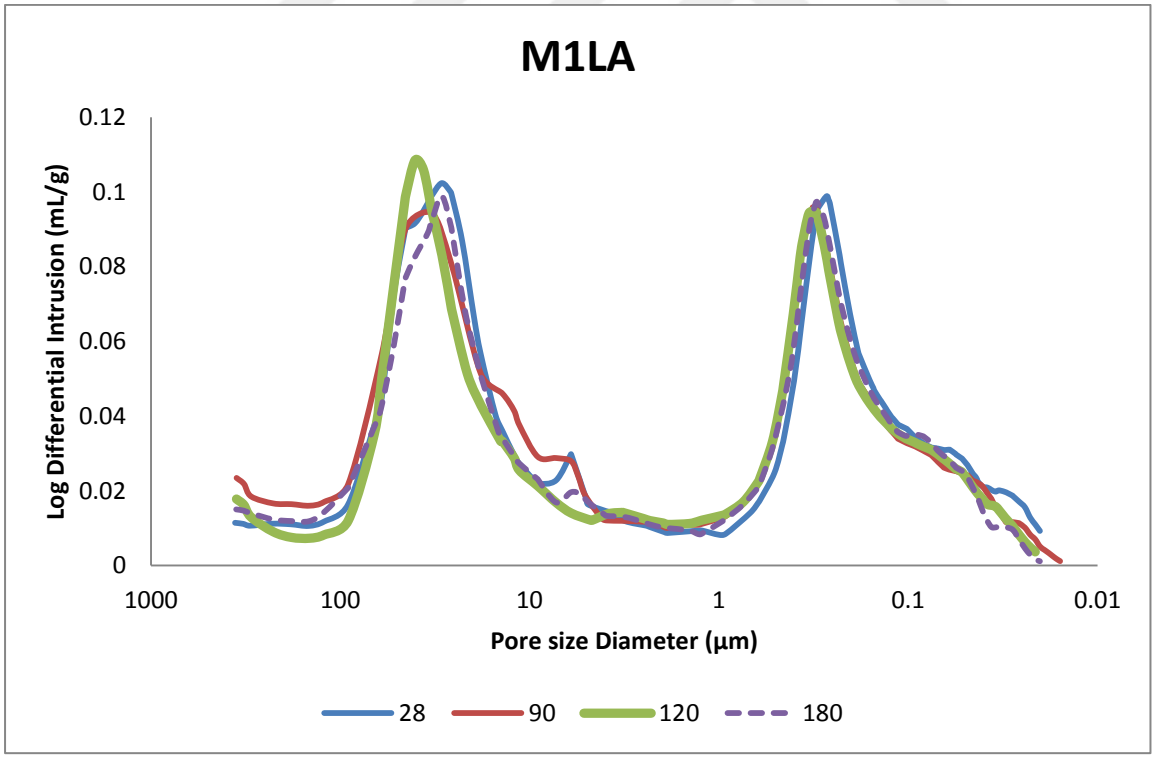


Figure 5.1- 37. Pore size distribution of sample M1LA in tested periods

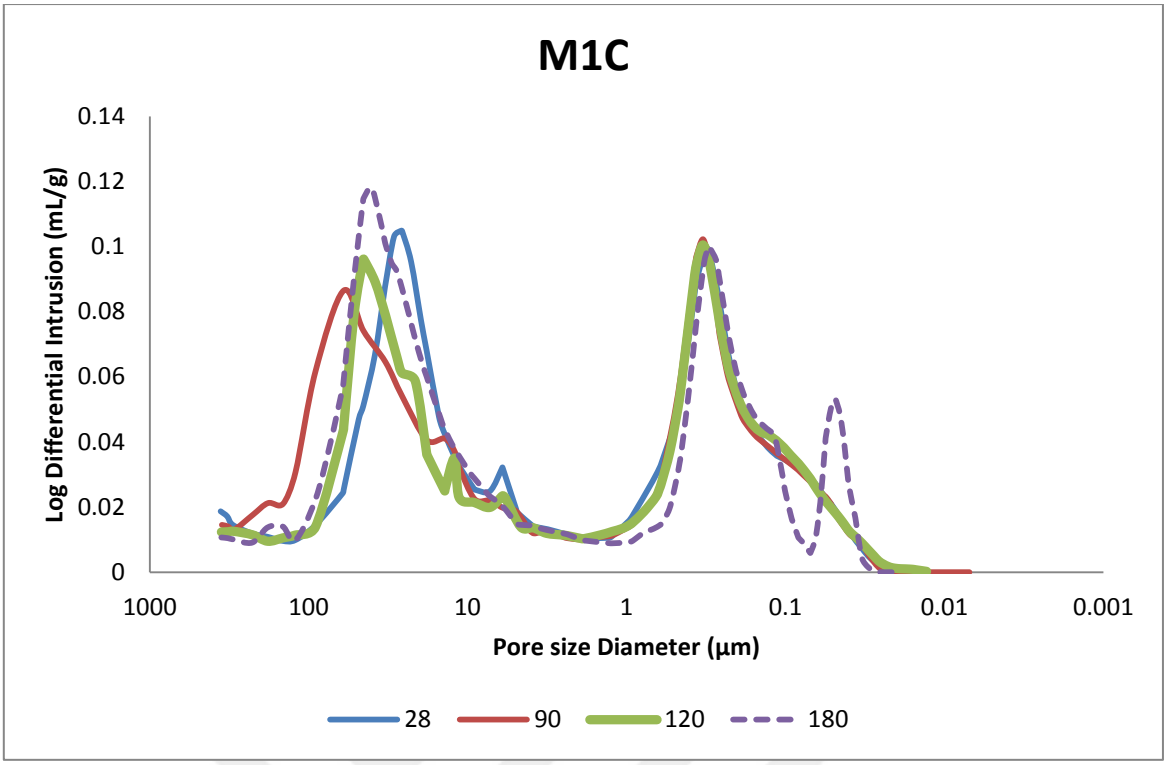


Figure 5.1- 38. Pore size distribution of sample M1C in tested periods

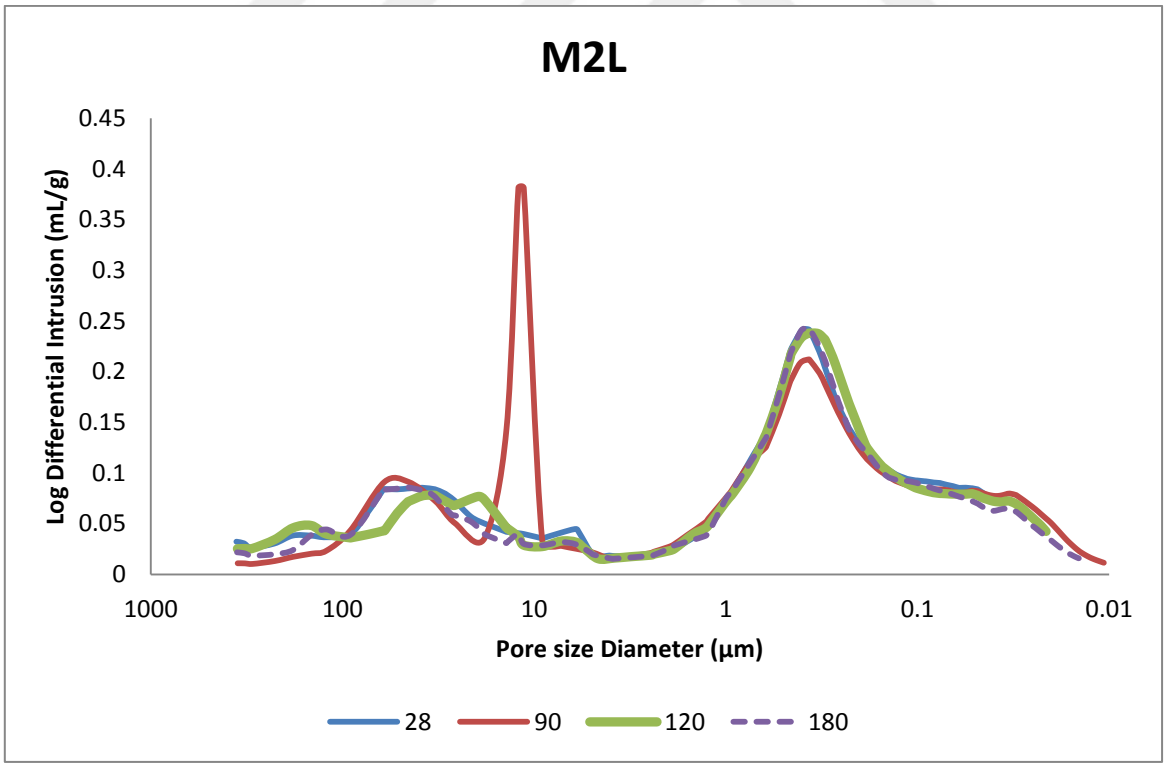


Figure 5.1- 39. Pore size distribution of sample M2L in tested periods

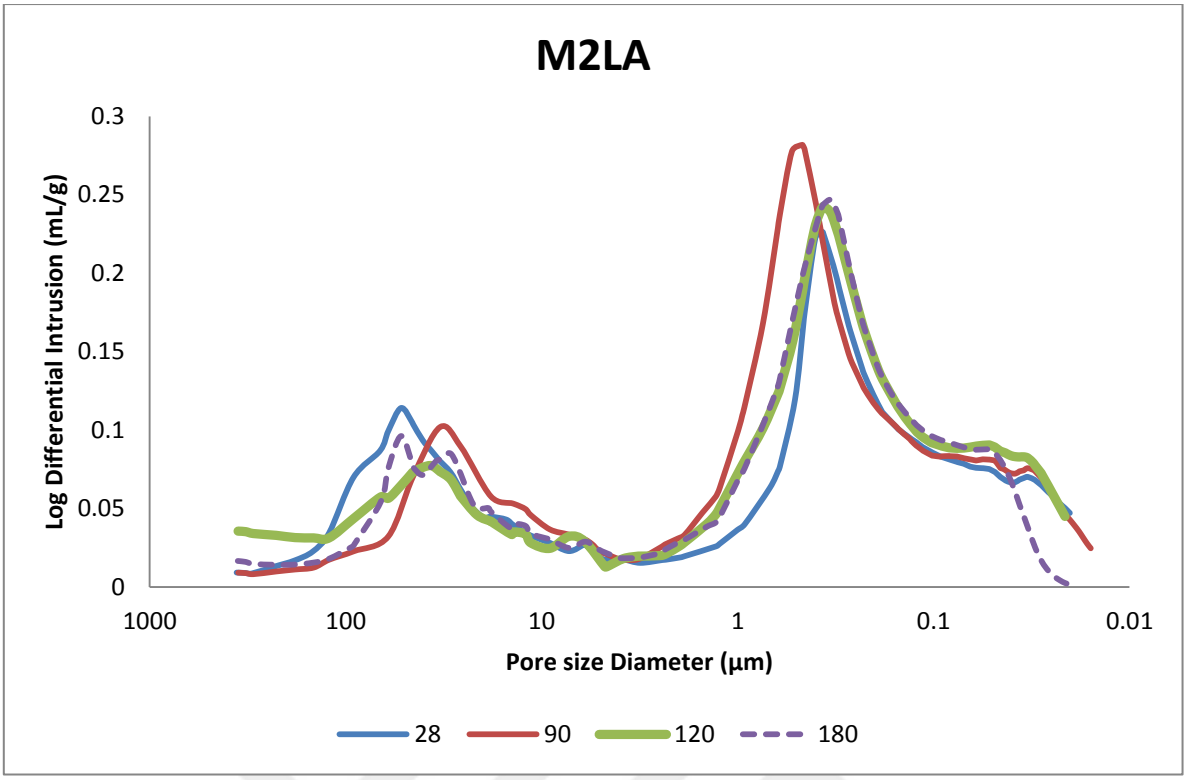


Figure 5.1-40. Pore size distribution of sample M2LA in tested periods

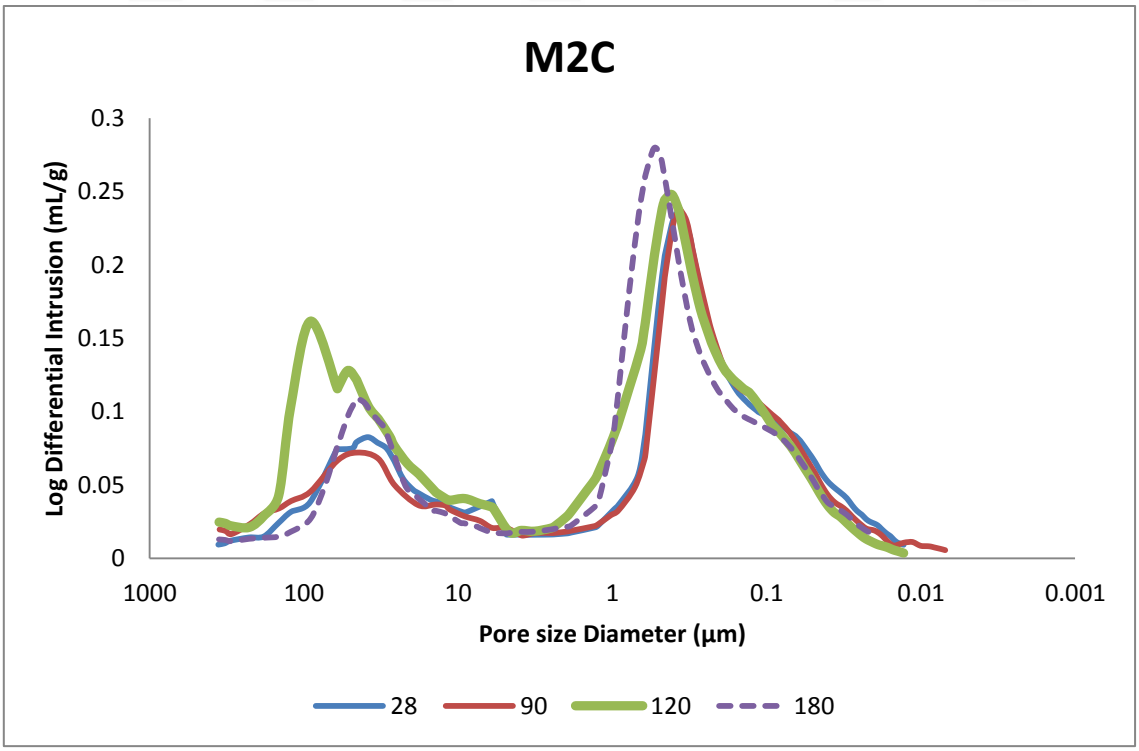


Figure 5.1- 41. Pore size distribution of sample M2C in tested periods

Pores between 0.1µm to 100µm were capillary pores that contribute to the water transfer through capillary action. Capillary pores were interconnected and in charge of the moisture and air transfer (Thomson et al. 2004; Lourenço, 2014; Groot, 2016) Small capillary pores (<1 µm) were formed in the binder when water evaporates and bigger capillary pores were formed in the spaces between binder and aggregate (Lourenço, 2014).

Sorption pores (< 0.1 µm) were gel pores that were developed in hydrated phases and coarser pores above 100 µm which form as entrapped air in the mixing process, lead water intake by permeability (Groot, 2016; Lourenço, 2014).

Pores around 0.1 µm in diameter were associated to the portlandite transformation to calcite (Lawrence, 2006). With the transformation of portlandite to calcite and the consequent volume rise, the largest and the smallest pores were plugged and total porosity falls (Izaguirre et al., 2010); however it does not imply a noteworthy change in pore size distribution (Thomson et al. 2004; Izaguirre et al. 2010)

The most noticeable change is seen in first modal of M1L mortars and second modal of M2LA mortars. shows how at 120 days the porosity between 20 and 8 µm disappeared in the M1L and M1LA mortars, and a tendency to decrease the size of M1L of larger pores when passing the trend from 70 µm to 30-40 µm, with no significant changes in pores of less than 1 µm in size.

In the M2 mortars the number of the macropores (100-10 µm) was lower than M1 mortars and their size and amount decrease with age. Large pores (> 50 µm) were present when aggregates were rounded which results in bad bonding between the lime and the aggregate, (Lanas et al. 2003)

In M2LA the number of micropores (< 1 µm) which was higher than M2L, also slightly decreases. Sorption pores below 0.1 µm, decrease at 180 days (Figure 5.1- 40)

Acording to (Thomson et al, 2004), the reason of the increase in porosity can be either the increase in the amount of pores, or the increase in pore diameter. So, the increase of total porosity in M1L at 180 days was related with the amount of pores (Figure 5.1- 36) while M2C mortars at 120 days was due to the increase in diameter of pore size in macropores (Figure 5.1- 41).

5.2 Results of physical analyses

5.2.1 Surface Hardness (Equotip) in 28, 90, 120 and 180 days of curing

Samples M1LA, M1C, M2L and M2LA had approximately same surface hardness close values at 28 days while M1L had lower and M2C had higher values (Table 5.2- 5).

Since the carbonation begins at the exterior layer, as time passes the surface hardness was supposed to increase during carbonation. There was no significant increase except for the use of the accelerator being still not so obvious. As it is illustrated in Figure 5.1- 42 all samples show increment in 90 and 120 days, notwithstanding that the highest increase was in the samples of M2LA which maintain the increase at 180 days as well incorporation of brick-tile dust and fragments favour the hardness of the mortars (Nežerka et al. 2015) and seems to had more hardness with accelerator. In addition, at 180 days the only mortar that its increase continues was M2LA with a ratio of 9 %. Herewith the highest hardness values belong to M2LA and M2C at 180 days. The high value of standard deviation of M2L at 180 days indicates the inhomogeneity in the carbonation.

Among M1 mortars, M1LA and M1C had similar values at 28, 90 and 120 days which were higher than M1L however the greater fall in the values occur at sample M1C at 180 days. In sample M1LA a higher hardness was reached from the beginning of the carbonation process, which tends to be maintained over time.

Table 5.2- 5. Surface hardness (leebs) of the samples (SD: standard deviation)

	28 days	SD	90 days	SD	120 days	SD	180 days	SD
M1L	206	6	211	5	214	2	205	5
M1LA	211	1	214	3	219	8	217	2
M1C	212	10	216	7	218	8	210	6
M2L	211	4	216	2	220	7	219	34
M2LA	213	12	224	4	225	1	233	6
M2C	230	7	237	7	238	4	234	4

In case of M2 mortars, curing in chamber seems to be favourable for carbonation according to high surface hardness from the early periods however; with accelerator there was a significant ever-increases within the time which reaches to the surface hardness of M2C (Figure 5.2- 42).

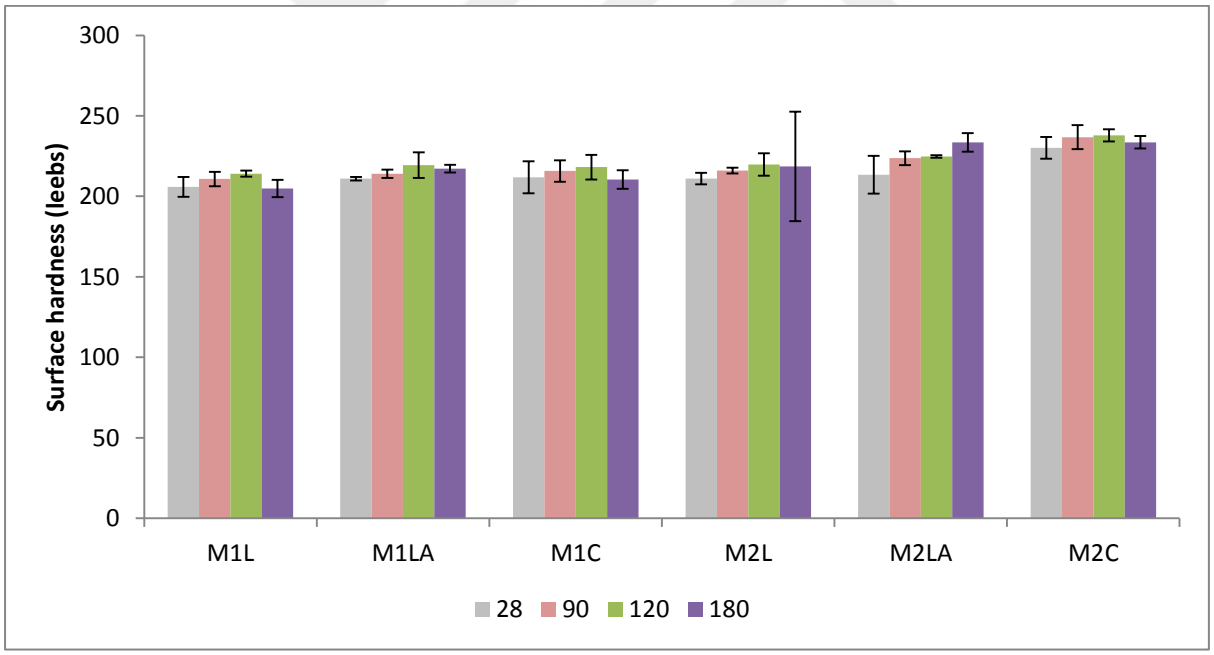


Figure 5.2- 42. Surface hardness values of the samples in tested periods

5.2.2 Air permeability in 28, 90, 120 and 180 days of curing

At 28 days, M1 samples had close air permeability values around 1700, M2LA shows lower value and M2L together withM2C had higher amounts.

Table 5.2-6. Air permeability (mD) of the samples in different periods

	28 days	SD	90 days	SD	120 days	SD	180 days	SD
M1L	1803	779	2404	525	3421	193	3052	367
M1LA	1666	714	2335	791	2267	426	2804	968
M1C	1709	154	1968	160	2260	493	2412	310
M2L	2234	786	2914	1887	3509	1230	2560	725
M2LA	1400	308	2243	777	2366	755	3105	1690
M2C	2344	1552	3207	2388	2629	755	4215	3544

As it is presented in Table 5.2-6 the higher air permeability of mortars was observed in M2 (medium value: 1993 mD) than M1 (medium value: 1726 mD). In both mortars the permeability tends to increase with the passing time being very important the value that was reached for M1L (3052 mD). In group M2, the increment over time was clear for M2LA (122%), although there were variations with intermediate times M2C shows an increase in the permeability between the initial and the final days reaching to the highest value among all mortars (4215 mD). Also, it should be underlined that standard deviations of M2 mortars were higher especially the M2C mortars which indicate the inhomogeneity of the samples.

From the point of curing condition, samples show consistency among each other. Accelerator used samples and chamber curing samples show non-linear increase while steady increase of laboratory samples interrupts at 180 days.

Air permeability is related to porosity and/or pore size. Theoretically, increasing carbonation leads fall in porosity and as well as the decrease in air permeability. The reason why the opposite was encountered in the samples should be related with the fissures and cracks. Nevertheless no correlation could be obtained between the air permeability and the porosity results. Total porosity of M1L sample show a sudden increase at final age contrarily

air permeability falls at 180 days. The same occurs at 120 days M2C mortars. So, the air permeability should be affected by not the total porosity but the distribution of the pores. This argument is valid for the average pore size diameter of the mortars other than chamber cured ones. As mentioned earlier in 8.1. Interconnected pores located between 0.1µm-100µm contribute to the water transfer through capillary action and were responsible for the water vapour and air transfer (Thomson et al., 2004; Lourenço, 2014; Groot, 2016). It could be confirmed that macropores between 80 and 100 µm were getting disappeared at 180 days which its air permeability falls as well. Likewise, the increase in the pores between 90 and 100 µm can be followed by ever increase in permeability of M1C. In M2 mortars the rising pores between 0.9 and 1 µ were responsible for the increase in air permeability.

The increase in air permeability may be due to the increase in total porosity as the change in the amount of pore sizes between 0.1 µm and 1 µm had an influence on it (Arizzi and Cultrone, 2012). In agreement with porosity, M2 mortars had in general higher air permeability than M1 mortars.

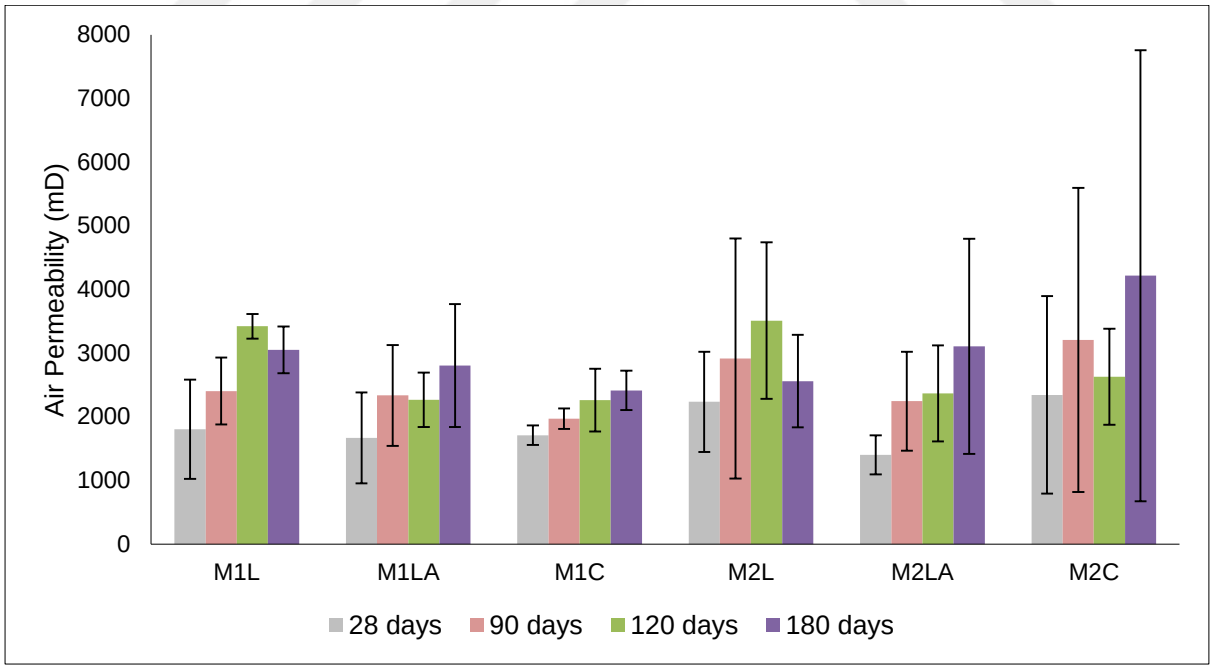


Figure 5.2- 43. Air permeability values of the samples in tested periods

5.2.3 Ultrasonic Pulse Velocity (UPV) in 28, 90, 120 and 180 days of curing

M1 had a higher ultrasonic pulse velocity (UPV) (average value: 1413 m/s, standard deviation: 65) than the mortar M2 (average value: 1093 m/s, standard deviation: 53)(Table 5.2-7). This would be produced by different components of the aggregates and amount of binder. The bricks had lower UPV than the quartz that had been used as aggregate in M1.

Table 5.2- 7. UPV(m/s) values of samples (SD: standard deviation)

	28 days	SD	90 days	SD	120 days	SD	180 days	SD
M1L	1335	84	1479	83	1502	103	1516	92
M1LA	1421	89	1490	84	1558	93	1509	66
M1C	1440	145	1520	82	1571	128	1551	108
M2L	1090	79	1060	63	1094	67	1070	53
M2LA	1113	117	1066	60	1121	73	1071	72
M2C	1244	314	1083	80	1125	78	1051	67

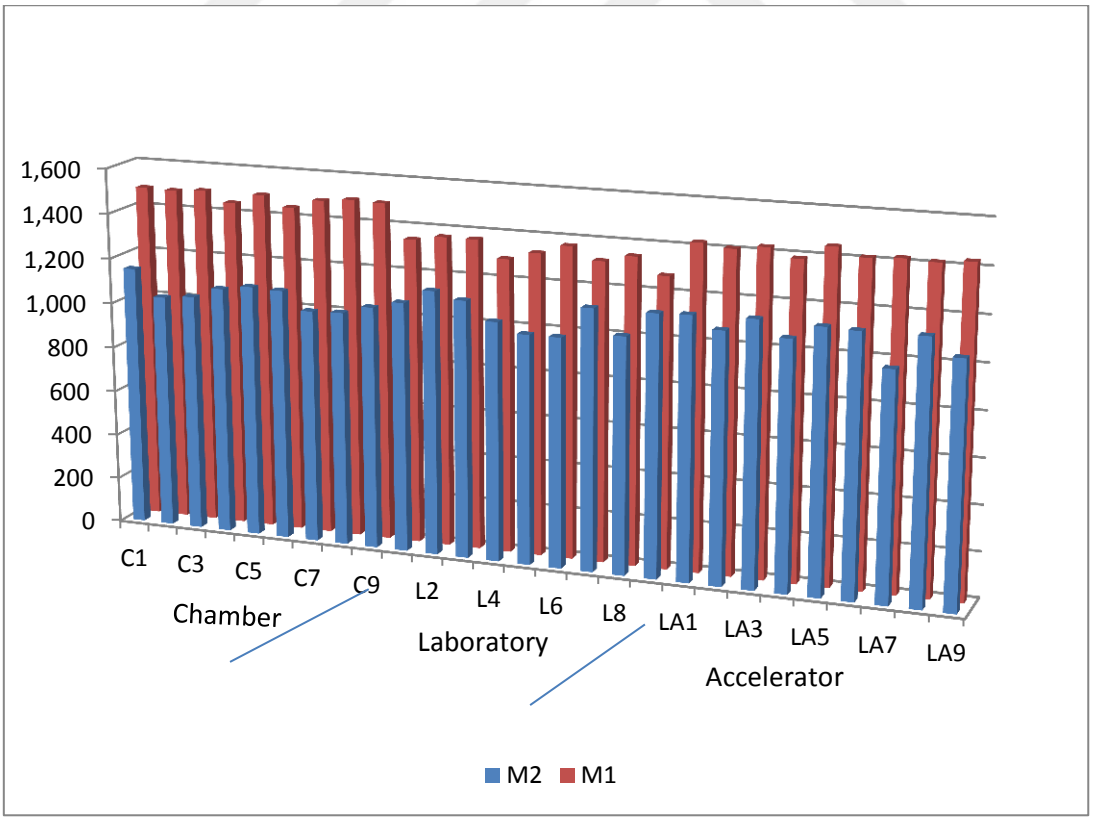


Figure 5.2- 44. UPV values of the samples at 28 days of curing

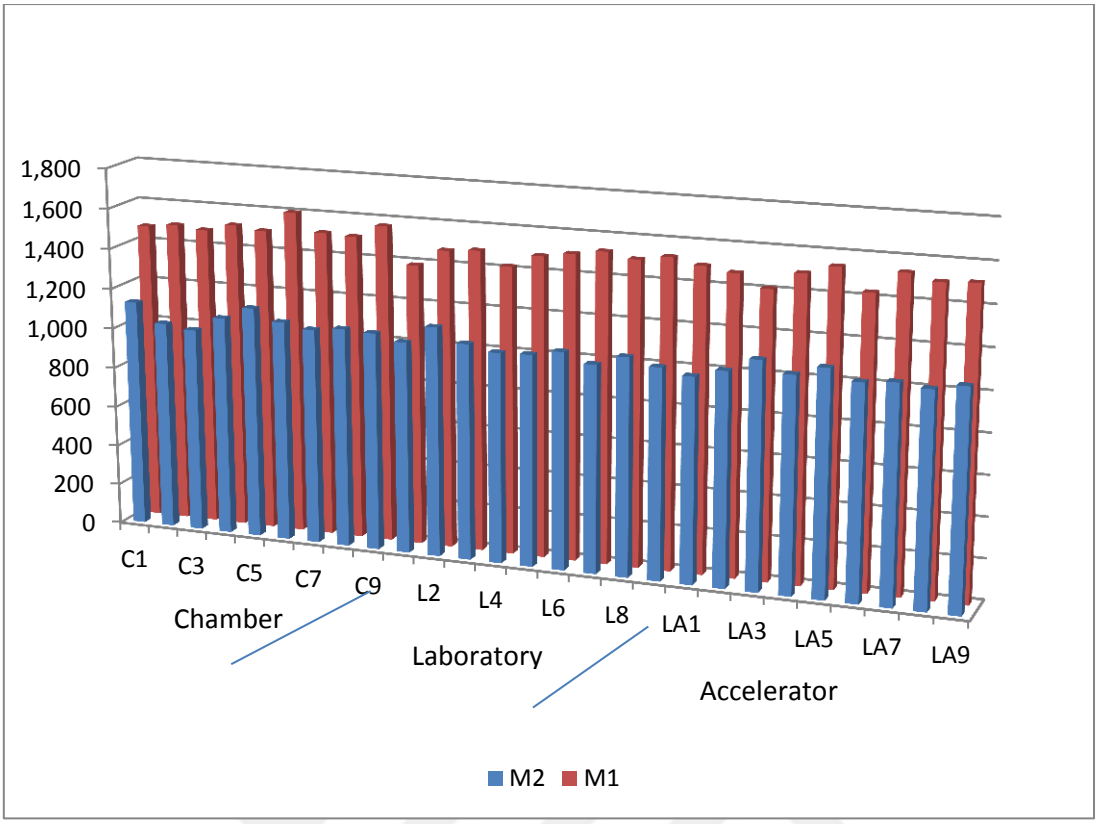


Figure 5.2- 45. UPV values of the samples at 90 days of curing

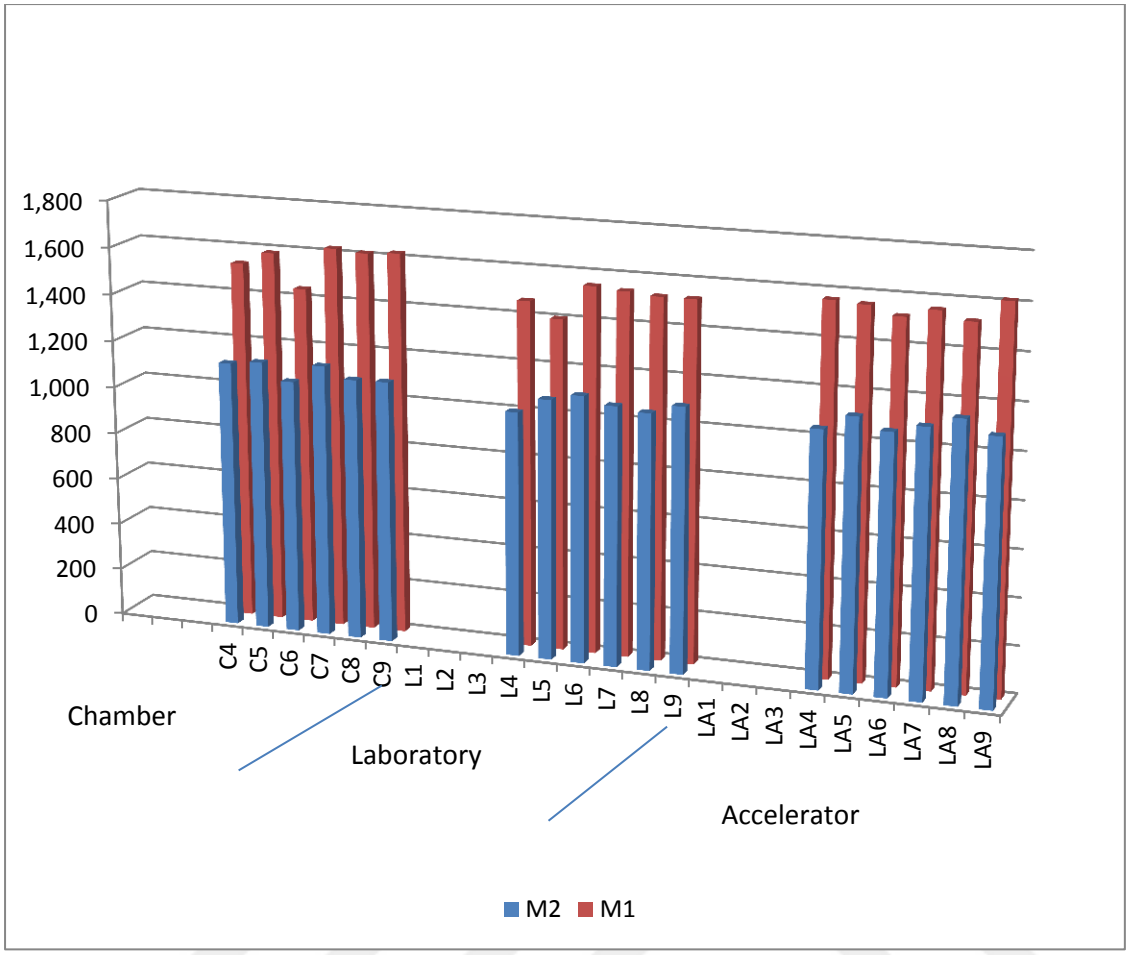


Figure 5.2- 46. UPV values of the samples at 120 days of curing

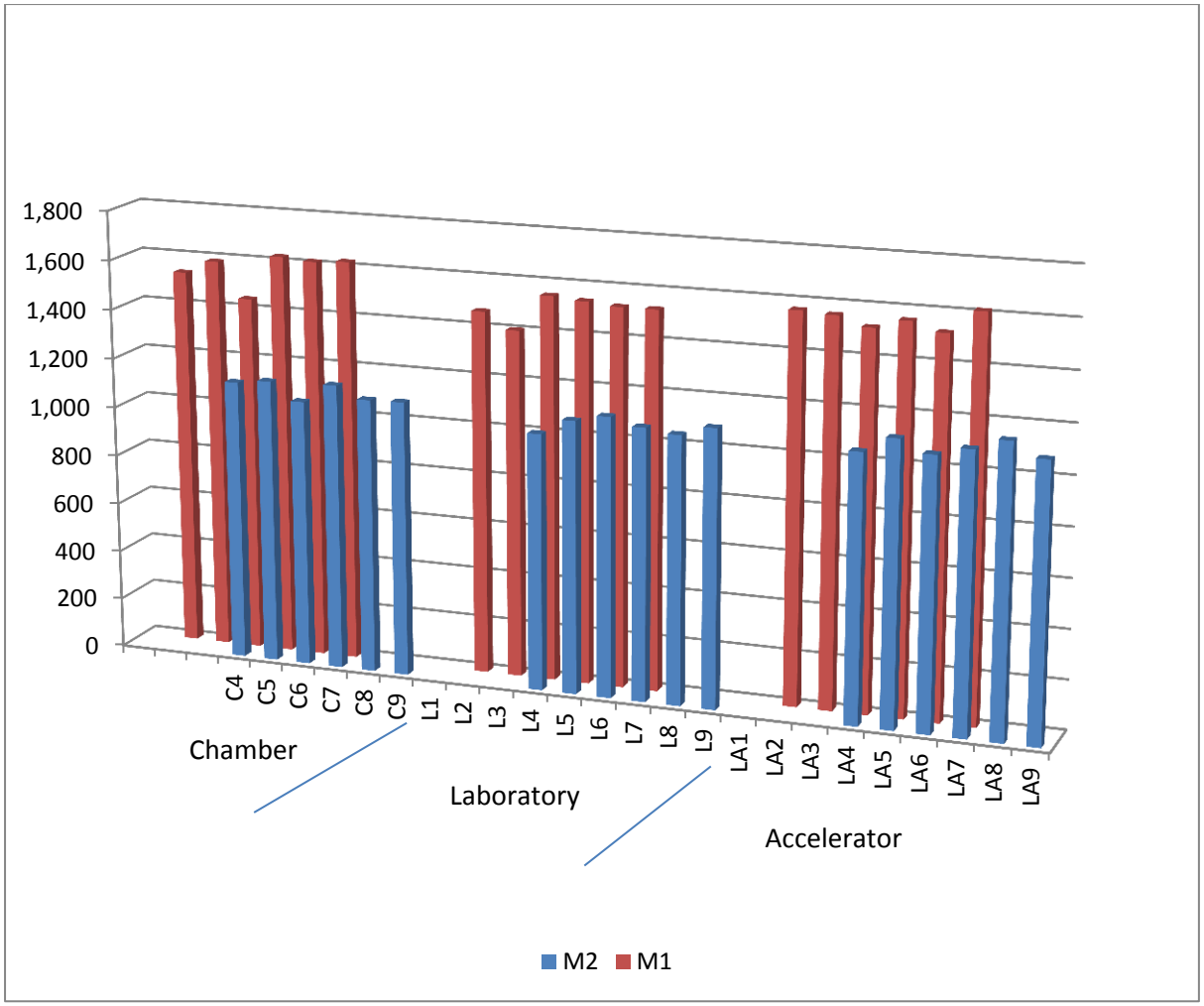


Figure 5.2- 47. UPV values of the samples at 180 days of curing

Laboratory samples having less velocity at 28 days show continual increase M1LA and M1C mortars had slightly higher values at all dates and then decrease at 180 days (Figure 5.2-44- Figure 5.2-47). By the advancing age reaching to 180 days velocity gains of 13.5 % in M1L, 6.2 % in M1LA and 7.7% in M1C mortars were recorded. On the contrary velocity of M2L decrease 1.9%, of M2LA falls 3.8% and 15.6% in M2C mortars at the end of 180 days of curing. Similarly new forming fissures and cracks should be related to the fall of velocity of mortars especially in chamber cured samples. In M2 group samples cured at laboratory conditions both with and without accelerator show no change with identical fluctuations, samples of M2C show the same fluctions in the advanced ages but higher UPV values at 28 days however high standard deviations indicate that samples had higher variations in velocity.

Mortars with ceramic aggregates show in all cases, in the first 120 days, slightly higher values of ultrasonic velocity, which can be attributed to their hydraulic characteristics.

The mortar M1, in the three forms of carbonation shows an increase of the UPV indicating a process of hardening of the mortar that reaches higher values under natural laboratory conditions in the laboratory (Figure 5.2-48). While the M2 does not show a significant increase and even in the carbonation chamber there was a decrease of the UPV that was possibly due to the fisuration of this mortar in these conditions.

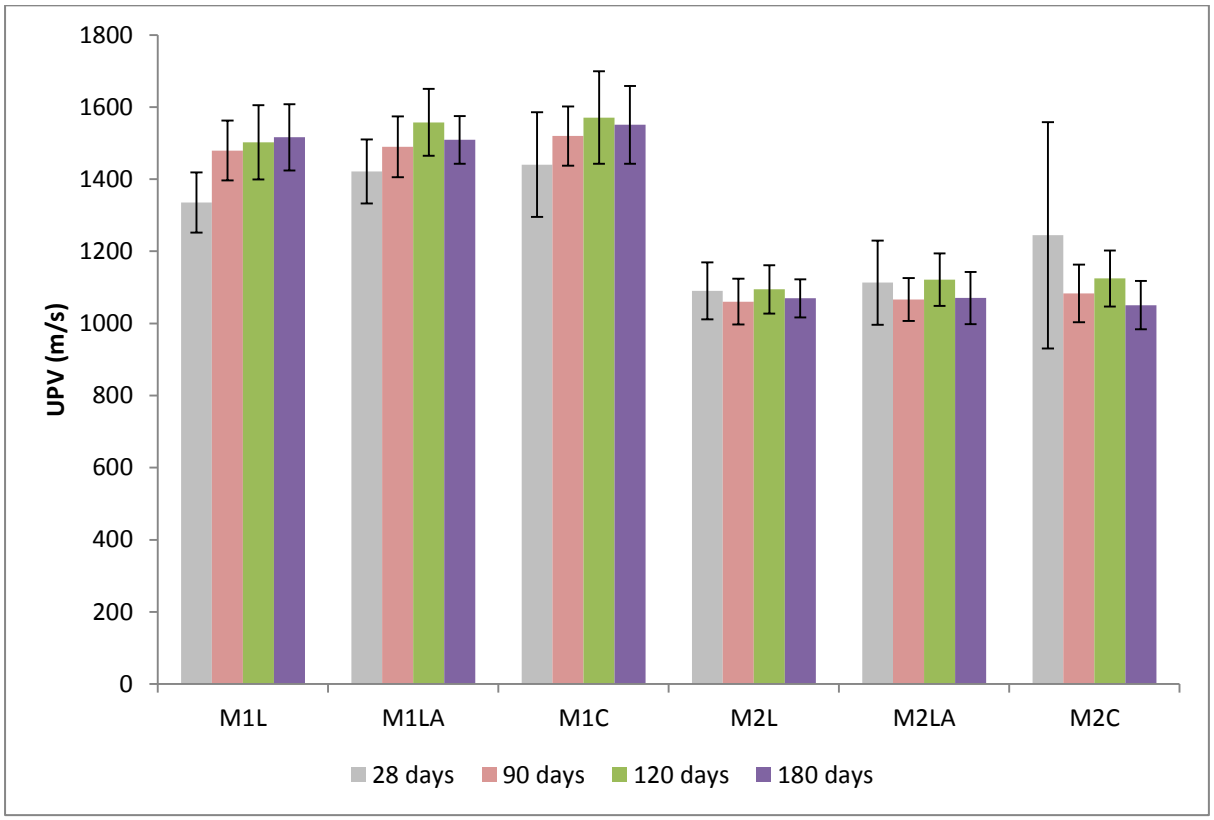


Figure 5.2-48. Average UPV values of the sample in tested periods

Expected increasing values were gathered in M1 mortars while there was no countable change in M2 mortars and even fall in M2C sample. Anisotropy (ΔM) results in chamber cured samples support more the carbonation an increase in M1C sample that velocity slightly raises anisotropy show a by far increment in 120 and 180 days. Similarly decrease was seen both in velocity and anisotropy of M2C (Figure 5.2-49). The former was due to the

interlocking carbonate crystals and the latter should be related with the cracks and fissures that prevent the ultrasonic propagation waves go faster.

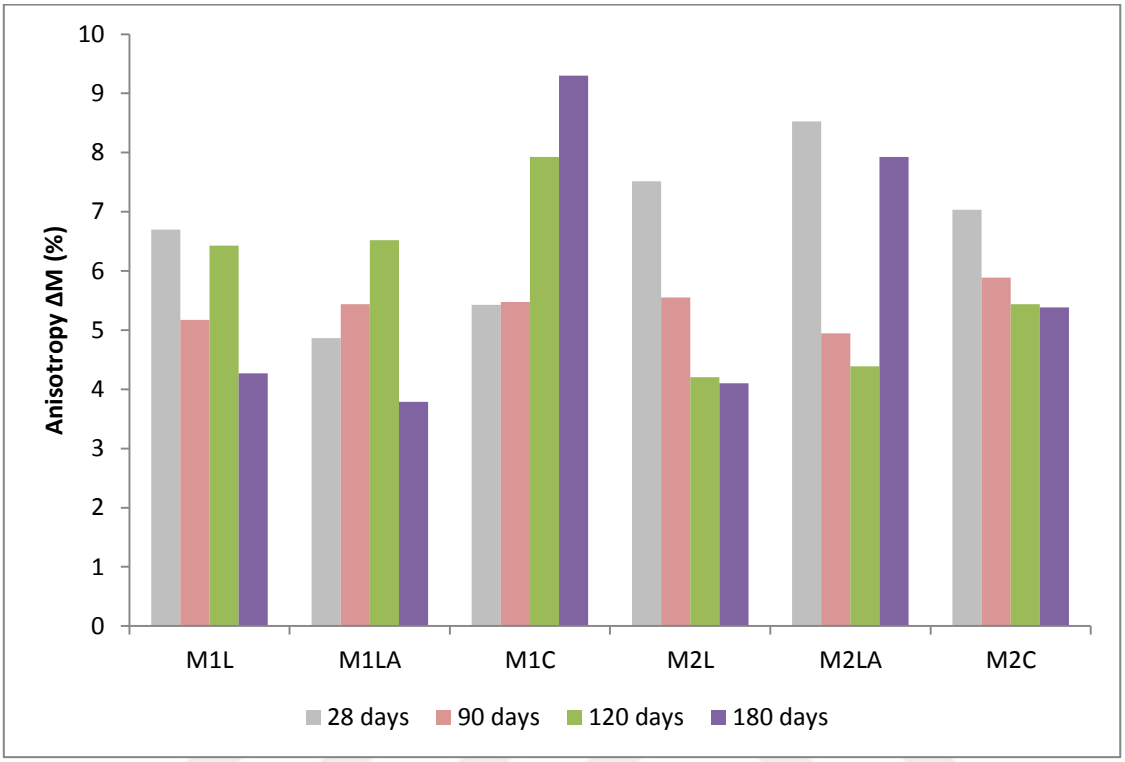


Figure 5.2-49. Anisotropy (%) of the samples

5.3 Results of hydric analyses

Hydric analyses saturation and capillary water absorption tests were presented below.

5.3.1 Saturation in 28, 90, 120 and 180 days of curing

As illustrated in Figure 5.3- 50 and Figure 5.3- 51, values of the saturation degree (water absorption) and open porosity under vacuum of the M2 samples were higher than the values of M1 samples. This was already expected due to the presence of bricks and the decrease in the values with the passing of time as theoretically pores decrease during the carbonation process. Apparently, at 28 days saturation of M2LA were the highest values and after steady few the decreases at 90 and 120 days ends up 34 % at 180 days a little higher than M2L. On the other hand, M2C does not show a significant decrease at 90 and 120 days and at 180 days a higher decrease results in 30% saturation.

In the M1 mortars having 17% degree of saturation at 28 days, slight decreases were observed at the end while the higher decreases occur in M2 mortars with sudden falls at 180 days of carbonation and consistently their water absorption capacity decreases. The decrease of open porosity was 27.2 % without carbonation accelerator and 29.1 % with accelerator whereas in M1 mortars the falls were 3.5 % and 2.9 %, respectively.

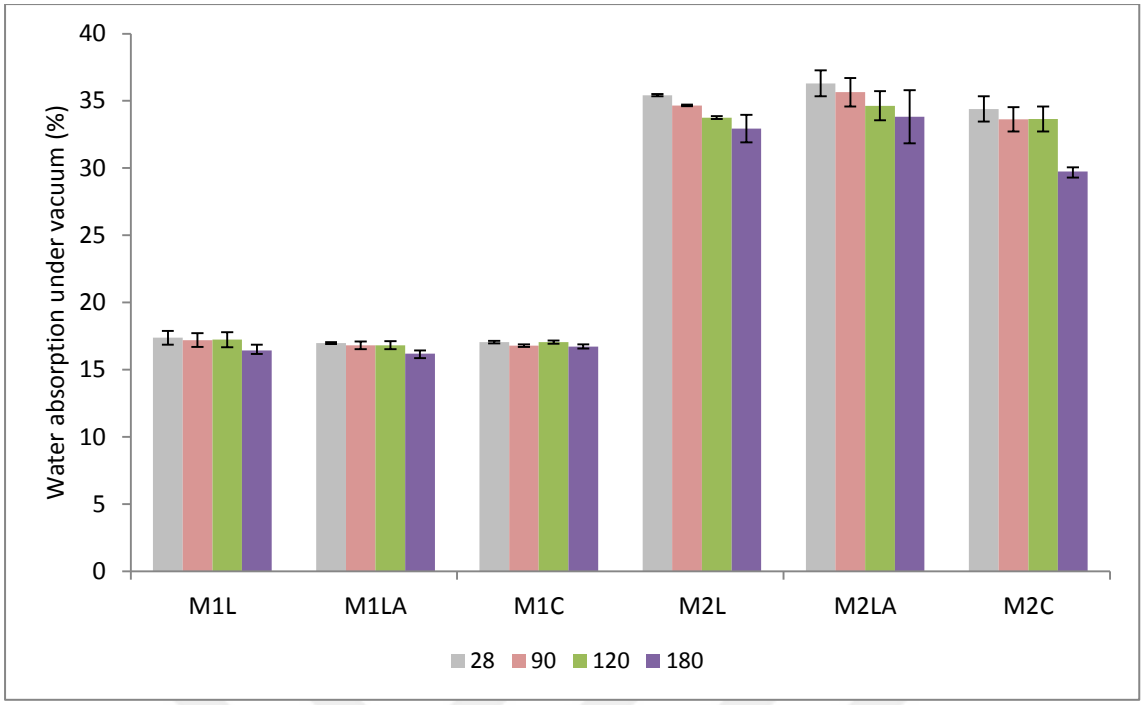


Figure 5.3- 50. Column graph showing the saturation values of the samples

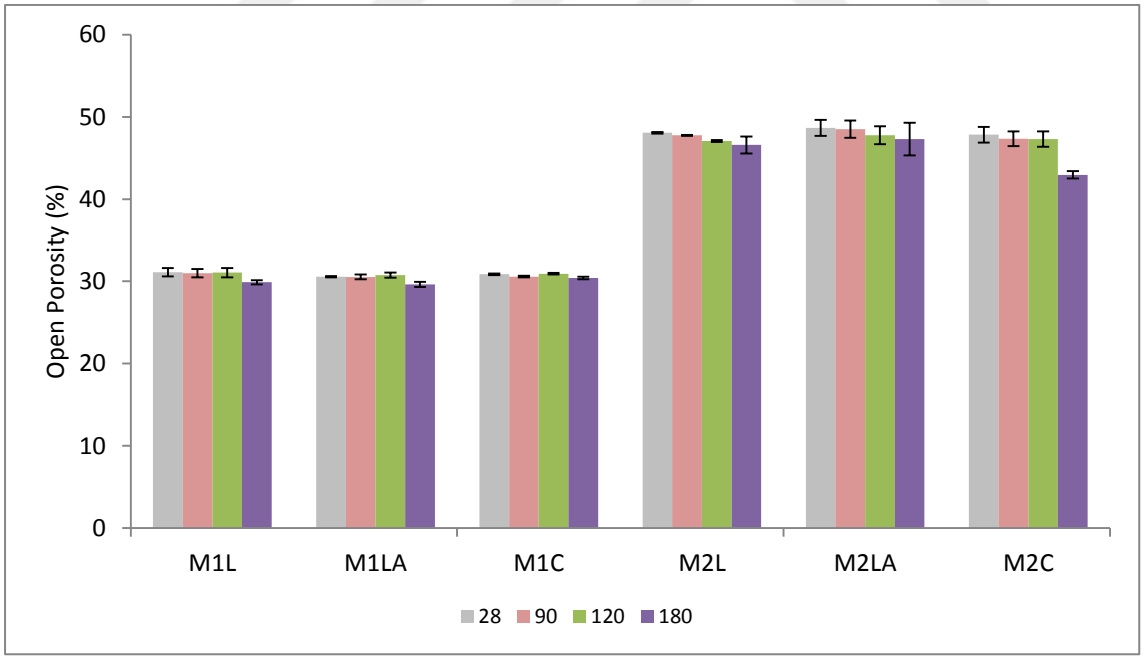


Figure 5.3- 51. Column graph showing the open porosity values of the samples

Table 5.3- 8. Physical properties of the samples in tested periods (D_r: real density, D_a: apparent density, CI: Compactness Index, OP: Open porosity, S: Saturation coefficient, SD: standard deviation)

Samples		D_r(g/cm³)	SD	D_a(g/cm³)	SD	CI	SD	OP(%)	SD	S (%)	SD
M1C	28	2.62	0.00	1.81	0.00	0.69	0.00	30.86	0.10	17.05	0.09
	90	2.62	0.01	1.82	0.00	0.69	0.00	30.57	0.15	16.79	0.10
	120	2.63	0.01	1.81	0.01	0.69	0.00	30.93	0.10	17.05	0.11
	180	2.61	0.00	1.82	0.01	0.70	0.00	30.41	0.21	16.72	0.16
M1L	28	2.60	0.00	1.79	0.02	0.69	0.01	31.09	0.62	17.38	0.51
	90	2.61	0.00	1.80	0.02	0.69	0.01	31.00	0.63	17.21	0.51
	120	2.62	0.00	1.80	0.02	0.69	0.01	31.06	0.67	17.23	0.56
	180	2.60	0.02	1.82	0.01	0.70	0.00	29.88	0.33	16.42	0.25
M1LA	28	2.59	0.02	1.80	0.01	0.69	0.00	30.56	0.15	16.98	0.08
	90	2.61	0.00	1.82	0.01	0.69	0.00	30.54	0.35	16.82	0.29
	120	2.64	0.04	1.83	0.01	0.69	0.01	30.75	0.67	16.82	0.30
	180	2.60	0.01	1.83	0.01	0.70	0.00	29.64	0.45	16.18	0.32
M2C	28	2.67	0.00	1.39	0.02	0.52	0.01	47.83	0.01	34.40	0.01
	90	2.67	0.00	1.41	0.02	0.53	0.01	47.33	0.01	33.63	0.01
	120	2.67	0.00	1.41	0.02	0.53	0.01	47.29	0.01	33.65	0.01
	180	2.53	0.04	1.44	0.00	0.57	0.01	42.95	0.01	29.74	0.01
M2L	28	2.61	0.01	1.36	0.00	0.52	0.00	48.06	0.11	35.43	0.09
	90	2.64	0.00	1.38	0.00	0.52	0.00	47.74	0.06	34.66	0.06
	120	2.64	0.00	1.39	0.00	0.53	0.00	47.08	0.08	33.76	0.12
	180	2.65	0.00	1.41	0.00	0.53	0.00	46.58	0.07	32.94	0.13
M2LA	28	2.61	0.01	1.34	0.02	0.51	0.01	48.65	0.62	36.31	0.97
	90	2.64	0.00	1.36	0.02	0.52	0.01	48.50	0.76	35.65	1.06
	120	2.64	0.00	1.38	0.02	0.52	0.01	47.75	0.79	34.64	1.08
	180	2.65	0.01	1.40	0.02	0.53	0.01	47.29	0.89	33.81	1.14

Increasing carbonation results in increase in mortar weight thus the percentage of weight gain was another parameter that was preferred by many researchers to measure the carbonation (Lawrence 2006; Cultrone et al 2008; Izaguirre at el 2010). It was seen that

among M1 mortars which were heavier than M2 mortars sample with accelerator had more weight at 28 days and the following periods (Figure 5.3- 52). On the other hand in M2 mortar group chamber cured samples had higher weights as well as the standard deviations.

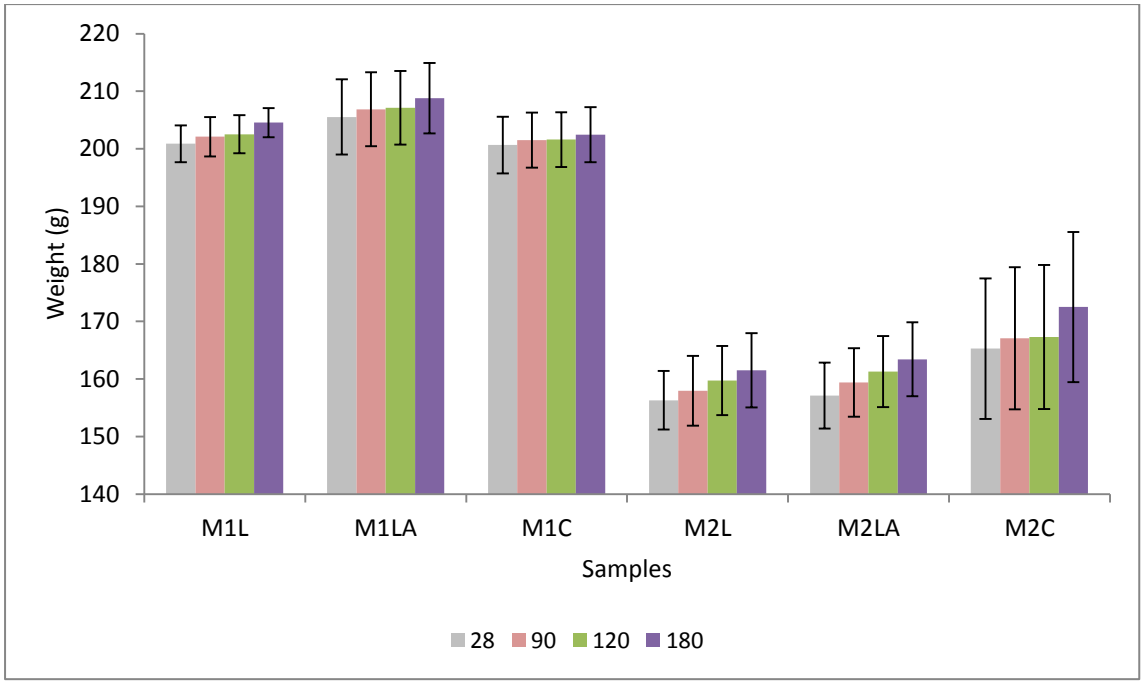


Figure 5.3- 52. Weight difference of mortars during carbonation

The increase in weight was higher in M2 group which was shown in the graph (Figure 5.3- 53). M2LA and M2L show similar increment trend being the weight gain of M2LA was higher. Having fluctuated increase M2C end up with greater weight gain at the end of 180 days.

The increase in weight in other words percentage of weight difference was close to each other in M1L and M1LA which end up 1.5% increase instead the increase of the mortars cured at chamber do not reach even 1%.

If the more weight gained sample group was considered as the more carbonated, M2C was by far the first despite the immobility it shows between 90 and 120 days. Contrarily, again

chamber cured mortar but belonging to M1 was supposed to be the least carbonated according to this approach.

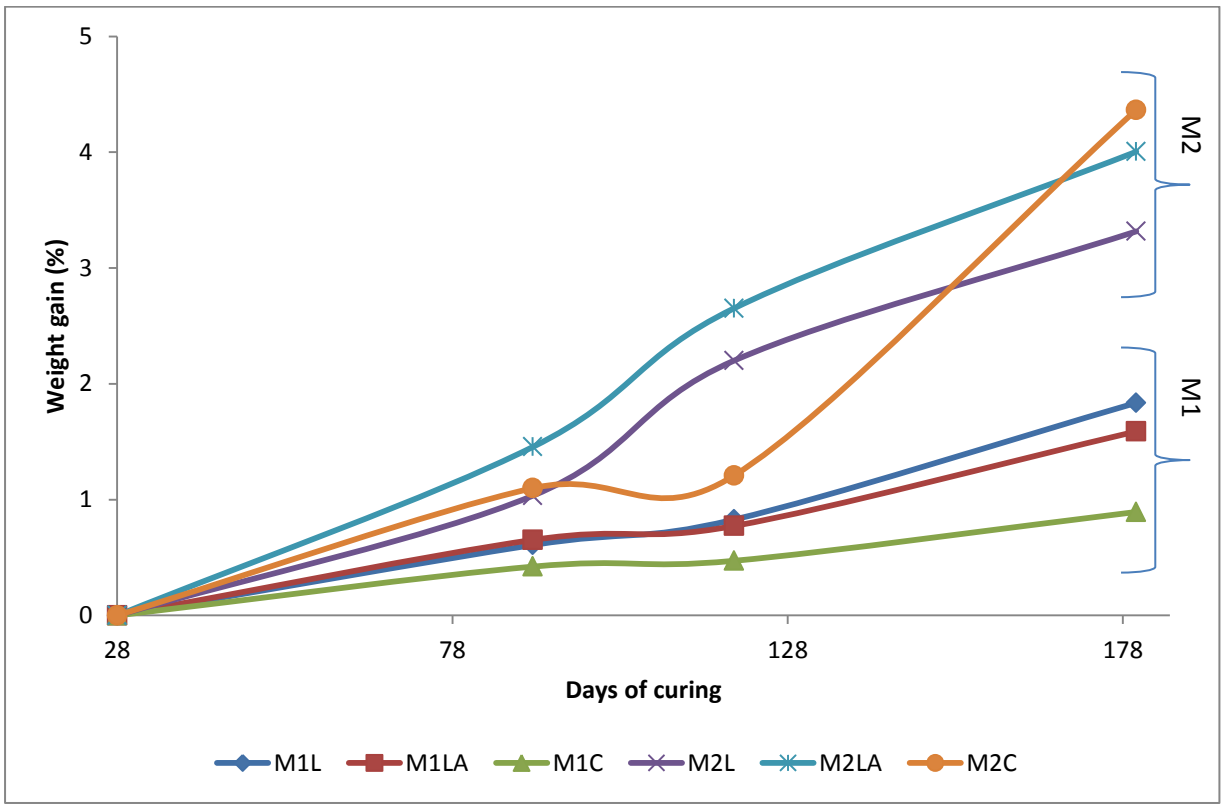


Figure 5.3- 53. Weight gain (%) of mortars during carbonation

5.1.8 Capillary absorption in 28, 90, 120 and 180 days of curing

Capillary coefficients of the samples at 5 minutes and 90 and 10 minutes were listed below (Table 5.3- 9, Table 5.3- 10). From Figure 5.3- 54 it can be seen better that samples generally show small early capillarity except M2C mortars at 120 and 180 days which had sudden high values. This was the indication of weakness of the mortars which was caused by the larger pores or connected cracks. The weak mortar properties with high CC5 was expected as old mortars show much slower initial water absorption rate through capillarity than the new

mortars (Veiga et al. 2004). On the other hand capillary coefficients between 90 and 10 minutes vary it was seen that at 28 days M2 mortars show higher capillarity than M1 mortars. M1L and M1C samples do not exhibit a significant change while the samples with accelerator increase to 2.5 kg/m^2.h$^{1/2}$ at rest of the days. In the graph (Figure 5.3- 55) M2L with increasing trend M2LA with decreasing trend locate more or less at 2.5 kg/m^2.h$^{1/2}$. Capillarity of M2C decreases from that point to the capillarity level of M1 mortars at 90, 120 and 180 days.

Table 5.3- 9. Capillary coefficients (kg/m^2.min^{0,5}) of the samples at 5 minutes in tested periods (SD: standard deviation)

	28 days		90 days		120 days		180 days	
	CC_5	SD	CC_5	SD	CC_5	SD	CC_5	SD
M1L	3.0	0.0	2.5	0.1	3.8	1.6	2.5	0.1
M1LA	2.9	0.2	4.4	0.3	4.4	0.3	4.2	0.3
M1C	3.0	0.1	2.5	0.1	2.7	0.2	2.8	0.3
M2L	4.8	0.4	4.1	0.2	3.3	0.2	3.3	0.3
M2LA	4.6	0.4	4.1	0.3	3.5	0.4	3.3	0.2
M2C	4.2	0.2	2.7	0.1	13.2	3.7	13.1	3.7

Table 5.3- 10. Capillary coefficients (kg/m^2.min^{0,5}) of the samples between 10 and 90 minutes in tested periods (SD: standard deviation)

	28 days		90 days		120 days		180 days	
	CC_{90-10}	SD	CC_{90-10}	SD	CC_{90-10}	SD	CC_{90-10}	SD
M1L	1.2	0.0	1.4	0.1	1.3	0.1	1.3	0.1
M1LA	1.2	0.2	2.5	0.4	2.4	0.5	2.4	0.5
M1C	0.9	0.1	1.1	0.1	1.1	0.1	1.0	0.1
M2L	2.3	0.2	2.7	0.4	2.3	0.1	2.5	0.1
M2LA	2.8	0.3	2.7	0.2	2.3	0.1	2.4	0.0
M2C	2.5	0.5	1.3	0.0	1.2	0.0	1.3	0.0

It is seen that mortars with ceramic aggregates had higher capillary coefficients which was already expected. The other expected phenomenon was decrease in capillarity with

carbonation. As the carbonation of the mortars was not completed yet they were all weak mortars and therefore early capillary coefficients were higher in all of the mortars (Figure 5.3-54, Figure 5.3- 55). M2C sample which had well marked increase at capillarity at 5 minutes at 120 and 180 days whereas shows small capillarity between 10 and 90 minutes at the same days. It can be inferred that newly forming cracks lead rapid capillary suction and saturation. Among M1 mortars accelerator cause higher capillarity after 90 and following days on the other hand both of the capillarity coefficients show decreasing trend in the samples of M2LA. This phenomenon implies better carbonation of the samples with ceramic aggregate and accelerator. This hydric behaviour of mortars was related to the modification of their pore structure, where calcium carbonates fill some pores after the calcium hydroxide enters to the ceramics aggregates and react (Nežerka et al. 2015)

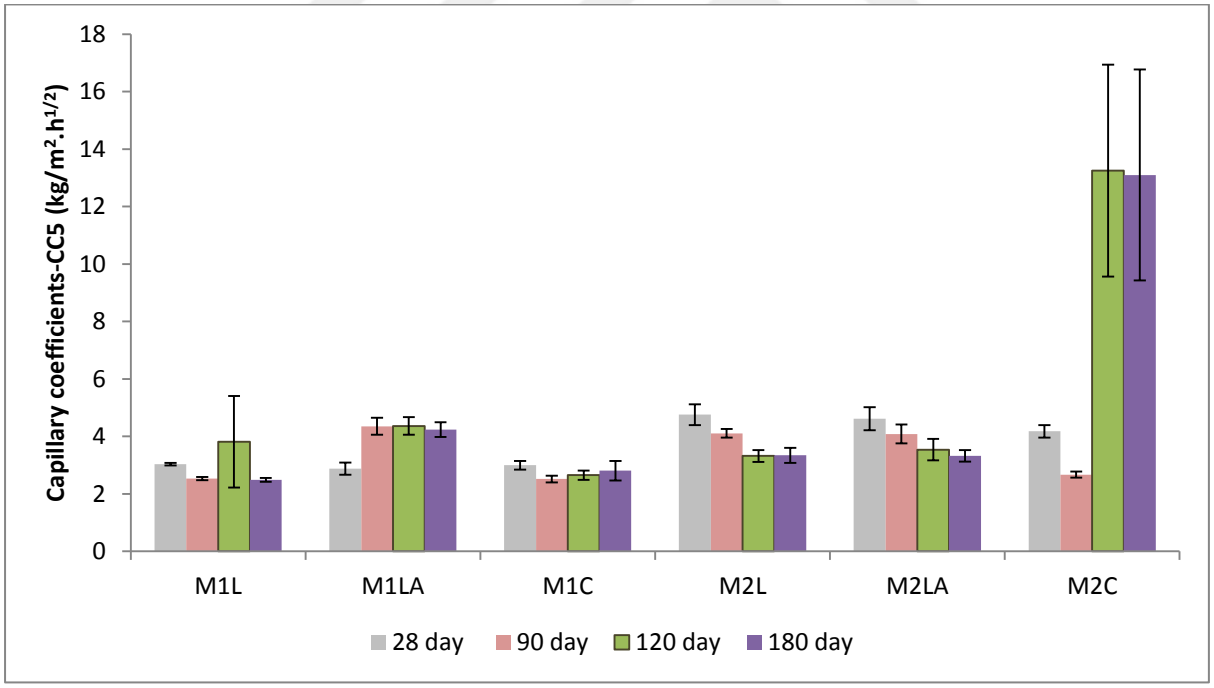


Figure 5.3- 54. Capillary coefficients of samples at 5 minutes

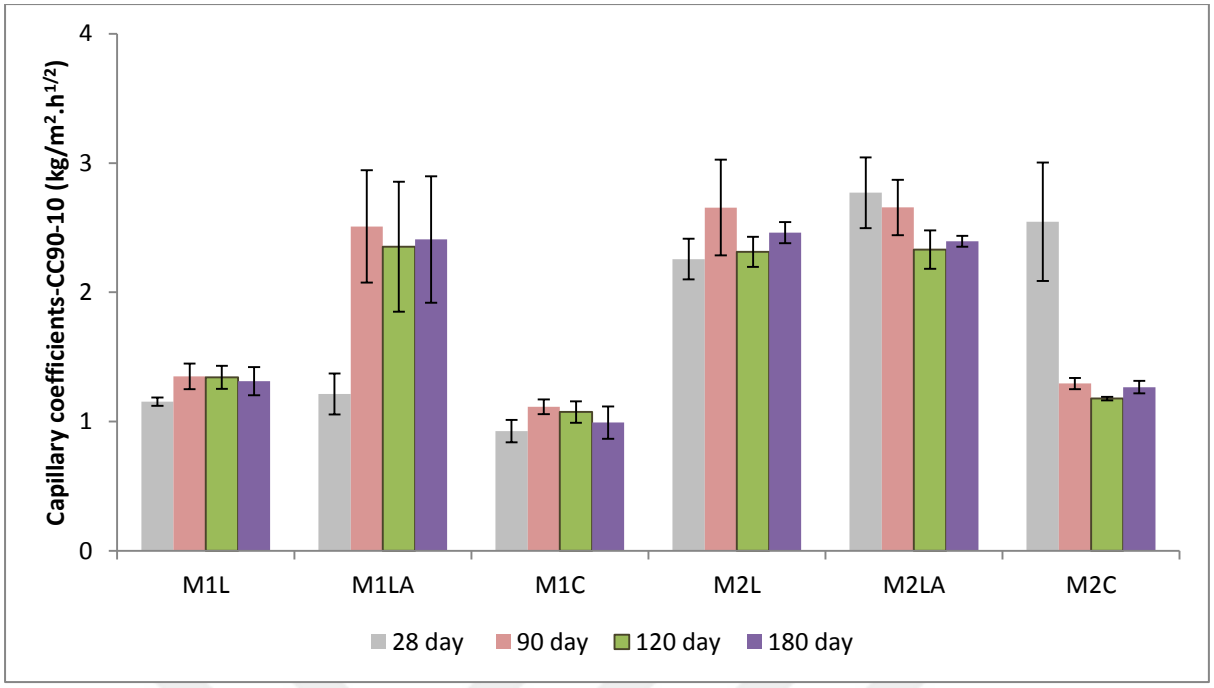


Figure 5.3- 55. Capillary coefficients of the samples between 10 and 90 minutes

Obviously, water absorption through capillarity is related with the open porosity and capillary pores (Veiga et al. 2004) and also directly related to temperature (Karagiannis et al 2016). In our case the measurements were done in the laboratory conditions with same temperature this factor was negligible. At 120 days the increase in the macropores (around 100 µm) of M2C should be responsible for the increase in early capillarity. Likewise, the increase in capillary rise in M1LA mortars were associated to the number of pore sizes between 8 and 20 µm at 90 days and overall increase in average pore size diameter towards 180 days (Figure 5.3- 20).

5.4 Results of mechanical tests

Flexural and compressive strengths were started to be done after 90 days.

5.1.9 Flexural Strength in 90, 120 and 180 days of curing

As shown in Figure 5.3- 56, 90 day-cured samples M2L and M2LA had slightly higher flexural strength (1.1 MPa), at 120 days only sample M1L shows a few increments and at the end of the 180 days M1L, M1LA, M2L exhibit the same force with 90 days, the others had ever-decrease if the slight increase of M2C was ruled out.

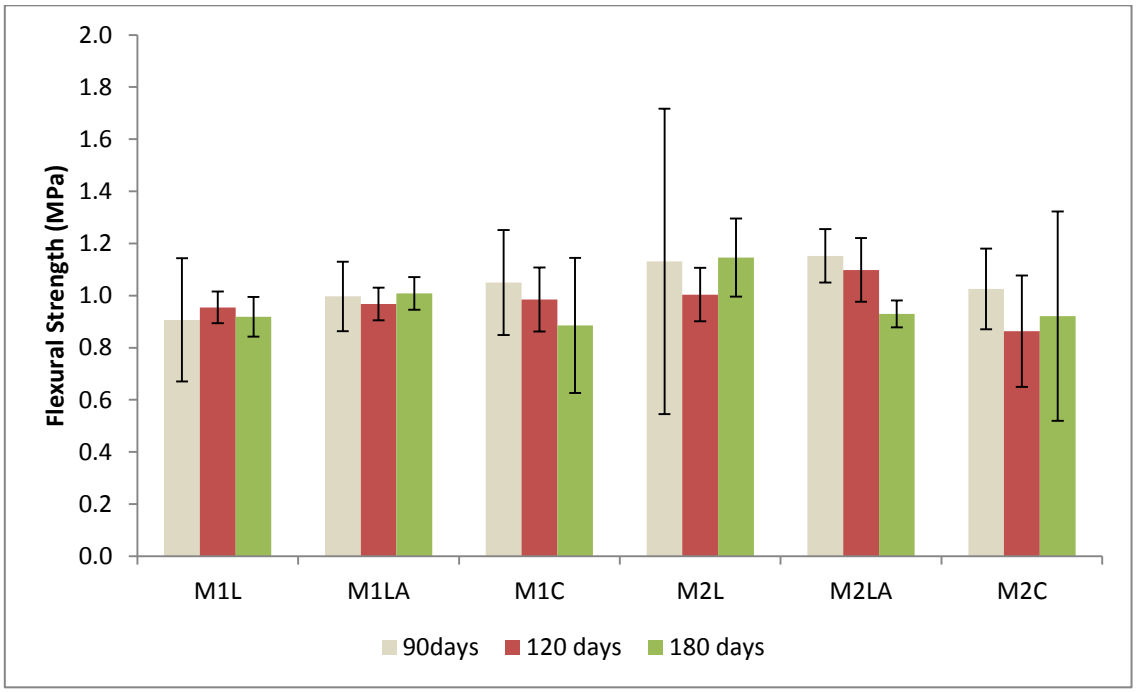


Figure 5.4- 56. Flexural strength values of the samples

5.1.10 Compressive Strength in 90, 120 and 180 days of curing

In the experimental time lapse, there was no significant change in the compressive strength of the mortars. This indicates that the strength which was gained at early age hardening, remains. As it is seen in Figure 5.3- 57, the uniaxial compressive strength values of M1 mortars were around 1.5 MPa.

At 90 days M2LA had highest (2.1 MPA) values then M2C follows it with 1.8 MPa. M1 mortars and M2L shows compressive strength around 1.5 MPa. The strength was supposed to increase

with the decrease in porosity (Moropolou et al. 1997; Lanas et al. 2004, Seabra et al. 2006). Nevertheles, in the samples M1L, M2LA and M2C the opposite of this trend was observed. After 180 days highest flexural strength was seen in M2C which was the same value of 90 days. Although M2LA mortar begins with the the highest strength, after the continous fall the end of 180 days strength was as low as M1 mortars. The strength reduction may be related to the cracks formed due to shrinkage that affects strength and more significantly the flexural strength (Lanas and Álvarez Galindo, 2003; Farinha et al. 2015)

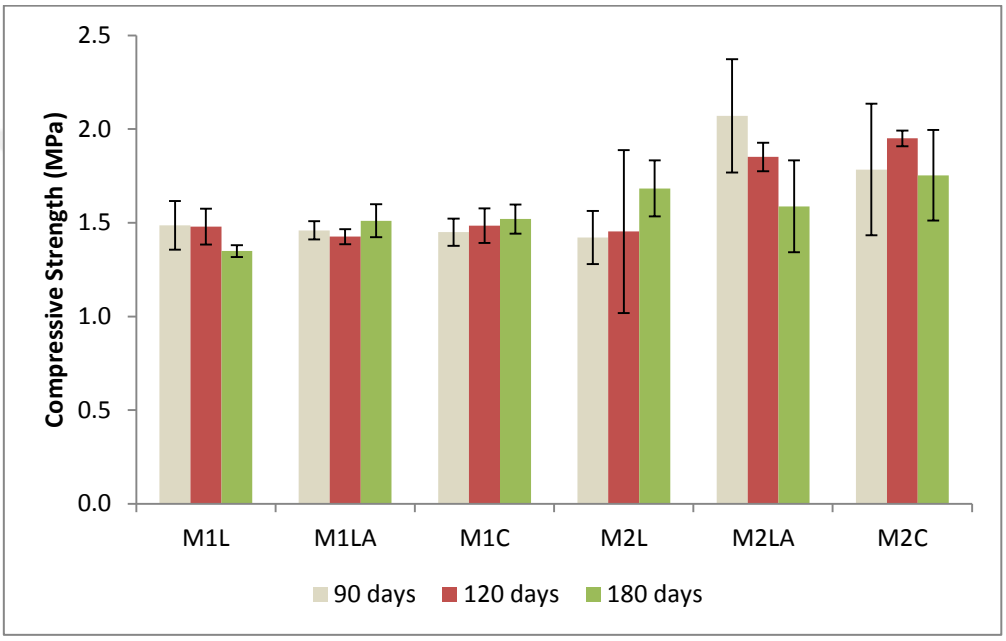


Figure 5.4- 57. Compressive strength of the samples

When we look at Figure 5.3- 58 comparing the uniaxial compressive strength and modulus of elasticity, the different tendencies of M1 and M2 mortars can be observed. As they had similar strength values, M1 mortars had higher elasticity and increase in time in all of the curing conditions. On the other hand, M2 mortars having lower elastic modulus values fluctuate in the compressive strength while no change occur in elasticity.

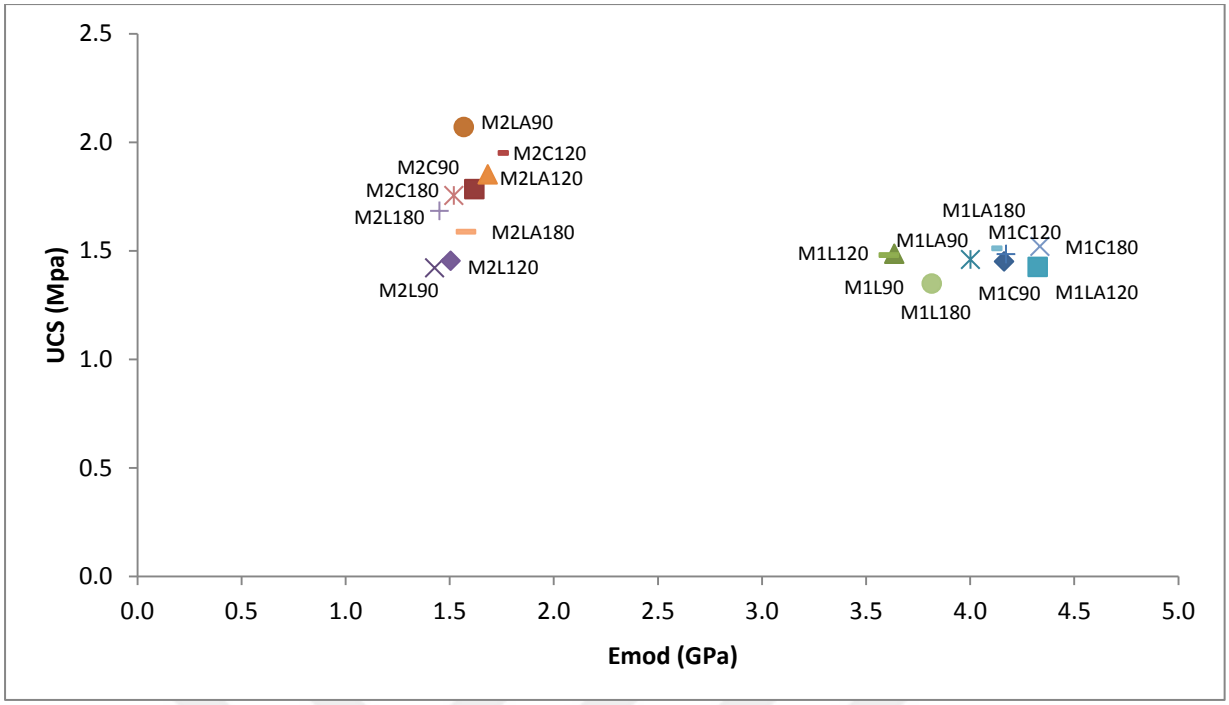


Figure 5.4- 58. Uniaxial compressive strength (MPa) vs modulus of elasticity (GPa) graph

As long as stable compounds form, porosity reduces and strength of mortar increases (Papayianni et al. 2001). Amorphous silica that was present in Roman bricks can promote the chemical reaction between the hydrated lime and ceramic and also the physical contribution to the bond (Franquelo et al. 2008; Stefanidou et al. 2015, 2016) justifying the better mechanical characteristics of M2 mortars. The fall in strength may be due to siliceous aggregates selection, because calcareous aggregates contribute to better bonding to lime matrix, so that results in higher strength and prevents cracking and consequent strength fall (Lanas et al, 2004).

C-S-H formations contribute more than $CaCO_3$ phases in the mechanical strength development of mortars (Çizer et al, 2010). Immediately after hydration reaction, when the carbonation reaction occurs both on the lime and on the hydrated phases, cause their decalcification, in other words, formation of more calcium carbonate (calcite and aragonite) crystals. Even though the open porosity was lowered by calcium carbonate crystals, the strength of mortars was significantly reduced (Çizer et al, 2010). Not so high

pozzolanic reactions have occurred because of the dry curing conditions, the higher fall in the strength of M2LA mortars could be ascribed to decalcification of the hydrated phases or to shrinkage.

6 Discussion of the Experimental Part

This chapter discusses the results of the tests that were repeated at 28, 90, 120 and 180 days of carbonation.

In the case of the Roman mortars, a different classification was made depending on two clearly distinguishable features such as the presence or absence of ceramic material during the elaboration. The procedure for studying the different types of mortar varies according to the characteristics of each one. *Opus signinum* type mortars, which were imitated conserving both the original material and their proportions, were prepared using the proportion and original Roman ceramics from the Complutum archaeological site. The repair mortars imitating the Roman mortars were cured in three different conditions. The first group was cured in laboratory conditions; the second was treated using an accelerator product, which was sprayed on the samples and exposed to laboratory conditions. The last group was cured in a climatic chamber with higher CO_2 exposure. It is important to keep in mind that the laboratory conditions were on average of 34% relative humidity, 25°C temperature and 703 ppm CO_2 concentration with little fluctuations. Meanwhile, the climatic chamber conditions were kept constant quite different from the natural carbonation process (60% RH, 20°C T and 1600 ppm CO_2) (Table 2.2-9). This chapter evaluates the results of trials.

Optical Microscopy: At 180 days, secondary calcite precipitation around the aggregates and inside the cracks was clearly observed in the samples of M1LA and all of the M2 mortars . In M1L, no significant change was recorded, whereas especially in the M2LA and M2C mortars the filling of the pores and cracks by re-precipitation of calcium carbonate were noted. Lubelli et al. (2011) claim that for this phenomenon primarily the dissolution is necessary and since the solubility of portlandite is much higher than that of calcium carbonate, it is expected to occur more in not-fully carbonated mortars.

XRD: In the XRD analysis, the main concern was to monitor the increased amounts of calcite and reduced amounts of portlandite in the samples. As a result, the decrease in portlandite was more visible than increase in calcite. Deviances at 90 and 120 days were observed, but found to be negligible. The highest rise of calcite was reached at 180 days in M1 mortars exposed to high CO_2, while in M2 version of chamber cured mortars the decrease in portlandite was higher. Overall, higher decrease in portlandite peaks were barely observed in chamber and with accelerator samples. Vaterite, a metastable polymorph of $CaCO_3$

(JCPDF 33-0268, a=7.147, c=16.61Å) with hexagonal symmetry was detected in the X ray diffraction profiles. In addition, the presence of aragonite, the orthorhombic variety of $CaCO_3$ (JCPDF= 760606, A=4.959, b=7.964, 5.737Å), more stable than the vaterite phase, was also detected both in the sample treated with DiloCarB (LA sample) as in the sample without any treatment (L sample) but exposed to laboratory conditions. However, some traces of both polymorphs were detected in XRD patterns, in the mortars inserted in the chamber (C sample) at early stages as well.

As decrease of portlandite and increase of calcite are not so pronounced in neither of periods, evaluation can be done through the presence of other calcium carbonate polymorph peaks (Table 6.1). In the M1L sample, at 28 days, vaterite peak, and then at 90 days, aragonite peak were detected. In later periods, no peaks of metastable polymorphs were seen. Keep in mind that, the absence of the peaks does not mean the absence of the crystals; however, it shows that the amount is not high enough to pass the XRD detection limit (4-5 %). The same was observed in M1LA, but there were two aragonite peaks at 120 days. The M1 sample that is cured in chamber had vaterite peaks at early periods and an aragonite peak at 120 days in the XRD graphs. In the samples with ceramic inclusion, the L and LA samples showed high amount of aragonite in all periods, and the same type of mortar cured in chamber at 28 days showed no peaks of metastable polymorphs. Two aragonite and one vaterite peaks were seen both at 90 and 120 days and at the end of 6 months only aragonite was present. Considering the fact that vaterite is less stable than aragonite, mortars with ceramic inclusion have advanced carbonation with an abundance of aragonite peaks. It is likely, that the absence of these peaks implies a more stable carbonation. In this sense, all M1 mortars had stable calcite crystals in the last period. Among M1 mortars, carbonation seems to take place in this order: C, L and LA, regarding the fact that the early calcite peaks (intensity and increase throughout the curing ages) were higher in C samples, and the L samples showed more progressive evolution in crystals than the LA samples.

Examination of the M2 mortars found that the chamber cured samples have higher amounts of calcite and show advanced carbonation regarding metastable polymorphs as well. Already at 28 days, the only present calcium carbonate polymorph was calcite. In the following periods other polymorphs appeared, and the number of peaks of aragonite was higher than vaterite whenever present. Among the other mortars, calcite peaks were low, and there was an abundance of aragonite, however, more stable carbonation can be inferred from the LA samples.

Table 6.1. The presence of metastable calcium carbonate peaks in XRD patterns (A: Aragonite and V: vaterite, the number of letters indicates the intensity and number of peaks)

	M1L	**M1LA**	**M1C**	**M2L**	**M2LA**	**M2C**
28 days	V	V	V	A A A A V	A A A	-
90 days	A	A	V	A A	A A A	A A V
120 days	-	A A	A	A A A V	A A A	A A V
180 days	-	-	-	A A A	A A V	A

TGA: The samples showed anomalies between 90 and 120 days. Lime consumption in the chamber cured M1 mortar was slightly higher than laboratory cured sample at 28 and 90 days; however the calcium carbonate formation is remarkably higher than others resulting the highest formation after 6 months of curing. It is important to note that, metastable polymorphs (vaterite, aragonite and ACC) decompose at the same weight loss temperature range associated with portlandite (Morandeau et al. 2014). Weight loss due to the evaporation of hygroscopic water was higher in the M2 specimens that included ceramic, which correlates with the amorphous phases seen in the XRD of ceramics.

Portlandite was not consumed that much in the M2L mortars in the early stages, while calcium carbonate formation was relatively higher. In the M2C mortars, it was clear that both the consumption of portlandite and calcium carbonate formation is high.

M2C had the highest carbonation ratio ending at 96%, and M1C follows in the earlier periods, but ended up with 80% like others. Among the other samples, carbonation began around 30% and ended up at approximately 80% carbonation.

SEM: The expected crystal evolution is for platelet and hexagonal portlandite crystals (Rodriguez Navarro et al. 1998; Cazalla et al. 2000) to turn into scalenohedral and then rosette shaped calcite crystals in advanced ages (Çizer et al. 2012a). The scalenohedral shape crystals transform from amorphous $CaCO_3$ crystals as a result of the dissolution re-precipitation phenomena with an excess of Ca^{2+} ions in a CO_2 rich environment (López Arce et al. 2011; Gomez Villalba et al. 2011; Çizer et al. 2012b). In the carbonation of the mortars,chamber cured samples are pioneers in crystal evolution. Even at 28 days scalenohedral calcite crystals formed next to the platelet portlandite crystals, with small ball-shaped vaterites above them and rarely dispersed needle-like aragonite crystals. In M2, the shape of the calcite crystal was likely to be short rhombohedral, but still the sharp edge was clearly seen and at 120 days transforms into tabular form. At 180 days, the microstructure changed, and plaques of amorphous calcium carbonate (ACC) appeared connected to aragonite flakes, where scalenohedral calcites were present on cauliflower shaped portlandites. In M1, tabular calcite crystals did not change their form, but at the end of 180 days they had more rounded edges. Decreasing porosity was better observed in chamber cured samples during the SEM observations. Anhydrous calcium carbonate polymorph aragonite was abundant in later stages developing acicular crystals. Vaterite, the metastable calcium carbonate polymorph, was present on top of portlandite crystals since it has a slower growth rate and attaches to the larger crystals (Gomez Villalba et al. 2011). Regarding the sizes of the formed crystals in chamber cured samples well-shaped scalenohedral calcite crystals were slightly getting smaller in M1 mortars and larger in M2 mortars (Table 6.3).

Lower humidity curing of the samples caused not very well defined crystal morphologies (Nezerka et al. 2014). The relevant research states that scalenohedral crystals transform into

rhombohedral crystals when exposed to high CO_2 (Table 6.2). However, the CO_2 exposure and relative humidity were higher than they were in our study. In laboratory conditions with little fluctuations low humidity is present and is not favorable for the formation of stable polymorph calcite. Therefore, in the early stages as the majority of the detected calcium carbonate crystals were aragonite and vaterite in the pseudo-hexagonal shape and platelet portlandite crystals. Nevertheless, at 120 days very well shaped scalenohedral crystals formed even though the RH is low, higher CO_2 concentration should have influenced it. An environment with low moisture content prevents the transportation to inner pores causing calcium carbonates to form on the surface of the portlandite crystals (Thiery et al. 2007; Morendou et al. 2014).

Accelerator created rounded shape crystal habit in M1 mortars, which were highly obvious at 90 days. Later on, they turned into rounded edge scalenohedral-like crystals at 120 days. Like the chamber cured M2 samples, ACC appeared at 180 days next to the portlandite, vaterite, aragonite and calcite crystals. In M2 mortars, aragonite, vaterite and portlandite were present in the early stages of curing, later on ACC formation next to needle-like aragonite was seen at 120 and 180 days like the M2L120 and M2C180 mortars. Scalenohedral calcites were dispersed on top of the portlandite crystals. Consequently, the effect of the accelerator on the microstructure was more visible in M1 mortars. In accelerator sprayed samples, crystals increased in size in M1 mortars fluctuated in M2 mortars. Acicular aragonite crystals were always present every time and the lengths of the crystals were changing. Note that, in the consolidations, manufacturer recommends to use DiloCarB after the product CaloSil. The research of Arizzi et al. (2015) found that CaloSil leads 1.8-2.8 μm aciform aragonite crystals and nano-size tabular calcite crystals, and in the research of Gomez-Villalba et al (2011; 2012) 2.2 μm size aragonites and nano-size rhombohedral calcite crystals were detected. Apparently, without the precursor nanolime Calosil, single use of DiloCarB causes larger crystals even in low relative humidity curing conditions.

Table 6.2. Calcite crystal shapes in the mortars at different curing times (- : calcite crystals were not detected)

	M1L	**M1LA**	**M1C**	**M2L**	**M2LA**	**M2C**
28 days	-	-	Scalenohedral	-	-	Rhombohedral
90 days	-	Penthagonal	Scalenohedral	-	modified Scalenohedral	Prismatic
120 days	Scalenohedral and modified Scalenohedral	modified Scalenohedral	Rhombohedral	Scalenohedral	Scalenohedral	Tabular
180 days	modified Scalenohedral	modified Scalenohedral	modified Scalenohedral	modified Scalenohedral	modified Scalenohedral	Tabular and modified Scalenohedral

The crystallinity and stability of the deposited calcium carbonates are influenced by surface tension fluctuations, water ratio, and energy released from the reactions (Gomez-Villalba et al. 2011). Unstable polymorph aragonite and vaterite were frequently seen in all samples. Aragonite was rarely detected in chamber cured samples at 28 days, but was detected in large sizes whenever present (larger in M1). In the later stages of curing ,the length of the acicular crystals decreased. In the laboratory cured samples no calcite was detected at early stages and, at 120 days scalenohedral shape calcite crystals were observed (Table 6.2). At the end of six months, portlandite crystals were still detectable with hexagonal forms in all of the samples and higher amounts in the L samples. Larger calcite crystals (3 μm) were found in M2C and M1LA, and the largest aragonite crystal were found in M1C.

Table 6.3. Crystal sizes of the repair mortar samples at different stages of curing (P: portlandite, Ca: calcite, Ar: aragonite, V: vaterite, ACC: amorphous calcium carbonate)

	M1L	**M1LA**	**M1C**	**M2L**	**M2LA**	**M2C**
28 days	3 μm (P) 1-2 μm (Ar) 40nm-1 μm (V)	3 μm (P) 50 μm (Ar) 0.5 μm (V)	1 μm (P) 2.5 μm (Ca) 50 nm (V) 16 μm (Ar)	1-2 μm (P) 10-50 μm, 0.2 mm (Ar) 0.3-0.5 μm (V)	2-3μm (P) 10 μm (Ar) 0.6 μm (V)	1-2 μm (P) 1 μm (Ca) 40nm-1 μm (V) 50 μm (Ar)
90 days	2.6 μm (P) 4 μm (Ar) 0.5 μm (V)	0.5 μm (V) 10 μm (Ar) 1 μm (Ca) 3 μm (P)	1 μm (P) 2.5 μm (Ca) 5 μm (Ar) 0.3 μm (V)	2 -3 μm (P) 0.3 μm (V) 5 μm (Ar) 10 μm (ACC)	1-2 μm (ACC) 8 μm (Ar) 2.5 μm (P)	1-1.5 μm (Ca) 50nm-1 μm (V) 1 μm (Ar)
120 days	1.5 μm (Ca) 0.3 μm (V) 5 μm (Ar) 3 μm (ACC)	1.3 μm (P) 1 μm (Ca) 5 μm (Ar) 0.4 μm (V) 5 μm (ACC)	1-2 μm (P) 5 μm (Ar) 0.3 μm (V) 1-2 μm (Ca)	2.5 μm (P) 10 μm (ACC) 7 μm (Ar) 1.5-2 μm (Ca)	1.5-2 μm (Ca) 5 μm (Ar)	1 μm (Ca) 8 μm (Ar) 0.3 μm(V) 1 μm (P)
180 days	1-2 μm (Ca) 4 μm (Ar) 0.3 μm (V) 1-2 μm (P)	3 μm (Ca) 5 μm (Ar) 0.3 μm (V)	1-2 μm (Ca) 6 μm (Ar) 0.3 μm (V) 3 μm (ACC)	2μm (P) 4 μm (Ar) 0.3 μm (V) 1-2 μm (Ca)	1 μm (Ca) 2 μm (Ar) 1-2 μm (ACC)	3 μm (Ca) 5 μm (Ar) 0.3 μm(V) 6 μm (ACC)

As Table 6.3 shows, crystal sizes were highly variable with larger aragonites and smaller vaterites. This can be associated with the Ostwald ripening phenomenon in which smaller crystals having higher solubility stick to the larger crystals that absorb them. New $CaCO_3$ has a tendency to precipitate on the larger crystal and smaller crystals continue to dissolve in order to reach the equilibrium. Thus it is possible for larger crytals to get larger while smaller ones get smaller (Gomez-Villalba et al. 2011).

Contrary to expectations, no pozzolanic activity products, C-S-H peaks, were observed in the X ray diffraction patterns even in the climatic chamber with higher humidity conditions. Nor

were they detected by the SEM analyses;however, other larger crystals could have masked the very small size of the C-S-H crystals. The use of low temperature-fired Roman bricks in addition to the use of both dust and fragments increased our understanding of the complexity of the microstructure and crystal growth. Nevertheless, it is clear that their presence in the mortar with chamber curing (higher RH and CO_2) caused better defined crystal morphology and a more compact matrix (Figure 6.1 - Figure 6.3).

Complutum regional geology includes clay content, among which illite, smectite, chlorite and kaolinite are the clay minerals reported by previous studies (Martinez Garrido et al. 2016). The ceramics used in the M2 mortars contained those clay minerals, and their transformed mineral phases provide information about their manufacture. The presence of high temperature mineral mullite which is transformed from kaolinite,and presence of gehlenite, a reaction product of illite and calcite, together with calcite and mica are the indicators of the firing temperature ranges (Barluenga et al. 2014; Matias et al. 2014a; Böke et al. 2006; Cultrone et al. 2004). In addition, the presence of hematite indicates the open air firing of the ceramics. Roman tiles were fired at temperatures above 900˚C (Figure 2.2-45), while Roman bricks were fired at lower temperatures between 800 and 900 ˚C (Figure 2.2-46). Firing tiles at high temperatures changes the amorphous structure of clay crystals and reduces the surface area and thus pozzolanicity as well (Böke et al. 2004). It can be observed that the humps between the 20 and 35 θ in the XRD patterns due to the vitrified amorphous calcined clay minerals are low (Figure 2.2-45,46).

The inclusion of clay rich Roman ceramics, which include several types of aluminosilicates, causes reactions with the lime binder and improves bonding (Böke et al. 2006); however the combined use of both tile and brick which have different levels of amorphous phases reduce the possibility of the formation of pozzolanic reaction products.

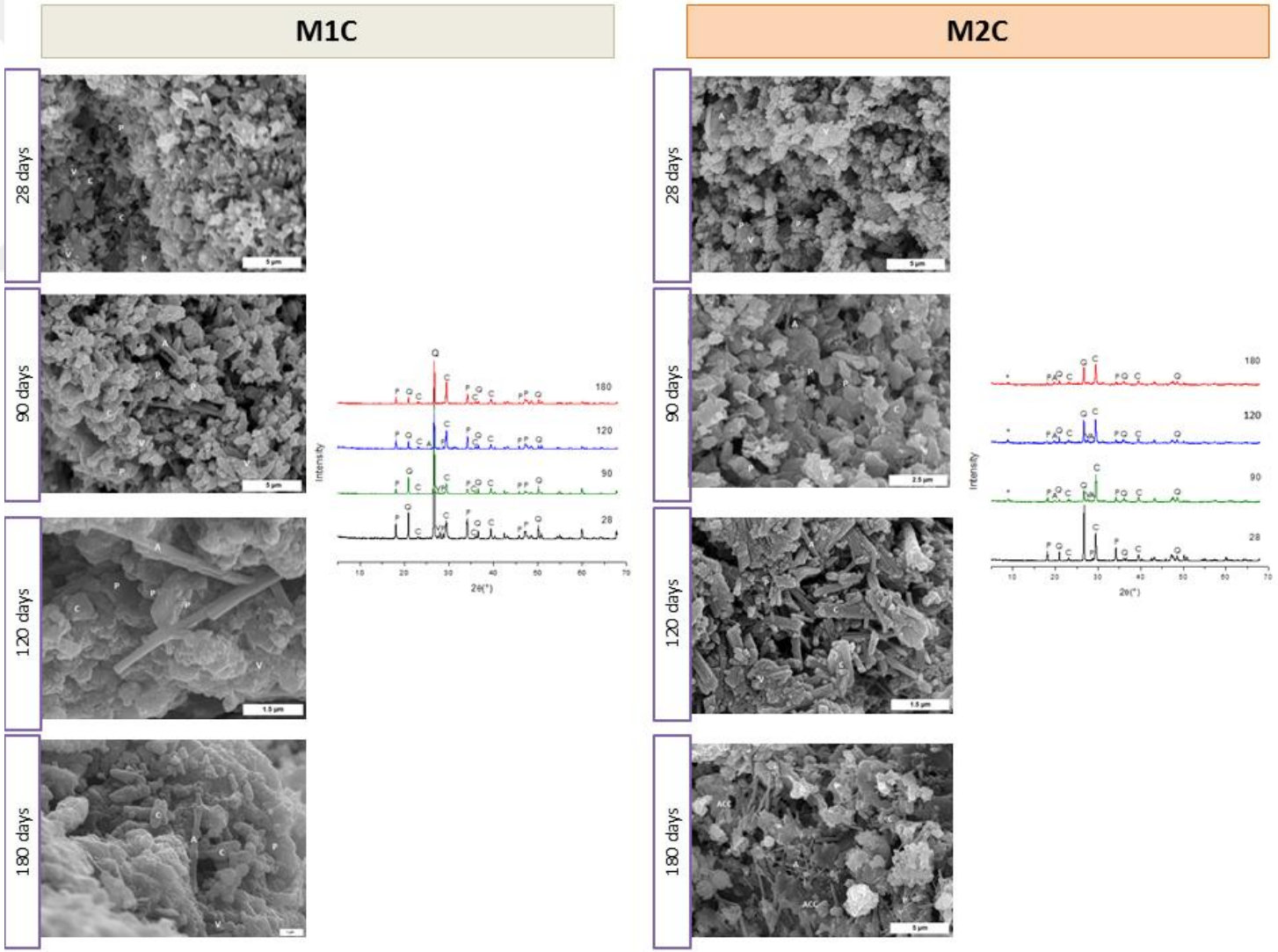


Figure 6.1.The evolution of carbonation of chamber cured mortar samples as determined by SEM and XRD

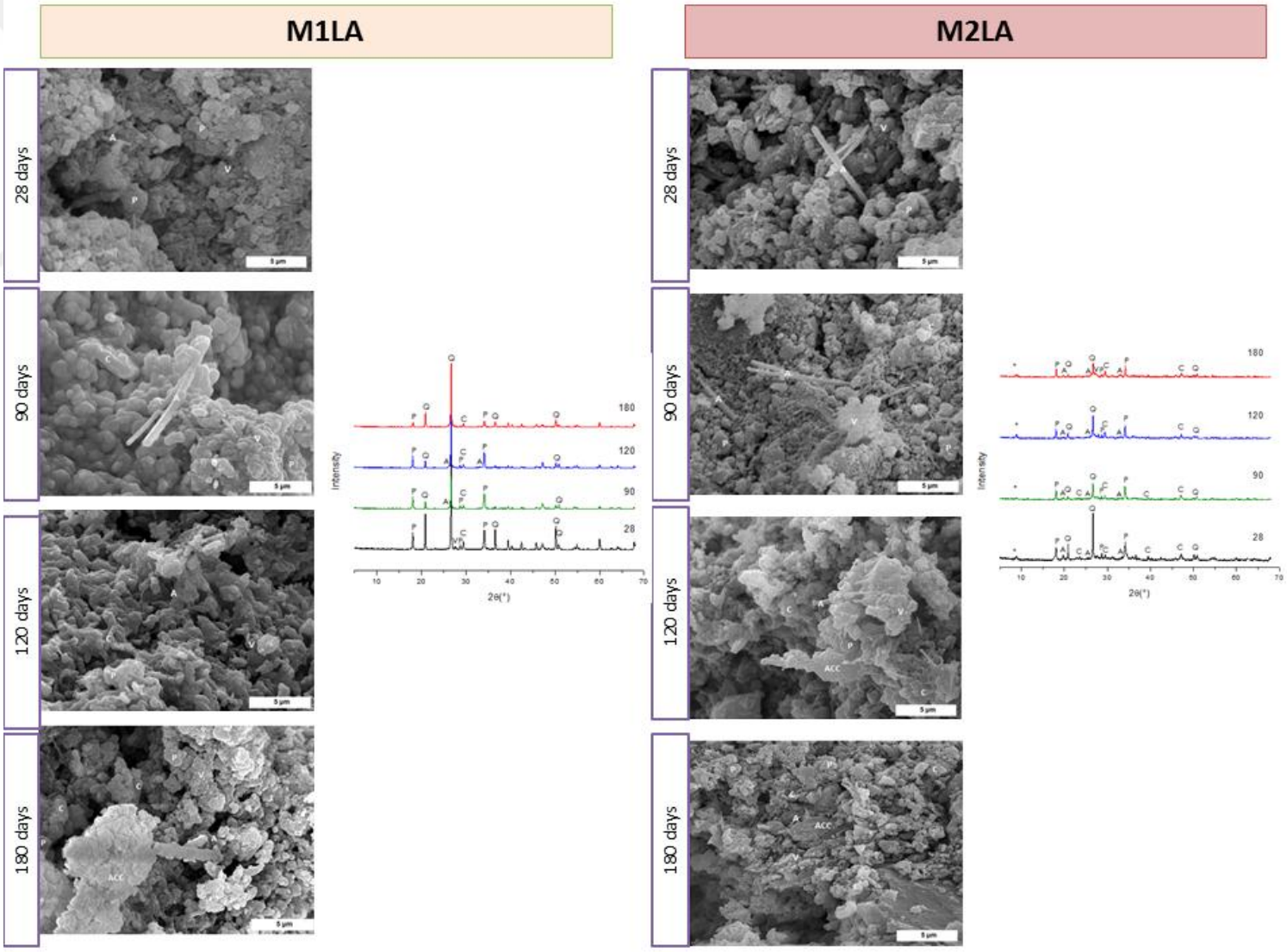


Figure 6.2. The evolution of carbonation of mortar samples with accelerator as determined by SEM and XRD

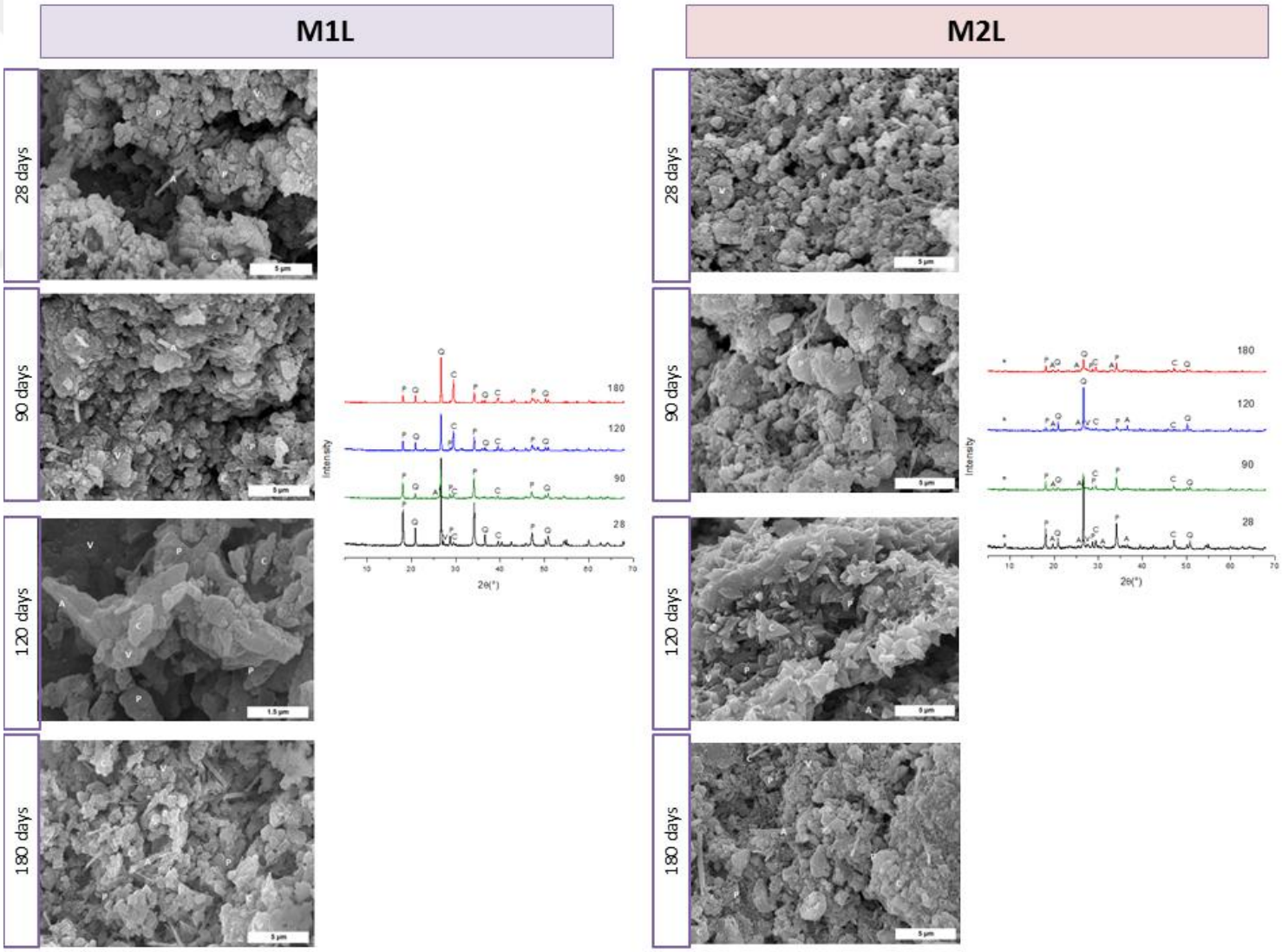


Figure 6.3. The evolution of carbonation of laboratory cured mortar samples as determined by SEM and XRD

Phenolphthalein: From 28 days mortar specimens cured at climatic chamber especially with ceramic inclusion show discernible carbonation front, on the other hand others have still hot pink in colour. At 28 days, the distinction between the pink zones associated with uncarbonated portlandite was in the core of the specimens, while in the rest of the periods the off-colour was dispersed on all measured surfaces. The other reason for not observing the sharp colour difference could be related to the presence of additives and aggregates. Lawrence (2006) and Cazalla et al (2000) did not find any significant colour change in their experiments with different aged lime putties before six months. This study's turn out colours imply that the exposure of CO_2 had a catalyser effect with phenolphthalein. On the other hand, keep in mind that, this method has drawbacks; as phenolate group in the phenolphthalein structure is deformed in the basic zone pH between 9 and 11.5 and cannot detect carbonation (Ŝevčík et al. 2016). As state Morandeau et al (2014), the $CaCO_3$ forming around portlandite prevents the absorption of the Phenolphtalein.

MIP: As expected due to the ceramic dust and fragment inclusion and the more porous ceramic aggregate, the M2 mortars had higher total porosity and specific surface area. In laboratory cured samples, porosity fell in M2 and rose in M1 specimens due to increased cracks. In M2 mortars, the amount of the pores between 1 and 0.01 μm are higher whereas in M1 mortars the intensity of the two models was the same. In the M2 mortars, the number of the macropores (100-10 μm) was lower than it was in the M1 mortars, and their size and amount decreased with age. This was probably due to better bonding between ceramic aggregate and lime. The calcium carbonate precipitates in the small pores (Arandigoyen et al. 2005). In the chamber cured specimens, at 180 days, micropores between 0.1 and 0.01 μm occurred, which is an indicator of connecting micropores since pores below 0.1 μm are not affected by carbonation (Lawrence et al. 2007). In M2LA, the number of micropores (< 1 μm) was higher at early ages and then slightly decreased. Sorption pores below 0.1 μm decreased at 180 days. Increasing numbers of capillary pores weaken the material (Lawrence, 2006). Surely, the formation of different calcium carbonate polymorphs makes a difference in the pore morphology and porosity as well. The SEM analysis found that the

pores are interconnected, and their sizes have a tendency to diminish with advancing carbonation.

Surface hardness: It is expected for surface hardness to increase as carbonation starts in the outer zones. There was no significant increase in any of the samples, except with the use of the accelerator. However, this is still not so remarkable. Among the M1 mortars, M1LA and M1C had similar values at 28, 90 and 120 days, which were higher than M1L; however the value fell more for sample M1C at 180 days. In sample M1LA, a higher hardness was reached from the beginning of the carbonation process, which was maintained over time. In the case of the M2 mortars, curing in chamber seemed to be favorable for carbonation and accordingly surface hardness from the early periods; however, with the accelerator there are significant increases in time for both of the mortar types. The increase in surface hardness until 180 days and then sudden decrease show that cracks occur in the interior of the mortar specimen until 6 months, while at 6 months superficial cracks occur as well. M2LA is not included in this hypothesis since its surface hardness increased continously. The cracks revealed from other analyses show that the fissures and cracks do not reach the surface.

Air permeability: The increase in air permeability may be due to the increase in total porosity since the change in pore sizes between 0.1 μm and 1 μm influences it (Arizzi et al. 2012). In concordance with the porosity results, the M2 mortars had general higher air permeability than the M1 mortars. M2C showed an increase in permeability between the initial and the final days reaching the highest value. It should also be underlined that the standard deviations of the M2 mortars were higher, especially in the chamber cured mortars, which indicates the inhomogeneity of the samples. From the standpoint of curing condition, the samples were consistent with each other. The mortar samples with accelerator and the chamber cured samples showed non-linear increases, and the other mortar samples cured in the laboratory showed steady increases until a sudden interruption at 180 days. This should be related with calcite formation at later ages. Furthermore, it was confirmed that macropores between 80 and 100 μm were getting disappearing at 180 days, which reduces air permeability as well.

UPV: During carbonation, velocity increase was recorded for the M1 mortars. TheLA and C mortars had slightly higher values in all periods until 180 days. This is a contradictory result considering the SEM analysis. At the ultimate age, the M1 mortar samples have abundant stable calcium carbonate crystals. Change in the microstructure should have generated cracks, and thus the velocity slightly decreased. The M2 mortars cured in laboratory conditions (L and LA) showed fluctuations probably due to the abundance of unstable calcium carbonate polymorphs and the chamber cured sample (C) show higher velocity at 28 days due to stable calcite formation. In the rest of the carbonation days, the velocity decreased and was similar to the others' low values and fluctuiations. The same phenomena could have occurred, and the fissures and cracks generated by stable calcite formation should be related to the fall of velocity. The velocity of calcite is higher than that of portlandite; however, the velocity of other present $CaCO_3$ polymorphs and the transitions between them should have an influence on ultrasonic velocity. Mineralogical composition, texture, density, porosity, compactness and environmental conditions (humidity, temperature) are the factors that affect velocity (Fort, 2008). In M1 mortars, the velocities of the minerals portlandite, calcite, vaterite, aragonite and ACC can be ascribed to velocities gathered from the binder, and the velocity of quartz can be considered velocities of aggregates. On the other hand, the high number of ingredients and the different size and form of crystals in the M2 mortars should be kept in mind. The same mineral velocities for the binder and the velocities of quartz, anorthite and clay minerals played a role as well. The addition of fine dust ceramic particles also increases the velocity (Fort, 2008). Researchers report that pores in the binder and the carbonation degree are the determinants for ultrasonic velocity (Arizzi et al. 2013). The MIP results correspond did so in the M1 mortars since silicic sand aggregate is not porous;however, porous ceramic aggregate in the M2 mortars once again complicated the issue. Although the carbonation degree was higher in M2 mortars, the propagation waves had a whole range of labyrinth-like paths to follow. The early age pronounced velocity of M2C and the subsequent decrease were also in concordance

with the other studies (Arizzi et al. 2013). At 28 days, the degree of carbonation was already 80% and the acceleration of carbonation degree deceased.

Weight gain: The weight of carbonate is 35% higher than hydroxide (Lawrence, 2006). Hence, the evolution in carbonation can also be followed by increase in weight. Ceramic is a lightweight aggregate. Therefore, M2 mortars are lighter than M1 mortars and showed higher weight increase, which indicates higher carbonation rates. M2C was by far the first, despite the immobility it showed between 90 and 120 days. On the other hand, surprisingly, M1C seems to be the least carbonated according to this approach even though the other analyses do not support this. The discrepancy between tests might be related to the micro weight of crystals and interconnection of the pores.

Water absorption capacity under vacuum: In the M1 mortars, slight decreases were observed at the end, while higher decreases occured in M2 mortars with sudden falls at 180 days of carbonation and consistently reduced water absorption capacity. At 28 days, the saturation of M2LA had the highest values and after steady decreases at 90 and 120 days ended up a little higher than M2L. On the other hand, M2C did not show a significant decrease.

Water absorption through capillarity: The M2C mortars showed high early capillarity at 120 and 180 days, which implied weakness caused by larger pores or connected cracks. The increase in the porosity and macropores at 120 days are indicators of the cracks that caused higher 5 minutes capillary coefficient. With capillary coefficients varying between 90 and 10 minutes at 28 days, the M2 mortars showed higher capillarity than the M1 mortars. According to capillarity, the M1L and M1C samples had better performance; however, the carbonation of the samples with ceramic inclusion was advanced.

Flexural and compressive strength: The M1 and M2 group mortar samples did not show very different strength values, and no significant change were recorded in 6 months. Early gained strength was conserved, and slight changes occurred due to generating cracks. Especially the mortars with ceramic inclusion were expected to have increased strength due to the

increase in carbonation (González Cortina, 2000). Unexpectedly, at advanced ages, the flexural strength of the samples fell in the M2LA, M2C and M1C samples. Although the change was not so significant, it was probbaly due to the cracks generated during accelerated carbonation. Nevertheless, it is necessary to point out that higher CO_2 exposure had a slightly negative effect on the mortars with ceramic inclusion. The M2C samples had lower flexural strength than other mortars of the same type. Apart from the cracks and fissures due to accelerated carbonation, crystal morphology played a role, too. Apparently, prismatic and tabular formed crystals cause lower flexural strengths (Table 6.2). In compressive strength, the highest values and highest falls were seen in mortars with ceramic inclusion and then the accelerator and chamber cured samples. The M1 group did not show a significant change, but the chamber cured samples showed a slight increase. The M2 laboratory cured sample was the only group increased compressive strength.

Consequently, the accelerator did not affect the mechanical strength so much when it was used only with sand aggregate. With ceramic inclusion the mortars showed higher values and higher decreases. Chamber curing did not affect compressive strength, but it did influence flexural strength negatively.

The mortars with coarser aggregates had lower porosities and capillary water absorption coefficients, but higher mechanical strengths (Lawrence, 2006). Mechanical strength values are important because repair mortar should have sufficient, but not excessive, strength. Low compressive and flexural strength ratios and low elastic modulus are preferred for repair mortars (Moropoulou et al. 2005). Veiga et al. (2001) report that the compressive strength of repair mortars should be between 0.4-2.5 MPa if used as rendering mortar, and the range for pointing mortars is 0.6-3 MPa at 90 days. Matias et al. (2014) found lower values for mortars with ceramic aggregates: between 0.2 and 1.5 MPa for compressive strength and between 0.2 and 0.3 MPa for flexural strength. Flexural strength is defined as 0.2-0.7 MPa for exterior mortars 0.4-0.8 MPa for pointing mortars (Veiga et al. 2001). In our case, compressive strength varied between 1.3-2.1 MPa which fits the range mentioned by other authors. Flexural strength values were between 0.9-1.2 MPa, higher than the upper limits mentioned

(Veiga et al. 2011; Matias et al. 2014). On the other hand, in the research of Çizer et al. (2010), theflexural strength of mortars cured in a humid environment were between 0.75-2.15 MPa. This result is surprising because the curing conditions were not humid enough in our study, and the water: binder: aggregate ratio may have influenced the higher fexural strength.

The M1L and M2LA compressive strength values fell in time. Increased total porosity resulted in falling compressive strength (Thomson et al., 2004). Related to the cracks generated by shrinkage, which especially affects flexural strength (Lanas and Álvarez Galindo, 2003; Farinha et al. 2015).

In repair mortars lower modulus of elasticity than the adjacent material is needed for concordance of movement. Modulus of elasticity values for rendering and pointing mortar are 2-5 GPa and 3-6 GPa, respectively (Veiga et al. 2011). Correspondingly, in our study; the M1 mortars with higher Emod (3.5-4.2 GPa) can be used as pointing mortars, while the M2 mortars with lower Emod (1.5-2.5 GPa) should be used as rendering mortars.

Considering the research questions asked at the beginning:

What are the factors that influence carbonation?

Carbonation is the process in which CO_2 diffuses from the open pores, dissolves in capillary pore water and reacts with $Ca(OH)_2$ to form $CaCO_3$ (Çizer et al. 2008). Supported by our experimental study as well, there are several factors that affectcarbonation (Figure 6.4). Porosity and pore size have determining roles in CO_2 transfer. Therefore, changing parameters such as water: binder: aggregate ratio influences porosity (Arandigoyen et al., 2005; Arandigoyen and Álvarez, 2007; Arizzi et al., 2013). The higher the binder ratio, the higher the carbonation produced. Nevertheless, a certain amount of aggregate is necessary since it prevents the formation of shrinkage cracks in the binder. In our study, the climatic chamber cured samples showed advanced carbonation; however, atlater ages,

deformation of the well-shaped crystals was also observed. A high concentration of CO_2 causes faster reactions, but this leads to the evaporation of capillary water due to the heat released by these reactions (Çizer et al., 2012a; Moorehead, 1986). This results in no more dissolving of diffused CO_2 apart from the blocking of the pores by carbonated crystals. Therefore, higher temperatures are not preferable due to the evaporation phenomena. The solubility of CO_2 also falls at higher temperatures (Cultrone et al. 2005) and the formation of calcium carbonate and hydraulic phases alters the microstructure. Thus, temperature and relative humidity, which have an effect on crystal size and morphology, also play crucial roles in carbonation . No crystalline $CaCO_3$ polymorphs were found other than calcite in the samples cured at conditions 20°C T 95% RH and 20% and 100% CO_2 concentration (Çizer et al. 2008), and 20°C T 60% RH and 450 ppm CO_2 concentration (Ševčík et al. 2016). Gomez-Villalba et al (2011) detected all three anhydrous and one hydrate polymorph in both 75% and 90% RH curing conditions and report that better crystallization is seen at former 75 % RH. In another study, aragonite was detected at 20 °C T and 50% RH atmospheric CO_2 environment (Martinez Ramirez et al. 2003). In our study, both in the chamber cured samples (20°C 60% RH and 1600 ppm CO_2 concentration) and in the laboratory cured samples (25°C 34% RH and 703 ppm CO_2 concentration) in the chamber cured samples at early curing ages well-formed scalenohedral calcite crystals were seen and aragonite appeared at later ages. Higher relative humidity together with CO_2 exposure favor stable crystallization. It can be concluded that higher RH (%) favors direct calcite precipitation without forming the precursor unstable crystals which can be regarded as better carbonation.

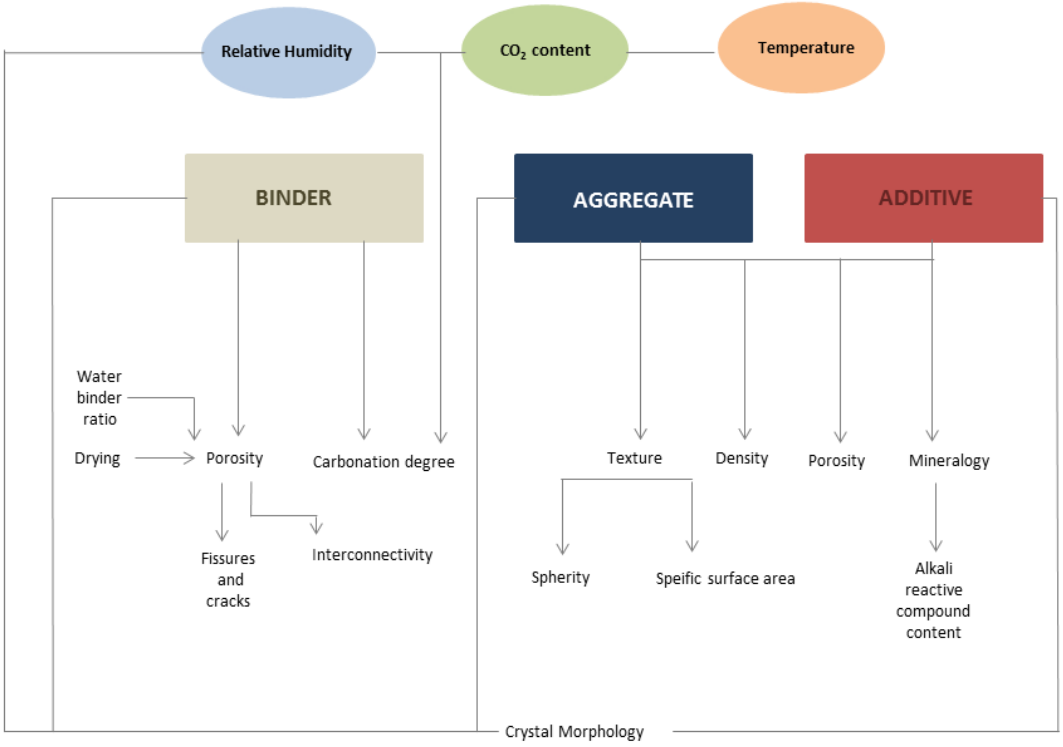


Figure 6.4. Diagram showing the factors that affect carbonation

Anomalies in the portlandite calcite amount in TGA-DSC are associated with the overlapping of the dehydration of portlandite and the decomposition of unstable calcium carbonate polymorphs. The ones in XRD can be explained by the different carbonation degrees in different specimens or inhomogeneity in the same specimen. Following the determined procedure in the beginning, in every period, the same spot of the specimenwas cut and used for the analyses; however, in some instances, this was not possible because the mortars were splintered by internal cracks. Using the same specimen to measure carbonation could minimize these anomalies. Nevertheless, in this case, carbonation would be interrupted periodically and probably new cracks would be generated by the cutting process. Hence this was not done in this research.

How different are the carbonation processes at different curing conditions?

In all curing conditions , themortars with ceramic inclusion showed greater carbonation than those without ceramic inclusion. Quantitatively, more advanced carbonationwas seen in the climatic chamber cured samples (M2>M1), and accelerator seemed to have more of an effect when the mortar had ceramic content. These conclusions were reached based on phenolphthalein, microscopic, XRD, TGA and MIP analyses. At the end of 6 months the carbonation degree was not different (even less) than the laboratory control samples, but it was clear that, if M2LA could have maintained its momentum until 120 days, it would be closer to M2C carbonation. Nevertheless, the crystal size diminished at advanced ages, probably the large crystals formed on the surface probably hindered the carbonation.

As mentioned, thechamber cured samples showed advanced carbonation that can be followed by all tests; however, the microstructure variability of the crystals should to be mentioned. At early ages, already stable and well crystallized calcium carbonates were present; however, they later transformed into columnar and rhombohedral forms and at last in irregular modified scalenohedral morphology. There were also many unstable polymorphs; aragonite, vaterite and ACC.

In the accelerator sprayed samples, rounded shape crystals werepredominant, especially at 90 days. Theydid not possess defined faces; perhaps due to the the uncontrolled precipitation (Rodriguez-Blanco et al. 2010). The pentagonal shapes seen evolved at later ages into modified scalenohedral calcite crystals, associated with platelet portlandite, ACC and acicular aragonite. The ACC abundance can also be deduced from the hump between 2θ 25-30 in the XRD patterns. In the dry conditions, calcite is not expected as explained above, but the higher CO_2 exposure at local conditions could have had an influence on it. Laboratory cured samples show the same trend at 120 days. In the mortars with ceramic inclusion, ACC and aragonite were dominant, however, calcites with irregular shapes appeared as well.

Undoubtedly, the sample submitted to treatment with DioloCarB behaved differently. This was easily observable in the form of calcite crystallization and the reaction times, as shown in sample M1 (with lime and sand), which was very different from sample M2 (with lime, sand and ceramic). As previously reported, calcium carbonate has an effect on mechanical properties depending on its shape (Ryu et al 2008).

Is it possible to have faster carbonation without worsening the mortars' properties?

Even though this research used technology aided curing conditions, they were intended to be kept not close to the real conditions of mortar production. Consequently, the evolution in carbonation is not pronounced as it is in some other studies (Cultrone et al, 2005; Çizer et al. 2010; Arizzi and Cultrone, 2012).

According to the results of the experiments, accelerated carbonation can be achieved. As expected, none of the samples showed fully carbonation at the end of 180 days; however, the highest carbonation degree was detected in the samples containing ceramic and cured in the climatic chamber. The accelerator product, DiloCarB, caused slightly higher carbonation and more with ceramic inclusion.

Nevertheless, SEM analysis showed that rapid carbonation led to irregular crystal formation, and probably due to the abundance of aragonite together with calcite causing instability and cracks, thus reducing the physical and mechanical values. Alternatively, capillary water evaporated during the portlandite-calcite transformation, which is an exothermic reaction, and therefore the solubility of the carbon dioxide reduced or closing pores due to carbonation blocked the path of carbon dioxide and carbonation could not continue (Cultrone et al, 2005).

Most of the pores of a mortar are produced by the evaporation of water in the drying process (Arandigoyen et al.2005; Arizzi et al. 2013). Early age carbonation is crucial to have at least the skeleton of the mortar because in later stages cracks and pores can befilled by secondary calcite precipitation. In addition, early age surface hardness is nearly preserved,

and no significant changes are observed in the later ages. In 120 and 180 days, chamber cured M2 sample generated cracks that caused an increase in 5 minutes capillary coefficient, which indicates the weakness of mortar. Similarly, anomalies were present in the carbonation. Longer durations of monitoring arenecessary to establish more stable carbonation.

The results expected before the experiments were mostly fullfilled.

Theoretically, excess CO_2 and accelerator should increase the carbonation rate.

Advanced carbonation was observed in the accelerator sprayed samples, and even more in the ones subjected to higher CO_2. Nevertheless, shrinkage cracks due to rapid carbonation reduced the performance of the samples. The forms of the pores in the M1 mortars were angular and/or irregular, and interconnected cracks due to evaporation of water and shrinkage were present. Furthermore, the tortuous shape of the pores and cracks raised greater difficulties in terms of the movement of diffused CO_2 gas and dissolution water that cause carbonation. Since these cracks are formed in the binder zone, they do not affect the bonding between the aggregate (Leslie and Hughes, 2002). In the M2 mortars, these fractures are frequent; however, there are round pores as well. Apparently, the re-precipitation of calcite around the borders of the pores is more frequent. Furthermore, rounded pores are seen in the mortars of both types with accelerator, which is related to the rounded crystal forms which are observed in SEM analysis.

If the ceramic aggregates are reactive enough and conditions are appropriate, pozzolanic reactions should occur.

Roman ceramics were proven to be highly reactive; however, this was deduced from thermogravimetric analysis, and was not supported by XRD and SEM. Probably the pozzolanic reaction products were too small to detect. Alternatively, the absence of pozzolanity may have been due to the low relative humidity curing conditions (Cazalla et al, 2000; Nezerka et al., 2014). Since more amorphous silica causes more pozzolanic activity

(Walker and Pavia, 2011), perhaps the Roman ceramic was not amorphous enough to promote more pozzolanic products. The higher amorphousness of the bricks than the tiles can be seen in their XRD patterns. As a result, mix use of them causedless pozzolanic effect.

Regarding properties, higher values are expected in mortars with ceramic aggregates due to better bonding.

As expected, the mortars with ceramics had higher values in the analyses. More stable calcium carbonate polymorphs were formed in M2 mortars. Roman ceramics used as aggregate are rich in clay minerals. This makes themicrostructure of the mortars more complicated with irregular morphology, but at the same time, the matrix has more compact appearance. Moreover, ceramic dust inclusion increases the specific surface area that reacts with the lime putty. Therefore, the physical, mechanical, and hydric properties of M2 mortars are higher. It also seems that mortar with ceramicsand accelerator showed better performance and more advanced carbonation in chamber curing. Water absorption through capillarity and ultrasonic pulse velocity were more influenced by the cracks when there was ceramic inclusion.

At the end of the experimental campaign, mortar blends may still be not fully carbonated even in the accelerated ones.

According to TGA results, at the end of 6 months, the uppermost level of the carbonation was 96 % in the mortar sample including ceramics and exposed to high CO_2. The rest of the samples were approximately 80% carbonated at the end of the experiment.

7 Compatibility of Roman and Repair Mortars

This chapter compares the values gathered by the analytical techniques and literature and discusses the compatibility of Roman and repair mortars.

The compatibility of the repair mortars is the first and most important concern in conservation and restoration of the historic monuments. Compatibility is defined as having similar properties and characteristics thus working in concordance with other building materials (Valek et al. 2000; Moropoulou et al. 2005; Velosa et al. 2010). Despite the fact that in this doctoral research the experimental part, study of repair mortars, is not planned specifically for one archaeological site, in this chapter, the results of the analyses of both Roman and new mortars are compared, where possible, to examine the compatibility. Indeed, properties of adjacent building materials are important in the compatibility issues however they are counted out concerning the scope of the study. In our research compatibility is evaluated through density, porosity, surface hardness and hydraulicity and mechanical strength of Roman mortars and new mortars at the end of 180 days of carbonation. Note that mechanical tests are not applied to Roman mortars due to the inconvenience of irregular forms; thus the strength of Roman mortars results from literature and our strength of new mortars is compared.

Among the analysed Roman mortars porosity values are close in both opus type of mortars in Spain cases there are differences in Turkey cases. *Opus signinum* mortars are more porous in Turkey mortars on the contrary in Spain it is opposite, being not so different. An average porosity value of *opus caementicium* mortars is 30% in Spain and 24% in Turkey. When we look at the M1 type repair mortars all of them have close values between two *opus caementicium* porosities (23-26%). An average porosity value of *opus signinum* is 29% in Spain and 40% in Turkey. When we look at the M2 type repair mortars they have higher porosity values closer to Turkey *opus signinum* porosities (37-47%).

Repair mortar should have equal or worse quality than the original ones; thus their porosity should be same or higher than the Roman mortars. Regarding the porosity new mortars in our study they are compatible with all of the Roman mortars because having lower porosity than the original mortars would be a problem but in our case it is beside the mark. Note that, M1L180 and M2L180 specimens with highly different values are discarded.

Average apparent density values of *opus caementicium* mortars are 1.71 and 1.70 g/cm^3 in Spain while 2.06 and 1.82 g/cm^3 in Turkey. Their so called replicas M1 mortars have density values between (1.75-1.82 g/cm^3). M1LA sample at 90 days have lower density values. The rest is between density values of mortars from two regions, higher than Spanish mortars lower than Turkish mortars, however the difference is so little therefore it can be acceptable.

Average apparent density values of *opus signinum* mortars are 1.73 and 1.66 g/cm^3 in Spain while 1.45 and 1.33 g/cm^3 in Turkey. Their so called replicas M2 mortars have density values between 1.28 and1.40 g/cm^3 lower than Spanish mortars close to Turkish mortars. Nevertheless it is regarded as compatible because the lower density is acceptable (Table 7.1, Table 7.2).

Another comment that can be added that the porosity and density are difficult to control; although the ceramics and the granulometry of Complutum mortars are used these parameters show distinctions.

Table 7.1. Porosity and apparent density of Roman mortars (Standard deviations are indicated in the paranthesis)

		Porosity (%)	**Apparent density (g/cm^3)**
Complutum	OC	30(11)	1.71(0.35)
	OS	29 (4)	1.73 (0.19)
Mérida	OC	30 (7)	1.70 (0.21)
	OS	29	1.66
Nysa	OC	23(9)	2.06 (0.01)
	OS	38 (12)	1.45 (0.02)
Labraunda	OC	25	1.82
	OS	42(10)	1.33 (0.3)

Table 7.2. Porosity and apparent density of repair mortars

Repair mortar samples		Porosity (%)	Apparent density (g/cm^3)
M1L	28	26	1.75
	90	24	1.82
	120	25	1.76
	180	38	2.98
M1LA	28	26	1.76
	90	23	1.52
	120	24	1.77
	180	25	1.81
M1C	28	25	1.77
	90	26	1.76
	120	24	1.77
	180	26	1.81
M2L	28	43	1.30
	90	47	1.37
	120	41	1.32
	180	28	0.92
M2LA	28	37	1.34
	90	42	1.28
	120	41	1.32
	180	39	1.35
M2C	28	37	1.34
	90	37	1.40
	120	46	1.35
	180	39	1.31

When compared the pore size diameter and porosity repair mortars are in the range of the majority of Roman mortars show. Figure 7.1 illustrates the values of the repair mortars at the end of 6 months and the values of Roman mortars.

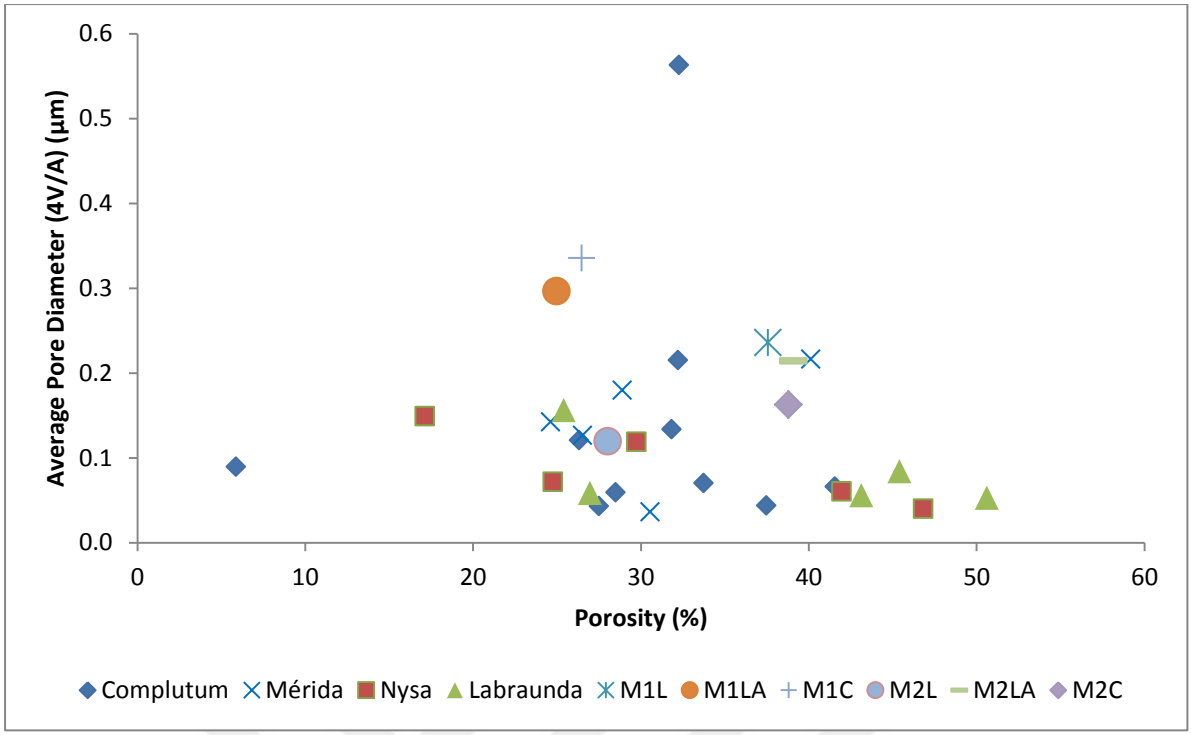


Figure 7.1. Average pore diameter vs porosity values of Roman mortars and repair mortars at the end of 6 months

Furthermore, in the pore size distribution of the Roman mortars the intensity of micropores are higher which indicates the deterioration (Figure 7.2). On the other hand, in the repair mortars micro and macropores have the almost same intensity, in other words equilibrium in the pore system was gathered which can be considered positive for the use of repair mortars in the conservation purposes. In M2 mortars the intensity of micro and macropores are not equal due to the particle size of the ceramic aggregates however still the less amount of micropores regarding to the Roman mortars are provided Figure 7.3).

The larger macropores are considered due to poor bonding between the binder and aggregate (Lanas et al. 2003) and the size of the macropores decrease with the carbonation in the pore borders. Whereas, it can also be thought that use of these repair mortars having more amount of macropores would be beneficial in terms that rainwater accumulate in them and prevent the saturation of the smaller pores. Meanwhile the pores will be filled with the dissolution recrystallization phenomena more strength can be gained

and the decreasing pore size would be happened after a long time in accordingly long term protection of the mortar and masonry can be provided.

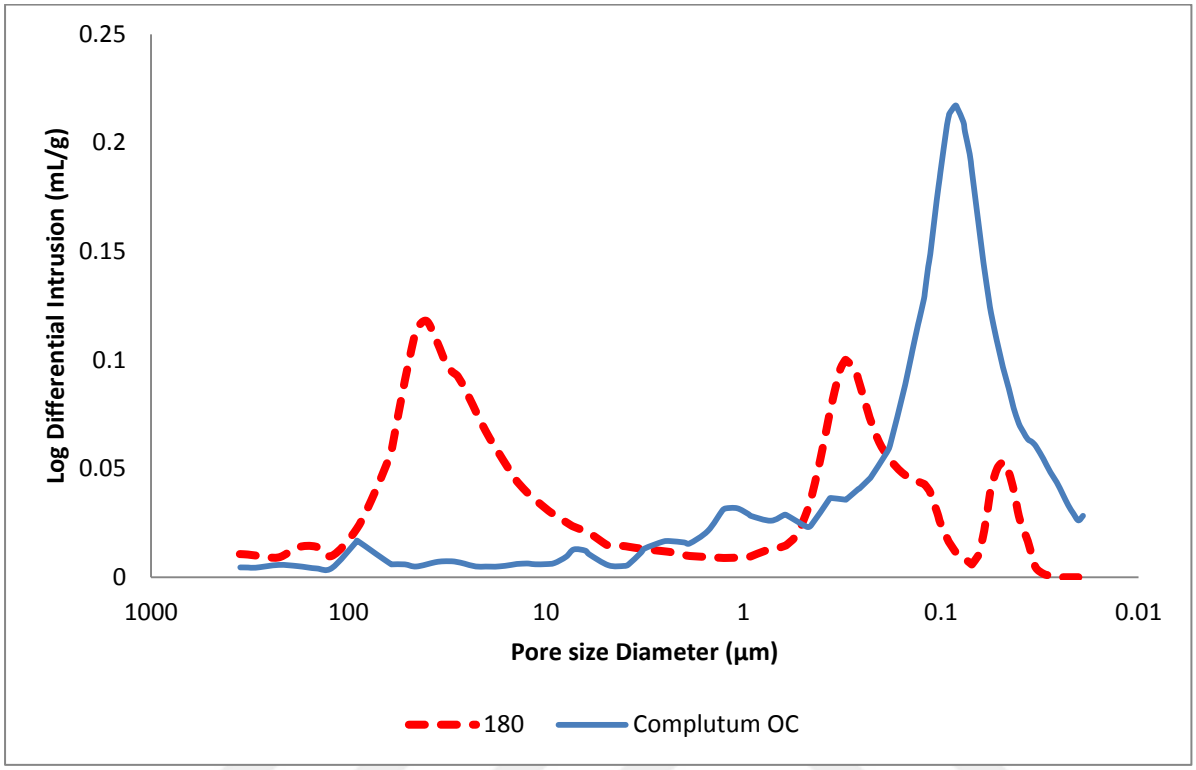


Figure 7.2. Pore size distributions of M1 sample in the chamber curing conditions at 180 days and *opus caementicium* sample from Complutum

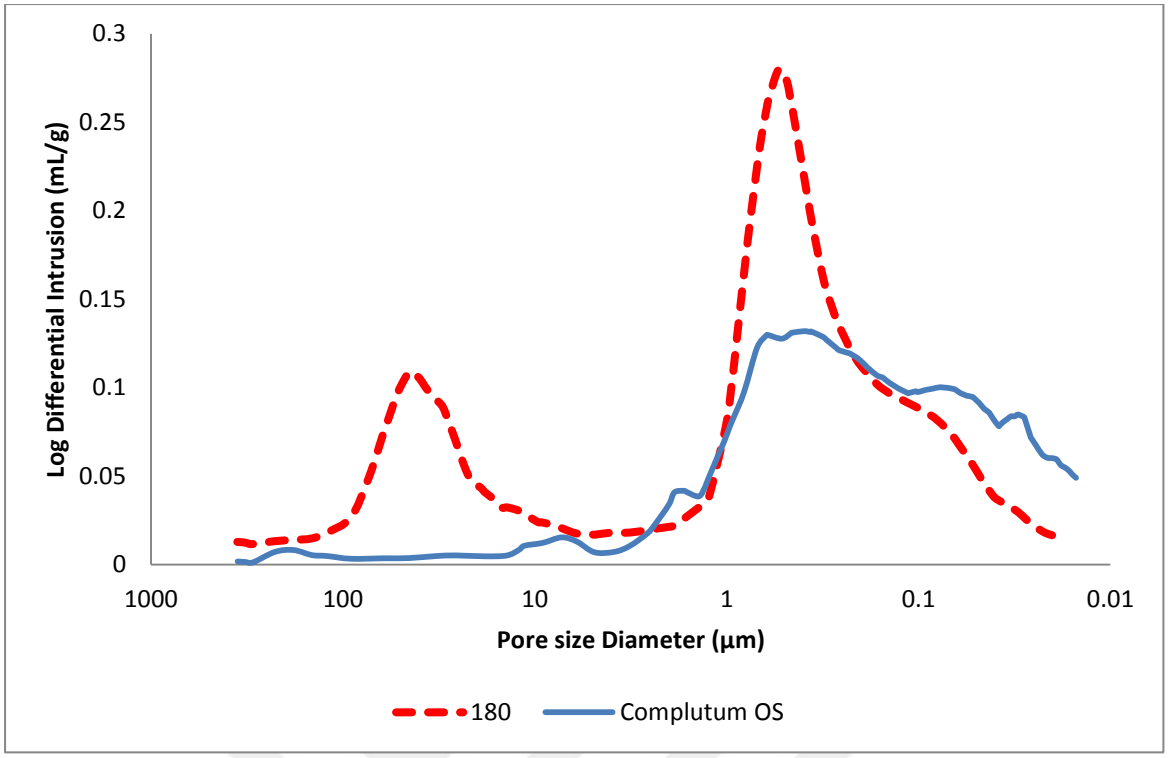


Figure 7.3. Pore size distributions of M2 sample in the chamber curing conditions at 180 days and *opus signinum* sample from Complutum

Surface hardness values of *opus caementicium* type Roman mortars vary between in Complutum mortars 143 and 442 leebs, in Mérida mortars 189 and 418 leebs, in Nysa mortars 172 and 318 leebs, in Labraunda mortars 149 and 200 leebs. Surface hardness values of *opus signinum* mortars vary between in Complutum 84 and 323 leebs, in Mérida 105 and 307 leebs, in Nysa 179 and 218 leebs and in Labraunda 78 and 239 leebs.

When compared the surface hardness values, in repair mortars there is no significant difference, among the specimens around 200 leebs and M2 mortars have higher values. On the contrary *opus signinum* mortars have lower values than *opus caementicium* mortars (Figure 7.4). It can be inferred that early superficial strength is gained in both of the types, although ceramic inclusion makes mortar have higher hardness values and in advancing time the strength reduces. It should be related to the fact that *opus signinum* mortars are more affected from deterioration. Repair mortars can be regarded as compatible to all of

the mortars as none of them have superior values. Besides, values are closer to the ones in the mortars of Turkey.

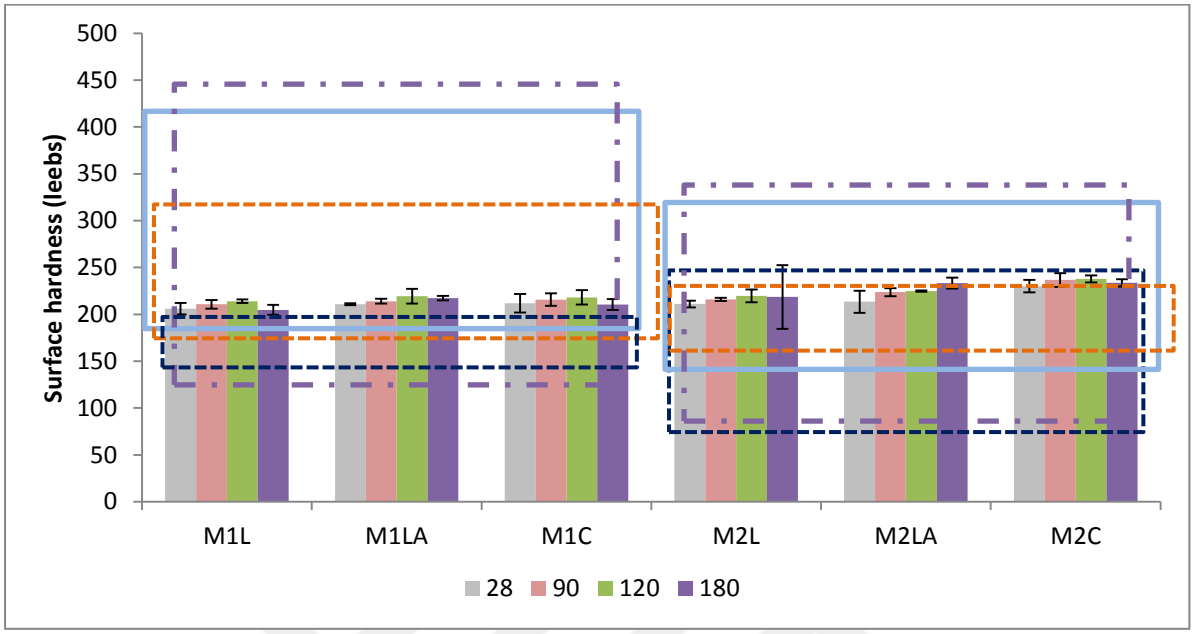


Figure 7.4. Surface hardness values of repair mortars and Roman mortars (whose ranges of surface hardness values are presented in boxes; are blue dashed line: Complutum, blue line: Mérida, orange dashed line: Nysa, black dashed line: Labraunda)

Data gathered from termogravimetric analysis is used to see the relation between inverse hydraulicity (CO_2/H_2O) and carbonate (CO_2) and the evolution of hydraulic character during carbonation is obvious (Figure 7.5). With the transformation of portlandite to calcium carbonate the values started to be shifted to the right. The values staying apart from others in every group -especially in 28 and 90 days- belong to chamber cured samples.

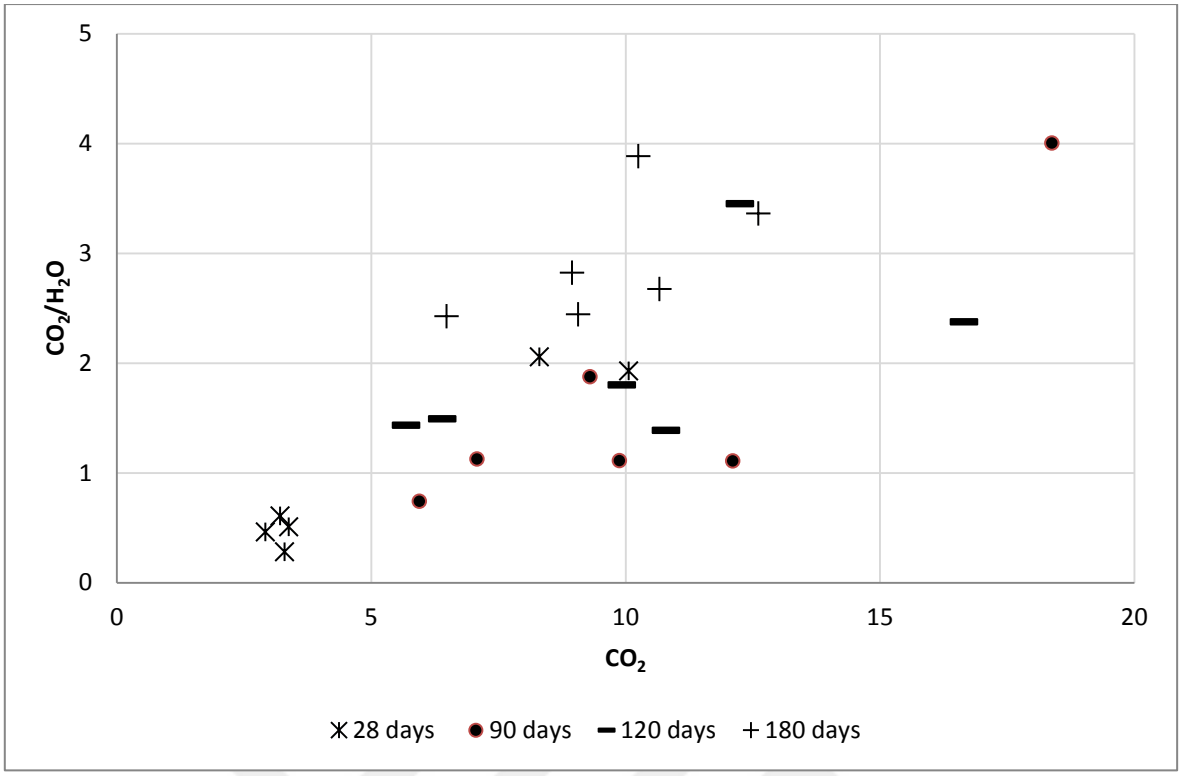


Figure 7.5. CO_2/H_2O vs CO_2 graph of repair mortars

It is possible to visualize the mortars when the values of repair mortars are placed into the comparison graph of Roman mortars (Figure 7.6). At 28 days mortars are accumulated below 5 in both axis, in which some Labranda and Complutum mortars are present as well. In the following days, mortars are situated in CO_2 5-15 % and CO_2/H_2O ratio below 5 in which the majority of Roman mortars lay down. Two chamber cured samples, M2C in 90 days and M1C in 120 days, are fall into the 15-20 % CO_2 where second intense distribution of the mortars, Mérida, Complutum and Nysa mortars are seen. In brief, all the mortars have hydraulic character after 90 days having the similar hydraulic character with Roman mortars.

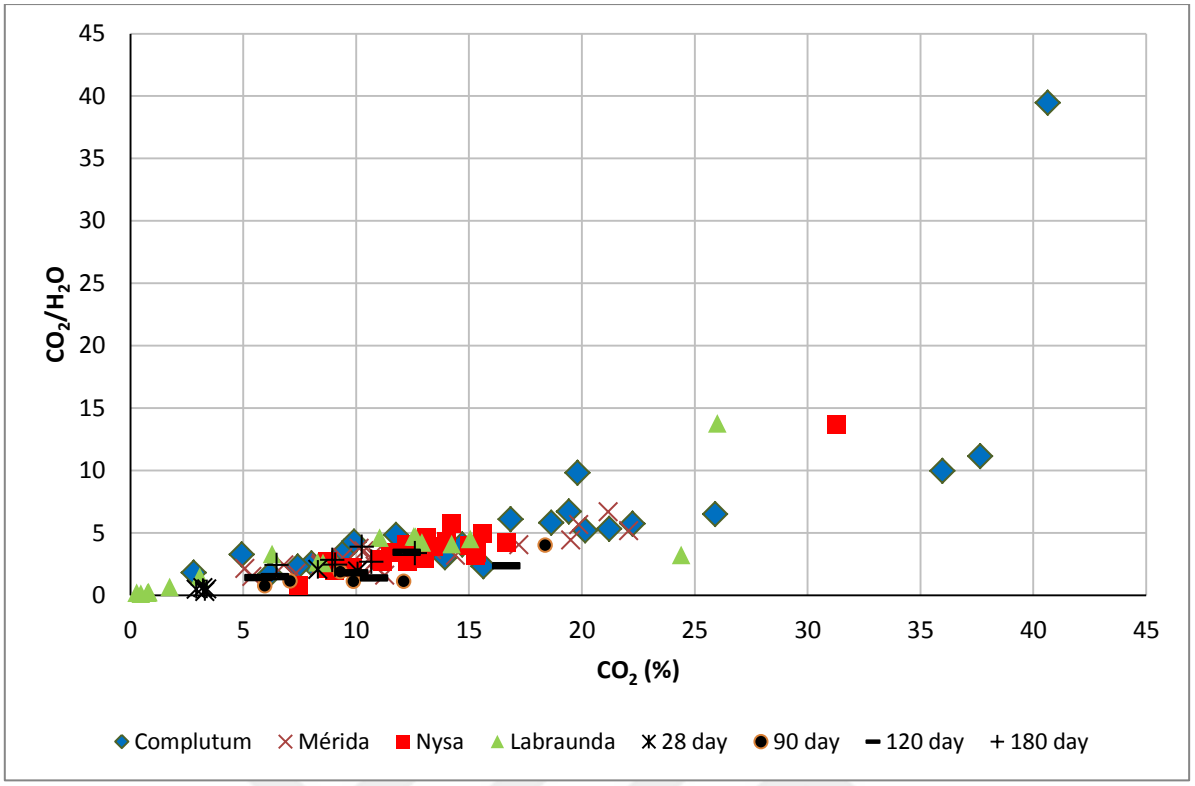


Figure 7.1. CO_2/H_2O vs CO_2 graph of Roman and repair mortars

The pore structures of the repair and Roman mortars have distinctive features; the pores are more angular and/or irregular in shape in not fully carbonated repair mortars with sand aggregate, in the Roman ones pores are found rounded shapes. Besides, interconnected cracks and fractures are frequent in the repair mortars. Leslie and Hughes (2002) state these fractures generating due to the loss of water and shrinkage have no influence on binder aggregate bonding. Considering the fact that microstructure Roman mortars have been changed with intrinsic and extrinsic factors throughout two millenniums, they have had probably tons of recrystallization phenomena and precipitation of secondary calcite in those cracks and fractures and edges of angular shape pores.

Regarding the mechanical resistance, that *opus caementicium* type mortars have compressive strength values between 0.5 and 3 MPa and *opus signinum* type mortars have above 1.5 MPa (Válek and Veiga, 2005; Válek and Bartos, 2001).

In our case compressive strength vary between 1.3-1.5 MPa in M1 mortars and 1.6-1.8 MPa in M2 mortars. The results fit the range of historic mortars therefore in terms of compressive strength they can be regarded as compatible with studied Roman mortars. Válek and Bartos (2001) remind that the strength steel-mold cured sample would be different from in-situ cured sample in the masonry since in the latter moisture suction of the adjacent material and bonding play important role as well. It might be inferred that the simulative values should be considered higher in the field. Consequently, M1 mortars would not pose a problem, while M2 mortars would be probably higher than the original mortar. Hence, lower ceramic content or more water ratio would be more appropriate as it lessen the strength of the mortars.

Another noteworthy property of the new mortars is the modulus of elasticity which shows higher values and increasing trend in M1 mortars and lower values together with no significant change in M2 mortars. Elasticity of the repair mortars is important in terms of the function of the mortar in the building. A mortar with high elastic property works in accordance with other building materials in the masonry. M1 mortars are suitable for joint mortar uses with load-bearing functions while M2 mortars are appropriate for rendering purposes.

When considered the other properties that are measured in repair mortars, without comparable results in our four Roman case studies, still the comparison can be done by the literature. Velosa et al. (2010) state that in historic mortars water absorption through capillarity should be evaluated in larger range considering the several time altered microstructure due to the deterioration. Therefore in order to determine the compatibility through capillarity the environmental conditions should be the first concern. Capillary coefficient of Roman mortars from amphitheatre in Mérida change between 1.93 and 5.96 kg m^{-2} $h^{-1/2}$ (Mota- López et al. 2016) and have values below 4 kg m^{-2} $h^{-1/2}$ in Coimbriga (Velosa et al. 2007). Therefore the capillary coefficients of the repair mortars (1-5 kg m^{-2} $h^{-1/2}$) can be considered compatible. Nevertheless, the higher values at 5 minutes capillarity of M2C mortars are related with deterioration therefore inappropriate for a repair mortar.

In the literature air permeability of historic mortars is not mentioned therefore the comparison cannot be done; however, it is possible to make reasoning. Walls with mortars with higher air permeability values can be regarded as so called "breathing" masonries as well. In our repair mortar study M2 mortars have higher values comparing to M1 mortars. It make sense when the aforementioned functions are given to the mortars; M2 rendering and M1 joint mortar.

8 Conclusion

This chapter presents the conclusion of the research.

The research questions that were asked in the beginning have been answered and the objectives of the thesis accomplished. One of its main aims of was to characterize the Roman mortars, two types according to their ceramic inclusion, *opus caementicium* and *opus signinum*, which were studied in four archaeological sites, two in Spain and two in Turkey.

After the characterization the following points were found for each site:

- In Complutum, mortars from different construction phases have different properties. The quantity of aggregate in the mortars increases as the centuries pass. This may be related to learning by trial and error that aggregates are necessary to prevent shrinkage cracks. The construction of the cuadrifrontal arch and the Zulema bridge may date back to first century AD since they have the similar proportions and geochemically match that period's floor and wall mortars.
- In Mérida, the San Lazaro aqueduct and the Circus, Moreria and the snow well are thought to have been constructed in the same period (first century AD) according to the rock fragment constituents. The Temple of Diana and the amphitheatre are known to have been built in first century BC, and the archaeological remains of Viñero and the Resti Bath with the same proportions and similar rock fragment constituents are thought to be constructed at same period.
- In Nysa, the mortars have uniformity, independent from function. All the mortars have similar properties. The monuments, whose construction periods have not been determined by by archaeologists, can may date back to the third century AD and later, according to the proportions and characteristics.
- In Labraunda, the mortars have a greater variety of characteristics. A higher amount of mortars include ceramic, which is related to the fact that number of water-related buildings is higher. In the south-eastern part of the Sanctuary, the mortars possess a very small amount of binder. It should be dissolution of lime if they are not made with those proportions at different period, which however is a slight possibility. The precise construction period of the hypostyle building is not known; however, its similar rock

fragments and high ceramic content imply that it was built in the first century AD as well.

The hypothesis of the comparative study claims that there should be distinctions between the Roman mortars of the two extremities of the Mediterranean Region. These are the findings:

- In all of the archaeological sites, the sands and rock fragments match the regional geologies. Raw materials were gathered from the vicinity not bought from a central manufacturer.
- Construction techniques were different in the two sides of the Mediterranean, and so are the mortars they used. The larger size aggregates (*caementea*) are found in the in the marble coating mortar and aqueduct mortar in the Spanish sites. On the other hand, in Turkey, *caementa* which prevents shrinkage cracks is not common. The coating mortar with the same function does not have this specific characteristic, which indicates the lack of technical knowledge and construction practice in Turkey, where lime mortars were used instead to joint irregular shape rubble stones and as rendering.
- Unlike the other sites, in Complutum, clean sand was used predominantly in aggregates. In the other sites, large dimension metamorphic rock fragments are frequently encountered in the mortars. As a result, the Complutum mortars have less minerals having silica-alumina leading to pozzolanic reactions with lime binder.
- In the mortars, the shape of the aggregates are sub-angular to sub-rounded, butin Labraunda angular sharp edge grains and rock fragments were more frequently used.
- The majority of the mortars studied have hydraulic character even though they had no function related to water (water contact or water vapour permeability). It can be interfered that hydraulicity was gained unintentionally by the raw materials as well.
- According to the surface hardness and porosity (mainly micro porosity) values, the state of conservation of the mortars is good. The mortars in Turkey are poorer than the mortars in Spain, although both of the archaeological sites are located next to

modern settlements and highways which would increase the deterioration. Whereas the air pollution-related gypsum was practically found in only two samples. Among the mortars studied, the highest ceramic and the least lime content, and accordingly, worse technology and performance, were found among the Labraunda mortars. This may be due to the kaolinite and illite content, which improves the pozzolanic activity, but lead to deterioration as well. The relatively high rainfall may be the reason for the decay. High rainfall may cause the dissolution of lime binder and prevent the re-precipitation of secondary calcite.

With this empirical knowledge, repair mortars were prepared by imitating the Roman mortars. They were cured at different conditions to accelerate carbonation and monitored periodically to see their evolution. The results of these analyses show that:

- In all curing conditions, the mortars with ceramic inclusion show higher carbonation than their peers without ceramic inclusion. Silica and clay mineral rich Roman bricks and tiles favor advanced carbonation with more stable calcium carbonate formation.
- The mortars cured in the climatic chamber showed advanced carbonation due to the high CO_2 exposure and higher RH. Stable calcite crystals were present at early ages as well, and the habits of the crystals changed according to the ceramic inclusion. There were scalenohedral to modified scalenohedral crystals in the mortars with sand aggregate. In the mortars with ceramic inclusion, calcite crystal is formed rhombohedral-like shapes. At later ages, they were seen in tabular habit, and finally not very well defined morphology. Cracks occured and crystals formed irregular shapes which cause a sudden decrease in the velocity and capillary absorption properties at the later ages, which slightly worsened their performance.
- Although accelerator did not cause specific difference, in the end better carbonation was observed and, these samples had a more steady carbonation process. Like the chamber cured samples, fissures and cracks occurred at the end of the experiment. In all cases, the mortars with ceramic content showed more sound

results. In terms of microstructure, accelerator caused rounded crystal habit, which then transformed into modified scalenohedral forms in the mortars with lime and sand aggregate.

- Anomalies in the TGA analyses occurred due to the juxtaposition of weight loss ranges of dehydration of portlandite and the decomposition of amorphous other instable calcium carbonate polymorphs. Anomalies in the portlandite-calcite in XRD analysis can either be related to the instability of the mortar mix at early ages. Metastable calcium carbonate polymorphs have the same thermal properties as calcium hydroxide. Therefore, the values probably are overlapped. Alternatively, different carbonation degrees due to the inhomogeneity of the same specimens may have caused the irregularities.

Linking the new mortars and the Roman mortars leads to the following implications:

- As expected carbonation of the new mortars are not completed at the end of six months. The difference between fully carbonated Roman mortar and newly carbonating mortar was clearly observed by TGA. Accordingly, the examining weight losses were different in the two studies.
- The newly carbonated mortars showed similar surface hardness values to the Roman mortars that were examined in the first part of the study. This confirms that t surface strength is gained at early ages of carbonation.
- Microscopic observations found that recrystallization can also occur at newly carbonating mortars at earlly ages.
- The density porosity and surface hardness values of the repair mortars were below and between the ranges of the Roman mortars and can thus be considered compatible.
- The pores are more angular and/or irregular in shape in not fully carbonated repair mortars. In the Roman mortars pores are found in rounded shapes. Besides, Interconnected cracks and fractures were frequent in the repair mortars, but did not affect the binder aggregate bonding. Consider that microstructure Roman mortars

have been altered many times throughout two millenniums, several recrystallization phenomena probably have occurred and re-precipitation of secondary calcite in the cracks-fractures and edges of angular shape pores.

- In the experimental part of the study, the use of ceramic positively affected every curing condition it can be applied to when repair mortars are needed. Only in Labruanda would more analysis be necessary due to the environmental conditions.
- The mechanical strength and modulus of elasticity of the M1 repair mortars are suitable for use in the field; however, those of the M2 mortars are probably higher than the original mortar. In order to lower the strength of the mortars, lessening the ceramic content or increasing the water ratio may work.
- In principle, it is highly recommended that repair mortars be prepared specifically for the archaeological site where they will be used; however, this research shows that a common repair mortar with average standards can be compatible when the climatic and geological conditions are similar enough. Curing in a higher CO_2 and RH environment accelerates carbonation; however, when the negative properties at the later ages are considered, the use of DiloCarB, which provides a slightly accelerated and steady carbonation, is appropriate for repair mortars.

This doctoral study used a multi-analytical approach. Here are the benefits of these techniques:

- Microscopic observations and XRD as traditional techniques served very well for defining the constituents of the mortars.
- TGA was a crucial technique for defining the hydraulic character of the mortars and served for characterization, and XRF served well as supporting technique and for geochemical clustering.
- In the repair mortar study, careful attention was paid to the preparation of samples, curing conditions and conducting the periodic analyses at short intervals to ensure the accuracy of the analytical techniques.

- XRD, TGA, SEM and phenolphthalein were useful to see the evolution of carbonation in the mortars.
- Physical, hydric and mechanical analyses were important to see the performance of the mortars at advanced ages.

This versatile doctoral study contributes useful information to the conservation science and especially mortar studies field. All objectives are achieved, although some difficulties were experienced. The data loggers placed in the archaeological sites in order to compare the climatic data lost their calibration or gave faulty data several times.

9 Contribution to the field

This chapter presents several contributions of this PhD thesis to the field.

- Above all, the thesis has an innovative approach aiming to built a bridge between the old and new mortars, the combination of comparative study and related experimental study had never been done before.
- Each case study in Roman mortar characterization serves for determining conservation-restoration strategies in each archaeological site.
- Second part of the thesis, repair mortar study is original regarding to the following points:
  - the use of original Roman raw material
  - until now DiloCarb has been mentioned in stone consolidation scientific literature, for the first time it is used as carbonation accelerating agent.
  - The comparison of different curing techniques; CO_2 diffusion in climatic chamber and accelerator
- High amount of data gathered from several analytical techniques are processed.

Scientific diffusions

Publications

2014 - Ergenç, D. Sánchez Montes, A.L. Fort, R. Sanz Arauz, D. Rascón Marqués, S. 2014. Los morteros de la ciudad romana de Complutum: Inicio de una investigación, Miradas a la investigación arquitectónica: construcción, gestión, tecnología Architectural research findings: building construction, management, technology, ed: M. M. Barbera-Barrera, F. Olivieri & J. Pinilla-Melo, ETSAM, Madrid, ISBN: 978-84-617-0504-7, pp. 34-39.

2015- Henry, O. Andersson, E. Bost,C. Çakmaklı, ÖD.Commito, A. Cormier-Huguet, M. de Staebler, P. Dupont, P.Ergenç, D. Frejman, A. Kepenek, B. Lebouteiller, P. Nilsson, H. Rojas, F. Vergnaud, B. 2015. Labraunda 2014. Anatolia Antiqua XXIII, pp. 301-394.

2015- Martínez-Garrido, M.I. Ergenç, D. Fort, R. 2015. Monitorización inalámbrica del yacimiento Complutum: evaluación de los elementos de protección para una conservación preventiva.in: Estudio y Conservación del Patrimonio Cultural. Actas ed: M. Morena Oliva,

M.A. Rogerio-Candelera, J.T. López Navarrete, V. Hernández Jolín, Málaga 2015. ISBN: 978-84-608-2452-7, pp. 9-13

2015- Ergenç, D. Sánchez Montes, A.L. Fort, R. 2015. Caracterización de pinturas murales en Casa de los Grifos de la ciudad romana Complutum, Alcalá de Henares, Estudio y Conservación del Patrimonio Cultural. Actas, ed: M. Morena Oliva, M.A. Rogerio-Candelera, J.T. López Navarrete, V. Hernández Jolín, Málaga 2015. ISBN: 978-84-608-2452-7, pp. 107-111.

2016- Henry, O. Anderson, E. Bost, C. Çakmakli, Ö. Cederling, F. Commito, A. Cormier-Huguet, M. Coutelas, A. Dolea, A. Ergenç, D. Freccero, A. Frejman, A. Lebouteiller, P. Lesguer, F. Löwenborg, D. Lungu, V. Marchand-Beaulieu, F. Sitz, A. de Staebler, P. Vergnaud. B. 2016. Labraunda 2015. Anatolia Antiqua XXIII, p. 339-457.

2016- Ergenç, D. Fort, R. 2016. Characterization of Roman mortars of Nysa in the ancient Caria, Turkey. Proceedings of the 4th Historic Mortars Conference HMC2016 10th-12th October 2016, Santorini, Greece Ed. I. Papayianni, M. Stefanidou, V. Pachta, Laboratory of Building Materials Department of Civil Engineering Aristotle University of Thessaloniki, ISBN: 978-960-99922-3-7

2016- Martinez-Garrido, M.I. Ergenç, D. Fort, R. 2016. Wireless Monitoring To Evaluate The Effectiveness Of Roofing Systems Over Archaeological Sites. Sensors and Actuators A Physical, DOI: 10.1016/j.sna.2016.10.038

2016- Mota-López, M.A. Fort, R. Álvarez de Buergo, M. Pizzo, A. Maderuelo-Sanz, R. Meneses-Rodríguez, J.M. Ergenç, D. 2016. Characterization of concrete from Roman buildings for public spectacles in Emerita Augusta (Mérida, Spain). Archaeological and Anthropological Sciences, DOI: 10.1007/s12520-016-0434-9

2017- Ergenç, D. Fort, R. 2017. Preliminary investigation of repair mortars for the Temple of Diana, Mérida, Ge-Conservacion, pp xx.

Poster presentations

2014- Ergenç, D. Sánchez Montes, A.L. Fort, R. Sanz Arauz, D., Rascón, S. 2014. Characterization of Historic Mortars of Complutum Roman Site, Madrid, Spain, YOCOCU 2014 Youth in the Conservation of Cultural Heritage, Agsu, Azerbaijan

2016- Ergenç, D. Martin Freire-Lista, D. Fort, R. 2016. Assessment of chemical analyses by means of portable XRF in the Roman mortars of Complutum archaeological site (Spain) in European Geosciences Union General Assembly (EGU 2016) 17-22 Abril 2016, Vienna, Austria

2016- Ergenç, D. Fort, R. Sanz Arauz, D. 2016. Influence of diethyl carbonate as an additive in the carbonation process of lime mortars, HMC 2016 4th Historic Mortars Conference, 10th October 2016

10. Future Lines of Work

Further research about Roman mortars to be explored includes:

- More statistical techniques (such as principal component analysis) are anticipated to serve the classification of the mortars according to their common properties and help to overcome the problem of excessive data.
- Including more case studies in different territories as well as the comparison of mortars used in different historical periods will enhance our level of understanding.
- Digital image and more microscopic analysis (SEM-EDS, TEM) applied to the Roman mortars would be helpful to examine the microstructure and correlate with the repair mortars.

Further research about repair mortars to be explored includes:

- XRD technique enhanced with the Rietveld refinement will be more useful for monitoring carbonation.
- The durability of repair mortars should be determined by ageing tests.
- Different additives and curing conditions should be tried, and new methodologies can be developed with super plasticizers and air entraining agents to cope with cracks.
- Higher relative humidity at early ages and fluctuating climatic conditions within the chamber should be tried to increase pozzolanic activity reactions.
- Carbonation and performance of the mortar should be monitored in situ to increase reliability.

References

A.....

- Adam, J.P. 1999. Roman building materials and techniques (First published in 1937). Translated by Anthony Mathews. London and New York, Routledge. ISBN: 0415208661
- Akman, M.S. Güner, A. and Aksoy. I.H. 1986. "The History and Properties of Khorasan Mortar and Concrete." In the proceedings of II. International Congress on the History of Turkish and Islamic Science and Technology, Vol I: Turkish and Islamic Science and Technology in the 16th Century, 101-112. İstanbul: İTÜ Research Center of History of Science and Technology.
- Akurgal, E. 1985. Ancient Civilisations and Ruins of Turkey: From Prehistoric Times Until the End of the Roman Empire, 2nd ed., pp.234-236, Istanbul
- Alba, M. 2005. Evolución y final de los espacios romanos emeritenses a la luz de los datos arqueológicos (pautas de transformación de la ciudad Tardoantigua y Altomedieval), en Augusta Emerita: Territorios, Espacios, Imágenes y Gentes en Lusitania Romana, Monografías Emeritenses 8, 207-253.
- Alvarez, J. I. Martín, A. García Casado, P.J. Navarro, I. Zornoza, I. 1999. Methodology and validation of a hot hydrochloric acid attack for the characterization of ancient mortars. *Cement and Concrete Research* 29, 7, 1061-1065.
- Alvarez, J.I. Navarro, I. García Casado, P.J. 2000. Thermal, mineralogical and chemical studies of the mortars used in the cathedral of Pamplona (Spain). Thermochimica Acta. vol. 365. pp.177-187.
- Alvarez de Buergo Ballester, M. 2012. técnicas de caracterización petrológicas: propiedades petrofísicas y técnicas no destructivas (tnd/ndt). in: Rafael Fort González, Elena Mercedes Perez Monserrat. (ed.) La conservación de los geomateriales utilizados en el patrimonio. Madrid.
- Anonymous, 1931. The Athens Charter for the Restoration of Historic Monuments. http://www.icomos.org/en/charters-and-texts/179-articles-en-

francais/ressources/charters-and-standards/167-the-athens-charter-for-the-restoration-of-historic-monuments access date: 13/01/2017

- Aoki, H. & Matsukura, Y. 2008. Estimating the unconfined compressive strength of intact rocks from equotip hardness. *Bulletin of Engineering Geology and the Environment,* 67**,** 23-29.
- Arandigoyen, M. & Alvarez, J. I. 2007. Pore structure and mechanical properties of cement–lime mortars. *Cement and Concrete Research,* 37**,** 767-775.
- Arandigoyen, M. Bernal, J. L. P. López, M. A. B. & Alvarez, J. I. 2005. Lime-pastes with different kneading water: Pore structure and capillary porosity. *Applied Surface Science,* 252**,** 1449-1459.
- Arizzi, A. & Cultrone, G. 2012. Aerial lime-based mortars blended with a pozzolanic additive and different admixtures: A mineralogical, textural and physical-mechanical study. *Construction and Building Materials,* 31**,** 135-143.
- Arizzi, A. Viles, H. & Cultrone, G. 2012. Experimental testing of the durability of lime-based mortars used for rendering historic buildings. *Construction and Building Materials,* 28**,** 807-818.
- Arizzi, A. Cultrone, G. 2013. The influence of aggregate texture, morphology and grading on the carbonation of non-hydraulic (aerial) lime-based mortars. Q. J. Eng. Geol. Hydrogeol. 46, 507–520.
- Arizzi, A. Martínez Martínez, J. Cultrone, G. 2013. Ultrasonic wave propagation through lime mortars: an alternative and non-destructive tool for textural characterization. Materials and Structures 46 pp.1321–1335. DOI 10.1617/s11527-012-9976-1
- Arizzi, A. & Cultrone, G. 2014. The water transfer properties and drying shrinkage of aerial lime-based mortars: an assessment of their quality as repair rendering materials. *Environmental Earth Sciences,* 71**,** 1699-1710.
- Arizzi, A. Molina, E. & Cultrone, G. 2016. Repair rendering mortars for the restoration of the Vargas Palace in Granada (Spain): a comparative study of the mortar behaviour in the laboratory and on site. *Prikryl, R., Torok, A., Gomez-Heras, M., Miskovsky, K. &*

Theodoridou, M. (eds) 2016. Sustainable Use of Traditional Geomaterials in Construction Practice. Geological Society, London, Special Publications, 416, 253–273.

- Arizzi, A. Gomez-Villalba, L. S. Lopez-Arce, P. Cultrone, G. & Fort, R. 2015. Lime mortar consolidation with nanostructured calcium hydroxide dispersions: the efficacy of different consolidating products for heritage conservation. European Journal of Mineralogy. 27(3) pp 311-323.
- Arizzi, A. & Cultrone, G. 2016. Inadequacy of different methods of assessing the correct dosages during the preparation of air-hardening lime mortars. *Geological Society, London, Special Publications,* 416**,** 275-283.
- Arizzi, A. Molina, E. and Cultrone, G. 2016. Repair rendering mortars for the restoration of the Vargas Palace in Granada (Spain): a comparative study of the mortar behaviour in the laboratory and on site', in Prikryl, R., Török, A., Gomez-Heras, M., Miskovsky, K. and Theodoridou, M. (ed.) Sustainable Use of Traditional Geomaterials in Construction Practice, London: Geological Society Special Publications 416.
- Artioli, G. 2010. Scientific Methods and Cultural Heritage An introduction to the application of materials science to archaeometry and conservation science. Oxford University Press. London

B.....

- Bakolas, A. Biscontin, G. Contardi, V. Franceschi, E. Moropoulou, A. Palazzi, D. Zendri, E. 1995. Thermoanalytical research on traditional mortars in Venice. Thermochimica Acta , 269 (270), pp. 817-828.
- Bakolas, A., G. Biscontin, A. Moropoulou, and E. Zendri. 1995. Characterization of the Lumps in the Mortars of Historic Masonry. Thermochimica Acta 269-270: 809-816. doi: 10.1016/0040-6031(95)02573-1.
- Bakolas, A., G. Biscontin, A. Moropoulou, and E. Zendri. 1998. "Characterization of Structural Byzantine Mortars by Thermogravimetric Analysis." Thermochimica Acta 321: 151-160. doi: 10.1016/S0040-6031(98)00454-7.

- Baran, A. 2010. The Sacred Way to Labraunda and Ancient Spring Houses, in: F. Kuzucu & M. Ural (eds.) Mylasa Labraunda Sanctuary of Karia and its Environs. Archaeology and Rural Architecture in Southern Aegean Region.
- Barbero Barbera, M.M. 2012. Mejora del comportamiento térmico de los morteros de cal aditivados y su empleo en rehabilitación de inmuebles (PhD Dissertation) Escuela Técnica Superior de Arquitectura. Universidad Politécnica de Madrid, Madrid
- Barbero-Barrera, M. Maldonado-Ramos, L. Van Balen, K. García-Santo, A. Neila-González, F.J. 2014. Lime render layers: An overview of their properties. Journal of Cultural Heritage 15, pp. 326–330.
- Barluenga, G. Estirado, F. Undurraga, R. Conde, J. F. Agua, F. Villegas, M. Á. & García-Heras, M. 2014. Brick masonry identification in a complex historic building, the Main College of the University of Alcalá, Madrid (Spain). Construction and Building Materials, 54, 39-46.
- Barroso, Y. Morgado, F.1996. Mérida, Patrimonio de la Humanidad. Conjunto monumental. Mérida: Consorcio de la Ciudad Monumental Histórico-Artística y Arqueológica de Mérida
- Bartz, W. & Filar, T. 2010. Mineralogical characterization of rendering mortars from decorative details of a baroque building in Kożuchów (SW Poland). *Materials Characterization,* 61, 105-115.
- Belfiore, C. M. Fichera, G. V. La Russa, M.F. Pezzino, A. Ruffolo, S. A. Galli, G. and Barca, D. 2015. Multidisciplinary approach for the archaeometric study of pozzolanic aggregate in roman mortars: the case of villa dei quintili (Rome, Italy), Archaeometry 57, 2 pp. 269–296, doi: 10.1111/arcm.12085
- Belfiore, C. M. Fichera, G. V. Ortolano, G. Pezzino, A. Visalli, R. & Zappalà, L. 2016. Image processing of the pozzolanic reactions in Roman mortars via X-Ray Map Analyser. *Microchemical Journal,* 125, 242-253.
- Bild, J. 2006. The Byzantine church at Labraunda, Master thesis. Uppsala University

- Blid, J. 2010. Roman and Byzantine Labraunda, F. Kuzucu & M. Ural (eds.), Mylasa Labraunda Sanctuary of Karia and its Environs. Archaeology and Rural Architecture in Southern Aegean Region.
- Bild, J. 2012. Felicium Temporum Reparatio: Labraunda in Late Antiquity (c. AD 300-600), Stockholm pp226-235.
- Biscontin, G. Birelli, M. P. & Zendri, E. 2002. Characterization of binders employed in the manufacture of Venetian historical mortars. Journal of Cultural Heritage, Vol 3, p. 31–37.
- Blanco-Varela, M. & Fortes-Revilla, C. 2004. Effect of Chemical Admixtures on Lime–Metakaolin Mortars Characteristics. COALITION, 7
- Bonazza, A. Sardella, A. Favoni, O. Rendini, P. Sabelli, R. 2009. Compatibility of repair mortars at the archaeological site of Villa Domizia on Giannutri Island, Italy in Workshop Repair Mortars for Historic Masonry. *In:* Groot, C. (ed.). RILEM Publications SARL.
- Bonazza, A. Ciantelli, C. Sardella, A. Pecchioni, E. Favoni, O. Natali, I. Sabbioni, C. 2013. Characterization of hydraulic mortars from archaeological complexes in Petra. Periodico di Mineralogia, 82(2), pp. 459-475.
- Boynton, R.S. 1980. Chemistry and Technology of Lime and Limestone, 2nd Ed. New York: John Wiley & Sons.
- Bozkurt, E. N. & Satır, M. 2000. The southern Menderes Massif (western Turkey): geochronology and exhumation history. Geological Journal, 35, 285-296.
- Böke, H. Çizer, Ö. İpekoğlu, B. Uğurlu, E. Şerifaki, K. & Toprak, G. 2008. Characteristics of lime produced from limestone containing diatoms. Construction and Building Materials, 22, 866-874.
- Böke, H. Akkurt, S. İpekoğlu, B., Uğurlu, E. 2006. Characteristics of brick used as aggregate in historic brick-lime mortars and plasters. Cement and Concrete Research 36. 1115–1122

- Brandon, C. J. Hohlfelder, R.L. Jackson, M.D. Oleson, J.P. 2014. Building for eternity : the history and technology of Roman concrete engineering in the sea, ISBN 978-1-78297-423-9.
- Bruno, P. Calabrese, Di Pierro, M. Genga, A. Laganara, C. Manigrassi, D.A.P. Traini, A. Ubbríaco P. 2004. Chemical–physical and mineralogical investigation on ancient mortars from the archaeological site of Monte Sannace (Bari—Southern Italy). Thermochimica Acta , Volume 418, p. 131–141.
- Budak, M., Akkurt, S., Böke, H., 2010, "Evaluation of heat treated clay for potential use in intervention mortars", Applied Clay Science, vol 49 pp.414-419.

C.....

- Callebaut, K., Elsen, J., Van Balen, K., Viaene, W. 2001. Nineteenth century hydraulic restoration mortars in the Saint Michael's Church (Leuven, Belgium): Natural hydraulic lime or cement? Cement Concrete Reserach. Vol 31. pp 397-403.
- Candeias, A. E., Nogeira, P., Miraõ, J., Silva, A. S., Veiga, R., Casal, M., Gil, M., Ribeiro, I. & Seruya, I. 2005. Characterization of ancient mortars: present methodology and future perspectives. *Extended Abstracts of CERC3 Workshop on Chemistry in the Conservation of Cultural Heritage, EU-ARTECH.*
- Caner-Saltık, E.N., Güney, A., Caner, E., Akoğlu, G., Ergenç, D., Dincer, Ş. 2011. "Development of Repair Mortars for the Ruined Stone Towers in Perge Archaeological Park Site", Conservation of Stone in Parks, Gardens and Cemeteries International Conference, Champs Sur Marne, France
- Cantisani, E., Cecchi, A., Chiaverini, I., Fratini, F., Manganafelli del Fá, C., Pecchioni, E. & Rescic, S. 2002. The binder of the «Roman Concrete» of the Ponte di Augusto at Narni (Italy). Periodico di Mineralogia, 71, 113-123.
- Cardoso, I., Macedo, M. F., Vermeulen, F., Corsi, C., Santos Silva, A., Rosado, L., Candeias, A. & Miraõ, J. 2014. A Multidisciplinary Approach to the Study of Archaeological Mortars from the Town of Ammaia in the Roman Province of Lusitania (Portugal). *Archaeometry,* 56**,** 1–24.

- Carran, D. Hughes, J. Leslie, A. Kennedy, C. 2012. A Short History of the Use of Lime as a Building Material Beyond Europe and North America, International Journal of Architectural Heritage: Conservation, Analysis, and Restoration, 6:2, 117-146, DOI: 10.1080/15583058.2010.511694
- Casadio F, Chiari G. Simon S. 2005. Evaluation of binder/aggregate ratios in archaeological lime mortars with carbonate aggregate: a comparative assessment of chemical, mechanical and microscopic approaches. Archaeometry 47(4) pp. 671–89.
- Casadio, F., Daher, C. & Bellot-Gurlet, L. 2016. Raman Spectroscopy of cultural heritage Materials: Overview of Applications and New Frontiers in Instrumentation, Sampling Modalities, and Data Processing. Topics in Current Chemistry, 374, 62.
- Cassar, M., Brimblecombe, P., Nixon, T., Price, C., Sabbioni, C., Saiz-Jimenez, C., Van Balen, K., 2004."Sustainable solutions in the conservation and protection of historic monuments and archaeological remains: a critical assessment of European research needs". In: Air Pollution and Cultural Heritage, C.Saiz-Jimenez (ed.), Balkema, Lisse, Netherlands, pp. 249-261.
- Cazalla, O. Rodriguez-Navarro,C. Sebastian, E. and Cultrone, G. de la Torre, M.J. 2000. Aging of Lime Putty: Effects on Traditional Lime Mortar Carbonation. J. Am. Ceram. Soc., 83 [5] pp. 1070–76.
- CEN, EN 1015-2: 1998. Bulk sampling of mortars and preparation of test mortars,1998, Brussels
- Coutelas, A. 2011. The selection and use of lime mortars on the building sites of Roman Gaul. Comm. Hum. Litt. Vol. 128, pp.139-151.
- Crisci, G. M., Franzini, M., Lezzerini, M., Mannoni, T. & Riccardi, M. P. 2004. Ancient mortars and their binder. Periodico di Mineralogia, 73, 259-268.
- Crupi, V. Galli, G. La Russa, M. F. Longo, F. Maisano, G. Majolino, D. Malagodi, M. Pezzino, A. Ricca, M. Rossi, B. Ruffolo, S. A. & Venuti, V. 2015. Multi-technique investigation of Roman decorated plasters from Villa dei Quintili (Rome, Italy). Applied Surface Science, 349, pp 924-930.

- Cultrone, G. Sebastián, E. & Huertas, M. O. 2005. Forced and natural carbonation of lime-based mortars with and without additives: Mineralogical and textural changes. Cement and Concrete Research, 35, 2278-2289.
- Çakmaklı, Ö.D. 2016. Labraunda'nin Yeni Bilmecesi: Su Kompleksi Kazıları 2013-2015 Kazı Sezonu Değerlendirmesi, Journal of History Culture and Art Research (ISSN: 2147-0626), DOI: 10.7596/taksad.v5i3.522
- Çamurcuoğlu, D. & Siddal, R. Plastering the Prehistory: Marl as a unique material to cover, maintain and decorate the Neolithic walls of Çatalhöyük. *In:* Papayianni, I., Stefanidou, M. & Pachta, V., eds. 4th Historic Mortars Conference, 2016 Santorini, Greece. Laboratory of Building Materials Department of Civil Engineering Aristotle University of Thessaloniki.
- Çizer, Ö. 2004. Investigation of Lime Mortar Characteristics for the conservation of the Ottoman baths in Seferihisar-Urla Region. Unpublished MSc. Dissertation ed. İzmir: İzmir Institute of Technology.
- Çizer, Ö. Van Balen, K. Elsen, J. Van Gemert, D. 2008. Crystal Morphology of Precipitated Calcite Crystals From Accelerated Carbonation of Lime Binders. In: Proc. ACEME08, 2nd International Conference on Accelerated Carbonation for Environmental and Materials Engineering, 1-3 October 2008, Rome, Italy, pp. 149-158.
- Çizer, Ö. Van Balen, K. & Van Gemert, D. 2010. Competition Between Hydration and Carbonation in Hydraulic Lime and Lime-Pozzolana Mortars. *Advanced Materials Research* 133-134, 241-246.
- Çizer, Ö. Rodriguez-Navarro, C, Ruiz-Agudo, E. Elsen, J. Van Gemert, D. & Van Balen, K. 2012a. Phase and morphology evolution of calcium carbonate precipitated by carbonation of hydrated lime. Journal of Materials Science, 47, 6151-6165.
- Çizer, Ö. Van Balen, K. Elsen, J. & Van Gemert, D. 2012b. Real-time investigation of reaction rate and mineral phase modifications of lime carbonation. *Construction and Building Materials,* 35, 741-751.

D.....

- Dawson, P. Hadfield, C. D. and Wilkinson, G. R. 1973. The polarized infrared and Raman spectra of Mg(OH)a and Ca(OH)M, J. Phys. Chem. Solids, 34, 1217-1225,
- Degryse, P. Elsen, J. and Waelkens. M. 2002. Study of Ancient Mortars from Sagalassos (Turkey) in View of Their Conservation. Cement and Concrete Research 32: 1457-1463. doi: 10.1016/S0008-8846(02)00807-4.
- Despotou, E. Schlegel, T. Shtiza, A. and Verhelst, F. 2014. Literature study on the rate and mechanism of carbonation of lime in mortars, 9th International Masonry Conference, Guimãraes.
- De Luca, R. Miriello, D. Pecci, A. Domínguez Bella, S. Bernal Casasola, D. Cottica, D. & Crisci, G. M. 2014. Mortars and plasters from the "Garum Workshop" at Pompei (Italy): An archeometric study. VIII Congresso Nazionale di Archeometria Scienze e Beni Culturali: stato dell'arte e prospettive Bologna 5 - 7 February 2014.
- Domingo C. Loste E. Gomez-Morales J. Garcia-Carmona J. Fraile J. 2006. Calcite precipitation by a high-pressure CO2 carbonation route. J. Supercritical Fluids 36, 202-215.
- Duran, A. Sirera, R. Pérez-Nicolás, M. Navarro-Blasco, I. Fernández, J. M. & Alvarez, J. I. Behaviour of air lime-metakaolin mortars modified with polynaphthalene sulfonate as superplasticizer. *In:* I. Papayianni, M. S., V. Pachta, ed. 4th Historic Mortars Conference - HMC 2016 2016 Santorini, Greece. Laboratory of Building Materials Department of Civil Engineering Aristotle University of Thessaloniki Thessaloniki, Greece, 383-390.
- Durán Cabello, R. M. 2004. El teatro y el anfiteatro de Augusta Emerita. Contribución al conocimiento histórico de la capital de Lusitania. Oxford: Archaeopress (BAR International Series; 1207). p 273.
- Duran, A. Perez-Rodriguez, J.L. Jimenez de Haro, M.C. Franquelo, M.L. Robador, M.D. 2011. Analytical study of Roman and Arabic wall paintings in the Patio De Banderas of Reales Alcazares' Palace using non-destructive XRD/XRF and complementary techniques. Journal of Archaeological Science. Vol 38.pp 2366-2377.

- Durán Fuentes, M. 2003. An endeavour to identify Roman Bridges. In: Actsbook of the first International Congress on Construction History. Instituto Juan de Herrera, E.T.S. de Arquitectura de Madrid.

E.....

- EDAMM, 2002. Environmental deterioration of ancient and modern hydraulic mortars Van Balen K, Toumbakari EE, Blanco-Varela M.T, Aguilera J, Puertas F, Palomo A, Sabbioni C, Riontino, C. Zappia G, Research Report No 15 Project No ENV4-CT95-0096.
- Edwards, H. G. M. Holder, J. M. Seaward, M. R. D. & Robinson, D. A. 2002. Raman spectroscopic study of lichen-assisted weathering of sandstone outcrops in the High Atlas Mountains, Morocco. Journal of Raman Spectroscopy, 33, 449-454.
- Elert, K. Rodriguez-Navarro, C. Sebastian Pardo, E. Hansen, E. & Cazalla, O. 2002. Lime mortars for conservation of historical buildings. Studies in Conservation 7(1), 62-75.
- Elsen, J. Mertens, G. Degryse, P. & Waelkens, M. 2005. Conservation of Ancient Mortars at Sagalassos-Turkey. International RILEM Workshop on Repair Mortars for Historic Masonry (pp. 94-98). RILEM Publications Pro 67.
- Elsen, 2006. Microscopy of historic mortars- a review. Cement and Concrete Research 36, pp 1416-1424.
- Elsen, J. Mertens, G. & Van Balen, K. 2011. Raw materials used in ancient mortars from the Cathedral of Notre-Dame in Tournai (Belgium). European Journal of Mineralogy, Volume 23, p. 871–882.
- Elsen J. Van Balen K. Mertens G. 2012. Hydraulicity in Historic Lime Mortars: A Review. in: Válek J., Hughes J., Groot C. (eds) Historic Mortars. RILEM Bookseries, vol 7. Springer, Dordrecht
- El-Turki, A. Ball, R.J. Allen, G.C. 2007. The influence of relative humidity on structural and chemical changes during carbonation of hydraulic lime. Cement and Concrete Research 37(8):1233–40.
- Ergenç, D. Sánchez Montes, A.L. Fort, R. Sanz Arauz, D. Rascón Marqués, S. 2014. Los morteros de la ciudad romana de Complutum: Inicio de una investigación, Miradas

a la investigación arquitectónica: construcción, gestión, tecnología Architectural research findings: building construction, management, technology, ed: M. M. Barbera-Barrera, F. Olivieri & J. Pinilla-Melo, ETSAM, Madrid, ISBN: 978-84-617-0504-7, pp. 34-39.

- Ergenç, D. Sánchez Montes, A.L. Fort, R. 2015. Caracterización de pinturas murales en Casa de los Grifos de la ciudad romana Complutum, Alcalá de Henares, Estudio y Conservación del Patrimonio Cultural. Actas, ed: M. Morena Oliva, M.A. Rogerio-Candelera, J.T. López Navarrete, V. Hernández Jolín, Málaga 2015. ISBN: 978-84-608-2452-7, pp. 107-111.
- Ergenç, D. Fort, R. 2016. Characterization of Roman mortars of Nysa in the ancient Caria, Turkey. Proceedings of the 4th Historic Mortars Conference HMC2016 10th-12th October 2016, Santorini, Greece Ed. I. Papayianni, M. Stefanidou, V. Pachta, Laboratory of Building Materials Department of Civil Engineering Aristotle University of Thessaloniki, ISBN: 978-960-99922-3-7

F.....

- Farci, A. Floris, D. Meloni, P. 2005. Water permeability vs. porosity in samples of Roman mortars. Journal of Cultural Heritage 6, pp.Perez Ema 55–59
- Faria, P. & Martins, A. 2013. Influence of Air Lime type and Curing Conditions on Lime and Lime-Metakaolin Mortars. *In:* De Freitas, V. P. D. & Delgado, J. M. P. Q. (eds.) *Durability of Building Materials and Components.* Berlin, Heidelberg: Springer Berlin Heidelberg.
- Farinha, C. de Brito, J. & Veiga, R. 2015. Incorporation of fine sanitary ware aggregates in coating mortars. *Construction and Building Materials,* 83, 194-206.
- Fernandes, F.M. Lourenço, P.B. and Castro, F. 2010. Ancient Clay bricks: manufacture and properties, in al., M.B.D.e. (ed.) Materials, Technologies and Practice in Historic Heritage.

- Figueiredo, M. O. Veiga, J. P. Silva, T. P. 2001. Materials and reconstruction techniques at the Aqueduct of Carthage since the Roman period. Historical Constructions, P.B. Lourenço, P. Roca (Eds.), Guimarães. pp 391-400.
- Fort, R. 1996. Características cromáticas de los materiales de construcción. In F. Mingarro (ed.): *Degradación y conservación del Patrimonio Arquitectónico*. Editorial Complutense. pp. 213-226
- Fort, R. 2008. Aplicación de la técnica de propagación de ondas ultrasónicas en el patrimonio petreo, in Proceeding of Durabilidad y Conservacion de materiales tradicionales naturales del patrimonio arquitectónico, Cáceres, pp 107-133.
- Franquelo, M. L. Robador, M. D. Ramírez-Valle, V. Durán, A. Jiménez de Haro, M. C. & Pérez-Rodríguez, J. L. 2008. Roman ceramics of hydraulic mortars used to build the Mithraeum house of Mérida (Spain). *Journal of Thermal Analysis and Calorimetry,* 92**,** 331-335.
- Freely, J. 2004. The Western Shores of Turkey. Discovering the Aegean and Mediterranean Coasts. Tauris Parke Paperbacks.
- Fusade, L. & Viles, H. 2016. Wood ash as an Additive: a Study of its Influence on the Physical Properties of Lime Mortars. *In:* I. Papayianni, M. S., V. Pachta ed. 4th Historic Mortars Conference 2016 Santorini, Greece. Laboratory of Building Materials Department of Civil Engineering Aristotle University of Thessaloniki Thessaloniki, Greece, 367-374.

G.....

- Gameiro, A. Santos Silva, A. Faria, P. Grilo, J. Branco, T. Veiga, R. Velosa, A. 2014. Physical and chemical assessment of lime-metakaolin mortars: Influence of binder:aggregate ratio. . Cement and Concrete Composites,, 45, 264-271.
- Gárate Rojas, I. 1994. Las Artes de la Cal (2nd ed). Ministerio de Cultura-ICBRBC. Madrid.
- Garcia Carmona J. Gomez Morales J. Rodriguez Clemente R. 2003. Rhombohedral–scalenohedral calcite transition produced by adjusting the solution electrical

conductivity in the system Ca(OH)2-CO2-H2O, J. Colloid and Interface Science 261, 434-440.

- Gedacht, D.C. 2004. Technology of Ancient Rome. The Rosen Publishing Group
- Genestar, C. Pons, C. & Más, A., 2006. Analytical characterisation of ancient mortars from the archaeological Roman city of Pollentia (Balearic Islands, Spain). Analytica Chimica Acta, Volumen 557, p. 373–379.
- Ghorab, H.Y. Ragai J. and Antar A. 1986. Surface and bulk properties of ancient Egyptian mortars. Part I: X-ray diffraction studies. Cement Concrete Research. Vol 16. pp 813-822.
- Giavarini, C. 2010. The Basilica of Maxentius and Its Construction Materials.in: BOŞTENADORU DAN, M., PŘIKRYL, R. & TÖRÖK, Á. (eds.) Materials, Technologies and Practice in Historic Heritage Structures. Dordrecht: Springer Netherlands DOI: 10.1007/978-90-481-2684-2_12, Springer, Chapter 12, pp. 209-234.
- Gliozzo, E. Dalconi, M. C. Cruciani, G. & Turbanti Memmi, I. 2009. Application of the Rietveld method for the investigation of mortars: a case study on the archaeological site of Thamusida (Morocco). European Journal of Mineralogy, 21, 457-465.
- Gleize, P.J.P. Motta, E.V. Silva, D.A. Roman, H.R. 2009. Characterization of historical mortars from Santa Catarina (Brazil). Cement & Concrete Composites. Vol 31. pp 342–346.
- Goedicke, C. 2004. Dating historical calcite mortar by blue OSL: results from known age samples. Radiation Measurements. vol 37. pp 409 – 415.
- Goldsworthy, H. & Zhu, M. I. N. 2009. Mortar Studies Towards The Replication Of Roman Concrete. Archaeometry, 51, 932-946.
- González Cortina, M. 2000. Recuperación de morteros romanos de cal y chamota en aplicaciones actuales. PhD Thesis. Universidad Politécnica de Madrid
- Gotti, E. Oleson, J. P. Bottalico, L. Brandon, C. Cucitore, R. & Hohlfelder, R. L. 2008. A Comparison of The Chemical And Engineering Characteristics of Ancient Roman

Hydraulic Concrete With A Modern Reproduction Of Vitruvian Hydraulic Concrete*. Archaeometry, 50, 576-590.

- Gomez-Villalba, L.S. López-Arce, P. Alvarez de Buergo, M. Fort. R. 2011. Structural Stability of a colloidal solution of a $Ca(OH)_2$ nanocrystals exposed to high relative humidity conditions. Appl. Phys. A 104(4), pp. 1249–1254
- Gomez-Villalba, L. S., López-Arce, P. & Fort, R. 2012. Nucleation of $CaCO_3$ polymorphs from a colloidal alcoholic solution of $Ca(OH)_2$ nanocrystals exposed to low humidity conditions. Applied Physics A, 106, 213-217.
- Gonzalez Cortina, M. 2000. Recuperacion de Morteros Romanos de Cal y Chamota en Aplicaciones Actuales. PhD Thesis, ETSAM, UPM
- Gordana A. Topličić-Ćurčić, Zoran J. Grdić, Nenad S. Ristić, Dušan Z. Grdić, Petar B. Mitković, Igor S. Bjelić, Ana J. Momčilović-Petronijević. 2014: Characterization of Roman mortar from the Mediana archeological site, Technical Gazette, Faculty of Mechanical Engineering in Slavonski Brod, Faculty of Electrical Engineering in Osijek, Faculty of Civil Engineering in Osijek, Vol 21, No1, ArticleNoTV-20130503131031, , Slavonski Brod, Croatia, ISSN1330-3651(M23)
- Groot, C. Bartos, P. Hughes, J. 2000. Characterisation of old mortars with a respect to their repair, in Proc. 12th International Brick/Block Masonry Conference, Madrid, p. 815-827.
- Groot, C. 2016. Repair mortars for historic masonry; Effects of the binder choice on durability. HERON 61.
- Gutman, M., Zupanek, B., Lesar Kikelj, M. & Kramar, S. 2016. Wall Paintings from the Roman Emona (Ljubljana, Slovenia): Characterization of Mortar Layers and Pigments. *Archaeometry,* 58**,** 297-314.
- Güney, B.A. 2012. Development of Pozzolanic Lime Mortars for the repair of Historic Masonry. PhD Thesis. Middle East Technical University. Ankara.

H.....

- Hale, J. Heinemeier, J. Lancaster, L. Lindroos, A. Ringbom, Å. 2003. Dating Ancient Mortar. American Scientist. Volume 91. pp 130-38.
- Hamey, L. A., Hamey, J. A. 1990. The Roman Engineers. Published in cooperation with Cambridge University Press. Lerner Publications Co.
- Hauptmann, A. Yalçın, Ü. 2000. Lime plaster, cement and the first puzzolanic reaction. In: Paléorient, vol. 26, n°2. La pyrotechnologie à ses débuts. Evolution des premières industries faisant usage du feu. pp. 61-68; doi: 10.3406/paleo.2000.4710 http://www.persee.fr/doc/paleo_0153-9345_2000_num_26_2_4710
- Hellström, P. 2007. Labraunda: a guide to the Karian sanctuary of Zeus Labraundos, Istanbul: Ege Yayınları.
- Henry, O. Andersson, E. Bost,C. Çakmaklı, ÖD.Commito, A. Cormier-Huguet, M. de Staebler, P. Dupont, P. Ergenç, D. Frejman, A. Kepenek, B. Lebouteiller, P. Nilsson, H. Rojas, F. Vergnaud, B. 2015. Labraunda 2014. Anatolia Antiqua XXIII, pp. 301-394.
- Hiesel, G. and Strocka, V. M. 2006. Die Bibliothek von Nysa am Mäander, Vorläufiger Bericht über die Kampagnen 2002–2006. Originalbeitrag erschienen in Archäologischer Anzeiger 2. 81-97.
- Hill, D. 1996. A History of Engineering in Classical and Medieval Times. Routledge.
- Hujer, W. H. F., T. Persaud, M. 2014. Estimating rock strength from non-destructive strength testing (equotip) and related benefits. EAGE Workshop on Geomechanics in the Oil and Gas Industry, 3.

I.....

- ICCROM, 1999, Arc Laboratory Handbook, ISSBN: 92-9077-157-7
- ICOMOS, 1964. International Charter For The Conservation And Restoration Of Monuments And Sites (The Venice Charter) http://www.icomos.org/charters/venice_e.pdf access date: 13/01/2017

- ICOMOS, 1990. Charter For The Protection And Management Of The Archaeological Heritage, http://www.icomos.org/images/DOCUMENTS/Charters/arch_e.pdf access date: 13/01/2017
- ICOMOS, 2003. Icomos Charter- Principles For The Analysis, Conservation And Structural Restoration Of Architectural Heritage, http://www.icomos.org/images/DOCUMENTS/Charters/structures_e.pdf access date: 13/01/2017
- İdil, V. 1999. Nysa ve Akharaka Nysa and Akharaka, İstanbul.
- Igea, J. Lapuente, P. Martínez-Ramírez, S. & Blanco-Varela, M. T. 2012. Characterization of mudejar mortars from St. Gil Abbot Church (Zaragoza, Spain): investigation of the manufacturing technology of ancient gypsum mortars. *Materiales de Construcción,* 62**,** 515-529.
- IGME, 1928. Mapa Geológico Nacional a escala 1:50.000 Hoja 50_560
- IGME, 1991. Mapa Geológico Nacional a escala 1:50.000 Hoja 0777
- Ingham, J. P. 2013. Geomaterials Under the Microscope. 8 - Mortar, plaster, and render. Boston: Academic Press.
- Ingo, G. M. Fragalà, I. Bultrini, G. de Caro, T. Riccucci, C. & Chiozzini, G. 2004. Thermal and microchemical investigation of Phoenician–Punic mortars. Thermochimica Acta, Volumen 418, p. 53–60.
- Izaguirre, A. Lanas, J. & Álvarez, J. I. 2010. Ageing of lime mortars with admixtures: Durability and strength assessment. Cement and Concrete Research, 40, 1081-1095.
- Izzo, F. Arizzi, A. Cappelletti, P. Cultrone, G. De Bonis, A. Germinario, C. Graziano, S. F. Grifa, C. Guarino, V. Mercurio, M. Morra, V. & Langella, A. 2016. The art of building in the Roman period (89 B.C. – 79 A.D.): Mortars, plasters and mosaic floors from ancient Stabiae (Naples, Italy). Construction and Building Materials, vol 117**,** 129-143.

J.....

- Jackson, M. D. J.M. Logan, B.E. Scheetz, D.D. Deocampo, C.G. Cawood, F. Marra, M. Vitti, and L. Ungaro. 2009. Assessment of Material Characteristics of Ancient

Concretes, Grand Aula, Markets of Trajan, Rome. Journal of Archaeological Science 36: 2481-2492. doi: 10.1016/j.jas.2009.07.011.

- Jackson, M.D. P. Ciancio Rossetto, C.K. Kosso, M. Buonfiglio, and F. Marra. 2011. Building Materials of the Theatre of Marcellus, Rome. Archaeometry 53(4):728-742. doi: 10.1111/j.1475-4754.2010.00570.x.
- Jackson, M. D. Chae, S. Mulcahy, S. R. Meral, Ç. Taylor, R. Li, P. Emwas, A.-H. M., Moon, J. Yoon, S. Vola, G. Wenk, H. R. & Monteiro, P. J. M. 2013. Unlocking the secrets of Al-tobermorite in Roman seawater concrete. *American Mineralogist,* 98**,** 1669–1687.
- Jung W. M. Kang S. H. Kim W.S. Choi C. K. 2000. Particle morphology of calcium carbonate precipitated by gas–liquid reaction in a Couette–Taylor reactor. Chemical Engineering Science 55, 733-747.

K.....

- Keay, S. 1988. Roman Spain, University of California Press
- Knapen, E. Çizer, Ö. Van Balen, K. & Van Gemert, D. 2009. Effect of free water removal from early-age hydrated cement pastes on thermal analysis. *Construction and Building Materials,* 23**,** 3431-3438.
- Kadıoğlu M & Kadıoğlu Y. K. 2008. Native of the marble in ancient city, Nysa on the Meander of Hellenistic and Roman Period, Aydin- Western Anatolia-Turkey. IOP Conf. Series: Earth and Environmental Science 2: 012-022 doi:10.1088/1755-1307/2/1/012022
- Kontoyannis, C. G. & Vagenas, N. V. 2000. Calcium carbonate phase analysis using XRD and FT-Raman spectroscopy. Analyst, 125, 251-255.
- Kourouniōtēs, K. 1924. Ellēnikai anaskaphai en Mikra Asia. Anaskaphai en Nusē tē epi Maiandrō, ADelt 7, 1921-22 Atina,
- Kramar, S. Zalar, V. Urosevic, M. Körner, W. Mauko, A. Mirtič, B. Lux, J. & Mladenović, A. 2011. Mineralogical and microstructural studies of mortars from the bath complex of the Roman villa rustica near Mošnje (Slovenia). *Materials Characterization,* 62**,** 1042-1057.

- Kurugöl, S. Güleç, A. 2015. Physico-Chemical, Petrographical and Mechanical Properties of Mortars used in an Ancient Roman Basilica in Amasra/Turkey. Gazi University Journal Of Science, [S.l.], v. 28, n. 4, p. 609-621, dec. 2015. ISSN 2147-1762. Available at: <http://gujs.gazi.edu.tr/article/view/1060001842>. Date accessed: 08 Apr. 2017.

L.....

- Lanas, J. Álvarez-Galindo, J. I. 2003. Masonry repair lime-based mortars: factors affecting mechancal behaviour, Cem. Conc. Res. 33(11) pp. 1867-76.
- Lanas, J. Pérez Bernal, J. L. Bello, M. A. & Alvarez Galindo, J. I. 2004. Mechanical properties of natural hydraulic lime-based mortars. *Cement and Concrete Research,* 34**,** 2191-2201.
- Lanas, J. Sirera, R. & Alvarez, J. I. 2006. Study of the mechanical behavior of masonry repair lime-based mortars cured and exposed under different conditions. Cement and Concrete Research*,* 36**,** 961-970.
- Lancester, L. Sotilli, G. Marra, F. & Ventura, G. 2011. Provenancing of lightweight volcanic stones used in ancient Roman concrete vaulting: Evidence from Rome. Archaeometry, 53, 707–727.
- La Russa, M.F. Ruffolo, S.A. Ricca, M. Rovella, N. Comité,V. Alvarez de Buergo, M. Crisci, G.M. Barc, D. 2015. Archaeometric approach for the study of mortars from the underwater archaeological site of Baia (Naples) Italy: Preliminary results. Periodico di Mineralogia 84, 3A (Special Issue), pp. 553-567, DOI: 10.2451/2015PM0031
- La Russa, M. F. Rovella, N. Pelosi, C. Rossi, D. Benucci, M. Romagnoli, G. Selva Bonino, V. E. Casoli, A. & Ruffolo, S. A. 2016. A multi-analytical approach applied to the archaeometric study of mortars from the Forty Martyrs rupestrian complex in Cappadocia (Turkey). Microchemical Journal, 125, 34-42.
- Lawrence, R. 2006. A Study of carbonation in nonhydraulic lime mortars, PhD Dissertation, Bath: University of Bath.

- Lawrence, R. Mays, T. Walker, P. & D'Ayala, D., 2007. Determination of carbonation profiles in non-hydraulic lime mortars using thermogravimetric analysis. Thermochimica Acta, Volumen 444 , p. 179–189.
- Leone, G. De Vita, A. Magnani, A. Rossi, C. 2016. Thermal and Petrographic Characterization of Herculaneum Wall Plasters. Archaeometry, DOI: 10.1111/arcm.12275.
- Leslie, A. B. & Hughes, J. J. 2002. Binder microstructure in lime mortars: implications for the interpretation of analysis results. Quarterly Journal of Engineering Geology and Hydrogeology, 35, 257-263.
- Lourenço, P.B. van Hees, R. Fernandes, F. Lubelli, B. 2014. Characterization and damage of brick masonry. DOI: 10.1007/978-3-642-39686-1_4
- Lucas, A. and Harris, J.R. 1962. Ancient Egyptian Materials and Industries. Edward Arnold. London.
- Luque, A. Cultrone, G. Sebastián, E. 2010. The Use of Lime Moratrs in Restoration Work on Architectural Heritage in: M.Bostenatu Dan et al. (eds.), Materials, Technologies and Practice in Historic Heritage Structures, DOI: 10.1007/978-90-481-2684-2-11
- Luxan, M.P. Dorrego, F. 2004. Characterization and selection of mortars in the restoration of the Kings Portal (Benavente, Zamora). Materials of Construction, Vol.54, no. 273
- Łydżba-Kopczyńska B. Madariaga J. M. 2016. Applications of Raman spectroscopy in art and archaeologyJ. Raman Spectrosc. 2016, 47, 1404–1407. DOI 10.1002/jrs.5067

M.....

- MacDonald, W. L. 1965. The Architecture of the Roman Empire. New Haven and London: Yale University Press.
- Magalhães, A. Veiga, R. 2009. Physical and mechanical characterisation of ancient mortars. Application to the evaluation of the state of conservation. Materiales de construcion. vol 59 no 295.pp 61-77.

- Malinowski, R. 1981. Ancient mortars and concretes. Durability aspects. Proceedings ICCROM Symposium. Rome, ICCROM, p. 341-349.
- Mamoli, M. 2007. Paper Space: The Library of Nysa Revisited. 11th Iberoamerican Society of Digital Graphics: Communication in the Visual Society. Mexico City: University La Salle.
- Maravelaki-Kalaitzaki, P. Bakolas, A. & Moropoulou, A. 2003. Physico-chemical study of Cretan ancient mortars. Cement and Concrete Research, Volume 33, p. 651–661.
- Maravelaki-Kalaitzaki, P. Bakolas, A. Karatasios, I. and Kilikoglou, V. 2005. Hydraulic lime mortars for the restoration of historic masonry in Crete, Cement and Concrete Research, 35, 8: 1577-1586.
- Marra, F. Deocampo, D. Jackson, M.D. Ventura, G. 2011. The Alban Hills and Monti Sabatini volcanic products used in ancient Roman masonry (Italy): An integrated stratigraphic, archaeological, environmental and geochemical approach. Earth-Science Reviews 108, pp.115–136.
- Marra, F. Danti, A. Gaeta, M. 2015. The volcanic aggregate of ancient Roman mortars from the Capitoline Hill: Petrographic criteria for identification of Rome's "pozzolans" and historical implications. *Journal of Volcanology and Geothermal Research,* 308**,** 113-126.
- Martinez-Garrido, M.I. Ergenç, D. Fort, R. 2016. Wireless Monitoring to Evaluate the Effectiveness of Roofing Systems Over Archaeological Sites. Sensors and Actuators A Physical, DOI: 10.1016/j.sna.2016.10.038
- Martinez-Ramirez, S. Sanchez-Cortes, S. Garcia-Ramos. J. Domingo, C. Fortes, C. Blanco-Varela, M.T. 2003. Micro-Raman spectroscopy applied to depth profiles of carbonates formed in lime mortar. Cement and Concrete Research, 33 (12), pp.2063-2068.
- Marzaioli, F. Nonni, S. Passariello, I. Capano, M. Ricci, P. Lubritto, C. De Cesare, N. Eramo, G. Antonio Quirós Castillo, J. Terrasi, F. 2013. Accelerator mass spectrometry 14C dating of lime mortars: Methodological aspects and field study applications at

CIRCE (Italy). Nuclear Instruments and Methods in Physics Research B. vol 294. pp 246–251.

- Matias, G. Faria, P. Torres, I. 2014a. Lime mortars with heat treated clays and ceramic waste: A review, Construction and Building Materials 73, pp. 125-136.
- Matias, G. Faria, P. Torres, I. 2014b. Lime mortars with ceramic wastes: characterization of components and their influence on the mechanical behaviour, Construction and Building Materials 73, pp. 523-534.
- Mellaart, J. 1967. Catal Hüyük: A Neolithic Town in Anatolia. New York: McGraw-Hill.
- Mertens, G. Snellings, R. Van Balen K. Bicer-Simsir, B. Verlooy, P. Elsen, J. 2009. Pozzolanic reactions of common natural zeolites with lime and parameters affecting their reactivity. Cement and Concrete Research 39, pp. 233–240.
- METU, 2013. Labranda 'Andron A' Restoration Project.
- Middendorf, B. Hughes, J. J. Callebaut, K. Baronio, G. & Papayianni, I. 2005a. Investigative methods for the characterisation of historic mortars—Part 1: Mineralogical characterisation. *Materials and Structures,* 38**,** 761.
- Middendorf, B. Hughes, J.J. Callebaut, K. 2005b. Investigative methods for the characterisation of historic mortars—Part 2: Chemical characterisation. Materials and Structures 38(8): 771-780. doi:10.1007/BF02479290
- Miriello, D. Barca, D. Bloise, A. Ciarallo, A. Crisci, G.M. De Rose, T. Gattuso, C. Gazineo, F. La Russa, M.F. 2010. Characterisation of archaeological mortars from Pompeii (Campania, Italy) and identification of construction phases by compositional data analysis. Journal of Archaeological Science. vol 37. pp 2207-2223.
- Miriello, D. Bloise, A. Crisci, G. M. Apollaro, C. & La Marca, A. 2011. Characterisation of archaeological mortars and plasters from kyme (Turkey). *Journal of Archaeological Science,* 38**,** 794-804.
- Miriello, D. Bloise, A. Crisci, G. M. Apollaro, C. Caracciolo, L. & La Marca, A. 2012. Archaeometric analysis of archaeological mortars and plasters from Kyme (Turkey). Arkeometri Sonuçları Toplantısı, 27.

- Montoya, C. Navarro, J. L. M. A., Casado, I., P. G. & Alvarez, J. I. 2003. Study of Ancient dolomitic mortars of the church of Santa María de Zamarce in Navarra (Spain). Comparison with simulated standards. Thermochimica Acta, 398(107-122).
- Moorehead D.R. 1986. Cementation by the Carbonation of Hydrated Lime. Cem. Conc. Res. 16, 700-708.
- Morandeau, A. Thiery, M. Dangla, P. 2014. Investigation of carbonation mechanism of {CH} and C-S-H in terms of kinetics, microstructure changes and moisture properties. Cement and Concrete Research. 56, pp. 153-170.
- Moropoulou, A. Bakolas, A. & Bisbikou, K. 1995. Characterization of ancient, byzantine and later historic mortars by thermal and X-ray diffraction techniques. *Thermochimica Acta,* 269**,** 779-795.
- Moropoulou, A. and Bakolas, A. 1998. Range of acceptability limits of physical, chemical and mechanical characteristics deriving from the evaluation of historic mortars, European Study Group on Physical, Chemical, Biological and Mathematical Tecqniques Applied to Archaeology, vol. 56, pp. 165-178.
- Moropoulou, A. Bakolas, A. & Bisbikou, K., 2000a. Physico-chemical adhesion and cohesion bonds in joint mortars imparting durability to the historic structures. Construction and Building Materials, Volumen 14, pp. 35-46.
- Moropoulou, A. Bakolas, A. Bisbikou, K. 2000b. Investigation of the technology of historic mortars, Journal of Cultural Heritage,vol. 1 pp 45-58.
- Moropoulou, A. Bakolas, A. and Aggelakapoulou, E. 2004. Evaluation of pozzolanic activity of natural and artificial pozzolans by thermal analysis, Thermochimica Acta, vol. 420, 135-140.
- Moropoulou, A. Bakolas, A. Moundoulas, P. Aggelakopoulou, E. & Anagnostopoulou, S. 2005. Strength development and lime reaction in mortars for repairing historic masonries. Cement and Concrete Composites, 27, 289-294.

- Moropoulou, A. and Polikreti, K. 2009. Principal Component Analysis in monument conservation: Three application examples, Journal of Cultural Heritage, vol. 10, pp. 73-81.
- Moropoulou, A. Apostolopoulou, M. Moundoulas, P. Aggelakopoulou, E. Siouta, L. Bakolas, A. Douvika, M. Karakitsios, P. and Asteris, P.G. 2016. The Role Of Restoration Mortars In The Earthquake Protection Of The Kaisariani Monastery, ECCOMAS Congress 2016 VII European Congress on Computational Methods in Applied Sciences and Engineering, Crete.Moropoulou, A., Bakolas, A. & Anagnostopoulou, S., 2005. Composite materials in ancient structures. Cement & Concrete Composites, Volumen 27, p. 295–300.
- Mosqueraa, M.J. Benitez, D. Perry, S.H. 2002. Pore structure in mortars applied on restoration Effect on properties relevant to decay of granite buildings. Cement and Concrete Research. Vol 32. pp 1883–1888.
- Mota López, M.I. 2015. Caracterización y Procedencia de los Materiales Geológicos Utilizados en el Teatro Y Anfiteatro de la Ciudad de Mérida en Época Romana, PhD thesis, Universidad Complutense de Madrid
- Mota-López, M. I., Fort, R., Álvarez de Buergo, M., Pizzo, A., Maderuelo-Sanz, R., Meneses-Rodríguez, J. M. & Ergenç, D. 2016. Characterization of concrete from Roman buildings for public spectacles in Emerita Augusta (Mérida, Spain). *Archaeological and Anthropological Sciences*, 1-16.

N.....

- Nežerka, V., Slížková, Z., Tesárek, P., Plachý, T., Frankeová, D. & Petráňová, V. 2014. Comprehensive study on mechanical properties of lime-based pastes with additions of metakaolin and brick dust. *Cement and Concrete Research,* 64, 17-29.
- Nežerka, V. Nemecek, J. Slížková, Z. 2015. Investigation of crushed brick-matrix interface in lime-based ancient mortar by microscopy and nanoindentation, Cement & Concrete Composites 55 , pp 122–128.

O.....

- Okay, A. 2001. Geological Map of Menderes Massif, Geology of Turkey,: http://web.itu.edu.tr/~okay/diagrams_%20maps/MapMenderesMassif.jpg (access date: 5.7.2014).
- Okay, A. 2007. Menderes Massif – A Nappe Pile or Stratigraphic Sequence? In TMMOB Jeologi Mühendisleri Odasi (ed) Menderes Masifi Kolokyumu: O. Özcan Dora Onuruna: Genişletilmiş bildiri özleri kitabı, Alsancak-İzmir.
- Ontiveros-Ortega, E., Rodríguez-Gutiérrez, O. & Navarro, A. D. 2016. Mineralogical and physical–chemical characterisation of Roman mortars used for monumental substructures on the Hill of San Antonio, in the Roman city of Italica (prov. Baetica, Santiponce, Seville, Spain). *Journal of Archaeological Science: Reports,* 7**,** 205-223.
- Ortega, L. A., Zuluaga, M. C., Alonso-Olazabal, A., Insausti, M. & Ibáñez, A. 2008. Geochemical Characterization of Archaeological Lime Mortars: Provenance Inputs. *Archaeometry,* 50**,** 387-408.
- Oğuz, C. Türker, F. Koçkal, N. U. 2014. Construction Materials Used in the Historical Roman Era Bath in Myra. The Scientific World Journal, vol. 2014, Article ID 536105, 9 pages, doi:10.1155/2014/536105
- Özkaya, Ö. Böke, H. 2009. Properties of Roman bricks and mortars used in Serapis temple in the city of Pergamon. Materials Characterization . vol 60. Pp 9995- 1000.
- Öztaner, S. H.,.Akdoğu, Arca, E.N. Gökalp Özdil, N. 2104. Nysa Ad Maeandrum'daki Yeni Bulgular Üzerine Bir Değerlendirme, In: Memoriam Filiz Öktem, 225-245

P.....

- Paamaa, L., PitkaÈnenb, I., RoÈnkkoÈmaÈkic, H. & Peraamaaki, P., 1998. Thermal and infrared spectroscopic characterization of historical mortars. Thermochimica Acta, Volumen 320 , pp. 127-133.
- Pahlavan, P., Manzi, S. & Bignozzi, M. C. Restorative Lime Mortars with Inclusion of Spent Cooking Oils. *In:* I. Papayianni, M. S., V. Pachta, ed. 4th Historic Mortars

Conference - HMC 2016 2016 Santorini, Greece. Laboratory of Building Materials Department of Civil Engineering Aristotle University of Thessaloniki Thessaloniki, Greece, 405-412.

- Palomo, A. Blanco-Varela, M.T. Martinez-Ramirez, S. Puertas, F. Fortes, C. 2004 Historic Mortars: Characterization and Durability. New Tendencies for Research, Eduardo Torroja Institute (CSIC). Madrid (Spain)
- Papayianni, I. Stefanidou, M. 2001.The Evolution of Porosity in Lime Based Mortars. in: 8th Euroseminar on Microscopy Applied to Building Materials, Athens
- Papayianni, I., Pachta, V. & Stefanidou, M. 2013. Analysis of ancient mortars and design of compatible repair mortars: The case study of Odeion of the archaeological site of Dion. *Construction and Building Materials,* 40**,** 84-92.
- Papayianni, I. & Stefanidou, M. 2006. Strength–porosity relationships in lime–pozzolan mortars. Construction and Building Materials, 20, 700-705.
- Papayianni, I. & Stefanidou, M. 2007. Durability aspects of ancient mortars of the archeological site of Olynthos. *Journal of Cultural Heritage,* 8**,** 193-196.
- Pavía. S. 2006. Repair mortars for masonry bridges. Bridge and Infrastructure Research in Ireland: Symposium, N.A.Ni Nuallain, A. O'Connor & K. Gavin Eds. Dept. Of Civil, Structural and Environmental Engineering, Trinity College Dublin. pp. 183-190.
- Pavia, S. & Caro, S. 2008. An investigation of Roman mortar technology through the petrographic analysis of archaeological material, Construction and Building Materials, 22, (8),1807 - 1811.
- Pavlík, V. & Užáková, M. 2016. Effect of curing conditions on the properties of lime, lime–metakaolin and lime–zeolite mortars. Construction and Building Materials, 102, Part 1, 14-25
- Pecchioni, E. Fratini, F. Cantisani, E. 2014. Atlante delle malte antiche in sezione sottile al microscopio ottico/ Atlas of the Ancient Mortars in thin section under optical microscope. 78 pp., ISSN: 2036-1122, ISBN: 978-88-404-4366-9.

- Pérez Ema, N. Álvarez de Buergo, M. Bustamante, R. 2013. Effects of Conservation Interventions on the Archaeological Roman Site of Mérida (Spain). Advance of Research. Procedia Chemistry. Vol. 8, pp. 269-278.
- Pérez-Monserrat, E. M. 2012. Técnicas de Caracterización Petrológicas (I): Microscopía Óptica de Polarización (Mop) y Difracción de Rayos X (DRX). In: Rafael Fort González, E. M. P.-M. (ed.) La conservación de los geomateriales utilizados en el patrimonio. Madrid.
- Pérez-Nicolás, M. Duran, A. Sirera, R. Navarro-Blasco, I. Fernández, J. M. & Alvarez, J.I. 2016. The use of a lignosulfonate superplasticizer in repair air lime-metakaolin mortars. *In:* I. Papayianni, M. S., V. Pachta ed. 4th Historic Mortars Conference - HMC 2016, 2016 Santorini, Greece Laboratory of Building Materials Department of Civil Engineering Aristotle University of Thessaloniki Thessaloniki, Greece, 375-382.
- Pizzo, A. 2007. Las técnicas constructivas de la arquitectura pública de Augusta Emerita. PhD Thesis, Universidad Autónoma de Madrid, 628 p..
- Polat-Pekmezci, I. Ersen, A. 2010. Characterization of Roman Mortars and Plasters in Tarsus (Cilicia-Turkey). 2nd Historic Mortars Conference HMC2010 and RILEM TC 203-RHM Final Workshop 22-24 September 2010, Prague, Czech Republic

R.....

- Ramírez Sábada, J.L. 2003: Catalogo de las inscripciones imperiales de Augusta Emerita, Cuadernos Emeritenses 21, Mérida.
- Rampazzi, L. Pozzi, A. Sansonetti, A. Toniolo, L. Giussani, B. 2006. A chemometric approach to the characterisation of historical mortars. Cement and Concrete Research. vol 36. pp 1108–1114.
- Rascón Marqués, S. Sánchez Montes, A. L. 2009. La basílica y los edificios administrativos del foro de la ciudad romana de Complutum. De los edificios de época de Claudio a la monumentalización urbana de los siglos III, IV y V. Anales de Arqueología Cordobesa, Nº 20, págs. 175 – 202.

- Rascón Marqués, S. Sánchez Montes, A. L. 2015. Complutum: modelo urbanístico para una ciudad romana privilegiada en los siglos III-IV d.C., en BRASSOUS, L. y QUEVEDO, A. (eds.): Urbanismo cívico en tiempos de cambio. Los espacios públicos de Hispania y del Occidente romano entre los siglos II y IV d.C. Collection de la Casa de Velázquez, Madrid.
- RILEM TC 25-PEM, 1980. Recommended test to measure the deterioration of Stone and to Access effectiveness of treatment methods. Materials and Structures, 75, pp. 175-253.
- RILEM TC 167-COM: 2005. Characterization of Old Mortars with Respect to their Repair: Prepared by: Van Balen, K., Papayianni, I., Van Hees, R., Binda, L., Waldum, A., Introduction to requirements for and functions and properties of repair mortars; Materials and Structures vol. 38 pp 781-785.
- RILEM TC 203-RHM. 2009. Repair mortars for historic masonry. Testing of hardened mortars, a process of questioning and interpreting. *Materials and Structures,* 42**,** 853-865.
- Ritzouli, K. Stefanidou, M. Konopisi, S. 2016. Analysis and evaluation of mortars in Santorini's construction technology from the Venetian period up to 19th century, Proceedings of HMC 2016 4th Historic Mortars Conference.
- Robador, M.D. Perez-Rodriguez, J.L. Duran, A. 2010. Hydraulic structures of the Roman Mithraeum house in Augusta emerita, Spain. Journal of Archaeological Science. Vol 37. pp 2426-2432.
- Rodriguez-Blanco, J.D. Shaw, S. Benning, L.G. 2011. The kinetics and mechanisms of amorphous calcium carbonate (ACC) crystallization to calcite, via vaterite. Nanoscale, 3, p. 265.
- Rodriguez-Navarro, C. Hansen, E. and Ginell, W.S. 1998. Calcium Hydroxide Crystal Evolution upon Ageing of Lime Putty. Journal of the American Ceramic Society 81(11): 3032-3034. doi: 10.1111/j.1151-2916.1998.tb02735.x.

- Rodríguez-Navarro, C. 2004. Binders in historical buildings: Traditional lime in conservation. *Seminario SEM 09*, 91-112.
- Rogers, S. B. 2011. Evaluation and Testing of Brick Dust as a Pozzolanic Additive to Lime Mortars for Architectural Conservation. (Masters Thesis). University of Pennsylvania, Philadelphia, PA.
- Ryu, M. Kim, H. & Ahn, J. 2008. Effect of Shape and Application Process of Precipitated Calcium Carbonate on Optical and Mechanical Properties of Recycled Paper, Geosystem Engineering, 11:4, 69-74, DOI: 10.1080/12269328.2008.10541288

S.....

- Sabbioni, C. Zappia, G. Riontino, Blanco-Varela, C. M.T. Aguilera, J. Puertas, F. Van Balen, K. Toumbakari, E.E. 2001. Atmospheric deterioration of ancient and modern vhydraulic mortars. Atmospheric Environment. Vol 35. pp 539-548.
- Sánchez-Moral, S. García-Guinea, J. Luque, L. González Martín, R. López Arce, P. 2004. Carbonation kinetic in Roman-like lime mortars. Mater. Constr. 54 (275), 23–37.
- Sanchez Montes, A.L. 2013. Oral documentation during the fieldwork.
- Sanchez-Moral, S. Luquea, L. Canaveras, J.C. Soler, V. Garcia-Guinea, J. Aparicio, A. 2005. Lime pozzolana mortars in Roman catacombs: composition, structures and restoration. Cement and Concrete Research. Vol 35. pp 1555 – 1565.
- Sandrolini, F. Franzoni, E. 2010. Characterization procedure for ancient mortars' restoration: The plasters of the Cavallerizza courtyard in the Ducal Palace in Mantua (Italy). Materials Characterization. vol 61. pp 97-104.
- Sanjurjo-Sánchez , J. Trindade, M.J. Blanco-Rotea, R. Benavides Garcia, R. Fernández Mosquera, D. Burbidge, C. Prudêncio, M.I. Dias, M.I. 2010. Chemical and mineralogical characterization of historic mortars from the Santa Eulalia de Bóveda temple, NW Spain. Journal of Archaeological Science. vol 37. pp 2346-2351
- Santos Silva, A. Paiva, M. Ricardo, J. Salta, M. Monteiro, A. M. Candeias, A. E. 2006a. Characterisation of roman mortars from the archaeological site of Troia. *Materials Science Forum,* 514, 1643-1647.

- Santos Silva, A. Ricardo, J. Salta, M. Adriano, P. Mirão, J. Candeias, A. E. Macias, A. 2006b. Characterization of Roman mortars from the historical town of Mértola. *In:* Fort, Alvarez De Buergo, Gomez Heras, Vasquez-Calvo (ed.) *Heritage Weathering and Conservation.* Madrid: Taylor & Francis.
- Santos Silva, A. Adriano, P. Magalhães, A. Pires, J. Carvalho, A. João Cruz, A. Mirão, J. Candeias, A. 2010. Characterization of Historical Mortars from Alentejo's Religious Buildings. International Journal of Architectural Heritage: Conservation, Analysis, and Restoration International Journal of Architectural Heritage. Vol 4 pp 138–154.
- Santos Silva, A. Gamiero. A. Grilo, J. Veiga, R. Velosa, A. 2014. Long-term behavior of lime–metakaolin pastes at ambient temperature and humid curing condition. *Applied Clay Science,* 88–89**,** 49–55.
- Schmidt, K. Hurd, J. & Thompson, D. 2011. Göbekli Tepe, Turkey Preliminary Site Conservation Inspection and First Mortar and Plaster Documentation Report. *Global Heritage Fund*.
- Schueremans, L. Çizer, Ö. Janssens, E. Serré, G. & Van Balen, K. 2011. Characterization of repair mortars for the assessment of their compatibility in restoration projects: Research and practice. Construction and Building Materials*,* 25**,** 4338-4350.
- Sepulcre-Aguilar, A. Hernández-Olivares, F. 2010. Assessment of phase formation in lime-based mortars with added metakaolin, Portland cement and sepiolite, for grouting of historic masonry. Cement and Concrete Research. Vol 40. Pp 66–76.
- Sepulcre-Aguilar, A. 2005. Influencia de las adiciones puzolánicas en los morteros de restauración de fábricas de interés histórico-artístico, PhD Thesis. E.T.S. Arquitectura. UPM
- Ševčík, R. Mácová, P. Sotiriadis, K. Pérez-Estébanez, M. Viani, A. & Šašek, P. 2016. Micro-Raman spectroscopy investigation of the carbonation reaction in a lime paste produced with a traditional technology. Journal of Raman Spectroscopy, 47, 1452-1457.
- Siddall, R. 2011. From kitchen to bathhouse: the use of waste ceramics as pozzolanic additives in Roman mortars. In Å. Ringbom, & R. L. Hohlfelder (Eds.), Building Roma

aeterna: current research on Roman mortar and concrete. The Finnish Society of Sciences and Letters., 128, 152-168.

- Siivola, J. Shmid R. 2007. List of Mineral Abbreviations, in Recommendations by the IUGS Subcommission on the Systematics of Metamorphic Rocks
- Silva, D.A. Wenk, H.R. Monteiro, P.J. M. 2005. Comparative investigation of mortars from Roman Colloseum and cistern. Thermochimica Acta. 438, pp. 35-40.
- Silva, J. de Brito, J. Veiga, R. 2009. Incorporation of fine ceramics in mortars. Construction and Building Materials 23. Pp. 556–564.
- Stanislao, C. Rispoli, C. Vola, G. Cappelletti, P. Morra, V. and de'Gennaro, M. 2011. Contribution to the knowledge of ancient Roman seawater concretes: Phlegrean pozzolan adopted in the construction of the harbour at Soli-Pompeiopolis (Mersin, Turkey). Periodico di Mineralogia, 80,471–488
- Stefanidou, M. & Papayianni, I. 2005. The role of aggregates on the structure and properties of lime mortars. Cement and Concrete Composites. Vol. 27, No. 9-10, pp. 914-919.
- Stefanidou, M. Papayianni, I. & Pachta, V. 2012. Evaluation Of Inclusions In Mortars Of Different. Archaeometry, 54(4), p. 737–751.
- Stefanidou, M. Anastasiou, E. & Georgiadis Filikas, K. 2014. Recycled sand in lime-based mortars. Waste Management, 34, 2595-2602.
- Stefanidou, M. Papayiani, I. Pachta, V. 2015. Analysis and Characterization of Roman and Byzantine fired bricks from Greece, Materials and Structures 48 (7), pp. 2251–2260.
- Stefanidou, M. 2016. Use of natural pozzolans with lime for producing repair mortars. *Environmental Earth Sciences,* 75**,** 758.
- Stefanidou, M. Papachristoforou, M. & Kesikidou, F. 2016. Fiber- reinforced lime mortars *In:* I. Papayianni, M. S., V. Pachta ed. 4th Historic Mortars Conference - HMC 2016 Santorini, Greece. Laboratory of Building Materials Department of Civil Engineering Aristotle University of Thessaloniki Thessaloniki, Greece, 422-430.

- Strabon, 2000. Antik Anadolu Coğrafyası (Geographica book XII – XIII – XIV), Ed. A. Pekman, N. Başgelen, Arkeoloji ve Sanat Yayınları, İstanbul.
- Strickland, M.H. 2010. Roman Building Materials, Construction Methods, and Architecture: the Identity of an Empire. Master Thesis. Clemson University

T.....

- Tekin, Ç. Kurugöl, S. 2012. Çeşitli Organik Katkilarin Kirecin Karbonizasyonu Üzerindeki Etkisi, Journal of the Faculty of Engineering and Arcchitecture of Gazi University, 27, 4, pp. 717-728.
- Theodoridou, M. Ioannou, I. & Philokyprou, M. 2013. New evidence of early use of artificial pozzolanic material in mortars. Journal of Archaeological Science, 40, 3263-3269.
- Thiery, M. Dangla, P. Villain, G. Platret, G. 2007. Investigation of the carbonation front shape on cementitious materials: effects of the chemical kinetics. Cement and Concrete Research 37. Pp. 1047-1058.
- Thomson, M.L. Lindqvist, J.E. Elsen, J. and Groot, C.J.W.P. 2004. Porosity of Historic Mortars, in: 13th International Brick and Block Masonry Conference Amsterdam.
- Tunçoku S.S. Caner-Saltık, E.N. 2006. Opal-A rich additives used in ancient lime mortars, Cement and Concrete Research, vol.36, pp 1886-1893.

V.....

- Uğurlu Sağın, 2012. Characteristics of Roman Mortars Produced From Natural and Artificial Pozzolans In Aigai and Nysa. Unpublished PhD Thesis, İzmir Institute of Technology
- Uğurlu, E. Böke, H. 2009. The use of brick–lime plasters and their relevance to climatic conditions of historic bath buildings. Construction and Building Materials 23, pp. 2442–2450.
- UNE 83-308-86 Ensayos de hormigón - Determinación de la velocidad de los impulsos ultrasonidos

- UNE-EN 1015-11:2007, Methods of test for mortar for masonry - Part 11: Determination of flexural and compressive strength of hardened mortar
- UNE-EN 1015-18:2003, Methods of test for mortar for masonry - Part 18: Determination of water absorption coefficient due to capillary action of hardened mortar
- UNE-EN 1936:2007, Natural stone test methods - Determination of real density and apparent density, and of total and open porosity (2007).
- UNESCO, 1956. Recommendations on International Principles Applicable to Archaeological Excavations. New Delhi.
- Uygun, F. 2013. Photogrammetric evaluation options for ancient structures in Hypokremnos, Pagos, Paradiso and Nysa, Master Thesis, İzmir Institute of Technology
- Válek, J. Bartos, P.J.M. 2001. Influences affecting compressive strength of modern non-hydraulic lime mortars used in masonry conservation. Transactions on the Built Environment vol 55, WIT Press, www.witpress.com, ISSN 1743-3509
- Válek, J. Hughes, J. & Bartos, P. 2005. Gas Permeability, Porosity and Carbonation of Modern Conservation Lime Mortar Mix. Materials for Buildings and Structures. Wiley-VCH Verlag GmbH & Co. KGaA.
- Válek, J. Veiga, R. 2005. Characterisation of mechanical properties of historic mortars – testing of irregular samples. Structural Studies, Repairs and Maintenance of Heritage Architecture IX, WIT Transactions on The Built Environment, Vol 83, WIT Press. ISSN 1743-3509 (on-line)
- Van Balen, K. & Van Gemert, D. 1994. Modeling lime mortar carbonation. Mater Struct, 27, 393–8.
- Van Balen, K. 2005, Carbonation reaction of lime, kinetics at ambient temperature", Cement and o Concrete Research 35.
- Van Hees, R. P. J. Binda, L. Papayianni, I. and Toumbakari, E. 2004. RILEM TC 167-COM: 'Characterisation of old mortars with respect to their repair' Materials and Structures / Matériaux et Constructions. Vol. 37. pp 644-648.

- Varas, M.J. Alvarez de Buergo, M. Perez-Monserrat, E. Fort, R. 2008, Decay of restoration render mortar of the church of San Manuel and San Benito, Madrid, Spain: Results from optical and electron microscopy, Materials Characterization vol. 59, pp 1531-1540.
- Vazquez-Calvo, C. Martinez-Ramirez, S. Alvarez de Buergo, M. and Fort, R. 2012. The Use of Portable Raman Spectroscopy to Identify Conservation Treatments Applied to Heritage Stone, Spectroscopy Letters, 45, 2,pp.146-150.
- Veiga, M. R. Aguiar, J. Santos Silva A. Carvalho, F. 2001. Methodologies for characterisation and repair of mortars of ancient buildings, in Proc. International Seminar of Historical Constructions 2001, Guimarães, Portugal, Universidade do Minho, , pp.353-362.
- Veiga, M. R. Velosa, A. & Magalhães, A. 2009. Experimental applications of mortars with pozzolanic additions: Characterization and performance evaluation. Construction and Building Materials, 23, 318-327.
- Veiga, M. R. F, A. Velosa, A.L. Magalhães, A.C. Margalha, G. 2010. Lime-Based Mortars: Viability for Use as Substitution Renders in Historical Buildings. International Journal of Architectural Heritage, 4, 177-195.
- Vejmelková, E. Keppert, M. Rovnanikova, P. Kersner, Z. and Cerny, R. 2012. Properties of lime composites containing a new type of pozzolana for the improvement of strength and durability, Composites Part B. Engineering, 43, pp. 3534-40.
- Velosa, A. L. Veiga, R. Coroado, J. Ferreira, V. M. & Rocha, F. 2010. Characterization of Ancient Pozzolanic Mortars from Roman Times to the 19th Century: Compatibility Issues of New Mortars with Substrates and Ancient Mortars. In: DAN, M. B., PŘIKRYL, R. & TÖRÖK, Á. (eds.) Materials, Technologies and Practice in Historic Heritage Structures. Dordrecht: Springer Netherlands., Chapter 13, pp. 235-257.
- Velosa, A. Veiga, M.R. 2001. The use of pozzolans as additives in lime mortars for employment in building rehabilitation. In: P.B. Lourenço, P. R., ed. Historical Constructions,, 2001 Guimarães. 373-380.

- Velosa, A. L. Coroado, J. Veiga, M. R. & Rocha, F. 2007. Characterisation of roman mortars from Conímbriga with respect to their repair. *Materials Characterization,* 58 1208–1216.
- Ventolà, L. Vendrell, M. Giraldez, P. Merino, L. 2011. Traditional organic additives improve lime mortars: New old materials for restoration and building natural stone fabrics. Construction and Building Materials. vol 25 . pp 3313–3318.
- Villain, G. Thiery, M. & Platret, G. 2007. Measurement methods of carbonation profiles in concrete: Thermogravimetry, chemical analysis and gammadensimetry. Cement and Concrete Research, Volumen 37, p. 1182–1192.
- Viles H. Goudie, A. Grab, S. 2011. The use of the Schmidt Hammer and Equotip for rock hardness assessment in geomorphology and heritage science: a comparative analysis, Earth Surface Processes and Landforms. 36, pp. 320–333.
- Vitruvius, 2005. Mimarlık Üzerine On Kitap (translation. S. Güven 2005). Şevki Vanlı Mimarlık Vakfı Mimarlığın Uluslarası Kaynakları. 14th ed.
- von Diest W. 1913. Nysa ad Maeandrum : nach Forschungen und Aufnahmen in den Jahren 1907 und 1909, Berlin.
- Walker, R. & Pavía, S. 2011. Physical properties and reactivity of pozzolans, and their influence on the properties of lime–pozzolan pastes. Mater Struct. 44: pp. 1139. doi:10.1617/s11527-010-9689-2
- Ward-Perkins, J.B. 1994. Roman Imperial Architecture. New Haven and London: Yale University Press. ISSN 0553-4755
- Weber, J. 2016. Pozzolanic Mortars. Notes from Microscopic techniques to study mineral materials in cultural heritage workshop, Vienna.
- Yalçiner , Ç.C, Bano, M. Kadıoğlu, M. Karabacaki,V. Meghraoui, M. Altunel, E. 2009. New temple discovery at the archaeological site of Nysa (western Turkey) using GPR method. Journal of Archaeological Science 36: 1680–1689

- Yurtsevenler, Ö. 2013. Development of a Presentation Framework for an Archaeological Site Case Study: Nysa On The Meander. Unpublished master's thesis, Department of Architecture, METU, Ankara.

Z.....

- Zamba, I.C. M.G. Stamatakis, F.A. Cooper, P.G. Themelis, and C.G. Zambas. 2007. Characterization of Mortars used for the Construction of Saithidai Heroon Podium (1st century AD) in Ancient Messene, Peloponnesus, Greece." Materials Characterization 58: 1229-1239. doi: 10.1016/j.matchar.2007.07.004.
- Zendri, E. Lucchini, V. Biscontin G. Morabito. Z. M. 2004. Interaction between clay and lime in "cocciopesto" mortars: a study by 29Si MAS spectroscopy in APPLIED CLAY SCIENCE, vol. 25, pp. 1-1 (ISSN 0169-1317)

https://es.climate-data.org/location/2021/

https://en.climate-data.org/location/10596/

https://es.climate-data.org/location/178/

www.labraunda.org

List of Figures

Chapter 1

Figure 1-1. Map of Roman Mediterranean (Laistner, 1929) 6
Figure 1- 2. Illustration showing the construction of bridge (Hamey and Hamey, 1990) 7
Figure 1- 3. Illustration showing the elements of a Roman bridge (redrawn after Hamey and Hamey, 1990) 9
Figure 1- 4. Construction of a Roman road (Hamey and Hamey, 1990) 10
Figure 1- 5. Section of a Roman road, according to the Vitruvius' description (Hamey and Hamey, 1990) 10
Figure 1- 6. Lime cycle 11
Figure 1.2 - 7. Europe map bringing Spain and Turkey to focus 26

Chapter 2

Figure 2-1The archaeological sites indicated in Figure 1.2-7 33
Figure 2.1- 2. Map showing the localization of Complutum (Aerial photograph from Google Earth) 34
Figure 2.1- 3. Geological map of Alcalá de Henares 35
Figure 2.1- 4. General plan of the Complutum archaeological site (bigger marked red area in the center is the forum and House of Grifos, next to it in the westHouse of Atrio House of Marte , and in the 6 blocks west Cuadrifrontal arch 36
Figure 2.1- 5. Plan of the forum of Complutum with sampling points (bigger red zone in Figure 2.1- 4) 37
Figure 2.1- 6. a) Criptoporticus b) Basilica c) North Bath separation wall between tepidarium and caldarium d) Monumental façade 41
Figure 2.1-7. a) North Bath frigidarium northern wall b) North Bath frigidarium floor c) South Bath separation wall between fragidarium and tepidarium d) South Bath separation wall between tepidarium and caldarium, elevation of hipocaustum 42
Figure 2.1- 8. a-d) sewerages e) Cuadriporticus western side floor f) House of Marte floor 43
Figure 2.1- 9. a) North Bath Caldarium b) House of Atrium fountain c) Pillars of Arch d) Zulema Bridge 44
Figure 2.1- 10. House of Grifos a) exterior b) interior c) meteorological station d) sensor network in earthen wall with wall painting 45
Figure 2.1- 11. Location map of Mérida 46
Figure 2.1- 12. Geological map of Mérida (IGME, 1991) 48
Figure 2.1- 13. Location of sampling points 49
Figure 2.1- 14. a, b) Circus c,d) Amphitheatre 51
Figure 2.1- 15. San Lazaro Aqueduct 52
Figure 2.1- 16. Drawing of San Lázaro (Prado and Mariño, 1798-1801) 53
Figure 2.1- 17. a) Alcazaba b) Moreria c, d) Temple of Diana 54
Figure 2.1- 18. a, c) archaeological remains of Viñero b, d) Resti Thermal Bath 55
Figure 2.1- 19. Aerial map of Turkey showing the region where Nysa is located 56
Figure 2.1- 20. Geological setting of Nysa and its surrounding (Okay, 2011) 59
Figure 2.1- 21. Plan of Nysa and sampled points 60
Figure 2.1- 22. 3D model of Nysa from south eastern view showing the gymnasium, stadium, theatre, bridges, agora and street system by Marie Saldaña (2014) 61
Figure 2.1- 23. a) cistern b) pillars of 1st bridge c) 2nd bridge d) Stadium from the two bridges 63
Figure 2.1- 24. Map of Nysa by Yurtsevenler((2013) pointing out the water road with the location of the Roman Bridge and tunnel 64
Figure 2.1- 25. a, b) Tunnel c,d) Geronticon 65
Figure 2.1- 26. Aerial photo of the site showing Stadium, Road, Cistern, Bridge and Theatre (altered from photo inNysa excavation archive, 2014) 66
Figure 2.1- 27. a) Stadium Suma Cavea b) Arched structure in the southern part of Gymnasium c) Library 67
Figure 2.1- 28. Nysa Library ground floor plan (Uygun, 2012 ; Heisel and Strocka, 2006) 68
Figure 2.1- 29. a) Basilica shops b) Theatre 69
Figure 2.1- 30. Agora Road in the middle, coating mortar near water tube on the left and floor on the right 69
Figure 2.1- 31. Thermal Bath 70
Figure 2.1- 32. Location map of Labraunda 71
Figure 2.1- 33. Labraunda sanctuary from northwest (2013) 72
Figure 2.1- 34. Geological map of Muğla-Aydın region (after Okay, 2001) 74
Figure 2.1- 35. Plan of the Sanctuary showing sampling points 75
Figure 2.1- 36. Building Andron A 77
Figure 2.1- 37. a, b) South Bath c,d) Andron C 78
Figure 2.1- 38. Tetraconch Building (Reconstruction by J. Bild on the left and the plan on the right, - www.labraunda.org, access date: 30.7.2015) 78
Figure 2.1- 39. Tetraconch Bath 79
Figure 2.1- 40. a) East Bath b, c) Hypostyle Building d) Pool (Natatio) 80
Figure 2.1- 41. Datalogger measuring CO2, T and RH in the warehouse 81
Figure 2.2- 42. Particle size distribution of standard sand 84

Figure 2.2- 43. a) Roman ceramics in Complutum archaeological site b,c) crushing and grinding machines d) sieving 84
Figure 2.2- 44. Different granolmetries of the ceramic aggregates 86
Figure 2.2- 45. Standard sand and the apparatus used for the separation 87
Figure 2.2- 46. Steps of manufacturing 87
Figure 2.2- 47. Manufactured samples 88
Figure 2.2- 49. Mortar samples in the climatic chamber 88
Figure 2.2- 49. Samples cured at laboratory conditions 89
Figure 2.2- 50. DiloCarb spraing on samples 90
Figure 2.2- 51. Schematic illustration of nomenclature of samples 90
Figure 2.2- 52. Illustration showing the sampling points in each simple (1: prism cut towards 4 cm inside, 2: 1 cm inside, Samples for A: phenolphthalein sprayed zone, B: XRD, C: TGA, D: SEM, E: MIP) 91
Figure 2.2-53. DiloCarb spraying on samples 92
Figure 2.2-54. Schematic illustration of nomenclature of samples 92
Figure 2.2-55. Illustration showing the sampling points in each simple (1: prism cut towards 4 cm inside, 2: 1 cm inside, Samples for A: phenolphthalein sprayed zone, B: XRD, C: TGA, D: SEM, E: MIP) 93
Figure 2.3- 56. Schematic illustration of conducted analytical researches 95
Figure 2.3- 57. Photo taken during the microscopic observations 97
Figure 2.3- 58. Diamond disc cutting machine 97
Figure 2.3- 59. XRF equipment PHILIPS Magix Pro (PW-2440) (photo taken from the website: http://cic.ugr.es/servicios-y-unidades/ficha.php?codServicio=1&unidad=7, accessed date: 10.2.2016) 113
Figure 2.3- 60. CIE Lab parameters 115
Figure 2.3-61. Spectrophotometry Konica Minolta (photo taken from http://www.laboratoriopetrofisica.es/equipamiento.html, acces date: 18.3.2016) 116
Figure 2.3- 62. Equotip rebound tester 118
Figure 2.3- 63. Porosímetry Autopore Iv 9520; Micromeritic 120
Figure 2.3- 64. HCl acid attack test 122
Figure 2.3- 65. SEM instrument in CNME 123
Figure 2.3- 66. pH scale classification. Calcium hydroxide average pH and Phenolphthalein changing colour start ranges (after Guimares, 2014; Lawrence 2006) 124
Figure 2.3- 67. Compression and the instrument 125
Figure 2.3- 68. Air permeameter 126
Figure 2.3- 69. Illustration of UPV measurements 127
Figure 2.3-70. Photograph showing UPV measurement 128
Figure 2.3- 71. Vacuum chamber used in the saturation test 130
Figure 2.3- 72. The experimental set up capillary test 131

Chapter 3

Figure 3.1- 1. Examples of Opus Caementicium mortars (CM03 on the left, CM18 on the right, scale: 1 cm) 134
Figure 3.1- 2. Examples of Opus Signinum mortars (CM10 on the left, CM07 on the right, scale: 1 cm) 135
Figure 3.1- 3- Lightness vs Saturation of Complutum mortars 136
Figure 3.1- 4. a* vs b* of Complutum mortars 137
Figure 3.1- 5. White index vs yellow index of Complutum mortars 138
Figure 3.1- 6. Surface hardness of Complutum mortars (grey: opus caementicium, red: opus signinum) 139
Figure 3.1- 7. Opus caementicium mortars (a) CM01 plane polarized light b) CM09 cross polarized light, c) CM11 plane polarized light, d) CM35 plane polarized light) 140
Figure 3.1- 8. Opus signinum mortars (a) CM05 cross polarized light b) CM07 plane polarized light, c) CM10 plane polarized light, d) CM24 plane polarized light) 141
Figure 3.1- 9. Lime lumps a) CM14 b) CM10 c) CM21 d) CM04 142
Figure 3.1- 10. Photomicrographs a) sandstone in the centre CM02b (cross polarized light), b) slate in CM04 (plane polarized light 142
Figure 3.1- 11. Rounded ceramic fragment in CM05 with reactions in the border 143
Figure 3.1- 12. Photomicrograph of CM02a 143
Figure 3.1- 13. Binder aggregate ratios of Complutum mortars (reds are opus signinum mortars) 150
Figure 3.1- 14. Grain size distribution graph of Complutum mortars 151
Figure 3.1- 15. XRD patterns of Complutum mortars (Q: quartz, C: calcite, F: feldspar, M: mica, G: gypsum) 153
Figure 3.1- 16. CO2/H2O vs CO2% graph of samples 155
Figure 3.1- 17. Thermogram of CM01 (left) CM02a (right) 156
Figure 3.1- 18. Thermogram of CM05 (left) and CM07 (right) 156
Figure 3.1- 19. Thermogram of CM08 (left) and CM14 (right) 157
Figure 3.1- 20. Thermogram of CM15 (left) and CM16 (right) 158
Figure 3.1- 21. acid in/soluble fraction vs CaCO3 (%) from TGA of Complutum mortars (blue circle: opus caementicium, red circle: opus signinum mortars) 159
Figure 3.1- 22. CaO+MgO vs SiO2+Al2O3+Fe2O3 graph of Complutum mortars 162
Figure 3.1- 23. TiO2/Fe2O3 vs SiO2/CaO graph of Complutum mortars 163
Figure 3.1- 24. CaO/MgO vs TiO2/Fe2O3 graph of Complutum mortars 164
Figure 3.1- 25. Ba/Sr vs Zr/Y graph of Complutum mortars 166
Figure 3.1- 26. Log differential intrusion versus pore size of the Complutum samples 170

Figure 3.2- 27. Examples of opus caementicium mortars in Mérida (on the left MM3 having both types of mortars and MM15 on the right) 171
Figure 3.2- 28. Straw in the sample MM5 171
Figure 3.2- 29. Examples of opus signinum mortars in Mérida (on the left coating mortar in Bath MM18 and mortar from amphitheatre MM22 on the right) 172
Figure 3.2- 30. Luminosity vs Chrome of Mérida mortars 172
Figure 3.2- 31. Chromatic parameters b* vs a* of Mérida mortars 173
Figure 3.2- 32. White index vs yellow index of Mérida mortars 174
Figure 3.2- 33. Surface hardness values of Mérida samples 175
Figure 3.2- 34. Opus caementicium mortars (a) MM2 plane polarized light b) MM14 plane polarized light, c) MM16 cross polarized light, d) MM26 plane polarized light) 176
Figure 3.2- 35. Opus signinum mortars (a) MM18 plane polarized light b) MM22 plane polarized light, c) MM21 plane polarized light, d) MM27 plane polarized light) 177
Figure 3.2- 36. Rock fragments encountered in Mérida mortars a) quartzite in MM10 b) monzogranite in MM2 C) slate like metamorphic rock in MM18 d) granodiorite in MM16 (cross polarized light) 178
Figure 3.2- 37. a) lime lump in MM7 b) reactive rock fragment and rim around it in MM26 c) angular ceramic fragment with reaction rim in MM5 d) in MM3 (plane polarized light) scale: 500 µm 179
Figure 3.2- 38. Binder aggregate ratios of Mérida mortars (reds are opus signinum) 183
Figure 3.2- 39. Grain size distribution graph of Mérida mortars 185
Figure 3.2- 40. XRD patterns of Mérida mortars (Q: quartz, C: calcite, F: feldspar, M: mica, Ch: Chlorite, A: Actinolite) 186
Figure 3.2- 41. CO2/H2O vs CO2% graph of samples 189
Figure 3.2- 42. Thermogram of MM3 caementicium (left) and signinum (right) 190
Figure 3.2- 43. Thermogram of MM5 on the left MM12 on the right 191
Figure 3.2- 44. Thermogram of opus signinum mortars (MM18 on the left and MM22 on the right) 192
Figure 3.2- 45. acid in/soluble fraction of Mérida mortars (red circle: opus signinum, blue circle: opus caementicium mortars) 192
Figure 3.2- 46. CaO+MgO vs SiO2+Al2O3+Fe2O3 graph of Mérida mortars 194
Figure 3.2- 47. TiO2/Fe2O3 vs SiO2/CaO graph of Mérida mortars 195
Figure 3.2- 48. CaO/MgO vs TiO2/Fe2O3 graph of Mérida mortars 196
Figure 3.2- 49. Ba/Sr vs Zr/Y graph of Mérida mortars 196
Figure 3.2- 50. Log differential intrusion versus pore size of the Mérida samples 198
Figure 3.3- 51. Examples of Opus Caementicium mortars (NM05 on the left, NM24 on the right) 204
Figure 3.3- 52. Examples of Opus Signinum mortars (NM13 on the left, NM16 on the right) 205
Figure 3.3- 53. Luminosity vs Chrome of Nysa mortars 206
Figure 3.3- 54. Chromatic parameters b* vs a* of Nysa mortars 207
Figure 3.3- 55. Surface hardness values of Nysa samples 208
Figure 3.3- 56. Opus caementicium mortars a) NM02 b) NM04 c) NM24 d) NM10 209
Figure 3.3- 57. Opus signinum mortars a) NM08 b) NM11 c) NM15 d) NM16 210
Figure 3.3- 58. Rock fragments found a) quartzite in NM02 b) schistositic metamorphic rock in NM04 c) metaquartzite in NM24 d) marble in NM26 211
Figure 3.3- 59. reaction rim around a) ceramic fragment in NM07 b) polycrystalline slicic rock in NM05 c) recarbonation and recrystallization around pores in NM15 d) old mortar relict in NM06 212
Figure 3.3- 60. Binder aggregate ratios of Nysa mortars 215
Figure 3.3- 61. Grain size distribution graph of Nysa mortars 217
Figure 3.3- 62. XRD patterns of Nysa mortars 218
Figure 3.3- 63. CO2/H2O vs CO2% graph of samples 222
Figure 3.3- 64. Thermogram of mortars from tunnel a) NM04 b) NM12 c)NM13 223
Figure 3.3- 65. Thermogram of mortar from arch of Basilica shops (NM07) (left) stadium (NM08) 223
Figure 3.3- 66. Thermogram of mortar from theatre (NM09) (left), arch in Thermal Bath (NM25) (right) 224
Figure 3.3- 67. acid in/soluble fraction vs CaCO3 (%) from TGA of Nysa mortars 225
Figure 3.3- 68. CaO+MgO vs SiO2+Al2O3+Fe2O3 graph of Nysa mortars 227
Figure 3.3- 69. . TiO2/Fe2O3 vs SiO2/CaO graph of Nysa mortars 228
Figure 3.3- 70. CaO/MgO vs TiO2/Fe2O3 graph of Nysa mortars 229
Figure 3.3- 71. Ba/Sr vs Zr/Y graph of Nysa mortars 229
Figure 3.3- 72. Log differential intrusion versus pore size of the Nysa samples 231
Figure 3.4- 73. Examples of Opus Caementicium mortars (LM04A on the left, LM06B on the right, scale: 1 cm) 234
Figure 3.4- 74. Examples of Opus Signinum mortars (LM06A on the left, LM08 on the right, scale: 1 cm) 235
Figure 3.4- 75. Luminosity vs Chrome of Labraunda mortars 236
Figure 3.4- 76. b* vs a* of Labraunda mortars 237
Figure 3.4- 77. White index vs yellow index of Labraunda mortars 237
Figure 3.4- 78. Surface hardness values of Labraunda samples (gray: Opus caementicium, red: Opus signinum) 238
Figure 3.4- 79. photomicrographs of opus caementicium mortars a) LM02 (cross polarized light) b) LM04A (plane polarized light) c) LM05 (plane polarized light) d) LM06B (plane polarized light) 240
Figure 3.4- 80. a)Photomicrograph of LM01A from Andron A (cross polarized light) showing recrystallization in the pore on the left and quartzite on the right b)LM04A Photomicrograph of the mortar sample LM04A from the wall of Tetraconch Bath showing gneiss fragment (cross polarized light) c) Photomicrograph of the sample LM05 from Andron C wall (plane polarized light) marble fragment on the left LM05 d) LM07A showing augen eye gneiss mica group 240

Figure 3.4- 81. Photomicrographs of opus signinum a) sample LM06A from the floor of East Bath (plane polarized light) showing ceramic fragment with its reaction rim in the centre b) LM04B (plane polarized light) Photomicrograph (x4p) of mortar sample from floor of Tetraconch Bath LM04B, showing the ceramic in the centre and metamorhphic rock fragment embedded in a porous lime binder with schrinkage cracks c) LM06C(cross polarized light) d) LM08 (plane polarized light) 240
Figure 3.4- 82. Photomicrograph of a) LM02 b) LM06A c) LM01C d) LM06C 242
Figure 3.4- 83. Binder aggregate ratios of Labraunda mortars (reds are opus signinum mortars) 246
Figure 3.4- 84. Grain size distribution graph of Labraunda mortars 247
Figure 3.4- 85. XRD patterns of Labraunda mortars (Q: quartz, C: calcite, F: feldspar, M: mica, K: kaolinite, A: amphibole) 249
Figure 3.4- 86. CO2/H2O vs CO2% graph of samples (blue circle: highly hydraulic, orange circle: hydraulic, green: non-hydraulic) 252
Figure 3.4- 87. Thermogram of LM01C (left) and LM04A (right) 253
Figure 3.4- 88. Thermogram of LM03 (left) and LM04B(right) 253
Figure 3.4- 89. Thermogram of LM07D (left) and LM08 (right) 254
Figure 3.4- 90. acid in/soluble fraction vs CaCO3 (%) from TGA of Labraunda mortars , same grouping with Figure 3.4- 86, blue circle: highly hydraulic, orange circle: hydraulic) 255
Figure 3.4- 91. CaO+MgO vs SiO2+Al2O3+Fe2O3 graph of Labraunda mortars 256
Figure 3.4- 92. TiO2/Fe2O3 vs SiO2/CaO graph of Labraunda mortars 257
Figure 3.4- 93. CaO/MgO vs TiO2/Fe2O3 graph of Labraunda mortars 258
Figure 3.4- 94. Ba/Sr vs Zr/Y graph of Labraunda mortars 260
Figure 3.4- 95. Log differential intrusion versus pore size of the Labraunda samples 262

Chapter 4

Figure 4. 1. Luminosity vs Chrome of opus caementicium samples 270
Figure 4. 2. Luminosity vs Chrome of opus signinum samples 271
Figure 4. 3. b* vs a* chromatic parameters of opus signinum mortars 271
Figure 4. 4. B/A vs CaCO3 (%) of mortars 272
Figure 4. 5. CO2/H2O vs CO2 plot of mortars 273
Figure 4. 6. CaO+ MgO vs SiO2+Al2O3+ Fe2O3 plot of mortars 275
Figure 4. 7. CaO+ MgO vs SiO2+Al2O3+ Fe2O3 plot of opus caementicium mortars 276
Figure 4. 8. CaO+ MgO vs SiO2+Al2O3+ Fe2O3 plot of opus signinum mortars 277
Figure 4. 9. CaO/MgO vs TiO2/Fe2O3 plot of mortars 278
Figure 4. 10. Ba/Sr vs Zr/Y plot of mortars 279
Figure 4. 11. Average Pore Diameter vs Porosity of mortars 280
Figure 4. 12. Ba/Sr vs. Zr/Y plot of mortars 281
Figure 4. 13. Average Pore Diameter vs. Porosity of mortars 282

Chapter 5

Figure 5.1- 1.Photomicrographs 28 days on the left 180 days on the right in the order, M1L, M1LA, M1C, M2L,M2LA, M2C, (M1LA180, M2L180, M2LA180, M2C180 are under cross polarized light) 296
Figure 5.1- 2. XRD patterns of sample M1L during carbonation 298
Figure 5.1- 3. XRD patterns of sample M1LA during carbonation 298
Figure 5.1- 4. XRD patterns of sample M1C during carbonation 299
Figure 5.1- 5. XRD patterns of sample M2L during carbonation 299
Figure 5.1- 6. XRD patterns of sample M2LA during carbonation 300
Figure 5.1- 7. XRD patterns of sample M2C during carbonation 300
Figure 5.1- 8. Derivative weight loss of the sample M1L in different curing periods 302
Figure 5.1- 9. Derivative weight loss of the sample M1LA in different curing periods 303
Figure 5.1- 10. Derivative weight loss of the sample M1C in different curing periods 303
Figure 5.1- 11. Derivative weight loss of the sample M2L in different curing periods 304
Figure 5.1- 12. Derivative weight loss of the sample M2LA in different curing periods 304
Figure 5.1- 13. Derivative weight loss of the sample M2C in different curing periods 305
Figure 5.1- 14. Carbonation reaction ratio throughout the ages 307
Figure 5.1- 15. SEM image of sample M1C at 28 days 308
Figure 5.1- 16. SEM image of sample M1L at 28 days 309
Figure 5.1- 17. SEM image of M2L at 28 days 310
Figure 5.1- 18. SEM image and EDS stick shape crystal in the sample M2LA at 28 days 310
Figure 5.1- 19. SEM image of sample M2C at 28 days 311
Figure 5.1- 20. SEM image of sample M1C at 90 days 312
Figure 5.1- 21. SEM image of M1LA at 90 days 312
Figure 5.1- 22. SEM image of sample M2C at 90 days 313
Figure 5.1- 23. SEM image of sample M2L at 90 days 314
Figure 5.1- 24. SEM image of M1C at 120 days 314
Figure 5.1- 25. SEM image of sample M2C at 120 days 315
Figure 5.1- 26. SEM image of M2L at 120 days 316
Figure 5.1- 27. SEM image of M1L at 180 days 316

Figure 5.1- 28. SEM image of M1LA at 180 days 317
Figure 5.1- 29. SEM image of sample M1C at 180 days 318
Figure 5.1- 30. SEM image of the sample M2C at 180 days 318
Figure 5.1- 31. SEM image of M2L at 180 days 319
Figure 5.1- 32. Phenophtalein sprayed samples after 28 days of curing 322
Figure 5.1- 33. Phenophtalein sprayed samples after 90 days of curing 323
Figure 5.1- 34. Phenophtalein sprayed samples after 120 days of curing 323
Figure 5.1- 35. Phenophtalein sprayed samples after 180 days of curing 325
Figure 5.1- 36. Pore size distribution of sample M1L in tested periods 328
Figure 5.1- 37. Pore size distribution of sample M1LA in tested periods 328
Figure 5.1- 38. Pore size distribution of sample M1C in tested periods 329
Figure 5.1- 39. Pore size distribution of sample M2L in tested periods 330
Figure 5.1- 40. Pore size distribution of sample M2LA in tested periods 330
Figure 5.1- 41. Pore size distribution of sample M2C in tested periods 333
Figure 5.2- 42. Surface hardness values of the samples in tested periods 335
Figure 5.2- 43. Air permeability values of the samples in tested periods 336
Figure 5.2- 44. UPV values of the samples at 28 days of curing 337
Figure 5.2- 45. UPV values of the samples at 90 days of curing 338
Figure 5.2- 46. UPV values of the samples at 120 days of curing 339
Figure 5.2- 47. UPV values of the samples at 180 days of curing 340
Figure 5.2- 48. Avarage UPV values of the sample in tested periods 341
Figure 5.2-49. Anisotropy (%) of the samples 343
Figure 5.3- 50. Column graph showing the saturation values of the samples 343
Figure 5.3- 51. Column graph showing the open porosity values of the samples 345
Figure 5.3- 52. Weight difference of mortars during carbonation 346
Figure 5.3- 53. Weight gain (%) of mortars during carbonation 348
Figure 5.3- 54. Capillary coefficients of samples at 5 minutes 349
Figure 5.3- 55. Capillary coefficients of the samples between 10 and 90 minutes 350
Figure 5.4- 56. Flexural strength values of the samples 351
Figure 5.4- 57. Compressive strength of the samples 351
Figure 5.4- 58. Uniaxial compressive strength (MPa) vs modulus of elasticity (GPa) graph 352

Chapter 6

Figure 6.1.The evolution of carbonation of chamber cured mortar samples as determined by SEM and XRD 363
Figure 6.2. The evolution of carbonation of mortar samples with accelerator as determined by SEM and XRD 364
Figure 6.3. The evolution of carbonation of laboratory cured mortar samples as determined by SEM and XRD 365
Figure 6.4. Diagram showing the factors that affect carbonation 373

Chapter 7

Figure 7.1. Average pore diameter vs porosity values of Roman mortars and repair mortars at the end of 6 months 381
Figure 7.2. Pore size distributions of M1 sample in the chamber curing conditions at 180 days and opus caementicium sample from Complutum 383
Figure 7.3. Pore size distributions of M2 sample in the chamber curing conditions at 180 days and opus signinum sample from Complutum 384
Figure 7.4. Surface hardness values of repair mortars and Roman mortars (whose ranges of surface hardness values are presented in boxes; are blue dashed line: Complutum, blue line: Mérida, orange dashed line: Nysa, black dashed line: Labraunda) 386
Figure 7.5. CO2/H2O vs CO2 graph of repair mortars 386
Figure 7.6. CO2/H2O vs CO2 graph of Roman and repair mortars 387

Appendix B

Figure V.1. Thin section images of sample CM01 477
Figure V.2. Thin section images of sample CM02a 478
Figure V.3. Thin section images of sample CM02b 479
Figure V.4. Thin section images of sample CM03 479
Figure V.5. Thin section images of sample CM04 480
Figure V.6. Thin section images of sample CM05 480
Figure V.7. Thin section images of sample CM06a 481
Figure V.8. Thin section images of sample CM06b 482
Figure V.9. Thin section images of sample CM07 482
Figure V.10. Thin section images of sample CM07 (continue) 483

Figure V.11. Thin section images of sample CM08 483
Figure V.12. Thin section images of sample CM09 484
Figure V.13. Thin section images of sample CM10 484
Figure V.14. Thin section images of sample CM11 485
Figure V.15. Thin section images of sample CM14 485
Figure V.16. Thin section images of sample CM14 (continue) 486
Figure V.17. Thin section images of sample CM15 486
Figure V.18. Thin section images of sample CM16a 487
Figure V.19. Thin section images of sample CM16b 487
Figure V.20. Thin section images of sample CM16b (continue) 488
Figure V.21. Thin section images of sample CM18a 488
Figure V.22. Thin section images of sample CM18b 489
Figure V.23. Thin section images of sample CM20 489
Figure V.24. Thin section images of sample CM21 489
Figure V.25. Thin section images of sample CM24a 490
Figure V.26. Thin section images of sample CM25 490
Figure VI.1. Thin section images of sample MM2 491
Figure VI.2. Thin section images of sample MM2 continue 492
Figure VI.3. Thin section images of sample MM2 continue 493
Figure VI.4. Thin section images of sample MM2 continue 494
Figure VI.5. Thin section images of sample MM3 495
Figure VI.6. Thin section images of sample MM3 continue 496
Figure VI.7. Thin section images of sample MM3 continue 497
Figure VI.8. Thin section images of sample MM3 continue 498
Figure VI.9. Thin section images of sample MM3 continue 499
Figure VI.10. Thin section images of sample MM3 continue 500
Figure VI.11. Thin section images of sample MM5 501
Figure VI.12. Thin section images of sample MM5 (continue) 502
Figure VI.13. Thin section images of sample MM5 (continue) 503
Figure VI.14. Thin section images of sample MM6 504
Figure VI.15. Thin section images of sample MM6 (continue) 505
Figure VI.16. Thin section images of sample MM6 (continue) 506
Figure VI.17. Thin section images of sample MM7 507
Figure VI.18. Thin section images of sample MM7 (continue) 508
Figure VI.19. Thin section images of sample MM7 (continue) 509
Figure VI.20. Thin section images of sample MM7 (continue) 510
Figure VI.21. Thin section images of sample MM7 (continue) 511
Figure VI.22. Thin section images of sample MM8 512
Figure VI.23. Thin section images of sample MM10 513
Figure VI.24. Thin section images of sample MM10 (continue) 514
Figure VI.25. Thin section images of sample MM11 515
Figure VI.26. Thin section images of sample MM12 516
Figure VI.27. Thin section images of sample MM12 (continue) 517
Figure VI.28. Thin section images of sample MM14 518
Figure VI.29. Thin section images of sample MM14 (continue) 519
Figure VI.30. Thin section images of sample MM15 520
Figure VI.31. Thin section images of sample MM15 (continue) 521
Figure VI.32. Thin section images of sample MM16 522
Figure VI.33. Thin section images of sample MM16 (continue) 523
Figure VI.34. Thin section images of sample MM16 (continue) 524
Figure VI.35. Thin section images of sample MM18 525
Figure VI.36. Thin section images of sample MM20 526
Figure VI.37. Thin section images of sample MM20 (continue) 526
Figure VI.38. Thin section images of sample MM21 526
Figure VI.39. Thin section images of sample MM22 527
Figure VI.40. Thin section images of sample MM22 (continue) 528
Figure VI.41. Thin section images of sample MM25 529
Figure VI.42. Thin section images of sample MM26 530
Figure VI.43. Thin section images of sample MM26 (continue) 531
Figure VI.44. Thin section images of sample MM27 532
Figure VI.45. Thin section images of sample MM27 (continue) 533
Figure VII.1. Thin section images of sample NM01 535
Figure VII.2. Thin section images of sample NM01 (continue) 536
Figure VII.3. Thin section images of sample NM02a 537
Figure VII.4. Thin section images of sample NM02a (continue) 538
Figure VII.5. Thin section images of sample NM03 539
Figure VII.6. Thin section images of sample NM04 540
Figure VII.7. Thin section images of sample NM04 (continue) 541
Figure VII.8. Thin section images of sample NM05a 542
Figure VII.9. Thin section images of sample NM05a (continue) 542
Figure VII.10. Thin section images of sample NM05a (continue) 543

Figure VII.11. Thin section images of sample NM06 543
Figure VII.12. Thin section images of sample NM06 (continue) 544
Figure VII.13. Thin section images of sample NM07 545
Figure VII.14. Thin section images of sample NM07 (continue) 546
Figure VII.15. Thin section images of sample NM07 (continue) 547
Figure VII.16. Thin section images of sample NM08 548
Figure VII.17. Thin section images of sample NM09 549
Figure VII.18. Thin section images of sample NM09 (continue) 550
Figure VII.19. Thin section images of sample NM10b 551
Figure VII.20. Thin section images of sample NM10b (continue) 552
Figure VII.21. Thin section images of sample NM11 553
Figure VII 22. Thin section images of sample NM11 (continue) 554
Figure VII 23. Thin section images of sample NM15 555
Figure VII 24. Thin section images of sample NM15 (continue) 555
Figure VII 25. Thin section images of sample NM15 (continue) 556
Figure VII 26. Thin section images of sample NM15 (continue) 557
Figure VII.27. Thin section images of sample NM16 558
Figure VII.28. Thin section images of sample NM16 (continue) 559
FigureVII.29. Thin section images of sample NM16 (continue) 560
FigureVII.30. Thin section images of sample NM22 560
Figure VII.31. Thin section images of sample NM22 (continue) 561
Figure VII.32. Thin section images of sample NM22 (continue) 562
Figure VII.33. Thin section images of sample NM23 563
Figure VII.34. Thin section images of sample NM23 (continue) 564
Figure VII.35. Thin section images of sample NM23 (continue) 565
Figure VII.36. Thin section images of sample NM24 565
Figure VII.37. Thin section images of sample NM24 (continue) 566
Figure VII.38. Thin section images of sample NM24 (continue) 566
Figure VII.39. Thin section images of sample NM24 (continue) 567
Figure VII.40. Thin section images of sample NM26 568
Figure VII.41. Thin section images of sample NM26 (continue) 568
Figure VII.42. Thin section images of sample NM26 (continue) 569
Figure VIII.1. Thin section images of sample LM01A 571
Figure VIII.2. Thin section images of sample LM01A (continue) 572
Figure VIII.3. Thin section images of sample LM01A (continue) 573
Figure VIII.4. Thin section images of sample LM01C 574
Figure VIII.5. Thin section images of sample LM02 575
Figure VIII.6. Thin section images of sample LM02 (continue) 576
Figure VIII.7. Thin section images of sample LM04A 576
Figure VIII.8. Thin section images of sample LM04A (continue) 577
Figure VIII.9. Thin section images of sample LM04A (continue) 578
Figure VIII.10. Thin section images of sample LM04A (continue) 579
Figure VIII.11. Thin section images of sample LM04B 580
Figure VIII.12. Thin section images of sample LM04B (continue) 581
Figure VIII.13. Thin section images of sample LM05 581
Figure VIII.14. Thin section images of sample LM05 (continue) 582
Figure VIII.15. Thin section images of sample LM05 (continue) 583
Figure VIII.16. Thin section images of sample LM05 (continue) 584
Figure VIII.17. Thin section images of sample LM06C 585
Figure VIII.18. Thin section images of sample LM06C (continue) 585
Figure VIII.19. Thin section images of sample LM06C (continue) 586
Figure VIII.20. Thin section images of sample LM07A 586
Figure VIII.21. Thin section images of sample LM07A (continue) 587
Figure VIII.22. Thin section images of sample LM07B 588
Figure VIII.23. Thin section images of sample LM07C 589
Figure VIII.24. Thin section images of sample LM08 590

Appendix C

Figure IX.1. Log differential intrusion vs pore size diameter of CM02 591
Figure IX.2. Log differential intrusion vs pore size diameter of CM06 591
Figure IX.3. Log differential intrusion vs pore size diameter of CM07 592
signinum sample from Complutum
Figure IX.4. Log differential intrusion vs pore size diameter of CM09 592
Figure IX.5. Log differential intrusion vs pore size diameter of CM15 593
Figure IX.6. Log differential intrusion vs pore size diameter of CM16 593
Figure IX.7. Log differential intrusion vs pore size diameter of CM27 594
Figure IX.8. Log differential intrusion vs pore size diameter of CM31 594
Figure IX.9. Log differential intrusion vs pore size diameter of CM38 595

Figure X.1. Log differential intrusion vs pore size diameter of MM8 597
Figure X.2. Log differential intrusion vs pore size diameter of MM10 597
Figure X.3. Log differential intrusion vs pore size diameter of MM14 598
Figure X.4. Log differential intrusion vs pore size diameter of MM22 598
Figure X.5. Log differential intrusion vs pore size diameter of MM26 599
Figure XI.1. Log differential intrusion vs pore size diameter of NM12 601
Figure XI.2. Log differential intrusion vs pore size diameter of NM16 601
Figure XI.3. Log differential intrusion vs pore size diameter of NM23 602
Figure XI.4. Log differential intrusion vs pore size diameter of NM24 602
Figure XI.5. Log differential intrusion vs pore size diameter of NM25 603
Figure XII.1. Log differential intrusion vs pore size diameter of LM03 605
Figure XII.2. Log differential intrusion vs pore size diameter of LM06A 605
Figure XII.3. Log differential intrusion vs pore size diameter of LM07A 606
Figure XII.4. Log differential intrusion vs pore size diameter of LM07C 606
Figure XII.5. Log differential intrusion vs pore size diameter of LM09 607

Appendix D

Figure D.1. DiloCarB Technical Leaflet 614

List of Tables

Chapter 2

Table 2.1- 1. Description of the samples 36
Table 2.1- 2. Collected samples from Mérida 48
Table 2.1- 3. Sampled mortars in Nysa on Meander 60
Table 2.1- 4. Sampled mortars in Labraunda 74
Table 2.2- 5. Information gathered from the of previous studies 81
Table 2.2- 6. Proportions of the prepared mortars 82
Table 2.2- 7. Granulometric distribution of the ceramic and sand aggregate (weight percentage%) 83
Table 2.2- 8. Density of the constituents and wáter ratio of lime putty 84
Table 2.2-9. Environmental conditions in the laboratory between the test days (T: temperature, RH: relative humidity) 90
Table 2.2- 10. Schedule showing the mortar samples used for every experiment (M1: Lime and sand, M2: Lime, sand and ceramic, C: Chamber, L: Laboratory; LA: Accelerator,Mi: Microstructural tests, H: hydric tests, P: physical tests, Me: mechanical tets, every code of mortar specimen refers the number of specimen used in each test) 93
Table 2.3- 11. Some microscopic observations in the literature 97
Table 2.3- 12. Number of examined thin sections 98
Table 2.3- 13. XRD findings in the literature 101
Table 2.3- 14. Number of mortar samples analysed by XRD 102
Table 2.3- 15. Number of mortar samples analysed by TGA 106
Table 2.3- 16. Weight losses and their corresponding compounds 107
Table 2.3-17. Percentages (%) of major elements found in other mortar samples in previous studies 111
Table 2.3- 18. Number of Roman mortar samples analysed by XRF 112
Table 2.3- 19. Number of mortar samples analysed by Colour 115
Table 2.3-20. Number of mortar samples analysed by Equotip 117
Table 2.3- 21. Number of mortar samples analysed by Mercury Intrusion Porosimetry 119
Table 2.3- 22. Binder: aggregate ratios of the mortars from the previous studies 120
Table 2.3- 23. Number of mortar samples analysed by acid attack 121

Chapter 3

Table 3.1- 1. Petrographical constituents of Complutum mortars (Qtz: quartz, Fel: feldspar, mica, shr: shrinkage, pol: Qtz polycrystalline, crp: Qtz cryptocrstalline, aug: augite, pyx: pyropxene, opq: opaque plg, biot: biotite, ferric incl) 145
Table 3.1- 2. Acid soluble insoluble ratios (%) of Complutum mortars 148
Table 3.1- 3. Weight passing each sieve in Complutum mortars 150
Table 3.1- 4. Semiquantitative XRD analysis of Complutum mortars (++++: primary mineral, ++: secondary mineral, +: present, tr: trace) 152
Table 3.1- 5. Weight losses (%) of the mortar samples 154
Table 3.1- 6. Major elements in Complutum mortars (%) (LOI: Loss of ignition) 161
Table 3.1- 7. Parameters gathered by mercury intrusión (P: Porosity, APD: Average Pore Diameter (4V/A), BD: Bulk density, AD: Apparent density) 166
Table 3.1- 8. Pore size distribution and percentages of micro and macropores 167
Table 3.2- 9. Petrographical constituents of Mérida mortars 181
Table 3.2- 10. Binder and aggregate ratios (%) of Mérida mortars 183
Table 3.2- 11. Weight passing each sieve in Mérida mortars 185
Table 3.2- 12. Semiquantitative XRD analysis of Mérida mortars (++++: primary mineral, ++: secondary mineral, +: present, tr: trace) 187
Table 3.2- 13. Weight losses (%) of the mortar samples 189
Table 3.2- 14. Major elements of the Mérida mortars (%) (LOI: Loss of ignition) 194
Table 3.2- 15. Parameters gathered by mercury intrusión (P: Porosity, APD: Average Pore Diameter (4V/A), BD: Bulk density, AD: Apparent density) 198
Table 3.2- 16. Pore size distribution and percentages of micro and macropores 200
Table 3.3- 17. Mineralogical composition of the mortars (qtz: quartz, fel: feldspar, cal: calcite, mica: mainly biotite, opq: opaque mineral) 214
Table 3.3- 18. Binder and aggregate ratios (%) 215
Table 3.3- 19. Weight passing each sieve (%) 217
Table 3.3- 20. Semiquantitative XRD analysis of Nysa mortars (++++: primary mineral, ++: secondary mineral, +: present, tr: trace) 220
Table 3.3- 21. Weight losses (%) of the mortar samples 221
Table 3.3- 22. Major elements of the Nysa mortars (LOI: Loss of ignition) 227
Table 3.3- 23. Parameters gathered by mercury intrusion (P: Porosity, APD: Average Pore Diameter (4V/A), BD: Bulk density, AD: Apparent density) 231
Table 3.3- 24. Pore size distribution and percentages of micro and macropores 232
Table 3.4- 25. Petrographic constituents of Labraunda mortars (Qtz: quartz, plg: plagioclase, cal: calcite, 245

tour: tourmaline, opq: opaque mineral)
Table 3.4- 26. Binder and aggregate ratios (%) 246
Table 3.4- 27. Weight passing each sieve (%) 248
Table 3.4- 28. Semiquantitative mineralogical distribution of Labraunda mortars (Q: quartz, C: calcite, F: feldspar (albite, anorthite), K: kaolinite, Am: amphibole, M: Mica (muscovite, biotite), +++: abundant, ++: major, +: present, tr: traces found) 251
Table 3.4- 29. Weight losses (%) of the mortar samples 252
Table 3.4- 30. Elemental composition of the Labraunda mortars (%) (LOI: Loss of ignition) 260
Table 3.4- 31. Parameters gathered by mercury intrusión (P: Porosity, APD: Average Pore Diameter (4V/A), BD: Bulk density, AD: Apparent density) 262
Table 3.4- 32. Pore size distribution and percentages of micro and macropores 263

Chapter 4

Table 4.1. Physical properties of the mortars 282
Table 4. 2. Mortar types according to function in the constructions, (OC: opus caementicium, OS: opus signinum) 289

Chapter 5

Table 5.1- 1. Results of TG-DSC analysis (WL: weight loss) 301
Table 5.1- 2. Portlandite and calcite amounts during carbonation 305
Table 5.1- 3. Raman peaks at different periods 320
Table 5.1- 4. Physical properties gathered from MIP 326
Table 5.2- 5. Surface hardness (leebs) of the samples (SD: standard deviation) 333
Table 5.2-6. Air permeability (mD) of the samples in different periods 334
Table 5.2- 7. UPV(m/s) values of samples (SD: standard deviation) 336
Table 5.3- 8. Physical properties of the samples in tested periods (Dr: real density, Da: apparent density, CI: Compactness Index, OP: Open porosity, S: Saturation coefficient, SD: standard deviation) 344
Table 5.3- 9. Capillary coefficients (kg/m2.min0,5) of the samples at 5 minutes in tested periods (SD: standard deviation) 347
Table 5.3- 10. Capillary coefficients (kg/m2.min0,5) of the samples between 10 and 90 minutes in tested periods (SD: standard deviation) 347

Chapter 6

Table 6.1. Crystal sizes of the repair mortar samples in different ages (Ca: calcite, Ar: aragonite) 357
Table 6.2. Calcite crystal shapes in the mortars at different curing times (- : calcite crystals were not detected) 360
Table 6.3. Crystal sizes of the repair mortar samples at different stages of curing (P: portlandite, Ca: calcite, Ar: aragonite, V: vaterite, ACC: amorphous calcium carbonate) 361

Chapter 7

Table 7.1. Porosity and apparent density of Roman mortars (Standard deviations are indicated in the paranthesis) 379
Table 7.2. Porosity and apparent density of repair mortars 380

Appendix A

Table I.1. Macroscopic description of the mortar samples from Complutum (OC: Opus Caementicium, OS: Opus Signinum) 455
Table II.2. Macroscopic description of the mortar samples from Mérida (OC: Opus Caementicium, OS: Opus Signinum) 461
Table III.3. Macroscopic description of the mortar samples from Nysa(OC: Opus Caementicium, OS: Opus Signinum) 469
Table IV.4. Macroscopic description of the mortar samples from Labraunda(OC: Opus Caementicium, OS: Opus Signinum) 473

Appendix D

Table D.1. Roman mortar samples analysed in each analytical technique 609
Table D.2. Equipment and centre for each analytical technique 613

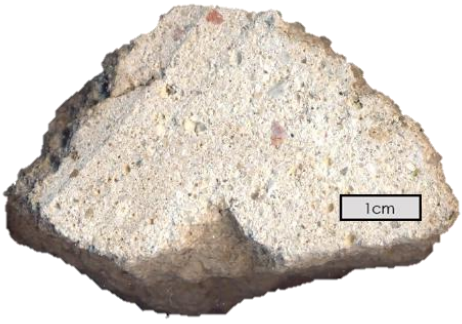
Appendices

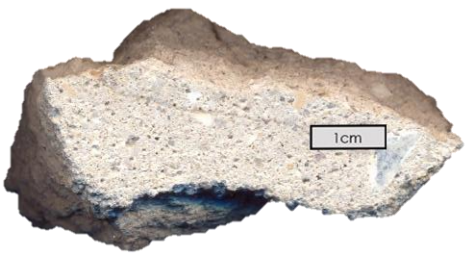
Appendix A

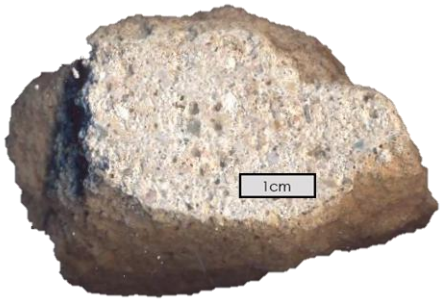
Macroscopic descriptions

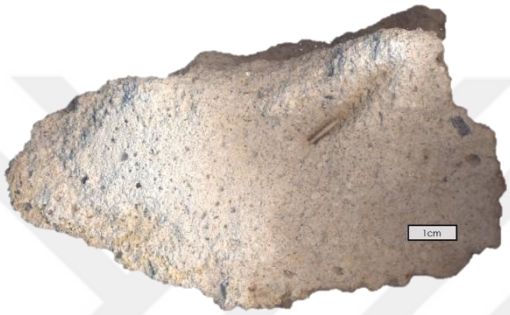
Appendix I- Complutum Archaeological Site

Table I.1. Macroscopic description of the mortar samples from Complutum (OC: Opus Caementicium, OS: Opus Signinum)

Sample	Photo	Description
CM01 **OC-Criptoporticus wall**		whitish colour mortar with high cohesion. Dark gray sub-angular to angular siliceous lithic aggregates (< 2 mm) are observed. Grain size distribution is medium-well sorted.
CM02a **OC-Criptoporticus wall**		Whitish colour mortar with very high cohesion. Binder has whitish creme colour and light and dark to light sub-angular to angular sand grains (< 1 mm) are observed. Grain size distribution is well sorted.
CM02b **OC-Criptoporticus wall**		Whitish colour mortar with high cohesion. Grains ra bigger than CM02a light and dark to light sub-angular to angular sand grains and lithic fragments (< 5mm) are observed. Grain size distribution is medium sorted.
CM03 **OC-North Bath wall**		Whitish colour mortar with high cohesion. light and dark to light sub-angular to angular aggregates (< 3 mm) and lime lumps are observed. Grain size distribution is medium sorted.

CM04 **OC-** **North Bath wall**		Mortar with low cohesion. Binder has creme colour and aggregates are not visible by naked eye.
CM05 **OS-** **North Bath coating**		Mortar with low cohesion. Binder has reddish colour and angular ceramic aggregates (< 50 mm) are observed. Grain size distribution is medium to well sorted.
CM06a **OC-** **North Bath floor**		Sample is a consistent mortar with medium cohesion. Binder has creme colour and grain size distribution is poorly sorted.
CM06b **OS-** **North Bath floor**		Sample is a consistent mortar with medium cohesion. Binder has reddish colour and rounded lime lumps and angular ceramic aggregates (< 5 mm) are well distributed.
CM07 **OS-** **North Bath coating**		Sample is a consistent mortar high cohesion. Large angular ceramic aggregates of sizes > 2.5 cm and 1 cm are embedded in white colour binder.
CM08 **OC-** **North Bath wall**		Dark colour aggregates and lime lumps are embedded in porous white colour binder. Medium cohesion.

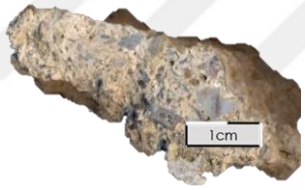
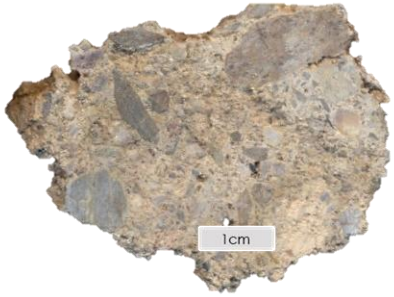
CM09 **OC-** **North Bath wall**		Sample is a consistent mortar with medium cohesion. Porous binder has creme colour angular white colour silicic rock fragments (< 2 mm)and elongated rounded dark colour rock fragments (5 mm). Grain size distribution is poorly sorted
CM10 **OS-** **North Bath coating**		Sample is a consistent mortar with medium cohesion. Porous binder has reddish brown colour angular dark colour aggergates are small in size (< 2 mm). Grain size distribution is well sorted.
CM11 **OC-** **Basilica wall**		Sample is a consistent mortar with medium to low cohesion. Porous binder has whitish colour angular aggergates are small in size (< 2 mm) and 1 cm size light colour rock fragments are observed. Grain size distribution is medium to well sorted.
CM14 **OC-** **South Bath wall**		Brown and dark colour aggregtaes (< 2 mm) are embedded in porous whitish binder
CM15 **OC-** **South Bath wall**		coating mortar is a mortar with medium cohesion. Porous binder has reddish colour angular ceramic aggregates (< 7,5 mm) are poorly sorted.

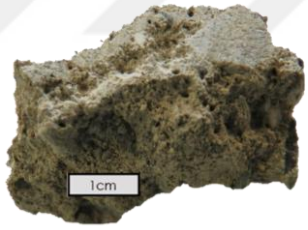
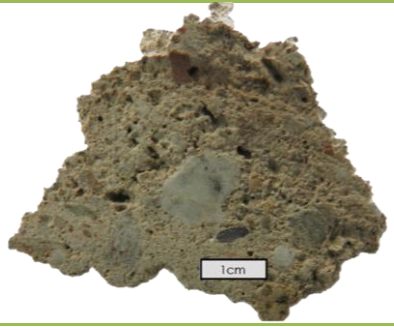
CM16a **OC-sewerage**		Sample is a consistent mortar with medium cohesion. Porous binder has white colour angular ceramic aggregates (< 1 mm) are medium to well sorted.
CM17 **OC-sewerage**		is a consistent mortar with high cohesion. Porous binder has whitish colour. Lime lumps (<3 mm) are detected. Phillite/slate is present as attached to the mortar sample. Grain size distribution is well sorted.
CM18 **OC-sewerage**		Very porous binder has light brown colour and light to dark colour sub-angular to angular elongated lithic aggregates (< 1 mm) are observed. Grain size distribution is medium sorted.

CM20 **OC-** **Monumental façade**		Sample has high cohesion. Porous binder has white-crème colour, Elongated lithic fragments (< 1 cm), ceramic aggregates (< 1 mm) and 4 mm size lime lumps are observed in crème colour binder. Grain size distribution is poorly sorted.
CM21 **OC-** **Cuadriportico foundation**		Sample has medium cohesion. Porous binder has creme colour, sand aggregates (< 1 mm) and lime lumps (< 2 mm) are observed. Grain size distribution is poorly sorted.
CM25 **OS-** **House of Atrium coating**		Sample has low cohesion. Porous binder has reddish colour, sand aggregates (< 7,5 mm) and ceramic fragments (< 4 mm) are observed. Grain size distribution is poorly sorted.

Appendix III. Nysa Archaeological Site

Table III.3. Macroscopic description of the mortar samples from Nysa (OC: *Opus Caementicium*, OS: *Opus Signinum*)

Code-Type	Photo	Description
NM01 **OC**		Sample collected from cistern is consistent mortar with high cohesion. Binder has creme colour and light and dark to light sub-angular to angular sand grains (< 30 mm) are observed. Lime lumps are present. Grain size distribution is well sorted.
NM02 **OC**		Sample collected from the west pillar of second bridge is a consistent mortar with high cohesion. Binder has creme colour and light and dark to light sub-angular to angular sand grains (< 50 mm) are observed. Grain size distribution is well sorted.
NM03 **OC**		Sample collected from the west pillar of first bridge is a consistent mortar with high cohesion. Binder has light brown creme colour and light and dark to light sub-angular to angular sand grains and lithic fragments (< 2 cm) are observed. Grain size distribution is poorly sorted.
NM04 **OC**		Sample collected from lower level of tunnel is a consistent mortar with high cohesion. Binder has brownish colour and light and dark to light sub-angular to angular sand grains (< 40 mm) and white colour quartz grains are observed. Grain size distribution is poorly sorted.
NM05 **OC**		Sample collected from the east pillar of second bridge is a consistent mortar with high cohesion. Binder has creme colour and light and dark to light rounded to angular aggregates and rock fragments (< 2 cm) are observed. Grain size distribution is poorly sorted.

NM06 **OC**		Sample collected from the Geronticon is a consistent mortar with high cohesion. Binder has creme colour and angular light and rounded dark aggregates (< 75 mm) are observed. Grain size distribution is medium to poorly sorted.
NM07 **OS**		Sample collected from the stone arch of basilica shops is a consistent mortar with medium cohesion. Highly porous binder has creme colour and angular light and rounded dark aggregates (< 2 cm) are observed. Grain size distribution is poorly sorted
NM08 **OS**		Sample collected from Stadium is a consistent mortar with low to medium cohesion. Highly porous binder has creme colour and angular light and rounded dark aggregates (< 1 cm) ceramic aggregates (< 50 mm) are observed. One of the collected samples includes lime inclusion (< 3 cm). Grain size distribution is medium sorted.
NM09 **OC**		Sample collected from Theatre is a consistent mortar medium cohesion. Highly porous binder has creme colour. Specimen is like a conglomerate that includes big dimension rock fragments cubic quarzitic rocks (1.5 cm), platelet phillite/slate fragment (4 cm). Grain size distribution is poorly sorted
NM10 **OC**		Sample collected from the wall of library is a consistent mortar with a conglomerate apperance and has medium to high cohesion. Binder has creme colour big dimension rock fragments cubic angular quartz and elongated rounded dark colour rock fragments (1-3 cm). Grain size distribution is poorly sorted.
NM11 **OS**		Sample collected from the wall of Gymnasium is a consistent mortar with high cohesion. Porous binder has creme colour angular white colour silicic rock fragments (< 2 cm)and elongated rounded dark colour rock fragments (50 mm). Grain size distribution is poorly sorted.

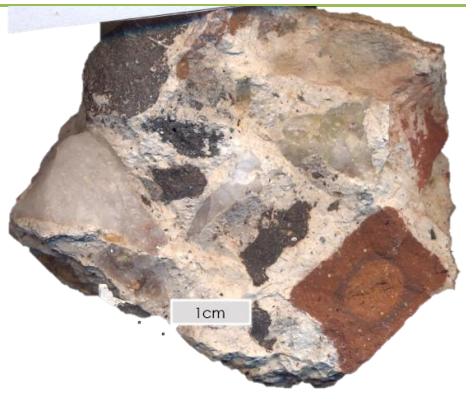
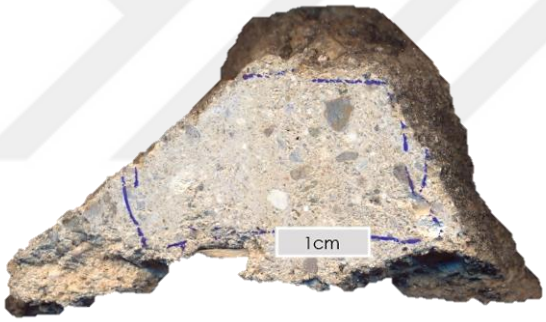
NM12 **OC**		Sample collected from higher level of tunnel is a consistent mortar with medium to low cohesion. Porous binder has reddish brown colour angular aggergates are small in size (< 20 mm). Grain size distribution is well sorted.
NM13 **OC**		Sample collected from lower level of tunnel is a consistent mortar with medium to low cohesion. Porous binder has reddish brown colour angular aggergates are small in size (< 20 mm) and 1 cm size light colour rock fragments are observed. Grain size distribution is medium to well sorted.
NM14 **OC**		Sample taken from the Agora road is very consistent. Binder has light brown colour angular aggergates ar enot visible by naked eye.
NM16 **OS**		Coating mortar found in Agora Road, is a consistent mortar with medium cohesion. Porous binder has reddish colour angular ceramic aggregates (< 1 cm) are medium to well sorted.
NM22 **OC**		Sample collected from the west pillar of second bridge is a consistent mortar with medium cohesion. Porous binder has light brown colour.
NM23 **OS**		Sample taken from Stadium (amphitheatre) is a consistent mortar with medium cohesion. Binder has reddish brown colour and light and dark gray sub-angular to angular siliceous lithic and aggregates (< 20 mm) are observed. Lime lumps (<30 mm) are detected. Phillite/slate is present as attached to the mortar sample. Grain size distribution is well sorted.

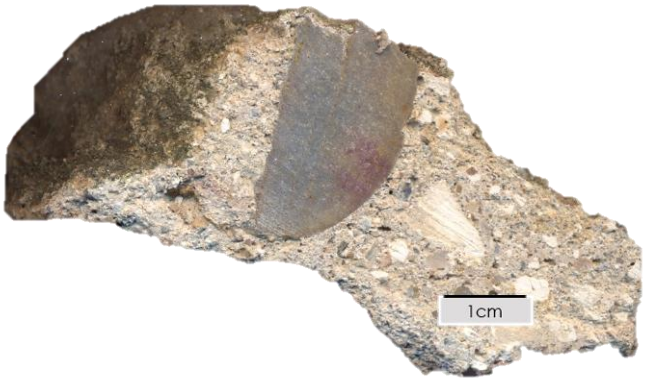
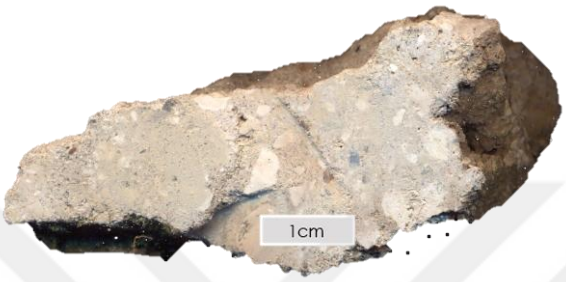
NM24 **OC**		Sample collected from the east pillar of second bridge is a consistent mortar with medium cohesion. Porous binder has light brown colour and light to dark colour sub-angular to angular elongated lithic aggregates (< 1 cm) are observed. Grain size distribution is medium sorted.
NM25 **OS**		Sample collected from the middle arch in the bath has high cohesion. Porous binder has white-crème colour, Elongated lithic fragments (< 1 cm), ceramic aggregates (< 40 mm) and 1 cm size lime lump are observed. Grain size distribution is medium to poorly sorted.
NM26 **OS**		Sample collected from the third arch in the bath has medium cohesion. Porous binder has reddish colour, sand aggregates (< 20 mm) and rock fragments (< 3cm) are observed. Biological colonization present in one of the samples. Grain size distribution is poorly sorted.
NM27 **OC**		Sample taken from the bath next to the water tube in the arch, is a consistent mortar with high cohesion. Porous binder has whitish creme colour and mainly agrregates are not visible by naked eye. Lithic fragments (<50 mm) are detected rarely and 1 cm x 2.5 cm lime inclusion is observed. Grain size distribution is poorly sorted.

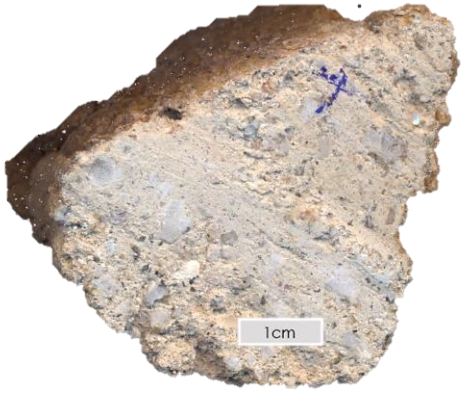
Appendix II- Mérida Archaeologic Complex

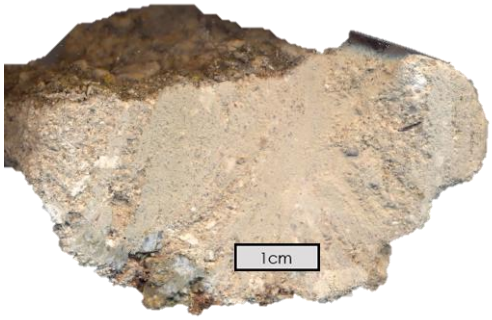
Table II.2. Macroscopic description of the mortar samples from Mérida (OC: Opus Caementicium, OS: Opus Signinum)

Code-Type	Photo	Description
MM1 **OC**		Sample collected from San Lazaro Aqueduct is consistent mortar with high cohesion. Binder has whitish creme colour and light and dark to light sub-angular to angular sand grains (< 2 mm) and fly ashes (< 1 mm) are observed. Lime lumps are present. Grain size distribution is well sorted.
MM2 **OC** **channel**		Sample taken from the San Lazaro Aqueduct Sample has high cohesion. light and dark to light sub-angular to angular sand grains (< 5 mm). Lime lumps are present. Grain size distribution is well sorted.
MM3 **OC OS** **channel**		Sample collected from the basemnet of San Lazaro Aqueduct has both types with very well observed fin elayer between them. Large fragments of ceramic and dark/light coloured lithic fragments are called caementa. Sample has high cohesion. Grain size distribution is well sorted.

MM5 **OC**		Sample collected from different level of basement of San Lazaro Aqueduct is similiar to MM3cae having large angular ceramic and dark/light colour rock fragments embedde in a white colour binder. Sample has high cohesion. Grain size distribution is well sorted.
MM6 **OC** **Alcazaba wall**		Sample taken from wall of Alcazaba has high cohesion. Light and dark to light rounded to angular lithic fragmnets are present (< 1.5 cm). Grain size distribution is poorly sorted.
MM7 **OC**		Sample taken from wall of Alcazaba has high cohesion. Light and dark to light rounded to angular sand grains (< 5 mm). Lime lumps are present. Grain size distribution is poorly sorted.
MM8 **OC** **Moreira wall**		Sample taken from wall of Moreria has medium cohesion. Binder has light brown creme colour. Light and dark to light sub-angular to angular sand grains (< 3 mm) are medium sorted. Visible lime lumps are present.
MM9 **OC**		Sample collected from Moreria wall has light brown colour, has high porosity and medium cohesion. Light and dark to light sub-angular to angular sand grains (< 3 mm) are medium sorted.

MM10 OC **Temple floor**		Creme colour sample collected from the floor of Temple of Diana includes large (2 cm) elongated rounded edge dark colour lithic fragment and up to 1 cm white colour fragments apart from small aggregates (<2 mm). Grain size distribution is poorly sorted.
MM11 OC		Whitish creme colour sample collected from the basement of granite ashlar in Temple of Diana has large (1 cm) subangular white and dark colour small aggregates which are poorly sorted. Sample shows high consistency and low porosity.
MM12 OC		Sample collected from the vault of the channel in Temple of Diana has biological colonization and medium cohesion. Grain size distribution is poorly sorted.
MM13 OC		Sample collected from the pillar basement in Temple of Diana has medium cohesion. Grain size distribution is poorly sorted. Highly porous fly ashes exist.

MM14 **OC**		Whitish creme colour sample collected from the wall of Temenos part in Temple of Diana has higher porosity and dark and light rounded to sub angular (5 mm) grains.
MM15 **OC**		Sample collected from the wall of Temenos Temple of Diana has light brown creme colour and rarely up to 1 cm dark colour lithic fragments. Medium-high porosity is observed.
MM16 **OC**		Whitish colour sample collected from wall of Vrinero includes small dark colour aggregates (<2 mm). Grain size distribution is medium sorted. Lime lumps exist.
MM17 **OC**		Sample collected from another wall of Vrineo has whitish creme colour. Sample has high porosity and low consistency. Aggregates are smaller than 5mm fly ashes are present.

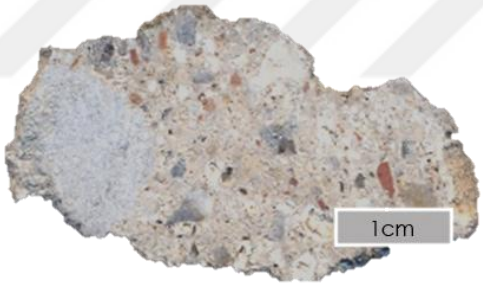
MM18 **OS**		Coating mortar sample collected from Resti Bath has reddish binder and up to 1 cm angular ceramic fragments. Some of the aggregates have higher sphericity. Mortar has medium cohesion.
MM19 **OC**		Sample collected from Resti Bath has low cohesion. Binder has light brown colour and aggregates are not viisble by naked eye.
MM20 **OC**		Sample from wall of Circo has creme colour and small grains (1-2 mm)

MM21 **OS**		Sample from wall of Circo has reddish colour and small grains (1-2 mm)
MM22 **OS** **Amphithe atre**		Sample collected from Sum cavea of Amphitheatre has creme colour. Porous mortar has 1 cm rounded lithic fragment and angular white colour and small grains (1, 2mm and <5mm). Grain size distribution is medium sorted.
MM24 **OC**		Sample collected from Sum cavea of Amphitheatre has creme colour. Porous mortar has 1 cm rounded lithic fragment and angular white colour and small grains (1, 2mm and <5mm). Grain size distribution is medium sorted.

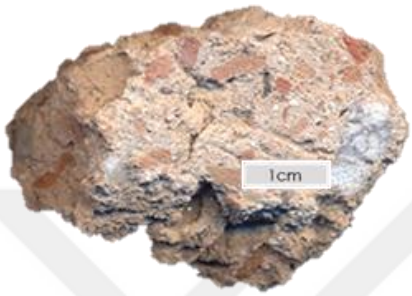
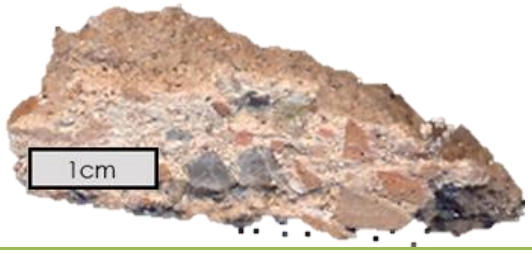
MM25 **OC**		Sample collected from Sum cavea of Amphitheatre has whitish colour. Porous mortar has 1 cm rounded lithic fragment and angular white and dark colour lithic fragments (5mm) and schistic rock (4 cm) are adhered to the mortar. 1mm dark colour minerals are dispered to the mortar.
MM26 **OC**		Sample collected from snow well has whitish colour and well distributed grains up to 2 mm are embedded in lime binder.
MM27 **OS** **Snow well**		Sample collected from snow well hasreddish colour and well distributed grains up to 3 mm are embedded in lime binder. Grey colour rock fragment is adhered to the sample.

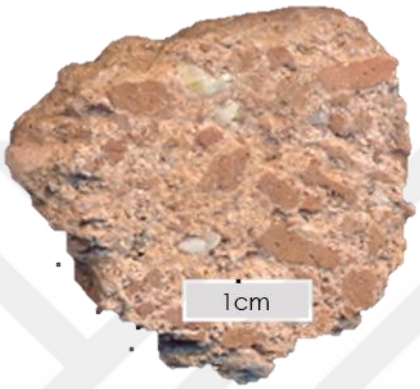
Appendix IV- Sanctuary of Labraunda

Table IV.4. Macroscopic description of the mortar samples from Labraunda (OC: *Opus Caementicium*, OS: *Opus Signinum*)

Sample	Photo	Description
LM01A		Binder has creme color, well sorted aggregates including ceramics (< 7.5 mm) are angular to sub-angular in shapeSample is a consistent mortar with high cohesion Binder has creme colour and light and dark gray sub-angular to angular siliceous lithic and reddish colour ceramic aggregates (< 50 mm) are observed. Lime lumps (<10 mm) are detected as well. Grain size distribution is well sorted.
LM01C		Whitish colour lime plaster sample aggregates are not visible by naked eye. LM01C is plaster sample with whitish colour, aggregates are not visible and porosity is low .
LM02		Binder has whitish colour bigger than 1cm rounded rock fragment and small angular aggregates (< 3mm) are embedded in the binder. Grain size distribution is poorly sorted. Sample LM02 is a consistent mortar with high cohesion (Figure 4). Binder has white colour and light to dark gray sub-angular to angular siliceous lithic and reddish colour ceramic aggregates (< 10 mm) are observed. Frequent lime lumps (<10 mm) are detected. Grain size distribution is poorly sorted
LM03		Crème light brown colour mortar with medium cohesion. Aggregates are not visible, mortar is highly porous. Sample LM03 is a consistent mortar with high cohesion and there was biological colonization outer surface of the sample. Porous binder has whitish colour and dark gray sub-angular to angular siliceous lithic (< 10 mm) and reddish colour ceramic aggregates (< 50 mm) are observed. Lime lumps (<10 mm) are detected. Grain size distribution is poorly sorted

LM04A		Aggregatesare poorly sorted in the light brown colour lime binder. Sample LM04A is a consistent mortar with medium cohesion Binder has white colour and high porosity and light gray rounded to sub-angular siliceous lithic (< 1 mm) and reddish colour ceramic aggregates (< 5 mm) are embedded on it. Grain size distribution is poorly sorted
LM04B		Binder has reddish colour aggregtaes are not visible by naked eye. Sample LM04B is a consistent mortar with medium cohesionPorous binder has light brown - creme colour and aggregates are poorly sorted. Sub-angular siliceous lithic (< 1 cm) and reddish colour ceramic aggregates (< 5 mm) are seen
LM05		Small fragments (2 cm) of mortars are sampled. Highly porous binder has crème colour and aggregates are not visible. Sample LM05 is a consistent mortar with medium cohesion. Porous binder has light brown colour angular ceramic aggregates (< 7.5 mm) are seen. Grain size distribution is poorly sorted
LM06A		Sample LM06A is a consistent mortar with medium cohesion Binder has light brown- reddish colour and high porosity, angular ceramic aggregates (< 1 cm) are embedded on it. Grain size distribution is well sorted

LM06B		Sample LM06B is a consistent mortar with medium cohesion (Figure 14). Porous binder has creme colour and apart from large aggregates (>1 cm) angular aggregates (< 5 mm) are not visible by naked eye. Grain size distribution is well sorted .
LM06C		Creme reddish colour mortar has large ceramic fragments (<1 cm) and (<1.5 cm) lime inclusion. Shows low cohesion. Sample LM06C is a consistent mortar with medium cohesion (Figure 16). Binder has creme colour and high porosity, 1 cm elongated rock fragments and angular ceramic aggregates (< 50 mm) and lime lumps (3-4 mm) are observed. Grain size distribution is well sorted.
LM07A		Sample LM07A is a mortar with medium cohesion. Binder has creme colour and high porosity, dark colou and cubic ceramic aggregates (< 50 mm) and lime lump (3-4 mm) are observed. Grain size distribution is poorly sorted .
LM07B		Sample LM07B is a mortar with medium cohesion. Binder has reddish light brown colour and high porosity, ceramic aggregates (< 1 cm) are observed by naked eye).
LM07C		Sample LM07C is a mortar with medium cohesion. Binder has creme colour and high porosity, dark colour grains and cubic ceramic aggregates (< 50 mm) are observed. Grain size distribution is poorly sorted (Figure 22).

LM07D		Small fragments (2 cm) of mortars are sampled. Highly porous binder has brown colour and aggregates are not visible. LM07D has medium cohesion. Binder is porous and crème in colour. Aggregates are not visible by naked eye.
LM08		Red colour mortar has ceramic aggregtaes (< 1 cm), silicic aggregates are visible as well. Sample LM08 is a mortar with medium cohesion. Binder has reddish colour and high porosity, dark colour grains and cubic ceramic aggregates (< 75 mm) are observed. Grain size distribution is poorly sorted.
LM09		Porous brown colour mortar has low cohesion. Aggregates are not visible by naked eye. Sample LM09 is a mortar with low cohesion (Figure 26). Binder has red colour and high porosity, dark colour 10 mm aggregates and cubic ceramic aggregates (< 50 mm) and lime lump (3-4 mm) are observed. Grain size distribution is poorly sorted.

Appendix B

Thin section images

Appendix V- Complutum Archaeological Site

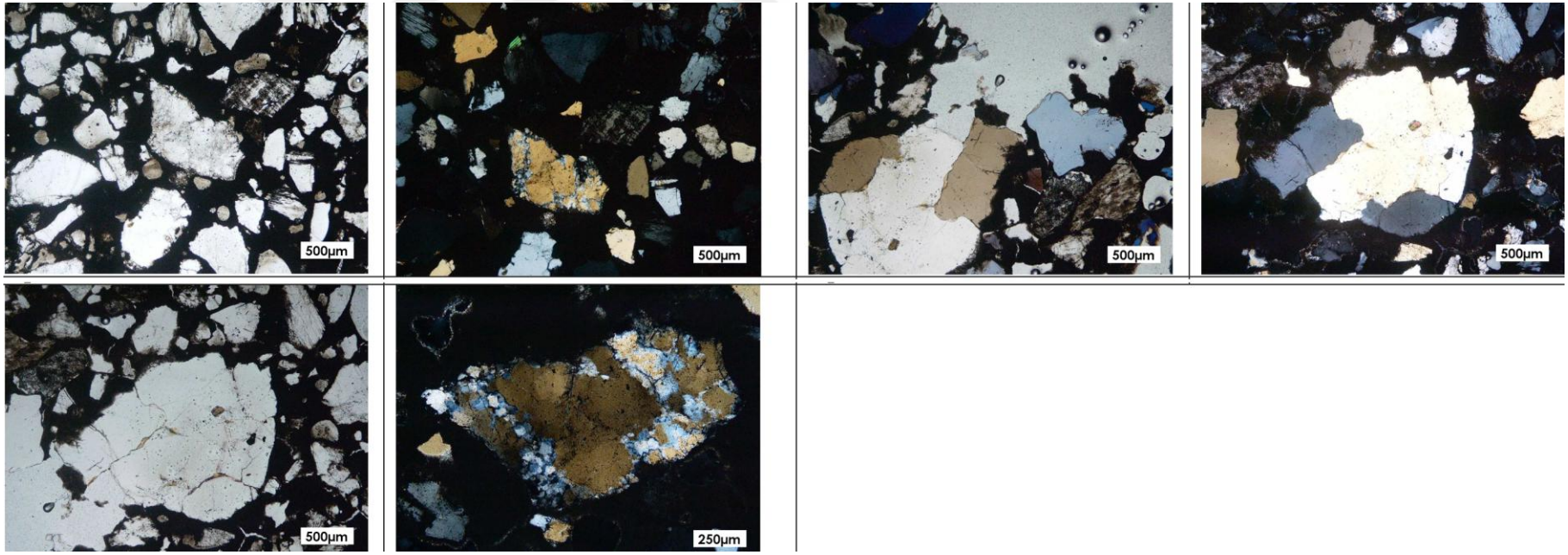


Figure V.1. Thin section images of sample CM01

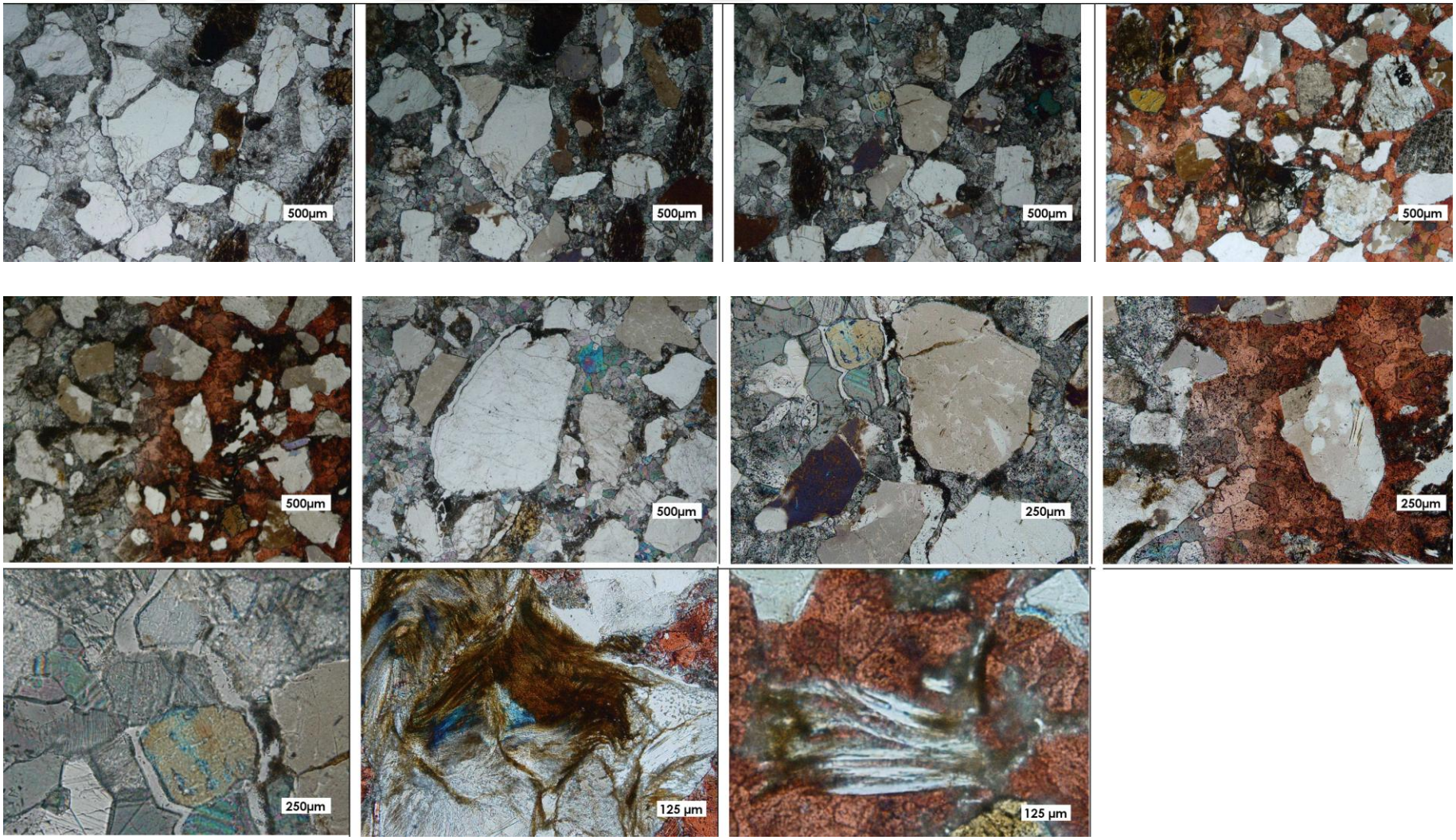


Figure V.2. Thin section images of sample CM02a

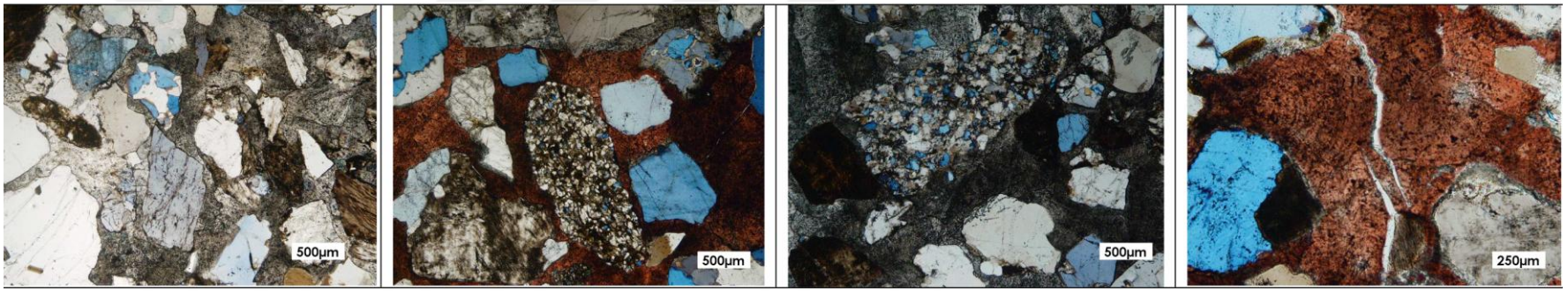


Figure V.3. Thin section images of sample CM02b

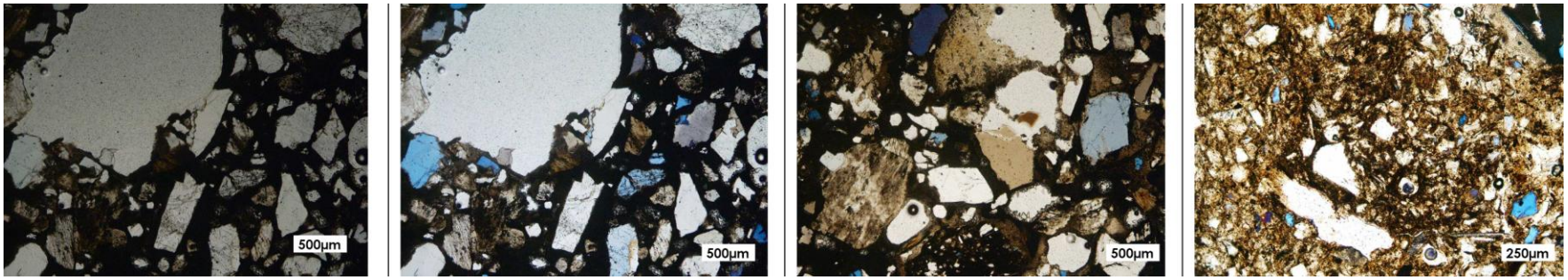


Figure V.4. Thin section images of sample CM03

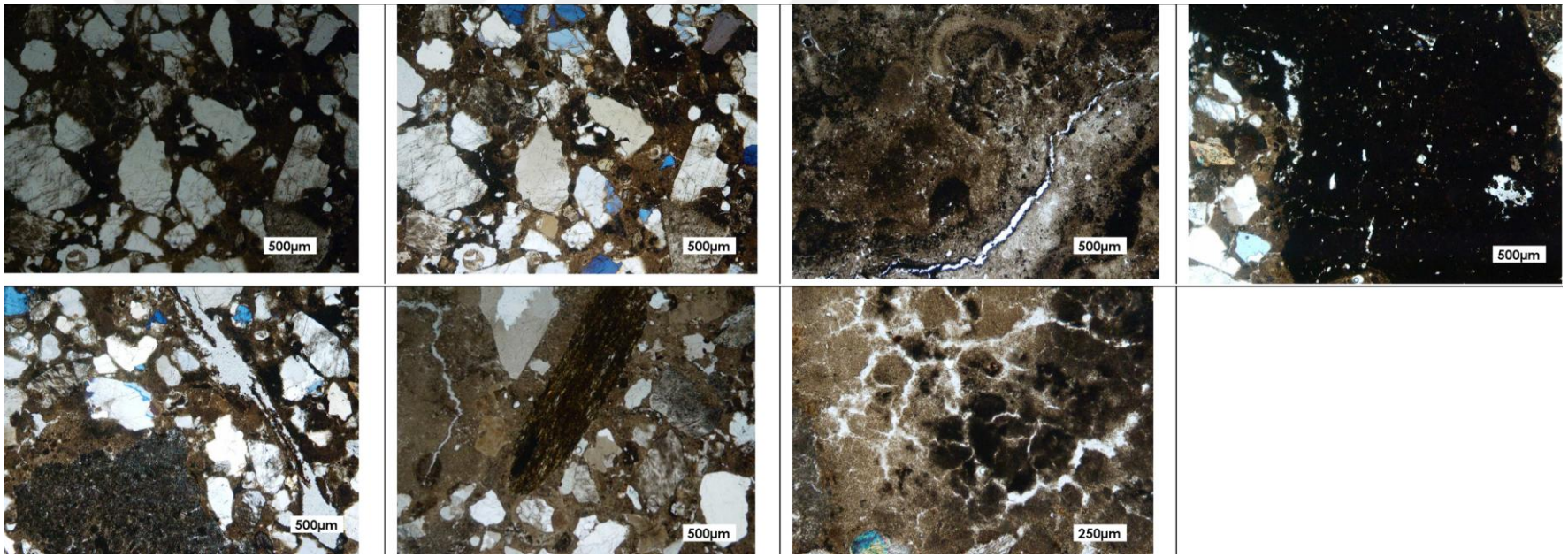


Figure V.5. Thin section images of sample CM04

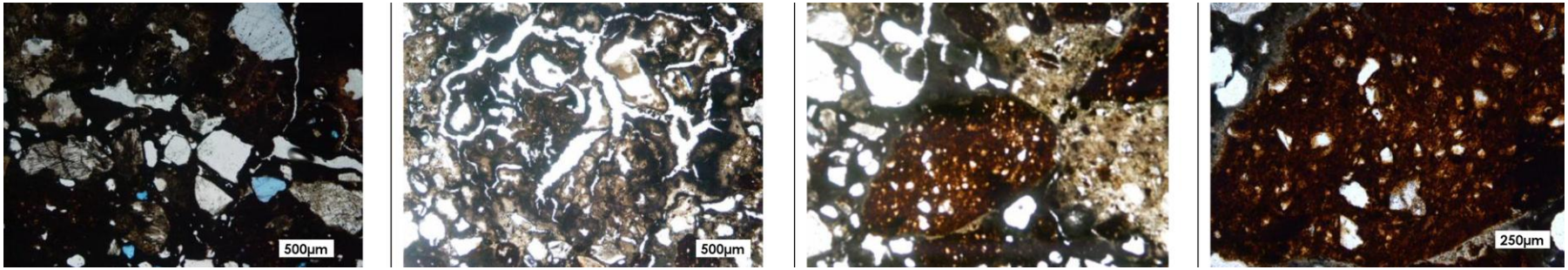


Figure V.6. Thin section images of sample CM05

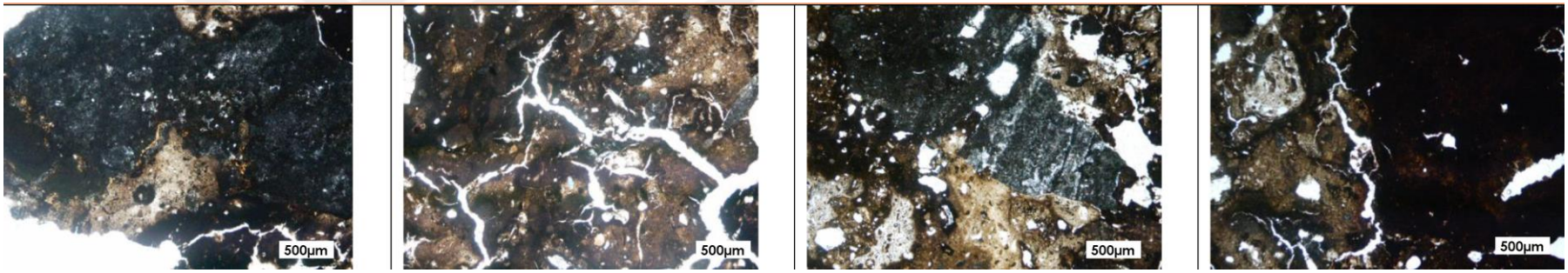


Figure V.7. Thin section images of sample CM06a

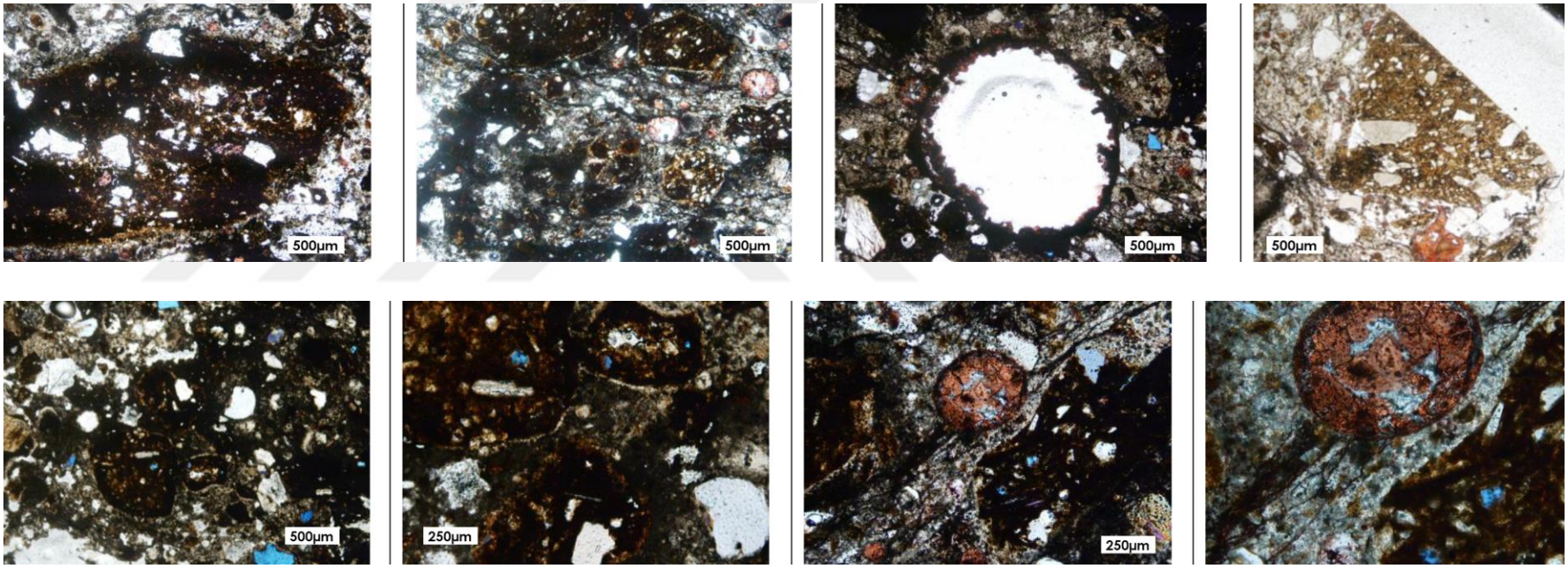


Figure V.8. Thin section images of sample CM06b

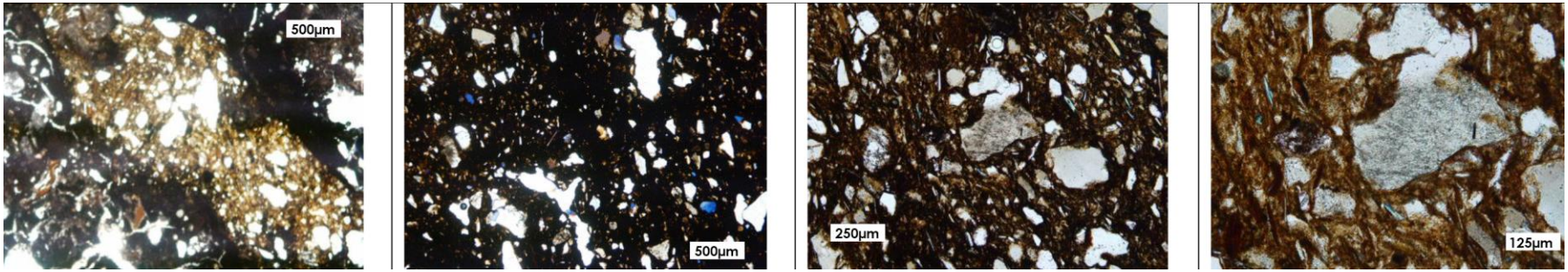


Figure V.9. Thin section images of sample CM07

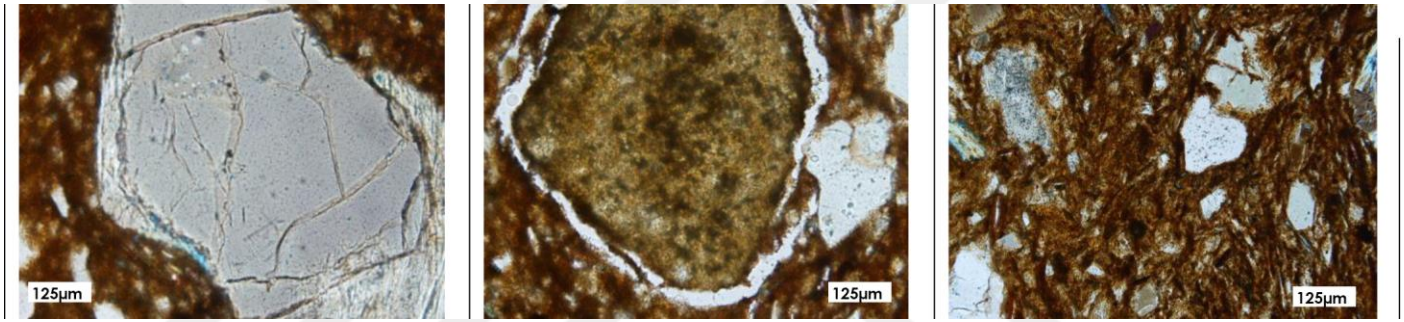


Figure V.10. Thin section images of sample CM07 (continue)

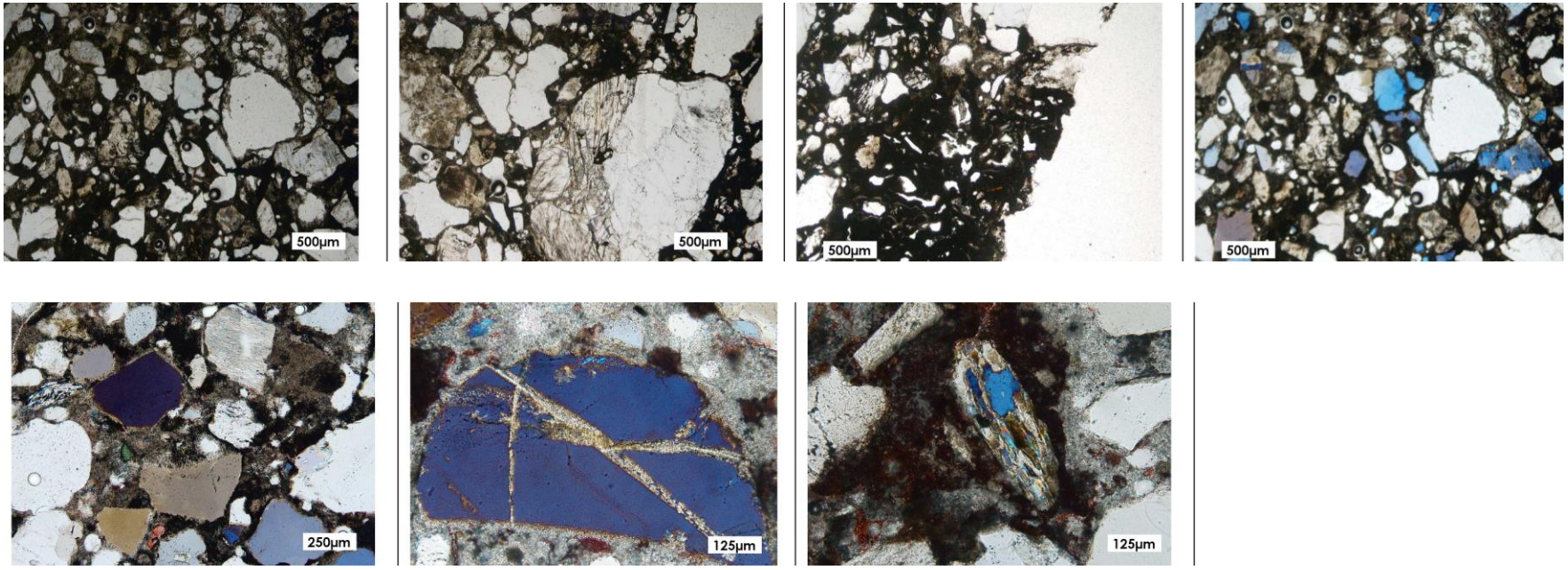


Figure V.11. Thin section images of sample CM08

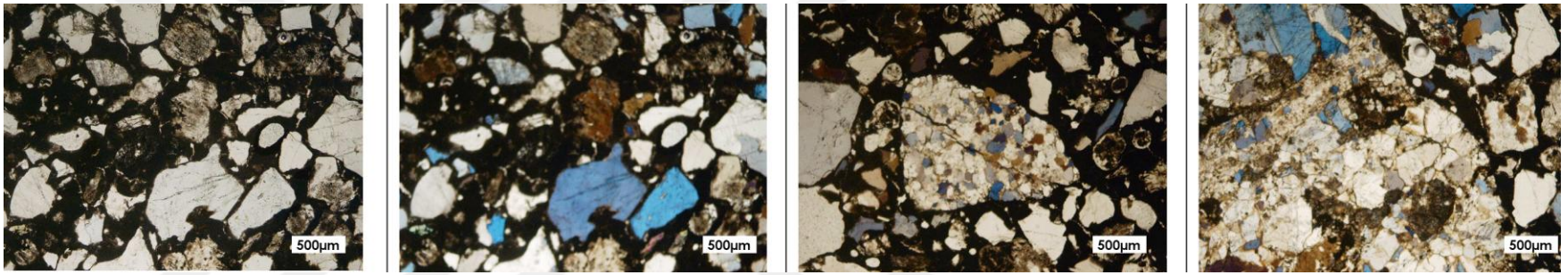


Figure V.12. Thin section images of sample CM09

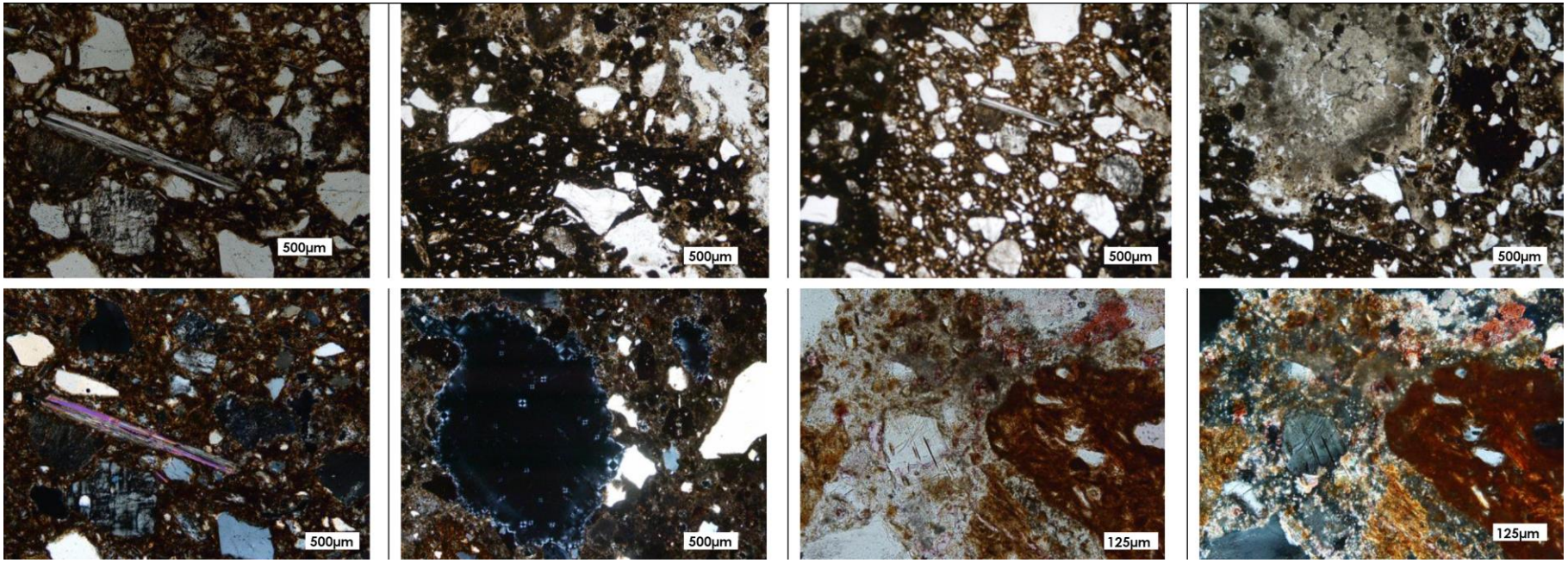


Figure V.13. Thin section images of sample CM10

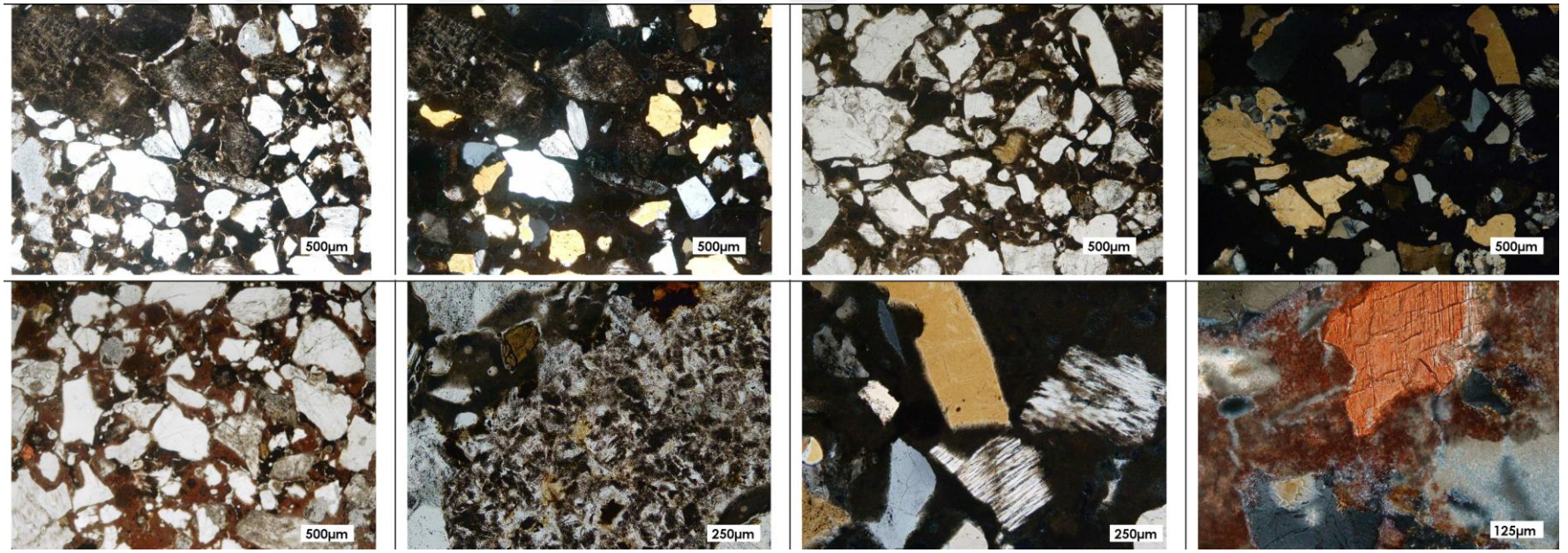


Figure V.14. Thin section images of sample CM11

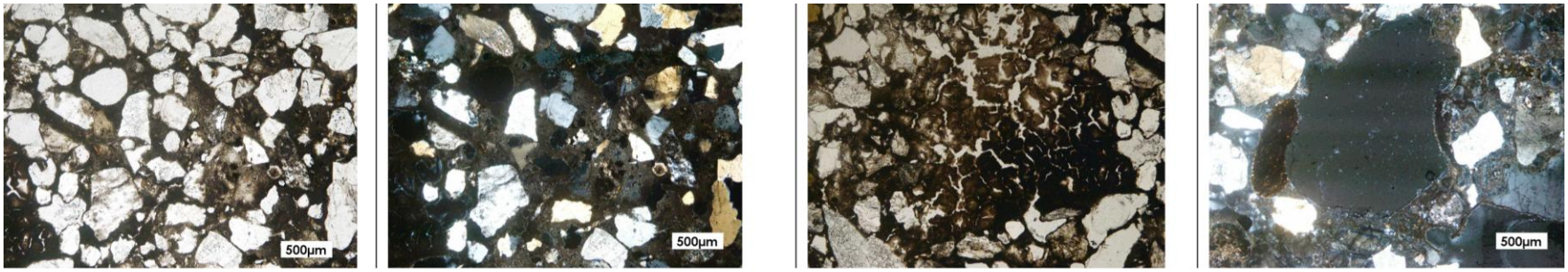


Figure V.15. Thin section images of sample CM14

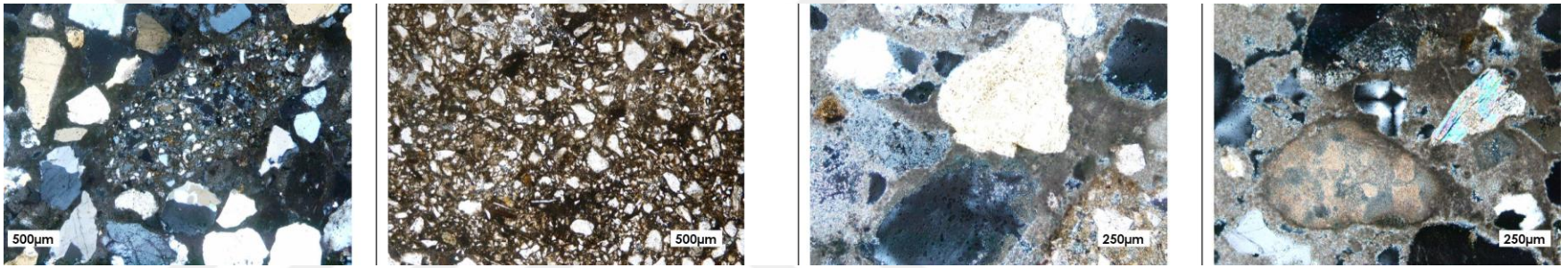


Figure V.16. Thin section images of sample CM14 (continue)

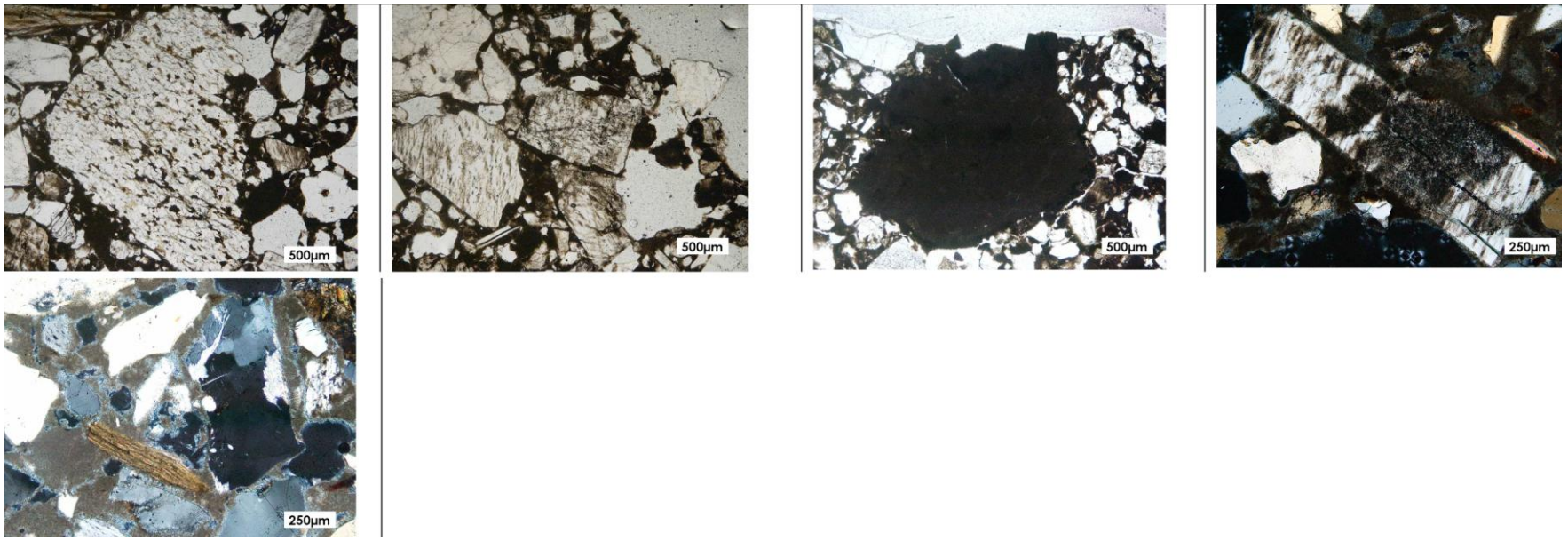


Figure V.17. Thin section images of sample CM15

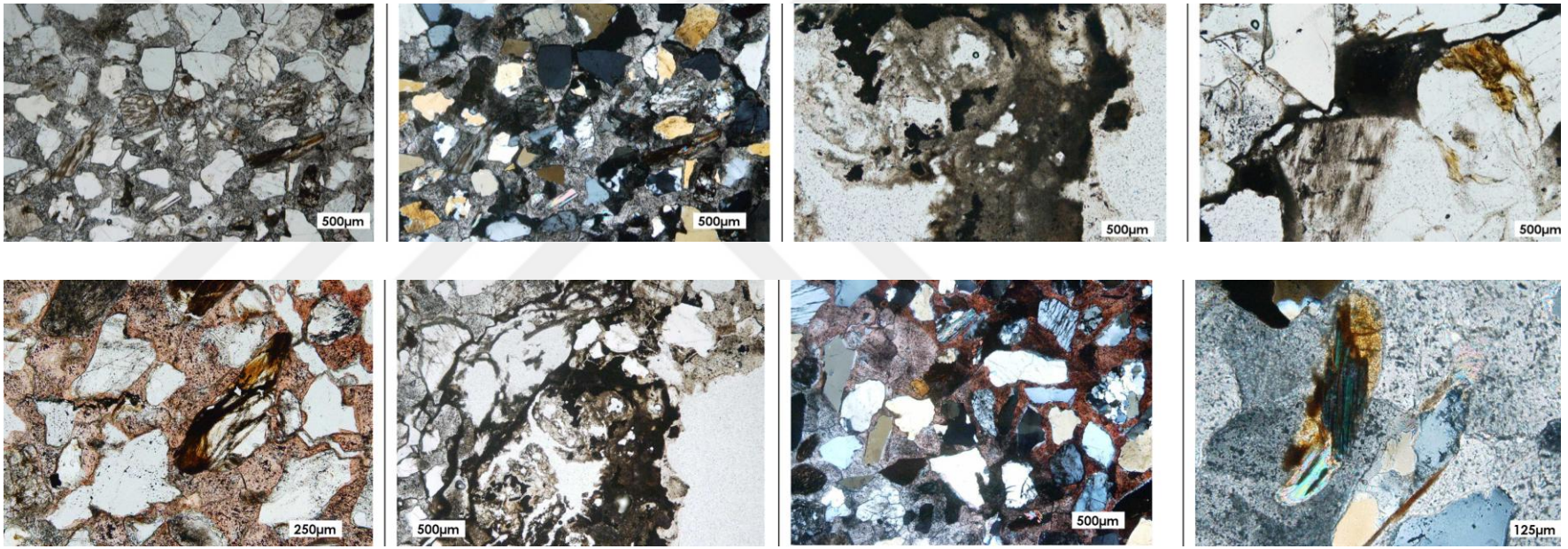


Figure V.18. Thin section images of sample CM16a

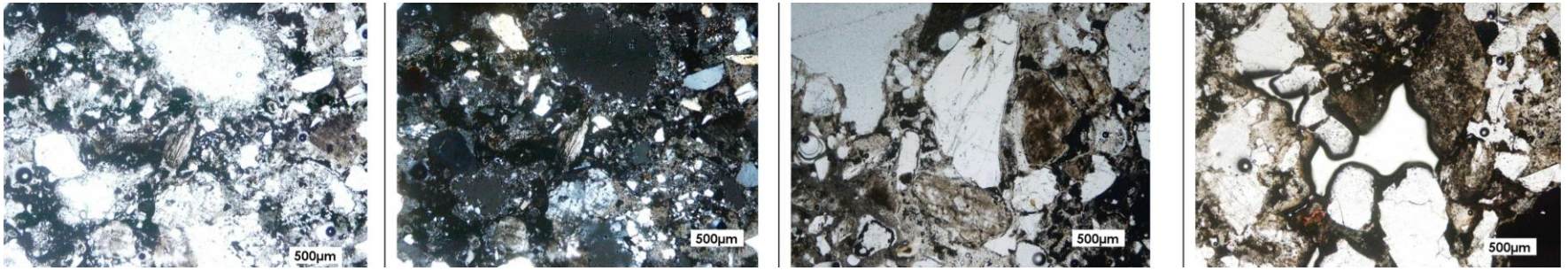


Figure V.19. Thin section images of sample CM16b



Figure V.20. Thin section images of sample CM16b (continue)

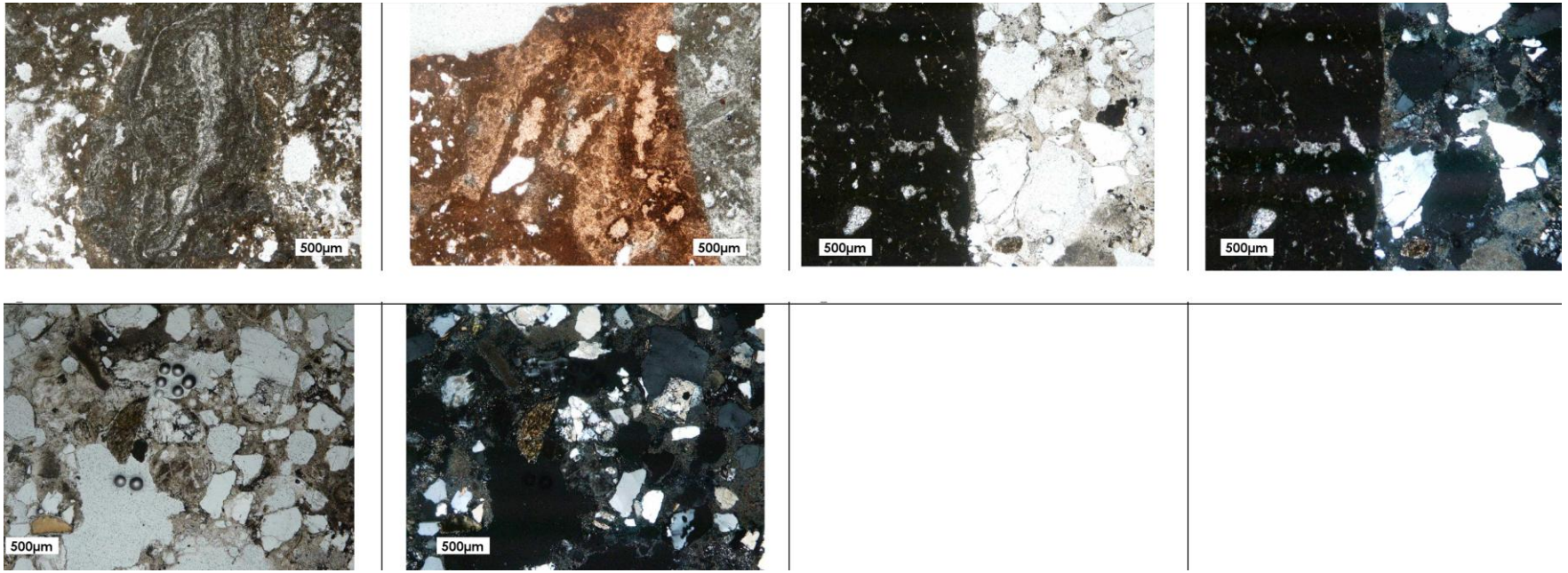


Figure V.21. Thin section images of sample CM18a

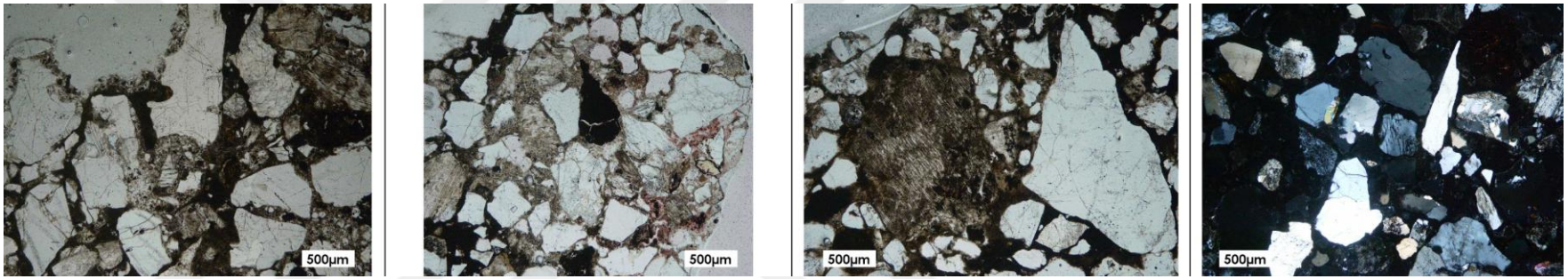


Figure V.22. Thin section images of sample CM18b

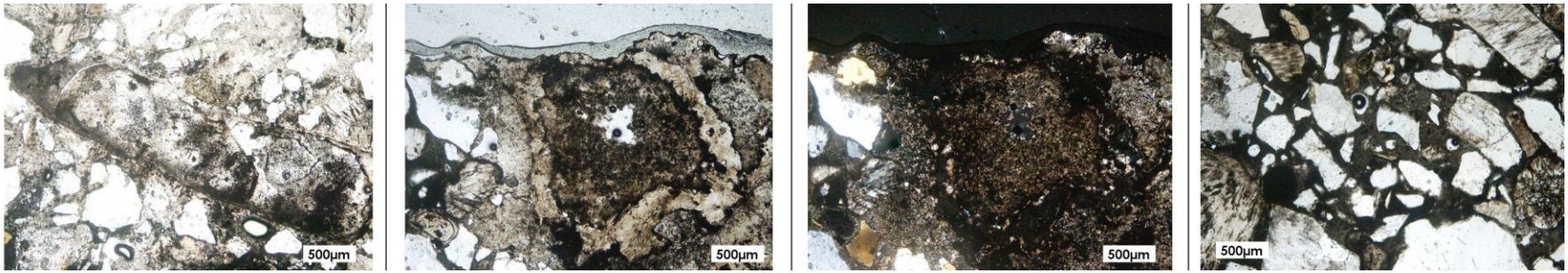


Figure V.23. Thin section images of sample CM20

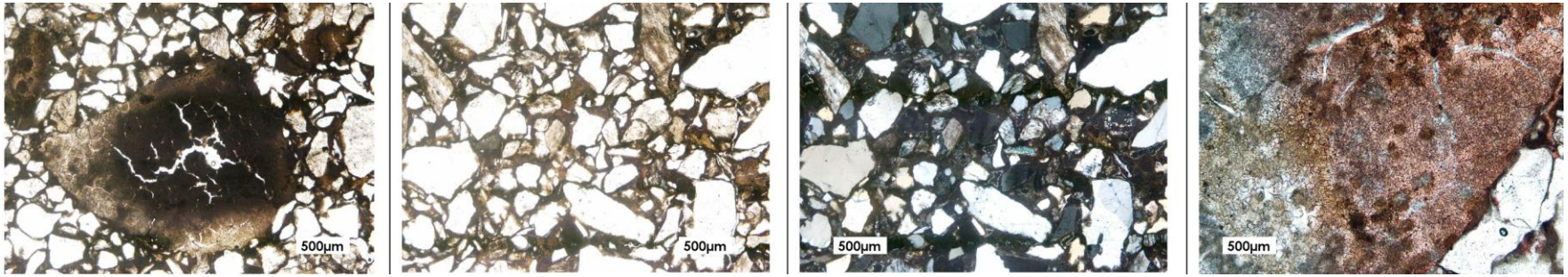


Figure V.24. Thin section images of sample CM21

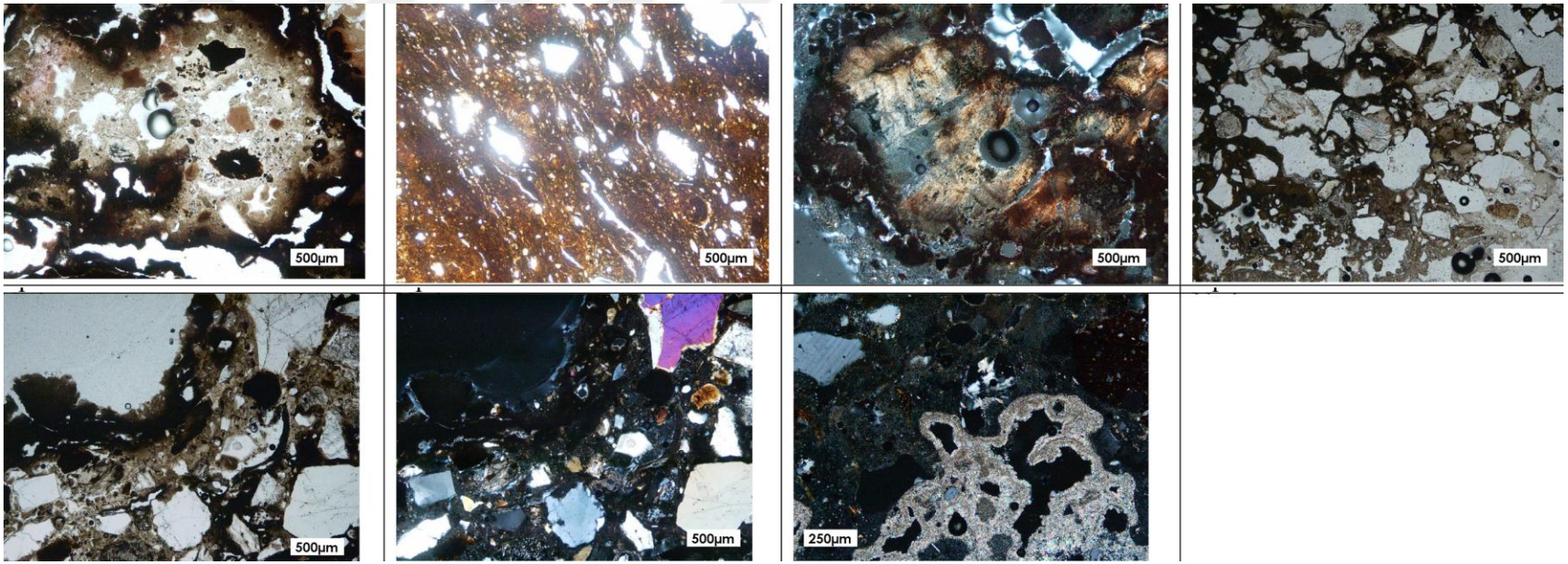


Figure V.25. Thin section images of sample CM24a

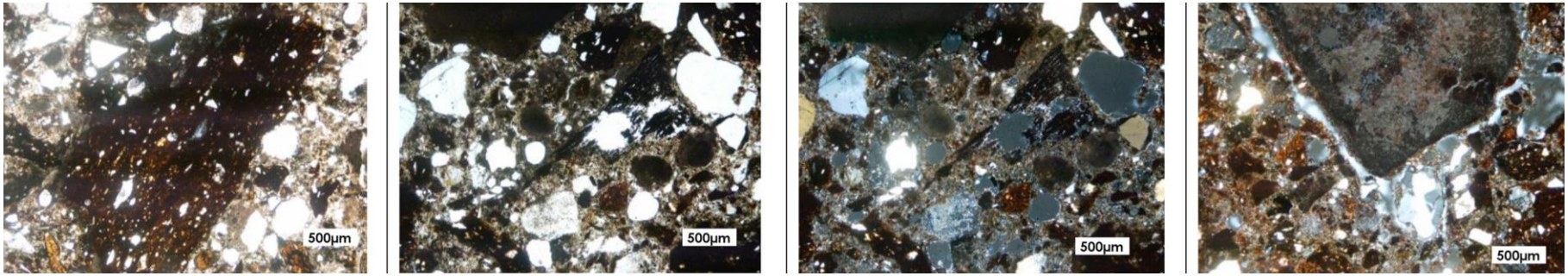


Figure V.26. Thin section images of sample CM25

Appendix VI- Mérida Archaeologic Complex

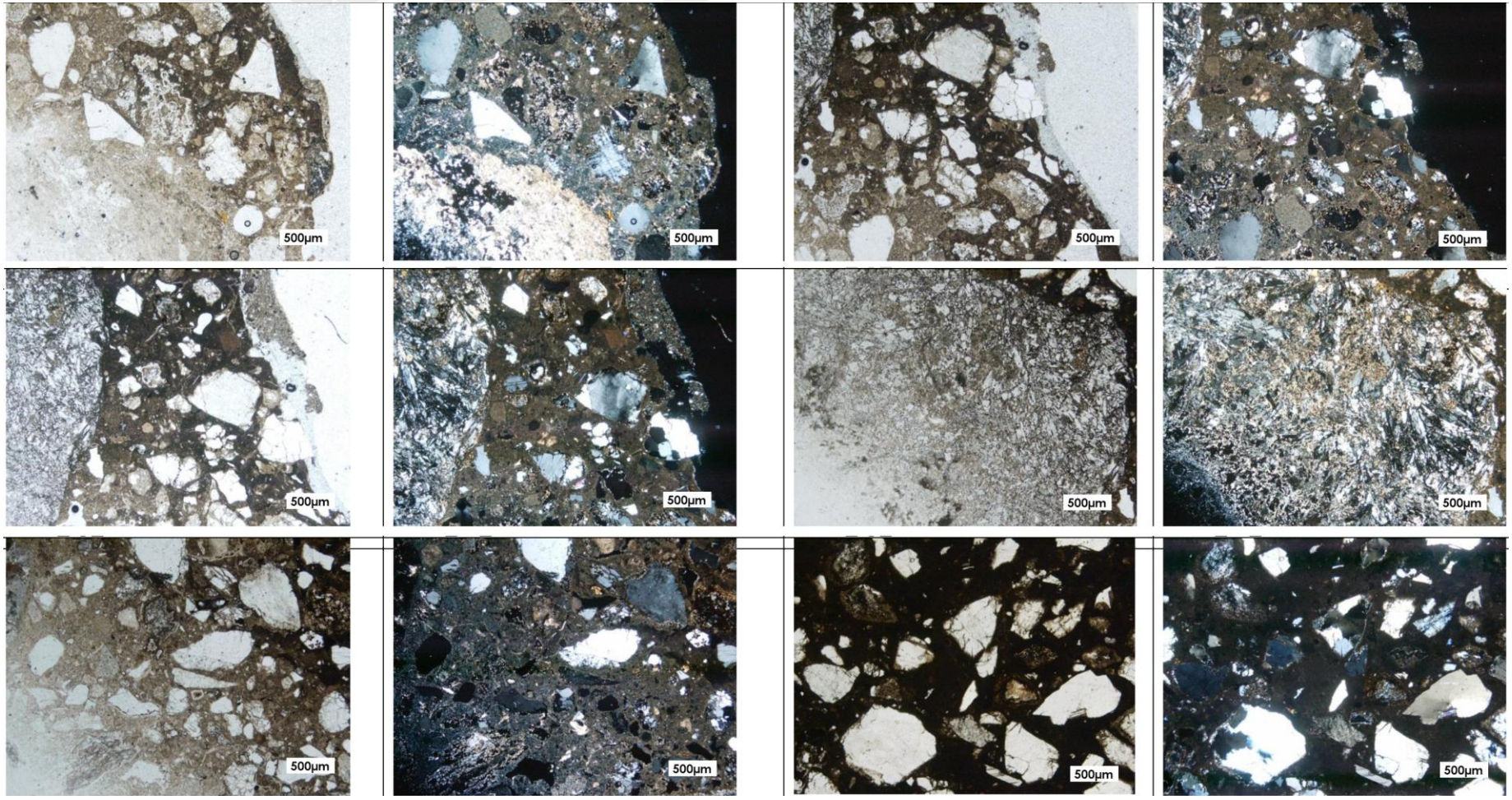


Figure VI.1. Thin section images of sample MM2

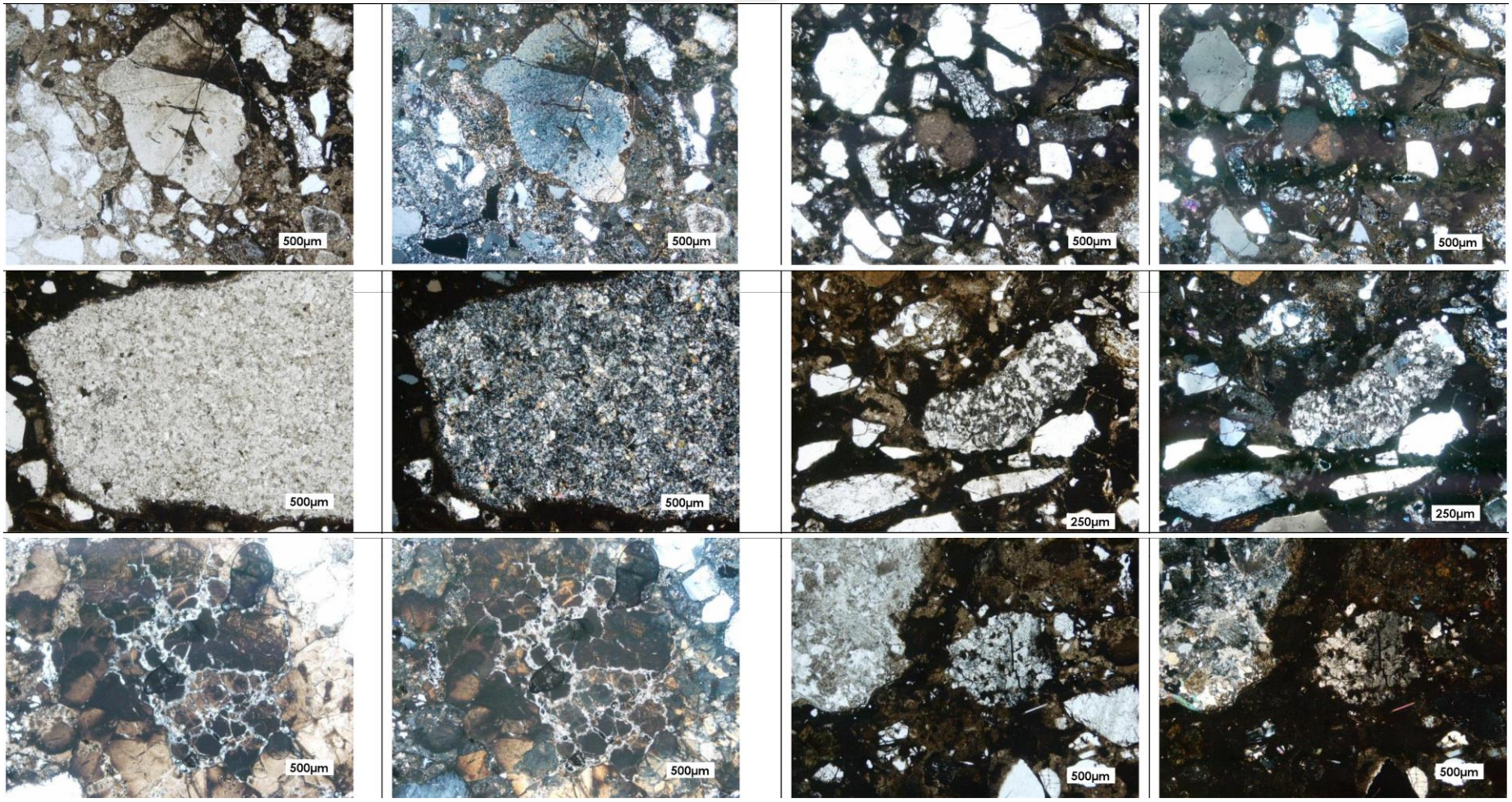


Figure VI.2. Thin section images of sample MM2 continue

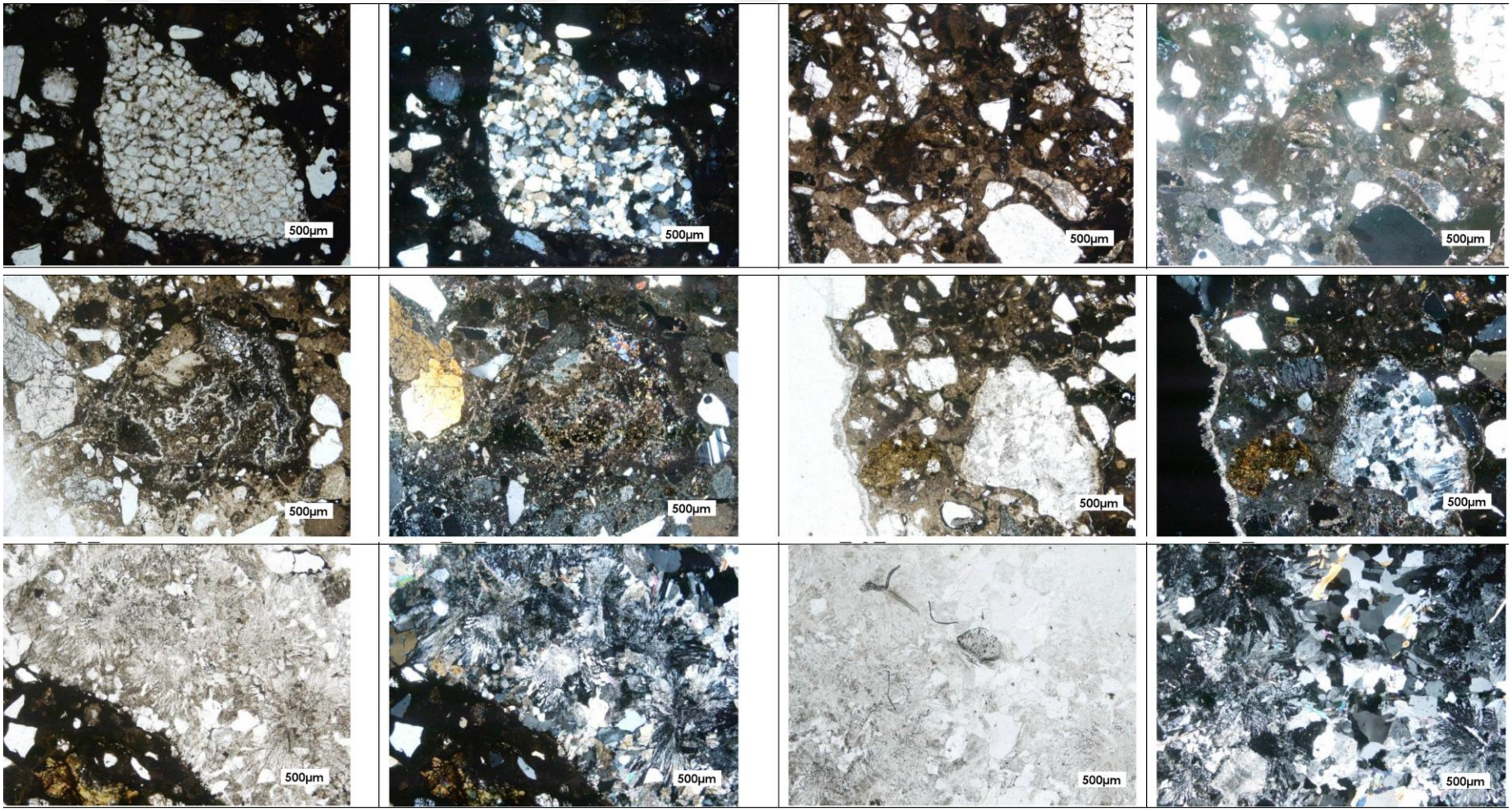


Figure VI.3. Thin section images of sample MM2 continue

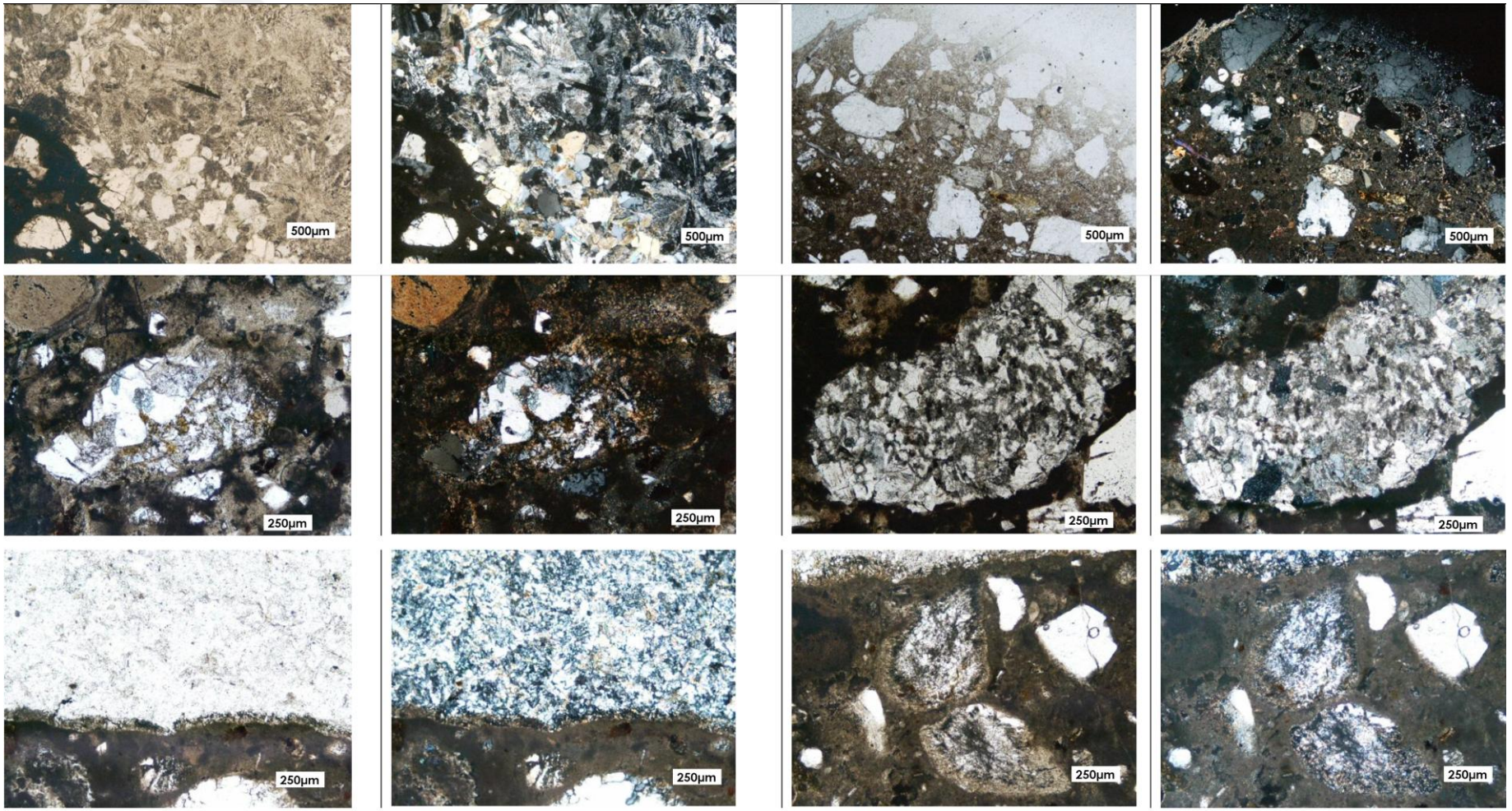


Figure VI.4. Thin section images of sample MM2 continue

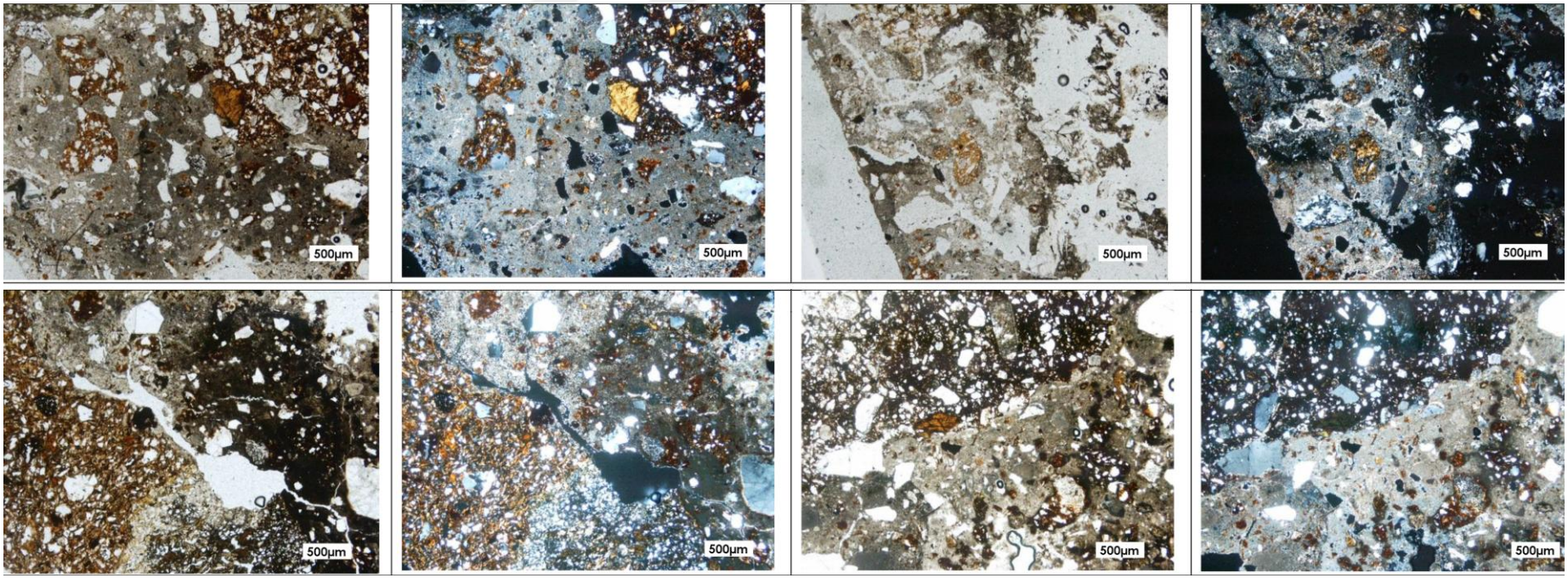


Figure VI.5. Thin section images of sample MM3

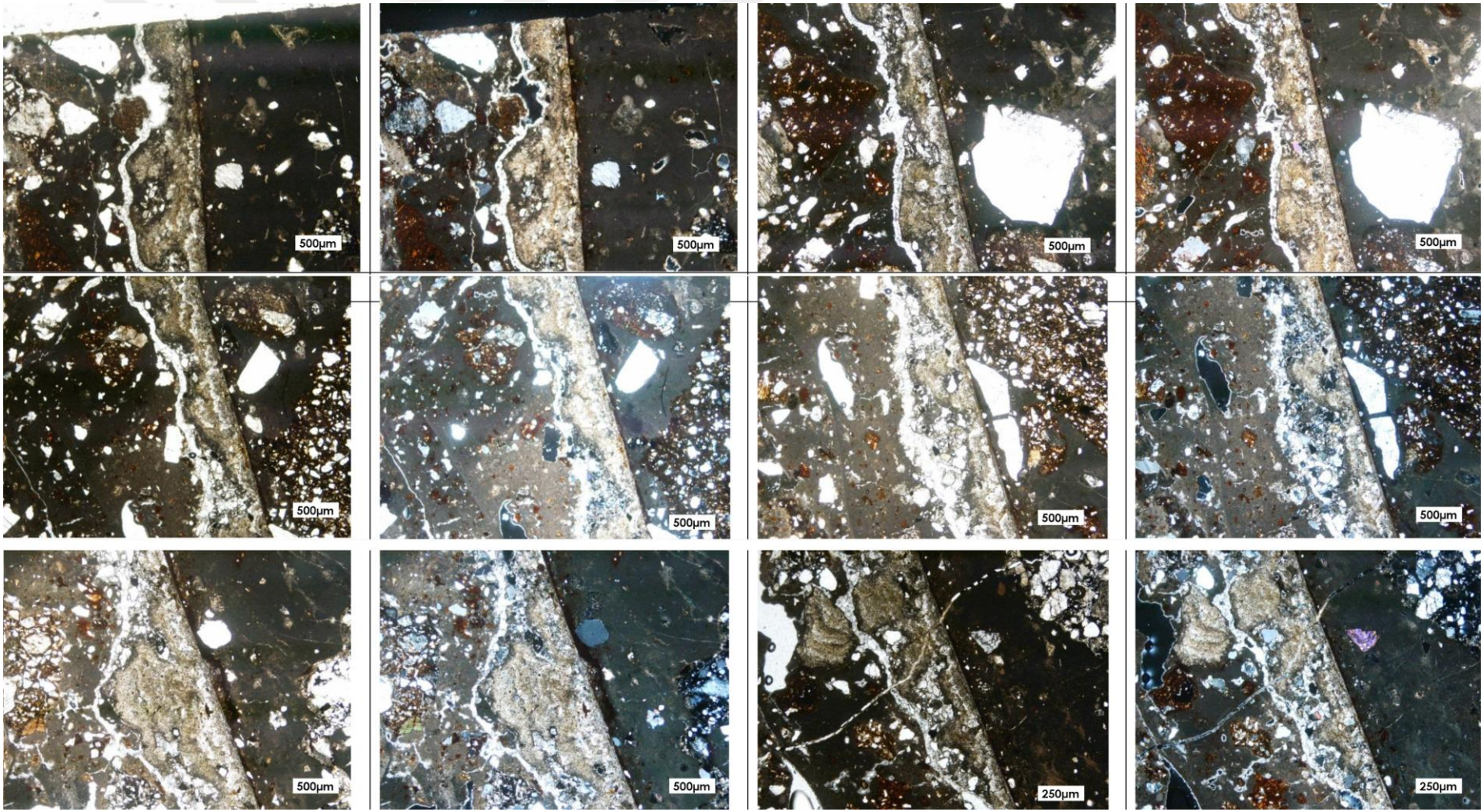


Figure VI.6. Thin section images of sample MM3 continue

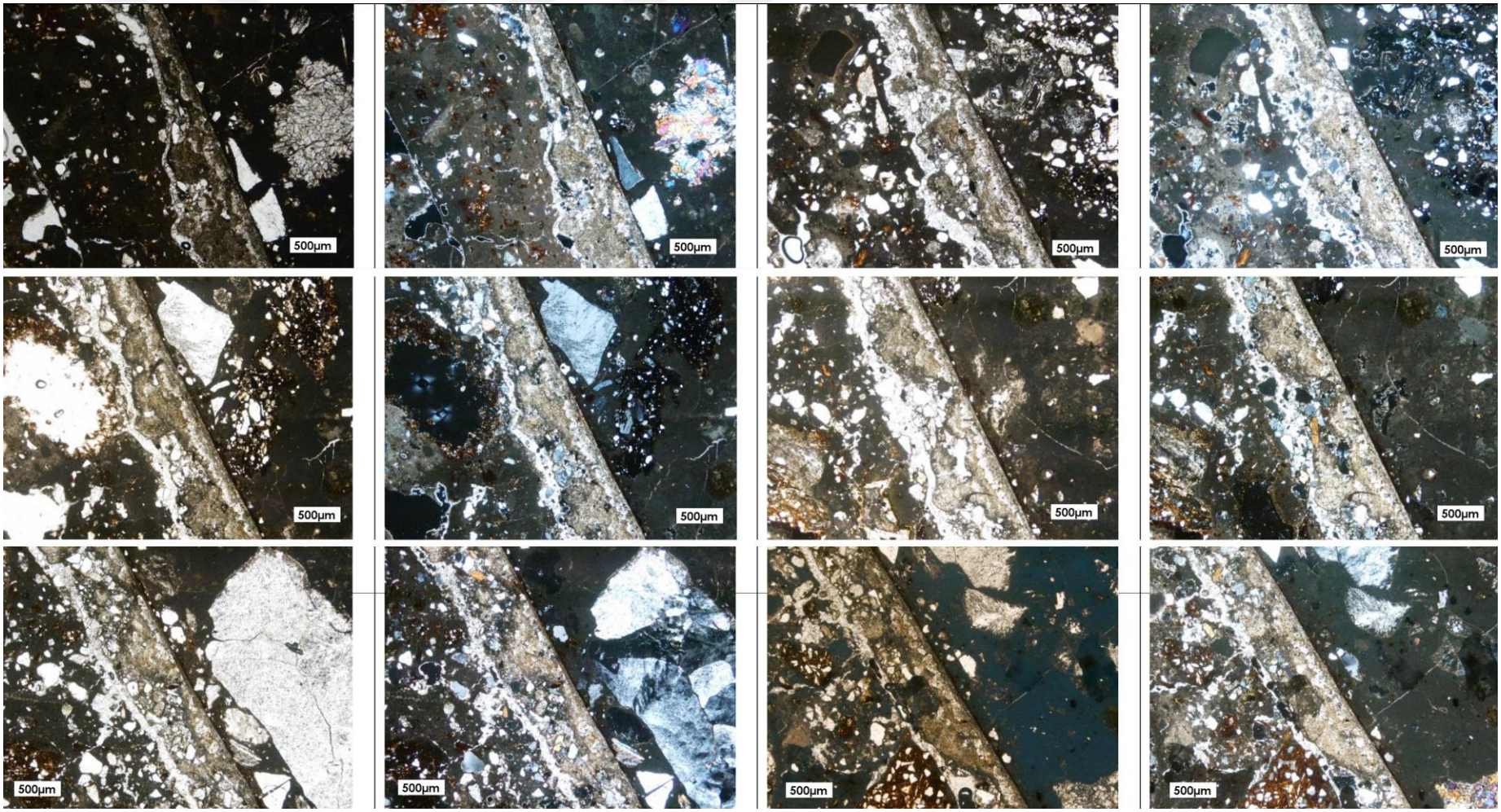


Figure VI.7. Thin section images of sample MM3 continue

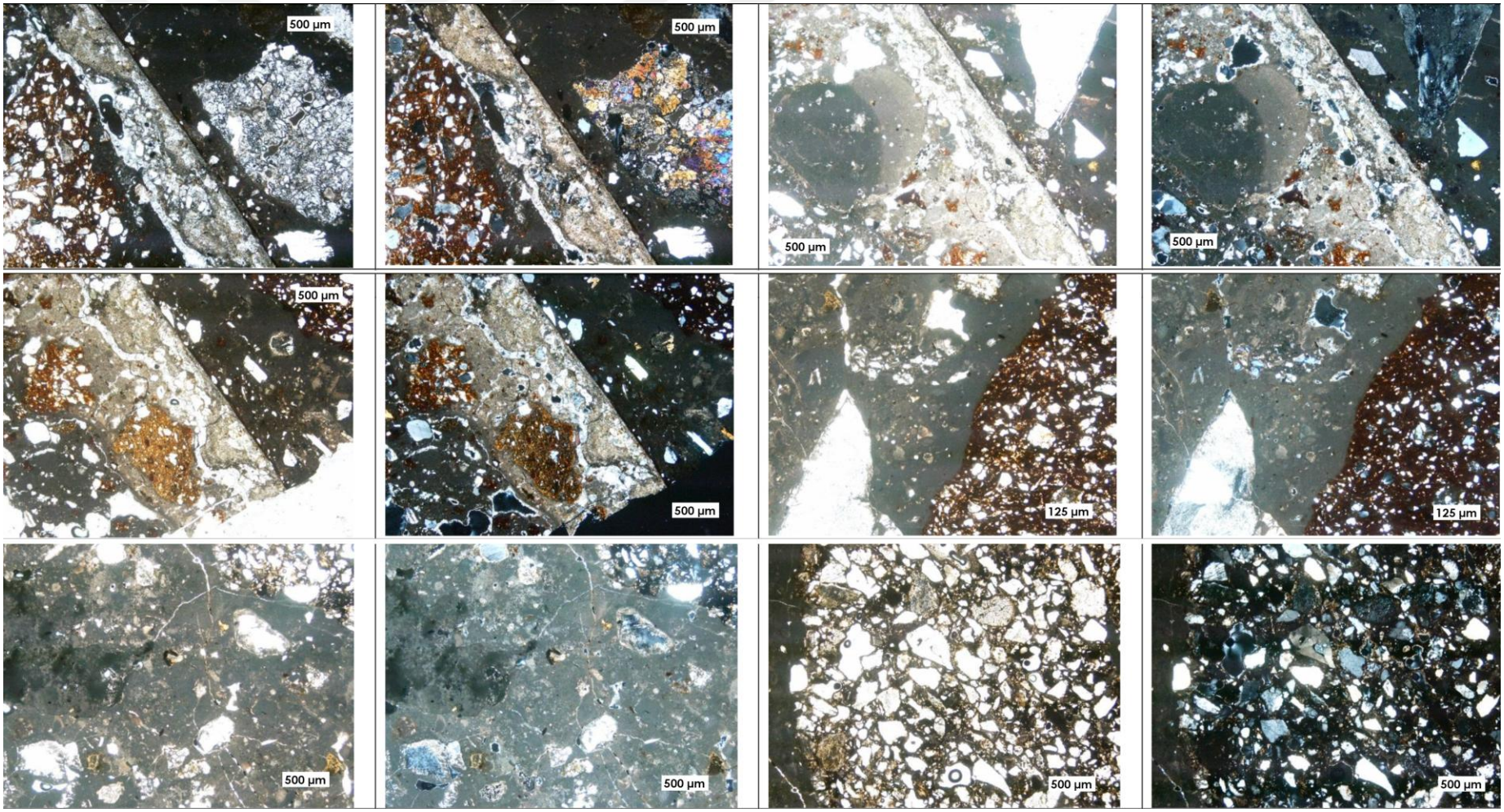


Figure VI.8. Thin section images of sample MM3 continue

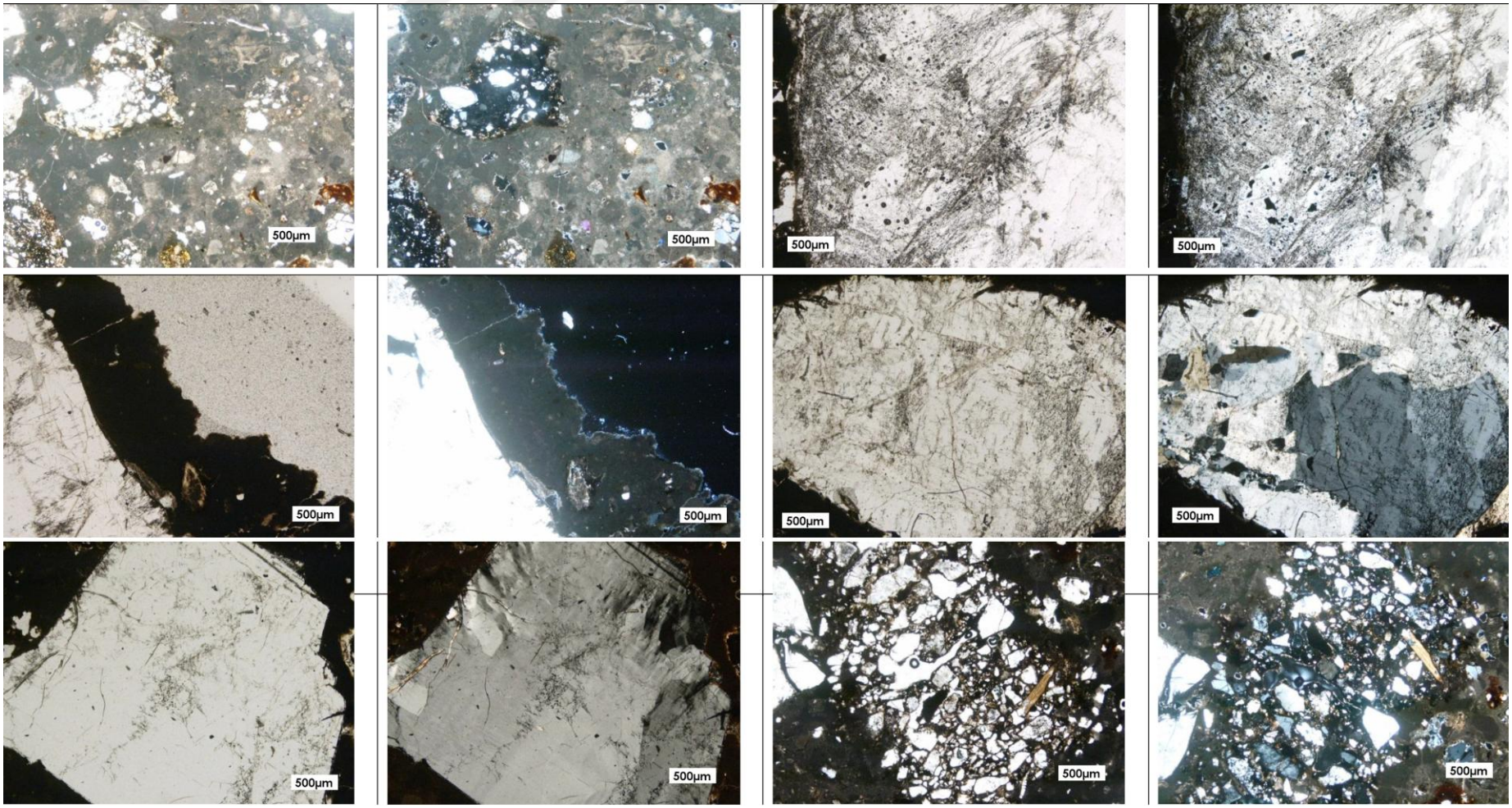


Figure VI.9. Thin section images of sample MM3 continue

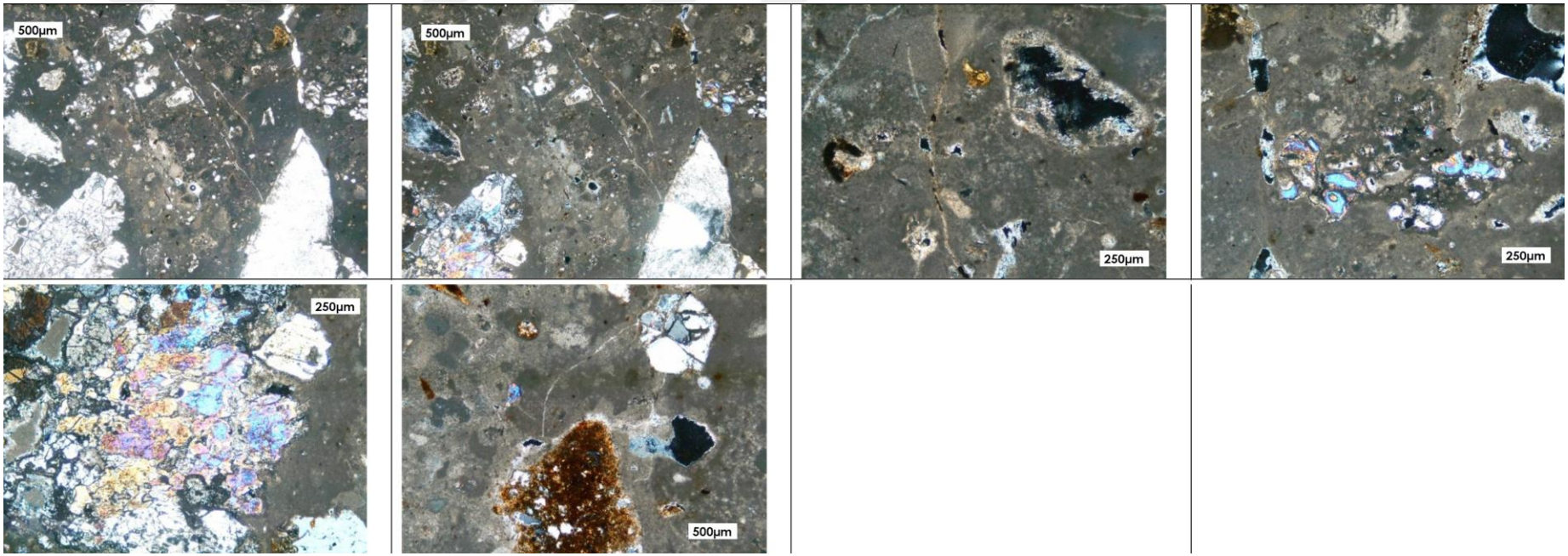


Figure VI.10. Thin section images of sample MM3 continue

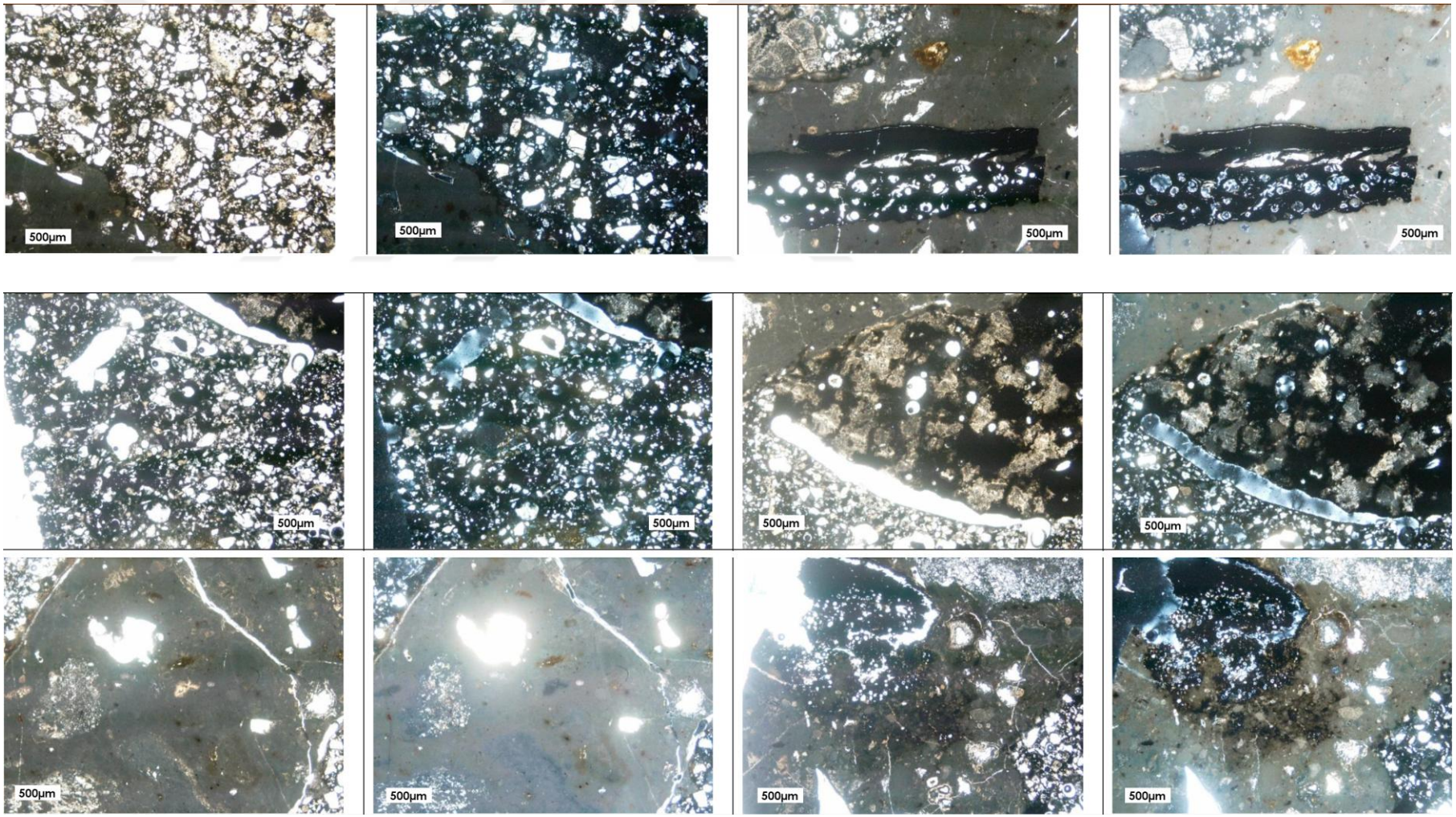


Figure VI.11. Thin section images of sample MM5

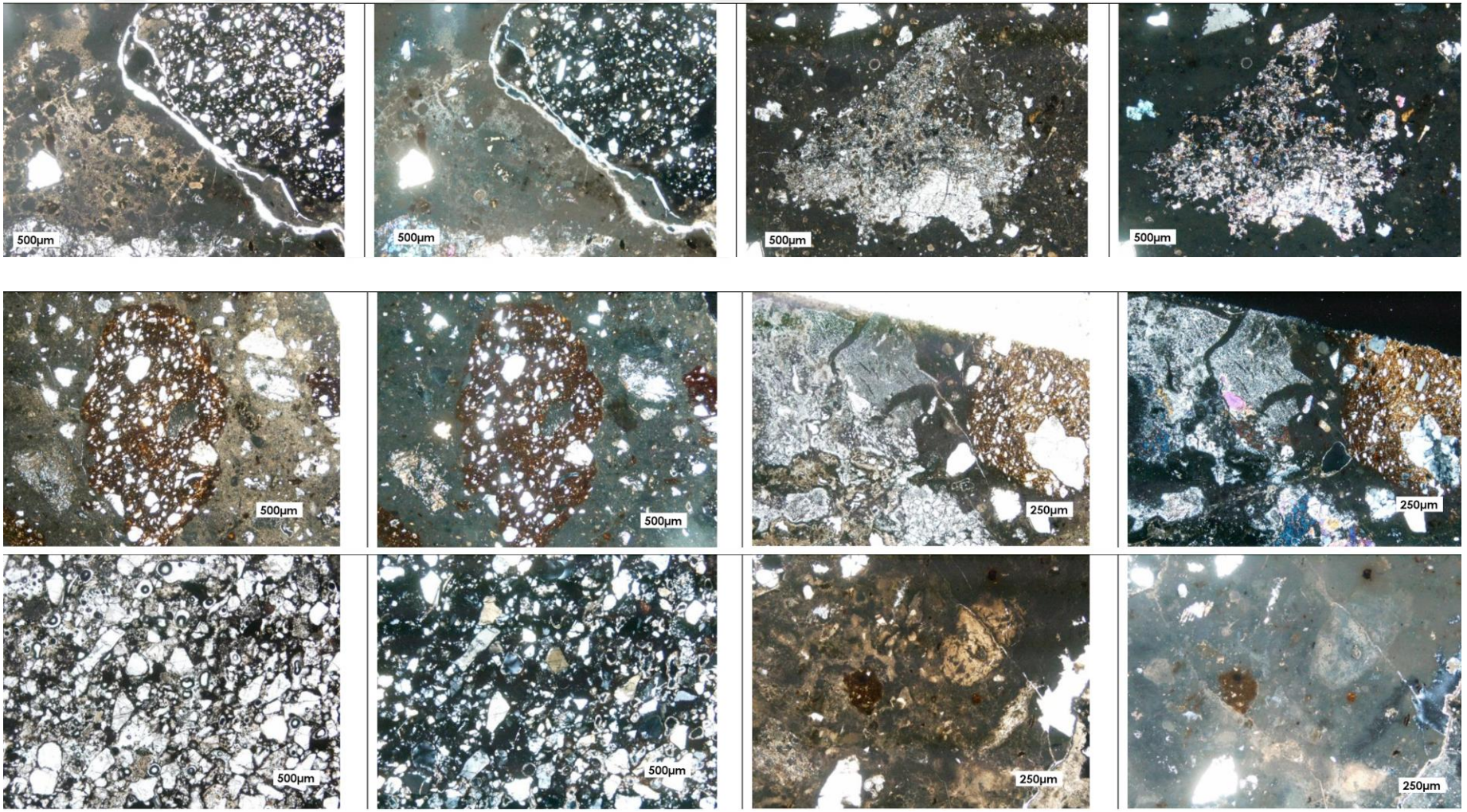


Figure VI.12. Thin section images of sample MM5 (continue)

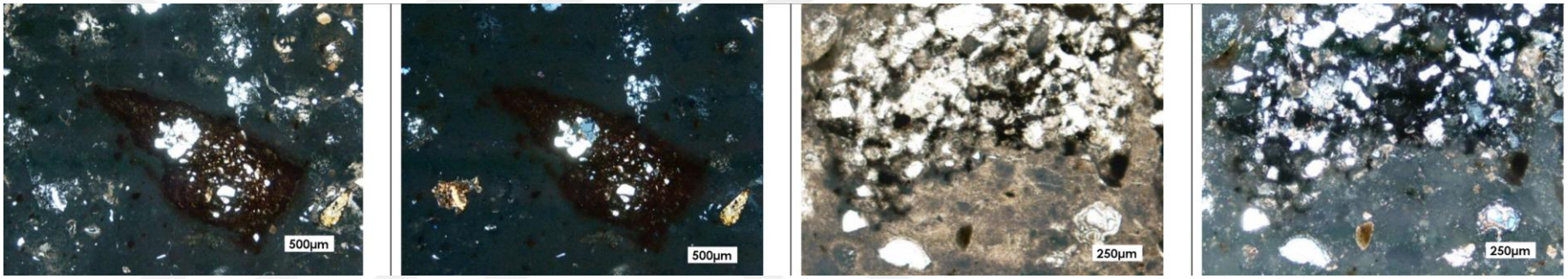


Figure VI.13. Thin section images of sample MM5 (continue)

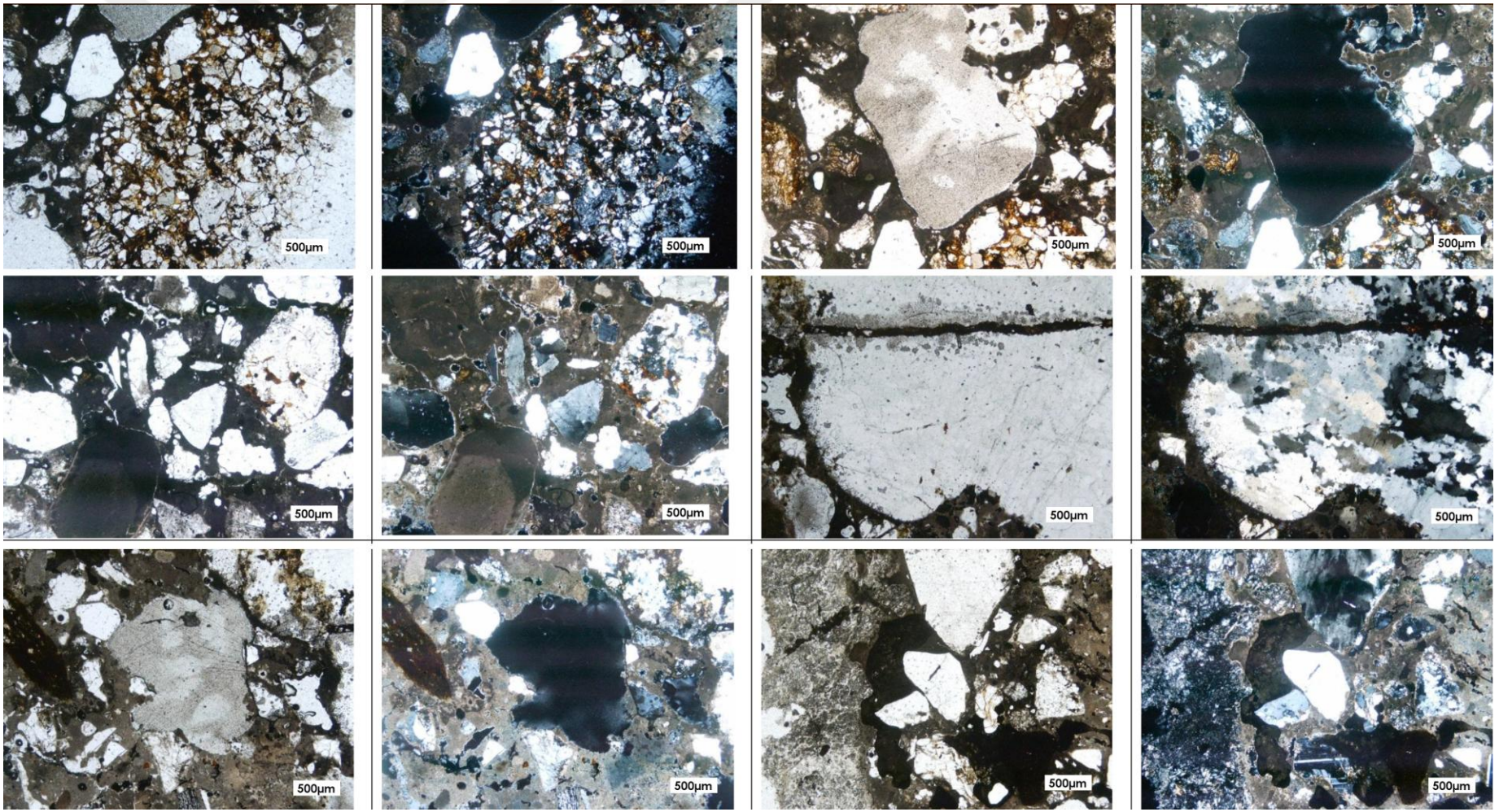


Figure VI.14. Thin section images of sample MM6

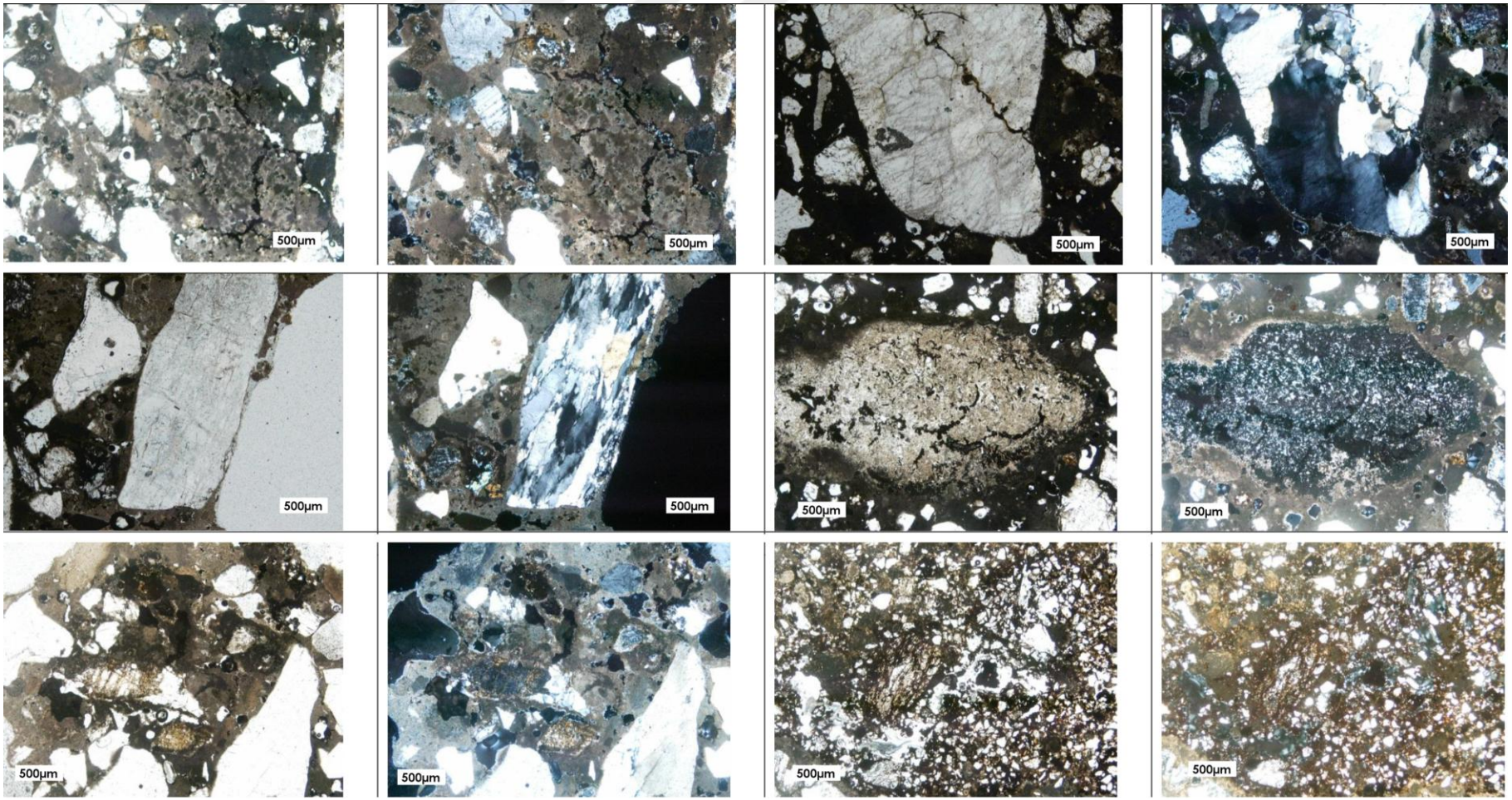


Figure VI.15. Thin section images of sample MM6 (continue)

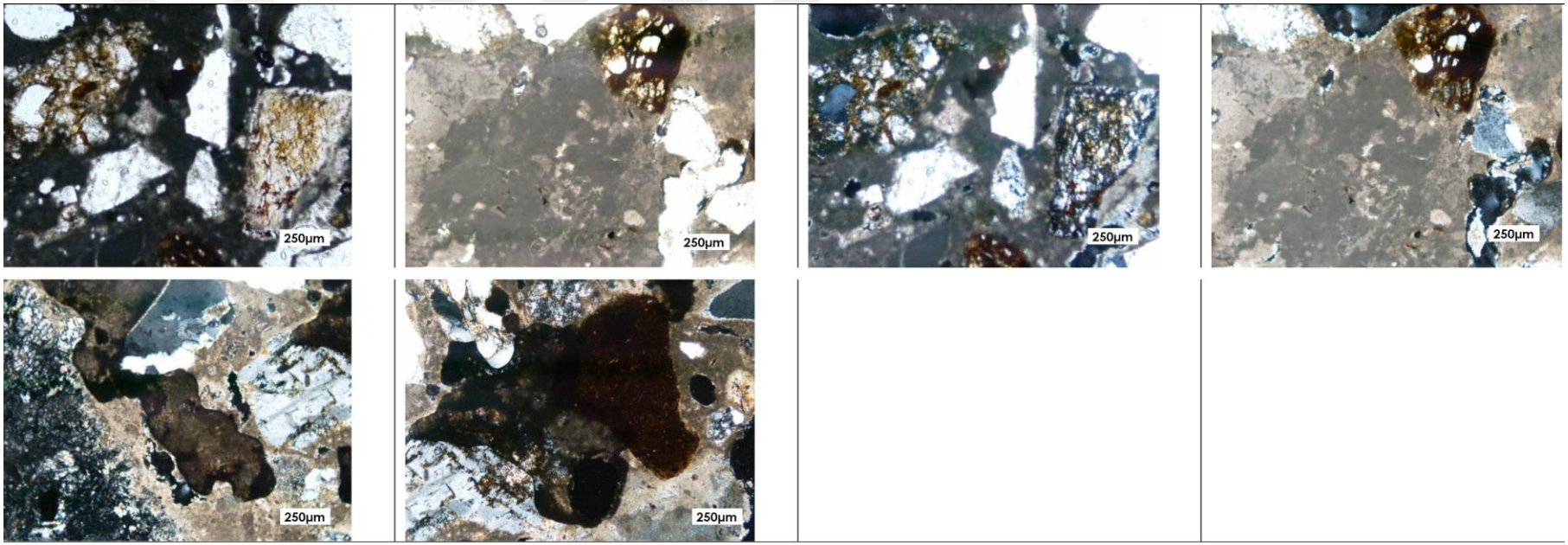


Figure VI.16. Thin section images of sample MM6 (continue)

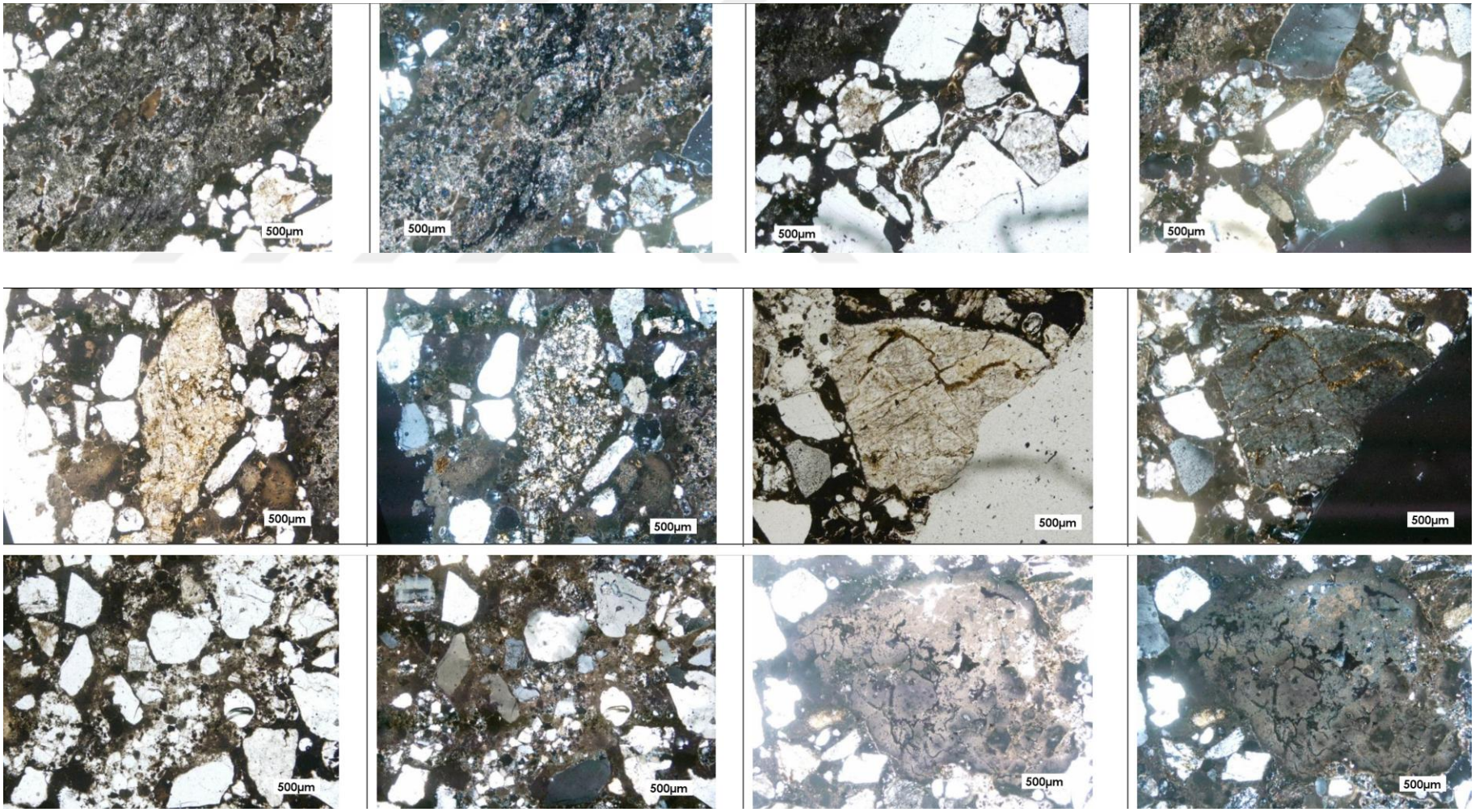


Figure VI.17. Thin section images of sample MM7

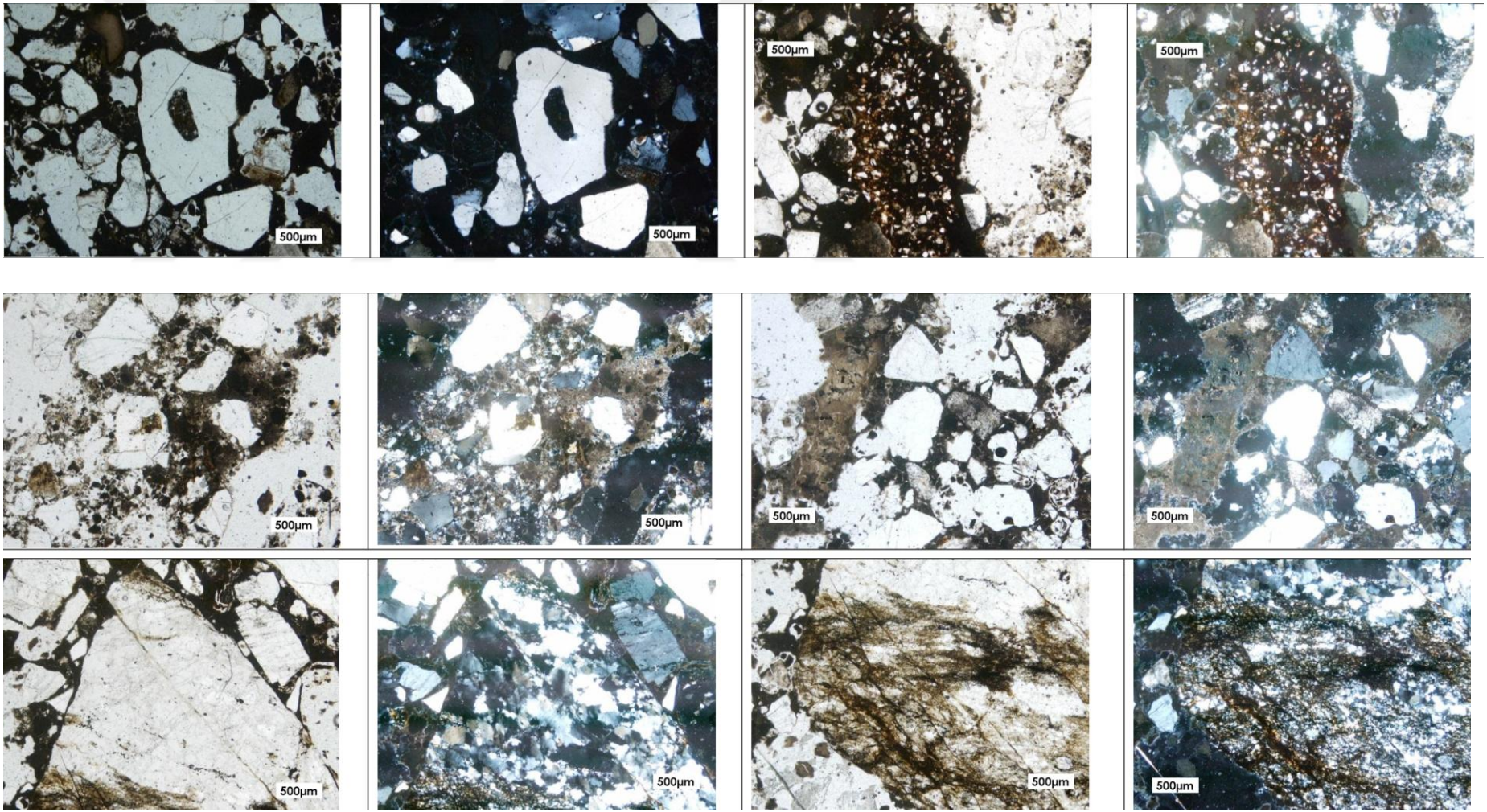


Figure VI.18. Thin section images of sample MM7 (continue)

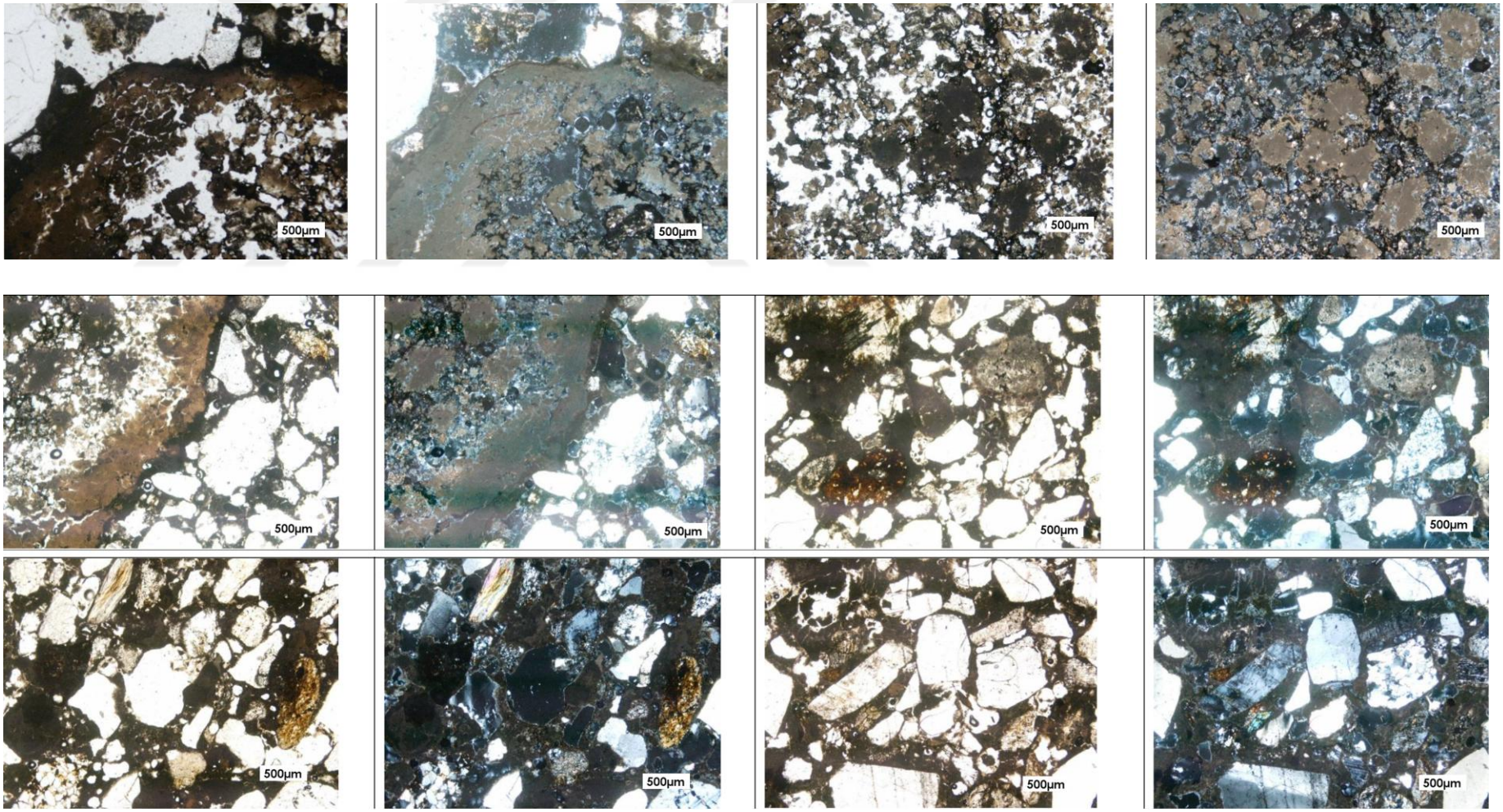


Figure VI.19. Thin section images of sample MM7 (continue)

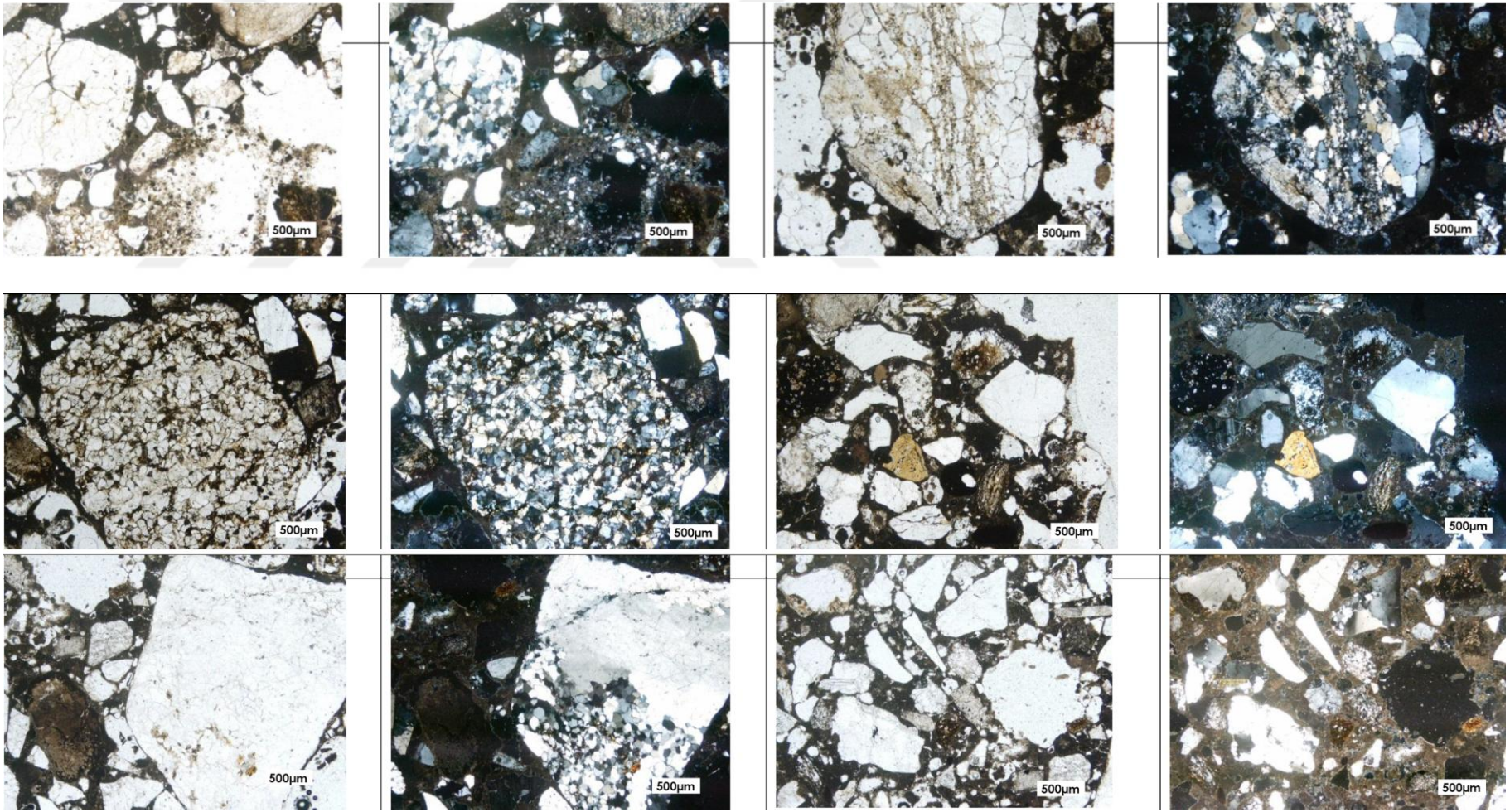


Figure VI.20. Thin section images of sample MM7 (continue)

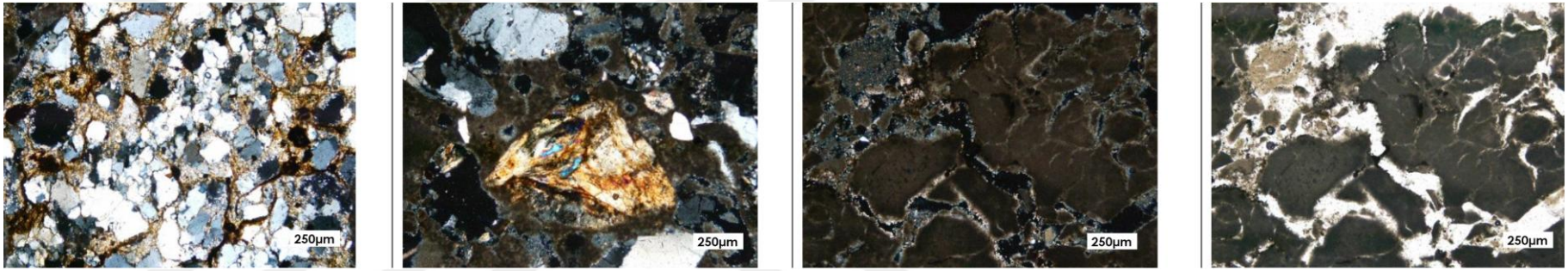


Figure VI.21. Thin section images of sample MM7 (continue)

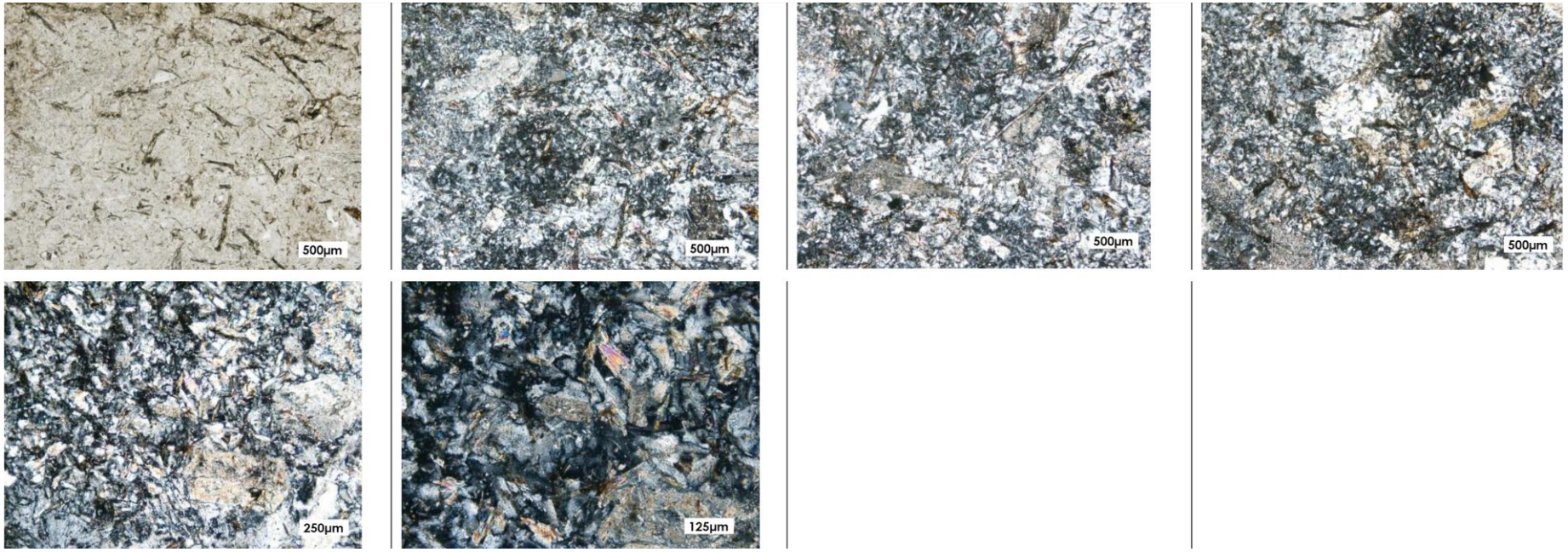


Figure VI.22. Thin section images of sample MM8

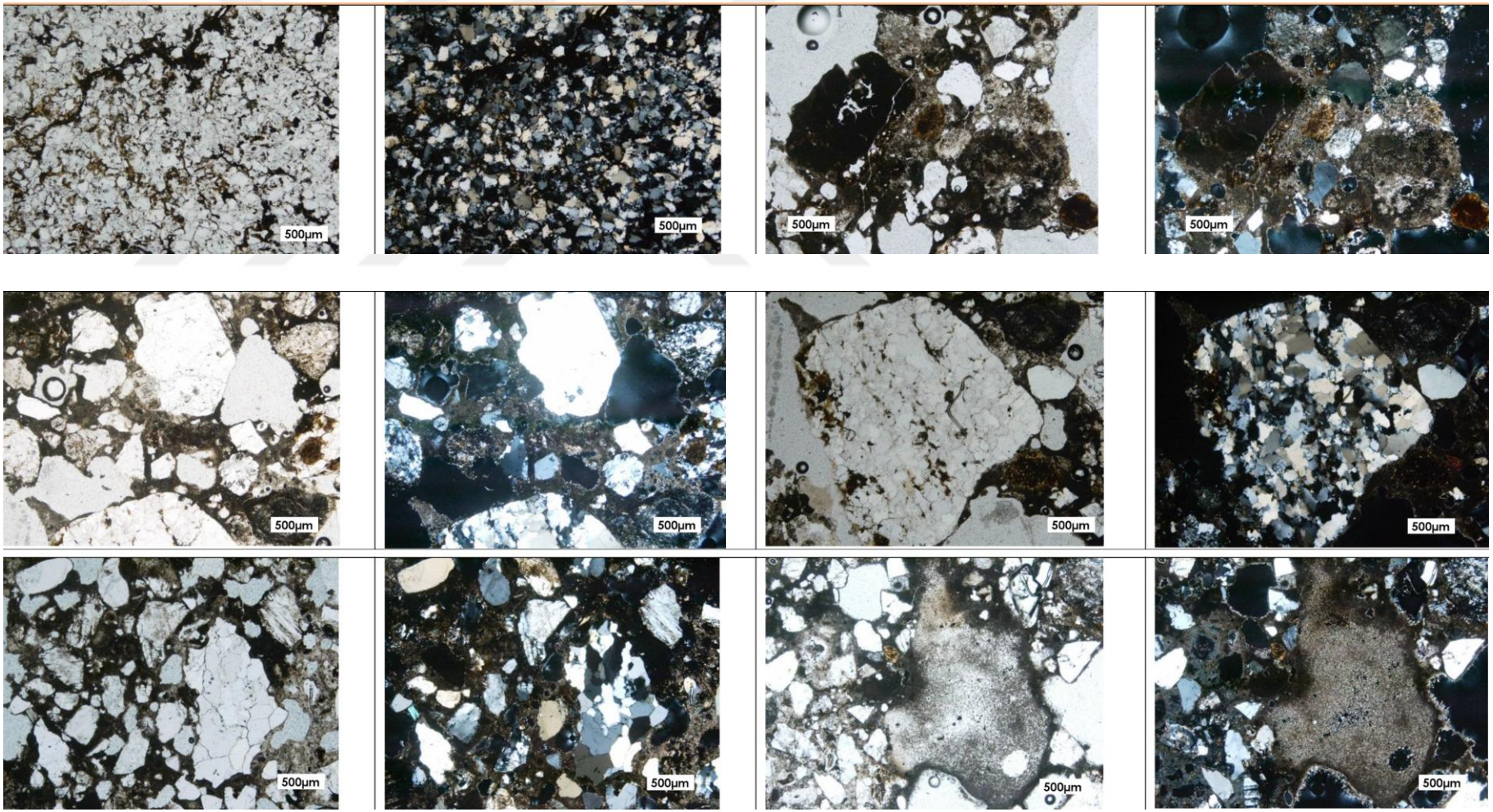


Figure VI.23. Thin section images of sample MM10

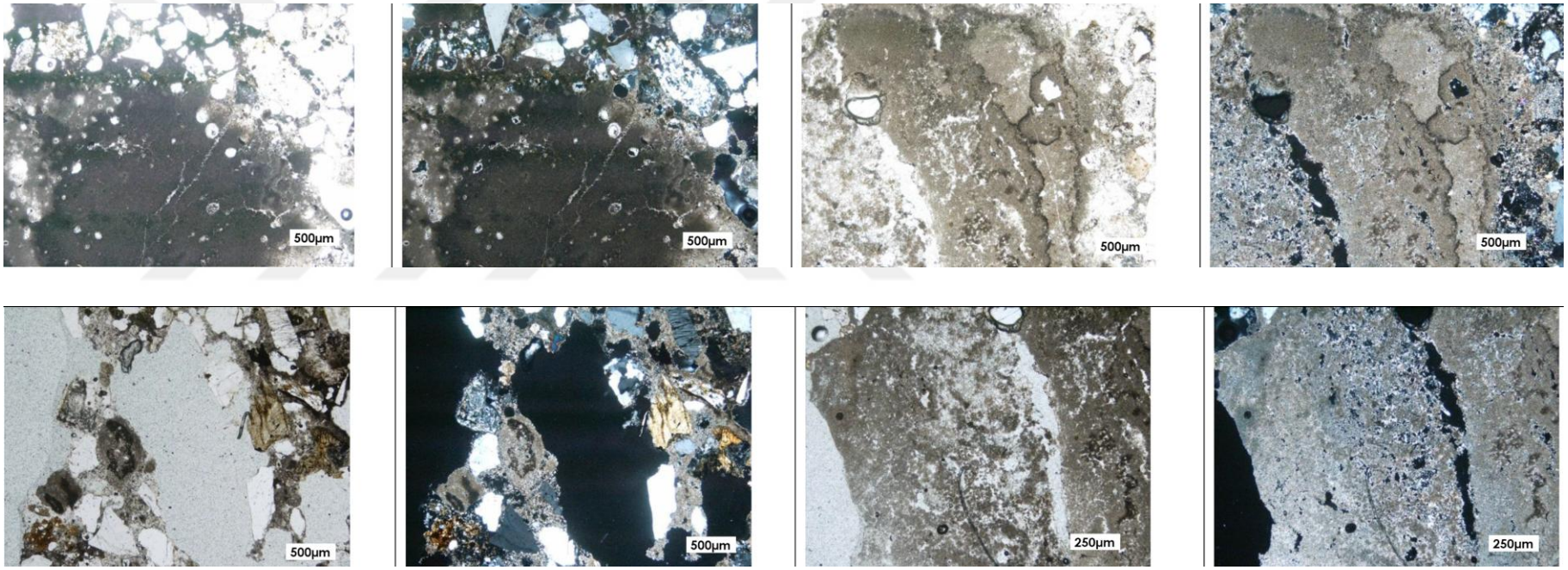


Figure VI.24. Thin section images of sample MM10 (continue)

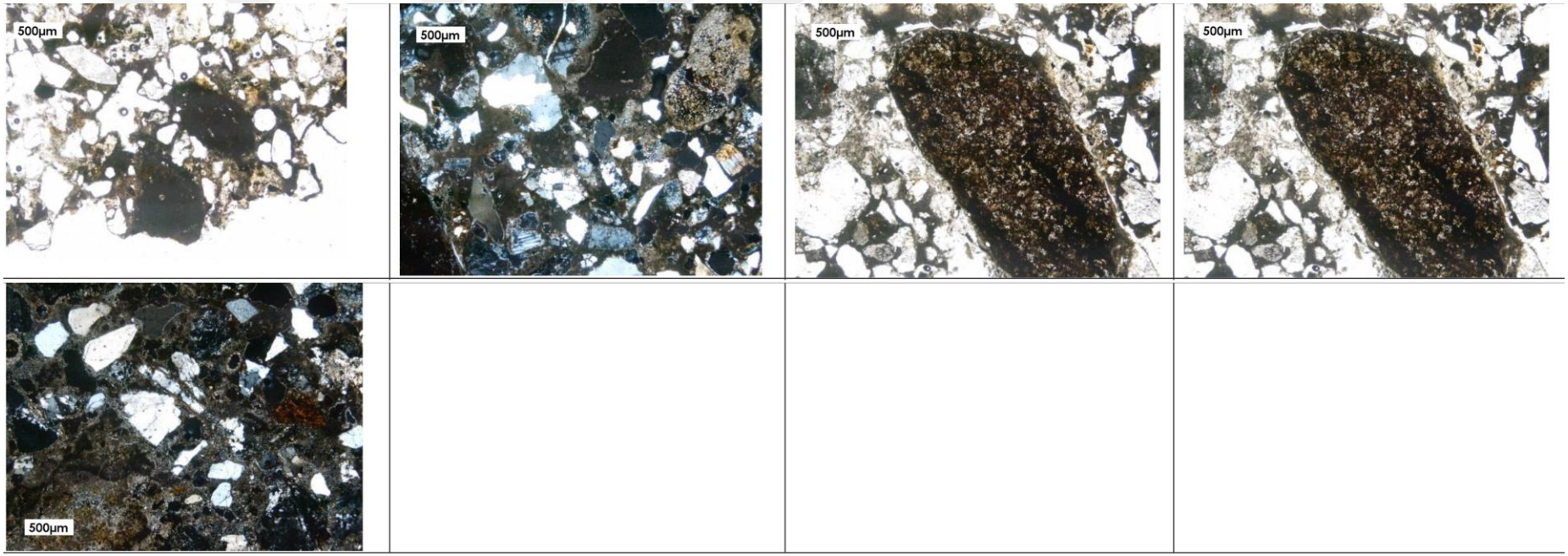


Figure VI.25. Thin section images of sample MM11

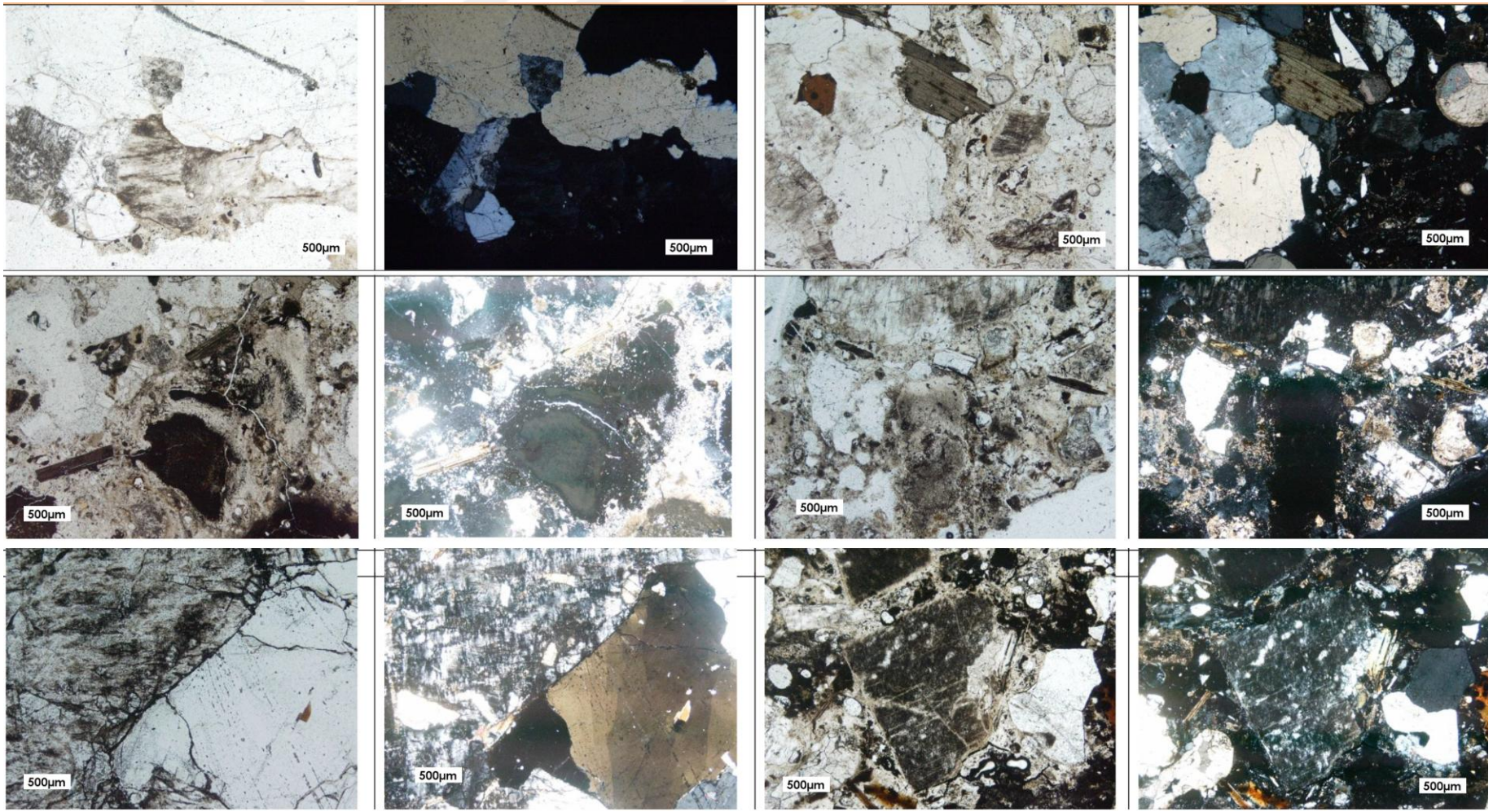


Figure VI.26. Thin section images of sample MM12

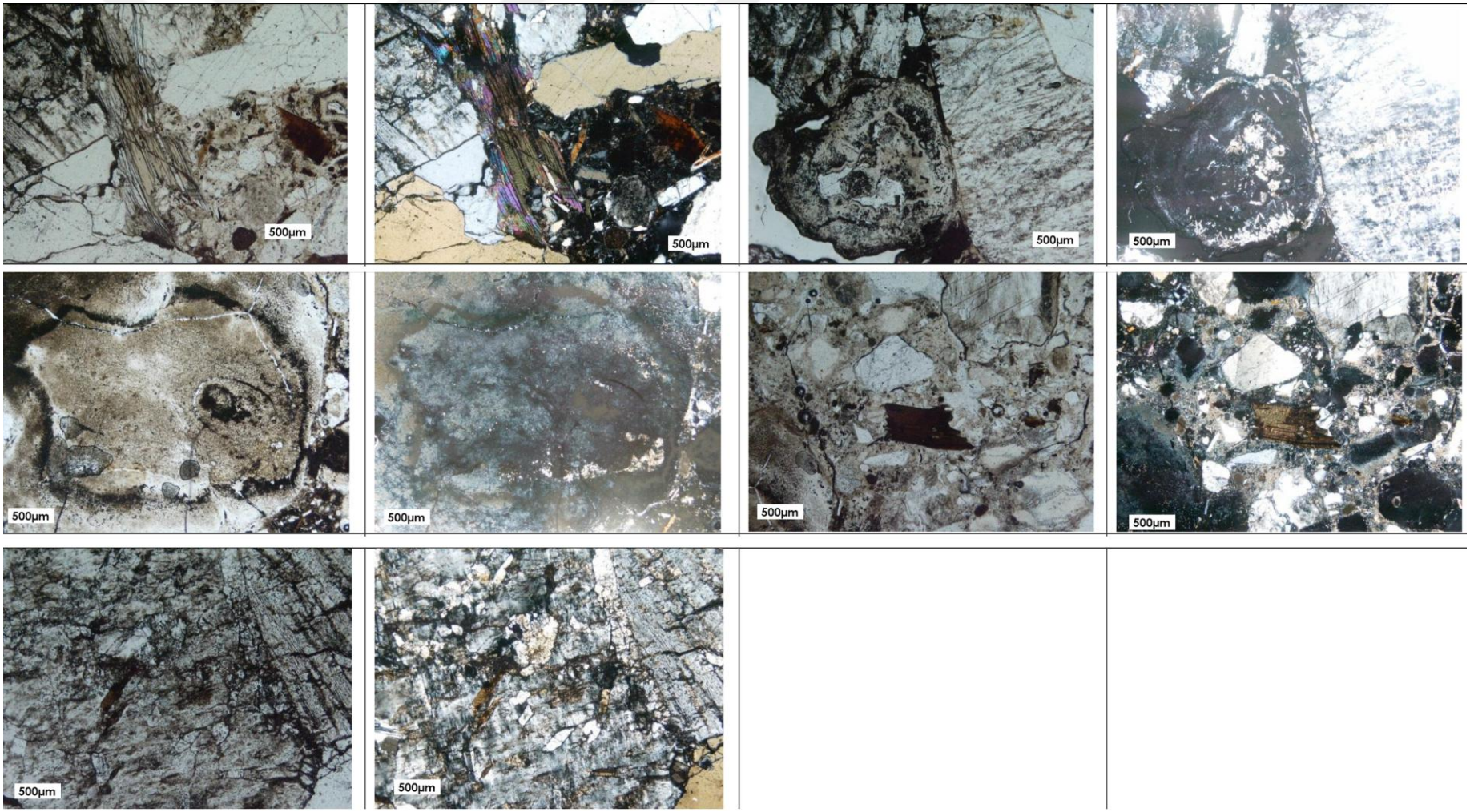


Figure VI.27. Thin section images of sample MM12 (continue)

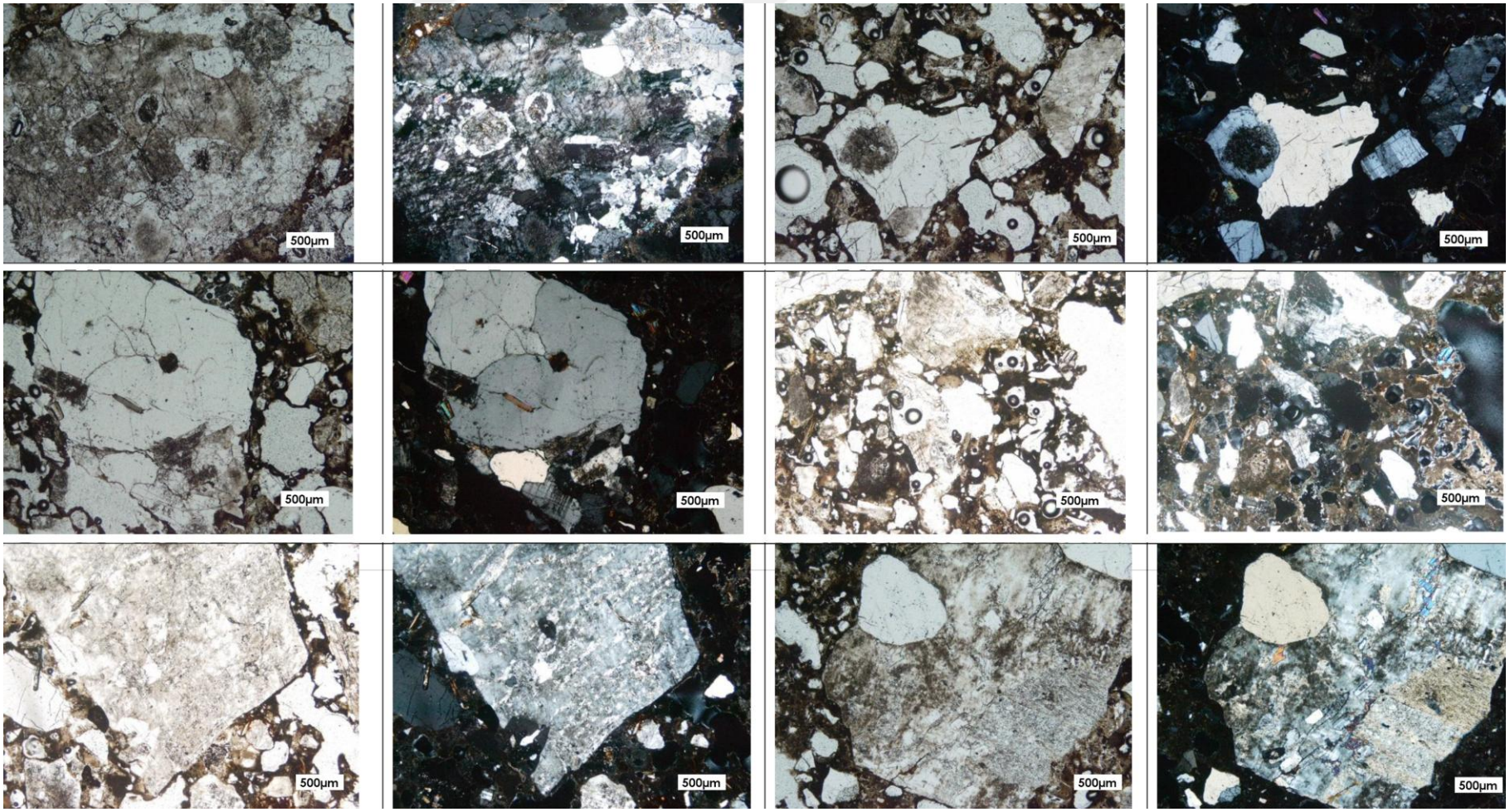


Figure VI.28. Thin section images of sample MM14

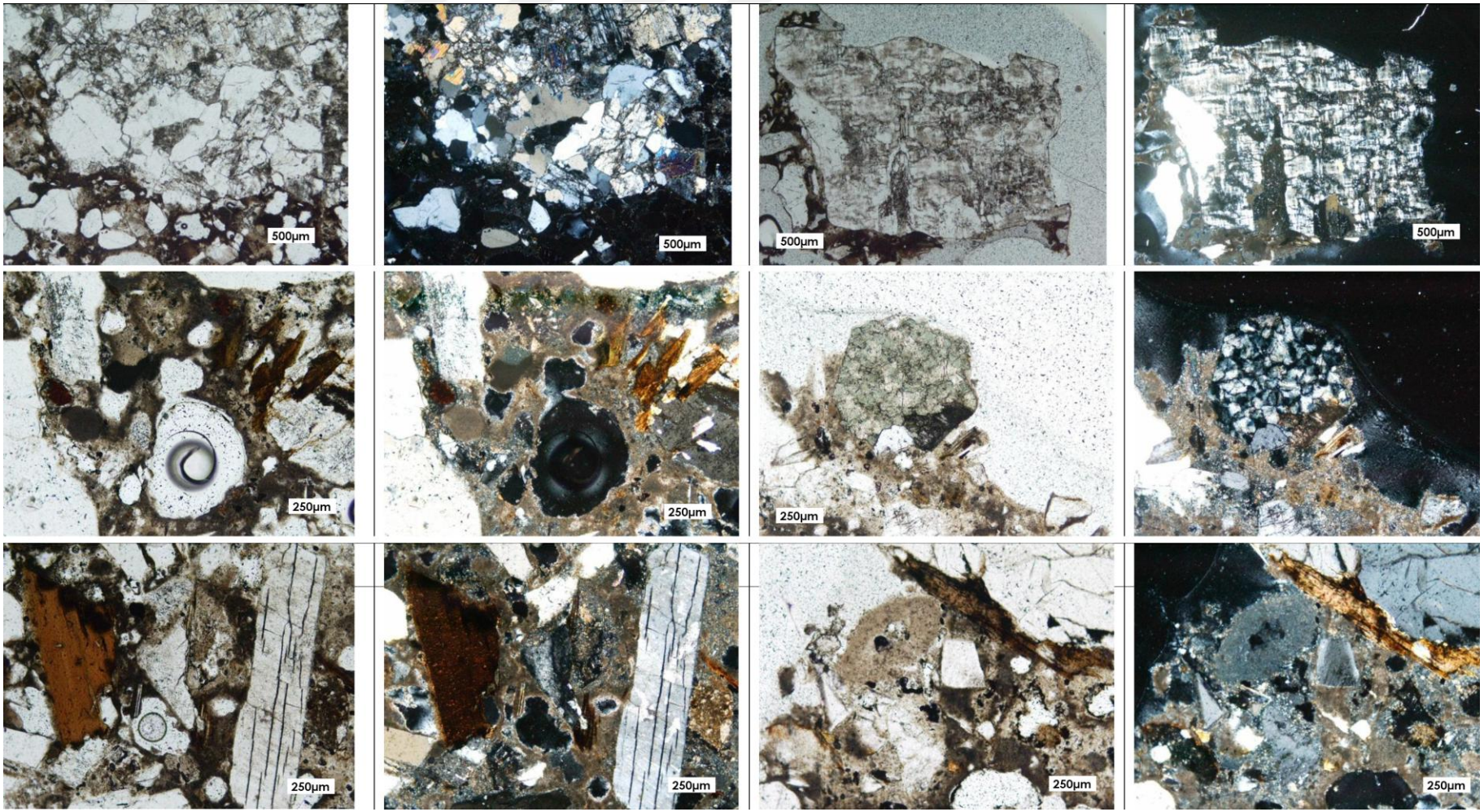


Figure VI.29. Thin section images of sample MM14 (continue)

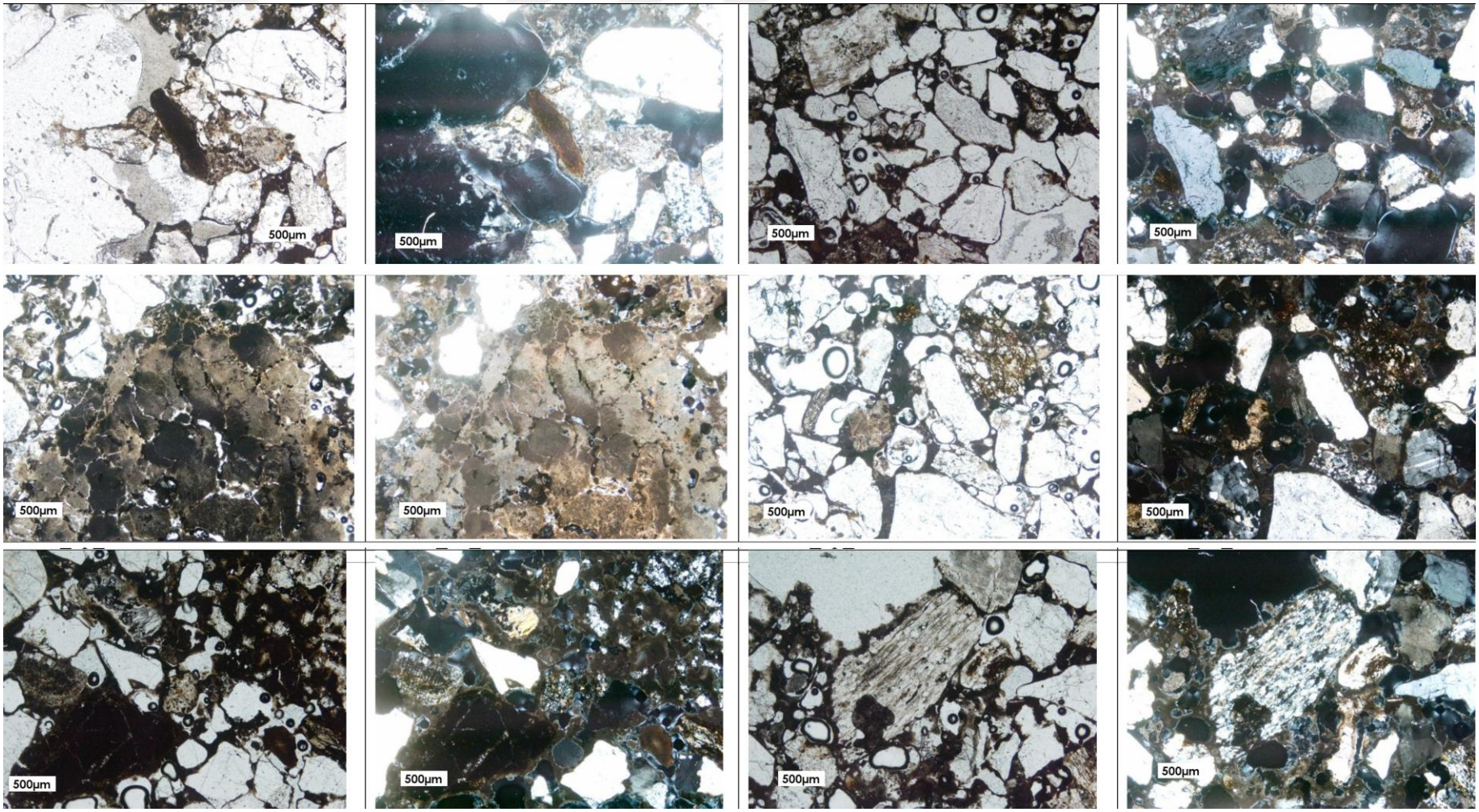


Figure VI.30. Thin section images of sample MM15

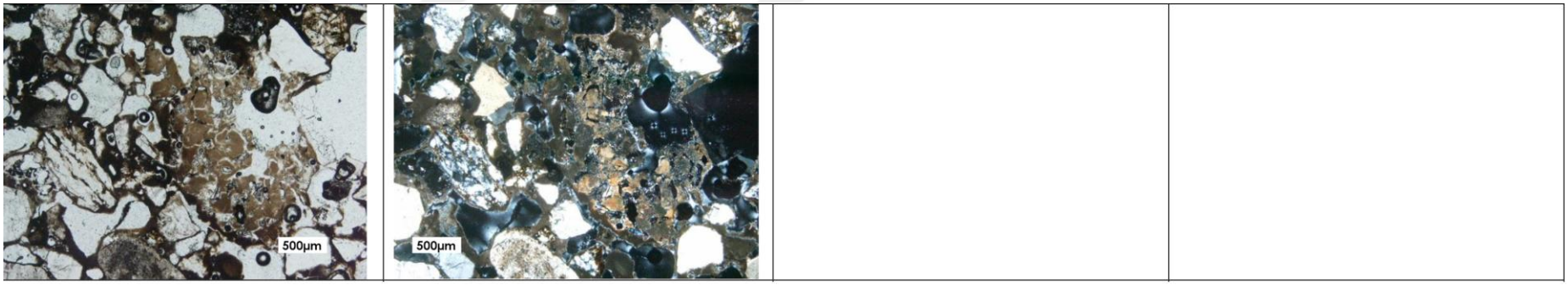


Figure VI.31. Thin section images of sample MM15 (continue)

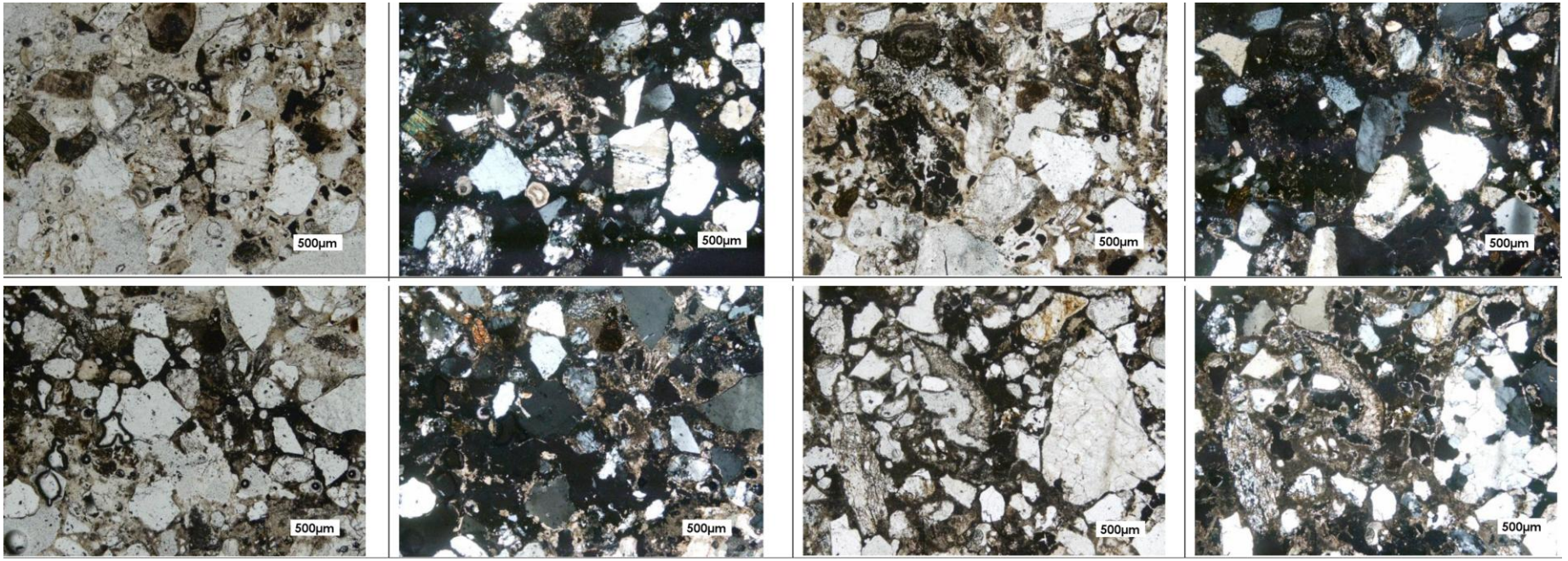


Figure VI.32. Thin section images of sample MM16

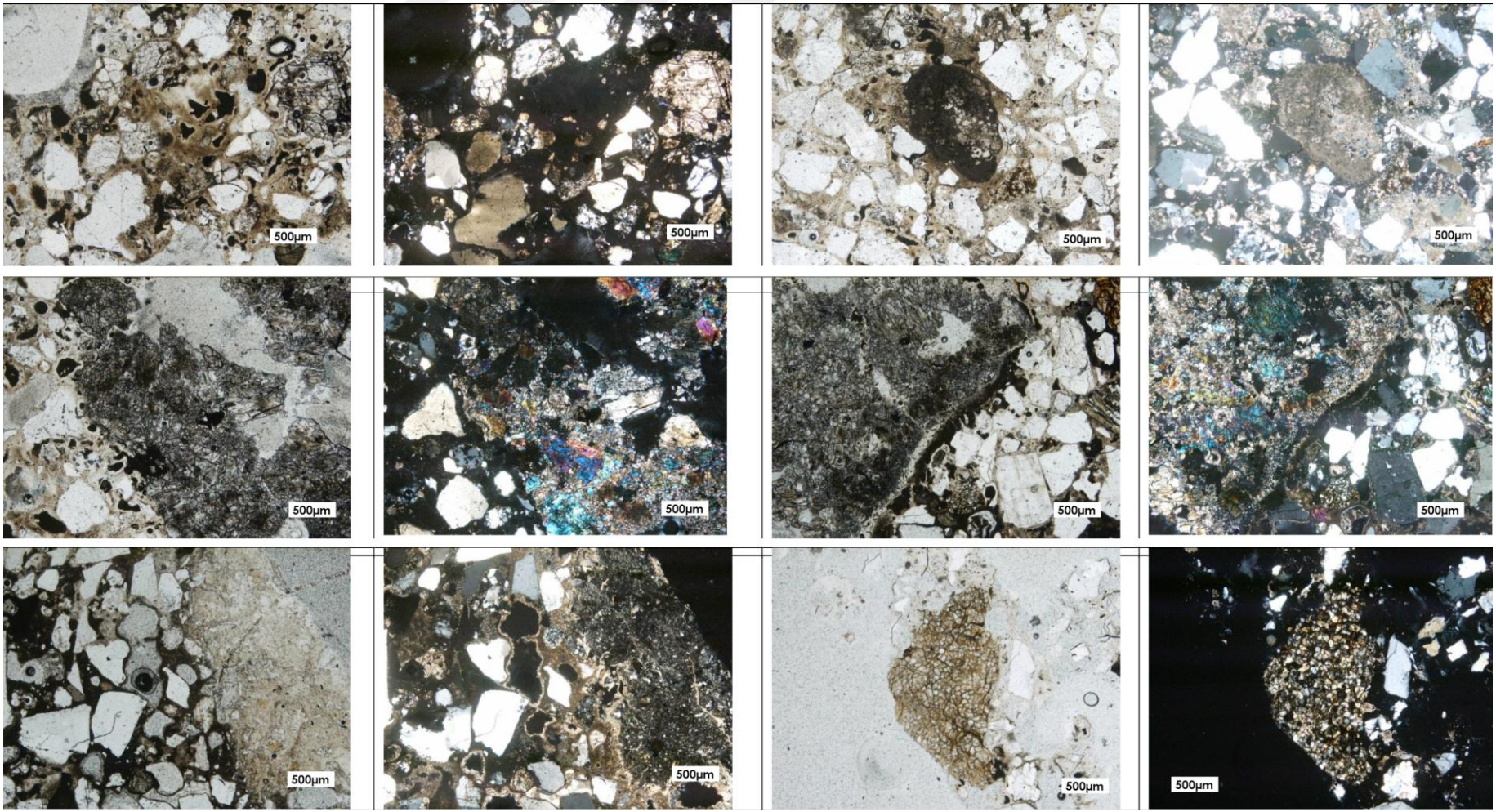


Figure VI. 33. Thin section images of sample MM16 (continue)

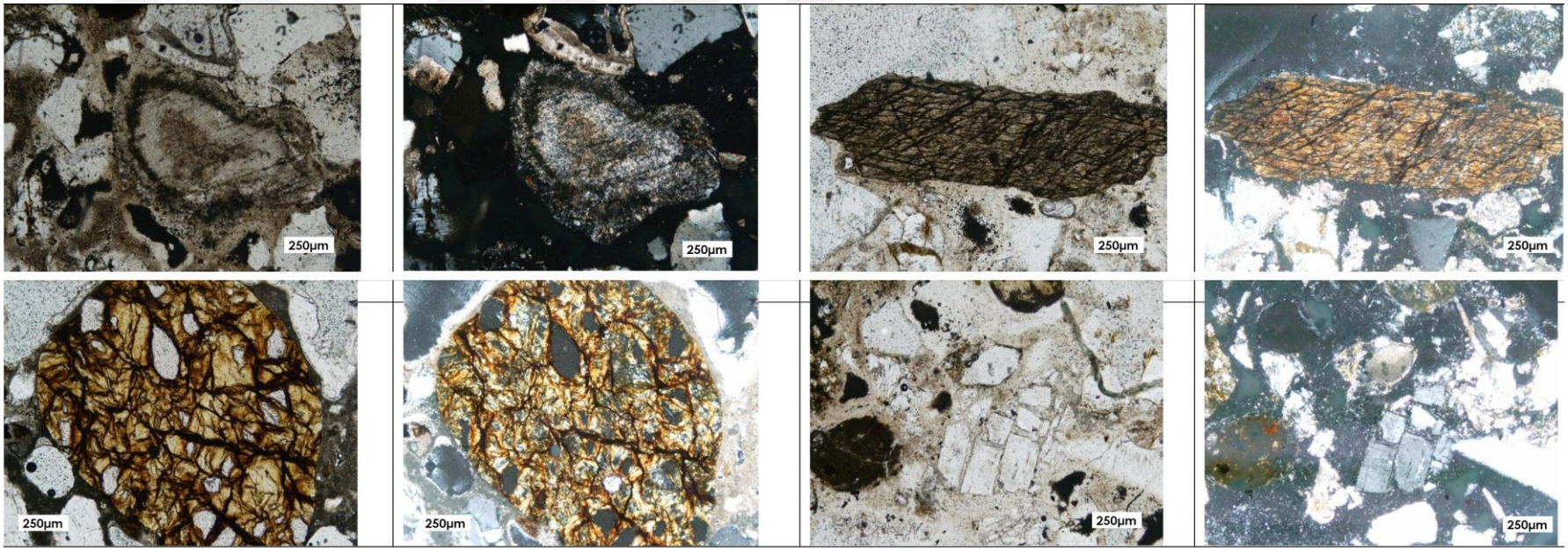


Figure VI.34. Thin section images of sample MM16 (continue)

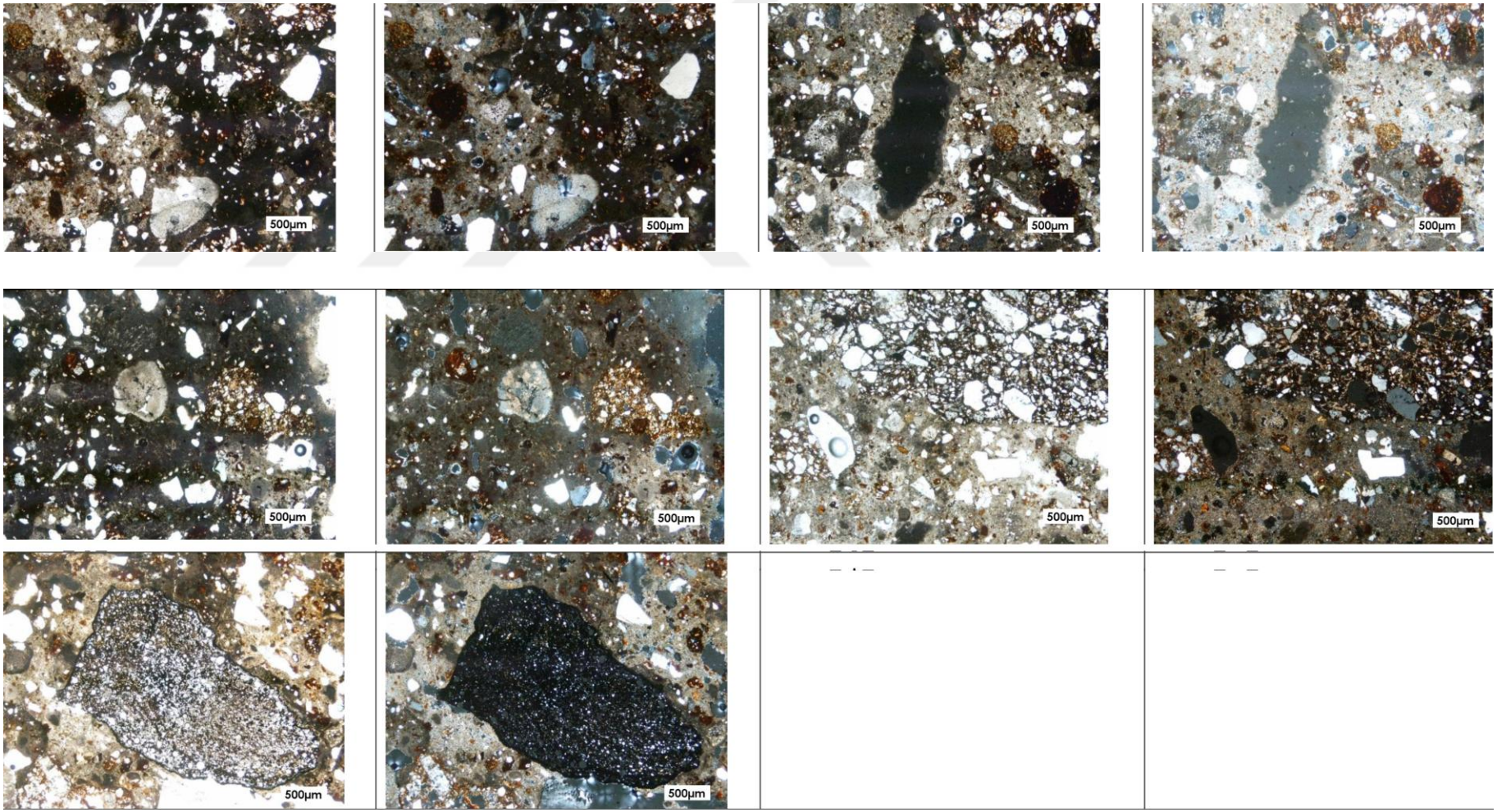


Figure VI.35. Thin section images of sample MM18

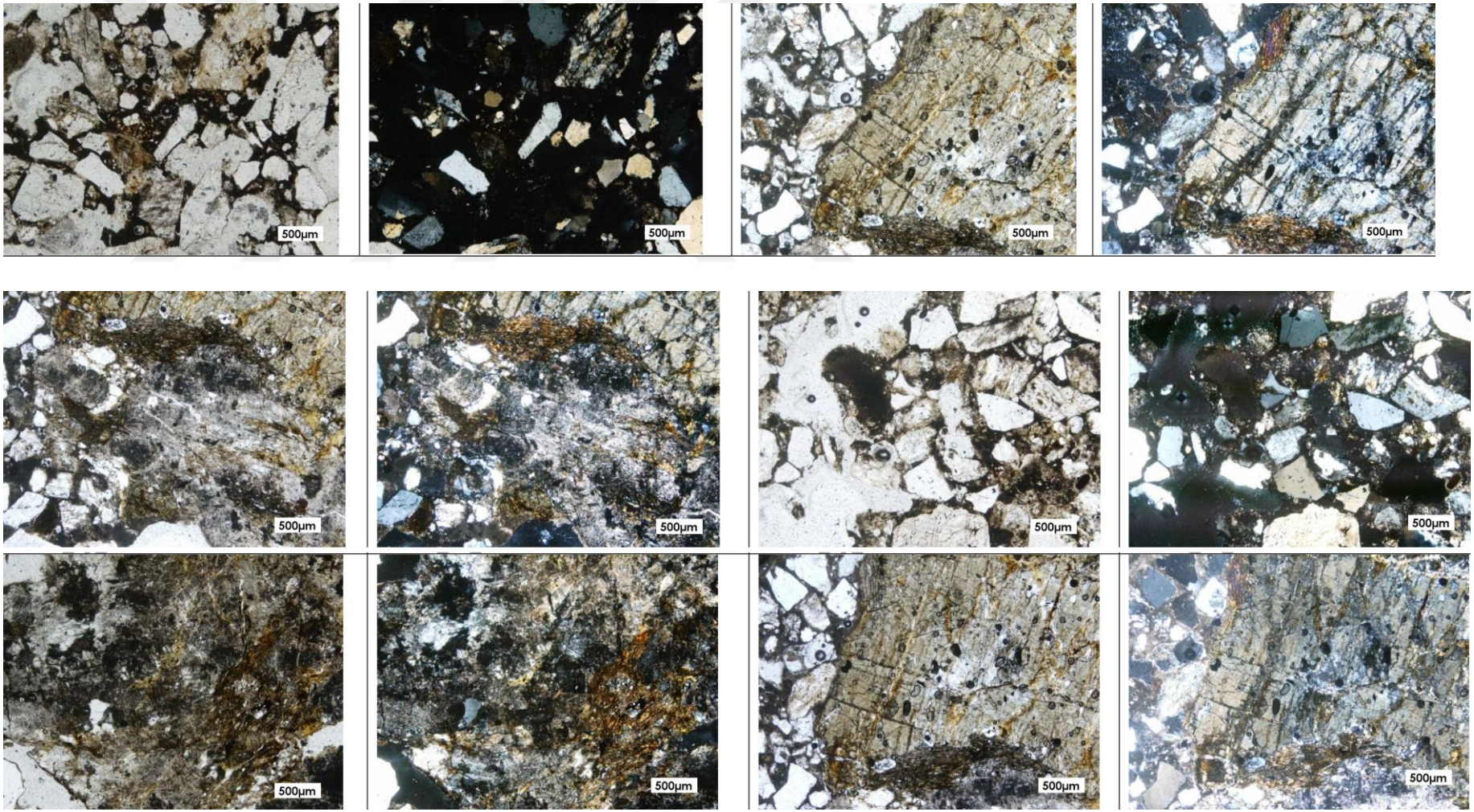


Figure VI.36. Thin section images of sample MM20

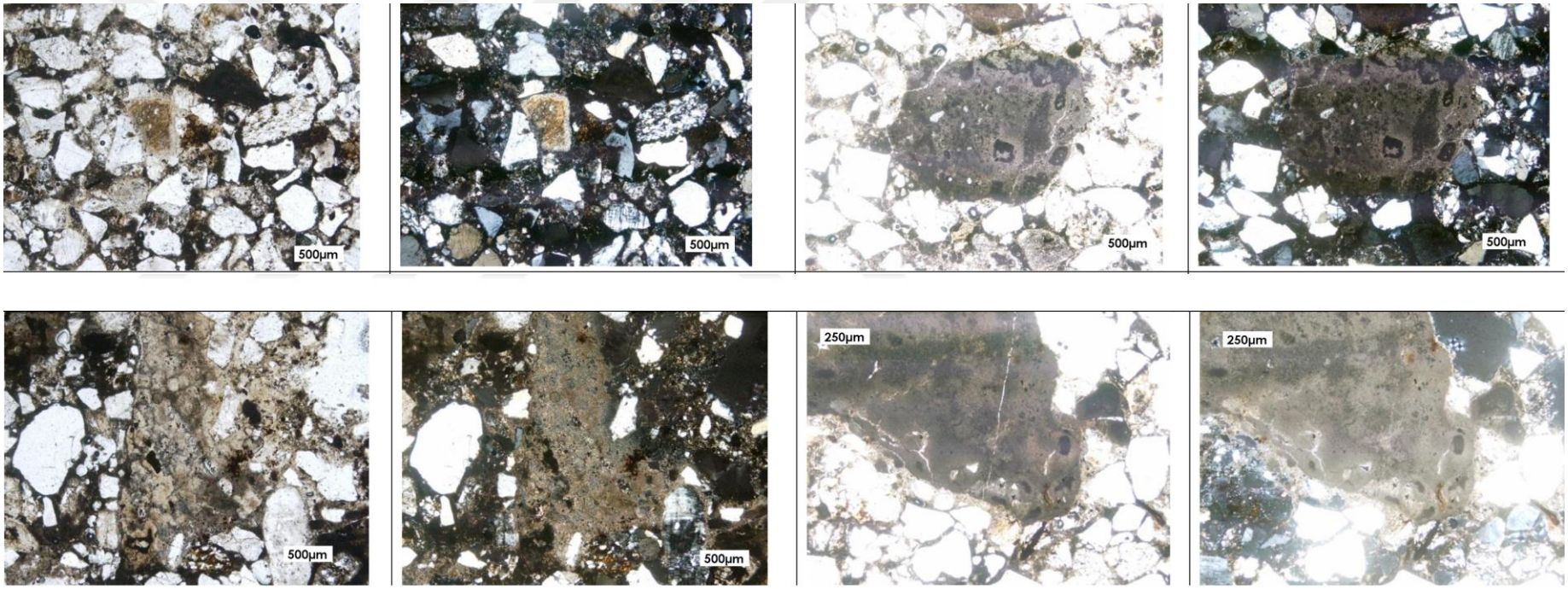


Figure VI.37. Thin section images of sample MM20 (continue)

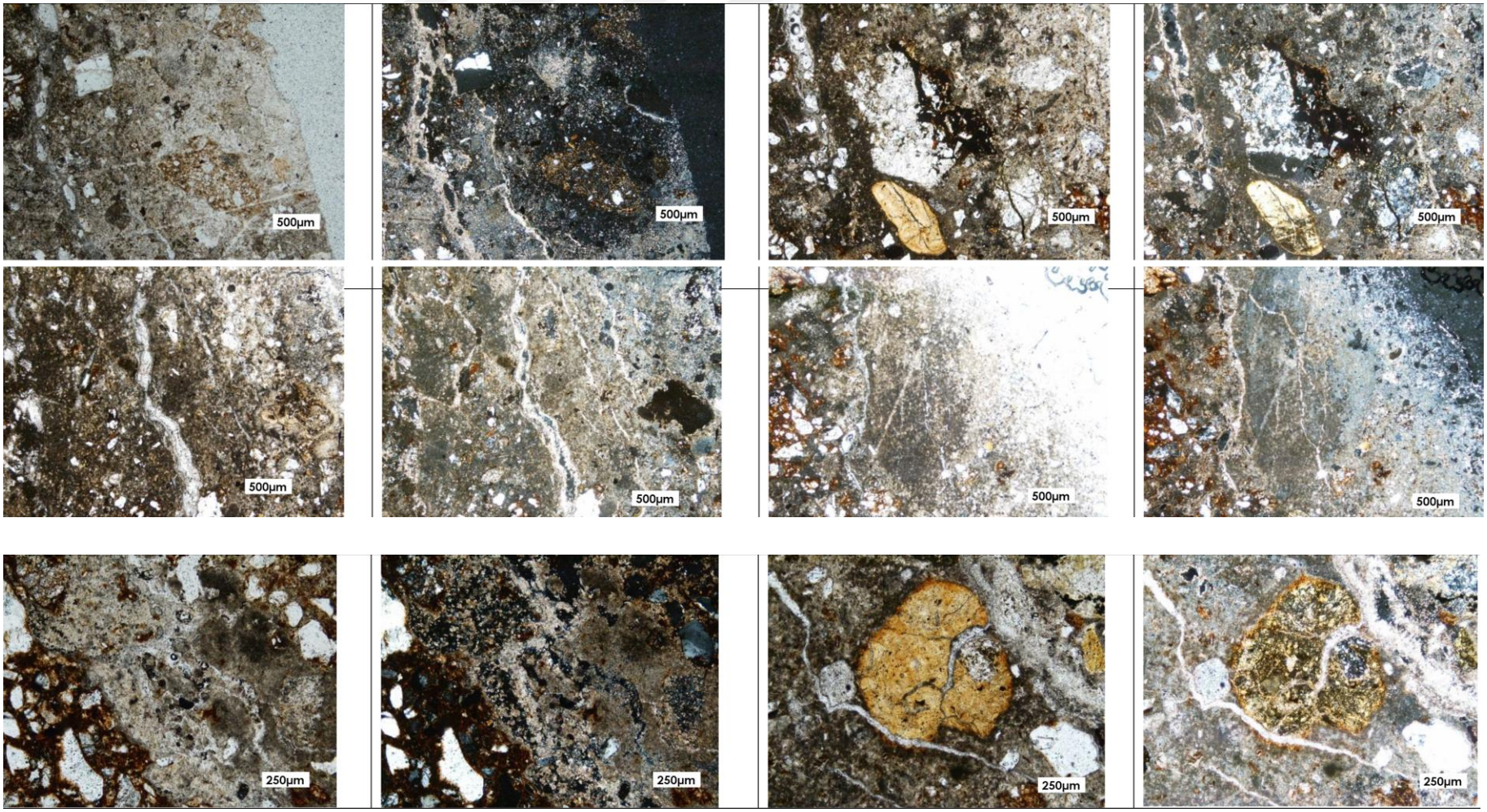


Figure VI.38. Thin section images of sample MM21

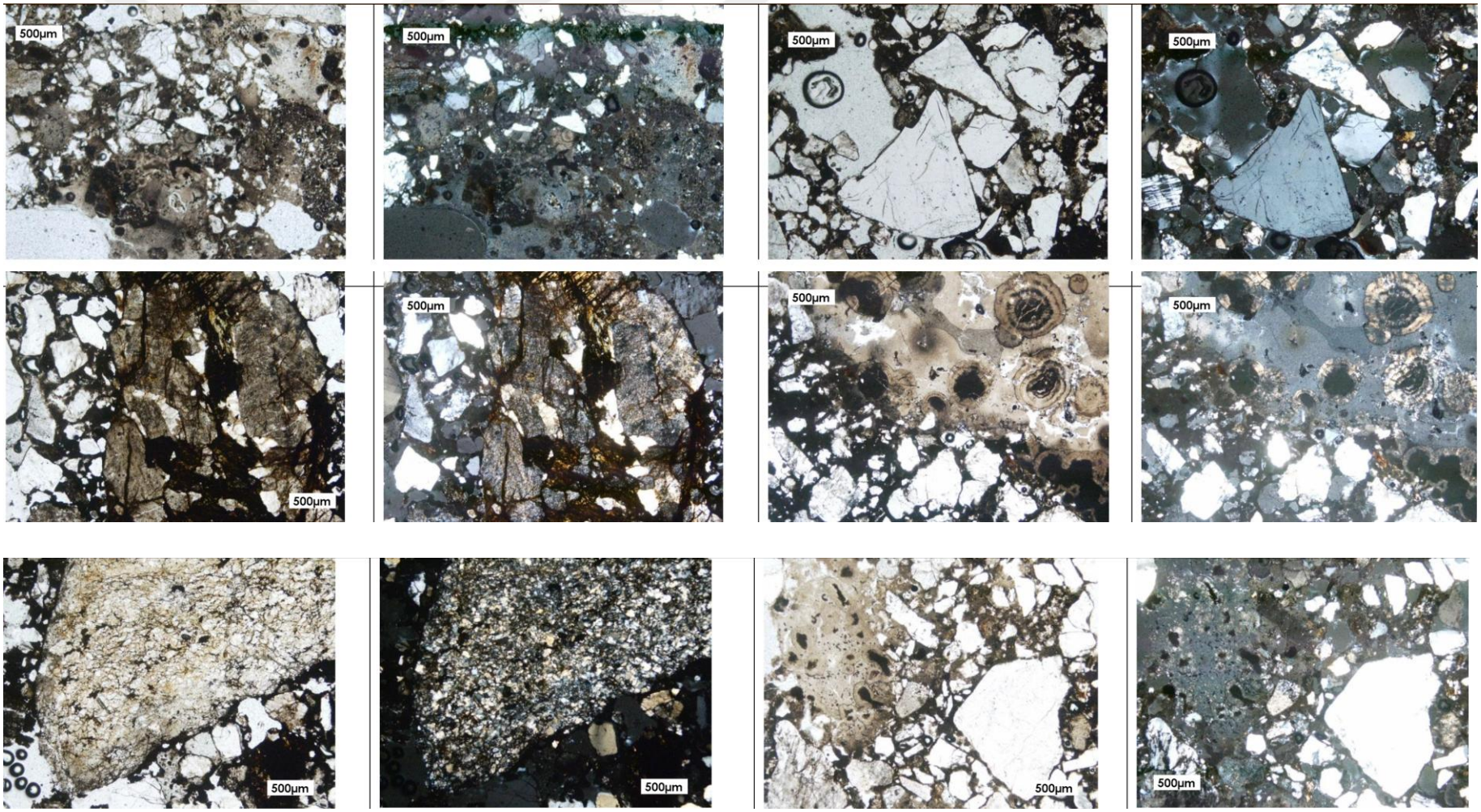


Figure VI.39. Thin section images of sample MM22

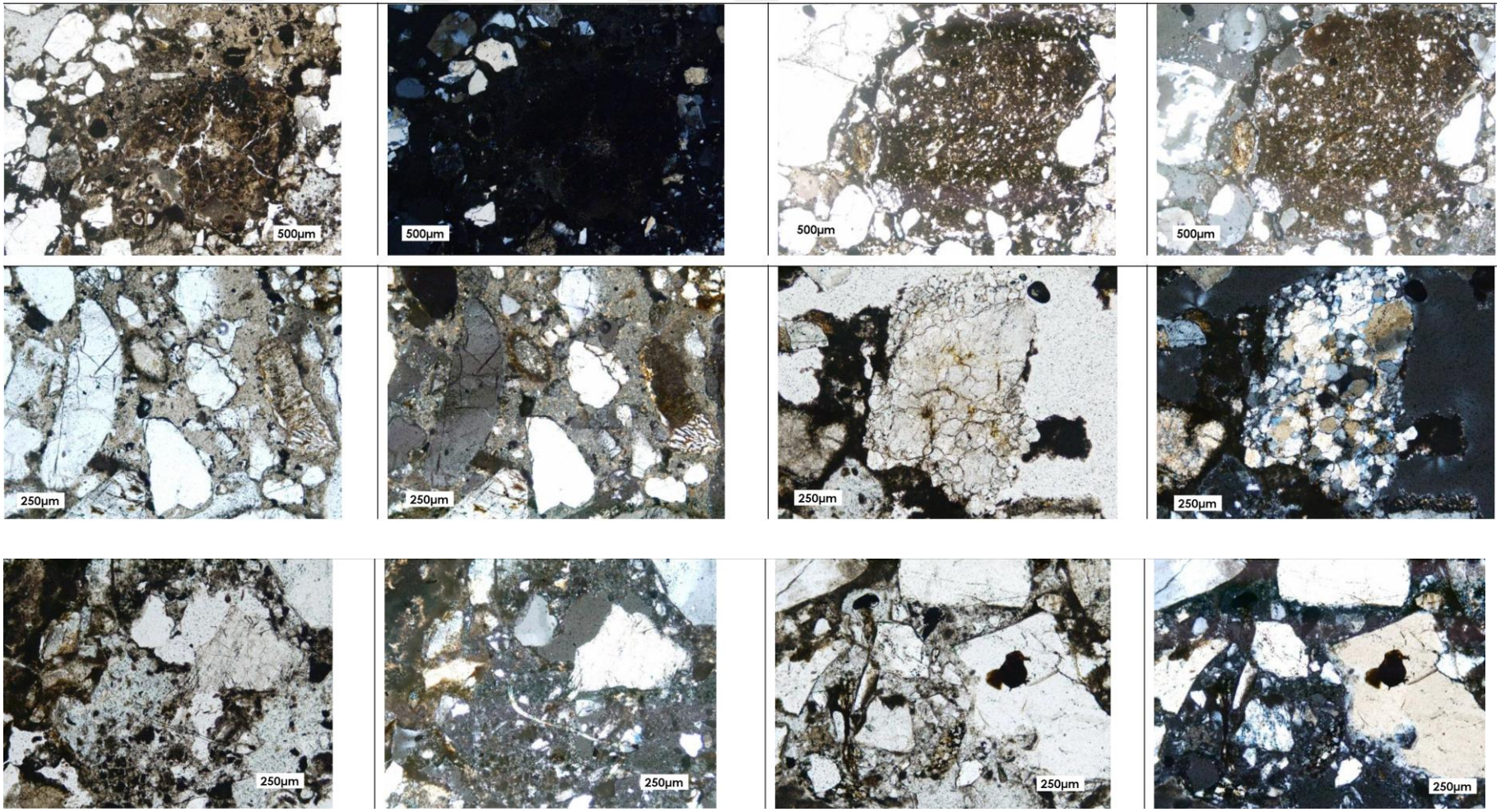


Figure VI.40. Thin section images of sample MM22 (continue)

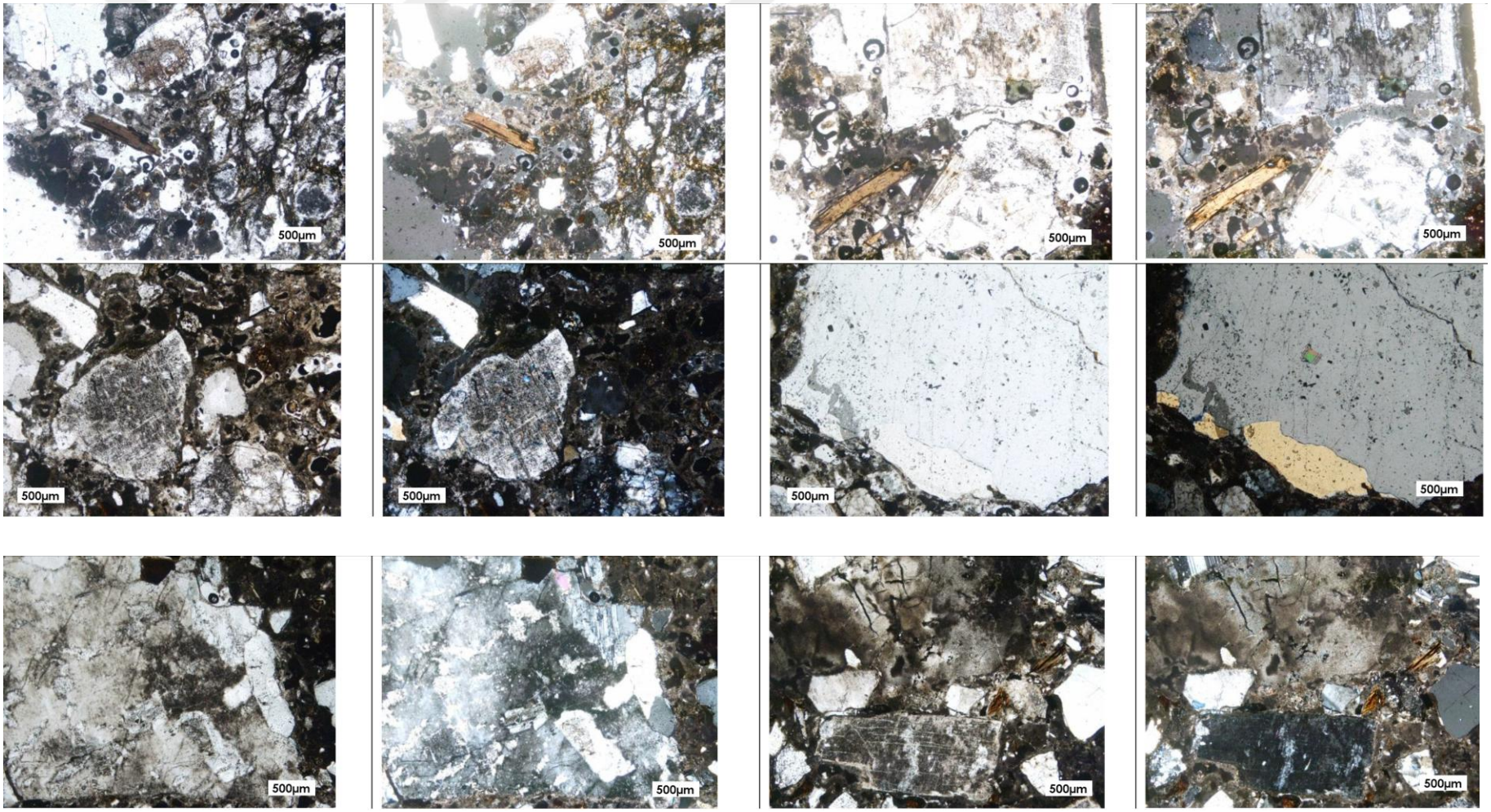


Figure VI.41. Thin section images of sample MM25

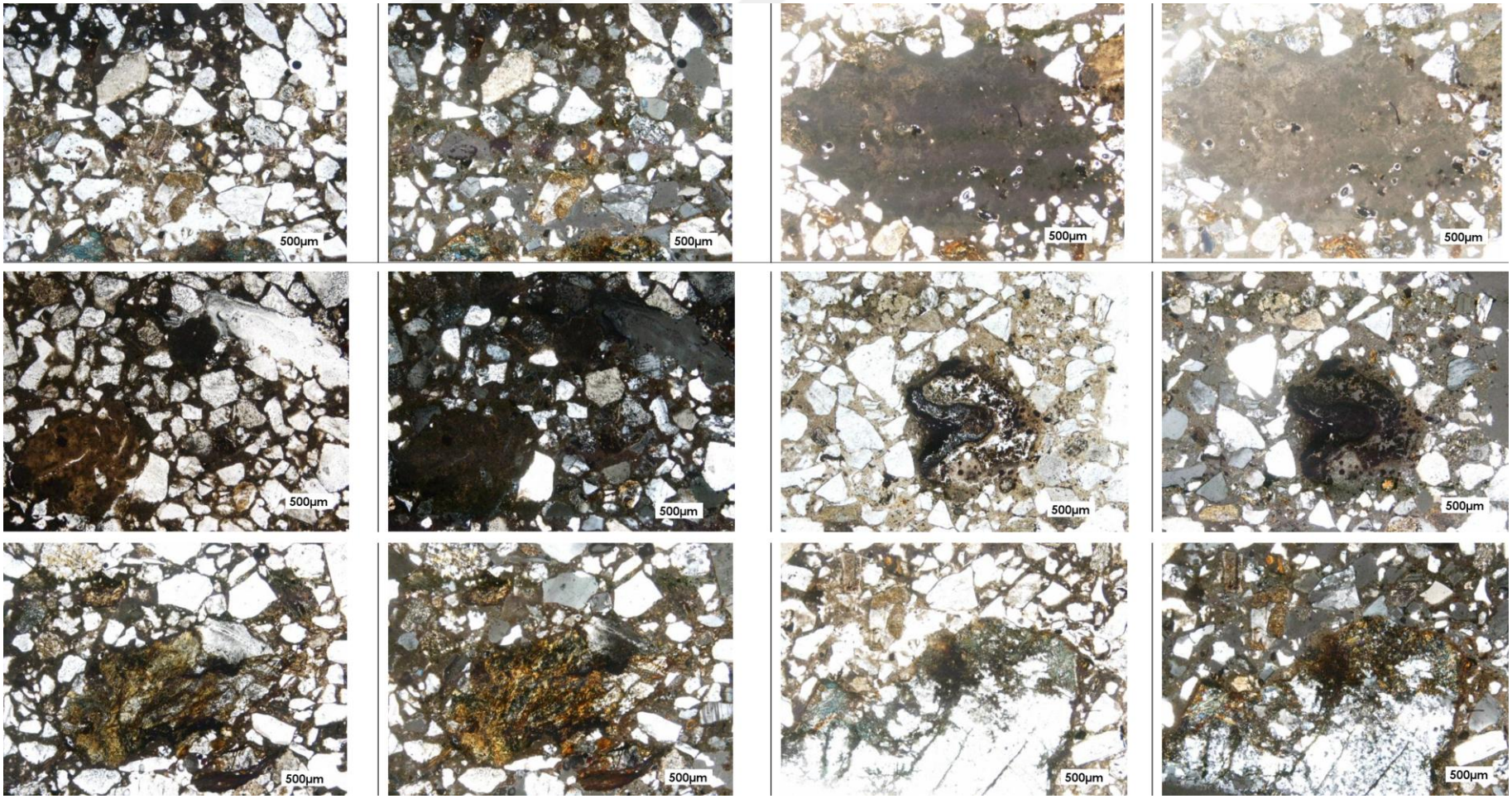


Figure VI.42. Thin section images of sample MM26

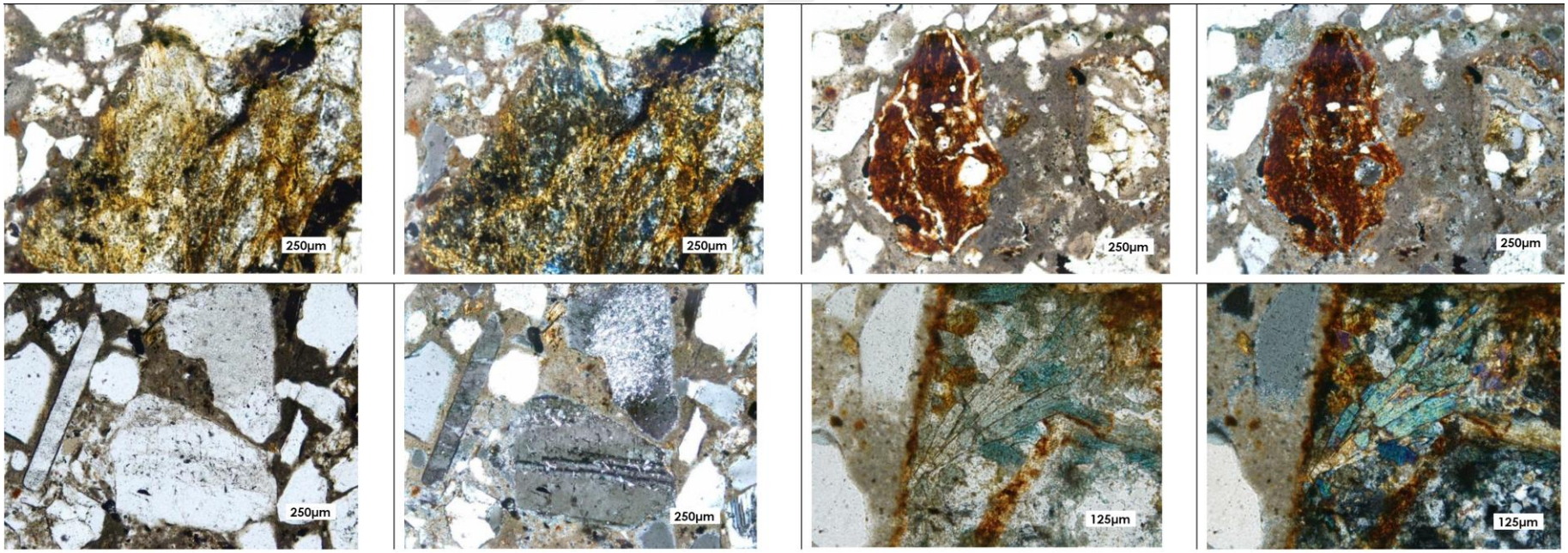


Figure VI.43. Thin section images of sample MM26 (continue)

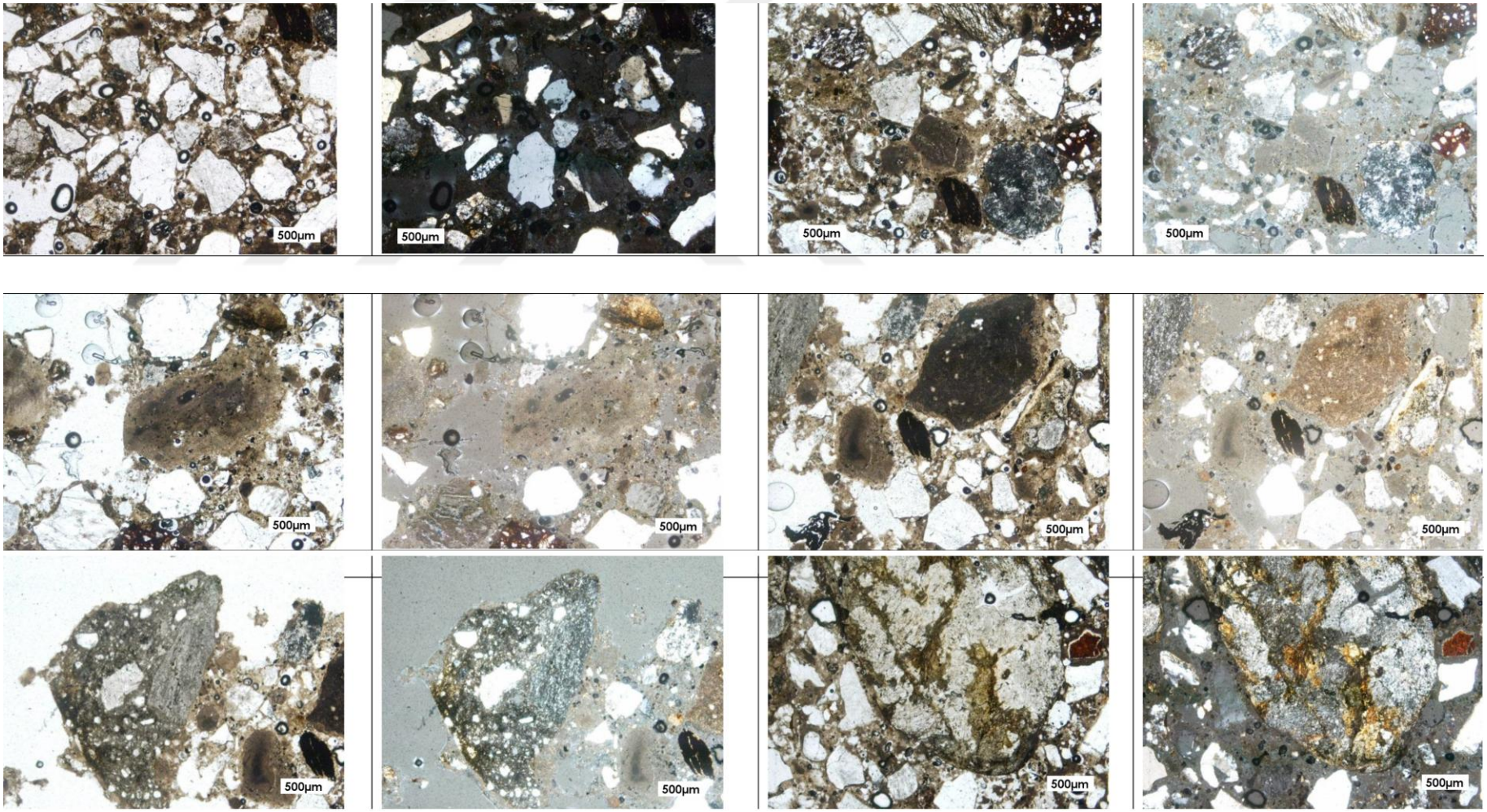


Figure VI.44. Thin section images of sample MM27

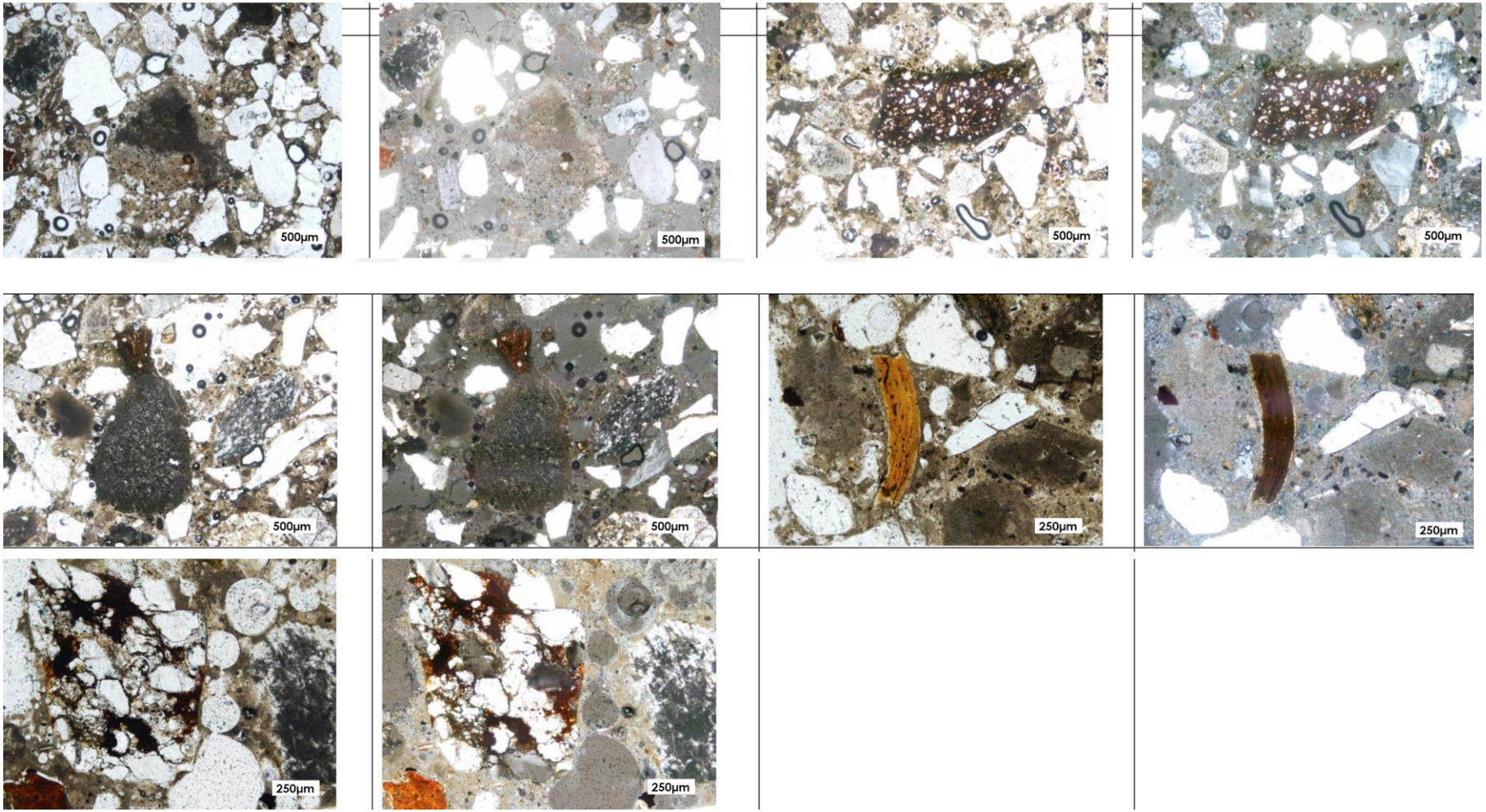


Figure VI.45. Thin section images of sample MM27 (continue)

Appendix VII- Nysa Archaeological Site

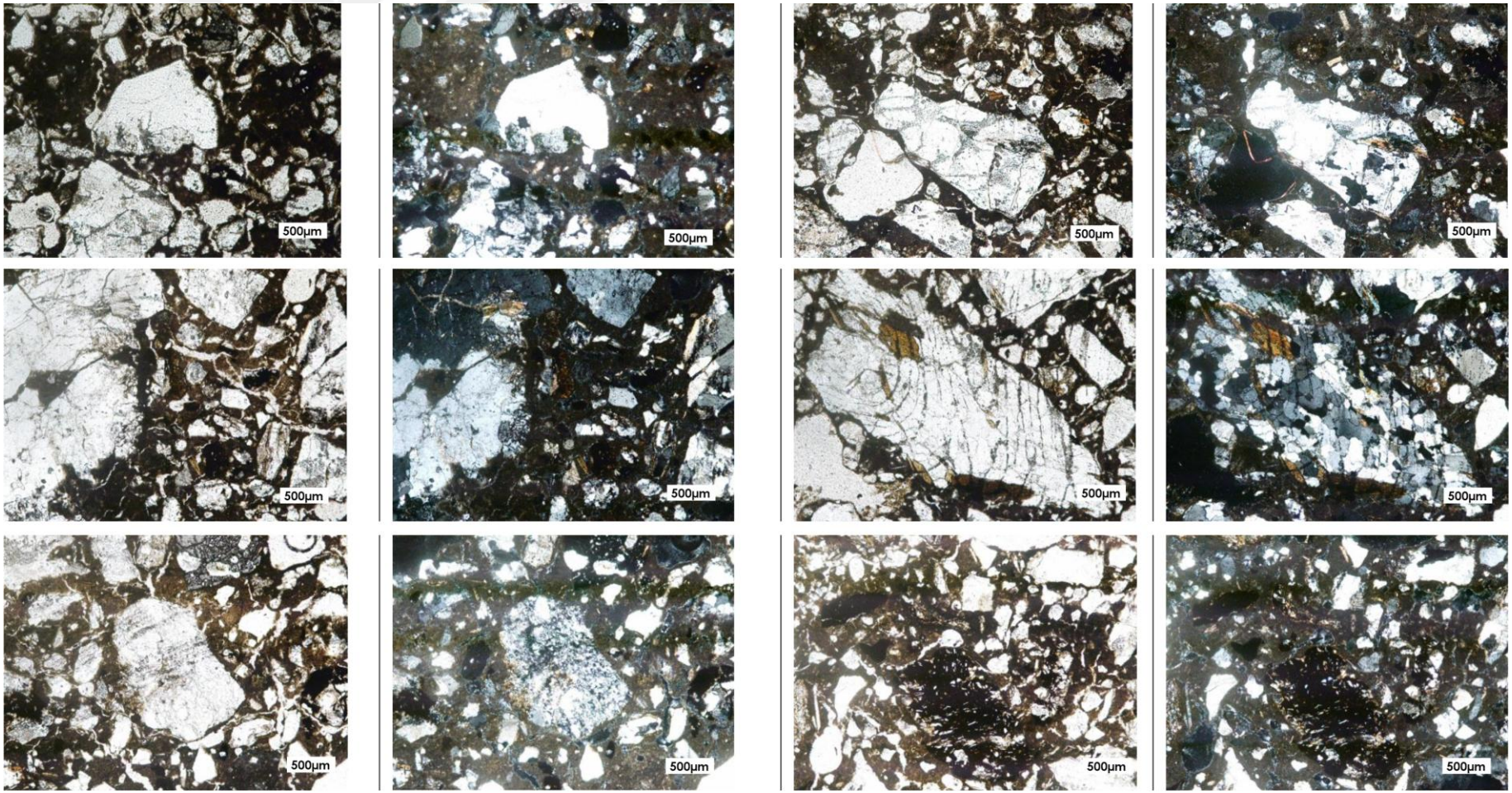


Figure VII.1. Thin section images of sample NM01

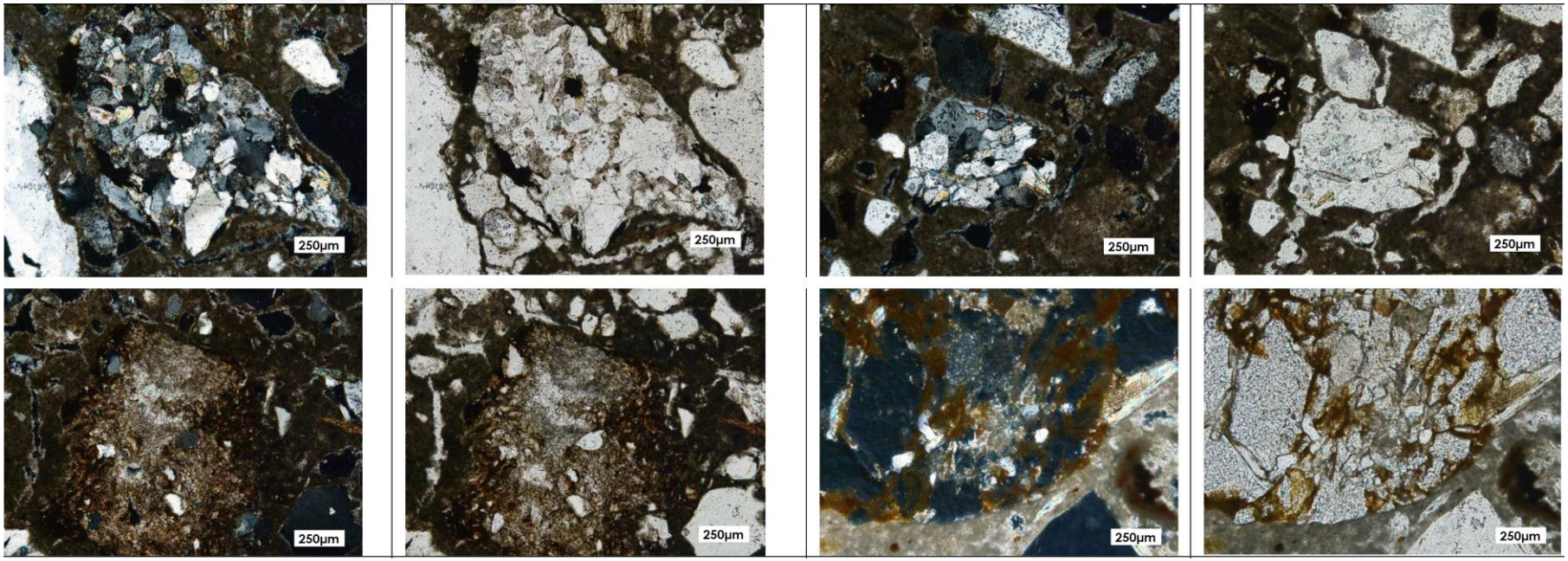


Figure VII.2. Thin section images of sample NM01 (continue)

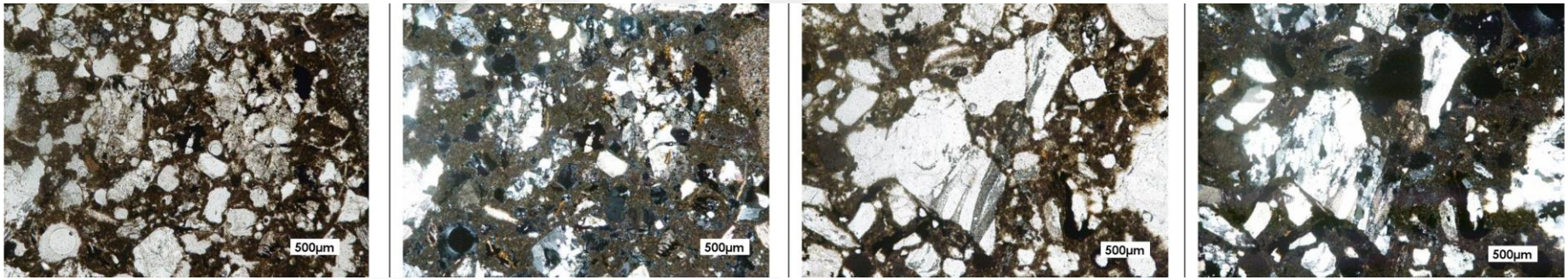


Figure VII.3. Thin section images of sample NM02a

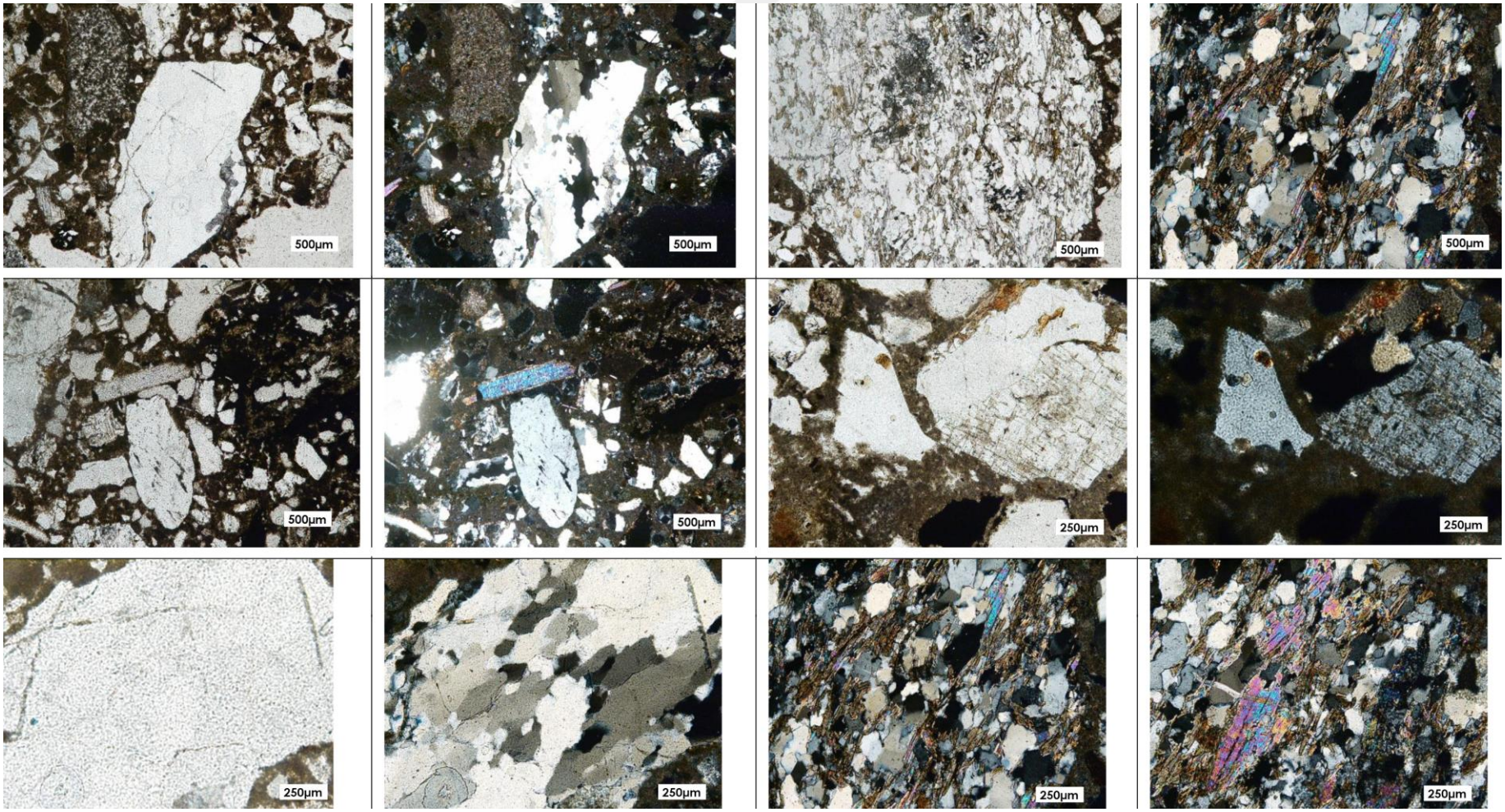


Figure VII.4. Thin section images of sample NM02a (continue)

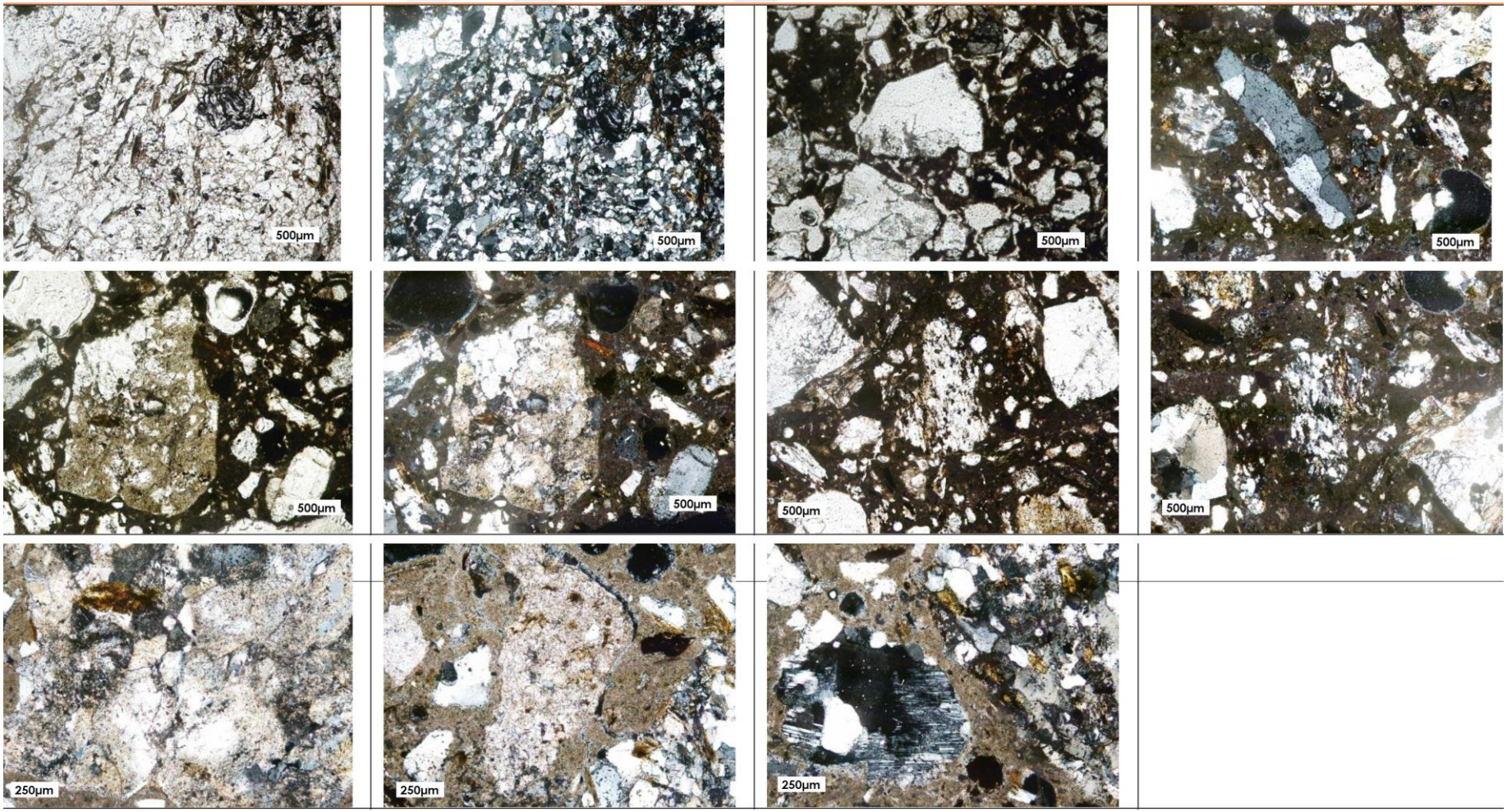


Figure VII.5. Thin section images of sample NM03

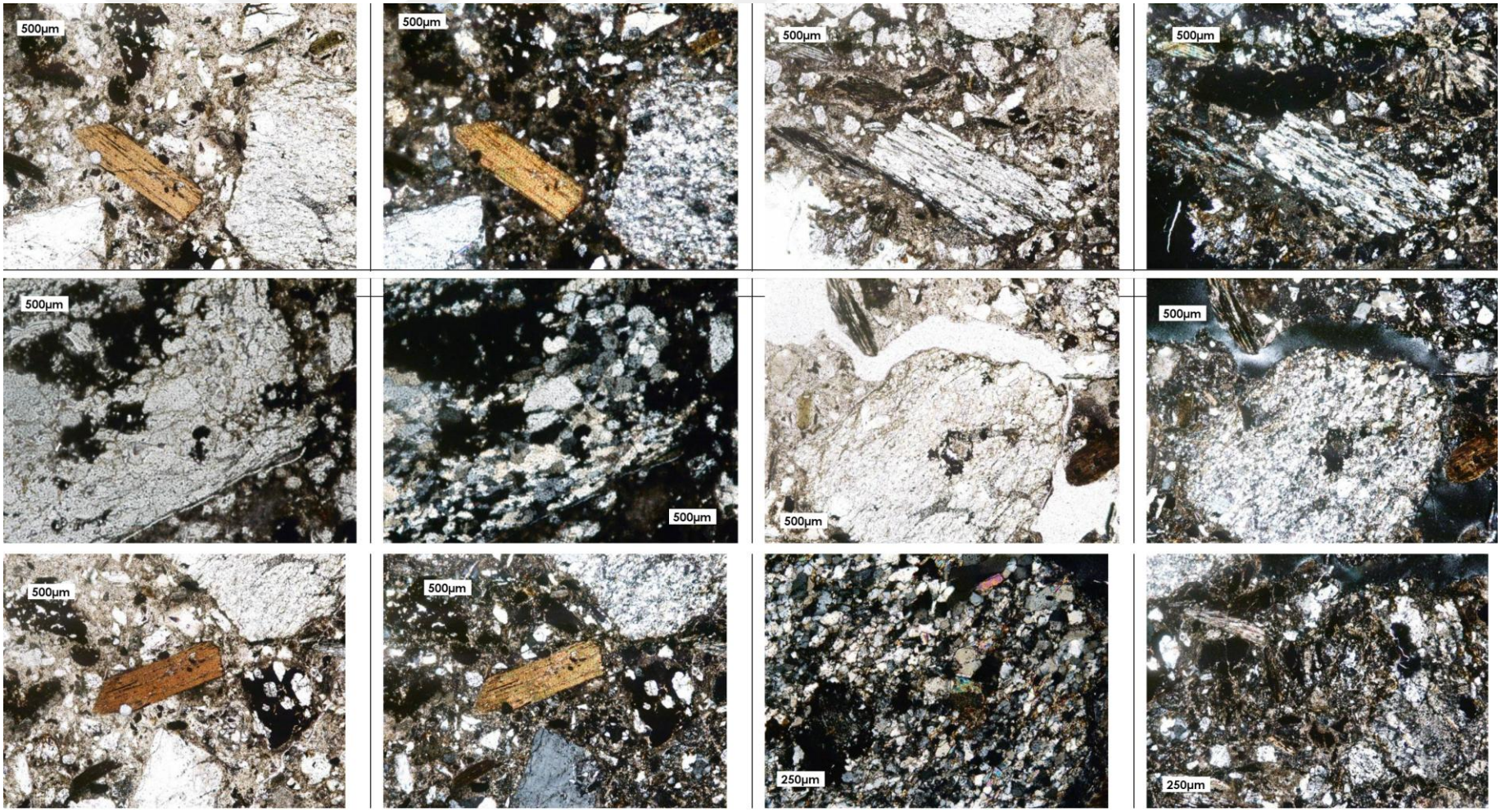


Figure VII.6. Thin section images of sample NM04

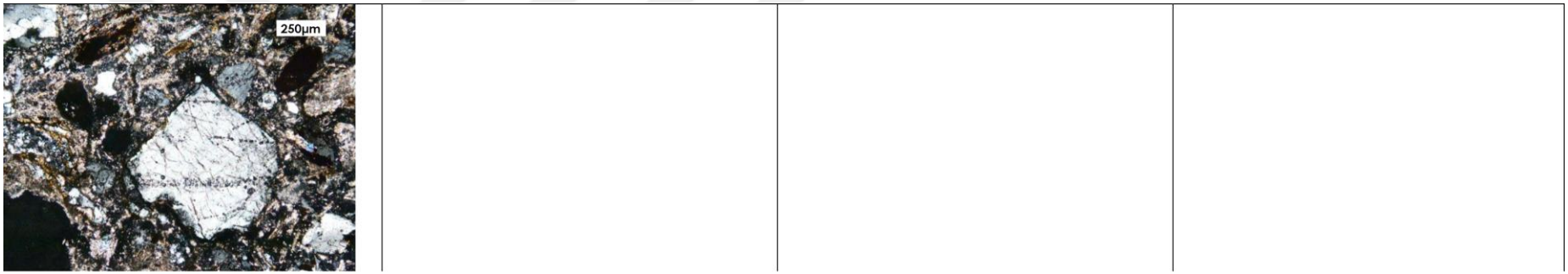


Figure VII.7. Thin section images of sample NM04 (continue)

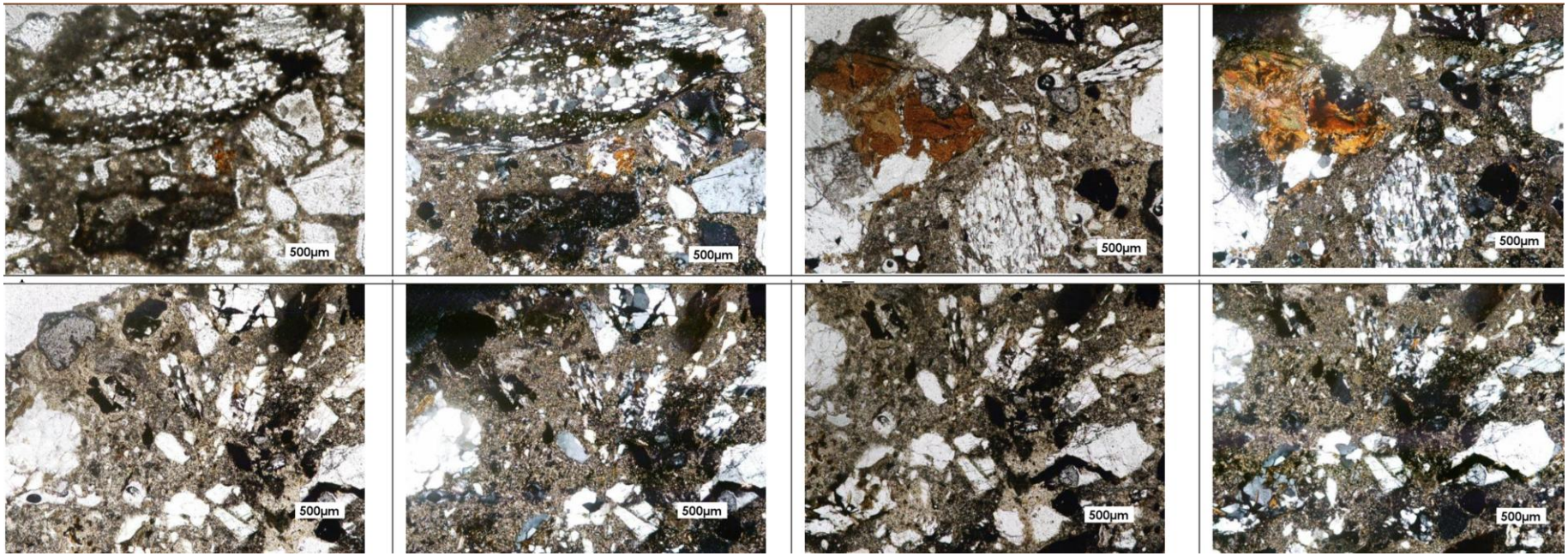


Figure VII.8. Thin section images of sample NM05a

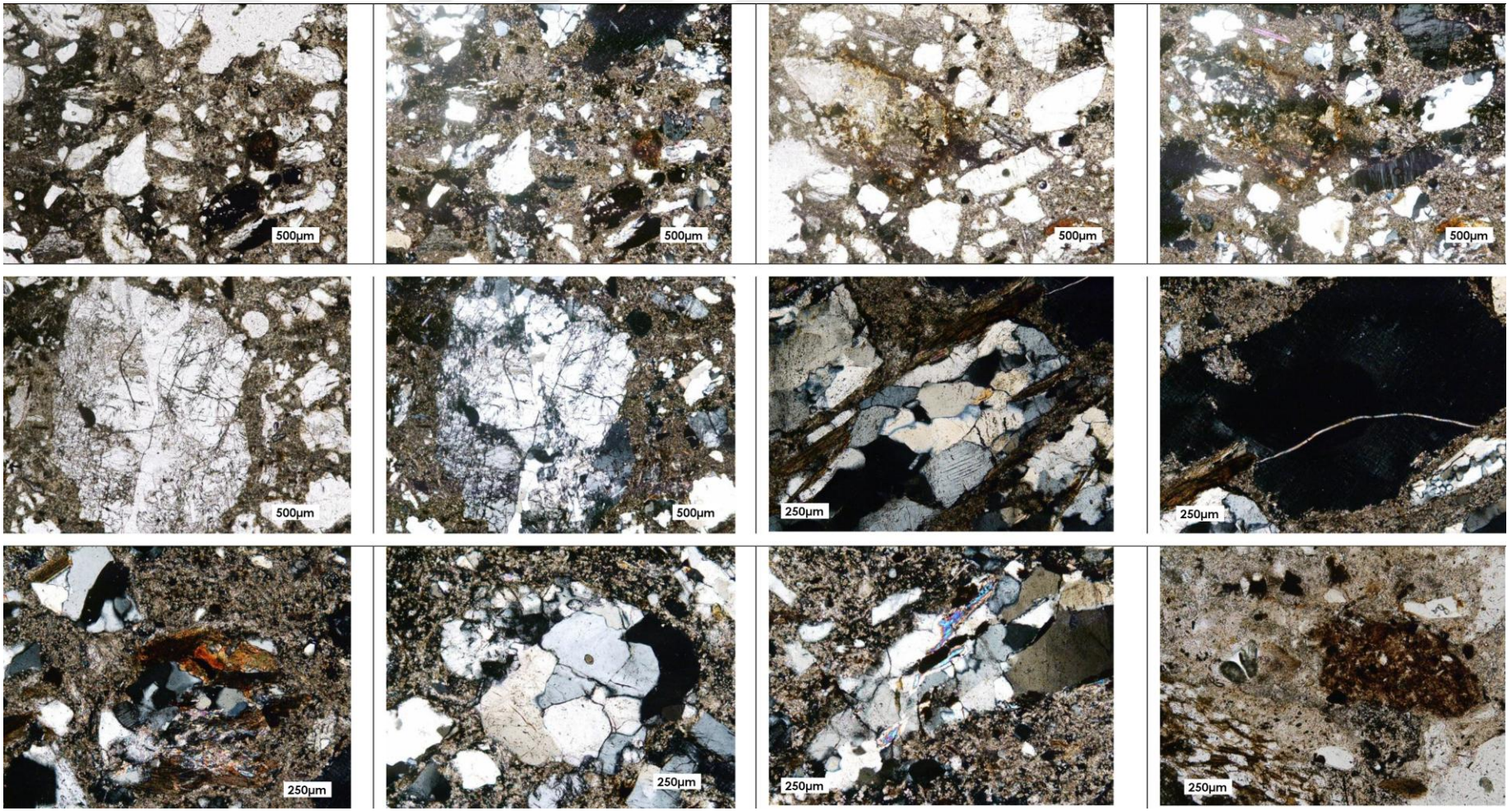


Figure VII.9. Thin section images of sample NM05a (continue)

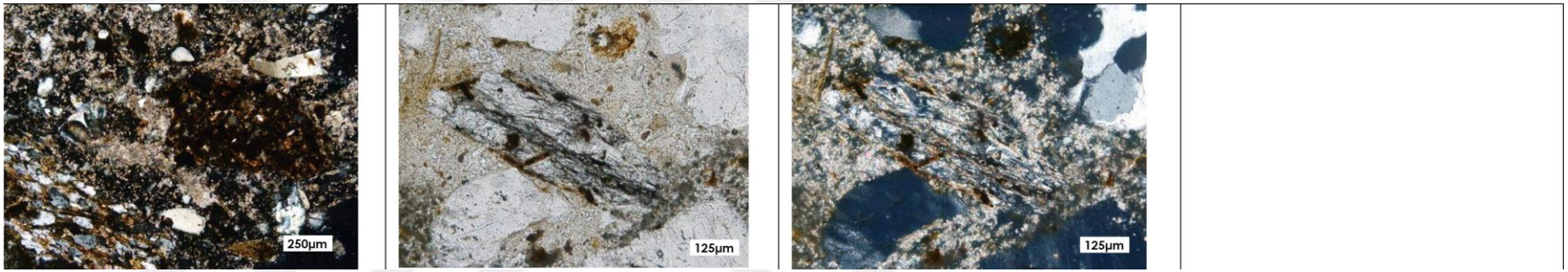


Figure VII.10. Thin section images of sample NM05a (continue)

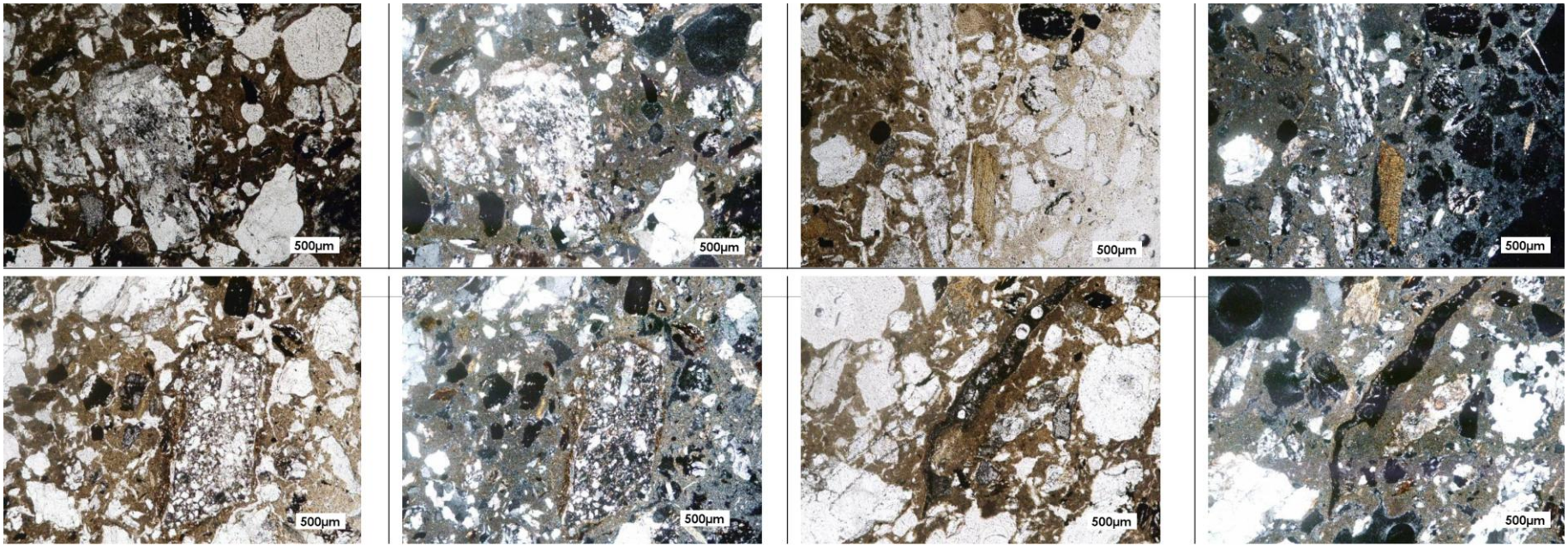


Figure VII.11. Thin section images of sample NM06

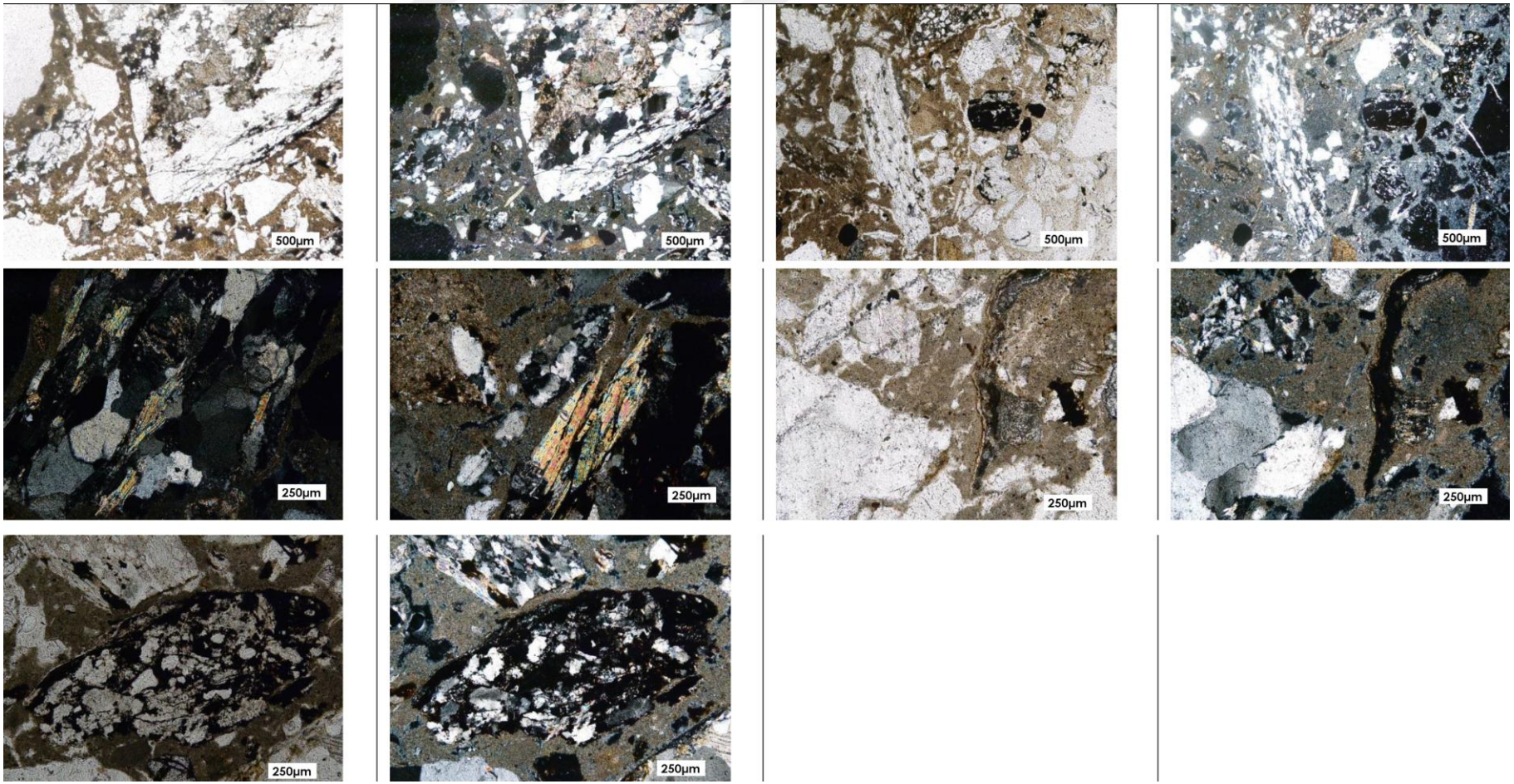


Figure VII.12. Thin section images of sample NM06 (continue)

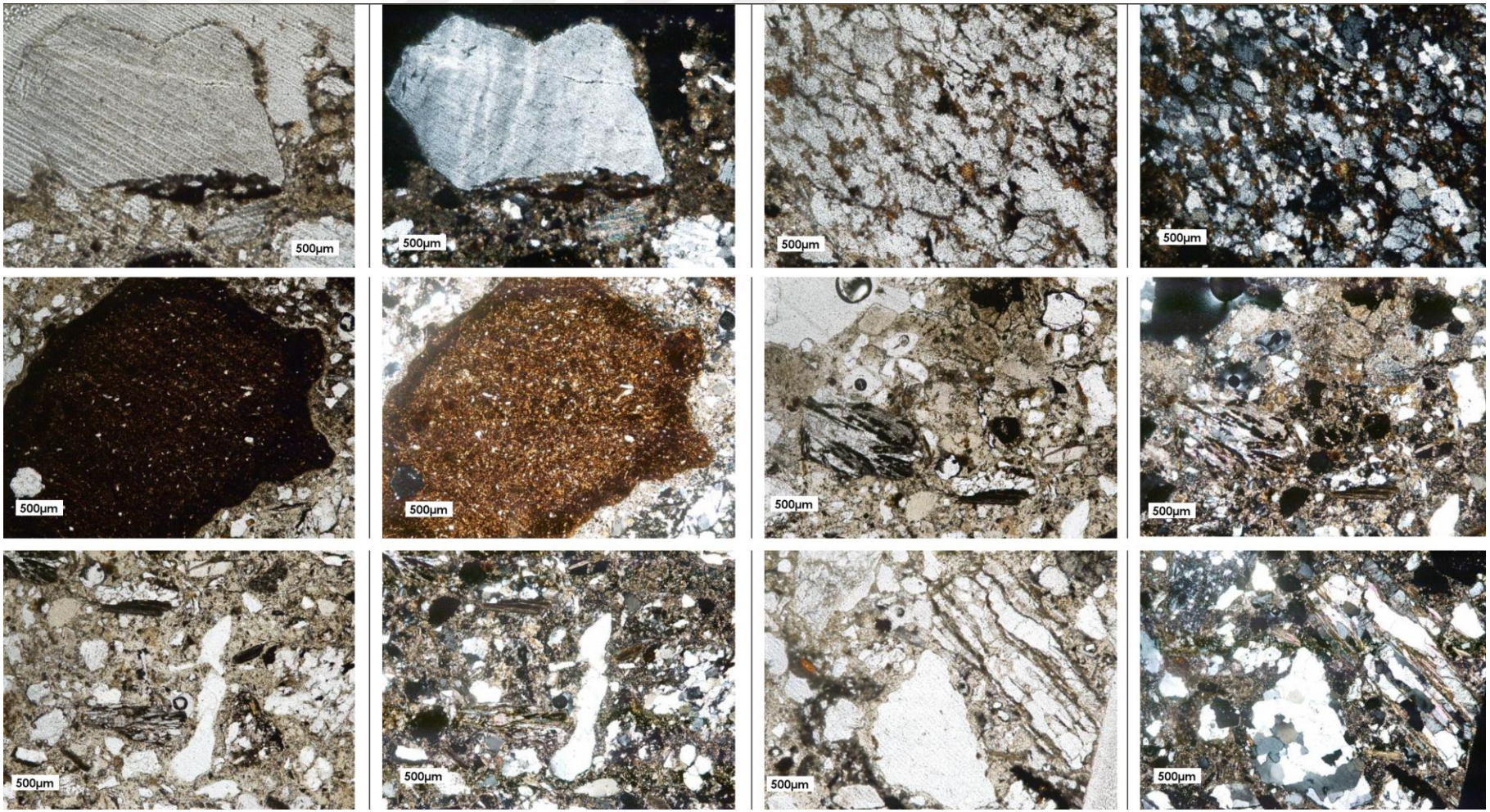


Figure VII.13. Thin section images of sample NM07

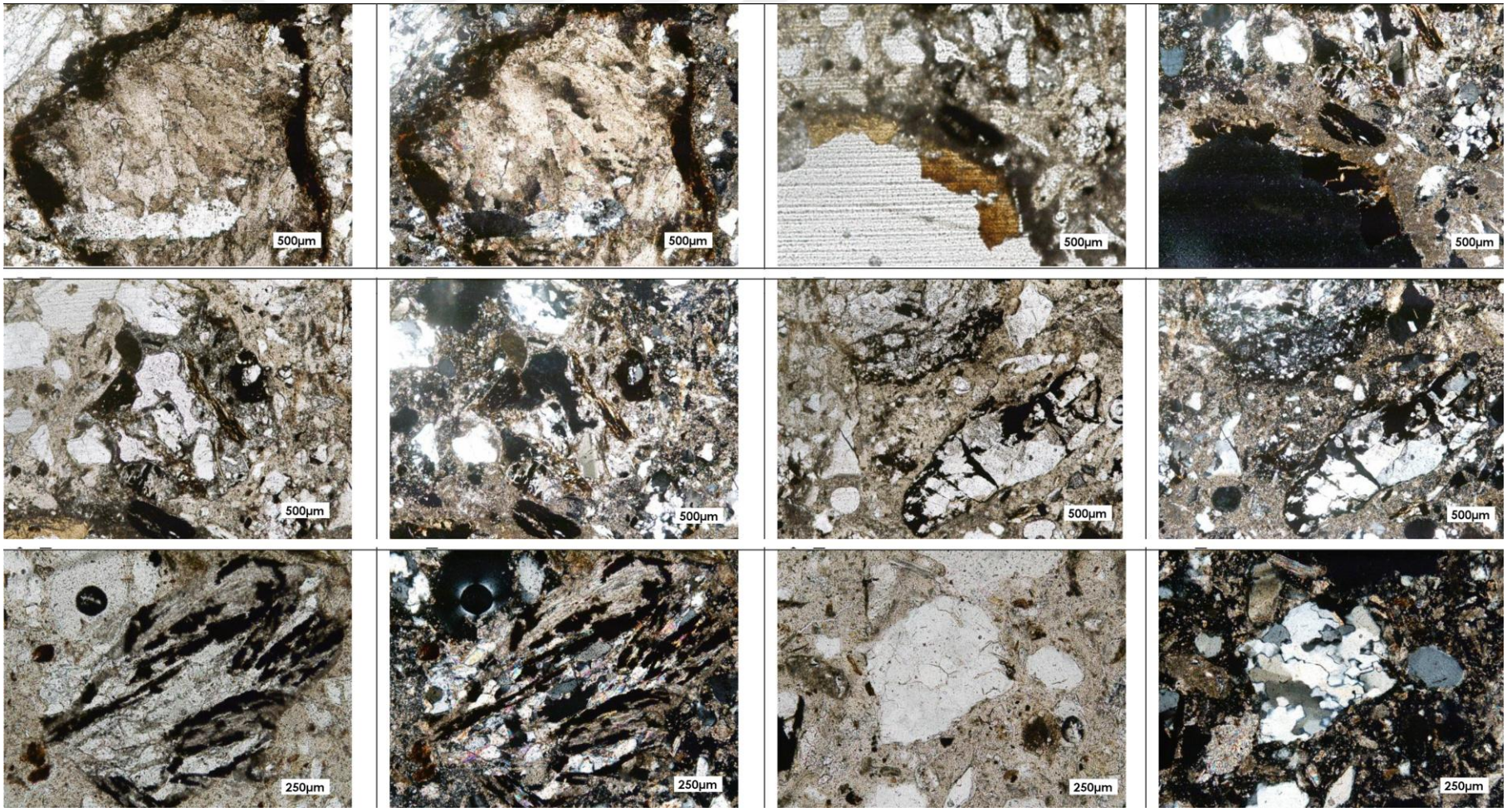


Figure VII.14. Thin section images of sample NM07 (continue)

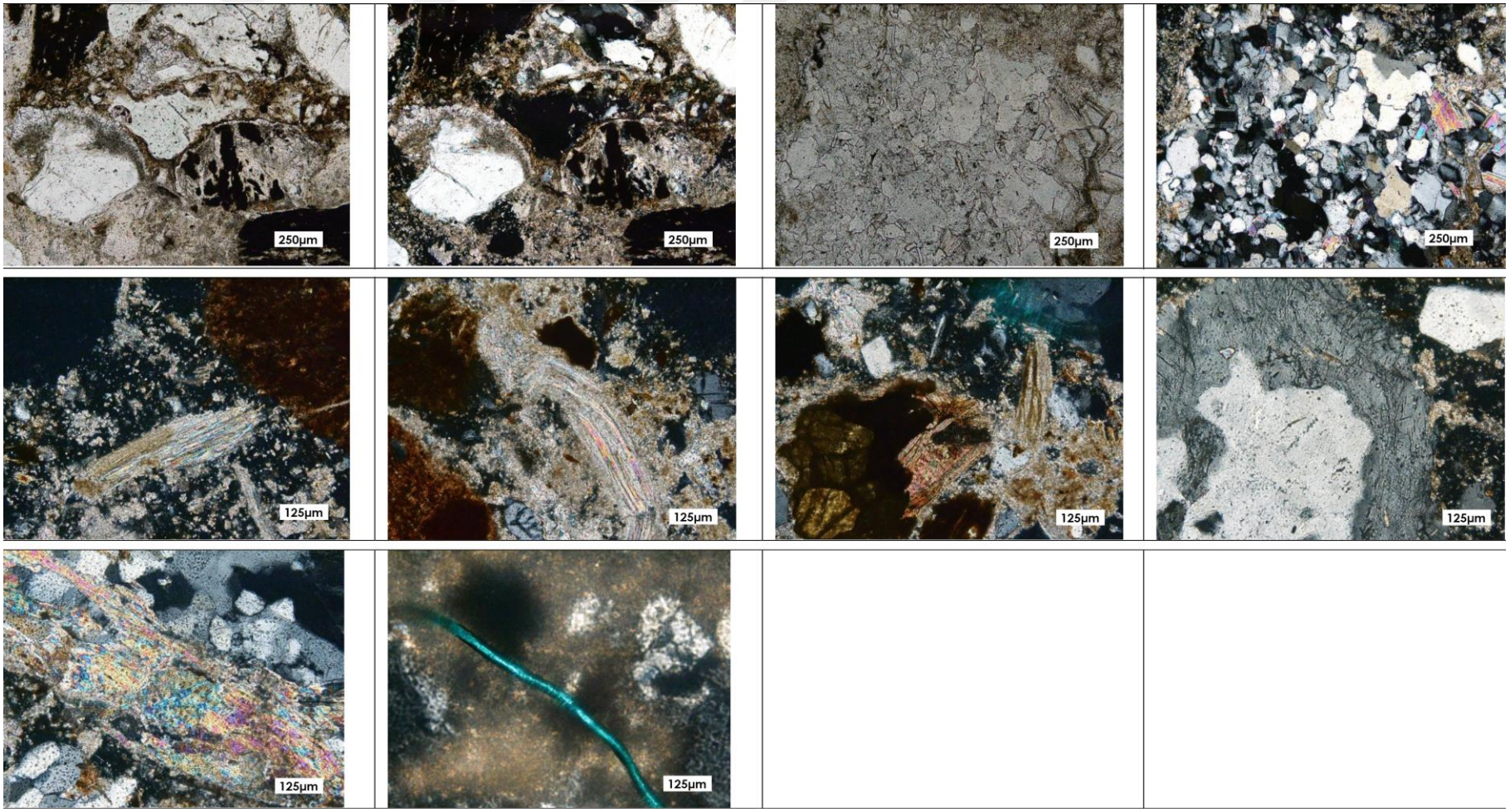


Figure VII.15. Thin section images of sample NM07 (continue)

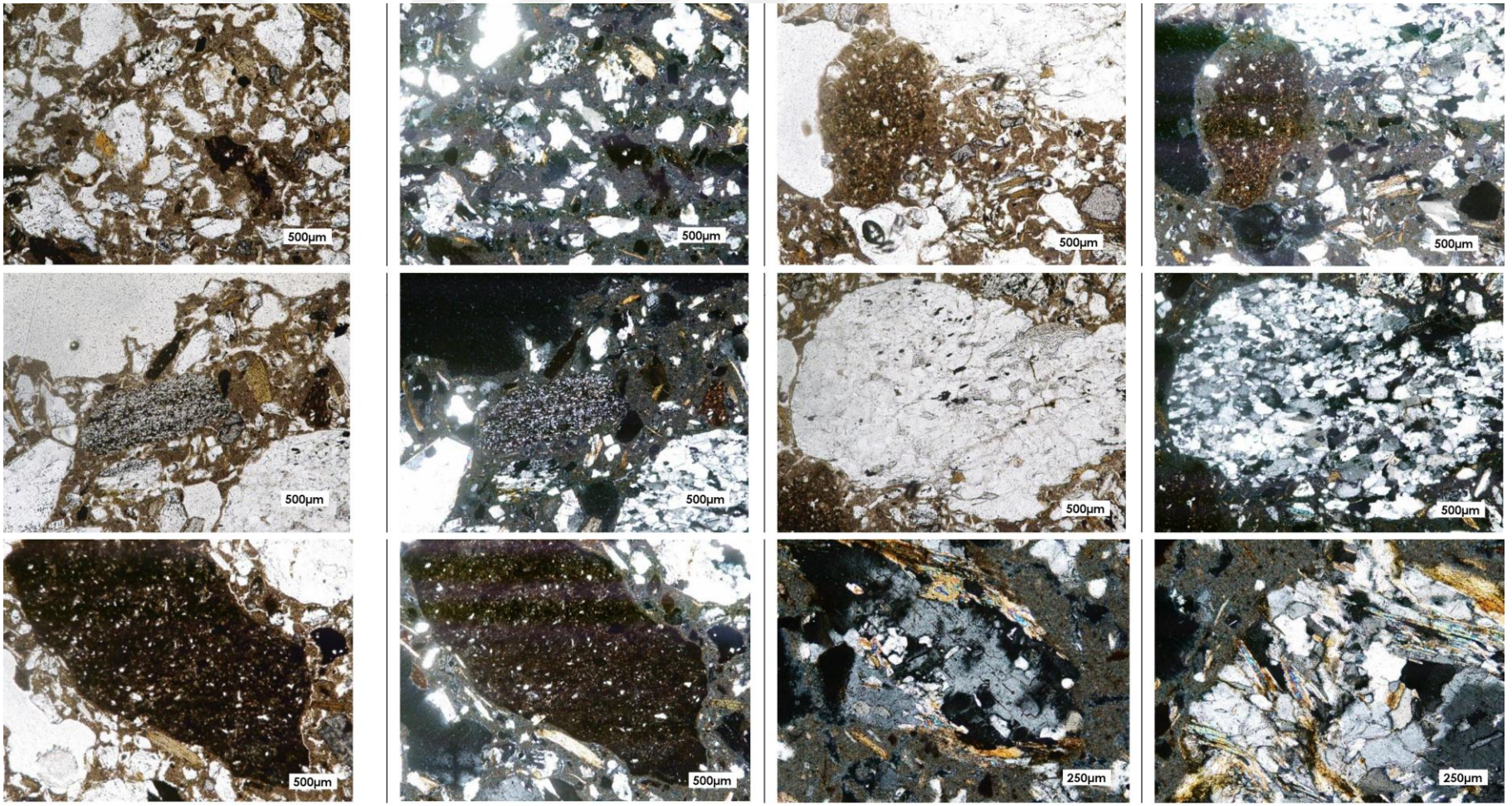


Figure VII.16. Thin section images of sample NM08

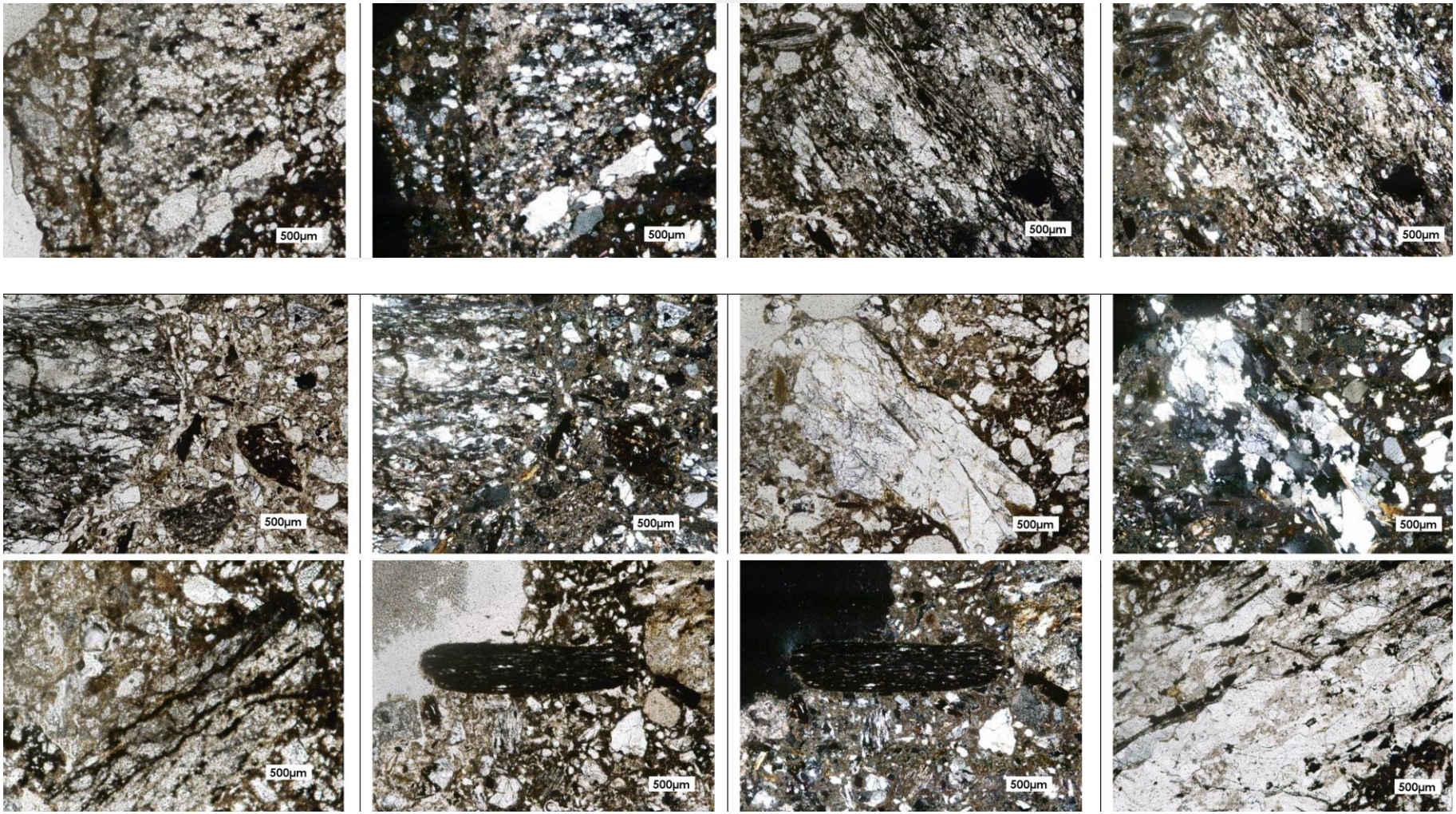


Figure VII.17. Thin section images of sample NM09

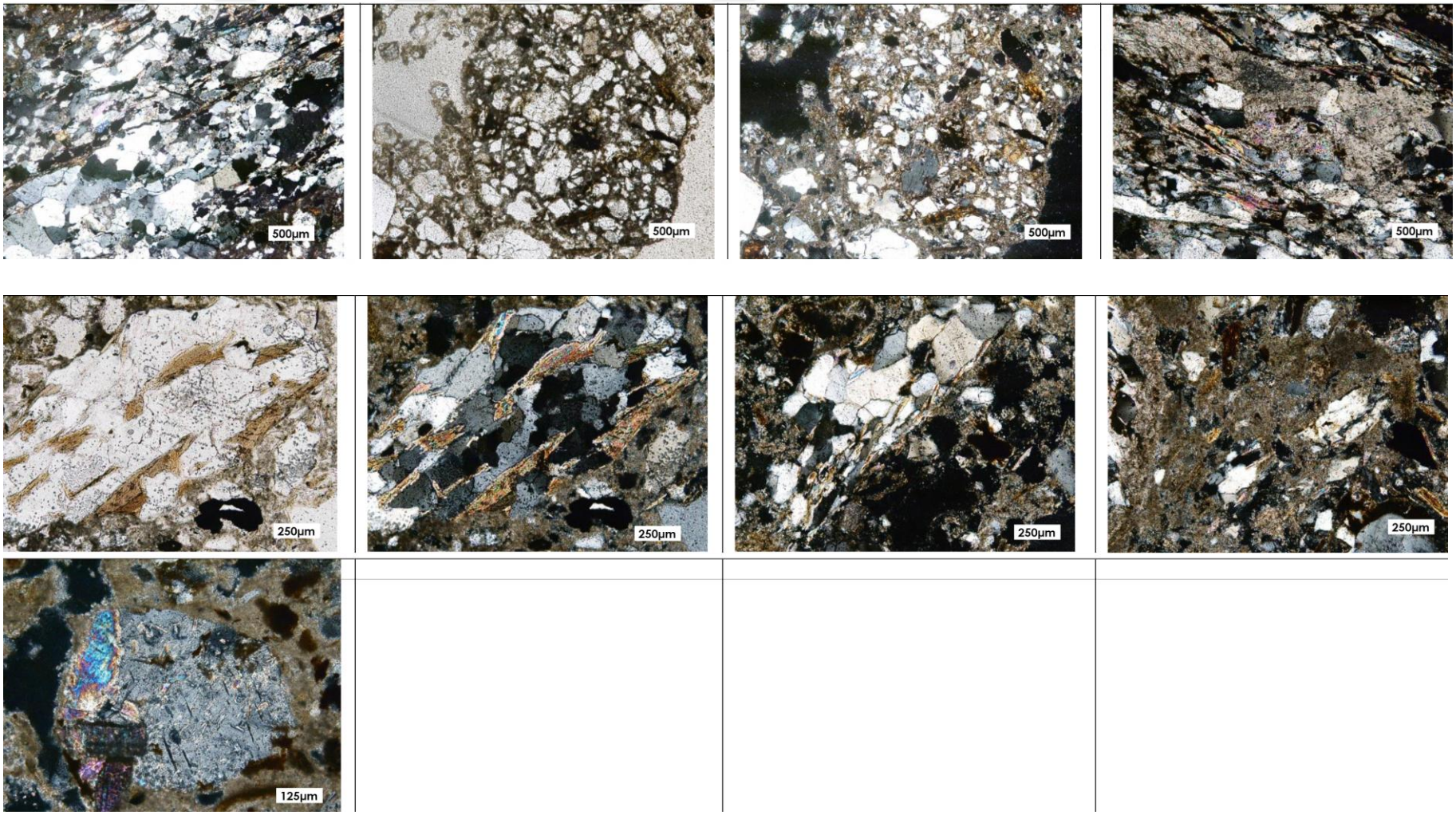


Figure VII.18. Thin section images of sample NM09 (continue)

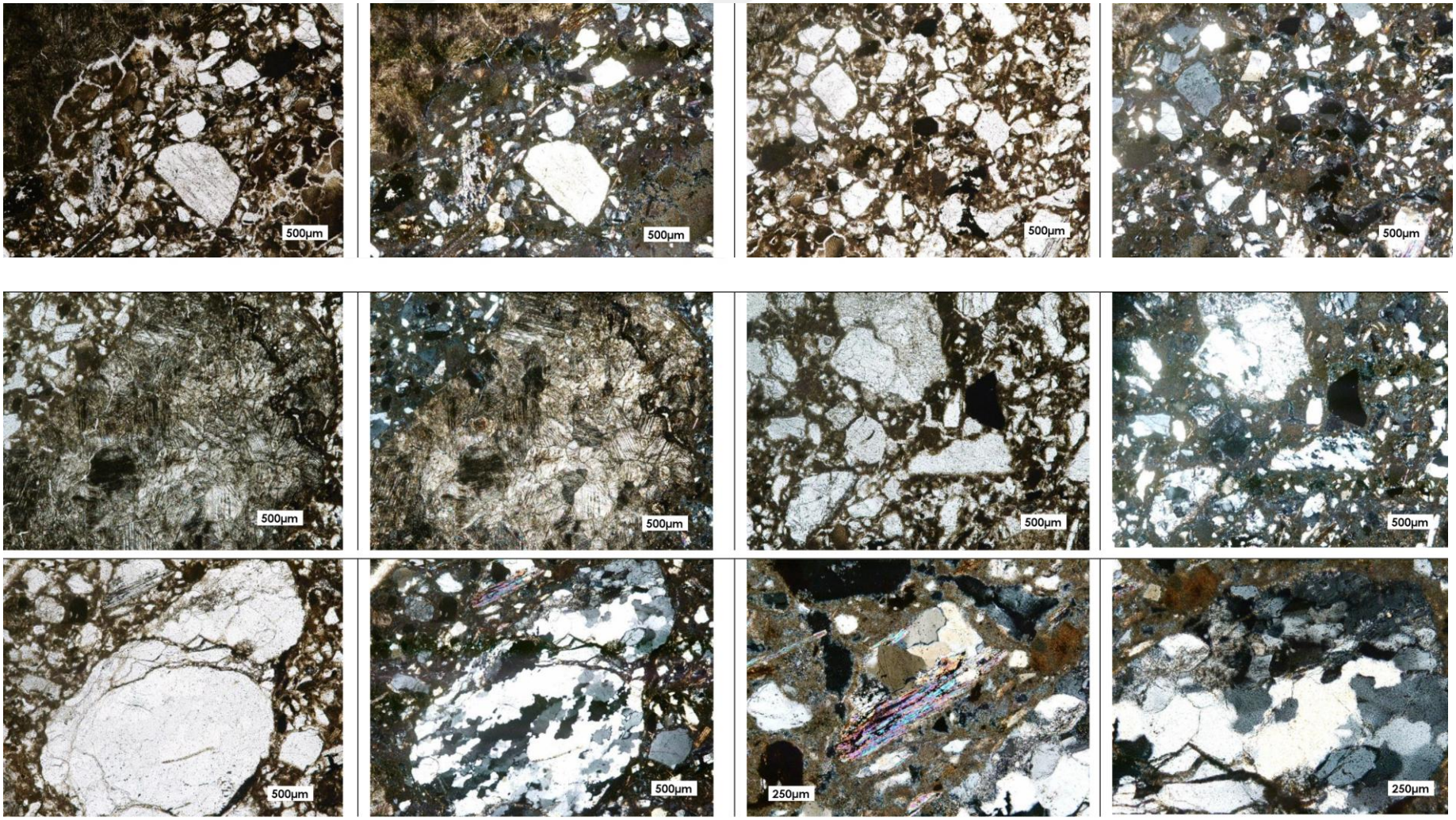


Figure VII.19. Thin section images of sample NM10b

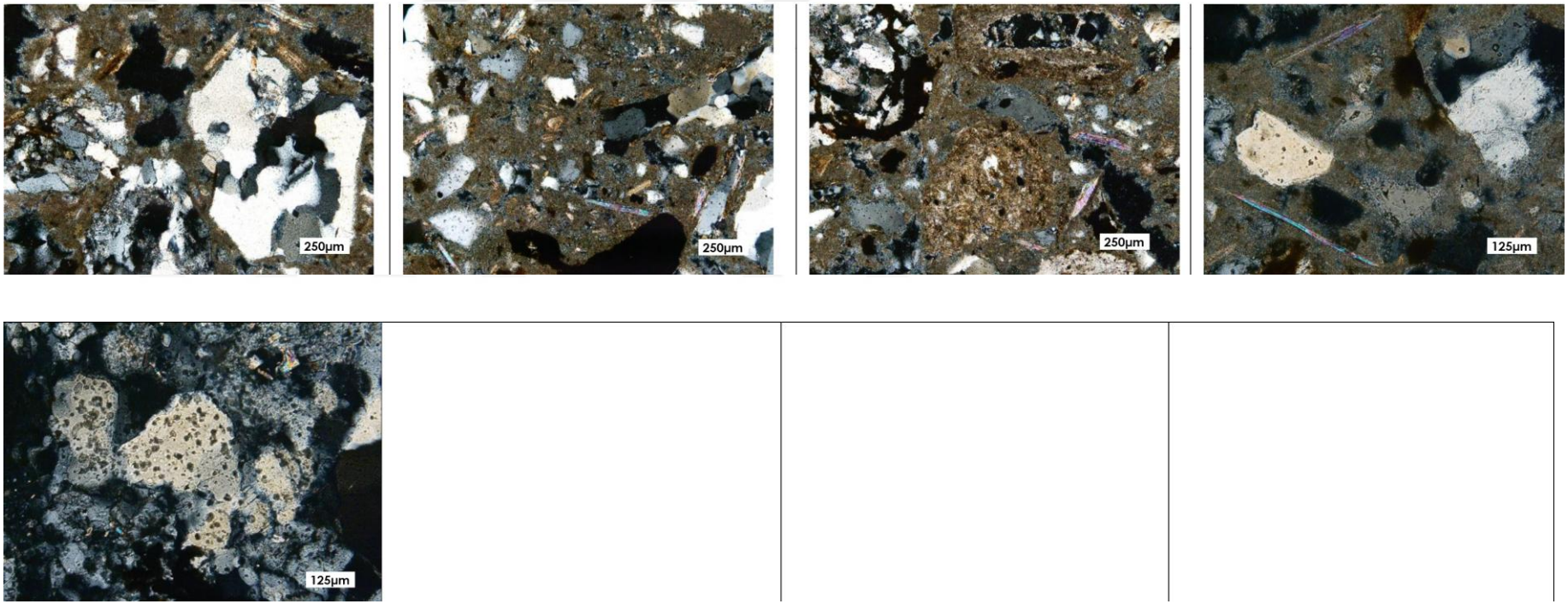


Figure VII.20. Thin section images of sample NM10b (continue)

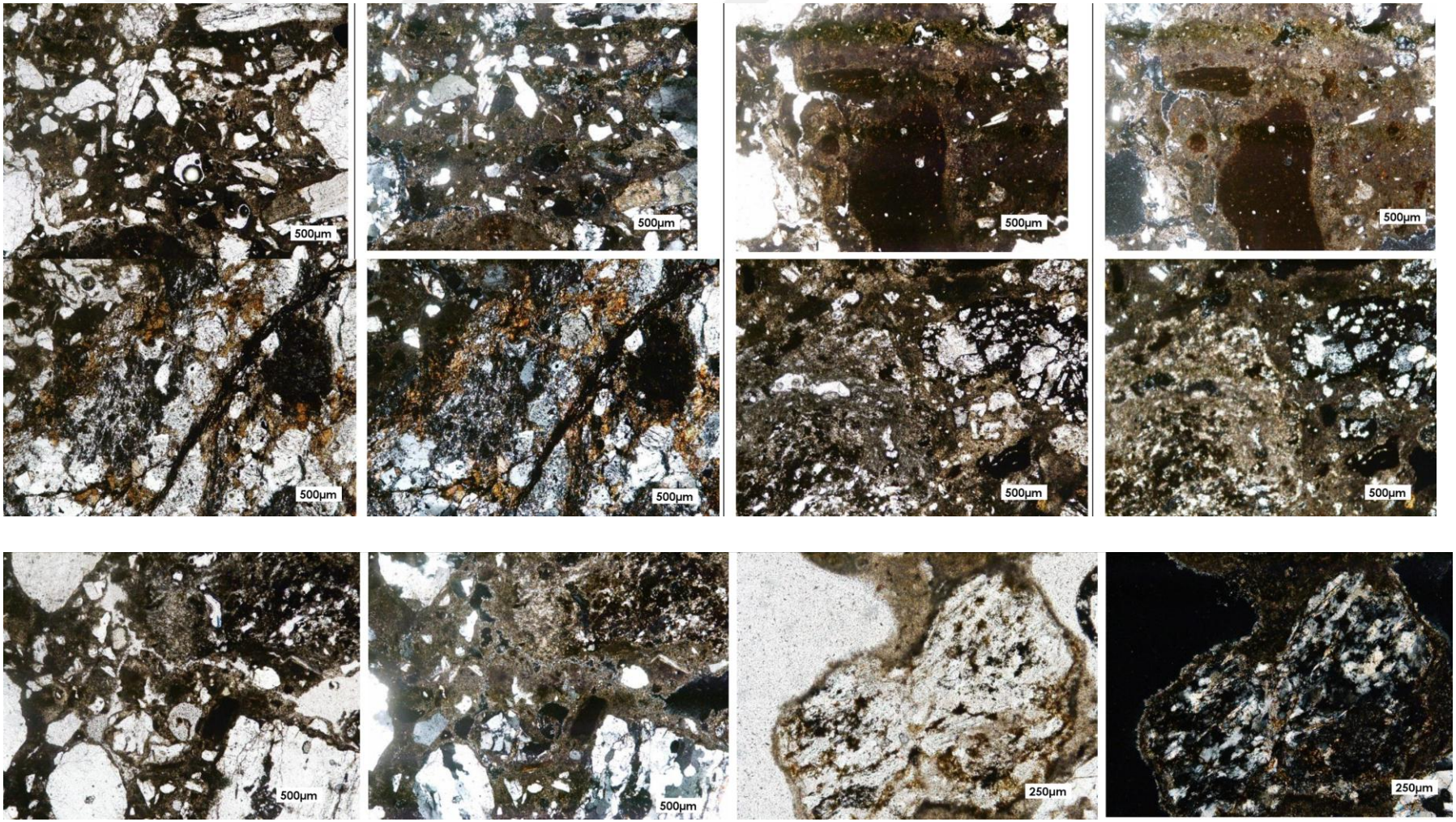


Figure VII.21. Thin section images of sample NM11

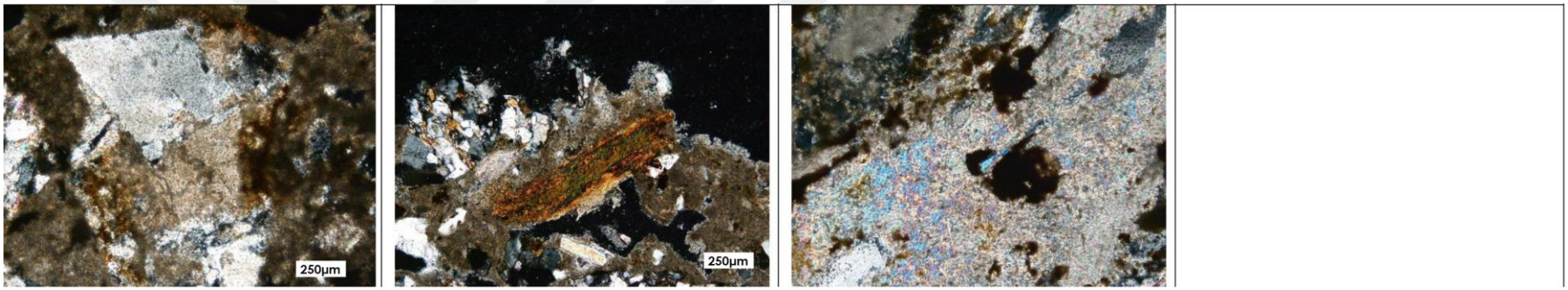


Figure VII.22. Thin section images of sample NM11 (continue)

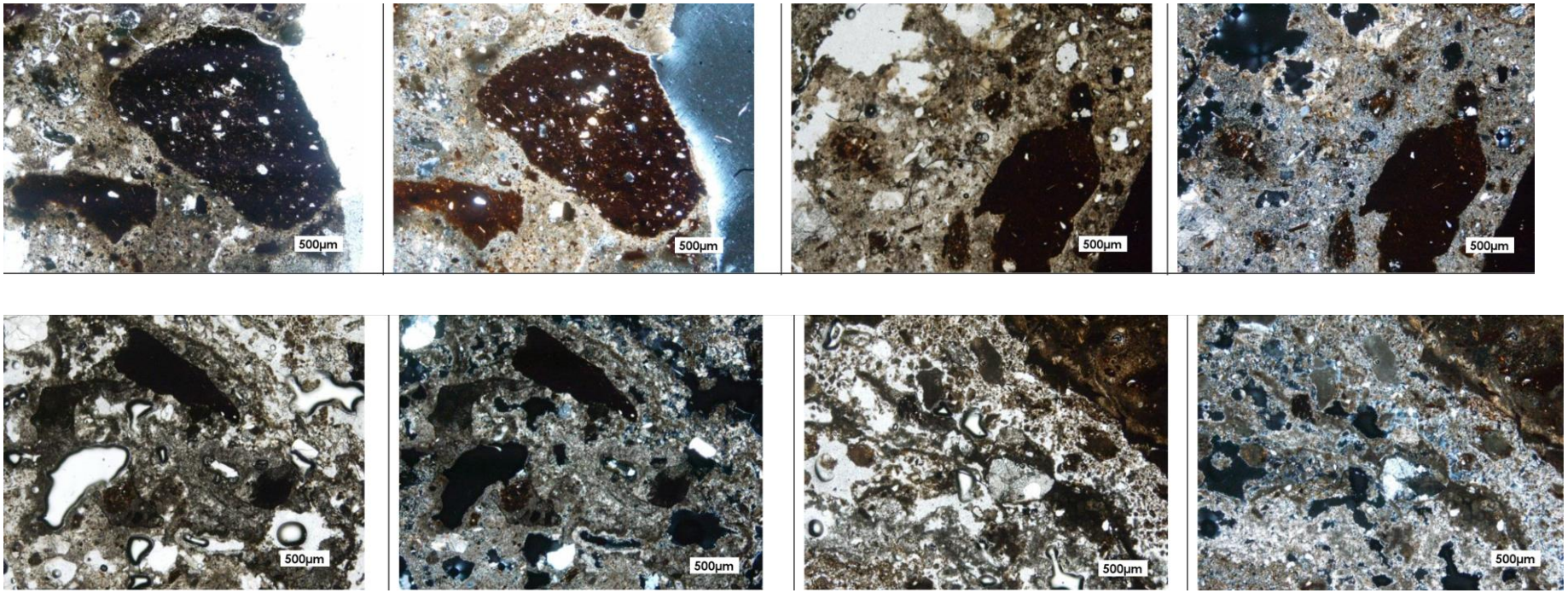


Figure VII.23. Thin section images of sample NM15

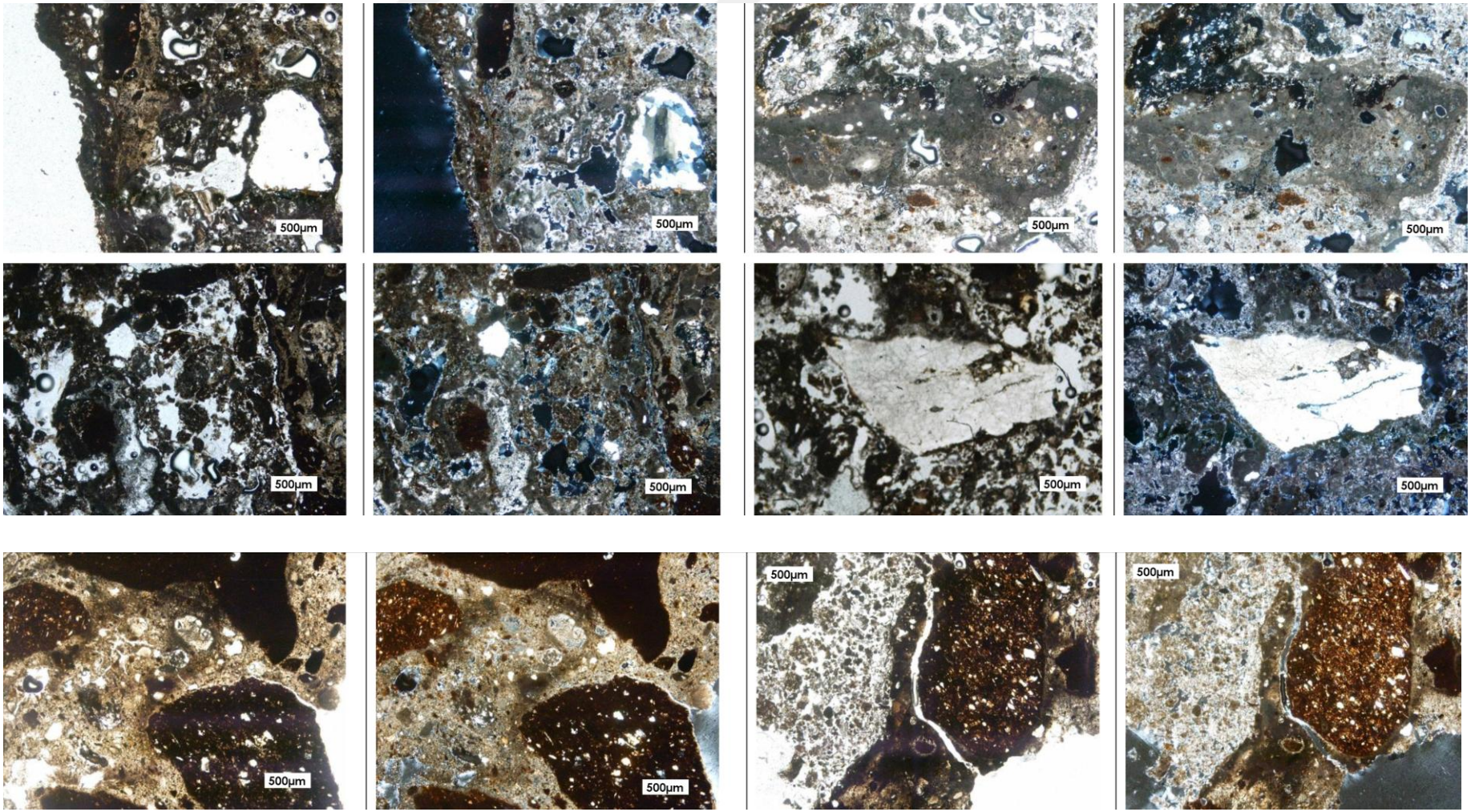


Figure VII.24. Thin section images of sample NM15 (continue)

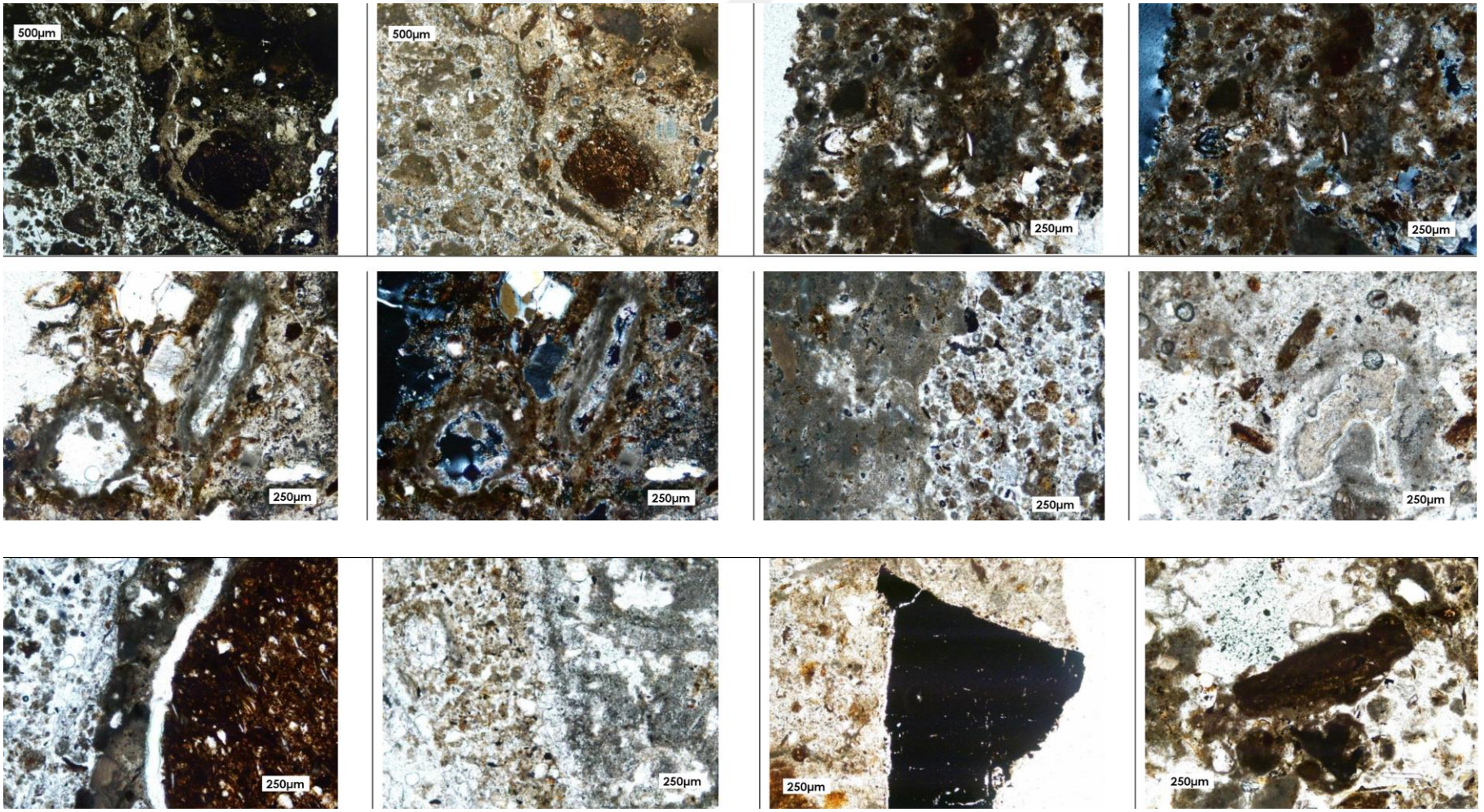


Figure VII.25. Thin section images of sample NM15 (continue)

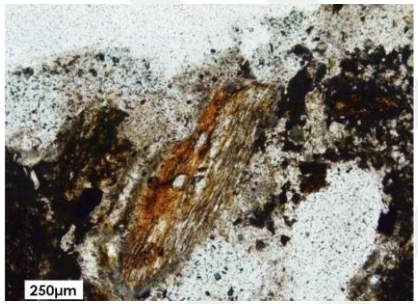


Figure VII.26. Thin section images of sample NM15 (continue)

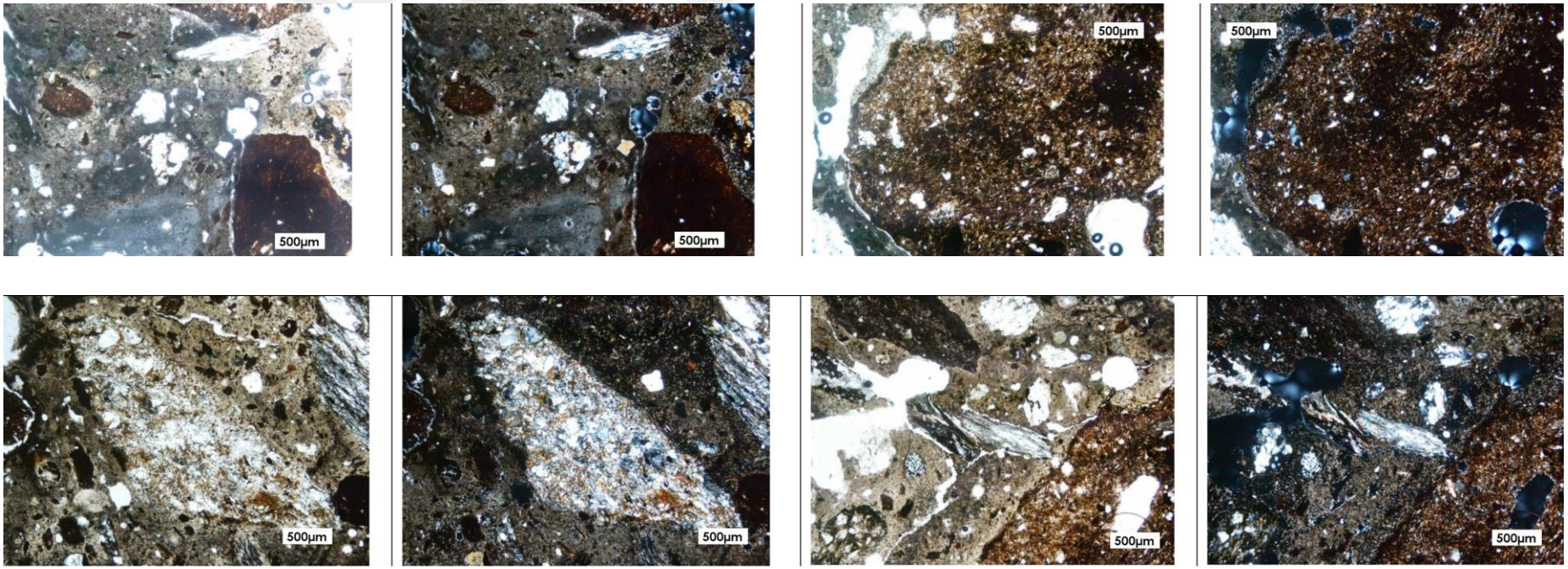


Figure VII.27. Thin section images of sample NM16

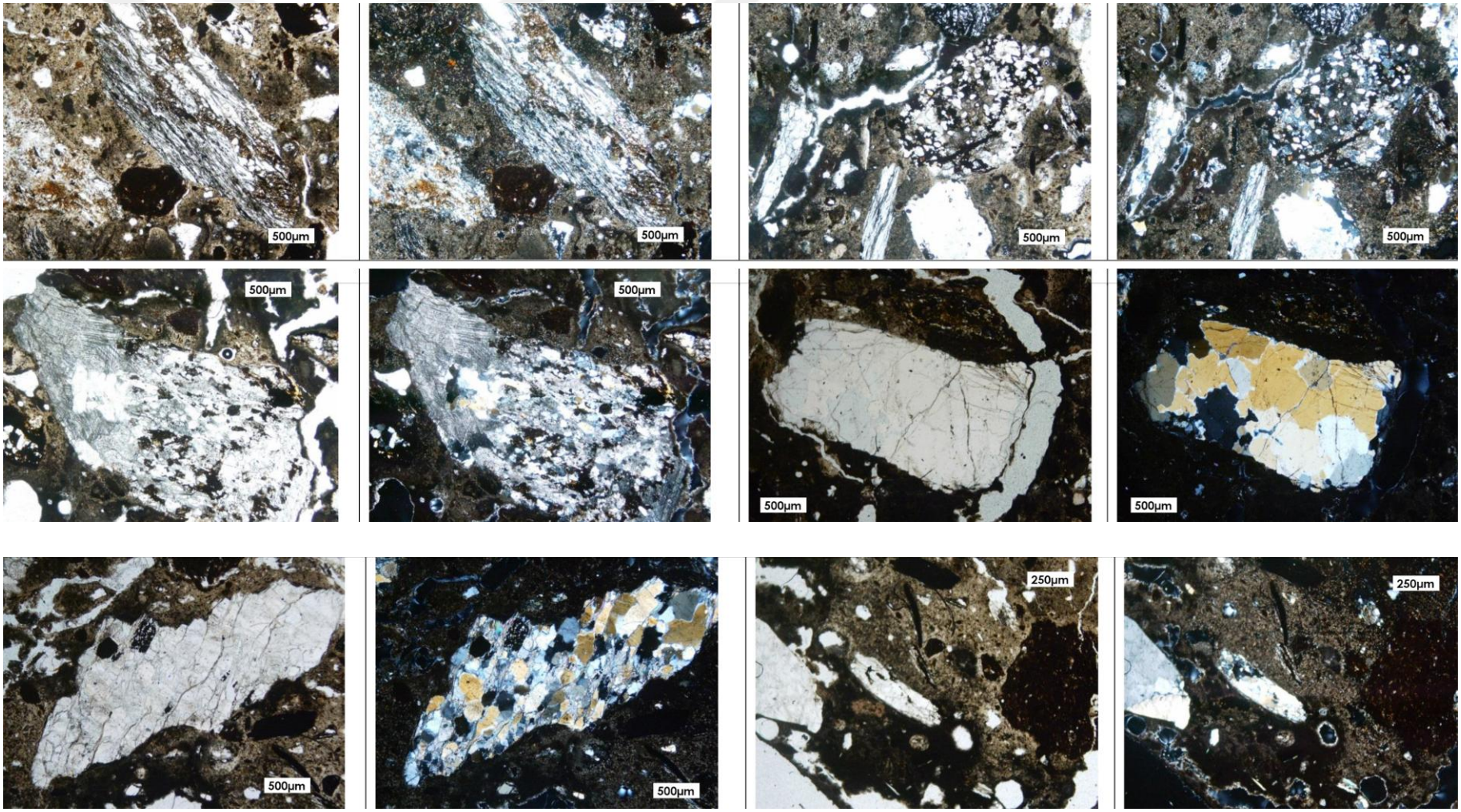
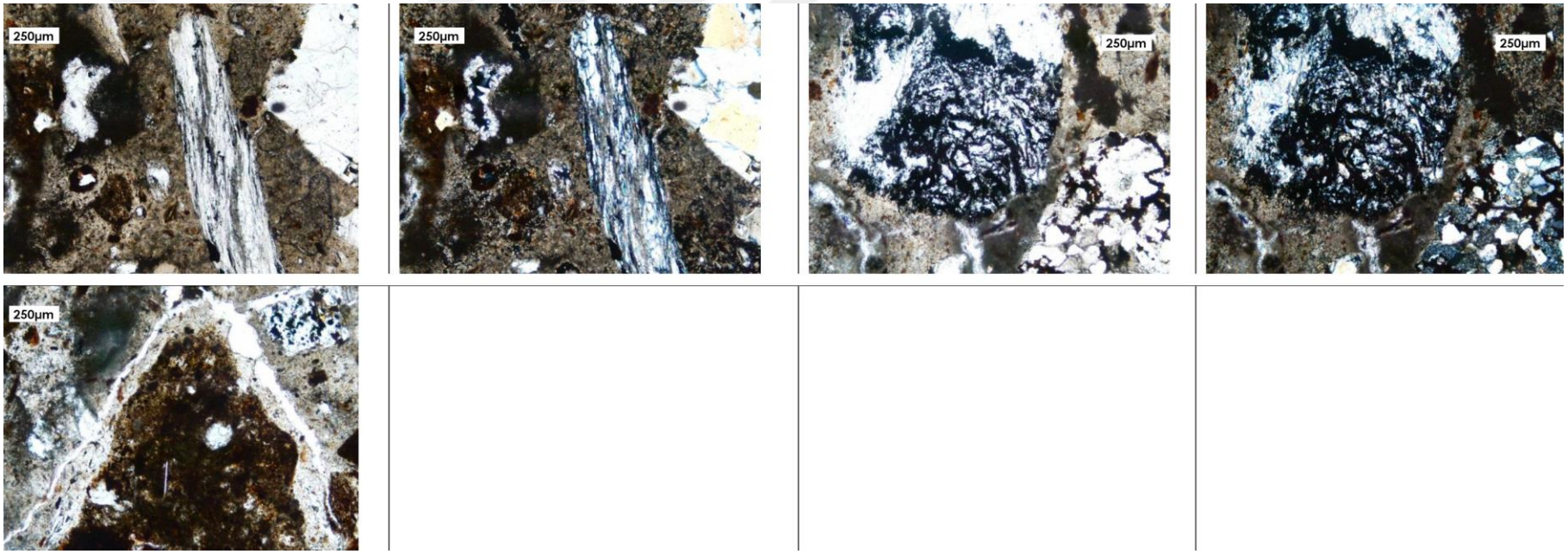
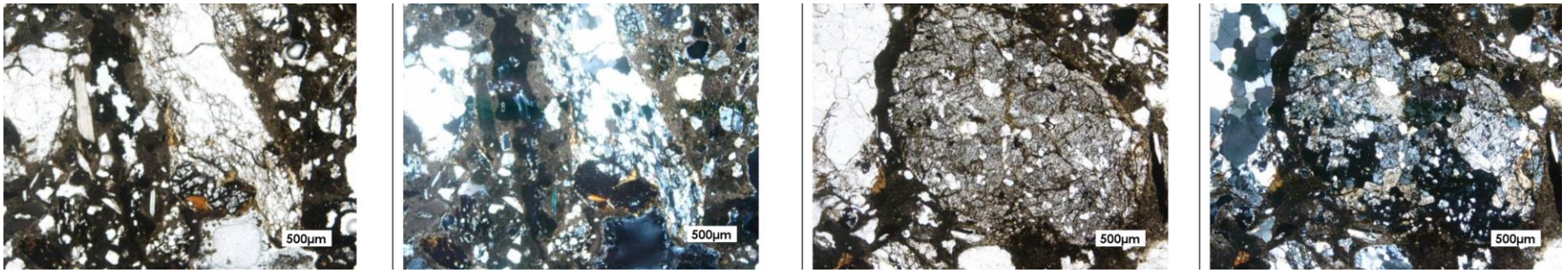


Figure VII.28. Thin section images of sample NM16 (continue)



FigureVII.29. Thin section images of sample NM16 (continue)



FigureVII.30. Thin section images of sample NM22

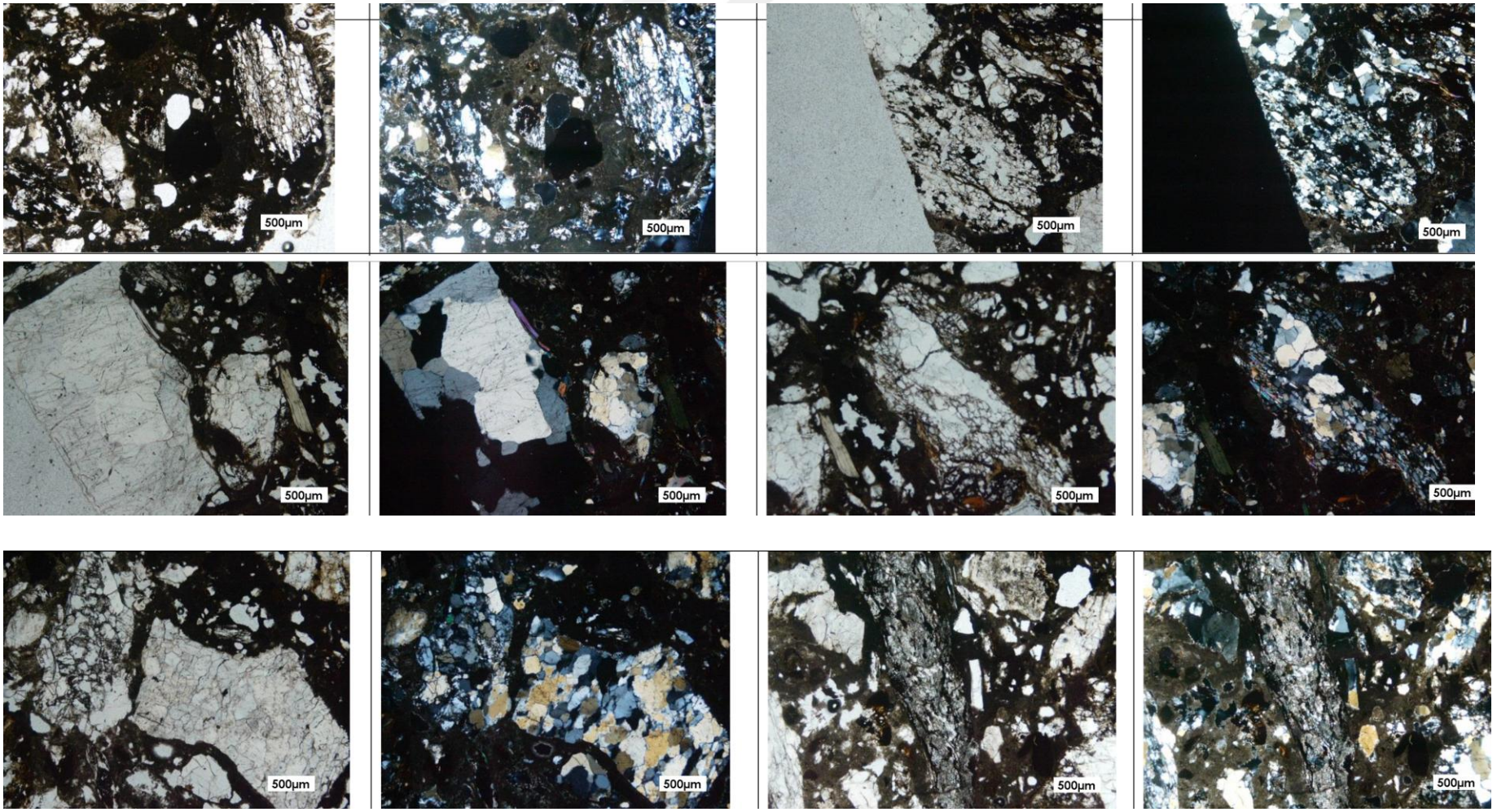


Figure VII.31. Thin section images of sample NM22 (continue)

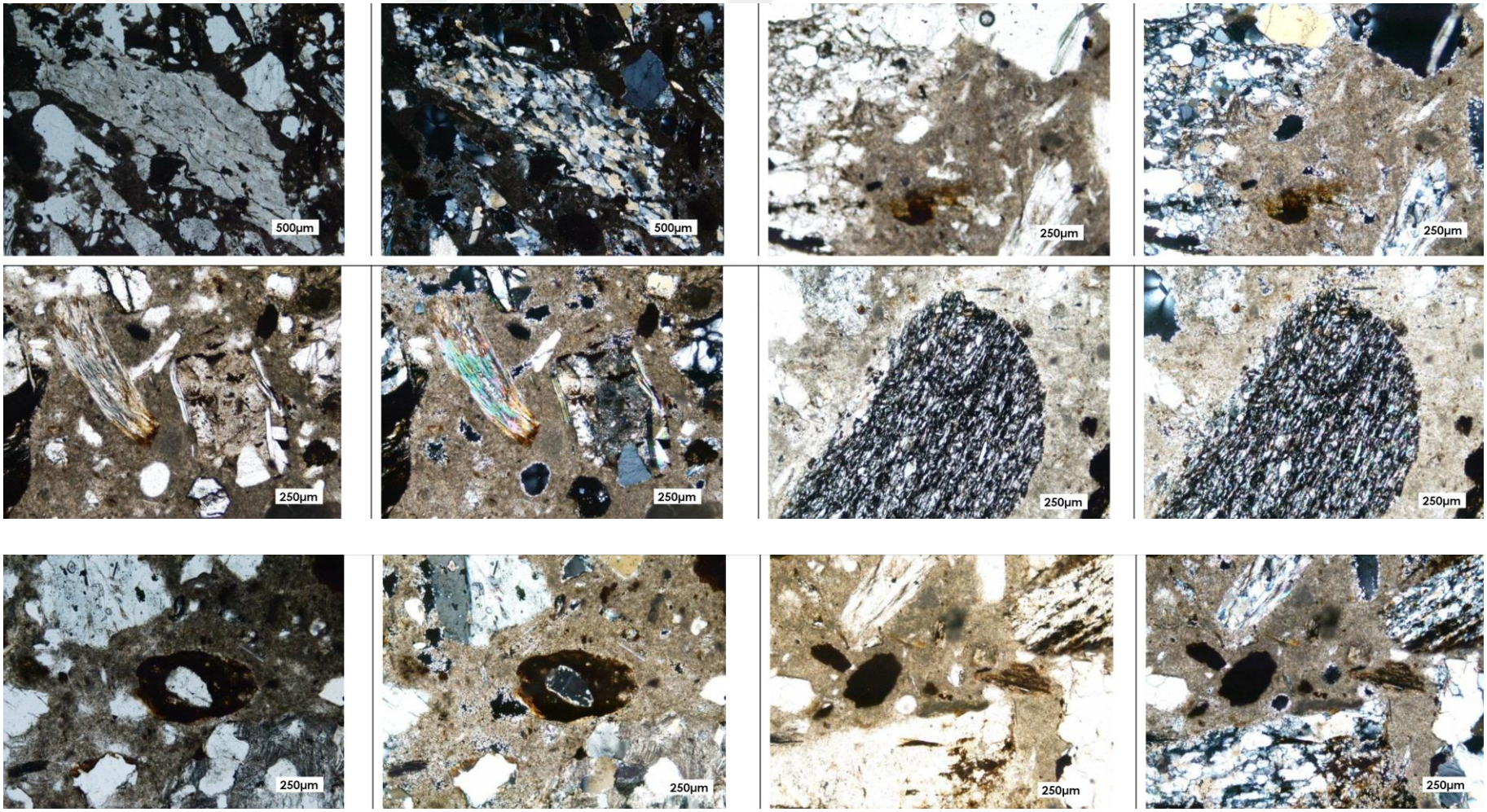


Figure VII.32. Thin section images of sample NM22 (continue)

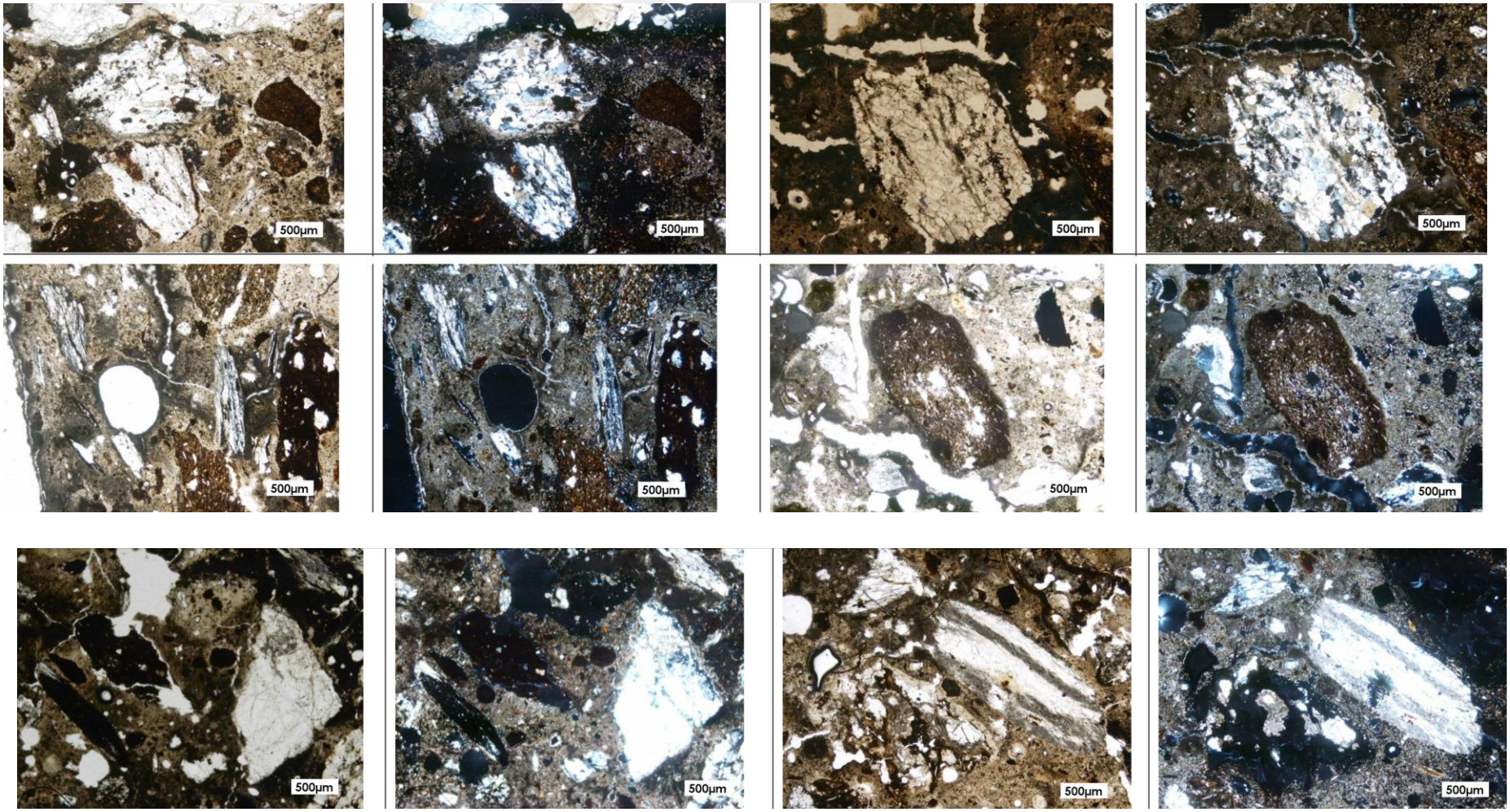


Figure VII.33. Thin section images of sample NM23

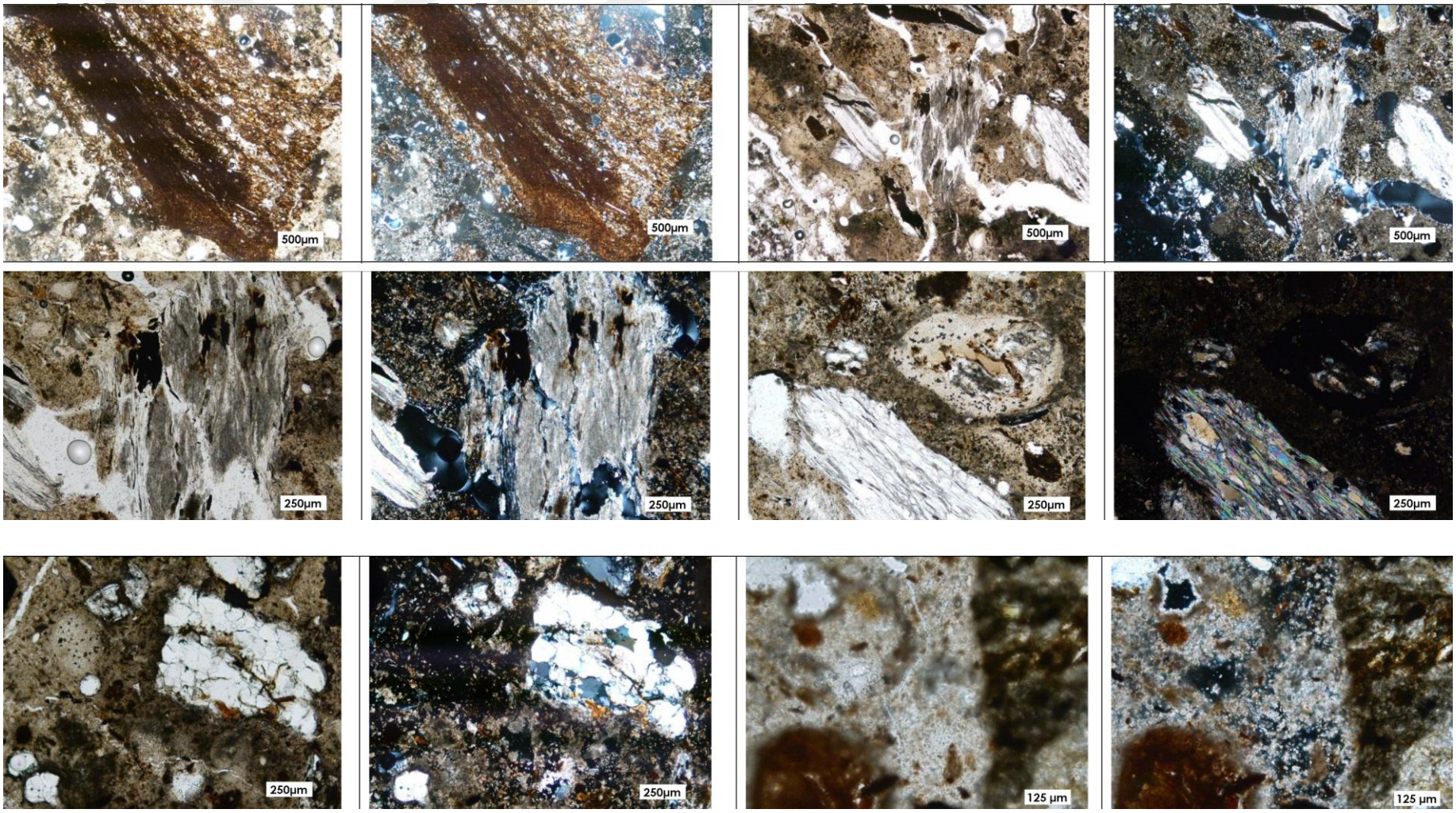


Figure VII.34. Thin section images of sample NM23 (continue)

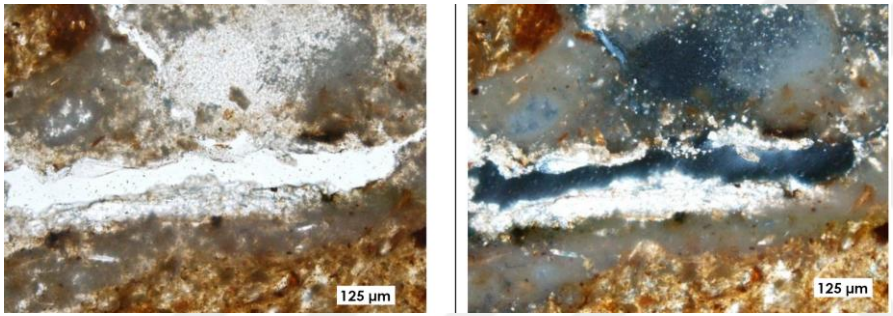


Figure VII.35. Thin section images of sample NM23 (continue)

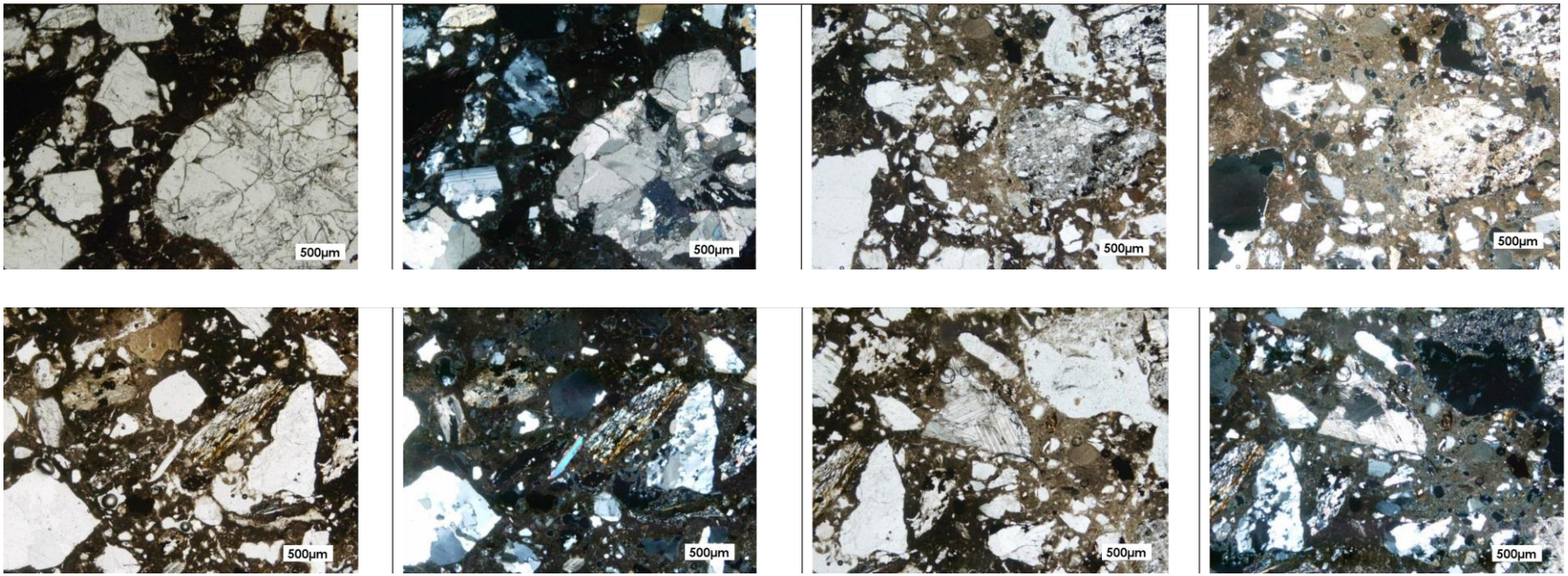


Figure VII.36. Thin section images of sample NM24

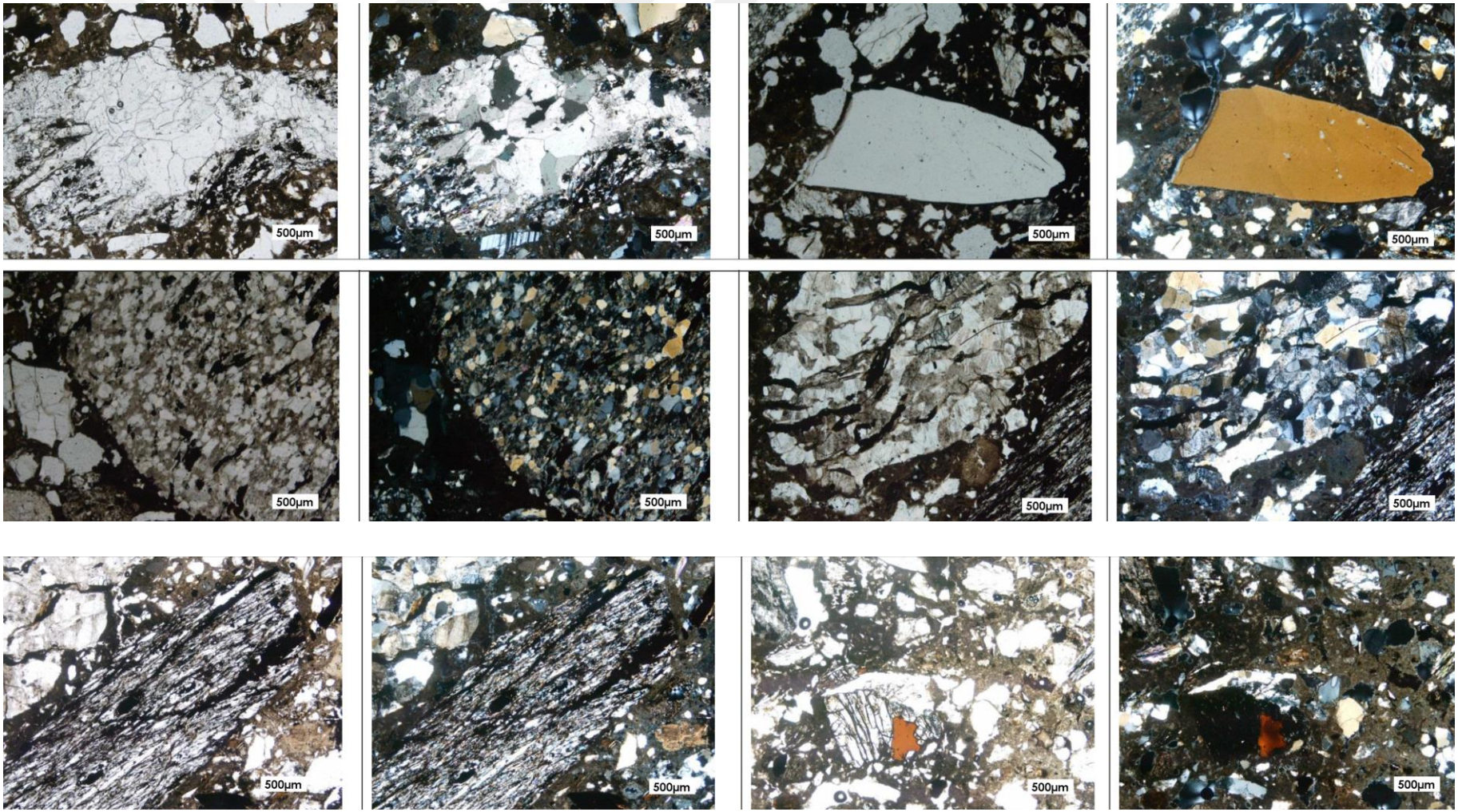


Figure VII.37. Thin section images of sample NM24 (continue)

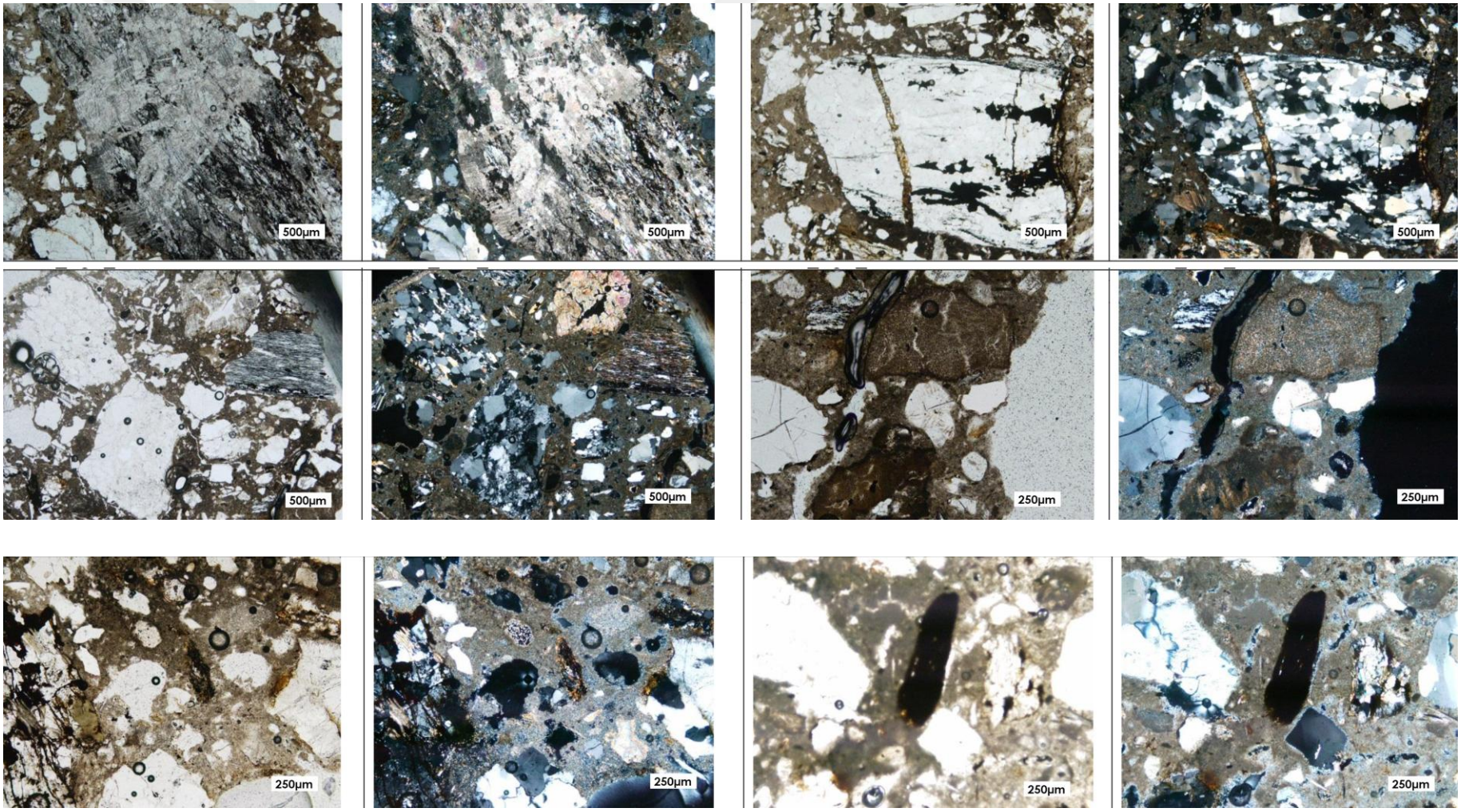


Figure VII.38. Thin section images of sample NM24 (continue)

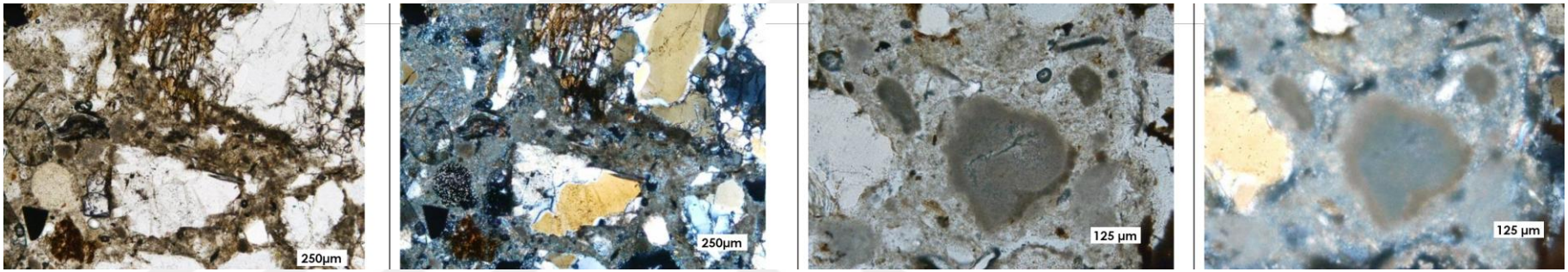


Figure VII.39. Thin section images of sample NM24 (continue)

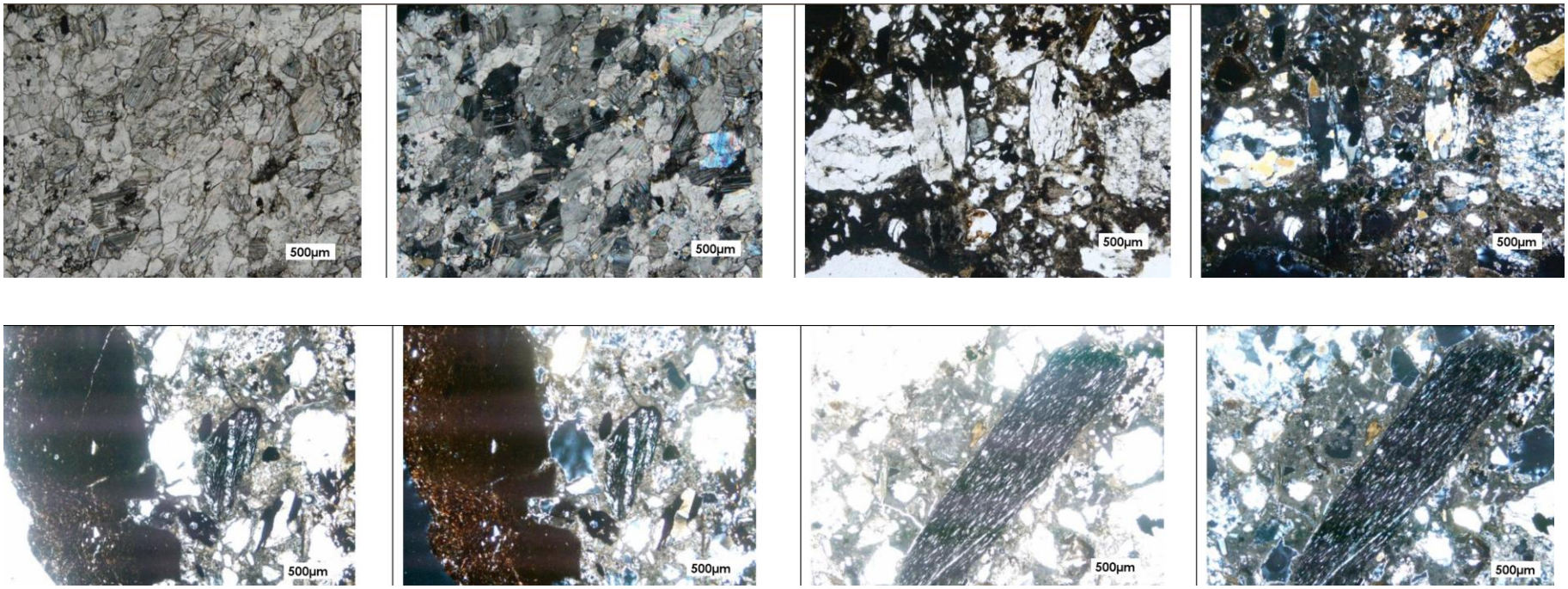


Figure VII.40. Thin section images of sample NM26

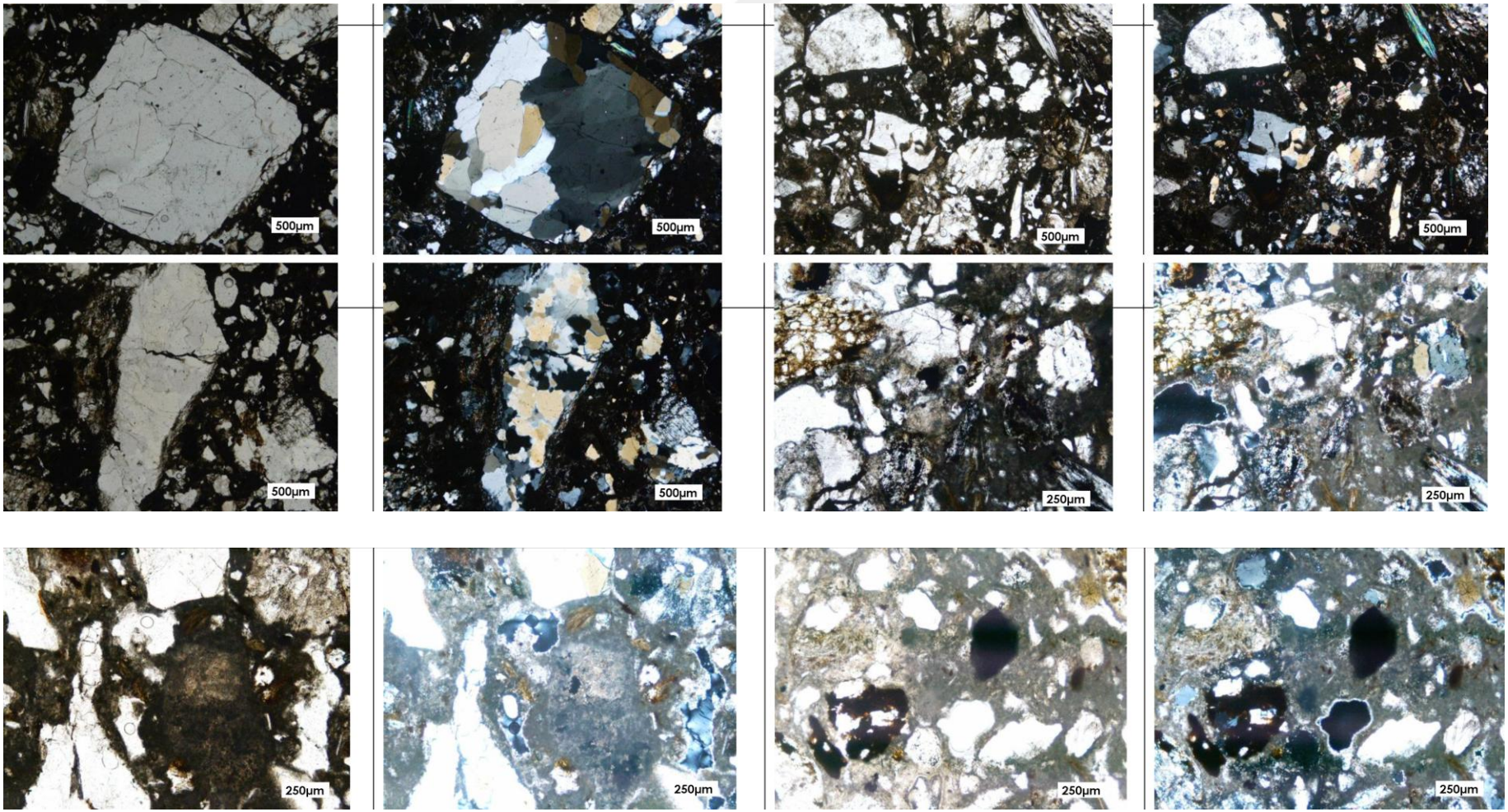


Figure VII.41. Thin section images of sample NM26 (continue)

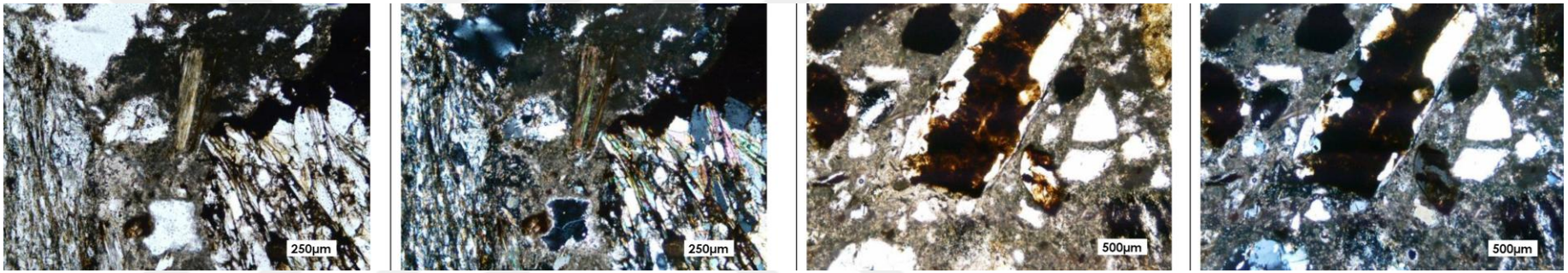


Figure VII.42. Thin section images of sample NM26 (continue)

Appendix VIII- Sanctuary of Labraunda

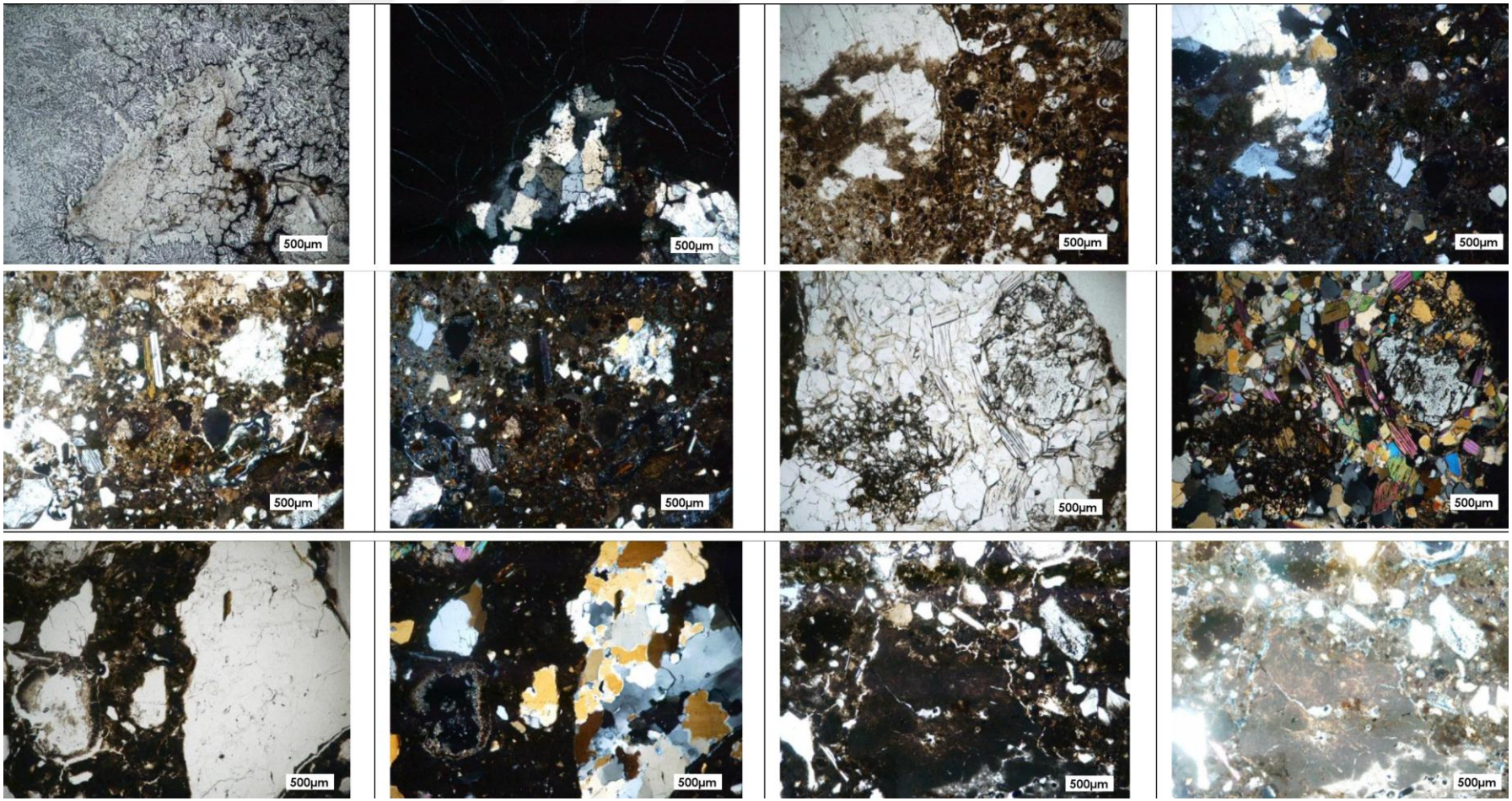


Figure VIII.1. Thin section images of sample LM01A

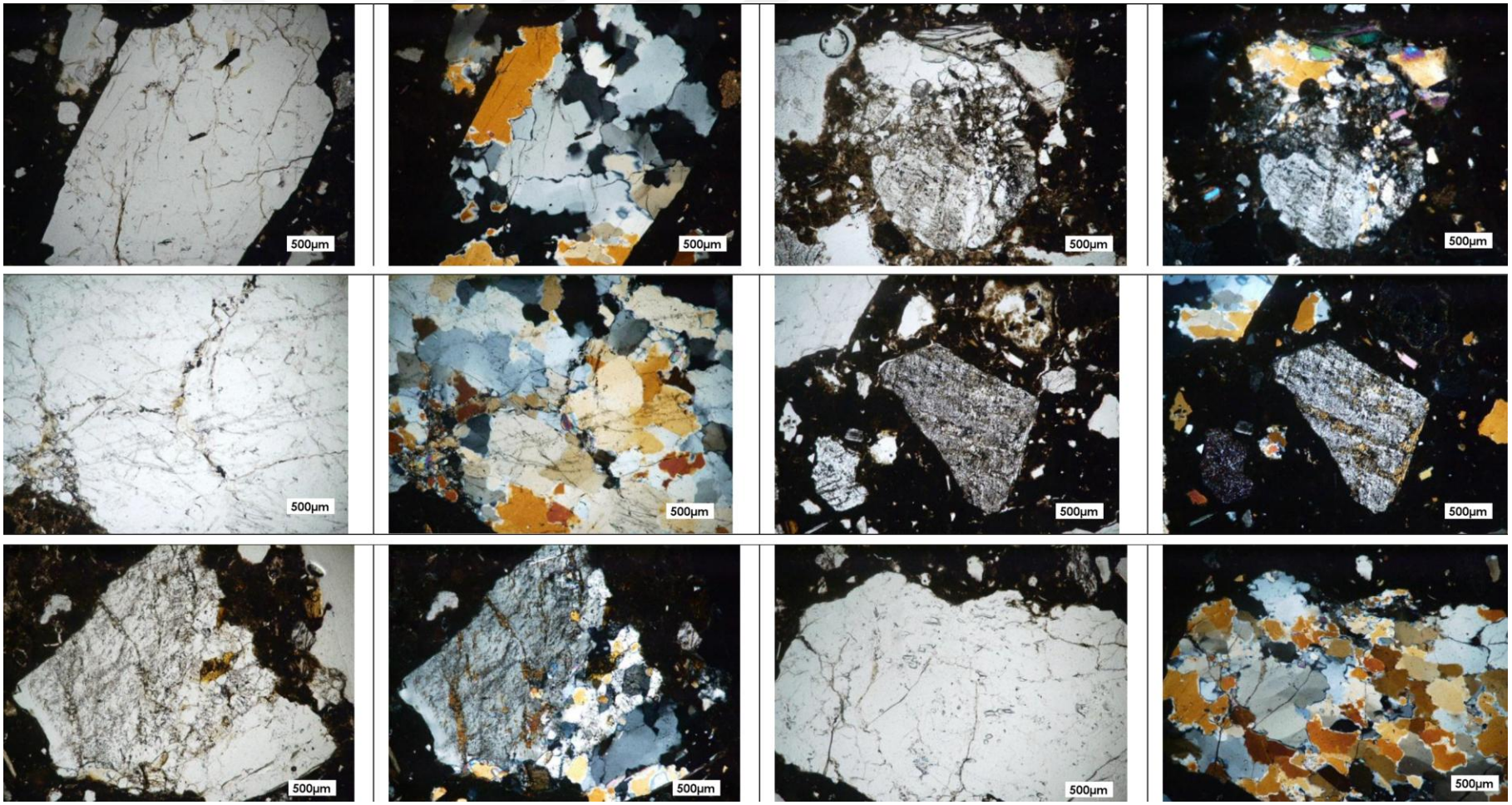


Figure VIII.2. Thin section images of sample LM01A (continue)

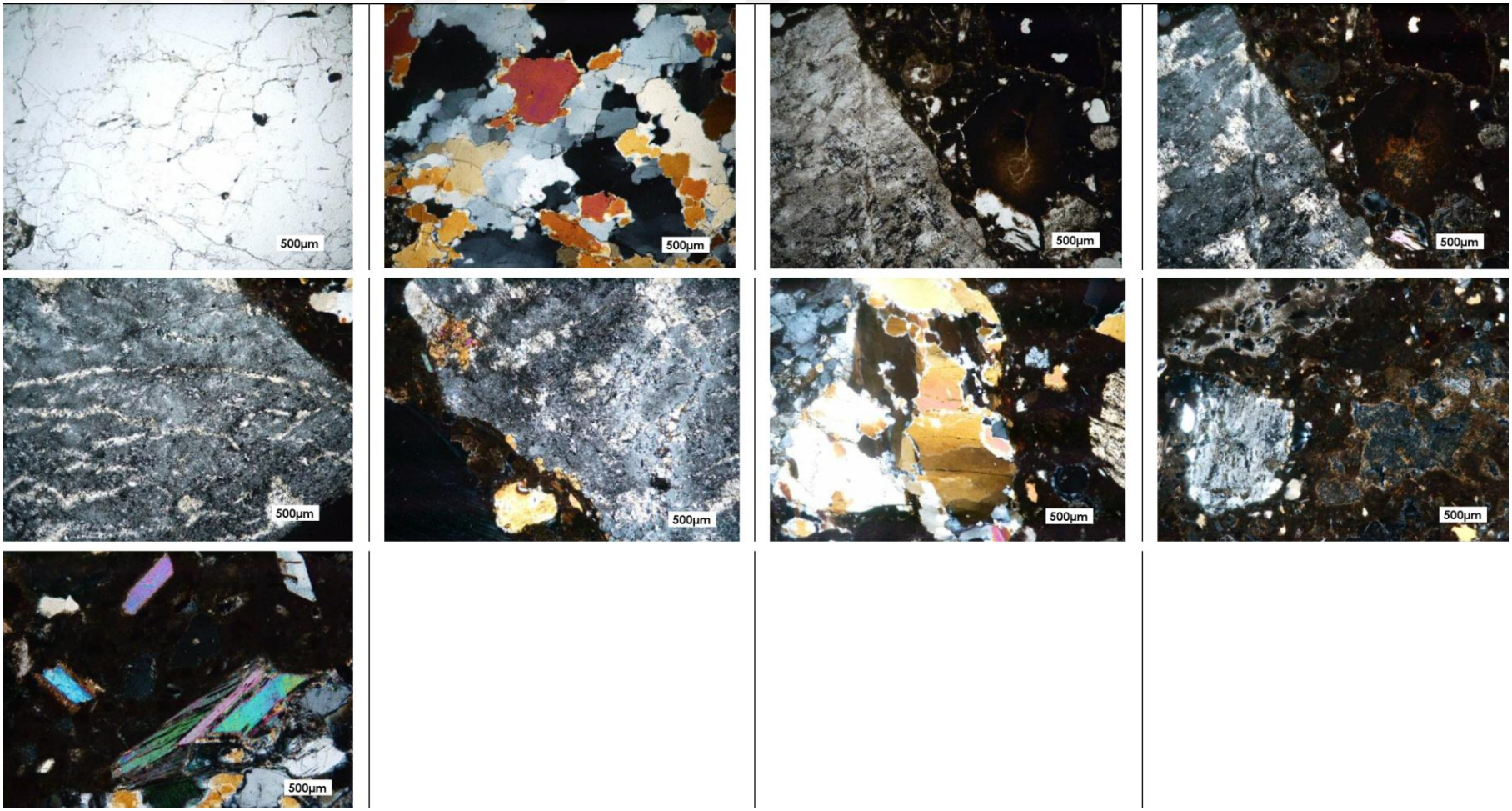


Figure VIII.3. Thin section images of sample LM01A (continue)

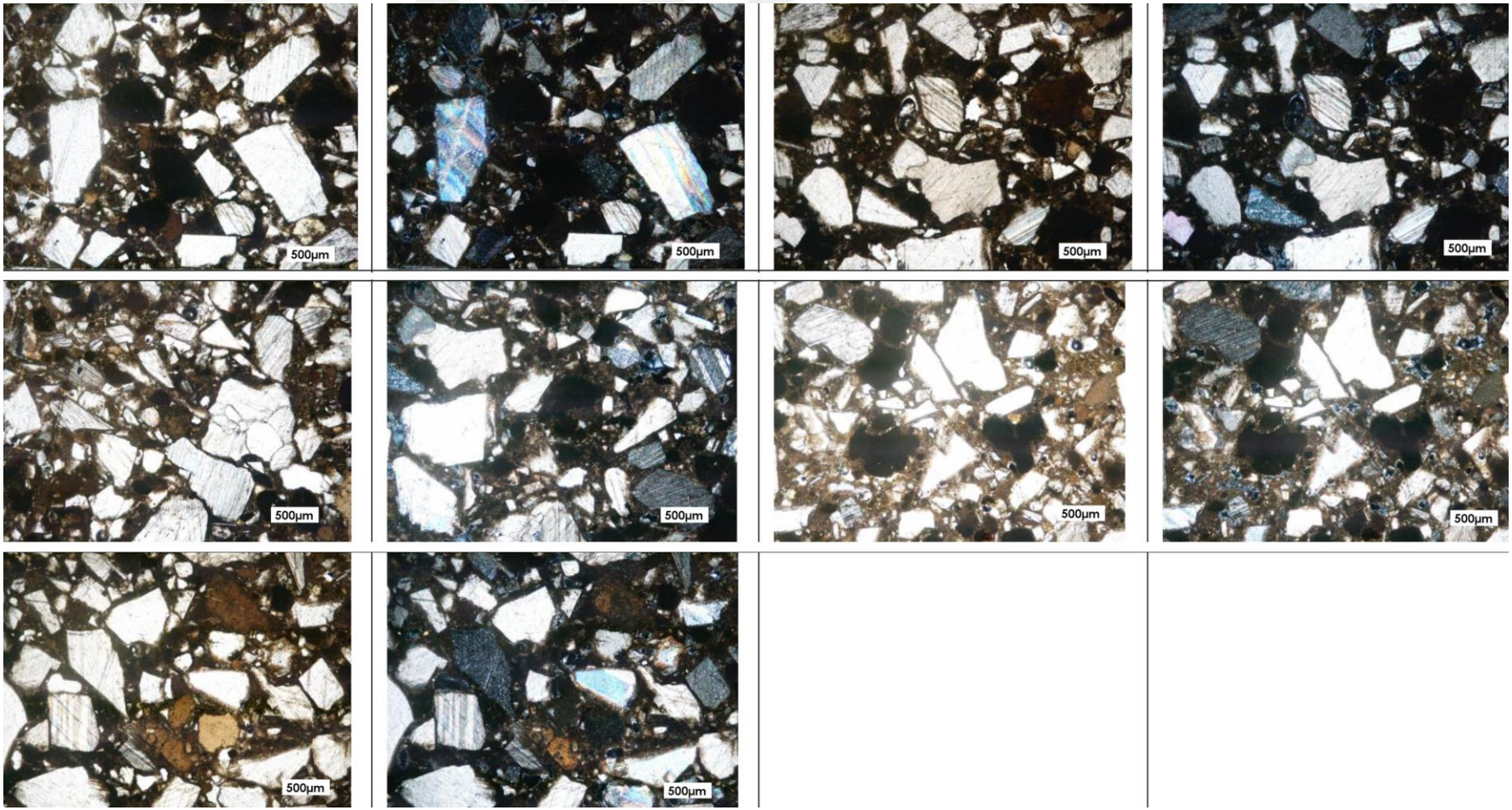


Figure VIII.4. Thin section images of sample LM01C

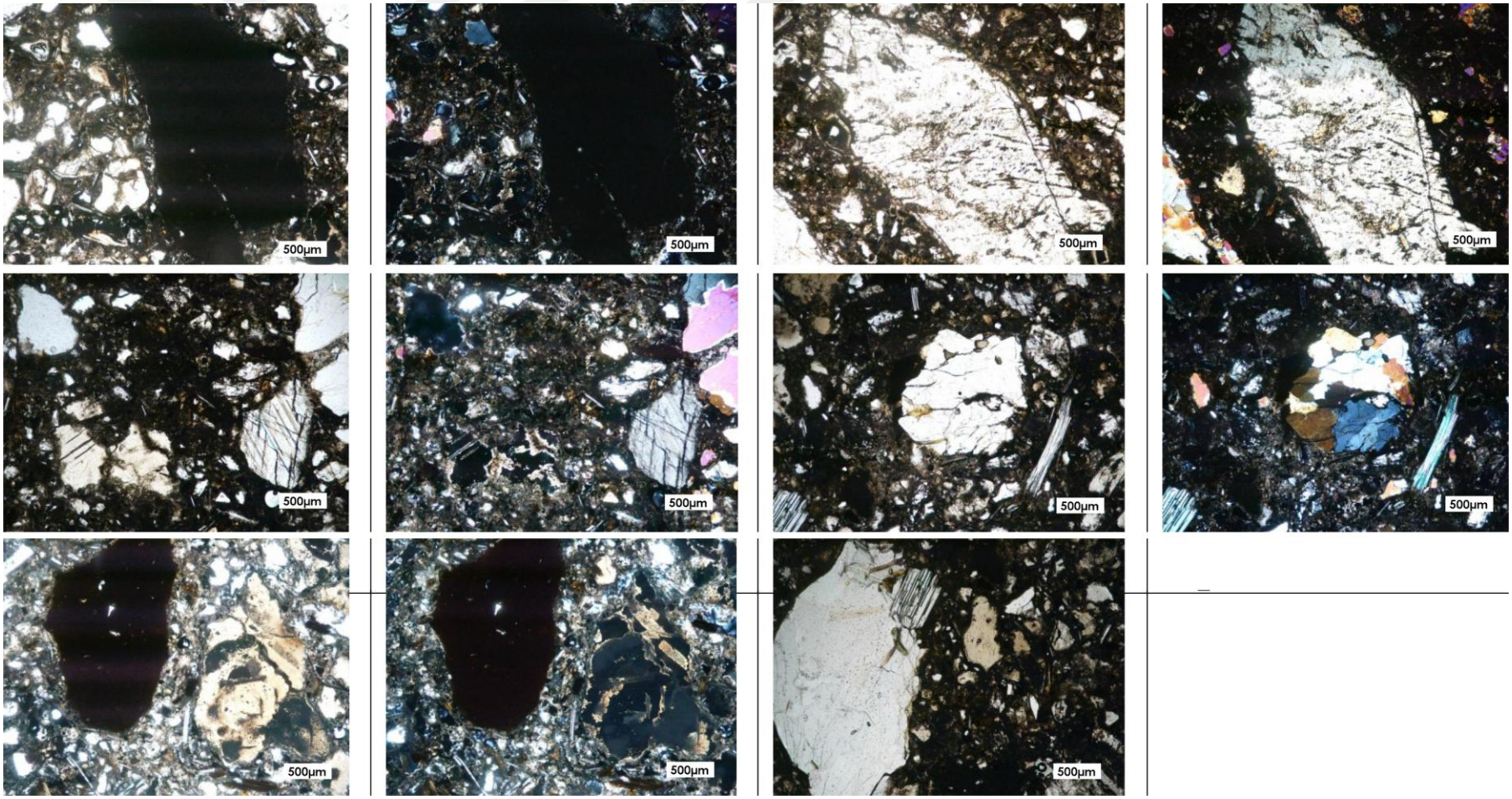


Figure VIII.5. Thin section images of sample LM02

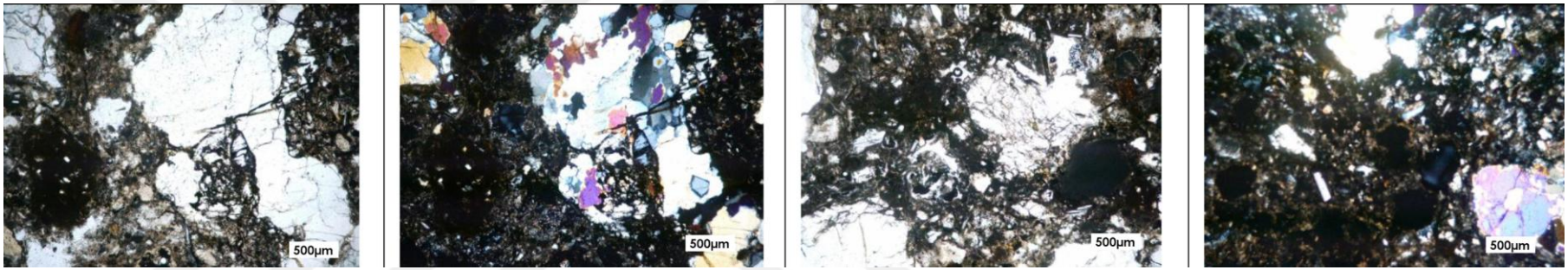


Figure VIII.6. Thin section images of sample LM02 (continue)

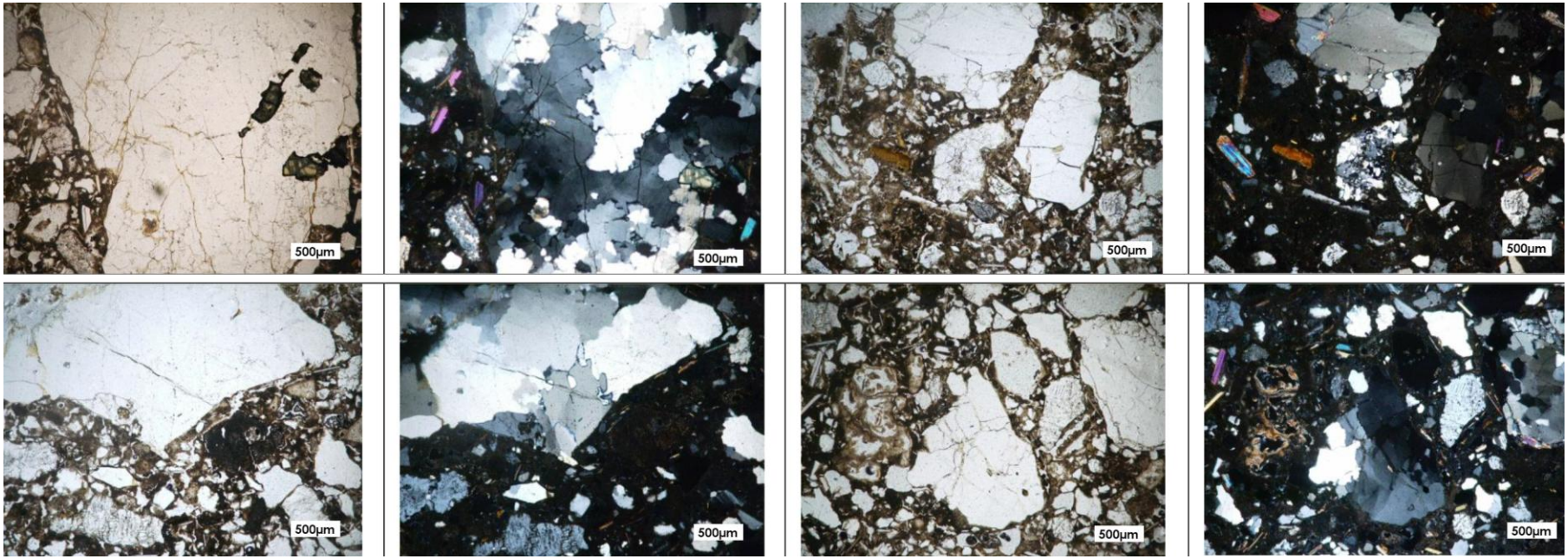


Figure VIII.7. Thin section images of sample LM04A

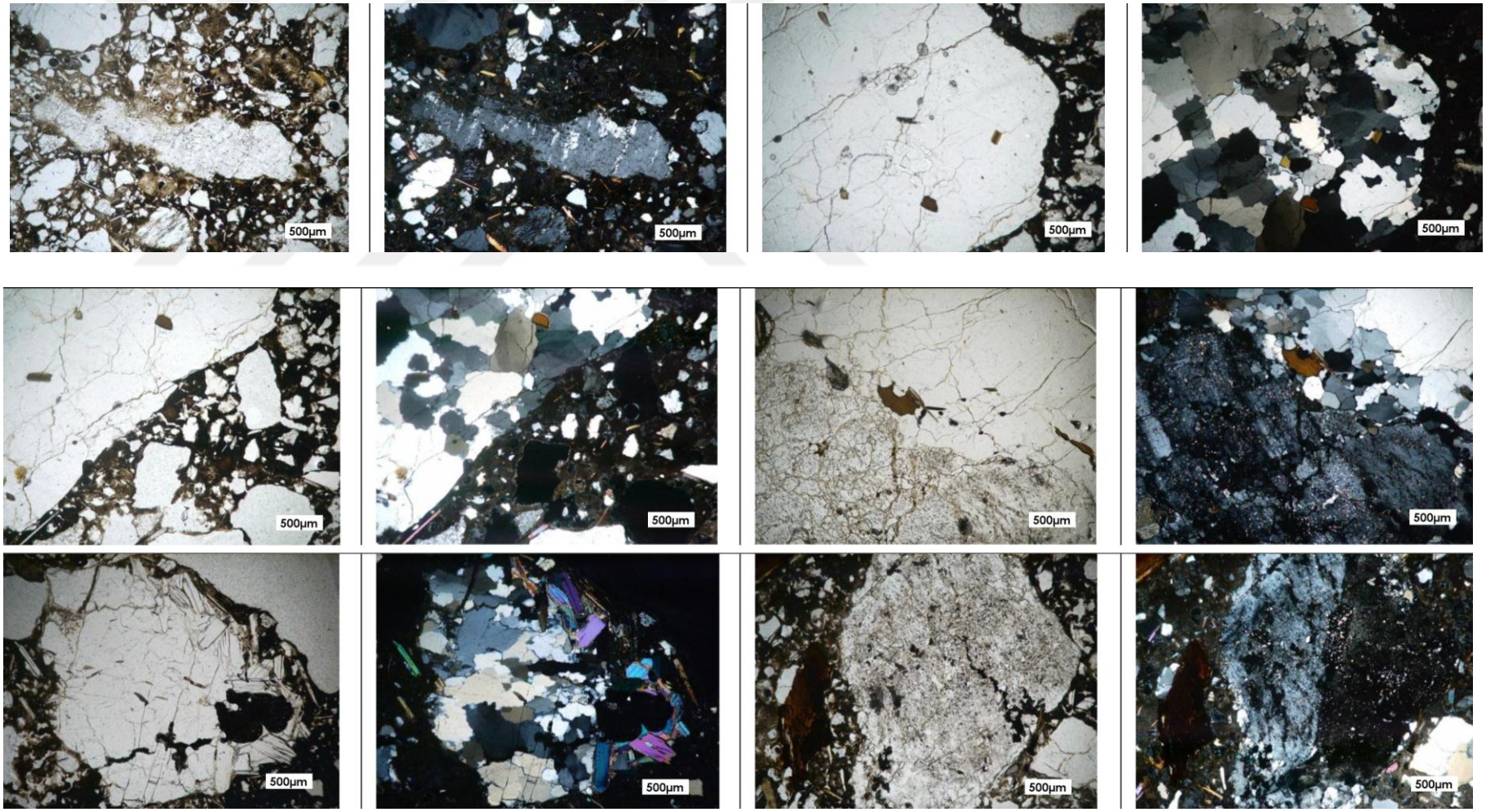


Figure VIII.8. Thin section images of sample LM04A (continue)

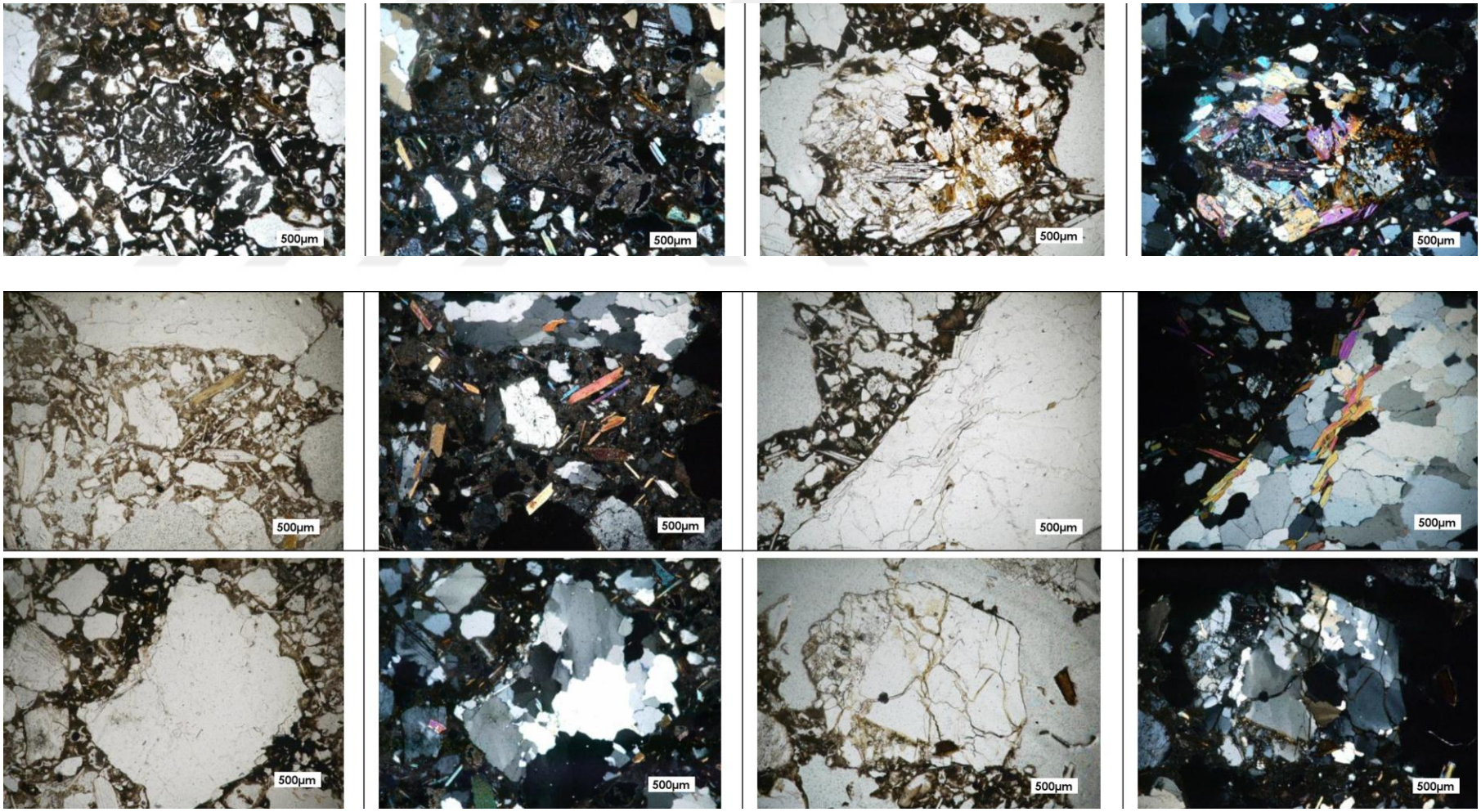


Figure VIII.9. Thin section images of sample LM04A (continue)

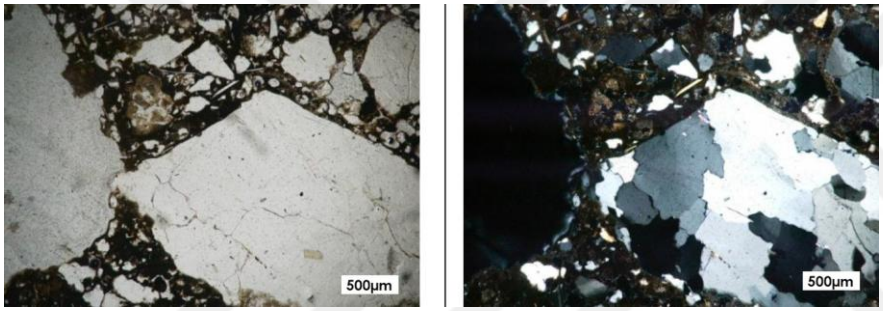


Figure VIII.10. Thin section images of sample LM04A (continue)

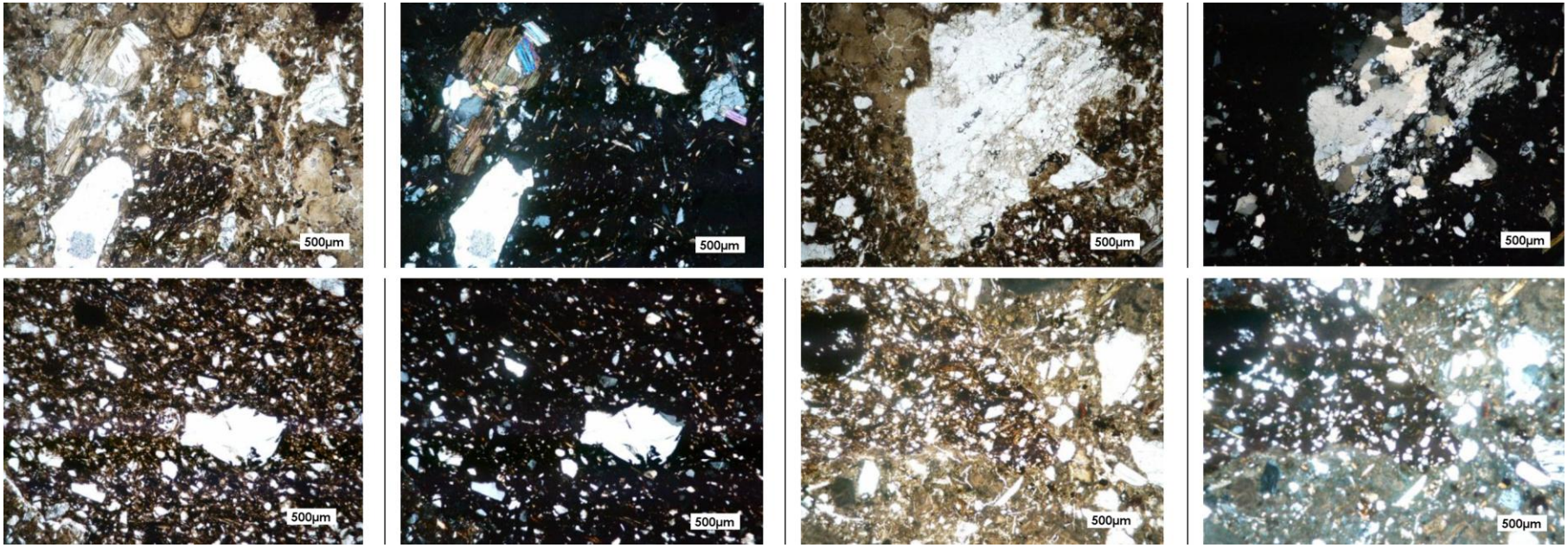


Figure VIII.11. Thin section images of sample LM04B

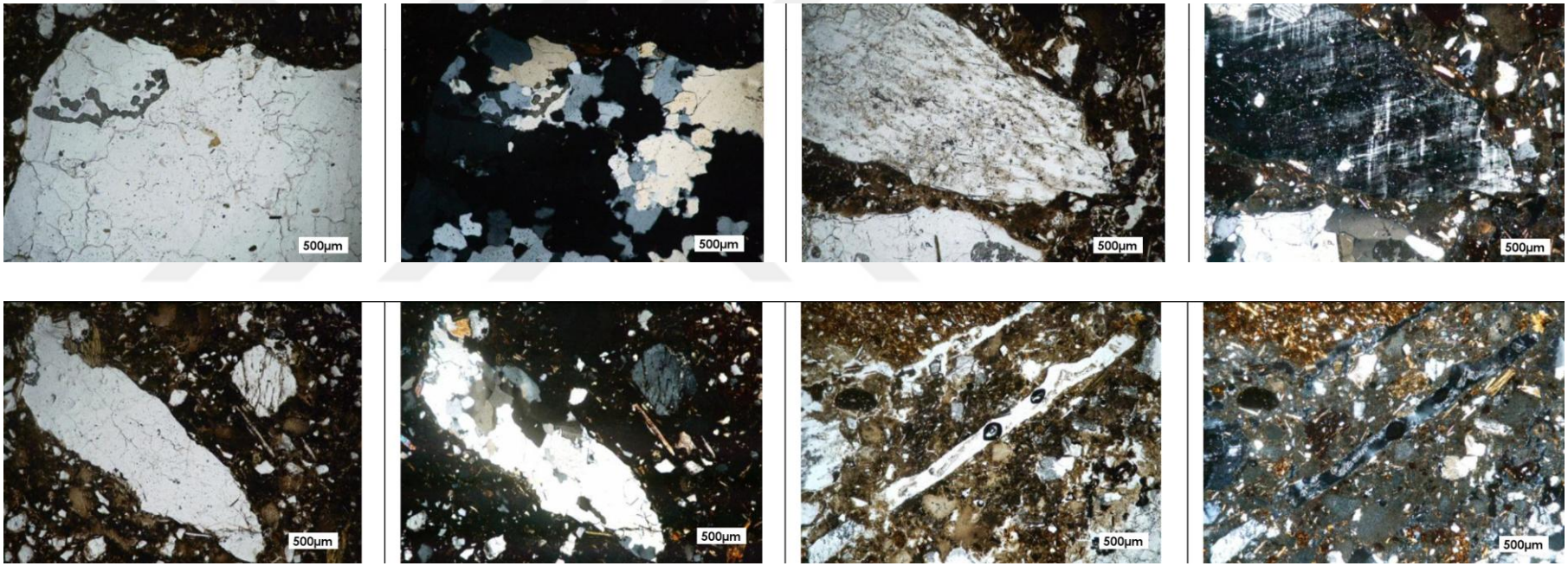


Figure VIII.12. Thin section images of sample LM04B (continue)

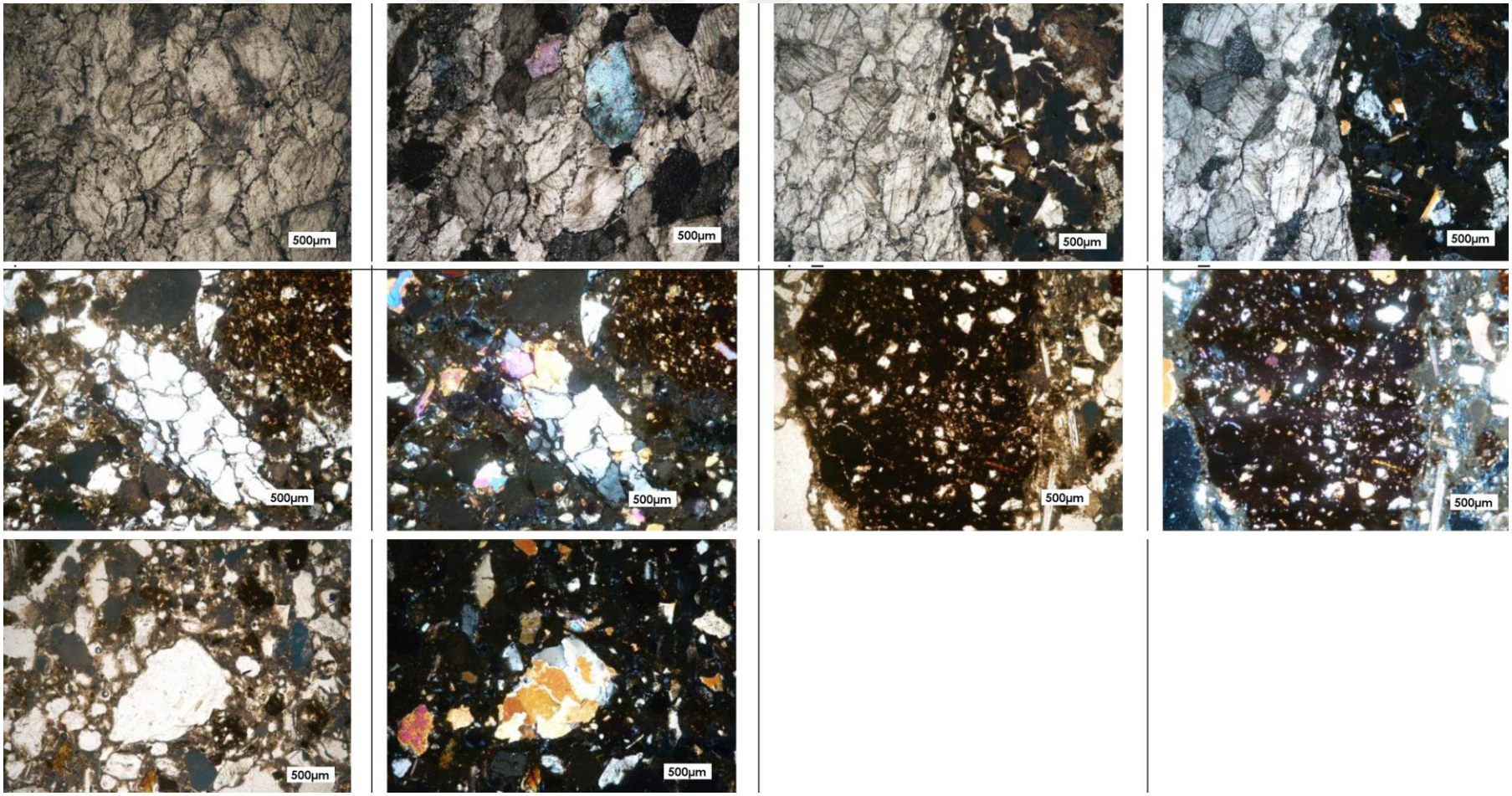


Figure VIII.13. Thin section images of sample LM05

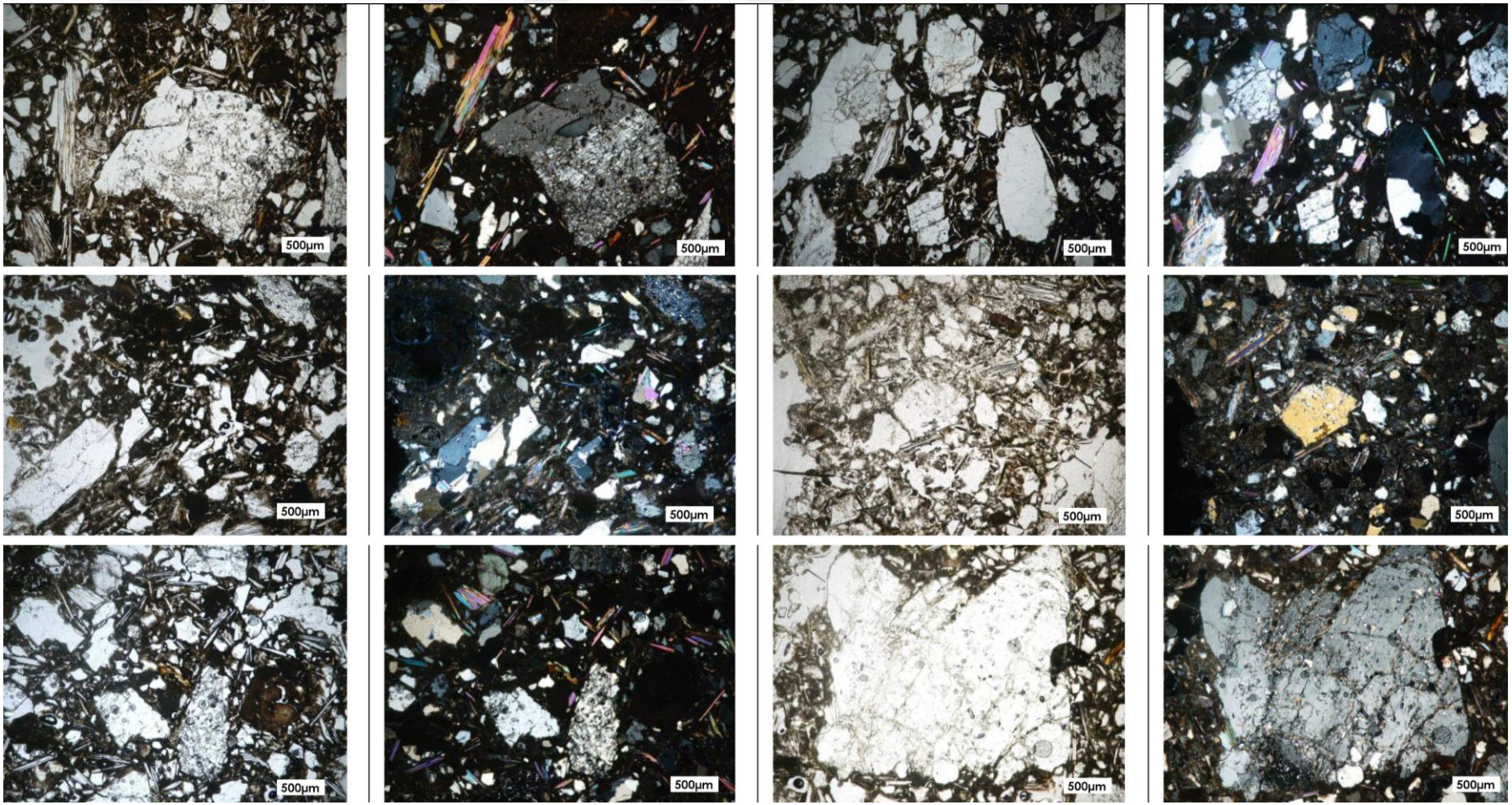


Figure VIII.14. Thin section images of sample LM05 (continue)

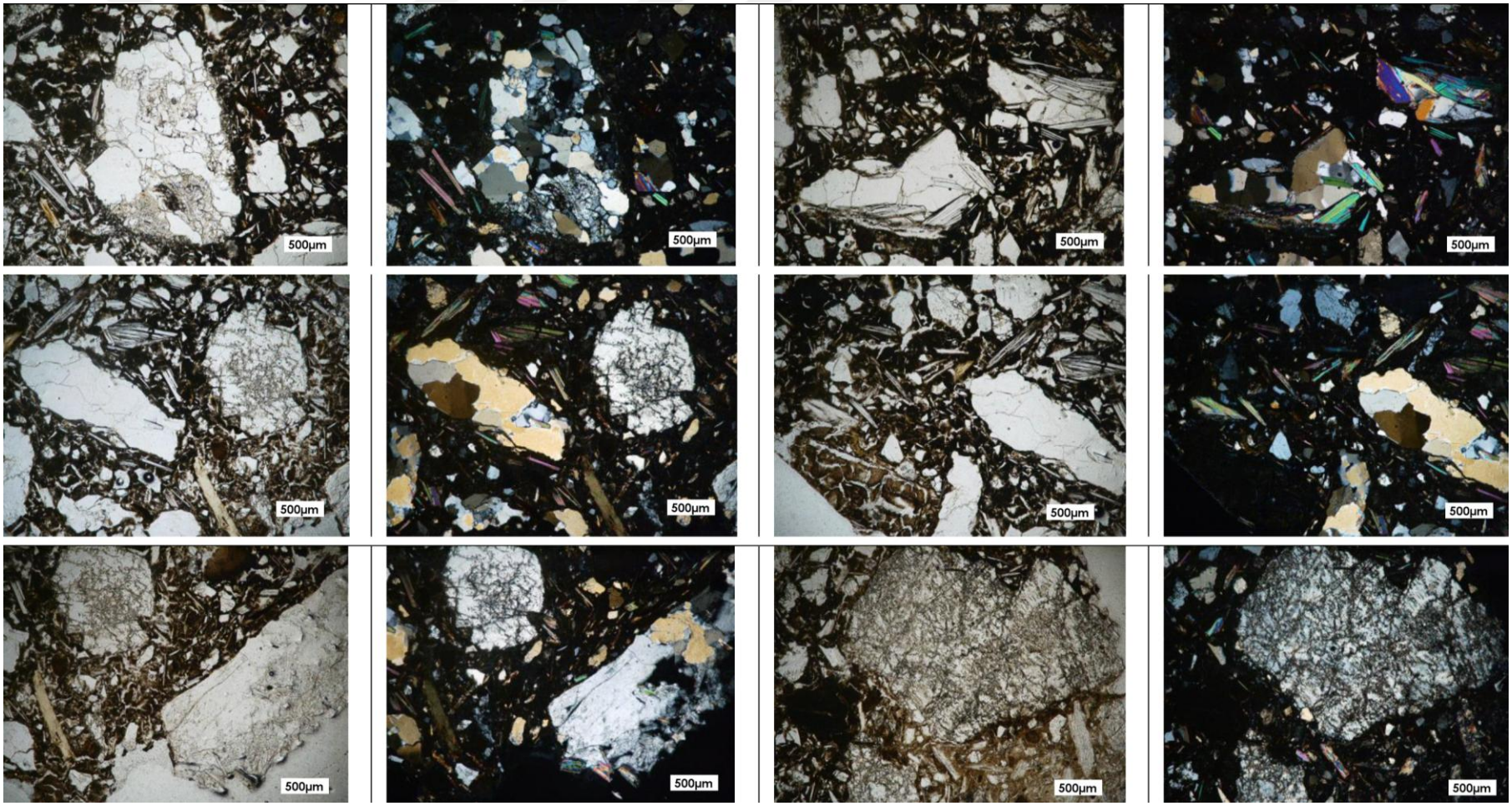


Figure VIII.15. Thin section images of sample LM05 (continue)

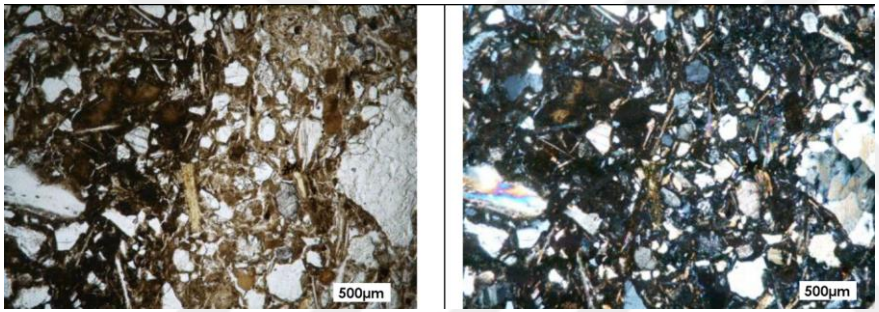


Figure VIII.16. Thin section images of sample LM05 (continue)

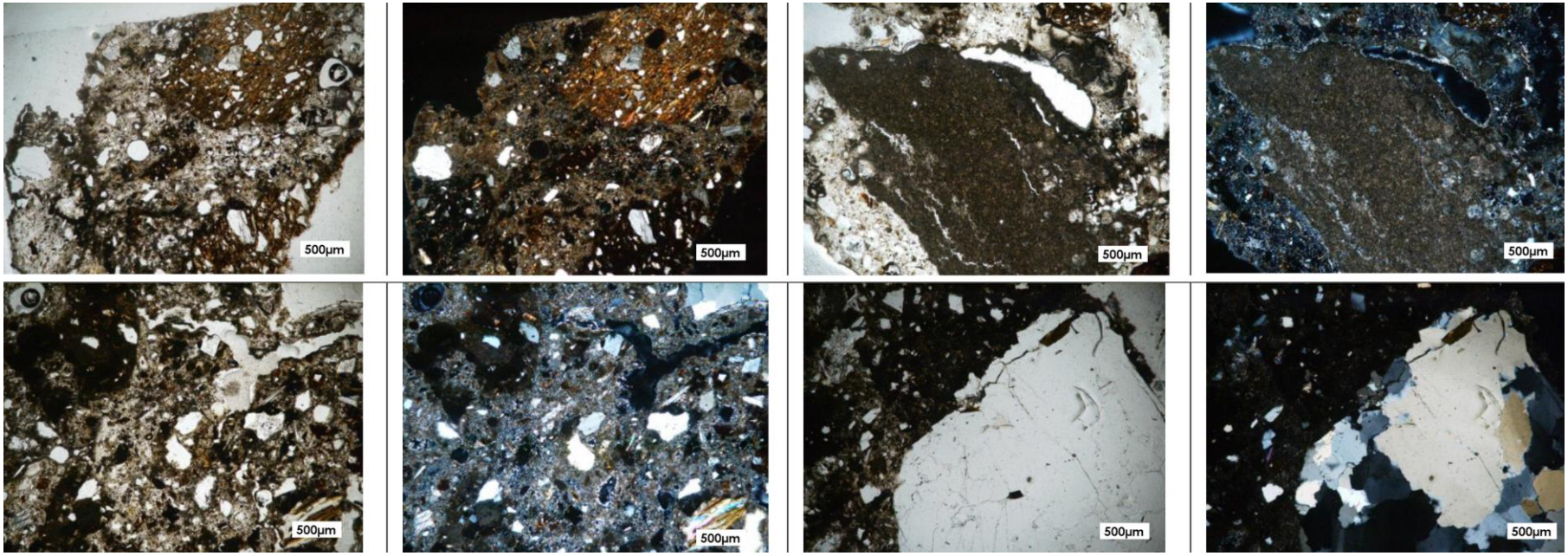


Figure VIII.17. Thin section images of sample LM06C

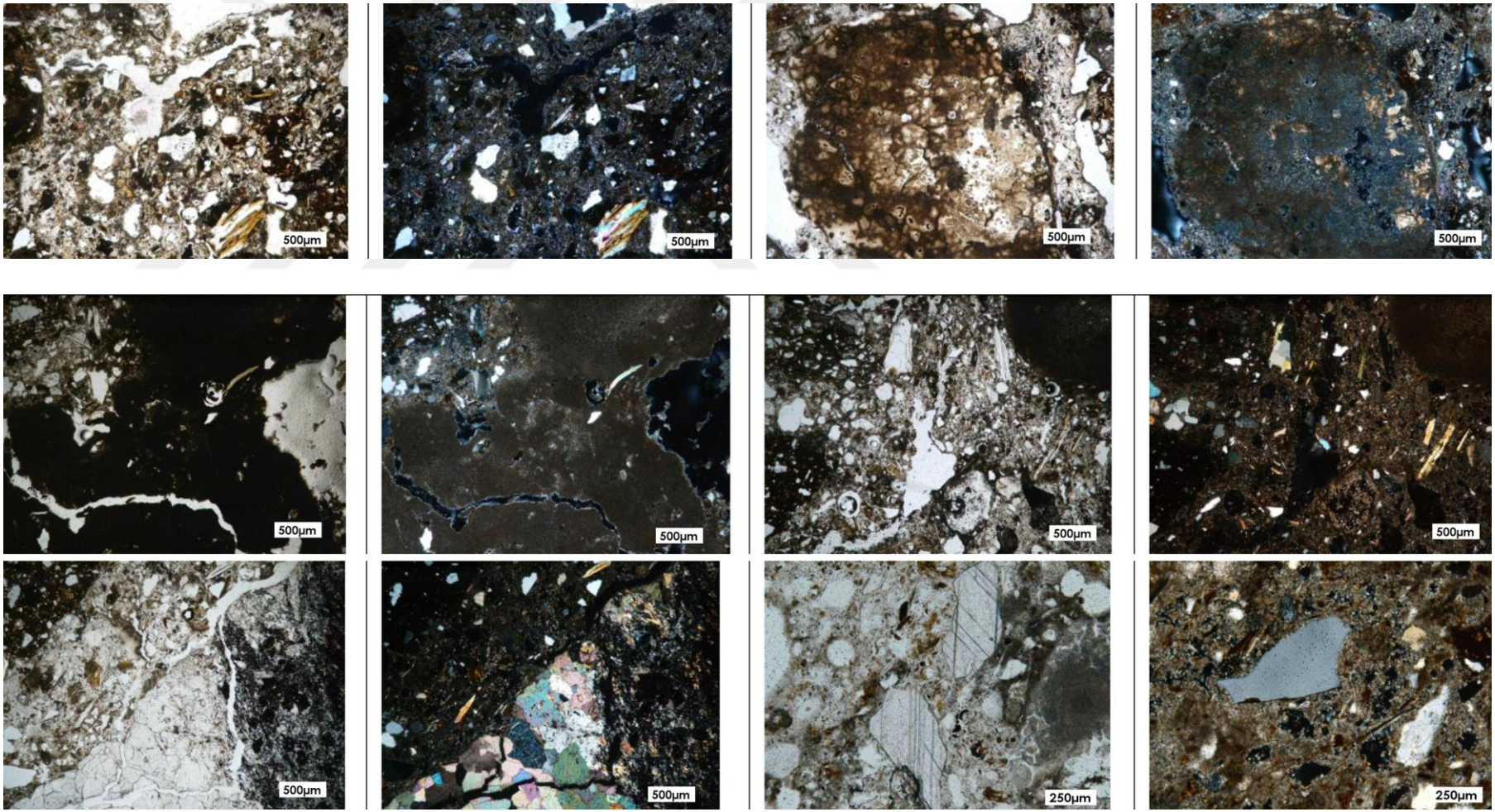


Figure VIII.18. Thin section images of sample LM06C (continue)

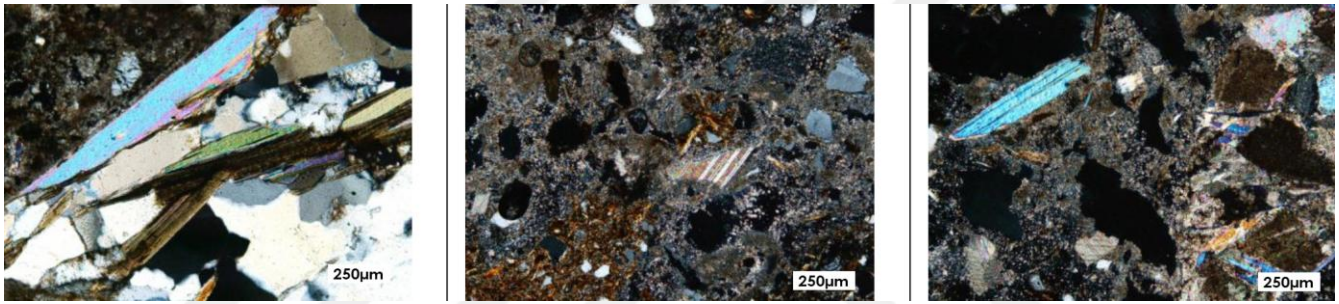


Figure VIII.19. Thin section images of sample LM06C (continue)

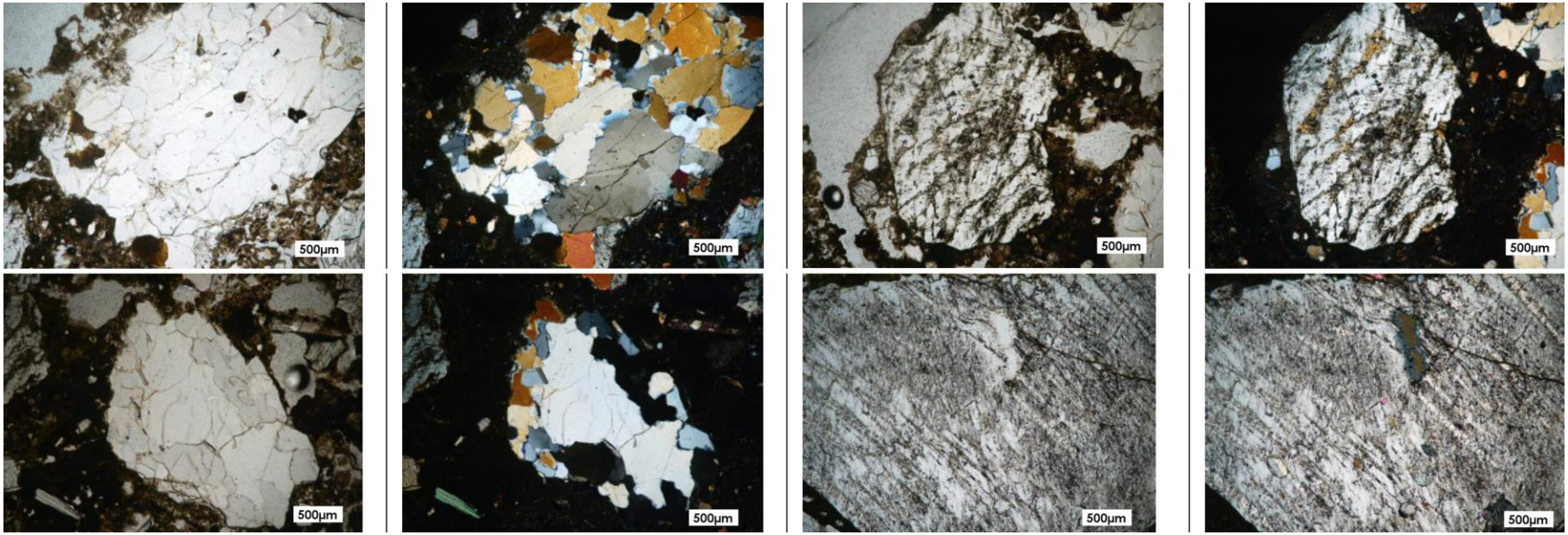


Figure VIII.20. Thin section images of sample LM07A

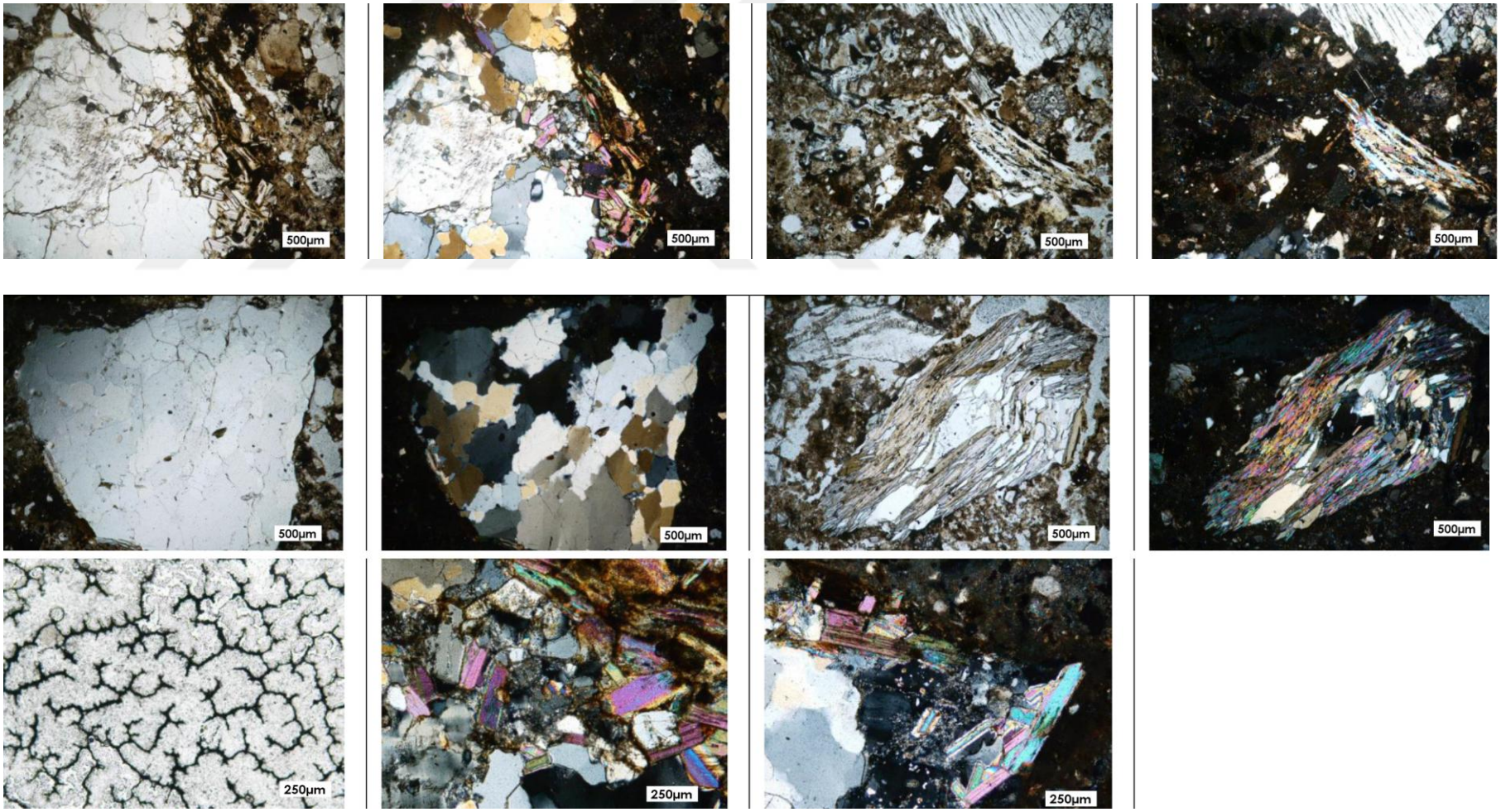


Figure VIII.21. Thin section images of sample LM07A (continue)

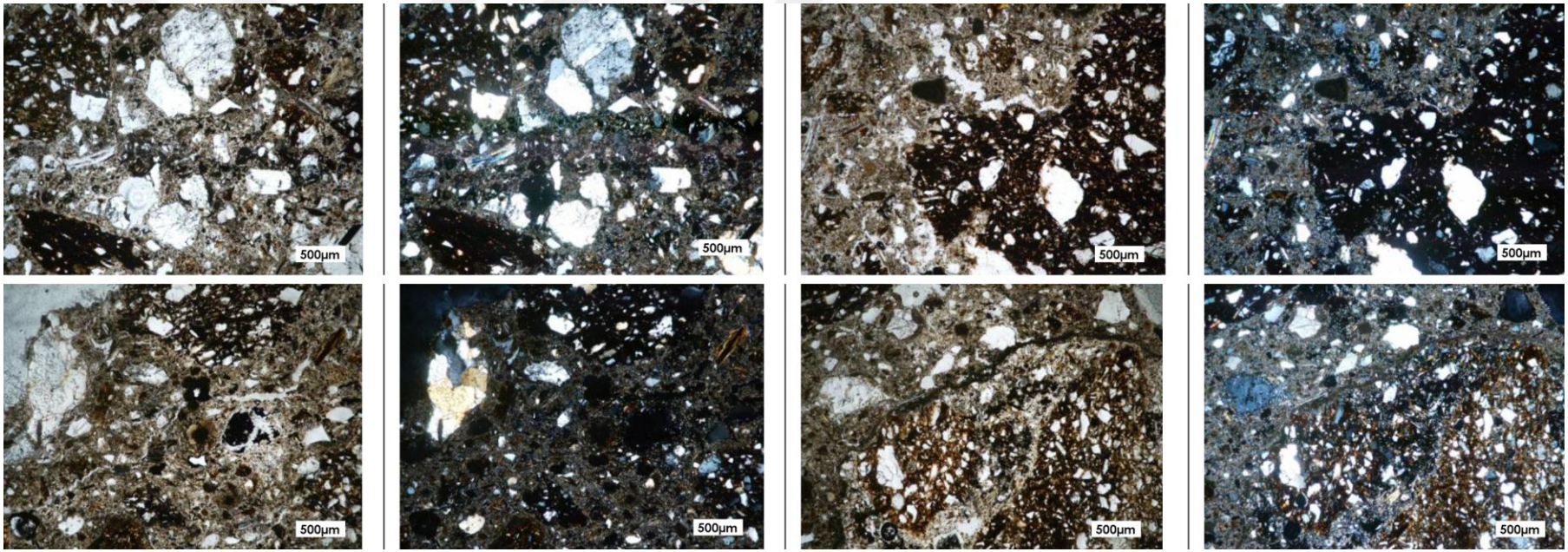


Figure VIII.22. Thin section images of sample LM07B

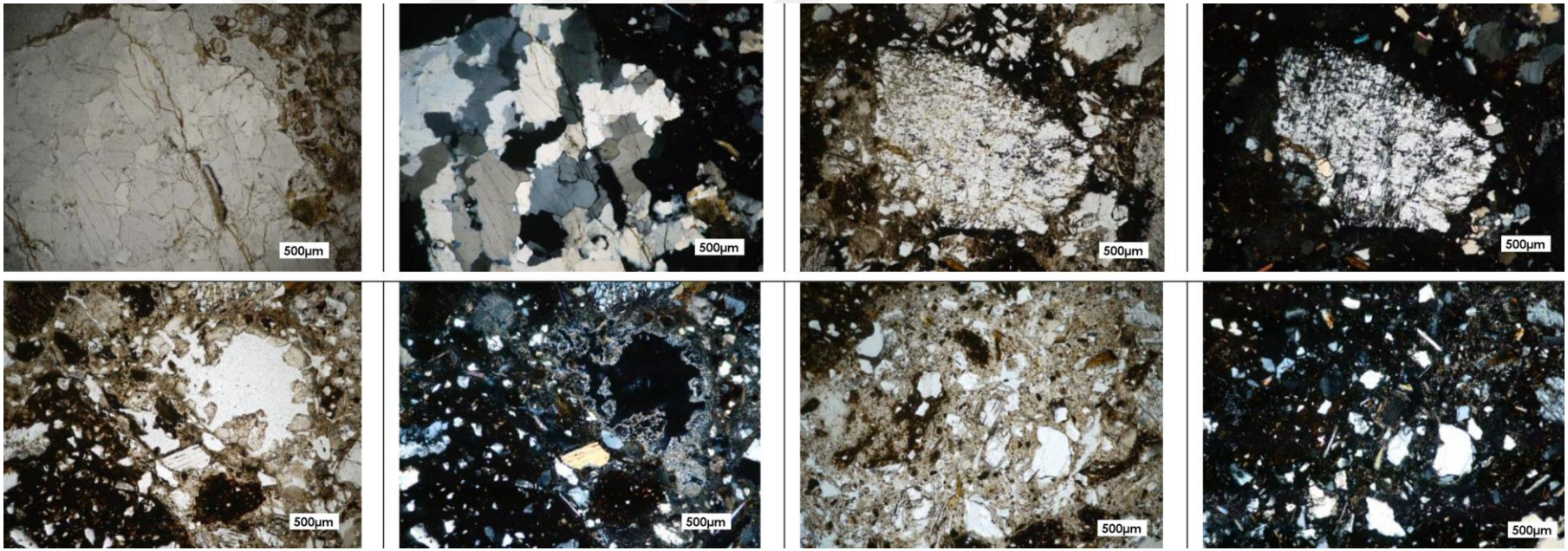


Figure VIII.23. Thin section images of sample LM07C

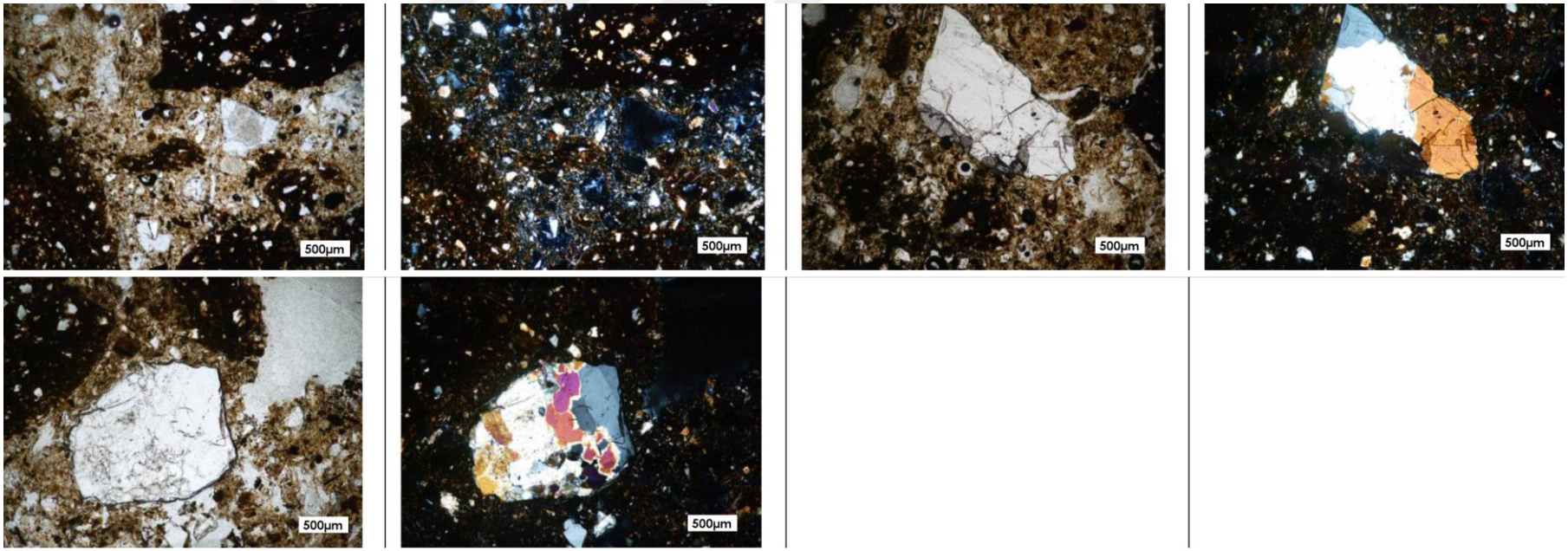


Figure VIII.24. Thin section images of sample LM08

Appendix C

MIP graphical data

Appendix IX – Complutum Archaeological Site

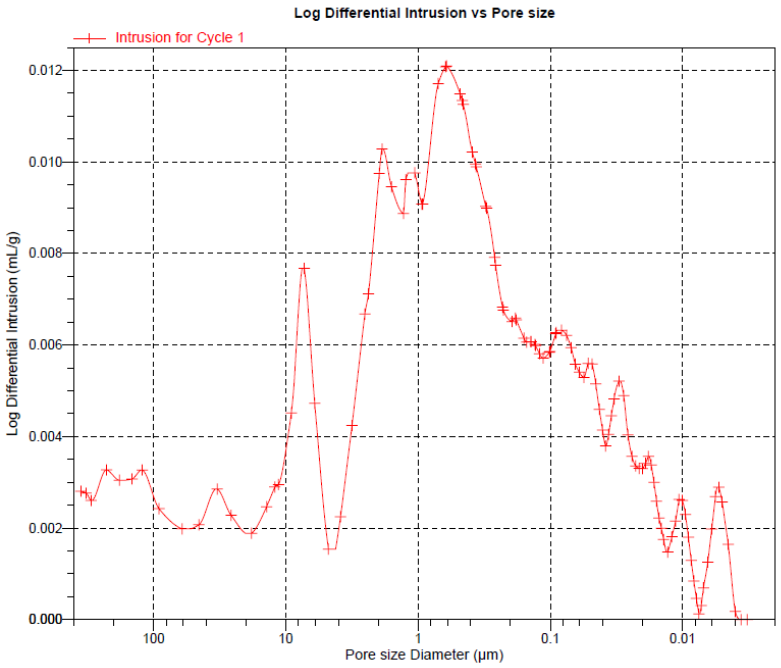


Figure IX.1. Log differential intrusion vs pore size diameter of CM02

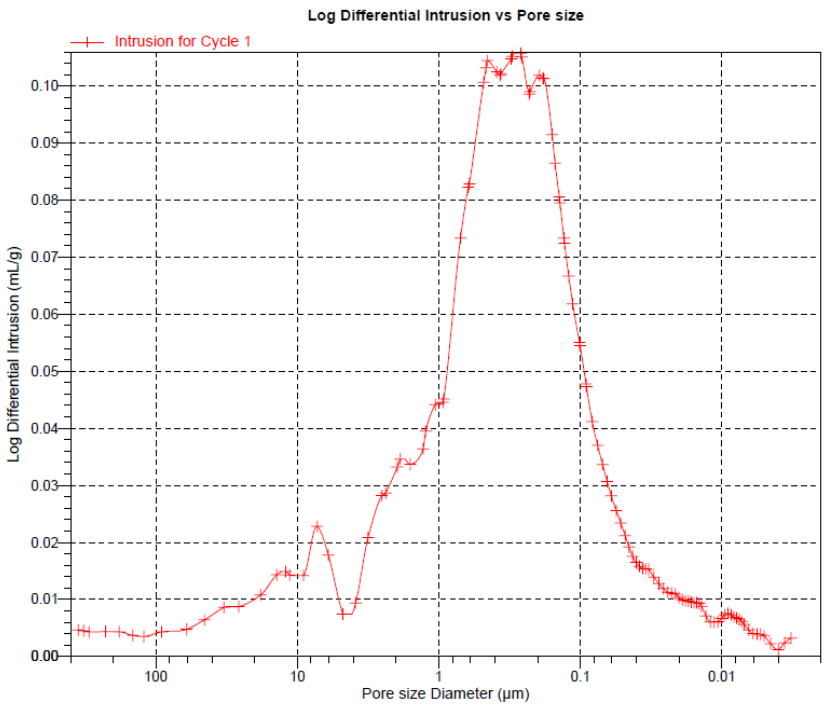


Figure IX.2. Log differential intrusion vs pore size diameter of CM06

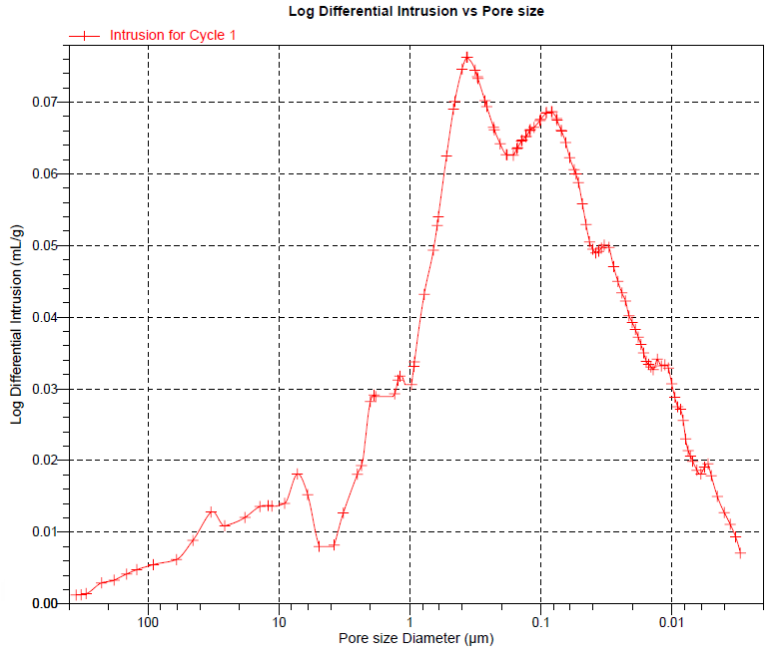


Figure IX.3. Log differential intrusion vs pore size diameter of CM07

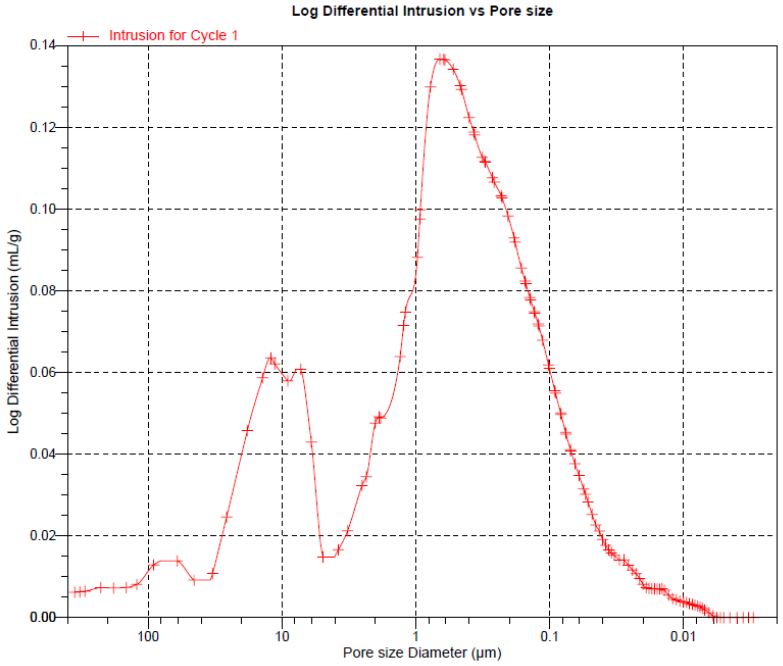


Figure IX.4. Log differential intrusion vs pore size diameter of CM09

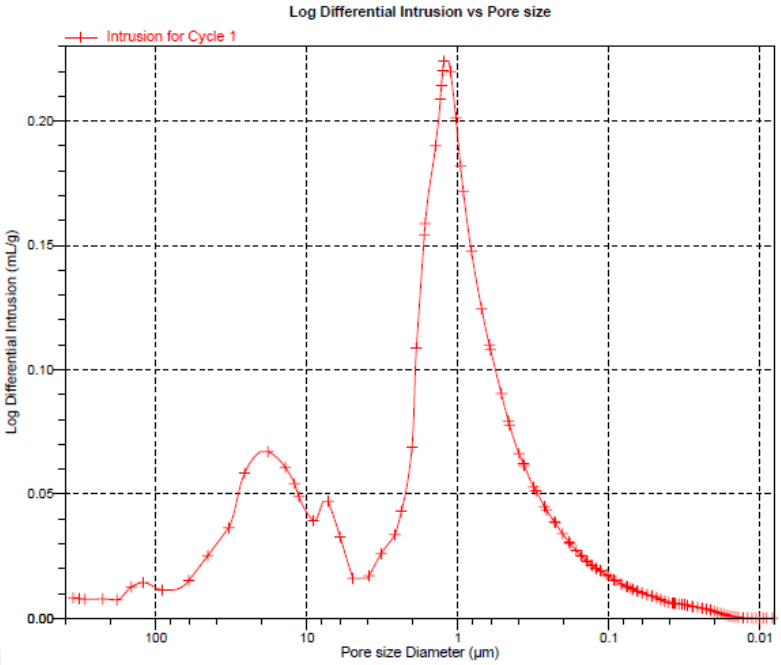


Figure IX.5. Log differential intrusion vs pore size diameter of CM15

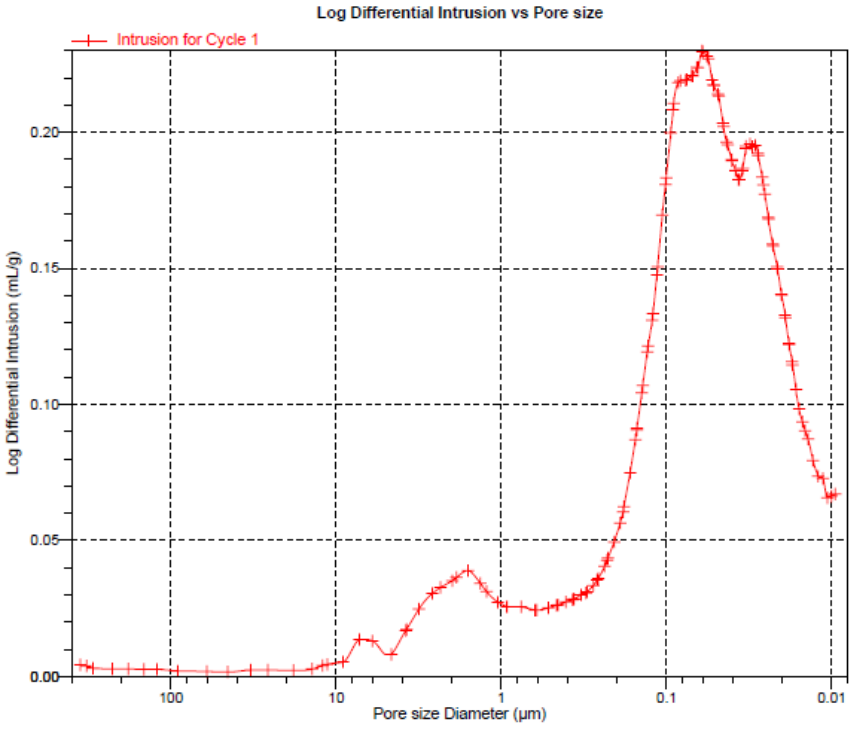


Figure IX.6. Log differential intrusion vs pore size diameter of CM16

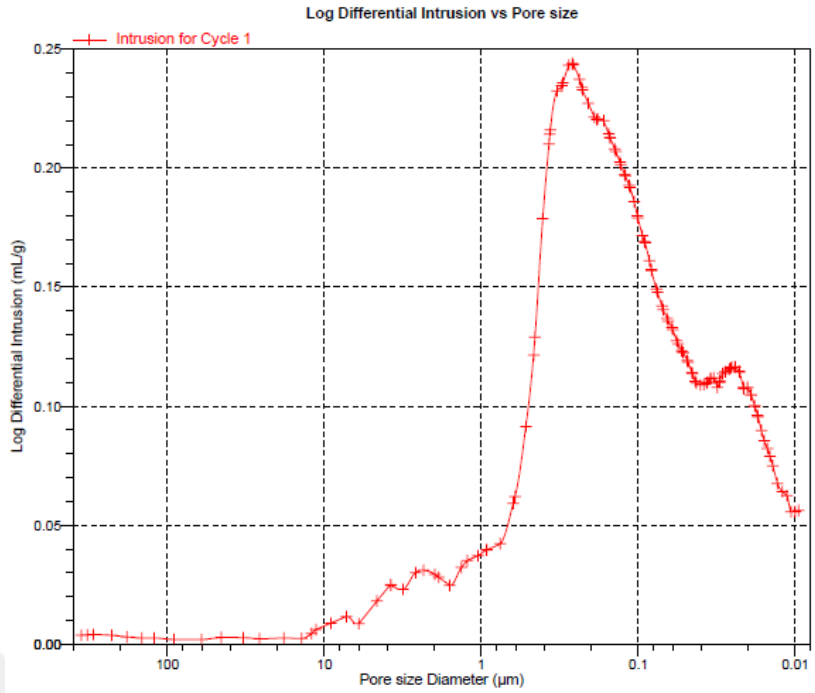


Figure IX.7. Log differential intrusion vs pore size diameter of CM27

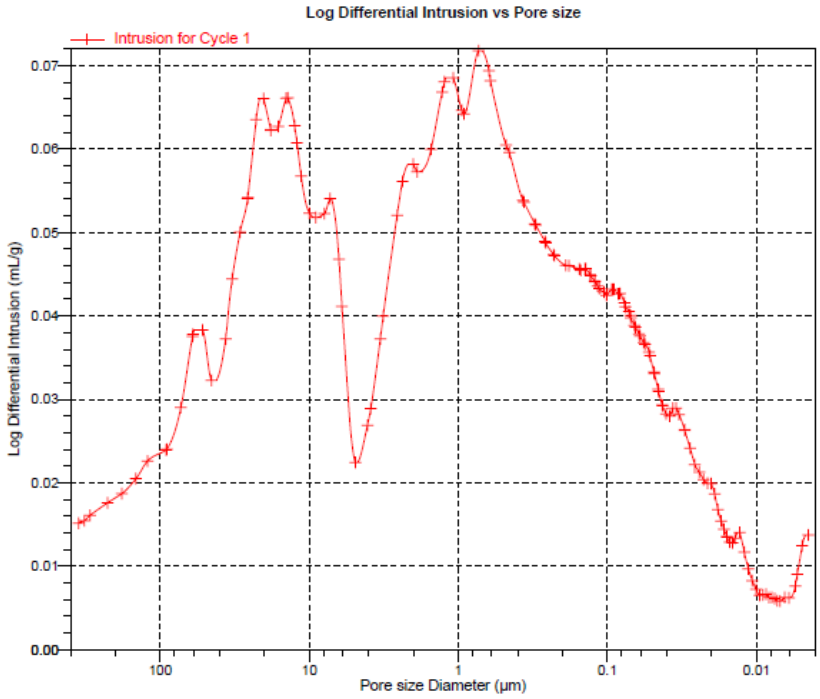


Figure IX.8. Log differential intrusion vs pore size diameter of CM31

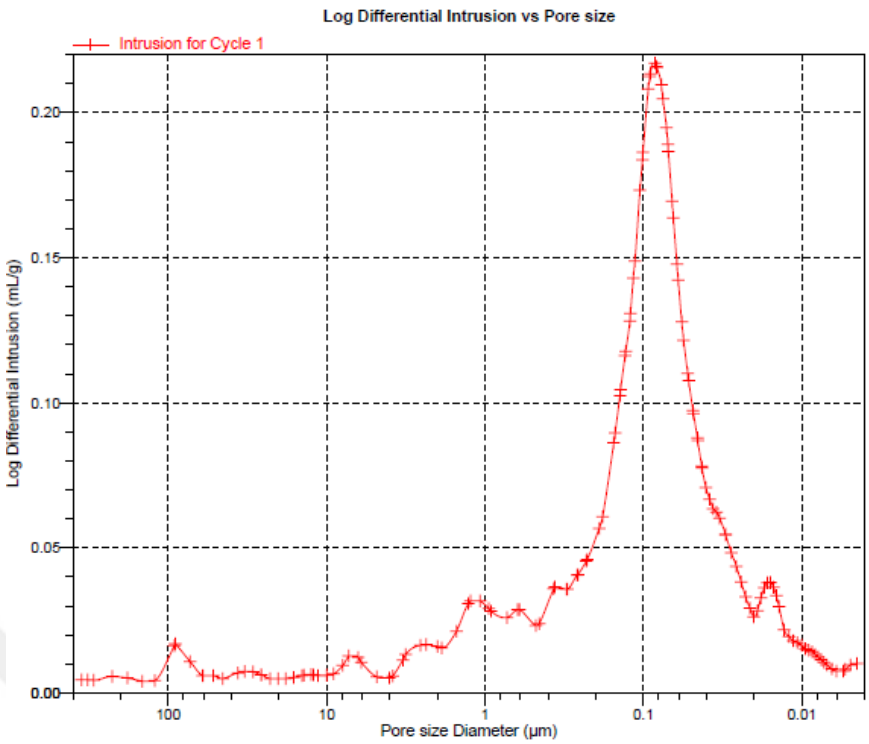


Figure IX.9. Log differential intrusion vs pore size diameter of CM38

Appendix X- Mérida Archaeologic Complex

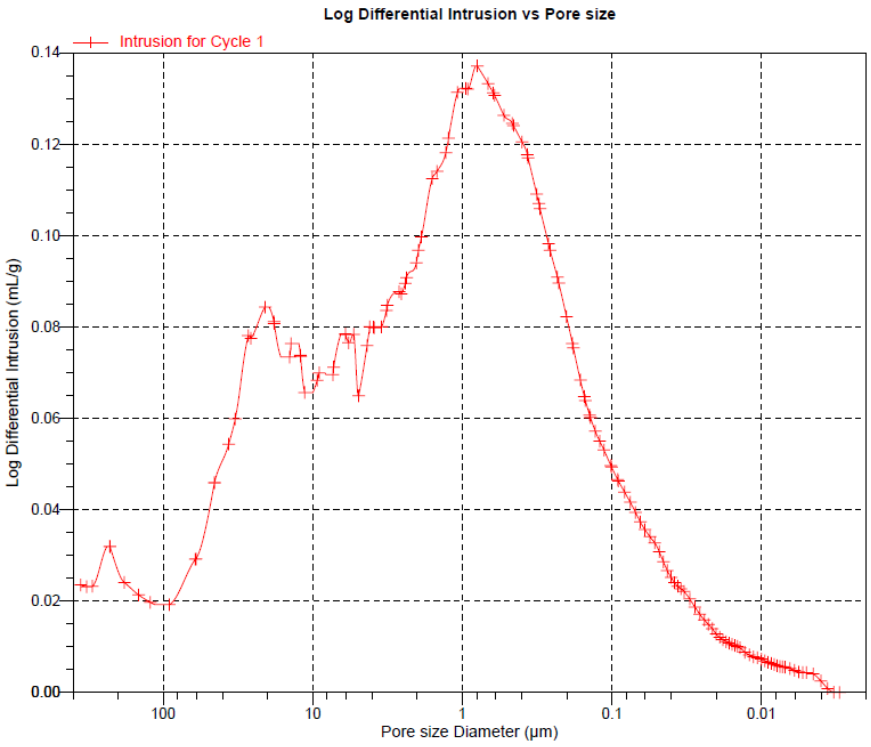


Figure X.1. Log differential intrusion vs pore size diameter of MM8

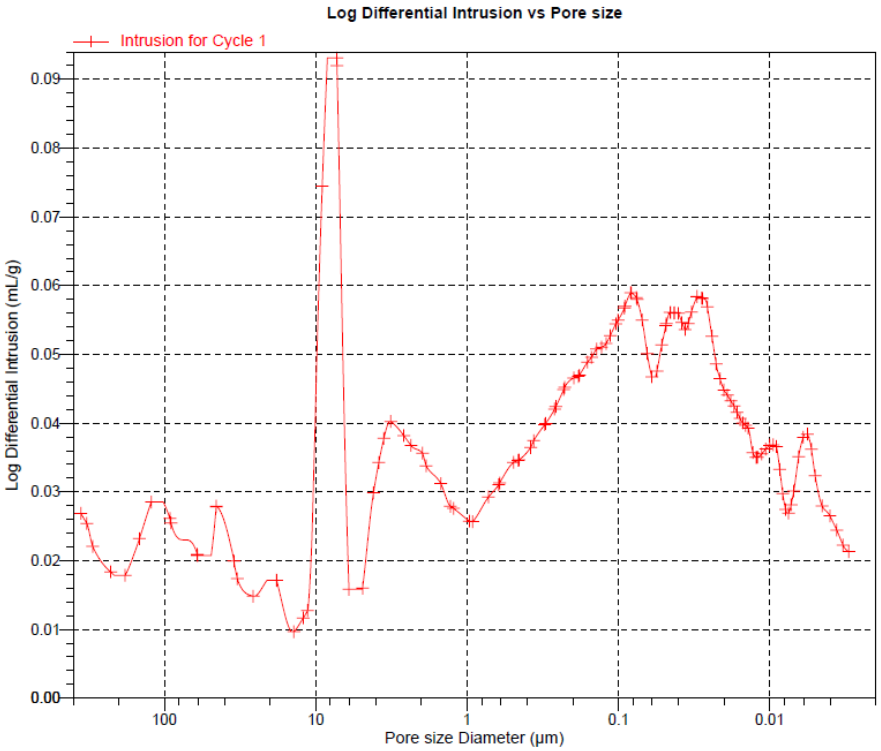


Figure X.2. Log differential intrusion vs pore size diameter of MM10

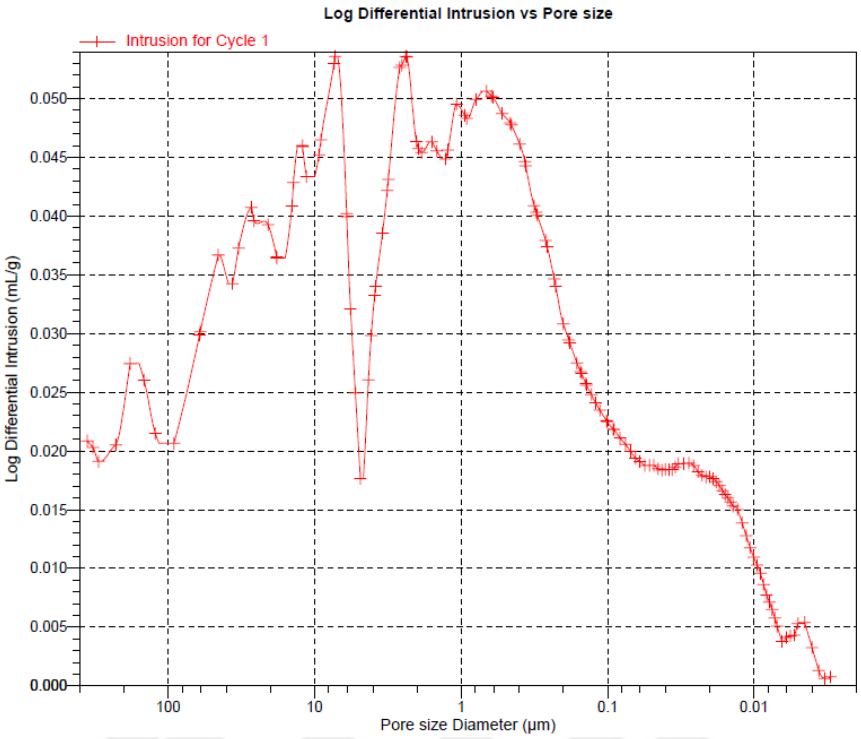


Figure X.3. Log differential intrusion vs pore size diameter of MM14

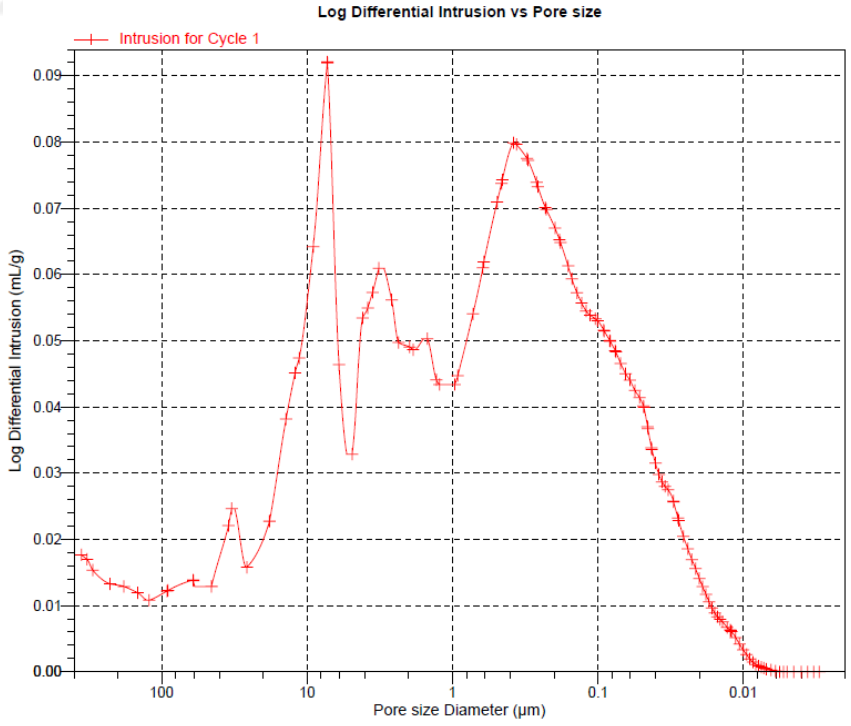


Figure X.4. Log differential intrusion vs pore size diameter of MM22

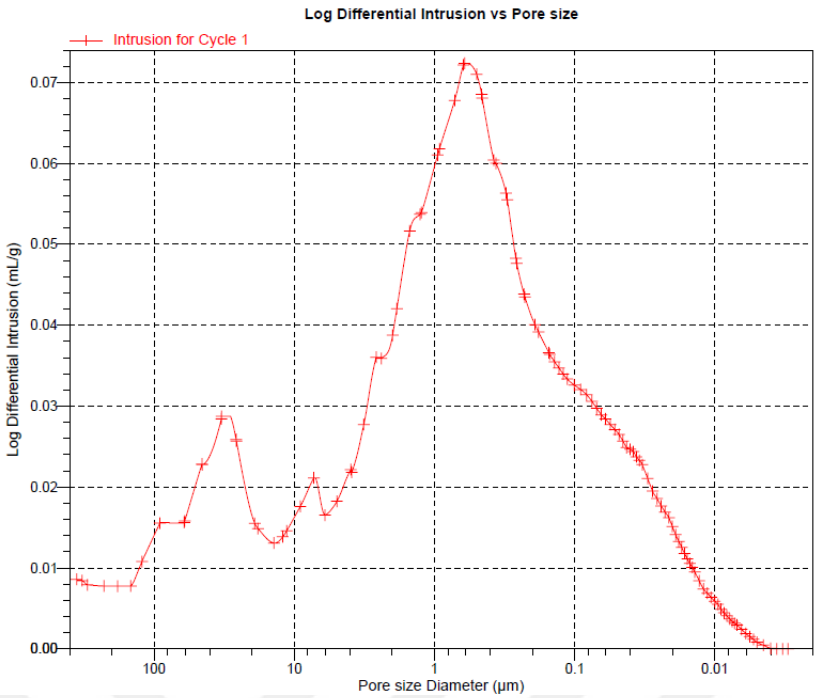


Figure X.5. Log differential intrusion vs pore size diameter of MM26

Appendix XI – Nysa Archaeological Site

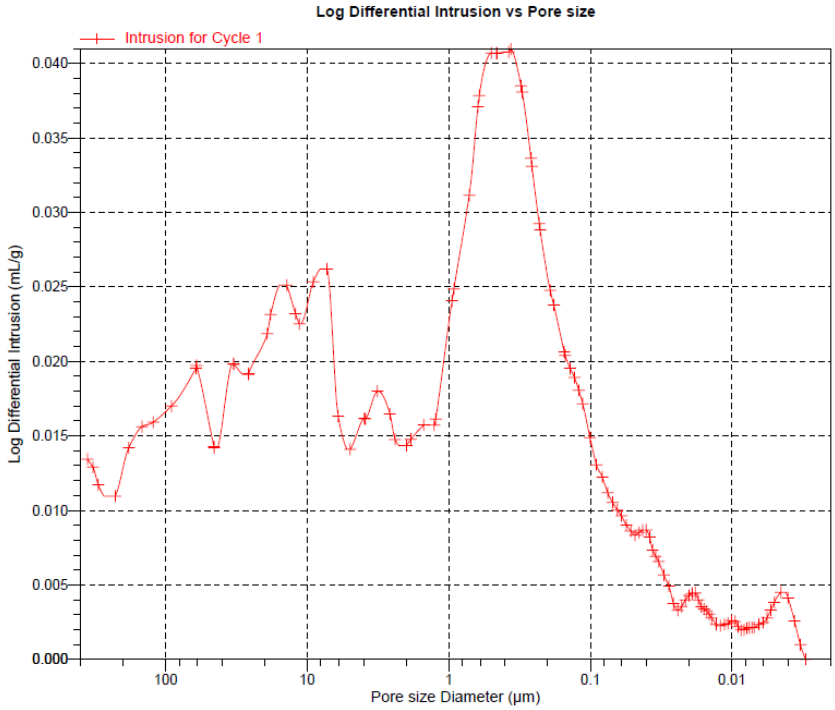


Figure XI.1. Log differential intrusion vs pore size diameter of NM12

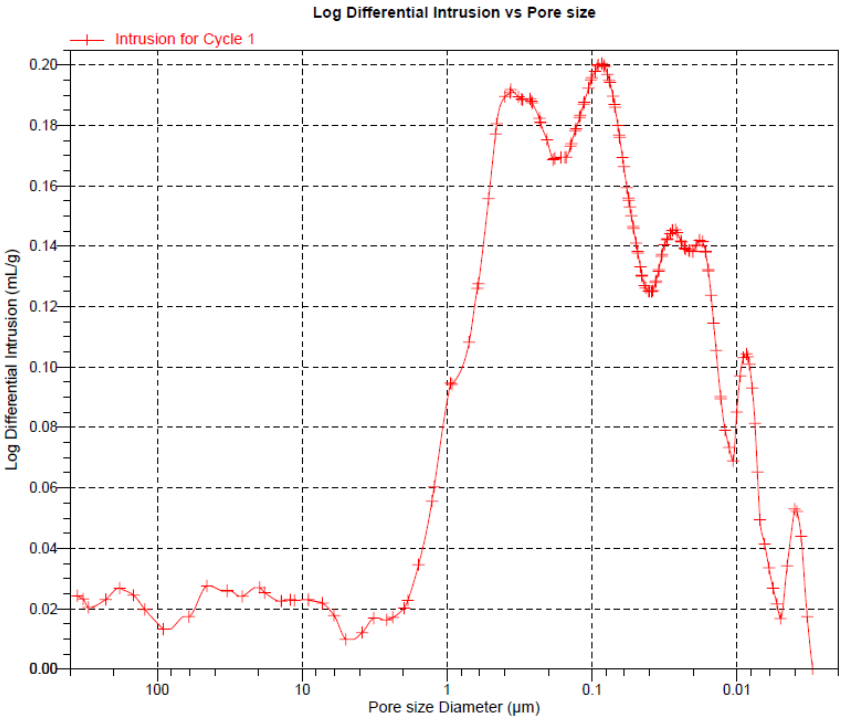


Figure XI.1. Log differential intrusion vs pore size diameter of NM16

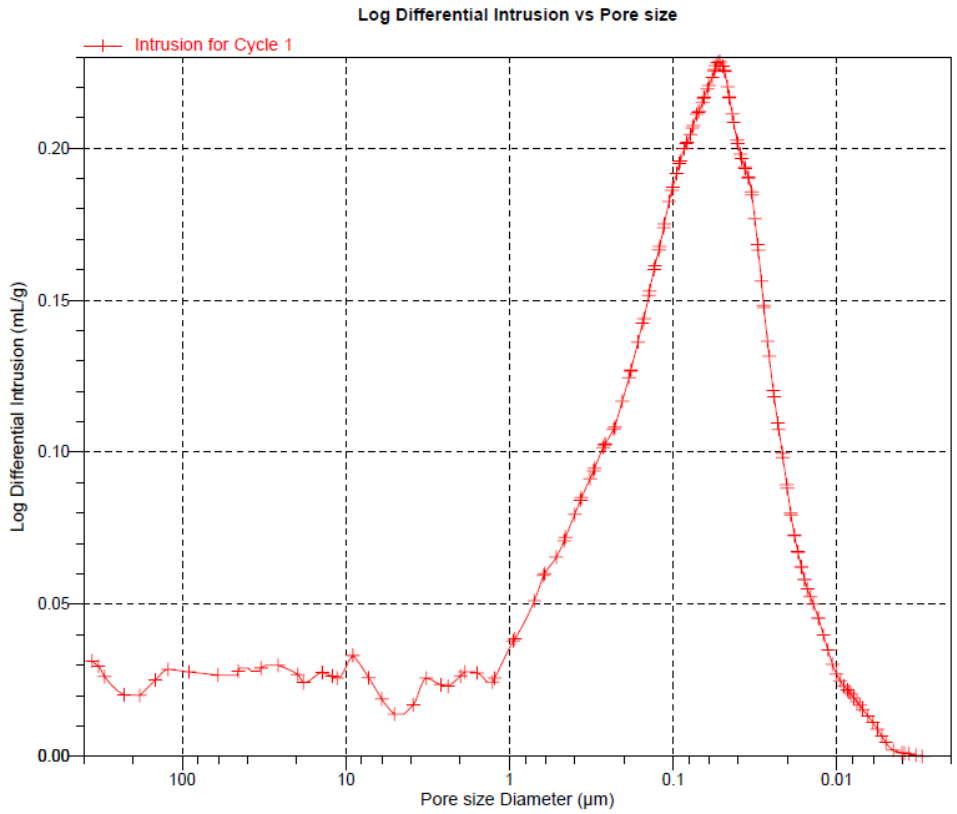


Figure XI.2. Log differential intrusion vs pore size diameter of NM23

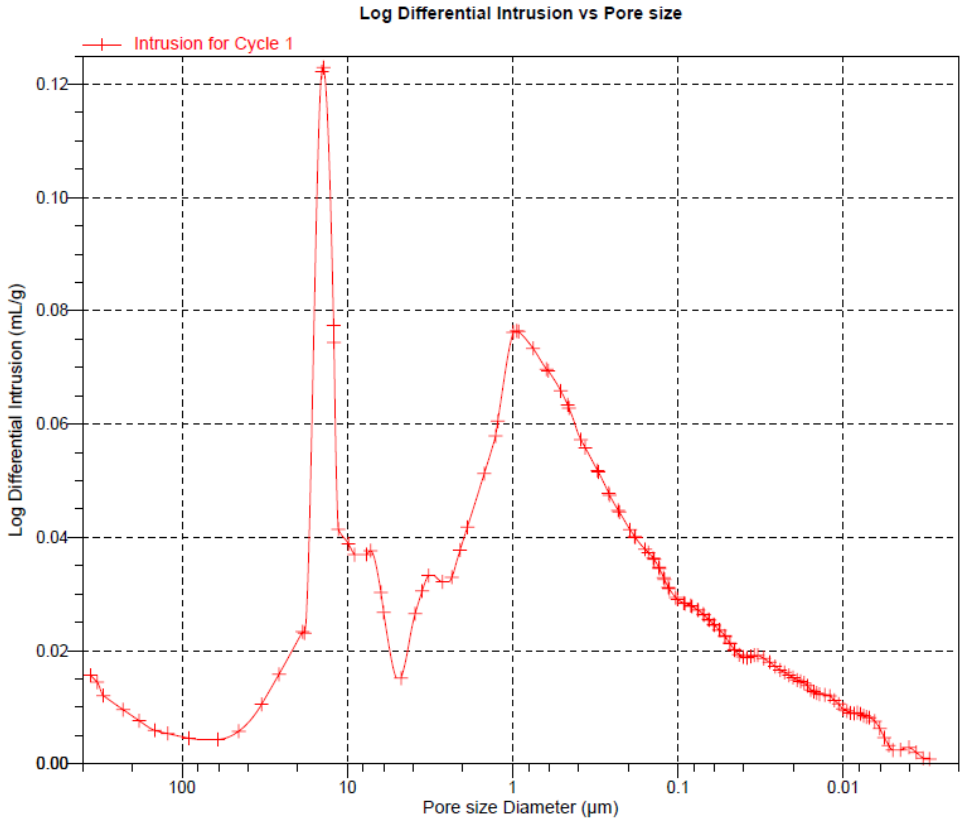


Figure. XI.3. Log differential intrusion vs pore size diameter of NM24

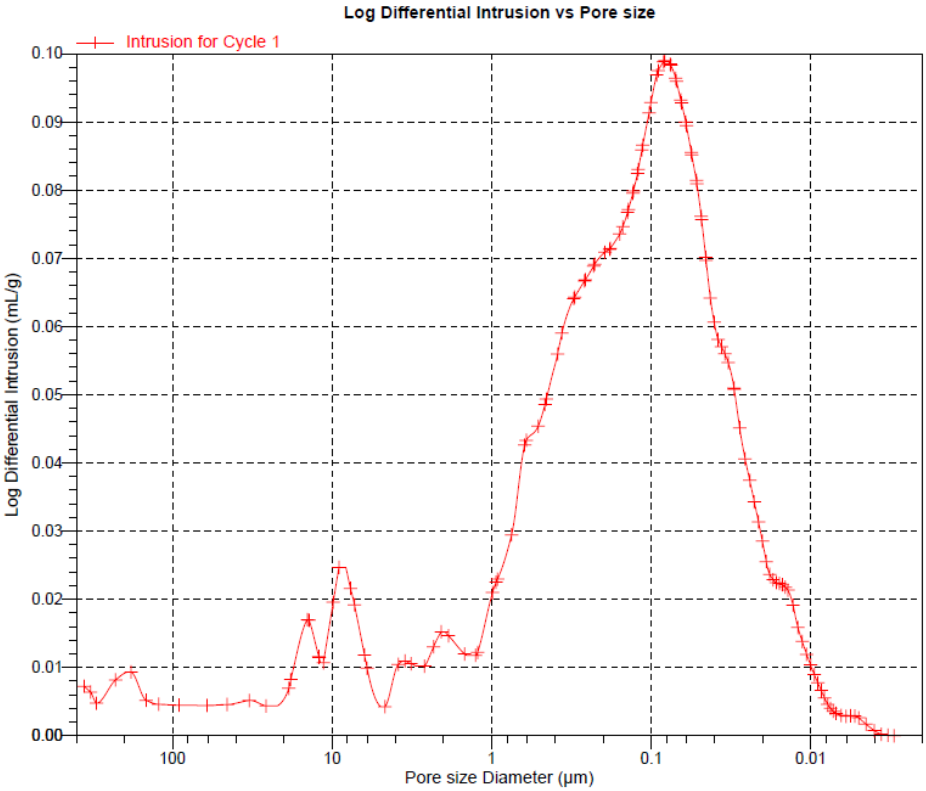


Figure XI.4. Log differential intrusion vs pore size diameter of NM25

Appendix XII- Sanctuary of Labraunda

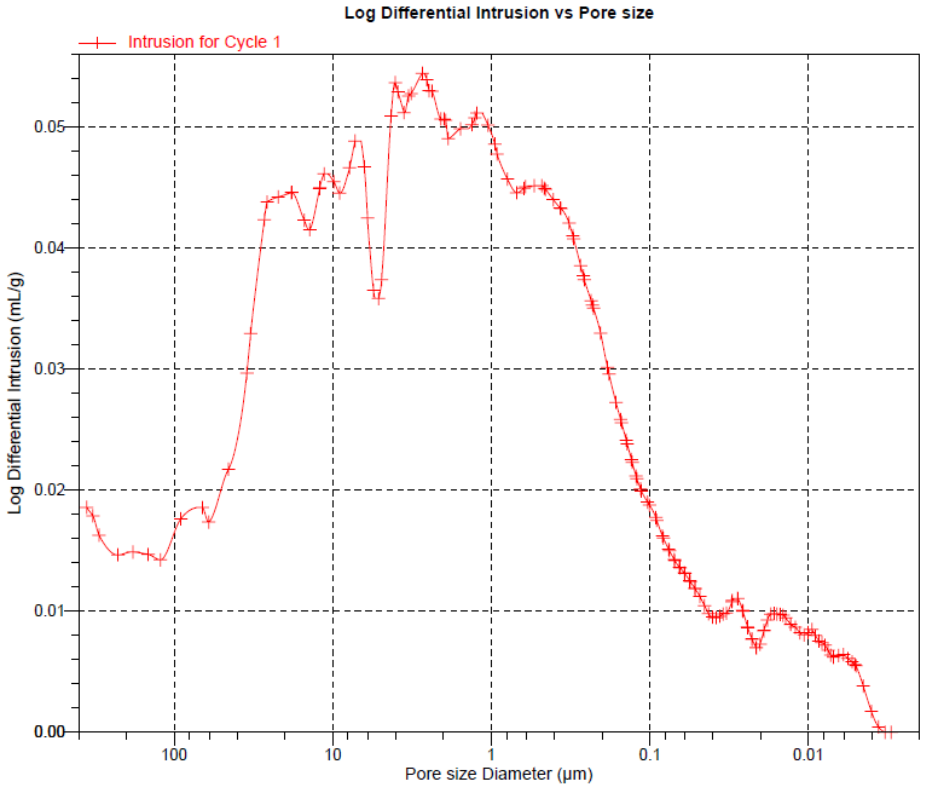


Figure XII.1. Log differential intrusion vs pore size diameter of LM03

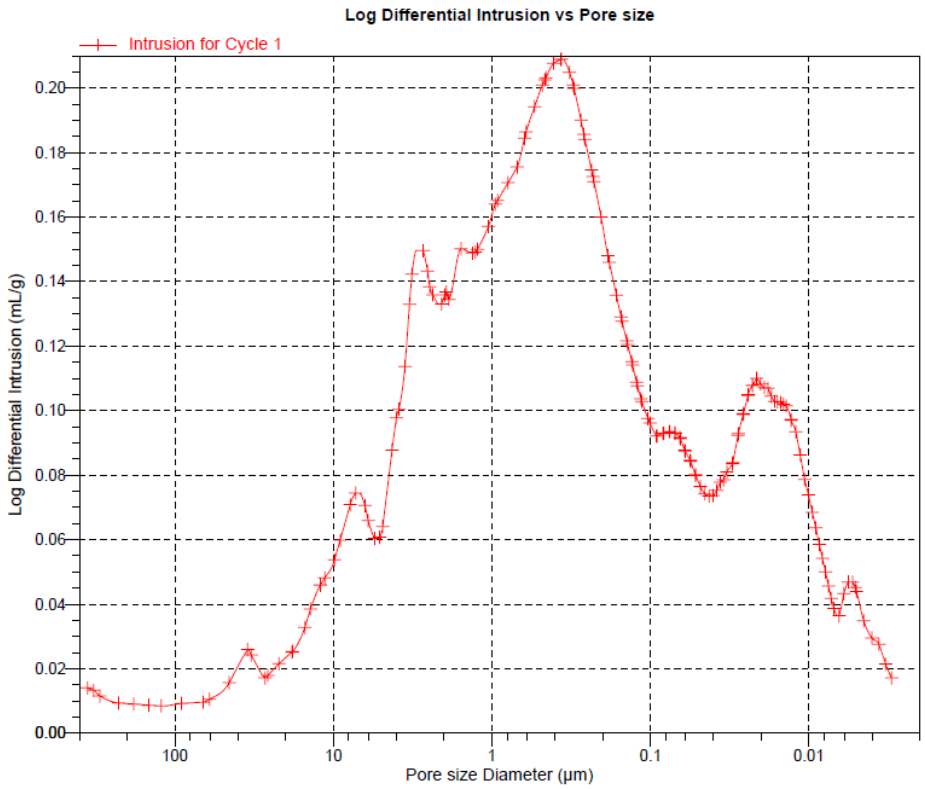


Figure XII.2. Log differential intrusion vs pore size diameter of LM06A

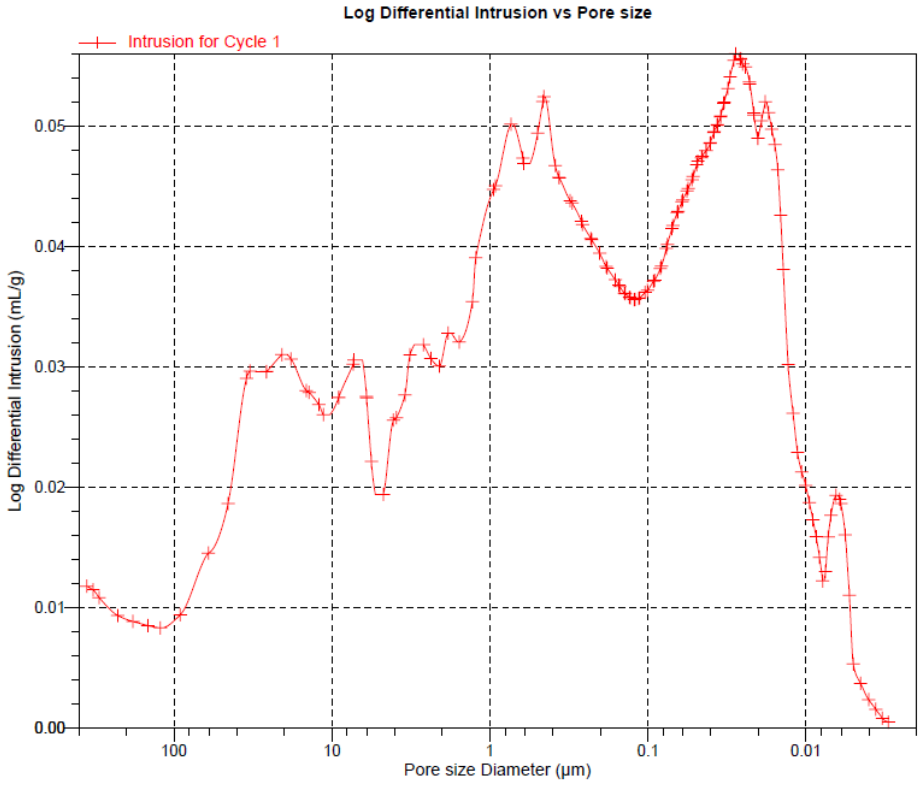


Figure XII.3. Log differential intrusion vs pore size diameter of LM07A

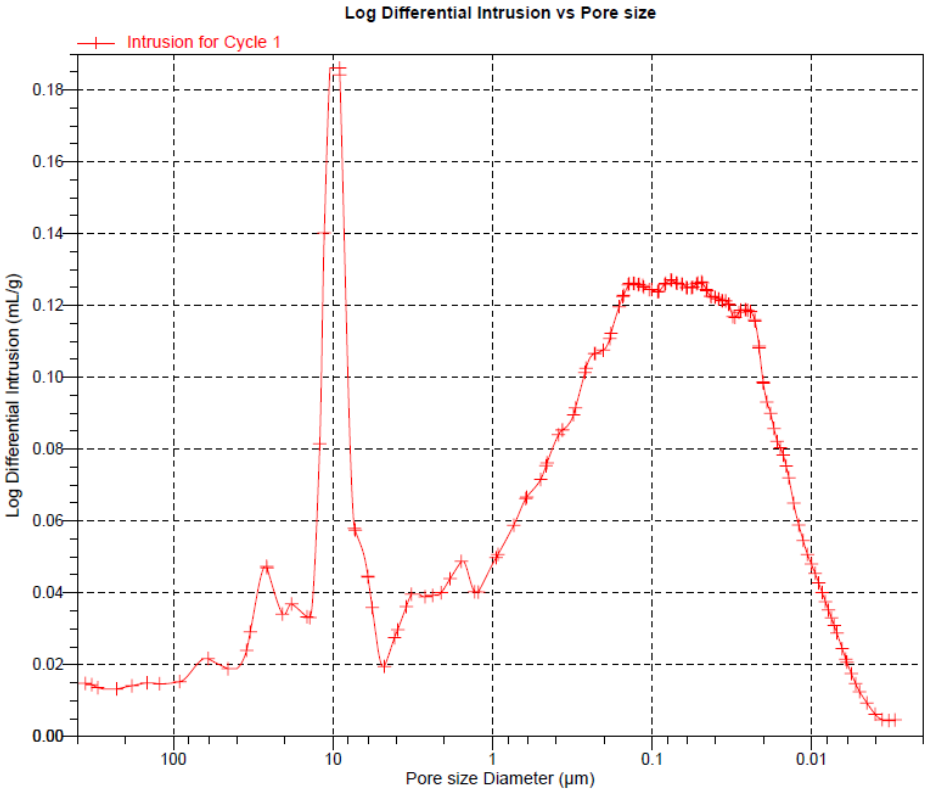


Figure XII.4. Log differential intrusion vs pore size diameter of LM07C

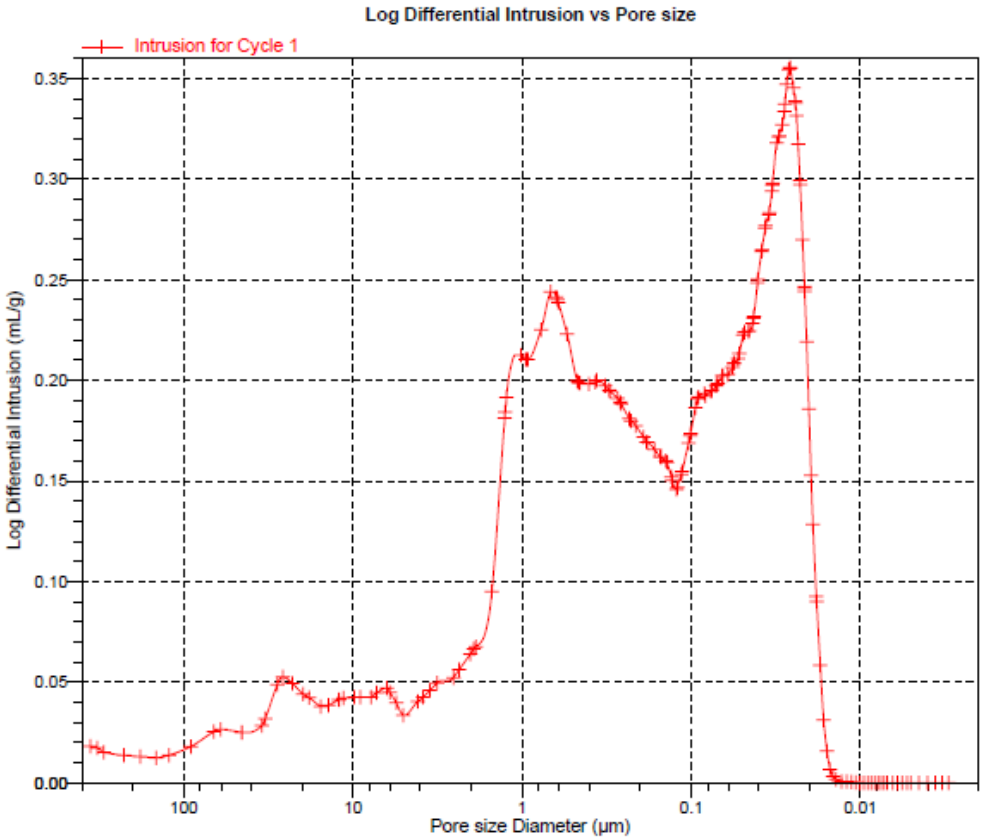


Figure XII.5. Log differential intrusion vs pore size diameter of LM09

Appendix D

Samples and laboratories used in experiments

Table D.1. Roman mortar samples analysed in each analytical technique (Complutum)

		OPM	XRD	Colour	Equotip	XRF	B:A Ratio	GSD	TGA-DSC	MIP
Complutum	CM01	X	X	X	X	X	X	X	X	
	CM02A	X	X	X	X	X	X	X	X	X
	CM03	X	X	X	X					
	CM04	X	X	X	X					
	CM05	X	X	X	X	X	X	X	X	
	CM06	X	X	X	X		X	X	X	X
	CM07	X	X	X	X	X	X	X	X	X
	CM08	X	X	X	X	X	X	X	X	
	CM09		X				X	X		X
	CM10	X	X	X	X	X	X	X	X	X
	CM11	X	X	X	X					
	CM12	X	X	X	X					
	CM13		X							
	CM14	X	X	X	X	X	X	X	X	
	CM15	X	X	X	X	X	X	X	X	X
	CM16A	X	X	X	X	X			X	X
	CM17	X	X	X	X					
	CM18	X	X	X	X		X	X	X	
	CM19									
	CM20	X	X	X	X					
	CM21		X							
	CM22		X				X	X	X	
	CM23		X							
	CM24	X	X	X	X					
	CM25	X	X	X	X					
	CM26		X				X	X	X	
	CM27		X						X	X
	CM28		X						X	
	CM29		X			X	X	X		
	CM30		X							
	CM31	X	X	X	X	X	X	X	X	X
	CM32		X							
	CM33	X	X	X	X	X	X	X	X	
	CM34		X				X	X		
	CM35	X	X	X	X	X			X	
	CM36									
	CM37	X		X	X				X	
	CM38						X	X		X

Table D.1cont. Roman mortar samples analysed in each analytical technique (Mérida)

		OPM	XRD	Colour	Equotip	XRF	B:A Ratio	GSD	TGA-DSC	MIP
Mérida	MM1						x	x		
	MM2	x	x	x	x	x	x	x	x	
	MM3	x	x	x	x	x	x	x	x	
	MM4									
	MM5	x	x	x	x				x	
	MM6	x	x	x	x	x	x	x	x	
	MM7	x	x	x	x				x	
	MM8	x	x	x	x	x	x	x	x	x
	MM9									
	MM10	x	x	x	x	x	x	x	x	x
	MM11	x	x	x	x				x	
	MM12	x	x	x	x				x	
	MM13									
	MM14	x	x	x	x	x	x	x	x	x
	MM15	x	x	x	x				x	
	MM16	x	x	x	x	x	x	x	x	
	MM17									
	MM18	x	x	x	x	x			x	
	MM19									
	MM20	x	x	x	x	x	x	x	x	
	MM21	x	x	x	x				x	
	MM22	x	x	x	x	x	x	x	x	x
	MM23									
	MM24		x			x	x	x		
	MM25	x	x	x	x				x	
	MM26	x	x	x	x				x	x
	MM27	x	x	x	x	x	x	x	x	

Table D.1. cont. Roman mortar samples analysed in each analytical technique (Nysa)

		OPM	XRD	Colour	Equotip	XRF	B:A Ratio	GSD	TGA-DSC	MIP
Nysa	NM01	X	X	X	X				X	
	NM02A	X	X	X	X	X	X	X	X	
	NM03	X	X	X	X				X	
	NM04	X	X	X	X	X	X	X	X	
	NM05A	X	X	X	X	X	X	X	X	
	NM06	X	X	X	X				X	
	NM07	X	X	X	X	X			X	
	NM08	X	X	X	X		X	X	X	
	NM09	X	X	X	X				X	
	NM10B	X	X	X	X		X	X	X	
	NM11	X	X	X	X	X	X	X	X	
	NM12		X	X	X		X	X	X	X
	NM13		X				X	X	X	
	NM14		X	X	X				X	
	NM15	X	X	X	X				X	
	NM16	X	X	X	X		X	X	X	X
	NM22	X	X	X	X		X	X	X	
	NM23	X	X				X	X	X	X
	NM24	X	X						X	
	NM25		X	X	X		X	X	X	X
	NM26	X	X	X	X		X	X	X	
	NM27		X	X	X				X	

Table .D.1.cont. Roman mortar samples analysed in each analytical technique (Labraunda)

		OPM	XRD	Colour	Equotip	XRF	B:A Ratio	GSD	TGA-DSC	MIP
Labraunda	LM01A	X	X	X	X				X	
	LM01B			X	X					
	LM01C	X	X	X	X				X	
	LM02	X	X	X	X				X	
	LM03			X	X	X	X	X		X
	LM04A	X	X	X	X	X			X	
	LM04B	X	X	X	X				X	
	LM05	X	X	X	X	X			X	
	LM06A	X	X	X	X	X	X	X	X	X
	LM06B	X	X	X	X		X	X	X	
	LM06C	X	X	X	X		X	X	X	
	LM07A	X	X	X	X	X	X	X	X	X
	LM07B	X	X	X	X		X	X	X	
	LM07C	X	X	X	X		X	X	X	X
	LM07D			X	X	X	X	X		
	LM08	X	X	X	X		X	X	X	
	LM09	X	X	X	X	X	X	X	X	X

Table D.2. Equipment and centre for each analytical technique

Analytical Technique	Equipment	Centre
OPM	Olympus BX51 (equipped with a digital camera Olympus DP12	Department of Petrology and Geochemistry UCM
XRD	Bruker D8 Advance X-ray diffractometer	IGEO (CSIC-UCM)
TGA-DSC	TA Instruments SDT-Q600, DSC Q-200 and General V4.1C DuPont 2000	CAI Geológicas of UCM
XRF	PHILIPS Magix Pro (PW-2440) with 4 kW X-Ray Generator	Centre of Scientific Instrumentation of University of Granada
Colour Spectrophotometry	CM 700d-Minolta	Petrophysics Laboratory – IGEO (CSIC-UCM)
Raman Spectroscopy	Inspector Raman Delta Nu	Petrophysics Laboratory – IGEO (CSIC-UCM)
MIP	Micromeritics' AutoPore IV 9500 Series	Petrophysics Laboratory – IGEO (CSIC-UCM)
SEM_EDS	JEOL JSM 6400	The National Microscopy Centre (CNME)
Surface Hardness	Rebound microdurometer Leeb Equotip 3D Proceq	Petrophysics Laboratory – IGEO (CSIC-UCM)
Acid in/soluble test	HCl	Petrophysics Laboratory – IGEO (CSIC-UCM)
Carbonation front	Phenolphthalein	Petrophysics Laboratory – IGEO (CSIC-UCM)
Flexural and compressive strength test	SCM3000 95	Construction laboratory of ETSAM UPM
Air permeability	Tiny-Perm-II by Vindum Engineeering New England Research Inc	Petrophysics Laboratory – IGEO (CSIC-UCM)
UPV	PUNDIT CNS ELECTRONICS	Petrophysics Laboratory – IGEO (CSIC-UCM)
Water absorption under vacuum	Vacuum chamber to test on rocks Rc-002; Test Systems, S.L	Petrophysics Laboratory – IGEO (CSIC-UCM)
Water absorption through capillarity	Vessel	Petrophysics Laboratory – IGEO (CSIC-UCM)

Technical Leaflet

IBZ-Salzchemie GmbH & Co.KG

DiLoCarB

Agent for enhanced carbonation

Natural carbonation of lime mortars and plasters is based on the reaction with atmospheric carbon dioxide. This is a very complex process, which depends on many factors, for example humidity, air circulation and temperature. The process is slow and needs weeks, sometimes years. Complete drying of the mortars as well as low humidity stops carbonation and the mortar will never achieve the required properties.

DiLoCarB allows a fast and complete carbonation process by a directed chemical reaction. DiLoCarB consists of ethanol, diethyl carbonate and water. The active component -diethyl carbonate- decomposes as soon as in contact with calcium hydroxide to ethanol and carbonate ions. These are able to react with present calcium ions. calcium carbonate is formed. This reaction is much faster than carbonation by reaction with atmospheric carbon dioxide and allows the conversion of calcium hydroxide into $CaCO_3$ also on places, where the contact with air is possible in a limited extent only.

Applications

DiLoCarB is often used in combination with *CaLoSiL®* products, but it can be also applied for the carbonation of mortars or plasters based on white lime hydrate. When CaLoSiL® is applied in a first step, then DiLoCarB should be used when the alcohol from CaLoSiL® has been evaporated. The material is fully saturated with DiLoCarB, for example by capillary suction, spraying, or injection. DiLoCarB is a clear solution with a low viscosity and a high penetration capacity. It forms fine calcium carbonate crystals.

The reaction time is between 30 and 240 minutes, depending on the reactivity of the present calcium hydroxide. During that time evaporation of DiLoCarB has to be prevented, for example by covering with plastic foil or humid cloths.

The success of the DiLoCarB application depends on many factors, for example

- Reactivity of the present calcium hydroxide.
- Suction capacity and porosity of the materials to be treated.
- Moisture and salt content.

Before using in large scale we recommend to treat a small test field with DiLoCarB in order to find out the most favourable application method.

Packaging

DiLoCarB is available in 500 mL, 1 L and 5 L containers.

Storage

DiLoCarB has to be stored between +5 °C and +30 °C. In unopened, original containers, storage for at least one year is possible.

Safety

DiLoCarB is flammable/combustible. Keep away from oxidisers, heat, sparks and flames. Avoid spilling, skin and eye contact. Ventilate well, avoid breathing vapours. Do not breathe vapour or mist. Do not smoke. Keep containers closed. Wash thoroughly after handling. Keep away from sources of ignition. Please store in tightly closed containers in a cool and dry place. Further information concerning safety during transport, storage and handling as well as for disposal can be found in our latest Material Safety Data Sheet. Follow the given instructions and if there are more questions, do not hesitate to contact us.

The information mentioned above is state of the art and has been developed by intensive research and development. The application of our products and their use is beyond the range of our influence. Therefore IBZ-Salzchemie GmbH & Co. KG cannot take any liability from events that result from the information contained in this leaflet. Careful and considered use of DiLoCarB is highly recommended.

IBZ-Salzchemie GmbH & Co.KG

Schwarze Kiefern 4 • 09633 Halsbrücke • Germany • Tel.:+49 3731 200155 • Fax: +49 3731 200156 •
www.ibz-freiberg.de • info@ibz-freiberg.de